HORT PAPERS IN—

strogeology

conomic geology

tuarine hydrology

oods

eochemistry

eochronology

eophysics

eothermal
instrumentation

acial geology

round water

arine geology

ineralogy

leontology

trology

uality of water

emote sensing

ratigraphy

rface water

GEOLOGICAL SURVEY RESEARCH 1971

Chapter C

GEOLOGICAL SURVEY PROFESSIONAL PAPER 750–C

GEOLOGICAL SURVEY RESEARCH 1971

Chapter C

GEOLOGICAL SURVEY PROFESSIONAL PAPER 750–C

Scientific notes and summaries of investigations in geology, hydrology, and related fields

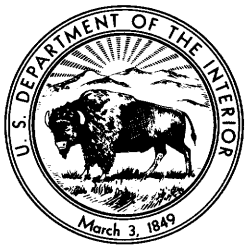

UNITED STATES GOVERNMENT PRINTING OFFICE, WASHINGTON: 1971

UNITED STATES DEPARTMENT OF THE INTERIOR

ROGERS C. B. MORTON, Secretary

GEOLOGICAL SURVEY

W. A. Radlinski, Acting Director

For sale by the Superintendent of Documents, U.S. Government Printing Office
Washington, D.C. 20402 - Price $2.75

CONTENTS

GEOLOGIC STUDIES

GEOLOGICAL SURVEY RESEARCH 1971

This collection of 40 short papers is the second published chapter of "Geological Survey Research 1971." The papers report on scientific and economic results of current work by members of the Geologic and Water Resources Divisions of the U.S. Geological Survey.

Chapter A, to be published later in the year, will present a summary of significant results of work done in fiscal year 1971, together with lists of investigations in progress, reports published, cooperating agencies, and Geological Survey offices.

"Geological Survey Research 1971" is the twelfth volume of the annual series Geological Survey Research. The eleven volumes already published are listed below, with their series designations.

Geological Survey Research	*Prof. Paper*
1960	400
1961	424
1962	450
1963	475
1964	501
1965	525
1966	550
1967	575
1968	600
1969	650
1970	700

GRAIN-SIZE DISTRIBUTION AND THE DEPOSITIONAL HISTORY OF NORTHERN PADRE ISLAND, TEXAS

By KENDELL A. DICKINSON, Corpus Christi, Tex.

Abstract.—Northern Padre Island, part of the Texas gulf coast barrier island system, consists of 5–10 feet of fine sand ($M_{\bar{X}} = 2.5\phi$) overlying slightly coarser sand ($M_{\bar{X}} = 2.3\phi$). The finer sand is being supplied from the north and the coarser sand from the south. The lower sand was largely derived from the Rio Grande near the south end of the island when (1) longshore drift from the south extended farther north, (2) sediment discharge from the Rio Grande was larger, or (3) the mouth of the Rio Grande was located farther north. Variation of size parameters across the surface of the island indicates that sand from the two sources has been mixed mostly in deflation basins in the younger barrier flats where the wind has eroded deeply. Lack of regular decrease in grain size with depth on northern Padre Island indicates that the island is not prograding. It is of special interest that grain size decreasing with depth, as in Galveston Island, is not a relation found in all barrier islands.

Padre Island off the south coast of Texas is a 110-mile-long barrier island that ranges in width from about 1 to 4 miles and extends southward from near Corpus Christi Bay to Port Isabel near the mouth of the Rio Grande (figs. 1 and 2). The island is a body of fine sand that is lenticular in cross section and ranges in thickness from about 5 feet in the southern part to about 60 feet in the northern part (fig. 3). It is separated from the mainland by a narrow body of shallow water, Laguna Madre. Grain size is one of the fundamental properties that has been useful in distinguishing sediments from different sources in the area.

Curray (1960) showed that in the Gulf of Mexico, sediment masses may be characterized by grain-size modes. Hayes (1964, 1965) applied mean grain size and other size parameters to differentiate sediment masses on the surface of Padre Island. He found that sand of the southern part of the island is of larger mean grain size (about 2.2ϕ) than that of the northern part (about 3ϕ), and he delineated a transitional area (fig. 1) in the central part of the island. Bullard (1942) demonstrated that heavy minerals reflect a similar pattern on Padre Island. In Laguna Madre, Rusnak (1960) has shown that a difference in feldspar content is related to source of sediment. Longshore drift, which is generally southerly on northern Padre Island and northerly on the southern part, seems to account for the distribution pattern of sediment on the surface. The convergence of these currents is discussed in detail by Lohse (1955) (fig. 1).

This report describes the sand-size characteristics of the surface and subsurface samples from the segment of the northern part of the island that is within the South Bird Island 7½-minute quadrangle and infers source areas and depositional history (figs. 1 and 2).

METHODS

Surface samples were collected from 80 stations along A–A' (fig. 2). The sample stations were generally located 100 feet apart along the gulfward half of the traverse and 200 feet apart along the lagoonward half of the traverse. An additional 21 surface samples from various locations in central and southern Padre Island were collected and analyzed for purposes of comparison.

One hundred and sixty subsurface samples were collected from rotary drill cuttings from 14 drill holes (fig. 4). Because these samples were to some degree contaminated by uphole caving during drilling, their usefulness is somewhat limited, though not completely destroyed. Contamination generally increases with depth.

Grain-size analyses were made by the settling-tube method of Emery (1938). Prior to analysis, shell fragments were removed with hydrochloric acid, sodium hexametaphosphate was added for dispersion, and the sample was reduced to about 3 grams with a sample splitter. Results of the settling-tube analyses of surface samples compared closely with those of the sieve analyses of Hayes (1965). However, Hayes found that the sand from a northern source was somewhat finer than the present work indicates. This difference and other differences noted may result from the different analytical methods used.

The mean grain size, $\bar{X}_\phi$; standard deviation, σ_ϕ; skewness, Sk_ϕ; and kurtosis, K_ϕ; were calculated by the method of moments (Griffiths, 1967, p. 90–91). $M_{\bar{X}}$, M_σ, M_{Sk}, and M_K are the averages of $\bar{X}_\phi$, σ_ϕ, Sk_ϕ and K_ϕ, respectively, for various depth levels and depositional environments. First derivative frequency-distribution curves (Curray, 1961) were plotted for the surface samples and for one subsurface sample, commonly from the 20-foot-depth level for each drill hole.

U.S. GEOL. SURVEY PROF. PAPER 750-C, PAGES C1-C6

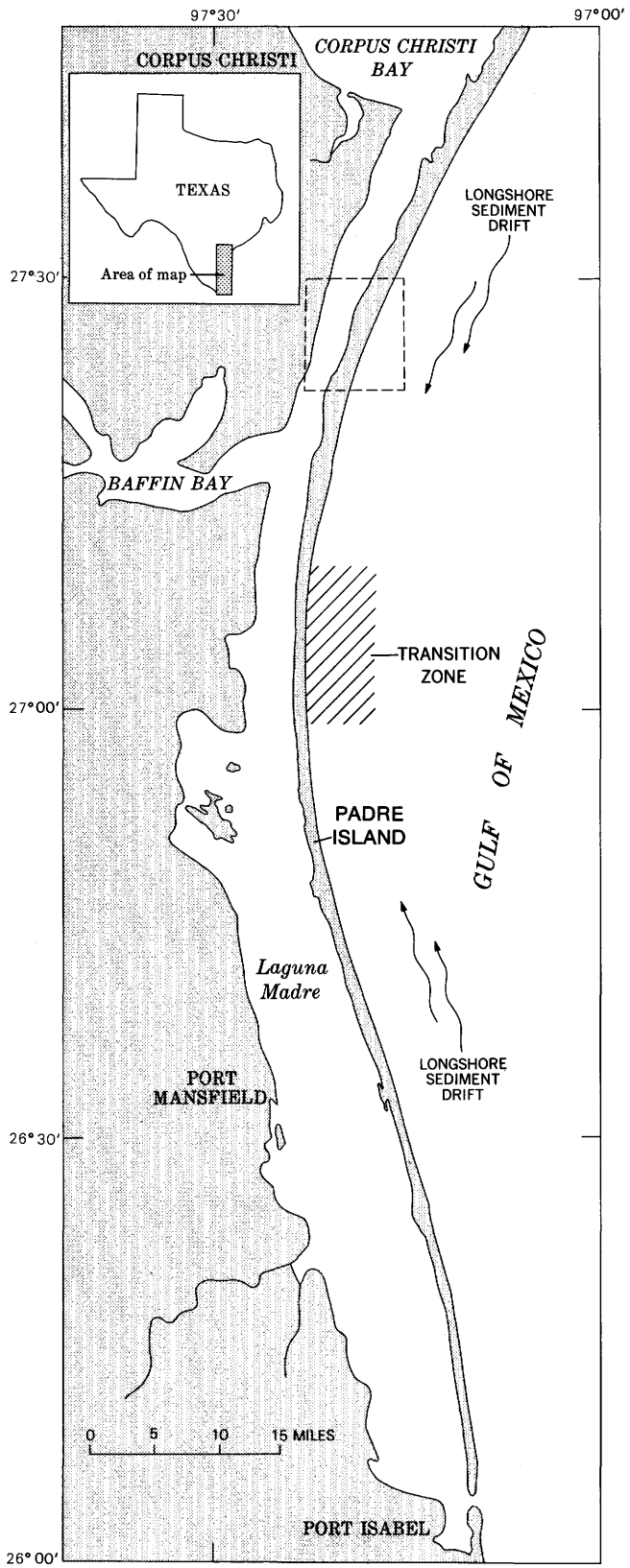

Figure 1.—Index map showing area of report, Padre Island, Tex. Mixing of sands from southern and northern sources occurs in the transition zone (Hayes, 1964). Dashed rectangle in upper part of map shows location of South Bird Island 7½-minute quadrangle (fig. 2).

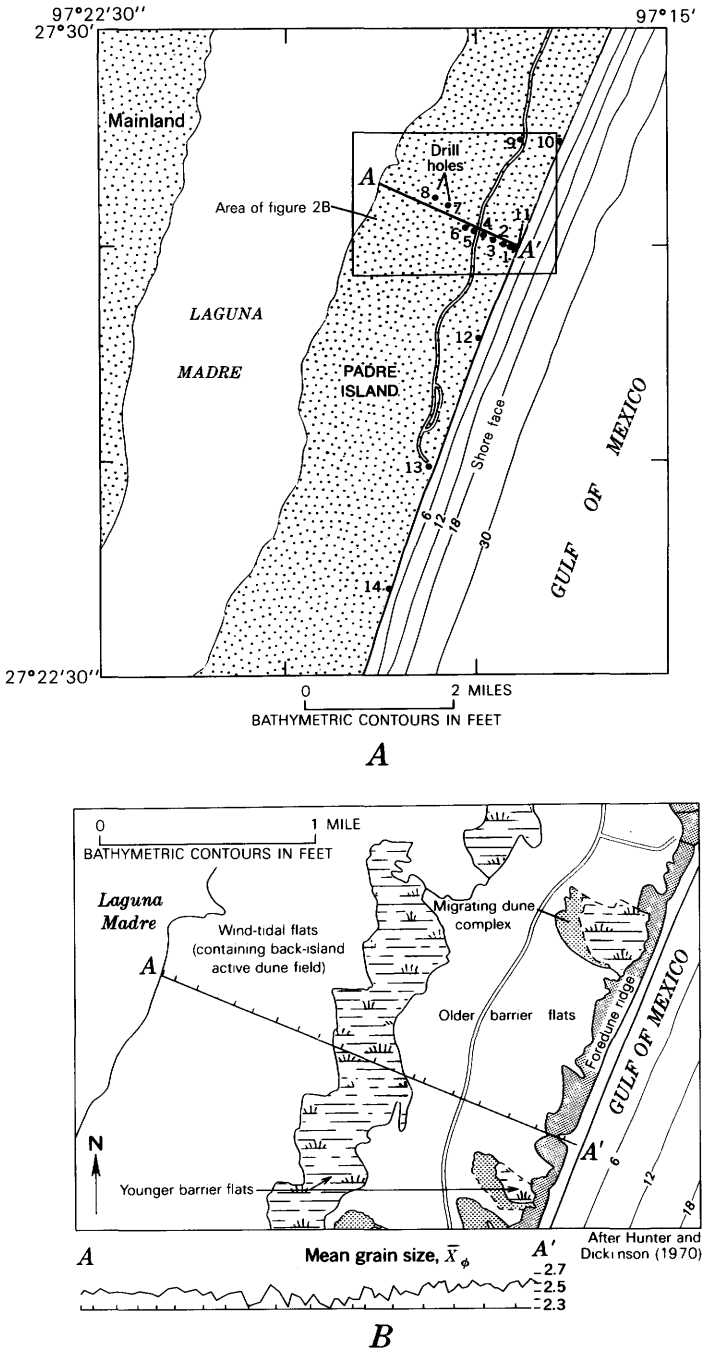

Figure 2.—Location of drill holes, *A*, and distribution of sediments and location of surface sample stations, *B*, on the segment of Padre Island, Tex., within South Bird Island 7½-minute quadrangle. Graph under map shows grain-size variations along traverse *A*–*A'*.

GRAIN-SIZE DISTRIBUTION IN THE SUBSURFACE

Samples analyzed from the 14 drill holes (figs. 2 and 4) show that a surface layer of fine to very fine ($M_{\bar{X}}$=2.5ϕ) sand overlies slightly coarser ($M_{\bar{X}}$=2.3ϕ) sand which makes up most of the island body in this area (table 1, figs. 4, 5). The upper layer ranges in thickness from about 5 to 10 feet, except in

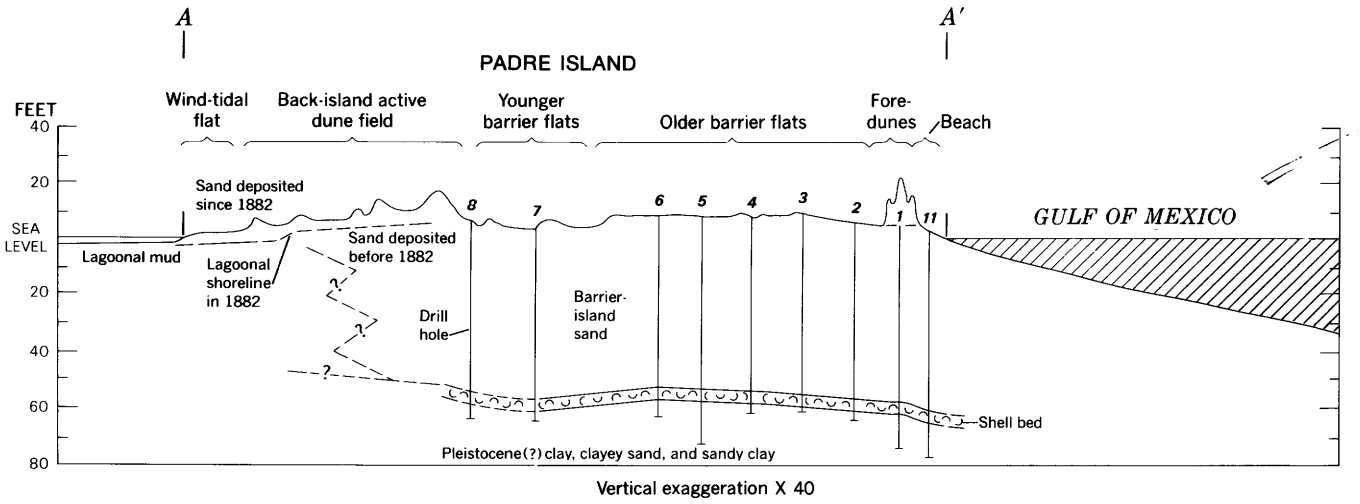

Figure 3.—Cross section A–A' of Padre Island, Tex., within South Bird Island 7½-minute quadrangle. Shells of *Mulinia* sp. from a bed at a depth of 62 feet yielded carbon-14 dates (Texas Univ. at Austin, 1970) of 27,380±1,100 and 29,980±1,070 years B.P. See figure 2*A* for location of cross section. Modified from Hunter and Dickinson (1970, section A–A').

Table 1.—M_X, M_σ, M_{Sk}, M_K *for samples from various depths from borings in northern Padre Island, South Bird quadrangle, and the probability,* P, *based on Student's* t *test, that the different parameters from various depths could be from the same normal population as the surface samples*

	Surface (14 samples)	Depth 10 feet (14 samples)	20 feet (11 samples)	30 feet (12 samples)
$M_{\bar{X}}$	2.52	2.30	2.29	2.30
P		< .001	<.001	<.001
M_σ.....	.32	.36	.34	.35
P		.001–.005	.1–.2	.05–.1
M_{Sk}....	–.19	–.17	–.05	–.08
P		.07–.8	.005–.01	.05–.1
M_K	.30	.36	–.42	–.56
P		.5–.6	.4–.5	.05–.1

dune areas, where it locally exceeds 30 feet. Table 1 shows the variation with depth of the mean of mean grain sizes, $M_{\bar{X}}$, and the probability that $M_{\bar{X}}$ for each depth level and $M_{\bar{X}}$ for the surface layer could be from the same normal population of $\bar{X}_\phi$. In each case the probability is less than 0.001. In most of the drill holes, mean sand size decreases slightly below 30 feet (fig. 4); this could mean that the island was prograding in its early stages. The grain sizes from greater depths are known with less certainty because of the contamination problem mentioned earlier.

Other grain-size parameters also vary with depth. An increase in standard deviation with depth (fig. 4) is expectable because the deeper samples are mixed with uphole material during drilling. A slight increase of negative skewness is apparent at greater depth, but the significance is questionable (table 1). The samples become more platykurtic at deeper intervals, but based on the Student's t test, the increase is not significant at a 95-percent confidence level.

SURFACE DISTRIBUTION OF GRAIN-SIZE PARAMETERS

Statistical parameters of sand grain size indicate significant differences among the environments of deposition along the traverse (fig. 3, A–A') that extends across Padre Island at a right angle to the shoreline from the gulf beach to the lagoon. As discussed, these differences apparently result from local wind erosion and grain-size stratification within the island. The greatest differences are shown in mean grain diameters as indicated by $\bar{X}_\phi$ and $M_{\bar{X}}$ (fig. 2, table 2). Sk_ϕ shows some significant variation with depositional environment; K_ϕ shows little or none. This is contrary to the results of Hayes (1965), which indicated that skewness and kurtosis were very sensitive to the mixing of different size modes. The several environments shown on figures 3 and 5 are (1) beach, (2) foredune ridge, (3) older barrier flats, (4) younger barrier flats, and (5) wind-tidal flats (Hunter and Dickinson, 1970). For this study,

Table 2.—*Sand-grain size parameters for surface samples from different depositional environments*

	Number of samples	$M_{\bar{X}}$	M_σ	M_{Sk}	M_K
Beach and foredune ridge.	11	2.56	0.30	–0.24	–0.30
Older barrier flat.	31	2.52	.34	– .32	– .08
Younger barrier flat.	17	2.41	.36	– .27	– .42
Wind-tidal flat.	21	2.46	.31	– .25	– .30

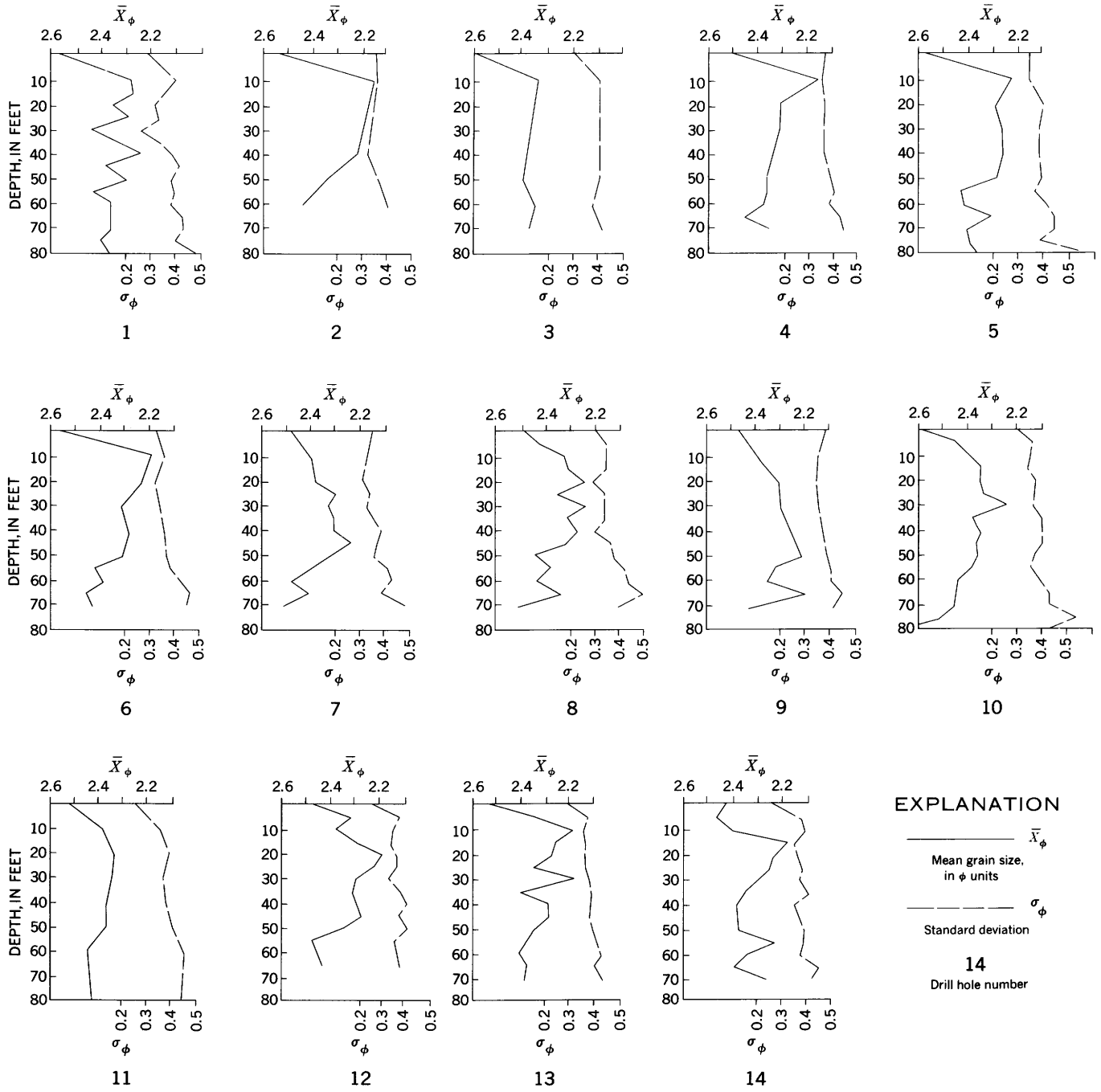

Figure 4.—Variation of mean grain size and standard deviation with depth in drill holes on northern Padre Island, Tex.

beach and foredune ridge results have been combined, as no significant differences between them were found in this study or in earlier studies by Boker (1956) or Hayes (1965).

The mean grain size for the beach and foredune ridge (2.56ϕ) is smallest of all the environments, and for the older barrier flats, which lie behind the foredune ridge, it is only slightly larger (2.52ϕ) (fig. 2, table 2). The coarsest sand (2.41ϕ) was found in the younger barrier flats. The wind-tidal flats, which contain the back dune fields, have an intermediate mean grain size (2.46ϕ). The probability, based on Student's t test of distributions of the various sand size parameters ($\bar{X}_\phi$, σ_ϕ, Sk_ϕ, K_ϕ) for each environment of deposition, that the parameters from different environments could be from the same normal population, is given in table 3. If a 95-percent confidence level is assumed, all differences in $\bar{X}_\phi$ and all differences in σ_ϕ except between wind-tidal flats and beach and foredune ridge are significant at 95-percent confidence. Skewness differences are significant between older barrier flats

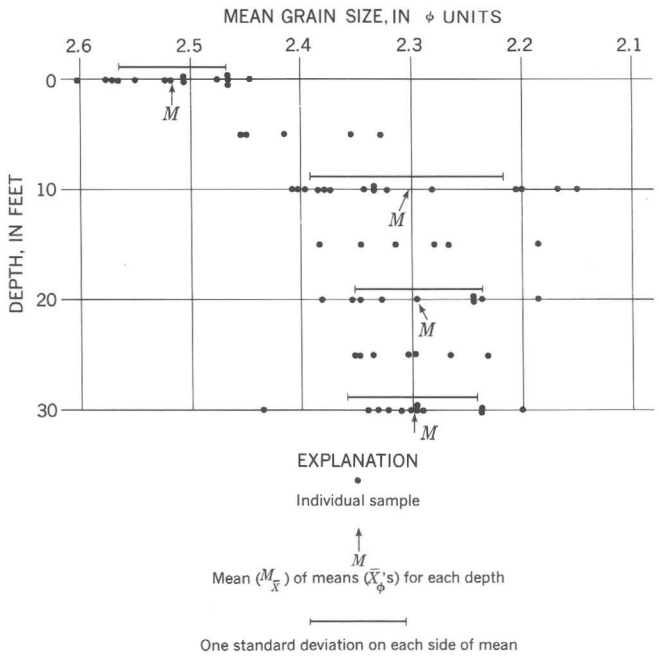

Figure 5.—Distribution of mean grain sizes with depth in drill holes in South Bird Island 7½-minute quadrangle, northern Padre Island, Tex.

Table 3.—*The probability,* P, *based on Student's* t *test of the distributions of parameters in each environment, that parameters from different environments could be from the same normal population*

	Beach and foredune ridge	Older barrier flat	Younger barrier flat
Older barrier flats.	$P_{\bar{X}} = 0.01–0.02$ $P_\sigma < .001$ $P_{Sk} < .001$ $P_K = .10–.20$		
Younger barrier flats.	$P_{\bar{X}} < .001$ $P_\sigma < .001$ $P_{Sk} = .10–.20$ $P_K = .20–.25$	$P_{\bar{X}} < 0.001$ $P_\sigma = .025–.05$ $P_{Sk} < .001$ $P_K = .20–.25$	
Wind-tidal flats.	$P_{\bar{X}} < .001$ $P_\sigma = .05–.10$ $P_{Sk} = .70–.80$ $P_K = .90$	$P_{\bar{X}} < .001$ $P_\sigma < .001$ $P_{Sk} = .01–.02$ $P_K = .10–.20$	$P_{\bar{X}} = 0.025–0.05$ $P_\sigma < .001$ $P_{Sk} = .05–.30$ $P_K = .05–.30$

and beach and foredune ridge, and between older barrier flats and wind-tidal flats. In no case was the difference in kurtosis significant.

The distribution of grain sizes on the surface of Padre Island within South Bird Island quadrangle results primarily from the mixing of grains from different sources during eolian transport of sand from the beach across the island westward into the lagoon and from wave action on the beach. Direction of eolian sand movement in this area is west-northwestward most of the year. Pronounced deflation basins were eroded into the underlying coarser sand during drought years, 1948–56, 1962–64, and 1967 (Hunter and Dickinson, 1970). Earlier deflation basis in what are now the older barrier flats probably also formed during dry periods but were later filled as subsequent dune migrations crossed the surface. A buried soil horizon (fig. 6) was found beneath the foredune ridge for some distance under the older barrier flats at a depth of about 1 to 3 feet along profile $A–A'$. The larger grain size beneath this soil horizon indicates that sand was coarser at the surface during an earlier depositional phase.

Figure 6.—Trench in older barrier flats just behind foredune ridge along profile $A–A'$, Padre Island, Tex., showing old soil horizon (top of dark layer). Sand above is finer ($\bar{X} = 2.5\phi$) than that below ($\bar{X} = 2.1\phi$).

BARRIER ISLAND MIGRATION

Many geologists believe that Gulf coast barrier islands are prograding except where they are associated with the destructive phase of delta building (Price, 1958; Bernard and others, 1962). Preserved beach ridges and a downward decrease in grain size are the chief evidence supporting this hypothesis. On northern Padre Island, beach ridges are not preserved, nor is there a regular decrease in grain size with depth (fig. 4). The absence of a nearshore gulf facies near the base of Mustang Island, which lies just north of Padre Island, has led Shepard (1956) to believe that the island has not prograded. The same situation is apparently true along at least part of northern Padre Island. It is herein concluded that the location of the gulf side of northern Padre Island has been relatively stable for several thousand years. Moreover, it has been shown by Hunter and Dickinson (1970) that larger quantities of sand are being

transported landward across northern Padre Island by the wind. They report that the lagoon shore migrated an average of about 700 feet landward between 1948 and 1967. The movement of the sand across the island prevents deposition of a progradational layer on the beach face of the island.

BARRIER ISLAND MODELS AND ENVIRONMENTAL INTERPRETATIONS

Galveston Island has been generally accepted as a model for barrier island development on the basis of work by Bernard and others (1962). Studies of northern Padre Island indicate that not all barrier islands conform to this model; caution should be used in interpreting ancient deposits on the basis of sand-size distribution. Hayes (1964) also has shown that the effects of depositional environments on grain-size parameters may be completely obscured by modal mixing, and that the use of statistical sand-size parameters in determining these environments may produce erroneous results.

CONCLUSIONS

1. In the central part of the South Bird Island quadrangle area on Padre Island, a relatively thin layer of fine to very fine sand overlies slightly coarser sand.
2. The finer sand on the surface comes from a predominantly northern source, and the underlying sand is the result of mixing of sand from both northerly and southerly sources.
3. Variations in sand size across the island result from varying degrees of mixture between the surface and subsurface layers.
4. Mean grain size, $\bar{X}_\phi$, is the most significant indicator of the degree of mixing.
5. The gulf shore of northern Padre Island has been relatively stationary throughout most of the island's history. It is not a prograding island.

REFERENCES

Bernard, H. A., Leblanc, R. J., and Major, C. F., 1962, Recent and Pleistocene geology of southeast Texas, Field excursion No. 3, *in* Geology of the Gulf Coast and central Texas and guidebook of excursions, Geol. Soc. America, 1962 Ann. Mtg.: Houston, Tex., Houston Geol. Soc., p. 175–224.

Booker, T. A., 1956, Sand dunes on northern Padre Island: Kansas Univ., Lawrence, M.S. thesis, 100 p.

Bullard, F. M., 1942, Source of beach and river sands on Gulf Coast of Texas: Geol. Soc. America Bull., v. 53, no. 7, p. 1021–1043.

Curray, J. R., 1960, Sediments and history of Holocene transgression, Continental shelf, northwest Gulf of Mexico, *in* Shepard, F. P., and others, eds., Recent sediments, northwest Gulf of Mexico: Tulsa, Okla., Am. Assoc. Petroleum Geologists, p. 221–266.

—— 1961, Tracing sediment masses by grain size modes: Internat. Geol. Cong., 21st, Copenhagen 1960, Rept., pt. 23, p. 119–130.

Emery, K. O., 1938, Rapid method of mechanical analysis of sands: Jour. Sed. Petrology, v. 8, no. 3, p. 105–111.

Griffiths, J. C., 1967, Scientific method of analysis of sediments: New York, McGraw-Hill, Inc., 508 p.

Hayes, M. O., 1964, Grain size modes in Padre Island sands, *in* Depositional environments, south-central Texas coast: Gulf Coast Assoc. Geol. Socs., Ann. Mtg., 1964, Field Trip Guidebook, Austin, Tex., 1964, p. 121–126.

—— 1965, Sedimentation on a semi-arid wave dominated coast (South Texas) with emphasis on hurricane effects: Texas Univ., Austin, Ph. D. thesis, 350 p.

Hunter, R. E., and Dickinson, K. A., 1970, Map showing landforms and sedimentary deposits of the Padre Island portion of the South Bird Island 7.5-minute quadrangle, Texas: U.S. Geol. Survey Misc. Geol. Inv. Map I-659, scale 1:24,000.

Lohse, E. A., 1955, Dynamic geology of modern coastal region, northwest Gulf of Mexico: Soc. Econ. Paleontologists and Mineralogists Spec. Pub. 3, p. 78–98.

Price, W. A., 1958, Sedimentology and Quaternary geomorphology of South Texas: Gulf Coast Assoc. Geol. Socs. Trans., v. 8, p. 41–75.

Rusnak, G. A., 1960, Sediments of Laguna Madre, Texas, *in* Shepard, F. P., and others, eds., Recent sediments, northwest Gulf of Mexico: Tulsa, Okla., Am. Assoc. Petroleum Geologists, p. 153–196.

Shepard, F. P., 1956, Late Pleistocene and Recent history of the central Texas coast: Jour. Geology, v. 64, no. 11, p. 56–69.

Texas University at Austin, 1970, Radiocarbon dates VIII: Radiocarbon Jour., v. 12, p. 618–619.

ZIRCONIUM ON THE CONTINENTAL SHELF— POSSIBLE INDICATOR OF ANCIENT SHORELINE DEPOSITION

By CHARLES W. HOLMES, Corpus Christi, Tex.

Abstract.—Semiquantitative analyses of bottom samples from the northwestern Gulf of Mexico shelf indicate that the highest relative trace-element concentrations are in regions of the shelf that are actively receiving sediments. Zirconium is an exception to this general pattern in that its highest concentrations are in an area of slow deposition or nondeposition seaward of Galveston, Tex. Within this area, the highest concentrations of zirconium are in elongate zones that parallel linear topographic features on the shelf floor. The similarity of patterns of sediment distribution, zirconium concentration, and the morphological features of the shelf suggest that the topographic features are ancient shorelines that have been submerged during the post-Pleistocene rise in sea level.

As a means of understanding the sedimentary processes by which trace elements are transported and concentrated in the marine environment, a geochemical survey of the surficial shelf sediments in the northwestern Gulf of Mexico was undertaken. The purpose of the survey was to determine the distribution of trace elements and to relate trace-element content to sediment type as well as to the topographic features on the sea floor. For the study, 850 samples were analyzed for trace elements by the six-step semiquantitative method (Grimes and Marranzino, 1968). Most of the samples were taken from a relatively small region on the central shelf near Galveston, Tex. The remaining samples represent a broad reconnaissance survey from the mouth of the Rio Grande to the Mississippi River. The samples were collected by the U.S. Bureau of Commercial Fisheries as a part of a comprehensive study of the physical properties of sediments and their relation to benthic fauna of the shelf.

Acknowledgments.—I wish to acknowledge the help and support of Dr. Robert Stevenson and John R. Grady, U.S. Bureau of Commercial Fisheries, who made the sample material available to the U.S. Geological Survey. The spectrographic analyses were done by E. L. Mosier, K. C. Watts, J. Curray, J. Motooka, and E. F. Cooley, U.S. Geological Survey.

GEOLOGIC SETTING

In the northwestern Gulf of Mexico, the break in slope that marks the outer edge of the continental shelf occurs at a depth of about 65 fathoms (118.8 m). The shelf widens from 48 nautical miles seaward of the mouth of the Rio Grande to about 114 nautical miles off the Texas-Louisiana border; farther east, at the Mississippi River delta, the shelf is very narrow (fig. 1). The gradient across the shelf generally varies with depth, being very steep from the shoreline to the 7-fathom (12.8-m) isobath, relatively flat from 7 to 35 fathoms (12.8–64 m), and increasingly steep to 65 fathoms (118.8 m), where there is an abrupt change in slope.

The continental shelf in this region includes three major depositional-topographic features: the Rio Grande delta, expressed both by the broad seaward bulge of the shoreline and by the pattern of isobaths on the shelf; the composite delta of the Colorado and Brazos Rivers, which also forms a broad bulge on the shoreline and on the shelf; and the Mississippi River delta. The general smoothness of the shelf surface is broken by shallow areas of banks and by irregular topography near shore, both in the Rio Grande region and across the shelf seaward of Galveston.

The surface of the shelf in the area seaward of Galveston has two distinct sets of linear topographic features (fig. 2) that appear to be low ridges with associated depressions on their landward sides. From the shoreline to a depth of 13 fathoms (23.7 m), three distinct ridges and depressions parallel the present coast. Two of these lie seaward of Galveston; the third is south of Freeport.

Farther seaward on the middle and outer shelf, other ridges and associated depressions are oblique to the present coast and strike generally in an east-southeasterly direction. Most of these features have abrupt inner and outer terminations and extend across the shelf for short distances. None extend for the entire length of the shelf. One exception to the easterly trend of these features is the Louisiana channel, which trends northeast-southwest (Curray, 1960).

The sediments of the shelf have been described previously by Stetson (1953) and Curray (1960), whose investigations show that muds floor most of the shelf between the Rio Grande and the Colorado-Brazos deltas, where the bottom topography is relatively smooth, and that sands and alternating sands and muds floor the area where the bottom is rough. On the basis of these investigations, Curray (1960) constructed an

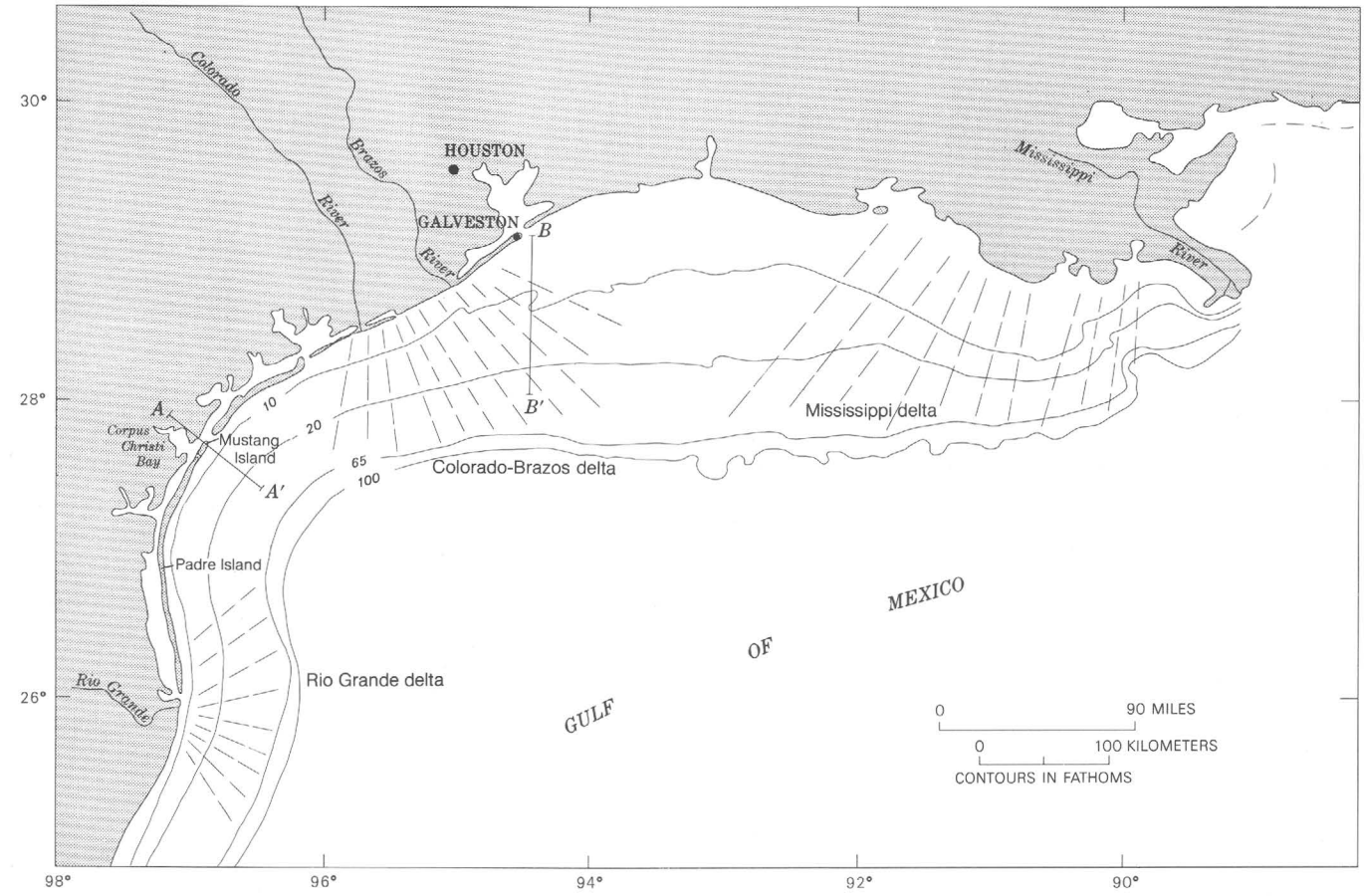

Figure 1.—Geography of the northwestern shelf of the Gulf of Mexico. A–A' and B–B' are lines of profiles shown in figure 4.

interpretative diagram which suggests that the areas where mud predominates are those regions (fig. 3) undergoing active sedimentation. That part of the shelf in the northwestern Gulf of Mexico where alternating sands and muds are the predominant types of bottom sediment is an area of little or no deposition.

A topographic profile normal to the present strand line northeast of Corpus Christi Bay, A–A' of figure 1, is shown in figure 4*A*. The profile crosses both the Pleistocene Ingleside barrier island and the Holocene Mustang barrier island. A north-south bathymetric profile, B–B', drawn from figure 2, is shown as figure 4*B*. The location of this profile was selected to coincide with a line of sediment samples reported by Stetson (1953) and a similar line by the Bureau of Commercial Fisheries. These profiles show the similarity in form of the present strand line and the submerged linear features on the shelf. Topographic highs in these profiles are above the average smoothed gradient of the shelf and are therefore concluded to be constructional in origin.

DISTRIBUTION OF ZIRCONIUM

The distribution of 30 trace elements along the continental shelf of the northwestern Gulf of Mexico shows a pattern that strongly reflects the depositional environments presently existing on the shelf. With the exception of zirconium, the highest elemental concentrations are in regions undergoing active sedimentation. Conversely, areas of slow deposition or nondeposition off Galveston and the mouth of the Rio Grande are depleted in trace elements, except for zirconium.

Zirconium content ranges from less than 0.01 percent in the area of active sedimentation to more than 0.1 percent in the region of nondeposition off Galveston. Higher zirconium concentrations occur in linear areas, which appear to have two distinct trends, one parallel to the coast and striking northeast and another oblique to the coast and striking generally southeast. The distribution is shown in figure 5.

In the sediments of the Gulf of Mexico, zirconium is found in the form of zircon, a stable heavy mineral that has been widely used as a provenance indicator, an index of soil chemical stability, and an index of sediment maturity. Its value for these uses is based on the fact that zircon tends to be concentrated in resistates. Because it is one of the minerals most resistant to chemical and physical attack, its presence in high concentrations is a good indicator of moderate- to high-energy environments such as the littoral zone.

Zircon makes up a significant portion of the heavy-mineral assemblages in the central shelf area of the northwestern Gulf

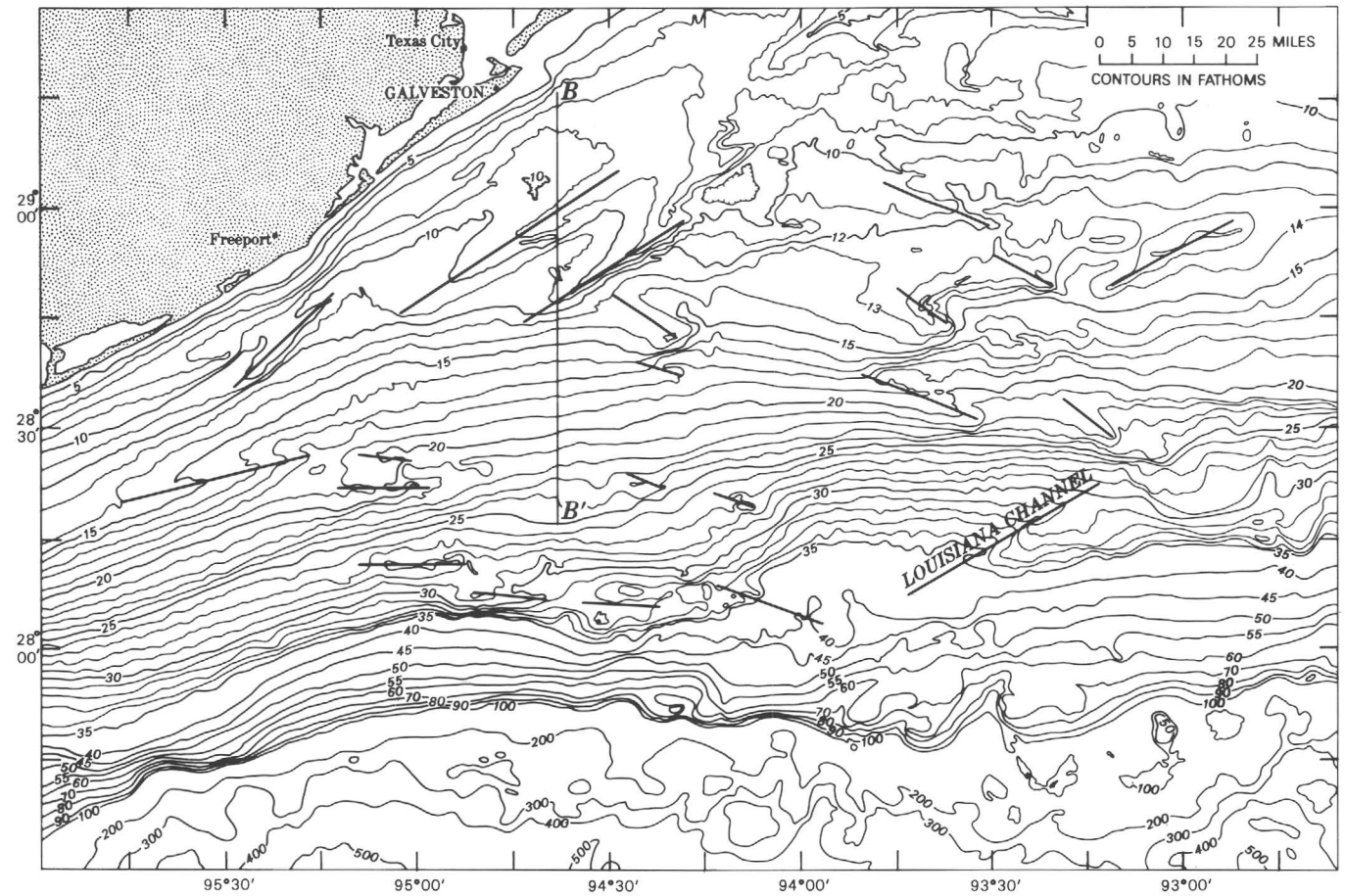

Figure 2.—Bathymetric chart of the central region of the northwest Gulf of Mexico with 1-fathom contour intervals from 5 to 60 fathoms. Solid lines approximate the axes of topographic ridges. B–B' same as on figure 1. Map from Curray (1960).

of Mexico. It has been shown to be derived from the weathering of Pleistocene deposits and from the effluent of the Colorado-Brazos system (Van Andel, 1960). These river systems were a major source of sediments during the Pleistocene, when they constructed a delta that forms a prominent bulge on the present continental shelf.

DISCUSSION

On the modern barrier islands of the south Texas coast, heavy minerals are concentrated in two distinct environments: the beach and the wind-tidal flat. In beach deposits, minerals are sorted by the winnowing action of waves and longshore currents whose combined forces produce heavy-mineral concentrations that are richer around deltas and the mouths of streams. Such deposits occur principally as lenses or patches in the sand of the beach (fig. 6*A*). On the tidal flats, heavy minerals are concentrated by the action of water and wind. During times of flooding in adjacent river systems, clastic material with associated heavy minerals is spread across tidal flats, where the heaviest particles settle in relatively quiet water. Subsequent draining of the flats exposes such deposits to wind action, which removes the light material and concentrates the heavier particles (fig. 6*B*). As a result of the conditions that prevail on southern Padre Island, heavy-mineral deposits are found on both sides of the island. Bradley (1967) reports similar heavy-mineral distributions on Mustang Island.

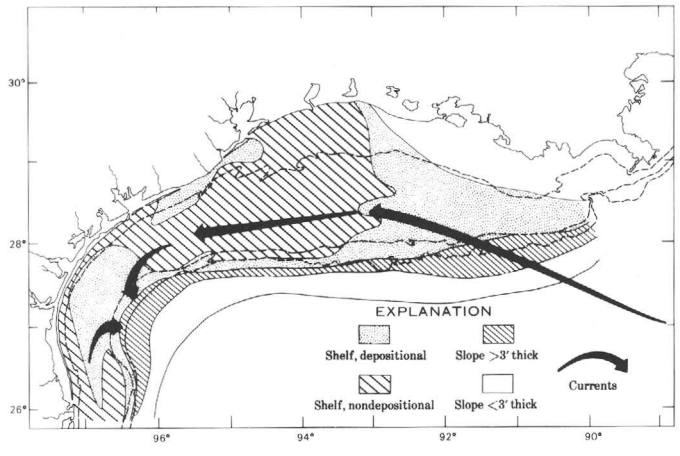

Figure 3.—Depositional regimes on the northwest Gulf of Mexico shelf. Modified from Curray (1960, fig. 17).

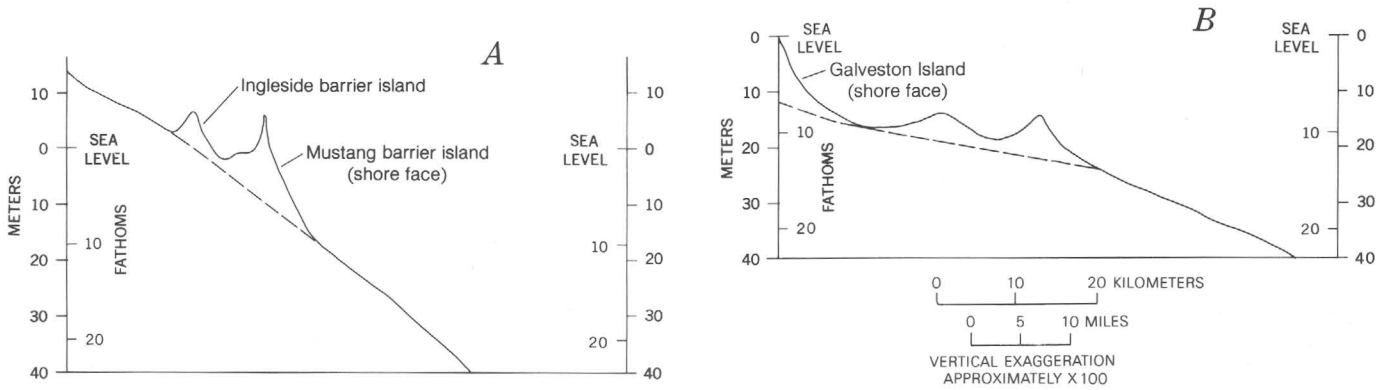

Figure 4.—Profiles extending from the Texas coast out into the northwestern Gulf of Mexico.
A. Profile normal to the present strand line north of Corpus Christi Bay. Line A–A' on figure 1.
B. Bathymetric profile across the shelf, showing the submerged topographic ridges off Galveston, Tex. Line B–B' on figures 1 and 2. Dashed lines show the average smoothed gradient of the shelf.

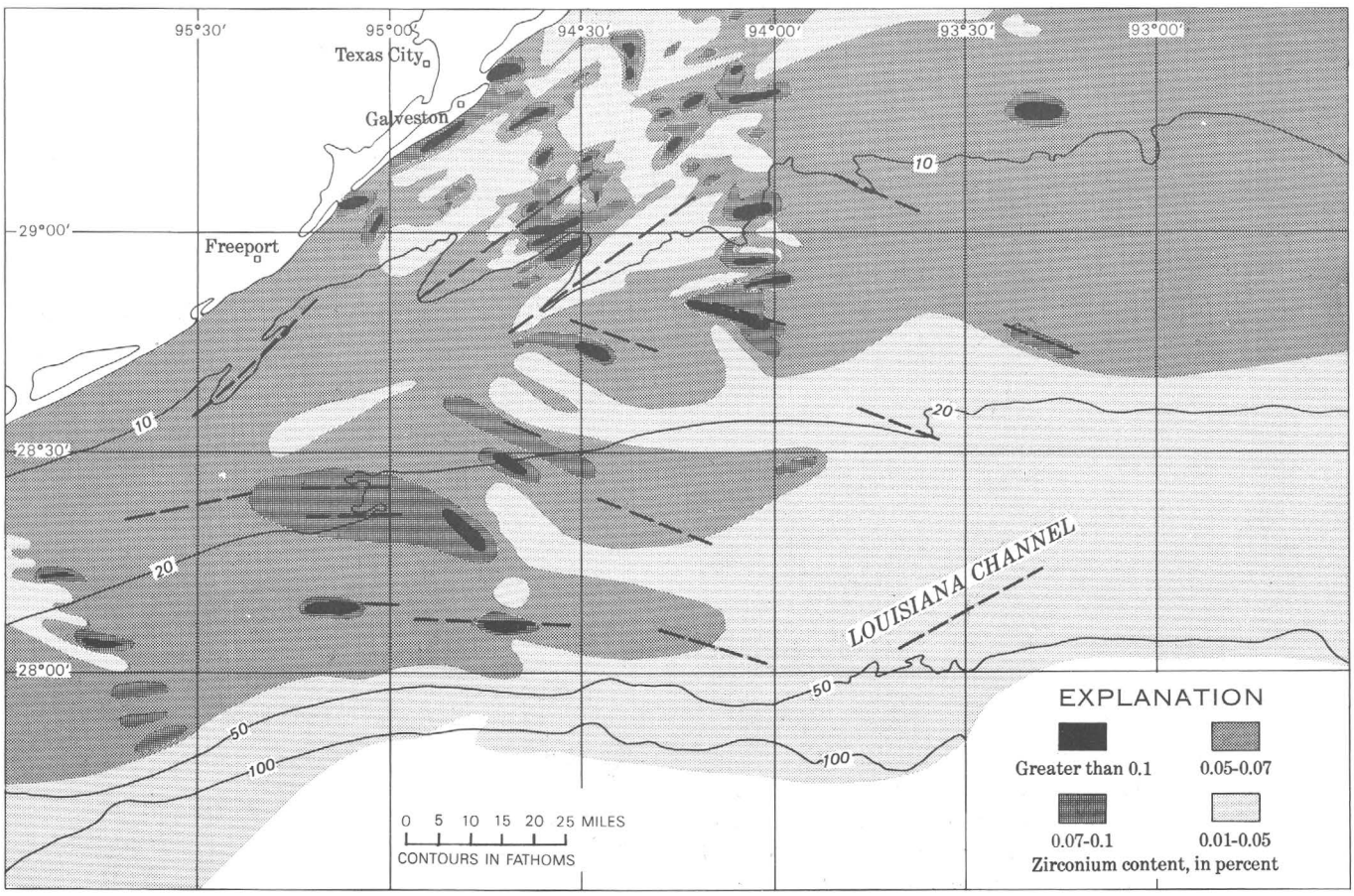

Figure 5.—Distribution of zirconium in the central part of the northwest Gulf of Mexico shelf. Dashed lines approximate the axes of the topographic ridges in figure 2.

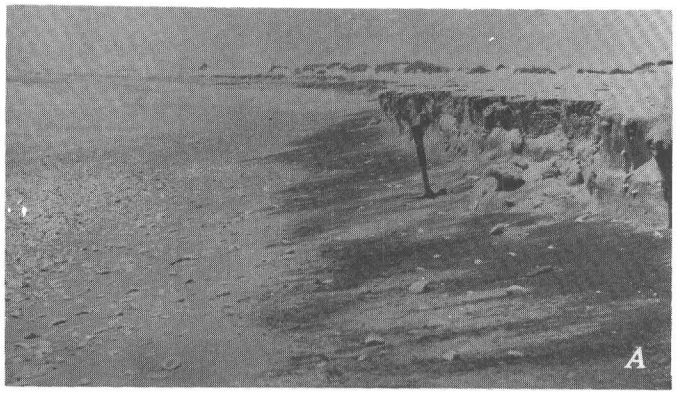

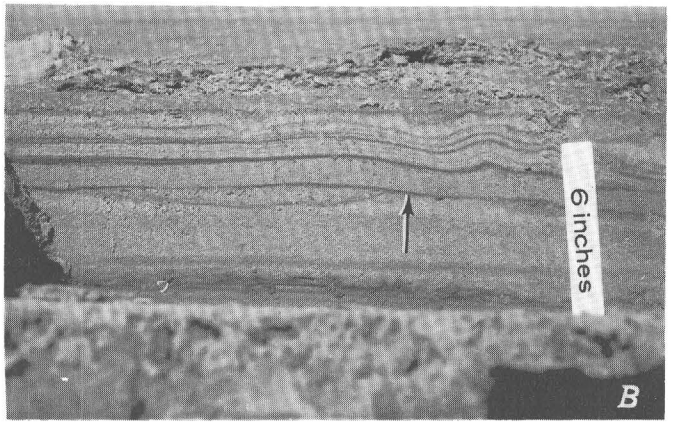

Figure 6.—Heavy-mineral concentrations on Padre Island, Tex.
A. Seaward face of island. The dark patches are heavy-mineral concentrations.
B. Wind-tidal flats, lagoon side of island. Dark heavy-mineral layers (arrow) are shown as they appear in a wall of a trench.

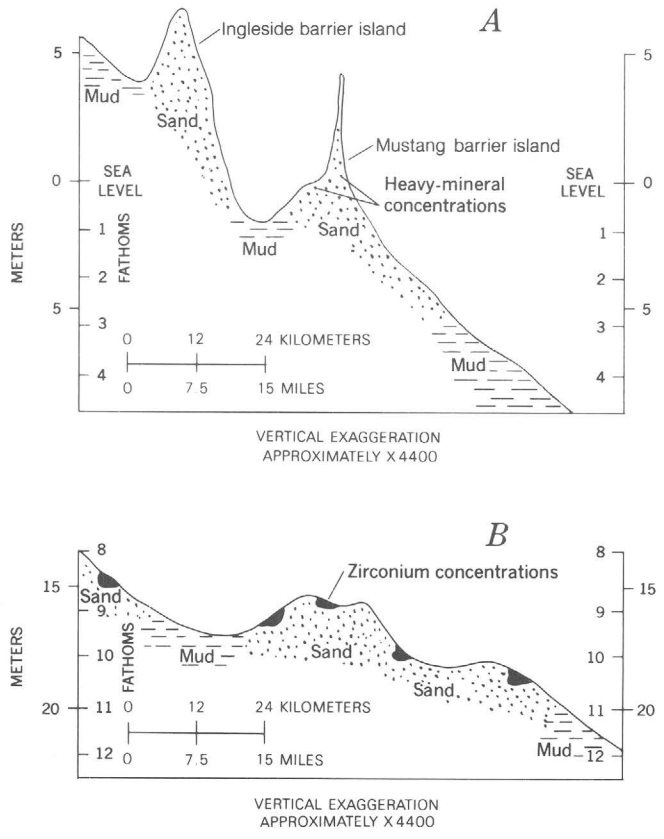

Figure 7.—Distribution of sediment type and heavy-mineral concentration along sections A–A' (partly exposed) and B–B' (submerged) on the Texas coast.
A. Section A–A' (fig. 1) across the present strand line north of Corpus Christi Bay. Enlargement of figure 4*A*.
B. Section B–B' (figs. 1 and 2) across the submerged ridges off Galveston, Tex. Enlargement of part of figure 4*B*.

A vertical section across the Ingleside-Mustang Islands complex in the Corpus Christi area shows that the sediments grade from mud in the lagoons to sand on the islands and back to mud offshore (fig. 7*A*). The sediment distribution across the inner depressions and ridges on the continental shelf also indicates the presence of mud in the inner depressions and sand on the ridges (fig. 7*B*). Heavy-mineral concentrations represented by zirconium accumulations are found on both sides of these shelf ridges in settings morphologically and sedimentologically similar to the Ingleside-Mustang Islands complex. These similarities of form, sediment distribution, and regional relations strongly suggest that the submerged linear features on the shelf are probably ancient barrier islands formed when sea level was approximately 13 fathoms below the present level.

The southeastward-striking ridges and depressions of the central and outer shelf have the same sedimentary patterns and morphology as those which parallel the shoreline. Heavy-mineral concentrations, however, are present only on the seaward side. This pattern of distribution is common along modern barrier islands of the Texas coast when environmental conditions preclude deposition of heavy minerals on the inshore side and the only source of heavy minerals is longshore drift.

The morphology and sedimentary facies of the outer-shelf ridges suggest that these features were barrier spits built outward during regressional episodes, which represented either hesitation in a transgressive sea or a general regression. These periods of regression prevented the establishment of a static system with a tidal-flat–lagoon complex where zirconium could be concentrated. Nevertheless, on the gulfward faces of the splits, energy was sufficient for heavy minerals to be concentrated.

The results of this investigation suggest that zirconium may be a useful indicator of depositional environments. On the northwestern Gulf of Mexico shelf, anomalous zirconium concentrations are associated with morphological features thought to be the submerged beaches of ancient barrier islands and spits.

Relatively large amounts of zirconium are the result of a combination of differential chemical weathering and initially high zircon concentrations of the source sediments. These concentrations further suggest that the sand bodies were deposited in a high-energy littoral environment and are sedimentologically mature.

REFERENCES

Bradley, J. S., 1957, Differentiation of marine and sub-aerial sedimentary environments by volume percentage of heavy minerals, Mustang Island, Texas: Jour. Sed. Petrology, v. 27, No. 2, p. 116–125.

Curray, J. R., 1960, Sediments and history of Holocene transgressions, continental shelf, northwest Gulf of Mexico, *in* Shepard, F. P., and others, ed., Recent sediments, northwest Gulf of Mexico: Tulsa, Okla., Am. Assoc. Petroleum Geologists, p. 221–266.

Grimes, D. G., and Marranzino, A. P., 1968, Direct-current arc and alternating-current spark emission spectrographic field methods for the semiquantitative analyses of geologic materials: U.S. Geol. Survey Circ. 591, 6 p.

Stetson, H. C., 1953, The sediments of the western Gulf of Mexico, pt. I, The continental terrace of the western Gulf of Mexico; its surface sediments, origin and development: Papers in Phys. Oceanography and Meteorology, Massachusetts Inst. Technology and Woods Hole Oceanog. Inst., v. 12, no. 4, p. 3–45.

Van Andel, T. H., 1960, Sources and dispersion of Holocene sediments, northern Gulf of Mexico, *in* Shepard, F. P., and others, ed., Recent sediments, northwest Gulf of Mexico: Tulsa, Okla., Am. Assoc. Petroleum Geologists, p. 34–55.

POTENTIAL STRIPPABLE OIL-SHALE RESOURCES OF THE MAHOGANY ZONE (EOCENE), CATHEDRAL BLUFFS AREA, NORTHWESTERN COLORADO

By JOHN R. DONNELL and A. C. AUSTIN,
Denver, Colo., Metairie, La.

Abstract.—Recent improvement of equipment used in strip mining coal deposits may make large tracts of oil-shale land in western Colorado amenable to strip mining. At present, it is technically possible to remove as much as 200 feet of overburden, and in the future it may be possible to remove as much as 400 feet. In four 7½-minute quadrangles in northwestern Colorado, about 75 square miles is underlain by the oil-shale-bearing Mahogany zone (in the Parachute Creek Member of the Eocene Green River Formation) where it has less than 400 feet of overburden. In the 75-square-mile area, the Mahogany zone has resources in the ground of 8 billion barrels of shale oil. Part of this area—approximately 25 square miles—is overlain by less than 200 feet of overburden and has resources in the ground of about 2.5 billion barrels of shale oil. The ratio of overburden thickness to Mahogany zone thickness ranges from 0 to 7:1. The area is underlain by several deeper rich oil-shale zones of unappraised thickness and richness that may also contain sodium minerals of potential economic interest.

Most economic studies of a future oil-shale industry utilize mining costs derived from conventional underground mining operations similar to those carried on by the U.S. Bureau of Mines and the combine of oil companies utilizing the Bureau's facilities near Rifle, Colo., and to those carried on by the Union Oil Co. and the Colony Development Co. in the Parachute Creek area.

Recently, Ertl (1965) and Cameron (1968) have discussed the feasibility of large-scale strip and open-pit mining in the Piceance Creek basin. In his article, Cameron speculates that a 1,000,000-ton-per-day open-pit operation will make the production of oil from oil shale competitive with oil produced anywhere. Both Ertl and Cameron deal in generalities in describing potential strippable or open-pit areas, mostly limiting consideration to areas near the center of the Piceance Creek basin, where hundreds of square miles of land are underlain by oil shale more than 1,000 feet thick and averaging 25 gallons of oil per ton.

DEPOSITS OF STRIPPABLE OIL SHALE

Several areas are delineated as being of potential interest for strip mining of the Mahogany zone (in the Parachute Creek Member of the Green River Formation) in the Cathedral Bluffs-Calamity Ridge area (fig. 1). This appraisal is based on recent geologic fieldwork, on assays of oil shale in the Mahogany zone published by the U.S. Bureau of Mines, and on new 7½-minute topographic maps published by the U.S. Geological Survey.

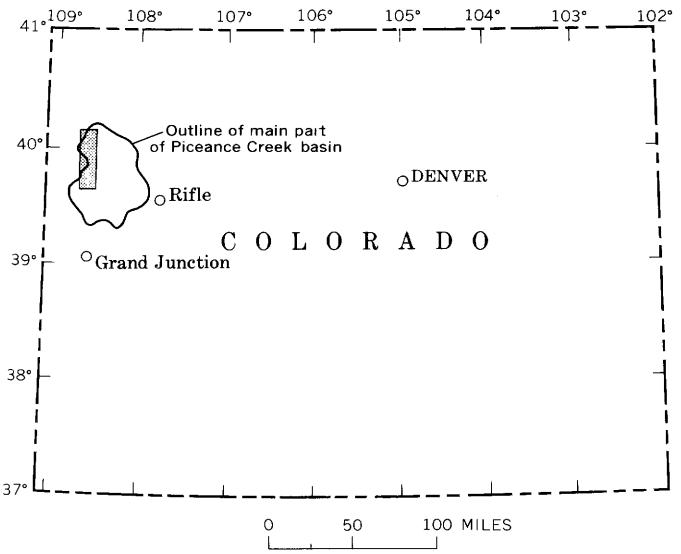

Figure 1.—Index map of Colorado, showing location of area (patterned) discussed in this report.

STRIPPABLE OIL SHALE DEFINED

Probably the closest analog to an oil-shale strip mining operation would be a somewhat comparable situation in the coal industry. Averitt (1970) discusses the coal strip mining industry in the United States; he traces the development of the small-capacity steam shovel of the early 1900's to the present electric-powered shovel of 200-yard capacity and states that a 300-cubic yard shovel is technically feasible. In 1969, a walking dragline with a 220-cubic yard capacity and a 310-foot boom capable of stripping 185 feet of overburden

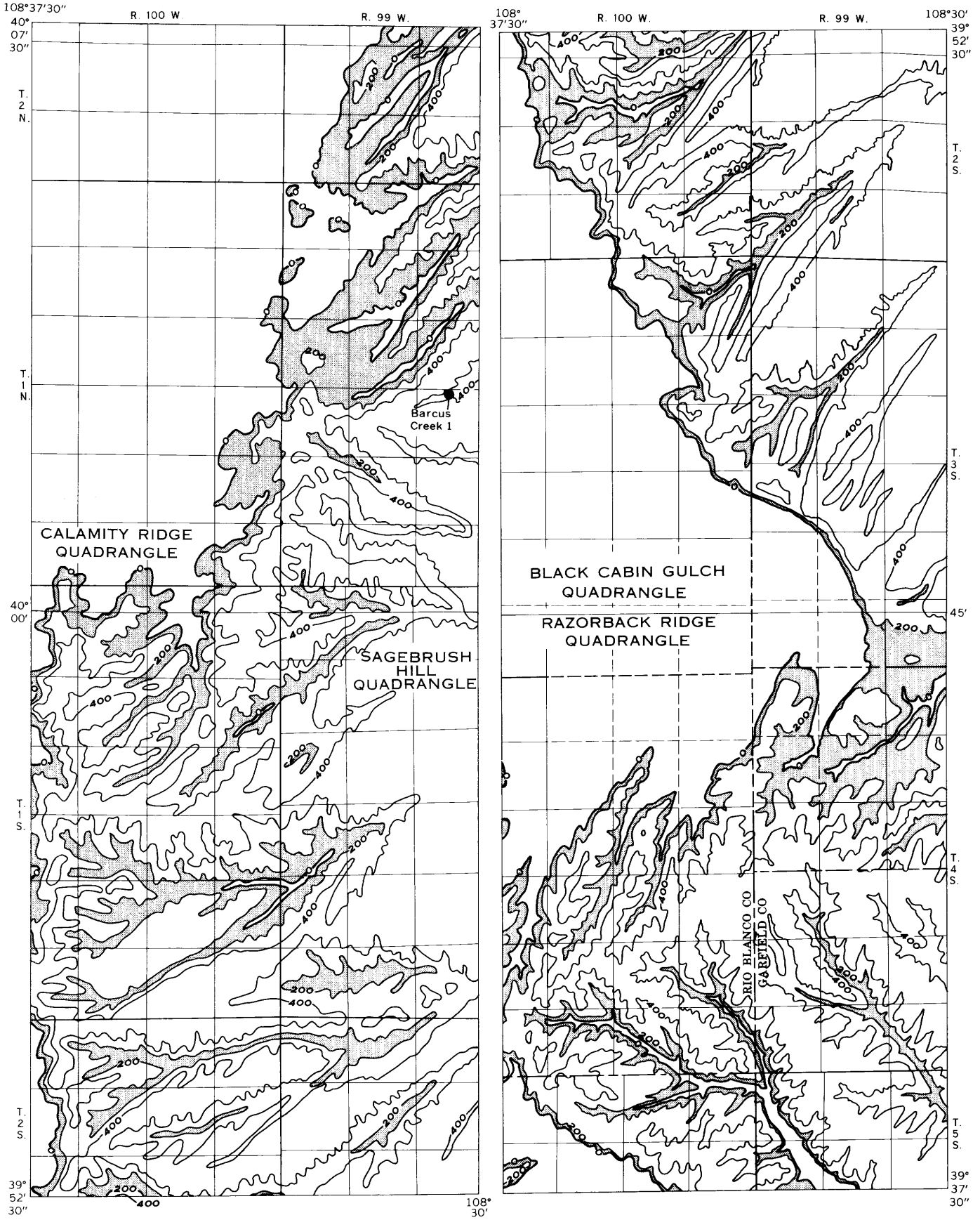
108°37'30"
R. 100 W.
R. 99 W.
108°30'
40°07'30"
39°52'30"
T. 2 N.
T. 1 N.
T. 1 S.
T. 2 S.
T. 2 S.
T. 3 S.
T. 4 S.
T. 5 S.
Barcus Creek 1
CALAMITY RIDGE QUADRANGLE
SAGEBRUSH HILL QUADRANGLE
BLACK CABIN GULCH QUADRANGLE
RAZORBACK RIDGE QUADRANGLE
40°00'
45'
39°37'30"
108°30'
RIO BLANCO CO
GARFIELD CO
0
200
400

Figure 2.

was operating, and an even larger dragline with a 500-foot boom is regarded as technically feasible. With equipment now available to industry and with technology available to construct and place into operation even larger equipment, it is technically possible that as much as 200 feet of overburden may be removed at present, and it is not beyond the realm of possibility that through advances in technology as much as 400 feet of overburden may be removed in the future. Areas delineated as strippable in this report have been so delineated only on the basis of thickness of overburden. An economic appraisal taking into account the size of area involved, character of overburden, thickness and grade of oil shale, waste disposal sites, and other technical problems is left to the mining engineer.

THICKNESS AND GRADE OF THE MAHOGANY ZONE

In this report, the Mahogany ledge or its subsurface counterpart, the Mahogany zone, is considered the minable unit. The Mahogany zone (fig. 2) ranges in thickness from about 65 feet in the western part of the Razorback Ridge quadrangle to about 145 feet in the eastern part of the Sagebrush Hill quadrangle. The zone as a whole ranges in grade from about 12 gallons of oil per ton in the western part of the Calamity Ridge and Razorback Ridge quadrangles to 26 gallons of oil per ton in the eastern part of the Black Cabin Gulch quadrangle. Select units in the Mahogany zone have higher oil contents than the average of the entire zone. A 10- to 15-foot-thick unit in the lower grade areas of the western part of the Calamity Ridge and Razorback Ridge quadrangles averages 30 gallons of oil per ton. A 90-foot-thick unit in the eastern part of the Black Cabin Gulch quadrangle, the richest part of the study area, averages 30 gallons per ton. There are several deeper rich oil-shale zones in the Green River Formation, in the 1,000- to 1,500-foot sequence below the Mahogany zone (Donnell and Blair, 1970). This is indicated by assays of core from the U.S. Bureau of Mines Barcus Creek hole in the report area (fig. 3) and by assays of core from holes drilled in adjoining areas to the east. Visual appraisal of oil shale in surface sections along the Cathedral Bluffs and Calamity Ridge indicates that the lower rich oil-shale zones underlie most of the report area, but assay information is insufficient to attempt a resource estimate of these zones in this report. The saline minerals nahcolite ($NaHCO_3$) and dawsonite [$NaAl(OH)_2CO_3$], which are of potential economic interest, are present in considerable quantities in the rich lower oil-shale zones and would be taken into consideration in an economic appraisal of a commercial oil-shale sequence. What little information is available thereon indicates that the amount of dawsonite and nahcolite in the Mahogany zone is very slight; therefore, no attempt is made in this report to estimate the resources of these saline minerals.

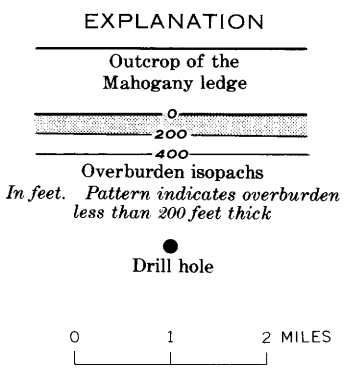

Figure 2.—Outcrop of the Mahogany ledge and thickness of overburden in the Calamity Ridge, Sagebrush Hill, Black Cabin Gulch, and Razorback Ridge quadrangles, Garfield and Rio Blanco Counties, Colo. The northern part of the report area is shown on the left, the southern part on the right.

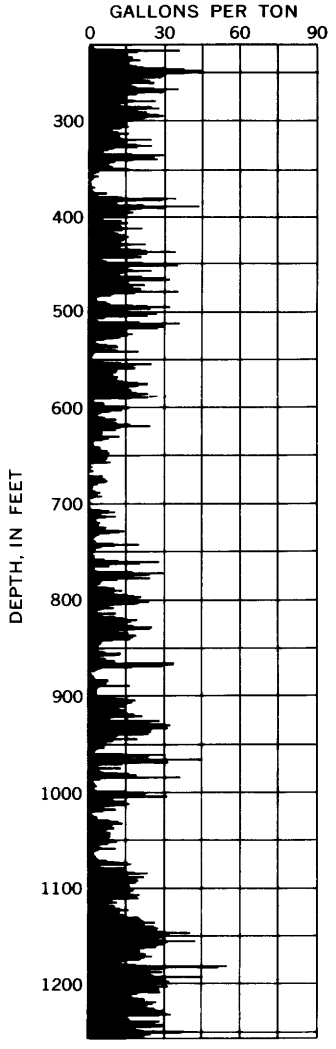

Figure 3.—Shale-oil assay histograms of U.S. Bureau of Mines Barcus Creek 1 core, NE¼NW¼ sec. 21, T. 1 N., R. 99 W., Rio Blanco County, Colo.

OVERBURDEN

For the purposes of this study, overburden is defined as the rock and soil that overlies the Mahogany zone. No differentiation is made in the character of the material that constitutes the overburden. In the Calamity Ridge quadrangle and in the northern part of the Sagebrush Hill quadrangle, the overburden is typified in the Bureau of Mines Barcus Creek 1 core. In this core, the 229 feet of overburden that overlies the Mahogany zone consists dominantly of sandstone or siltstone, which is probably highly tuffaceous. Less than 25 percent of the overburden sequence consists of oil shale, and of this only 2 feet assays more than 15 gallons of oil per ton. Conversely, in the southern part of the Sagebrush Hill quadrangle, in the Black Cabin Gulch quadrangle, and in the northern part of the Razorback Ridge quadrangle, the 300 feet of overburden that immediately overlies the Mahogany zone consists almost entirely of oil shale that averages 10 gallons of oil per ton. Thinner zones of this oil shale with an aggregate thickness of more than 50 feet will yield more than 15 gallons of oil per ton. In a commercial oil-shale mining operation, some of the richer oil-shale layers in what is considered overburden in this area might possibly be blended with oil shale from the Mahogany zone for retort feed.

RATIO OF OVERBURDEN THICKNESS TO OIL-SHALE THICKNESS

Coal strip mining operations in the United States as recently as 1965 have established an average overburden:coal thickness ratio of 10:1, and it was estimated that this ratio will have been increased to 11:1 by 1970 (Averitt, 1970). However, in some individual operations an overburden:coal thickness ratio as high as 30:1 has been obtained. The value of the mined product in a coal strip mining operation is probably at least two or three times greater than that in an oil-shale operation; therefore, the overburden ratio for oil shale must necessarily be less than that for coal. If the entire Mahogany zone is considered to be recoverable, then the overburden:oil shale ratio, in areas where the overburden is less than 200 feet thick, ranges from 0 to 3.5:1. If a select rich zone of oil shale that averages more than 30 gallons of oil per ton is considered to be recoverable, then in areas with 200 feet or less of overburden the overburden:oil shale ratio ranges from 0 to 20:1. The overburden:oil shale ratio on the Mahogany zone in areas containing 200 to 400 feet of overburden ranges from 1.4:1 to 7:1. The overburden:oil shale ratio on the select zone (30 gallons per ton) in the Mahogany zone, in these same areas, ranges from approximately 2:1 to 40:1.

STRIPPABLE RESOURCES OF THE MAHOGANY ZONE

The estimates of strippable oil-shale resources presented in this report are for resources in the ground. No attempt has been made to determine losses in mining or processing of the oil shale.

Table 1 lists resources, in place, of the Mahogany zone by township and range in two overburden categories—(1) deposits with less than 200 feet of overburden, and (2) deposits with 200 to 400 feet of overburden. The figures are tabulated in such a way that the resources in each overburden category may be totaled by individual 7½-minute quadrangles.

The Mahogany zone has less than 200 feet of overburden in an area of 16,537 acres (25.8 square miles), and in this area contains 2,541 million barrels of shale oil, or an average of about 154 thousand barrels per acre. In the northern part of this area, in T. 2 N., R. 99 W., no information is available on the quality of the oil shale in the Mahogany zone; therefore, no oil-shale resource appraisal was made for an area of 1,446 acres.

The Mahogany zone has more than 200 and less than 400 feet of overburden in an area of 34,572 acres (54 square miles) and in this area contains 5,524 million barrels of shale oil, or an average of about 160 thousand barrels per acre. In the northern part of this area, in T. 2 N., R. 99 W., no information is available on the quality of the oil shale in the Mahogany zone; therefore, no oil-shale resource appraisal was made for an area of 619 acres.

CONCLUSIONS

In an area of about 75 square miles along the western side of the Piceance Creek basin, Garfield and Rio Blanco Counties, Colo., the Mahogany zone has resources, in place, of about 8 billion barrels of shale oil under less than 400 feet of overburden. Approximately 2.5 billion barrels of this resource is under less than 200 feet of overburden. Additional rich oil-shale zones underlie the area, but data are not available for an accurate resource appraisal.

REFERENCES

Averitt, Paul, 1970, Stripping-coal resources of the United States—January 1, 1970: U.S. Geol. Survey Bull. 1322, 34 p.

Cameron, R. J., 1968, The outlook for oil shale [Paper presented at Am. Assoc. Petroleum Geologists 53d Ann. Mtg., Oklahoma City, Apr. 22-25, 1968]: Denver, Colo., Cameron and Jones, Inc., 13 p.

Donnell, J. R., and Blair, R. W., Jr., 1970, Resource appraisal of three rich oil-shale zones in the Green River Formation, Piceance Creek Basin, Colorado: Colorado School Mines Quart., v. 65, no. 4, Oct. 1970, p. 73–87.

Ertl, Tell, 1965, Mining Colorado oil shale *in* Second symposium on oil shale: Colorado School Mines Quart., v. 60, no. 3, p. 83–91.

Table 1.—*Potential strippable oil-shale resources in the Mahogany zone, Cathedral Bluffs area, Garfield and Rio Blanco Counties, Colo.*

Location			Area (acres)	Approximate range in thickness (ft)	Approximate range in value (gal of oil per ton)	Average oil content (bbl per acre, in thousands)	Resources (millions of bbls of oil)
T.	R.	Quadrangle[1]					
Deposits with less than 200 feet of overburden							
1 N.	99 W.	CR	2,631	100-130	12-20	150	394
1 N.	100 W.	CR	922	100-120	12-17	100	92
1 S.	99 W.	CR	137	120-145	17-23	175	24
1 S.	99 W.	SH	1,007	100-140	15-20	225	227
1 S.	100 W.	CR	231	100-130	12-22	100	23
1 S.	100 W.	SH	2,731	100-110	12-17	175	478
2 S.	99 W.	SH	441	120-140	17-23	200	88
2 S.	99 W.	BC	186	100-125	21-26	200	37
2 S.	100 W.	SH	778	100-130	12-21	185	144
2 S.	100 W.	BC	1,343	90-110	20-22	160	215
3 S.	99 W.	BC	361	85-115	18-24	170	61
3 S.	99 W.	RR	464	100-104	20-24	170	79
3 S.	100 W.	BC	664	85-100	18-22	140	93
4 S.	99 W.	RR	2,137	84-111	20-24	160	342
4 S.	100 W.	RR	1,780	70-90	15-22	100	178
5 S.	99 W.	RR	250	78-85	20-23	120	30
5 S.	100 W.	RR	474	65-80	15-22	75	36
Total			16,537				2,541

In an area of 1,446 acres in T. 2 N., R. 99 W., in the Calamity Ridge quadrangle, the oil-shale resource contained in the Mahogany zone is unappraised.

Deposits with 200 to 400 feet of overburden							
1 N.	99 W.	CR	3,232	100-130	12-20	150	485
1 N.	100 W.	CR	367	100-120	12-17	100	37
1 S.	99 W.	CR	387	120-145	17-23	175	68
1 S.	99 W.	SH	3,261	100-140	15-20	225	734
1 S.	100 W.	CR	186	100-130	12-22	100	19
1 S.	100 W.	SH	5,681	100-110	12-17	175	994
2 S.	99 W.	SH	1,452	120-140	17-23	200	290
2 S.	99 W.	BC	1,294	100-125	21-26	200	259
2 S.	100 W.	SH	2,019	100-130	12-21	185	374
2 S.	100 W.	BC	2,296	90-110	20-22	160	367
3 S.	99 W.	BC	2,523	85-115	18-24	170	429
3 S.	99 W.	RR	198	100-104	20-24	170	34
3 S.	100 W.	BC	1,387	85-100	18-22	140	194
4 S.	99W.	RR	3,873	84-111	20-24	160	620
4 S.	100 W.	RR	3,907	70-90	15-22	100	391
5 S.	99 W.	RR	909	78-85	20-23	120	109
5 S.	100 W.	RR	1,600	65-80	15-22	75	120
Total			34,572				5,524

In an area of 619 acres in T. 2 N., R. 99 W., in the Calamity Ridge quadrangle, the oil-shale resource in the Mahogany zone is unappraised.

[1] CR, Calamity Ridge; SH, Sagebrush Hill; BC, Black Cabin Gulch; RR, Razorback Ridge.

CLARK'S TERTIARY MOLLUSCAN TYPES FROM THE YAKATAGA DISTRICT, GULF OF ALASKA

By WARREN O. ADDICOTT; SABURO KANNO[1]; KENJI SAKAMOTO, and DON J. MILLER[2], Menlo Park, Calif.; Tokyo, Japan; Menlo Park, Calif.

Abstract.—Forty-six molluscan taxa described and illustrated by Clark in 1932 from the Oligocene and Miocene part of the Poul Creek and Yakataga Formations, Gulf of Alaska Tertiary province, Alaska, are reillustrated. One species from the Poul Creek Formation, *Turritella* sp., figured by Merriam in 1941 is also reillustrated. Clark's generic assignments have been reevaluated, in most cases necessitating changes in the generic classification of his species. Some of the collections used by Clark contain mixtures of species from both the Poul Creek and Yakataga Formations, and therefore the stratigraphic occurrence of these mollusks has also been restudied.

The Gulf of Alaska Tertiary province, extending in an arcuate belt from Prince William Sound (lat 60.5° N.) southeastward to the Fairweather Range (lat 58.5° N.), includes a thick sequence of marine and nonmarine strata that has been divided into two broad units: (1) indurated, strongly deformed rocks of early Tertiary age, and (2) less deformed and indurated rocks of middle and late Tertiary age (Plafker, 1967, 1971). Marine strata of Eocene through Pliocene age are characterized by abundant molluscan fossils. Although poorly known, these assemblages have provided the framework for age determination and correlation of the marine sequence of this province (MacNeil and others, 1961; Plafker, 1971).

Descriptive paleontologic documentation of the marine Tertiary sequence is limited to a very few reports (Clark, 1932; MacNeil, 1961, 1965, 1967). Other systematic studies, principally monographs of Pacific coast molluscan genera, touch on one or two taxa from the Gulf of Alaska Tertiary province (Schenck, 1931, 1936; Merriam, 1941; Parker, 1949; Keen, 1954; Smith, 1970). However, the only systematic treatment of Tertiary molluscan faunas was by Clark (1932), who described material from the Oligocene and Miocene part of the Poul Creek and Yakataga Formations of the Yakataga district (lat 60° N.). The collections were made by Taliaferro (1932) during the course of geologic mapping of the district. A systematic study of mollusks from the Yakataga district, principally from the Miocene section at Cape Yakataga, is being prepared by Kanno. It will treat many, but not all, of the species illustrated by Clark (1932), in addition to several species not previously recorded from the Yakataga district.

Clark's report stands as the principal reference for faunal correlation of the upper Oligocene to middle Miocene marine strata of this area. It has taken on added significance during the past few years on account of heightened geological exploration of the Gulf of Alaska Tertiary province by petroleum companies. Yet this unique report has proven to be difficult and in many ways unsatisfactory to use for biostratigraphic work, because of the exceptionally poor quality of the fossil illustrations, and because of the stratigraphic misallocation of many of the collections. Many of the illustrations are so poor that the specimens cannot even be determined generically. For example, divaricate sculpture cannot be detected on the figure of "*Nucula hamiltonensis*" [*Acila taliaferroi*] Clark (1932, pl. 14, fig. 14). The problem of stratigraphic assignment of collections was what led Clark (1932) to the incorrect conclusion that the mollusks from the Poul Creek and Yakataga Formations represented a single faunal unit or zone, and that none of his species were limited in stratigraphic occurrence to the Yakataga Formation. To the contrary, subsequent biostratigraphic studies have clearly indicated that several distinctive faunal units are indeed represented in these formations (MacNeil, in Miller, 1957 sheet 2, table 1; Plafker, 1971) and that there is a very pronounced faunal change at or near the Poul Creek-Yakataga Formation boundary.

The purpose of the present report is to make available high-quality photographs of Clark's molluscan types, to place these species in a modern framework of taxonomic classification, and, finally, to indicate as accurately as possible the stratigraphic occurrence of these specimens.

The photography in this report is by Sakamoto; stratigraphic allocation of Taliaferro's (1932) collections is by Miller; and taxonomic revisions are by Kanno and Addicott.

[1] Tokyo University of Education.
[2] Deceased, August 1961, formerly of U.S. Geological Survey.

Acknowledgments. —We are indebted to Wayne L. Frye and Joseph H. Peck, Jr., Museum of Paleontology, University of California, Berkeley, for permission to borrow and to photograph the fossil material included in this report. J. Wyatt Durham also of the University of California, Berkeley, provided assistance in evaluating the species of *Liracassis*. The report has been critically read by George Plafker, Richard C. Allison, and Ellen J. Moore. We appreciate their helpful comments.

STRATIGRAPHIC ALLOCATION OF COLLECTIONS

Neither Taliaferro's (1932) nor Clark's (1932) reports included locality descriptions. The localities were shown, however, on an index map by Clark (1932, fig. 1) at a scale of about 1 inch = 3 miles. Miller's formational assignments and notes on geographic occurrence of the fossil localities are shown in table 1. According to Joseph H. Peck, Jr., Museum of Paleontology, University of California, Berkeley (oral commun., December 1970), Miller searched Taliaferro's field notes and discussed the problems with Taliaferro during the early 1950's. Miller's comments, therefore, represent as thorough an evaluation as possible of the stratigraphic position of the fossil localities. The localities are from the coastal area between Yakataga Reef, on the west, and the head of Icy Bay, on the east. The geology of this part of the Yakataga district has been mapped by Miller (1957).

Table 1.—*Stratigraphic assignment of Taliaferro's collections from the Poul Creek and Yakataga Formations, Yakataga district, Alaska*
[Clark, 1932, fig. 1]

University of California (UCMP) locality No.	Description
3850	Poul Creek Formation, about 700 feet below top (locality approximate).
3851	Float, probably Poul Creek Formation. Not plotted on map; location of "Salmon Creek" not known.
3852	Float, probably Yakataga Formation; could include uppermost Poul Creek Formation.
3853	Yakataga Formation, lower part (locality approximate).
3854	Poul Creek Formation, about 2,000 feet below top.
3855	Probably Poul Creek Formation. Not plotted on map; locality not given in catalog. May be field number Y-9, float, Little River?
3856	Float, Poul Creek Formation and (or) Yakataga Formation. Not plotted on map; locality indefinite.
3857	Poul Creek Formation, middle or lower part (locality approximate).
3858	Float, Poul Creek Formation and (or) Yakataga Formation.
3859	Yakataga Formation, about 350 feet above base.
3860	Poul Creek Formation, upper 50 feet?
3861	Float, Poul Creek Formation and (or) Yakataga Formation. Not plotted on map; locality indefinite.
3863	Probably Poul Creek. Not plotted on map; locality not given in catalog.
3864	Unknown, Poul Creek Formation and (or) Yakataga Formation. Not plotted on map; locality not given in catalog. Locality is "Lawrence Creek" on Clark's list.
3868	Poul Creek Formation at least in part. Not plotted on map; locality not given in catalog. Locality is "Lawrence Creek" on Clark's list.
3869	Yakataga Formation(?) Locality indefinite; as plotted on Clark's map it falls in outcrop of Yakataga Formation, but list of fossils is more suggestive of Poul Creek Formation.
3870	Probably lower part of Yakataga Formation (locality approximate).
3871	Float, largely Poul Creek Formation, but may include some Yakataga Formation. Not plotted on map; locality indefinite.
3872	Float, Poul Creek Formation and (or) Yakataga Formation. Not plotted on map; locality indefinite.

BIOSTRATIGRAPHIC EVALUATION OF COLLECTIONS

Biostratigraphic criteria can also be used to evaluate the stratigraphic assignment of Clark's material. There is a very pronounced faunal change at or near the Poul Creek-Yakataga boundary, contrary to Clark's (1932, p. 799) conclusion that all the species in the Yakataga Formation range downward into the Poul Creek Formation. The diverse, relatively warm water fauna of the upper part of the Poul Creek is replaced, in the lower part of the Yakataga Formation, by a cool-water fauna of much different composition and of very low species diversity. The faunal change is striking as relatively few species are common to both formations (MacNeil, in Miller, 1957). This change is attributed to the onset of local glaciation and resultant cooling of shallow-water, nearshore marine environments.

Using stratigraphic ranges shown by MacNeil (in Miller, 1957), it seems clear that at least six of Clark's collections (UCMP locs. 3857, 3858, 3864, 3868, 3869, and 3870) contain stratigraphically anomalous associations. In other words, these collections contain species with mutually exclusive stratigraphic ranges. Kanno's unpublished biostratigraphic studies support these inferences. Two of the largest collections (UCMP locs. 3850 and 3854), however, do not appear to be mixed. Both are from the upper part of the Poul Creek Formation. Almost half the molluscan taxa figured by Clark (1932) are from these two localities. One of the three collections that Clark (1932, p. 799) maintained were from the Yakataga Formation (UCMP loc. 3859) also does not appear to be mixed, according to currently known stratigraphic ranges of the seven species listed by Clark.

This form of evaluation is limited, however, by the changing concepts for recognition of the Poul Creek-Yakataga boundary. The boundary recognized by Miller (1957) and MacNeil

(in Miller, 1957; MacNeil, 1961), for example, falls within the lower part of the Yakataga Formation as it is now recognized by Kanno and other geologists working in this area (George Plafker, oral commun., October 1970). The lowering of the boundary places it at or near the lowest occurrence of cool-water molluscan assemblages in the Poul Creek-Yakataga sequence at Cape Yakataga.

TAXONOMIC REVISION OF CLARK'S NAMES

Species described and illustrated by Clark (1932) are listed systematically in table 2. One of Clark's (1932) types, *Cancellaria alaskensis* (UCMP No. 12395), has been missing from the University of California type collection since 1933 (Joseph H. Peck, Jr., oral commun., October 1970). Taxonomic revisions are indicated in the right-hand column of the table and in brackets in the captions for figures 1-6. Systematic arrangement of gastropods is after Keen (1963); of pelecypods after McCormick and Moore (1969).

FOSSIL PHOTOGRAPHS

The initial entry on the plate descriptions (figs. 1-6) is the name used by Clark (1932, pls. 14-21). The spelling is as

Table 2.—*Correlation of Clark's (1932) names with names used in this report*

[Species preceded by an asterisk (*) are considered to be restricted, in stratigraphic occurrence, to the Yakataga Formation]

Clark (1932)	This report
Gastropods	
Turcicula turbonata n. sp.	*Bathybembix turbonata* (Clark).
Natica (Cryptonatica) n. sp	*Cryptonatica* aff. *C. clausa* (Broderip and Sowerby).
Polinices (Euspira) ramonensis Clark.	*Euspira ramonensis* (Clark).
Galeodea apta Tegland (pl. 21, figs. 1, 3).	*Liracassis apta* (Tegland).
Galeodea apta Tegland (pl. 21, figs. 2, 9, 15).	*Liracassis* aff. *L. petrosa* (Conrad).
Turritella hamiltonensis n. sp.	*Turritella hamiltonensis* Clark.
Turritella n. sp.	*Turritella* n. sp. Clark.
Turritella cf. *porterensis* Weaver.	*Turritella* aff. *T. diversilineata blakeleyensis* Weaver.
Colus rearensis n. sp.	*Ancistrolepis rearensis* (Clark).
**Neptunea* aff. *tabulatus* Baird	*Neptunea* aff. *N. tabulata* (Baird).
Fusinus cf. *hannibali* Clark and Arnold.	*Priscofusus* aff. *P. hannibali* (Clark and Arnold).
Psephaea corrugata n. sp.	*Musashia (Miopleiona) corrugata* (Clark).
Cancellaria (Progabbi) alaskensis n. sp.	*Cancellaria (Crawfordina) alaskensis* Clark.
Haminoea n. sp.?	*Haminoea* n. sp.? Clark.
Scaphander alaskensis n. sp.	*Scaphander alaskensis* Clark.
Pelecypods	
Nucula (Acila) gettysburgensis Reagan.	*Acila (Acila) gettysburgensis* (Reagan).
Nucula (Acila) gettysburgensis alaskensis n. var.	*Acila (Acila) gettysburgensis* (Reagan).
Nucula (Acila) hamiltonensis n. sp.	*Acila (Truncacila) taliaferroi* Schenck.
Nucula (Acila) yakatagensis n. sp.	*Acila (Truncacila) yakatagensis* (Clark).
**Leda fossa* Baird	*Nuculana (Borissia) olferovi sachalinensis* Krishtofovich.
**Pecten (Patinopecten) yakatagensis* n. sp.	*Patinopecten (Lituyapecten) yakatagensis* (Clark).
Thyasira bisecta Conrad	*Conchocele disjuncta* Gabb.
Venericardia hamiltonensis n. sp.	*Cyclocardia hamiltonensis* (Clark).
Venericardia yakatagensis n. sp.	*Cyclocardia yakatagensis* (Clark).
Cardium (Serripes) hamiltonensis n. sp.	*Papyridea? hamiltonensis* (Clark).

Clark (1932)	This report
Pelecypods (Continued)	
Cardium (Laevicardium) alaskensis n. sp.	*Nemocardium (Keenae?) alaskense* (Clark).
Cardium (Papyridea) brooksi n. sp.	*Clinocardium brooksi* (Clark).
Cardium (Ceratoderma) yakatagensis n. sp.	*Clinocardium yakatagensis* (Clark).
Mactra (Mactrotoma) californica equilateralis n. subsp.	*Spisula californica equilateralis* (Clark).
Spisula ramonensis Packard (pl. 14, figs. 1, 4; pl. 19, fig. 3).	*Spisula ramonensis* Packard.
Spisula ramonensis Packard (pl. 14, fig. 5).	*Spisula* aff. *S. ramonensis* Packard.
Schizothaerus? trapezoides n. sp.	*Spisula trapezoides* (Clark).
**Tellina* sp.	*Macoma?* cf. *M. arctata* (Conrad).
Macoma cf. *secta* Conrad (pl. 16, fig. 3).	*Macoma* aff. *M. calcarea* (Gmelin).
Macoma cf. *M. middendorffii* Dall.	*Macoma* cf. *M. incongrua* (von Martens).
Heterodonax? sp.	*Macoma* cf. *M. incongrua* (von Martens).
Macoma cf. *secta* Conrad (pl. 16, fig. 2).	*Macoma (Rexithaerus)* sp.
Macrocallista pittsburgensis Dall.	*Macrocallista pittsburgensis* (Dall).
Macrocallista? rearensis Clark	*Macrocallista rearensis* Clark.
**Chione securis alaskensis* n. subsp.	*Securella alaskensis* (Clark).
Mya salmonensis n. sp.	*Mya (Mya) salmonensis* Clark.
**Mya truncata* Linnaeus n. subsp.?	*Mya (Mya) truncata* Linné
Schizothaerus nuttallii Conrad n. subsp.?	*Mya* sp.
**Panomya (Arctica) turgida* Dall.	*Panomya arctica* (Lamarck).
**Panomya* n. sp.?	*Panomya* cf. *P. arctica* (Lamarck).
Saxicava pholadis Linnaeus	*?Panomya* sp.
Pandora (Kennerlia) yakatagensis n. sp.	*Pandora yakatagensis* Clark.
Thracia schencki Tegland (1933)	*Thracia schencki* Clark (1932).
Cephalopods	
Aturia angustata (Conrad) *alaskensis* Schenck.	*Aturia alaskensis* Schenck.

originally used and may contain typographical errors or lapses. If the name is followed by another one in brackets, that name represents our reevaluation of generic classification and of specific identification. Not all the species have been assigned to subgenera, in part owing to the poor quality of preservation and, in the case of some pelecypods, to the fact that hinges have not been exposed on most of the specimens. The intent of this report is to provide a current generic classification of Clark's (1932) taxa and not to evaluate the validity of his specific names. Nevertheless, some of the obvious misidentifications and synonyms are indicated by revised specific identifications in table 2. It is recognized that detailed systematic study of his material may prove that some of the other species are also synonyms.

In preparing his plates Clark (1932) cropped the matrix from around many of the photographs, and on some plates the resultant outline does not accurately depict the fossil specimen. In the interest of reproducing the type material as objectively as possible, this practice has not been followed in preparing illustrations of this report.

REFERENCES

Clark, B. L., 1932, Fauna of the Poul and Yakataga Formations (upper Oligocene) of southern Alaska: Geol. Soc. America Bull., v. 43, p. 797–846, pls. 14–21.

Keen, A. M., 1954, Five new species and a new subgenus in the pelecypod family Cardiidae: Bull. Am. Paleontology, v. 35, no. 153, 24 p., 1 pl.

——1963, Marine molluscan genera of western North America, an illustrated key: Stanford, Calif., Stanford Univ. Press, 126 p.

MacNeil, F.S., 1961, *Lituyapecten* (new subgenus of *Patinopecten*) from Alaska and California: U.S. Geol. Survey Prof. Paper 354-J, p. 225–239, pls. 35–46.

——1965, Evolution and distribution of the genus *Mya*, and Tertiary migrations of Mollusca: U.S. Geol. Survey Prof. Paper 483-G, 51 p., 11 pls.

——1967, Cenozoic pectinids of Alaska, Iceland, and other northern regions: U.S. Geol. Survey Prof. Paper 553, 57 p., 25 pls.

MacNeil, F. S., Wolfe, J.A., Miller, D. J., and Hopkins, D. M., 1961, Correlation of Tertiary formations of Alaska: Am. Assoc. Petroleum Geologists Bull., v. 45, no. 11, p. 1801–1809.

McCormick, Lavon, and Moore, R. C., 1969, Outline of classification [of Bivalvia], *in* Moore, R.C., ed., Treatise on invertebrate paleontology, pt. N, Mollusca 6, Bivalvia, v. 1: Lawrence, Kans. Univ. Kansas Press, p. N218–N222.

Merriam, C. W., 1941, Fossil Turritellas from the Pacific coast region of North America: California Univ., Dept. Geol. Sci. Bull., v. 26, no. 1, p. 1–214, pls. 1–41.

Miller, D. J., 1957, Geology of the southeastern part of the Robinson Mountains, Yakataga district, Alaska: U.S. Geol. Survey Oil and Gas Inv. Map OM–187, 2 sheets.

Parker, Pierre, 1949, Fossil and recent species of the Pelecypod genera *Chione* and *Securella* from the Pacific coast: Jour. Paleontology, v. 23, no. 6, p. 577–593, pls 89–95.

Plafker, George, 1967, Geologic map of the Gulf of Alaska Tertiary Province, Alaska: U.S. Geol. Survey Misc. Geol. Inv. Map I–484.

——1971, Possible future petroleum resources in the Pacific-margin Tertiary basin, Alaska: Am. Assoc. Petroleum Geologists Mem. 15 [In press].

Schenck, H. G., 1931, Cephalopods of the genus *Aturia* from western North America: California Univ., Dept. Geol. Sci. Bull., v. 19, no. 19, p. 435–490, pls. 66–78.

——1936, Nuculid bivalves of the genus *Acila:* Geol. Soc. America Spec. Paper 4, 149 p., 18 pls.

Smith, J. T., 1970, Taxonomy, distribution, and phylogeny of the cymatiid gastropods *Argobuccinum, Fusitriton, Mediargo,* and *Priene*: Bull. Am. Paleontology, v. 56, no. 254, p. 445–573, pls. 39–49.

Taliaferro, N. L., 1932, Geology of the Yakataga, Katalla, and Nichawak districts, Alaska: Geol. Soc. America Bull., v. 43, no. 3, p. 749–782.

[Figures 1–6 follow on pages C22–C33]

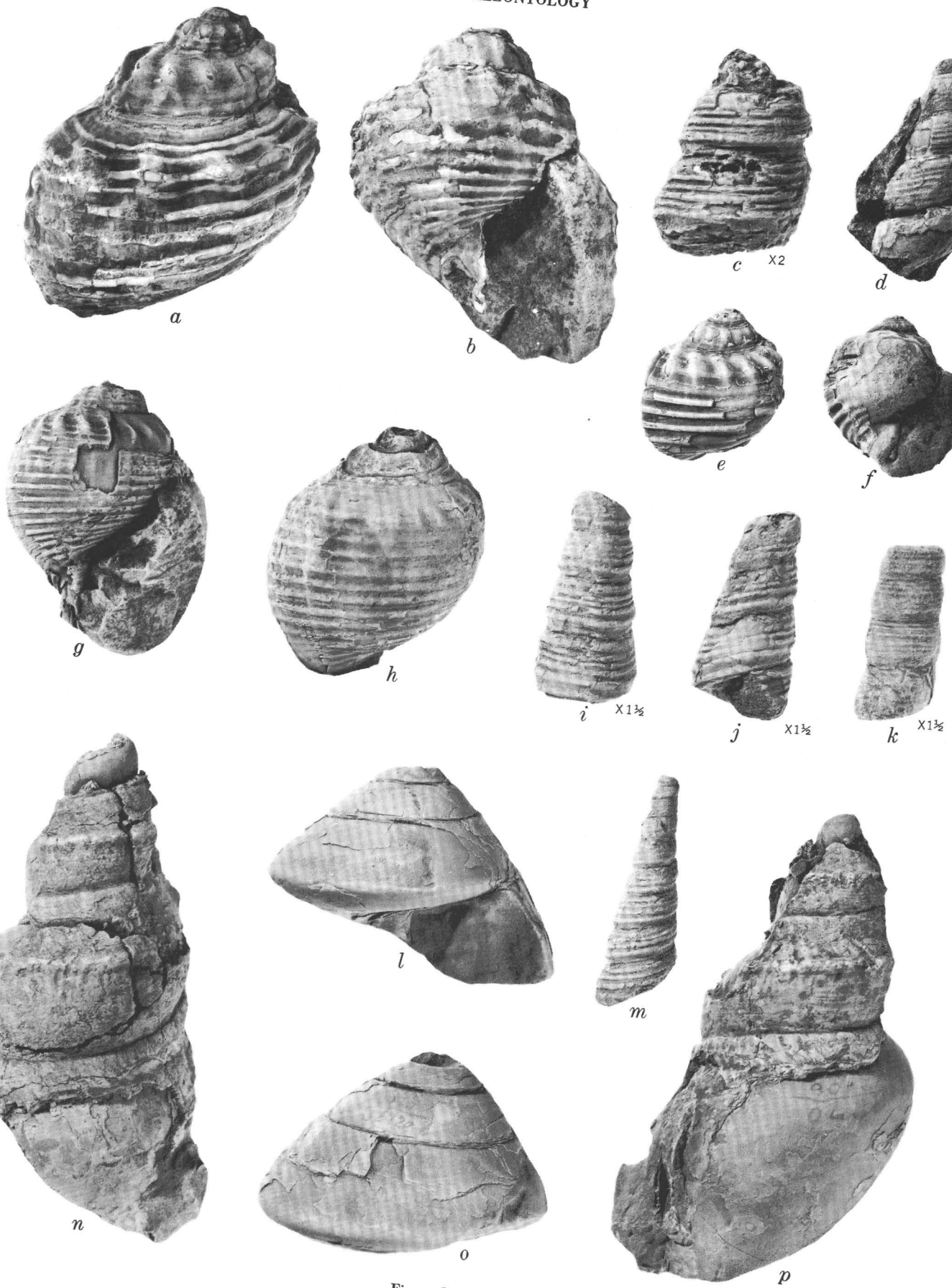

Figure 1.

Figure 1.—Molluscan fossils, from the Yakataga district, described by Clark (1932). All photographs natural size unless otherwise indicated.

a, b, e, f. Galeodea apta Tegland [*Liracassis* aff. *L. petrosa* (Conrad)].

a, b. UCMP 12404. UCMP loc. 3871. Clark (1932, pl. 21, fig. 15).

e, f. UCMP 12405. UCMP loc. 3871. Clark (1932, pl. 21, fig. 9).

c, k. Turritella cf. *porterensis* Weaver [*Turritella* aff. *T. diversilineata blakeleyensis* Weaver].

c. UCMP 31361. UCMP loc. 3868. Clark (1932, pl. 21, fig. 10).

k. UCMP 31440. UCMP loc. 3858. Clark (1932, pl. 21, fig. 16). A crushed specimen.

d. Turritella n. sp. Clark UCMP 31360. UCMP loc. 3871. Clark (1932, pl. 21, fig. 8).

g, h. Galeodea apta Tegland [*Liracassis apta* (Tegland)]. UCMP 12392. UCMP loc. 3850. Clark (1932, pl. 21, figs. 1, 3).

i, j, m. Turritella hamiltonensis Clark.

i, j. Holotype. UCMP 30281. UCMP loc. 3850. Clark (1932, pl. 21, fig. 14).

m. Paratype. UCMP 30280. UCMP loc. 3850. Clark (1932, pl. 21, fig. 13).

l, o. Turcicula turbonata Clark [*Bathybembix turbonata* (Clark)]. Holotype. UCMP 32420. UCMP loc. 3857. Clark (1932, pl. 20, fig. 11).

n, p. Neptunea aff. *tabulatus* Baird [*Neptunea* aff. *N. tabulata* (Baird)]. UCMP 12406. UCMP loc. 3870. Clark (1932, pl. 20, fig. 13).

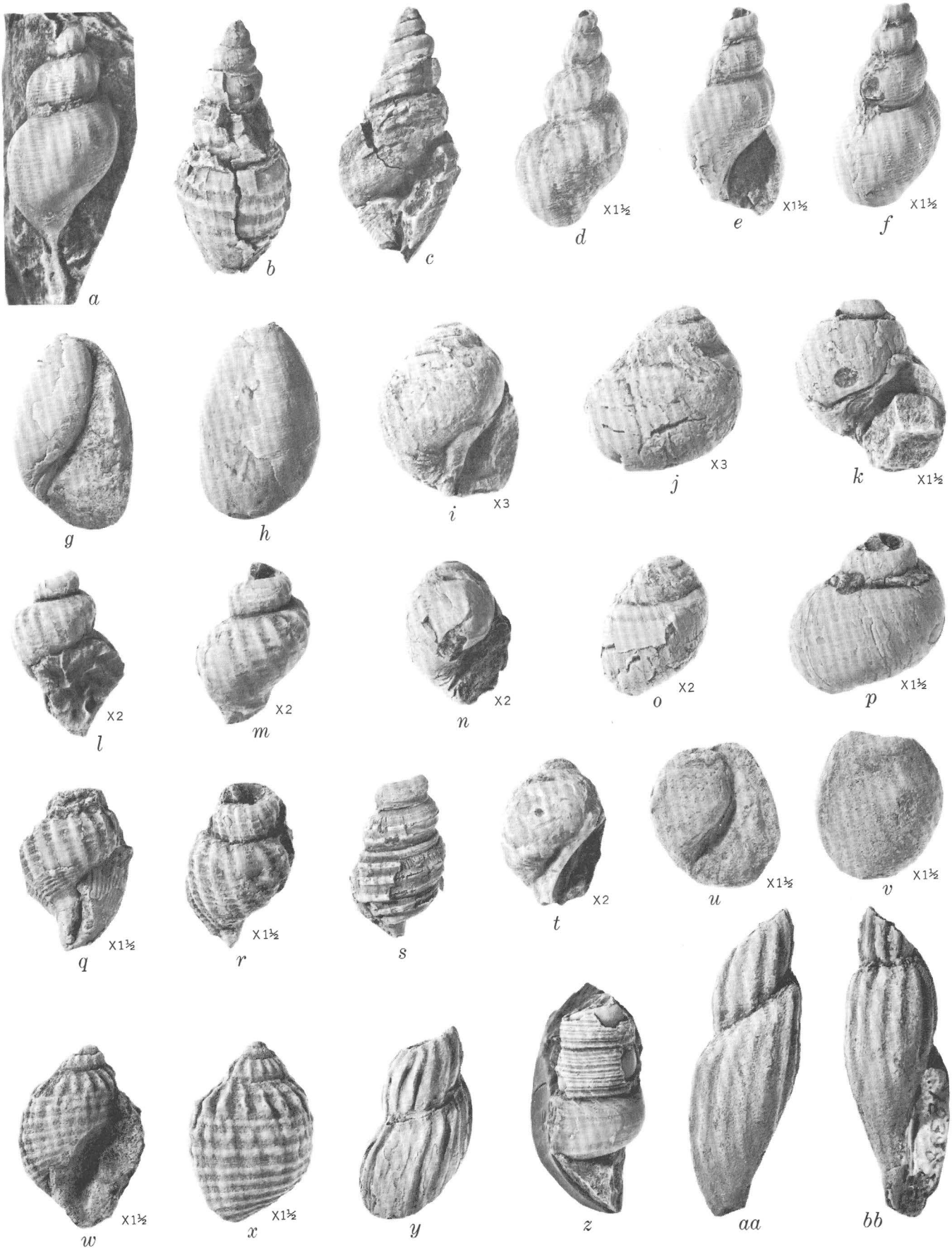
a
b
c
d X1½
e X1½
f X1½
g
h
i X3
j X3
k X1½
l X2
m X2
n X2
o X2
p X1½
q X1½
r X1½
s
t X2
u X1½
v X1½
w X1½
x X1½
y
z
aa
bb

Figure 2.

Figure 2.—Molluscan fossils, from the Yakataga district, described by Clark (1932). All photographs natural size unless otherwise indicated.

a, d-f. Fusinus cf. *hannibali* Clark and Arnold [*Priscofusus* aff. *P. hannibali* (Clark and Arnold)].

a. UCMP 31356. UCMP loc. 3850. Clark (1932, pl. 20, fig. 1).

d. UCMP 31358. UCMP loc. 3868. Clark (1932, pl. 20, fig. 2).

e, f. UCMP 31357. UCMP loc. 3868. Clark (1932, pl. 20, fig. 3).

b, c, s. Colus rearensis Clark [*Ancistrolepis rearensis* (Clark)].

b, c. Holotype. UCMP 12402. UCMP loc. 3868. Clark (1932, pl. 20, fig. 14).

s. Paratype. UCMP 12401. UCMP loc. 3868. Clark (1932, pl. 20, fig. 15).

g, h. Scaphander alaskensis Clark. Holotype. UCMP 12382. UCMP loc. 3854. Clark (1932, pl. 21, figs. 6, 7).

i, j, n, o, t Polinices (Euspira) ramonensis Clark [*Euspira ramonensis* (Clark)].

i, j. UCMP 12381. UCMP loc. 3854. Clark (1932, pl. 20, figs. 4, 5).

n, o. UCMP 12384. UCMP loc. 3854. Clark (1932, pl. 20, fig. 9). Specimen crushed, callus missing.

t. UCMP 12396. UCMP loc. 3854. Clark (1932, pl. 20, fig. 8).

k, p. Natica (Cryptonatica) n. sp. Clark [*Cryptonatica* aff. *C. clausa* (Broderip and Sowerby)]. UCMP 31359. UCMP loc. 3850. Clark (1932, pl. 20, figs. 6, 7).

l, m, q, r. Cancellaria (Progabbi) alaskensis Clark [*Cancellaria (Crawfordina) alaskensis* Clark]. The holotype of this species is lost.

l, m. Paratype. UCMP 31353. UCMP loc. 3868. Clark (1932, pl. 20, fig. 12).

q, r. Paratype. UCMP 31354. UCMP loc. 3868. Clark (1932, pl. 20, fig. 10).

u, v. Haminoea n. sp.? Clark UCMP 12397. UCMP loc. 3850. Clark (1932, pl. 21, fig. 12).

w, x. Galeodea apta Tegland [*Liracassis* aff. *L. petrosa* (Conrad)]. UCMP 12383. UCMP loc. 3860. Clark (1932, pl. 21, fig. 2).

y, aa, bb. Psephaea corrugata Clark [*Musashia (Miopleiona) corrugata* (Clark)].

y. Paratype. UCMP 12399. UCMP loc. 3871. Clark (1932, pl. 21, fig. 4).

aa, bb. Holotype. UCMP 12398. UCMP loc. 3850. Clark (1932, pl. 21, figs. 5, 11).

z. Turritella sp. Merriam. UCMP 15445. UCMP loc. 3854. Merriam (1941, pl. 40, fig. 6).

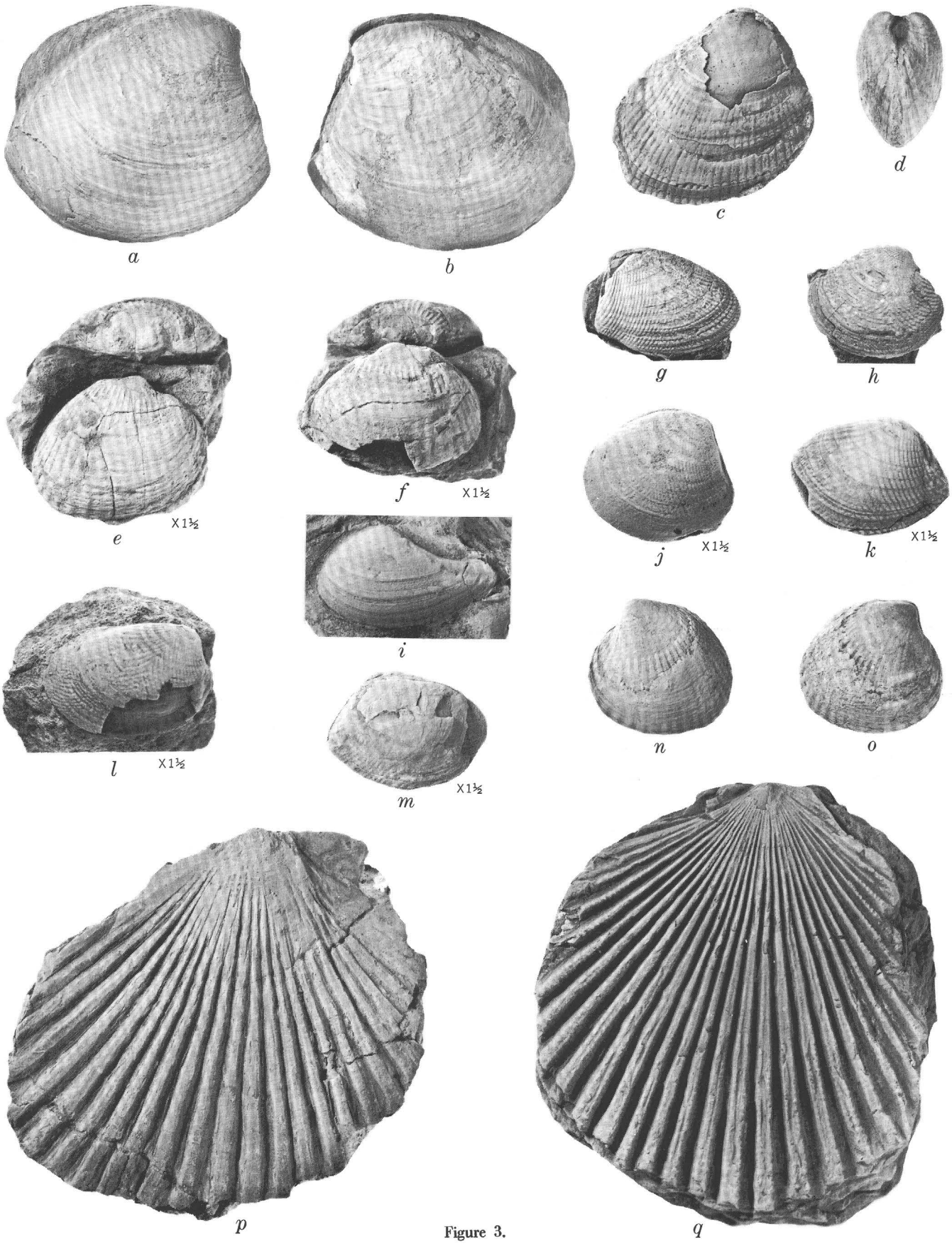

Figure 3.

Figure 3.—Molluscan fossils, from the Yakataga district, described by Clark (1932). All photographs natural size unless otherwise indicated.

a, b. Thyasira bisecta Conrad [*Conchocele disjuncta* Gabb]. UCMP 30385. UCMP loc. 3860. Clark (1932, pl. 14, fig. 2).

c. Cardium (Serripes) hamiltonensis Clark [*Papyridea? hamiltonensis* (Clark)]. Holotype. UCMP 30405. UCMP loc. 3855. Clark (1932, pl. 18, fig. 7).

d, n, o. Venericardia yakatagensis Clark [*Cyclocardia yakatagensis* (Clark)]. Holotype. UCMP 12409. UCMP loc. 3854. Clark (1932, pl. 14, figs. 6, 7).

e, f. Venericardia hamiltonensis Clark [*Cyclocardia hamiltonensis* (Clark)]. Holotype. UCMP 12408. UCMP loc. 3858. Clark (1932, pl. 14, figs. 9, 10.)

g. Nucula (Acila) gettysburgensis var. *alaskensis* Clark [*Acila (Acila) gettysburgensis* (Reagan)]. Holotype. UCMP 30388. UCMP loc. 3871. Clark (1932, pl. 14, fig. 15).

h, j. Nucula (Acila) hamiltonensis Clark [*Acila (Truncacila) taliaferroi* Schenck].

h. Paratype. UCMP 30375. UCMP loc. 3854. Clark (1932, pl. 14, fig. 11).

j. Holotype. UCMP 30376. UCMP loc. 3850. Clark (1932, pl. 14, fig. 14).

i. Leda fossa Baird [*Nuculana (Borissia) olferovi sachalinensis* Krishtofovich]. UCMP 12403. UCMP loc. 3858. Clark (1932, pl. 14, fig. 3).

k, m. Nucula (Acila) gettysburgensis Reagan [*Acila (Acila) gettysburgensis* (Reagan)]. UCMP 30400. UCMP loc. 3871. Clark (1932, pl. 14, fig. 12).

l. Nucula (Acila) yakatagensis Clark [*Acila (Truncacila) yakatagensis* (Clark)]. Holotype. UCMP 30393. UCMP loc. 3871. Clark (1932, pl. 14, fig. 13).

p, q. Pecten (Patinopecten) yakatagensis Clark [*Patinopecten (Lituyapecten) yakatagensis* (Clark)].

p. Paratype. UCMP 30382. UCMP loc. 3859. Clark (1932, pl. 15, fig. 8).

q. Holotype. UCMP 30381. UCMP loc. 3859. Clark (1932, pl. 16, fig. 1).

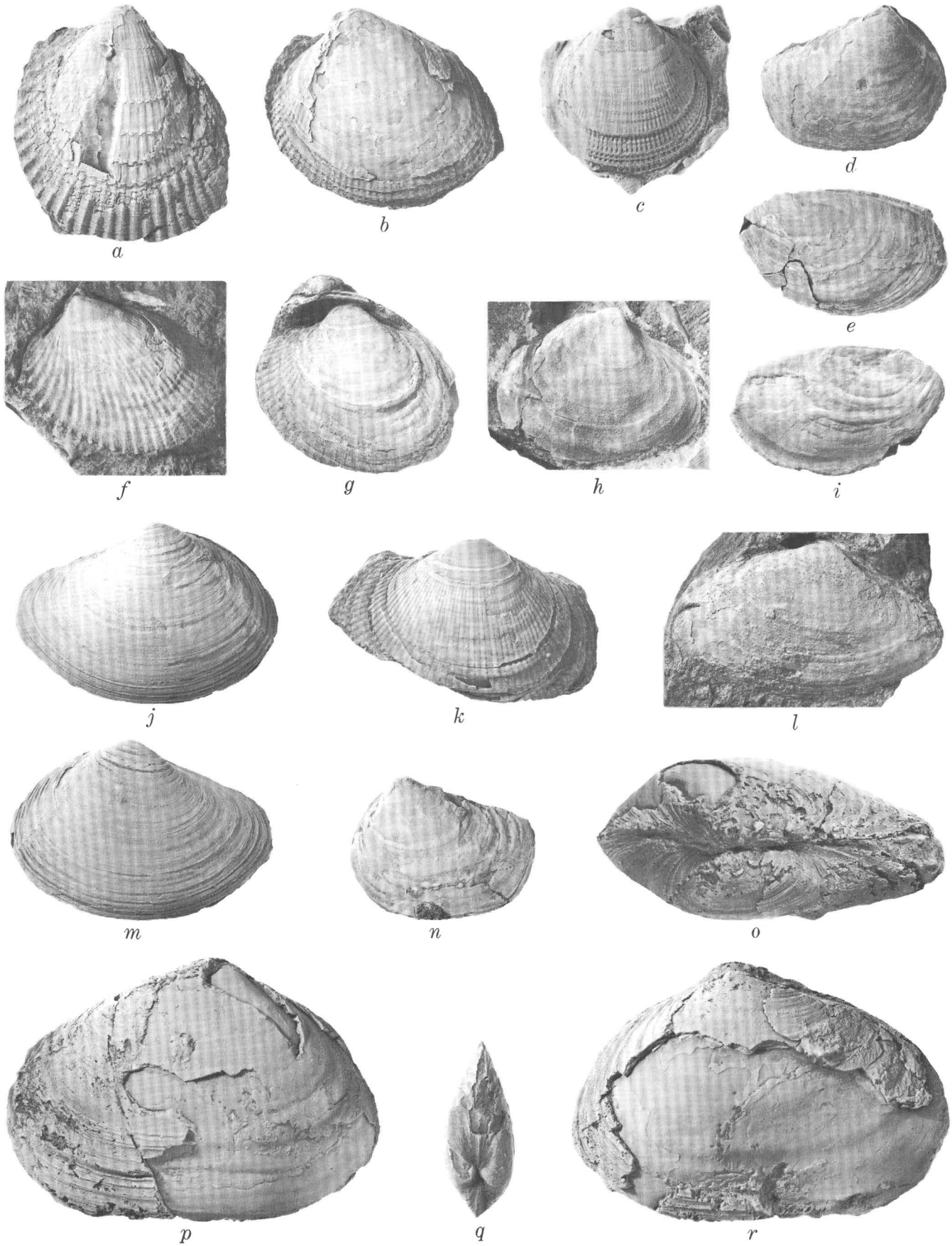

Figure 4.

Figure 4.—Molluscan fossils, from the Yakataga district, described by Clark (1932). All photographs natural size.

a. Cardium (Ceratoderma) yakatagensis Clark [*Clinocardium yakatagensis* (Clark)]. Holotype. UCMP 30384. UCMP loc. 3860. Clark (1932, pl. 18, fig. 8).

b, g, k. Cardium (Serripes) hamiltonensis Clark [*Papyridea? hamiltonensis* (Clark)].

b. Paratype. UCMP 30391. UCMP loc. 3850. Clark (1932, pl. 18, fig. 6).

g. Holotype. UCMP 30405. UCMP loc. 3855. Clark (1932, pl. 18, fig. 7).

k. Paratype. UCMP 30392. UCMP loc. 3850. Clark (1932, pl. 18, fig. 10).

c. Cardium (Laevicardium) alaskensis Clark [*Nemocardium (Keenae?) alaskense* (Clark)]. Holotype. UCMP 30389. UCMP loc. 3868. Clark (1932, pl. 18, fig. 4).

d, n, q. Schizothaerus? trapezoides Clark [*Spisula trapezoides* (Clark)]. Holotype. UCMP 30374. UCMP loc. 3850. Clark (1932, pl. 15, fig. 9). Specimen crushed along posterior dorsal margin.

e, i. Pandora (Kennerlia) yakatagensis Clark [*Pandora yakatagensis* Clark]. Holotype. UCMP 30399. UCMP loc. 3869. Clark (1932, pl. 17, figs. 1, 2).

f. Cardium (Papyridea) brooksi Clark [*Clinocardium brooksi* (Clark)]. Holotype. UCMP 30402. UCMP loc. 3850. Clark (1932, pl. 18, fig. 5).

h. Spisula ramonensis Packard. UCMP 32302. UCMP loc. 3850. Clark (1932, pl. 19, fig. 3).

j, m. Spisula ramonensis Packard [*Spisula* aff. *S. ramonensis* Packard]. UCMP 30394. UCMP loc. 3861. Clark (1932, pl. 14, fig. 5).

l.Mactra (Mactrotoma) californica equilateralis Clark [*Spisula californica equilateralis* (Clark)]. Holotype, UCMP 30390. UCMP loc. 3870. Clark (1932, pl. 14, fig. 8).

o, p, r. Schizothaerus nuttallii Conrad n. subsp.? Clark [*Mya* sp.]. UCMP 30380. UCMP loc. 3870. Clark (1932, pl. 15, figs. 1, 4).

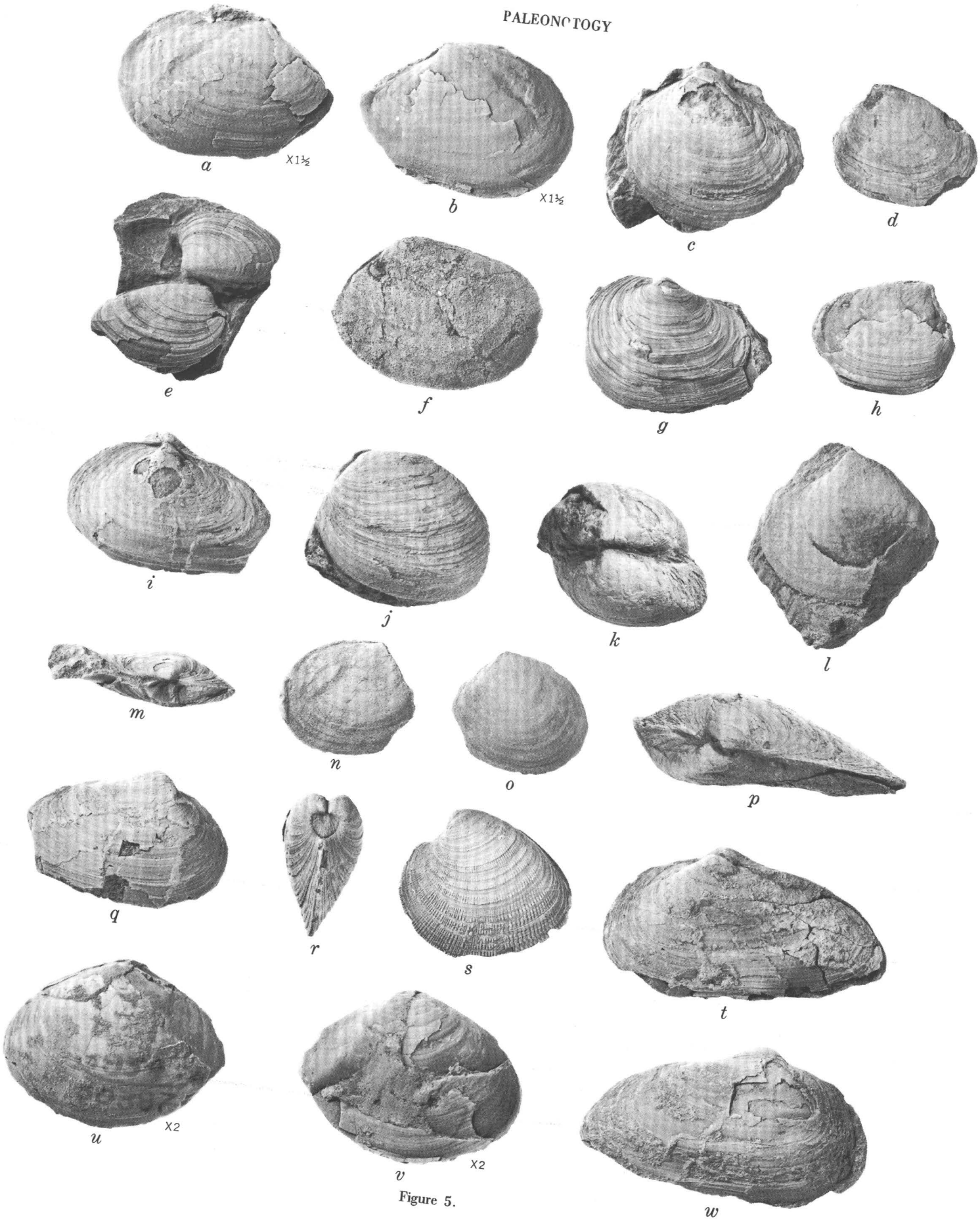

Figure 5.

Figure 5.—Molluscan fossils, from the Yakataga district, described by Clark (1932). All photographs natural size unless indicated otherwise.

a, b. Macoma cf. *secta* Conrad [*Macoma* aff. *M. calcarea* (Gmelin)]. UCMP 30386. UCMP loc. 3854. Clark (1932, pl. 16, fig. 3).

c, l. Spisula ramonensis Packard.

c. UCMP 30404. UCMP loc. 3850. Clark (1932, pl. 14, fig. 1).

l. UCMP 32301. UCMP loc. 3850. Clark (1932, pl. 14, fig. 4).

d, h. Heterodonax? sp. Clark [*Macoma* cf. *M. incongrua* (von Martens)]. UCMP 30383. UCMP loc. 3850. Clark (1932, pl. 15, figs. 6, 7).

e. Macrocallista pittsburgensis Dall [*Macrocallista pittsburgensis* (Dall)]. UCMP 31345. UCMP loc. 3854. Clark (1932, pl. 19, figs. 1, 2).

f. Tellina sp. Clark [*Macoma?* cf. *M. arctata* (Conrad)]. UCMP 31351. UCMP loc. 3859. Clark (1932, pl. 15, fig. 10).

g, m. Mya (Mya) truncata Linnaeus n. subsp.? Clark [*Mya (Mya)* truncata, Linné]. UCMP 30379. UCMP loc. 3868. Clark (1932, pl. 17, fig. 5).

i, p, q, t, w. Mya salmonensis Clark [*Mya (Mya) salmonensis* Clark].

i, q. Paratype. UCMP 30396. UCMP loc. 3851. Clark (1932, pl. 17, fig. 4).

p, t, w. Holotype. UCMP 30397. UCMP loc. 3851. Clark (1932, pl. 17, fig. 3).

j, k. Macrocallista? rearensis Clark. Holotype. UCMP 30378. UCMP loc. 3854. Clark (1932, pl. 18, fig. 1).

n, o. Macoma cf. *M. middendorffii* Dall [*Macoma* cf. *M. incongrua* (von Martens)]. UCMP 12407. UCMP loc. 3850. Clark (1932, pl. 16, fig. 4).

r, s. Chione securis alaskensis Clark [*Securella alaskensis* (Clark)]. Holotype. UCMP 30406. UCMP loc. 3868. Clark (1932, pl. 18, figs. 2, 3).

u, v. Macoma cf. *secta* Conrad [*Macoma (Rexithaerus)* sp.]. UCMP 30387. UCMP loc. 3854. Clark (1932, pl. 16, fig. 2).

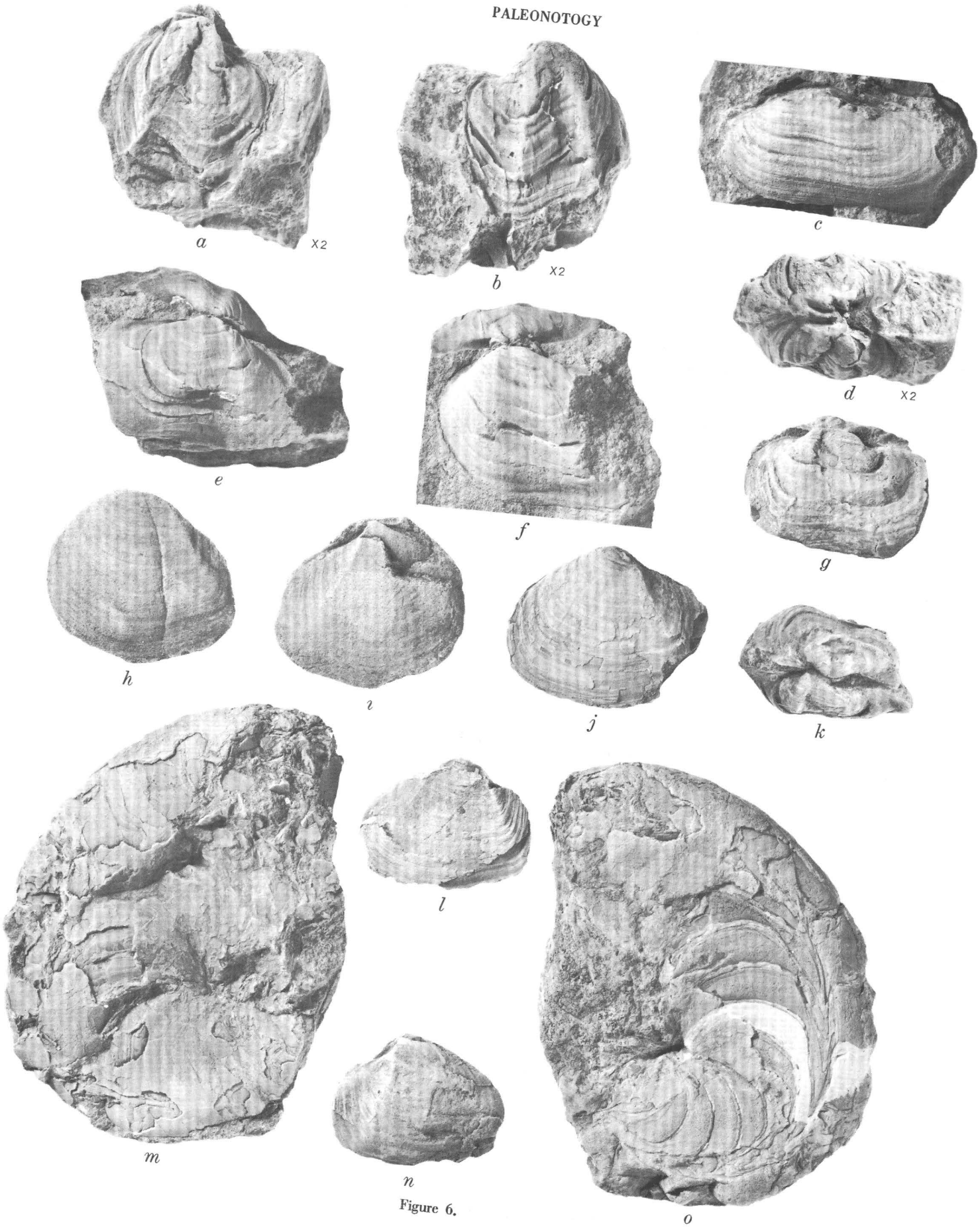

Figure 6.

Figure 6.—Molluscan fossils, from the Yakataga district, described by Clark (1932). All photographs natural size unless indicated otherwise.

a, b, d. Panomya n. sp.? Clark [*Panomya* cf. *P. arctica* (Lamarck)]. UCMP 30401. UCMP loc. 3858. Clark (1932, pl. 17, fig. 7).

c. Saxicava pholadis Linnaeus [?*Panomya* sp.]. UCMP 30395. UCMP loc. 3850. Clark (1932, pl. 18, fig. 9).

e, f, g, k. Panomya (Arctica) turgida Dall [*Panomya arctica* (Lamarck)].

e, f. UCMP 31347. UCMP loc. 3858. Clark (1932, pl. 17, fig. 9).

g, k. UCMP 30398. UCMP loc. 3864. Clark (1932, pl. 17, fig. 6).

h-j, l, n. Thracia schencki Tegland (1933) [*Thracia schencki* Clark].

h, i. UCMP 31342. UCMP loc. 3850. Clark (1932, pl. 15, fig. 3).

j. UCMP 31341. UCMP loc. 3854. Clark (1932, pl. 15, fig. 2).

l, n. UCMP 30377. UCMP loc. 3850. Clark (1932, pl. 15, fig. 5).

m, o. Aturia angustata (Conrad) *alaskensis* Schenck [*Aturia alaskensis* Schenck]. Holotype. UCMP 31362. UCMP loc. 3871. Clark (1932, pl. 16, figs. 5, 6).

PRIMITIVE SQUID GLADII FROM THE PERMIAN OF UTAH

By MACKENZIE GORDON, JR., Washington, D.C.

Abstract.—*Glochinomorpha* n. gen. (type species, *G. stifeli* n. sp.) of the family Glochinomorphidae n. fam. and suborder Glochinomorphina n. subord. is erected for small, nearly flat, longitudinally and radially lirate arrowhead-shaped fossils preserved in shale in the Meade Peak Phosphatic Shale Member of the Phosphoria Formation in northwest Utah. These fossils are interpreted as gladii of primitive squidlike coleoids having an extended rhachis, rather short lateral fields, and no conus. As the Middle Pennsylvanian genus *Jeletzkya* Johnson and Richardson, originally described as a squid, is here regarded as a true belemnite, these Permian fossils are the earliest squid remains on record.

The fossils upon which this paper is based were discovered by Peter B. Stifel in 1960 when mapping for his doctoral dissertation an area that included the Terrace Mountains, Box Elder County, Utah (Stifel, 1964). They were brought to my attention by E. L. Yochelson, who was studying the fauna of the Phosphoria Formation (Yochelson, 1968 a, b). Two of these unusual fossils were in the original collection. At Yochelson's request Stifel later made an additional collection at the same locality, which yielded 15 more specimens. The 17 examples collected by Stifel are the basis for a new suborder, family, genus, and species.

Acknowledgments.—I thank the following colleagues: E. L. Yochelson for providing the first specimens of this unusual fossil; P. B. Stifel, University of Maryland, for donating this material to the U.S. Geological Survey; J. A. Jeletzky, Geological Survey of Canada, for making available comparative material from the Jurassic of central Europe; and E. L. Yochelson, R. W. Imlay, and J. A. Jeletzky for reviewing this paper.

THE SQUID GLADIUS

The gladius or pen is the internal strengthening member, predominantly calcareous, located in the posterior dorsal part of the body of most squids. This internal shell is subdivided by its structure and fine surface ornamentation into central and lateral fields, commonly separated by hyperbolar zones (embayments in the concentric lines of growth.) At the posterior end of most gladii is a small, spoonlike chamber opening ventrally, known as the conus.

Jeletzky (1966, p. 32-39) has pointed out the analogy of the main part of the squid gladius to the proostracum and of the conus to the phragmocone of belemnites and phragmoteuthids. Hyperbolar zones are also characteristic features of belemnite and phragmoteuthid proostraca.

In some squid gladii the median zone extends forward as a free spikelike or daggerlike rhachis. This feature is particularly characteristic of the suborder Mesoteuthina, representatives of which are found in Jurassic and Cretaceous rocks. In this suborder, the rhachis generally continues to the apex of the conus as a keel on the dorsal side of the gladius.

In some mesoteuthid gladii, particularly those of the Late Jurassic genus *Kelaeno* Muenster, the conus has migrated forward and enlarged so that the gladius consists of rhachis and conus.

It is to the specialized squid gladii of the suborder Mesoteuthina that the Permian fossils under study bear a rather striking resemblance. Close examination, however, demonstrates that this similarity is largely superficial. Several important differences exist which require the erection of a new suborder to contain the Permian teuthids.

NEW SUBORDER OF PERMIAN SQUIDS

The Permian fossils here interpreted as squid gladii are foliate, composed of a roughly arrowhead-shaped posterior part and a forward-extending rhachis. Although some specimens lie flat on the shale interface, others have a gentle transverse curvature; the convex side is interpreted as the dorsal side. A reconstruction depicting how one of these fossils might have fitted into the body of an ancient squid is shown in figure 1.

In well-preserved specimens viewed from the dorsal side, the rhachis is visible only where it extends beyond the posterior part of the gladius. In partly decorticated specimens, however, or in specimens preserving the ventral side, the rhachis can be seen to extend approximately to the posterior tip of the gladius as a gradually narrowing low ridge or keel. The dorsal side is ornamented by straight or slightly curved lirae that radiate from the general area of the posterior tip. No concentric lirae can be positively identified, nor can any structure resembling a conus be distinguished. The possibility

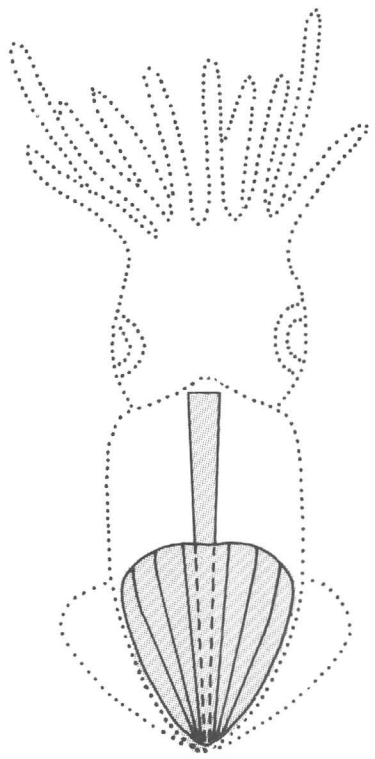

Figure 1.—Restoration of Permian squid gladius (patterned) of *Glochinomorpha*, showing its probable position in body of animal. Drawn approximately three times natural size.

that, as in the genus *Kelaeno*, the entire posterior part might represent the conus seems very unlikely because the radiating lirae converge toward the posterior tip of the gladius. In *Kelaeno* the apex of the conus is elevated and situated nearer the middle of the posterior part.

These Permian gladii resemble those of the suborder Mesoteuthina Naef that have the posterior part foliate and the anterior part extended as a free rhachis, but they differ in lacking identifiable hyperbolar zones and a conus and in having the rhachis posteriorly forming a ridge or keel on the ventral rather than the dorsal side. For these Permian gladii, the new suborder Glochinomorphina is proposed.

JELETZKYA REINTERPRETED AS A BELEMNITE

Recently, the fairly well preserved soft parts of a coleoid, consisting of a decapod tentacular crown, each arm bearing a double row of armhooks, was given the name *Jeletzkya douglassae* Johnson and Richardson (1968). The posterior part of the body of this animal lay buried in a concretion. In order not to risk destroying or injuring the specimen by normal methods of preparation, Johnson and Richardson had it X-rayed. This disclosed an elongate-oval structure terminating in a small cavity or chamber approximately at the point where the posterior part of the animal emerges from the concretion. The buried structure was interpreted by Johnson and Richardson as a squid gladius and the terminal cavity as the conus.

In preparing parts of the coleoid volume (M) of the "Treatise on Invertebrate Paleontology," J. A. Jeletzky and the writer have discussed thoroughly the classification of *Jeletzkya douglassae* within the general scheme of the coleoids. Both of us regard it as a belemnite, rather than a teuthid. All the available information at our disposal indicates that the decapod crown with each tentacle bearing a double row of hooks is restricted to the belemnitids and phragmoteuthids. Arm hooks are unknown in fossil teuthids, although some modern forms possess them. What Johnson and Richardson interpreted as a squid gladius complete with conus, we regard as a belemnitid proostracum with the final chamber of the phragmocone attached.

Jeletzky's investigation of thousands of Mesozoic belemnites from all over the world shows that the separation of the decaying body (including the proostracum and adoral part of the phragmocone) from the rest of the animal is normal in belemnites. The buoyancy of the phragmocone from gases released after death operating against the weight of the guard tended to break off the proostracum and with it commonly a little of the phragmocone. We believe that this is precisely what has happened to the holotype of *Jeletzkya douglassae*.

SYSTEMATIC PALEONTOLOGY

Phylum MOLLUSCA
Class CEPHALOPODA Cuvier
Subclass COLEOIDEA Bather
Order TEUTHIDA Naef, 1916
Suborder GLOCHINOMORPHINA n. subord.
Family GLOCHINOMORPHIDAE n. fam.

Genus GLOCHINOMORPHA n. gen.

[Derivation, Greek: Glochinos = arrow point; morphe = form]

Diagnosis.—Small teuthid having thin gladius, roughly arrowhead shaped in plan; posterior part subtriangular, having nearly smooth polished dorsal and ventral surfaces, split by protruding rhachis which forms longitudinal ridge or keel across ventral surface; dorsal surface gently convex toward anterolateral margins, radially lirate. Ventral surface very slightly concave, ornamented by faint concentric growth lines; no recognizable conus.

Description.—Gladius small, thin, leaflike, having subtriangular posterior part split by longitudinally fibrous rhachis that protrudes forward in stemlike elongation. Posterior part narrowly rounded and bullet shaped posteriorly; sides and front margins gently convex, strongly rounded anterolaterally. Dorsal and ventral surfaces almost smooth; dorsal surface nearly flat medially and posteriorly, gently convex toward lateral margins. Ventral surface very slightly concave to conform with convexity of dorsal side. Linear elevation along rhachis present on ventral side in some specimens, slightly higher anteriorly; rhachis forming central or subcentral longitudinal ridge at summit of elevation, continuing to posterior tip. Protruding part of rhachis gently convex on ventral side

and presumably depressed elliptical in cross section. Rhachis widening gradually from posterior to anterior end.

Ornamentation of dorsal surface consisting of moderately prominent paired radial lirae, normally six in number, that arise near posterior tip and extend forward to anterior margin; lirae straight to slightly sigmoidal; middle pair and next outer pair generally fairly well marked; less distinct third pair usually present near lateral margins; lirae normally divide posterior part of gladius into seven segments, each ornamented by finer indistinct subcontinuous radial lirae, approximately 13 of which occur in space of 1 mm. Linear structure also apparent in partly decorticated areas within gladius. Ornamentation of ventral surface consisting of very indistinct concentric growth lines over lateral fields that roughly parallel their anterior edge.

Type species.—*Glochinomorpha stifeli* n. sp.

Discussion.—So far as can be determined, this little coleoid gladius from the Meade Peak Phosphatic Shale Member of the Phosphoria Formation in northwest Utah is the earliest record of squid remains. It represents the only teuthid known from rocks of Paleozoic age. As discussed above, a decapod coleoid from the Middle Pennsylvanian Mazon Creek Formation of Illinois, *Jeletzkya douglassae* Johnson and Richardson (1968), described as an early squid, is considered by Jeletzky and the writer to be a belemnite.

The positioning of the presumed gladius within the body of the squid as seen from the dorsal side is depicted in figure 1. The dotted outline of the animal in this figure is intended to indicate that the form of the squid is purely conjectural. Nevertheless, the writer was guided somewhat in his assumptions by viewing, through the courtesy of J. A. Jeletzky, a remarkable specimen of a mesoteuthid coleoid in lithographic limestone preserving the outline of the animal with the gladius in place (labeled as *Kelaeno* sp. but differing from typical forms of that genus in the posterior position of the apex of the conus). This specimen is No. 1968 in the collection of the Staatlische Sammlung für Paläontologie und historische Geologie in Munich and came from the Ober Malm Plattenkalke (late Late Jurassic age) at Eichstätt, Blumenberg, Bavaria.

Lack of a recognizable conus in the gladius of *Glochinomorpha* is a puzzling feature and is one of the principal factors prompting its assignment to a new family. Its absence does not seem to be due to poor preservation as some of the gladii have very clear and sharp margins exhibiting no signs of breakage posteriorly.

Possibly the teuthids began with a simple flat foliate gladius of this type, which later gradually evolved a convex conus by partial enrollment of its posterior tip as a means of strengthening this internal apparatus. Such a suggestion, however, would argue against deriving the squid gladius from the phragmoteuthid proostracum and chambered phragmocone, as suggested for the origin of the gladius of the suborder Loligosepiina by Jeletzky (1966, p. 37-41). Rather, it would argue for development of the glochinomorphid gladius as an independent structure serving to strengthen the soft parts of a cephalopod lineage previously without an internal shell. More likely, however, the teuthids were polyphyletic, many of the teuthid suborders representing longstanding independent lineages.

Glochinomorpha n. gen. is closest in appearance to certain genera of the suborder Mesoteuthina which, like this Permian form, developed a rhachis. A photograph of a mesoteuthid in the Teyler Museum (catalog No. 15758), Haarlem, Holland, is shown in figure 2; this specimen exhibits a general configuration similar to that of *Glochinomorpha* except in the further development of concentric ribs that roughly conform to the concentric growth lirae of the Permian genus. The specimen comes from lithographic limestone of Late Jurassic (early Tithonian) age at an unknown locality in Bavaria, Germany. According to Jeletzky (oral commun., 1970), through whose kindness the figure was obtained, this shell probably belongs in a new genus related to *Beloteuthis* and *Palaeololigo* and possibly to *Celaenoteuthis*.

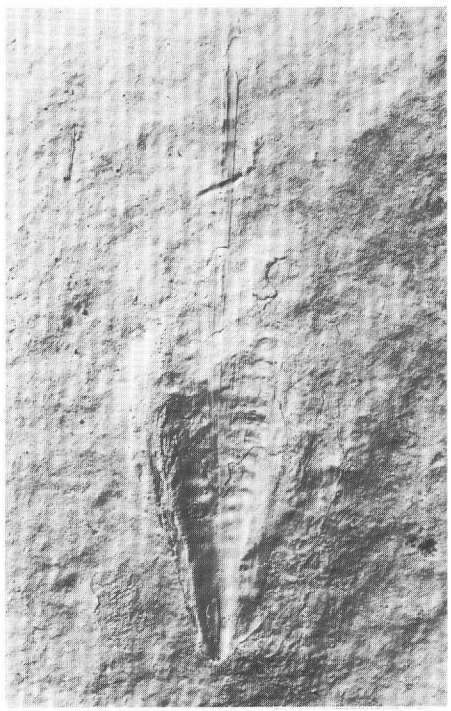

Figure 2.—Mesoteuthid squid gladius of Late Jurassic age from Bavaria, showing analogies to *Glochinomorpha*. × 1½.

Glochinomorpha stifeli n. sp.

Figure 3, a-h

Diagnosis.—Same as for the genus.

Description.—Same as for the genus.

Discussion.—The orientation of this species, by analogy with other squid gladii, is based on the assumption that the slightly convex side is dorsal. The gladius occupies a rearward and dorsal position in the body of the squid; its slightly convex

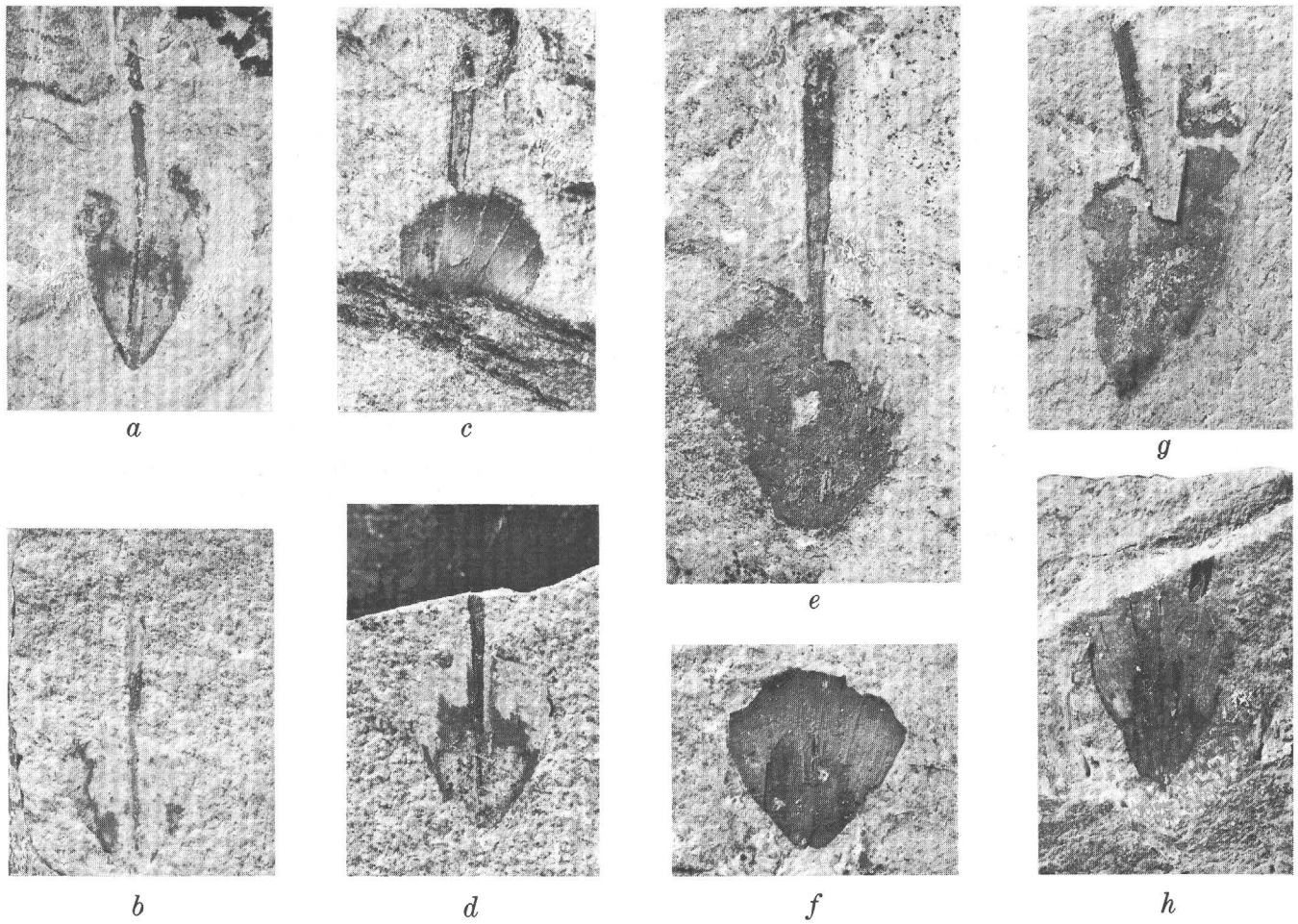

Figure 3.—*Glochinomorpha stifeli* n. sp. *a*, holotype, USNM 170606; *b*, paratype, USNM 170611; *c*, paratype, USNM 170612; *d*, paratype, USNM 170610; *e*, paratype, USNM 170607; *f*, paratype, USNM 170613; *g*, paratype, USNM 170608; *h*, paratype, USNM 170609. *a*, *b*, *d*, and *h* are interpreted as dorsal views, and *c*, *e*, *f*, and *g* as ventral views. All specimens from USGS locality 19020-PC, Terrace Mountains, Box Elder County, Utah. All figures X 4.

side would conform to the rounded surface of the squid (fig. 2).

The rhachis, contrariwise, has its best preserved convex surface on the opposite side in our specimens, continuing on some specimens as a low ventral ridge between the lateral fields. On others it can also be seen clearly in the plane of the lateral fields. From the dorsal side on many partly decorticated specimens the rhachis appears as a groove or depression. On two or three of the specimens the rhachis projects from some part of the anterior margin other than the center. These are interpreted as specimens from which the rhachis has been broken off, as indicated by the presence of sediment between the rhachis and the posterior part of these specimens. The dimensions, in millimeters, of the holotype and five paratypes are tabulated in the next column.

Number	Length	Length of posterior part	Maximum width
USNM 170608.....	[1]13.0	10.8	[2]6+
170607.....	[3]17.5	[3] 9.3	8.2
170606.....	11.1	7.2	5.3
170609.....	[1] 7.8	6.9	5.2
170610.....	[1] 8.4	6.7	5.2
170611.....	[1] 9.6	5.8	4.8

Convexity of posterior part ranges from approximately 1.0 to 1.5 mm; gladius is actually less than 0.5 mm thick, estimated as approximating 0.3 mm.

[1]Part of rhachis missing.
[2]Part of lateral field missing.
[3]Posterior tip missing.

Although the microscope structure of the interior of the gladius is not clearly preserved, it appears linear on a number of the specimens. On all of them the interior is filled with very fine limonitic material that presumably has replaced a predominantly calcareous filling. In some specimens the structure is porous with a slight suggestion of longitudinal alinement, but without any regularity in the size of the pores. The major longitudinal lirae on the dorsal surface can be recognized even where most of the filling of the gladius has been peeled away. Viewed from the ventral side they appear as narrow grooves.

Present in some specimens in which the limonitic filling is very fine and well preserved are short, tiny cracks which, as seen at fairly high magnifications (X 33), are regularly disposed, subparallel, and filled with dark-gray material, presumably calcite. In some areas they are parallel to the fine discontinuous lirae, but in others they cut at a slight angle across the lirae. These filled cracks are regarded as secondary. Their regularity may be controlled by the linear porous structure and their local diagonal elongation by strain accompanying diagenesis.

Types.—Holotype USNM 170606, paratypes USNM 170607-170615 (16 specimens).

Occurrence.—USGS locality 19020-PC. Box Elder County, Utah. Poorly exposed shale section in gully about 1 mile northeast of Green Spring, center W½NE¼ sec. 16, T. 7 N., R. 12 W., on southwest slope of Terrace Mountains. Phosphoria Formation, Meade Peak Phosphatic Shale Member, probably near middle. Collector, Peter B. Stifel.

REFERENCES

Jeletzky, J. A., 1966, Comparative morphology, phylogeny and classification of fossil Coleoidea: Kansas Univ. Paleont. Contr. Mollusca, art. 7, 162 p., 25 pls., 15 text figs.

Johnson, R. G., and Richardson, E. S., 1968, Ten-armed fossil cephalopod from Pennsylvanian of Illinois: Science, v. 159 p. 526-528, 4 figs.

Naef Adolf, 1916, Systematische Uebersicht der mediterranen Cephalopoden: Naples Sta. Zool. Pub., v. 1, p. 11-19.

Stifel, P. B., 1964, Geology of the Terrace and Hogup Mountains, Box Elder County, Utah [abs.]: Dissert. Abs., v. 25, no. 4, p. 2453.

Yochelson, E. L., 1968a, Biostratigraphy of the Phosphoria, Park City, and Shedhorn Formations *with a section on* Fish by D. H. Van Sickle; U.S. Geol. Survey Prof. Paper 313-D, p. 571-660, figs. 157-168, 5 tables.

——1968b, Charts showing distribution and abundance of fossils in the Phosphoria, Park City, and Shedhorn Formations in Wyoming, Idaho, Utah, and Montana: U.S. Geol. Survey open-file report, 8 sheets.

GONIATITES AMERICANUS N. SP., A LATE MERAMEC (MISSISSIPPIAN) INDEX FOSSIL

By MACKENZIE GORDON, JR., Washington, D.C.

Abstract.—*Goniatites americanus* n. sp. is the name proposed for a Late Mississippian ammonoid described and figured by various authors during the past 75 years, but not hitherto recognized as a distinct species. An important zonal fossil, it is found associated with several species of *Girtyoceras, Entogonites, Dimorphoceras,* and *Prolecanites* in an assemblage zone recognizable from northern Alaska to northern Arkansas. The *Goniatites americanus* Zone occurs at or near the top of the Meramec Series and its equivalents and is the lowest of three zones each characterized by different species of *Goniatites.* In terms of the northwest European section, this zone is equivalent to the lower part of the lower *Posidonia* (P_1) Zone of late Visean Age.

Throughout much of the American midcontinent and West and as far north as northern Alaska, the lower part of the stratigraphic interval characterized by ammonoids of the genus *Goniatites* contains an as yet unnamed species of that genus. Alaskan examples of this species were described by the writer (Gordon, 1957, p. 42-45) as "*Goniatites crenistria* Phillips, wide form." Arkansas specimens were later described (Gordon, 1964, p. 187-189) as "*Goniatites* aff. *G. crenistria* Phillips," further study having convinced the writer that these shells, although closely related to *G. crenistria,* should not be included in that species. It is now proposed that they be referred to a new species, *Goniatites americanus.* The description and illustrations of this new taxon are based upon specimens from the Chainman Shale of west-central Utah.

STRATIGRAPHIC SETTING AT THE TYPE LOCALITY

The beds containing *Goniatites americanus* and associated ammonoids are well exposed on the lower part of the northeast slope of Granite Mountain, Juab County, Utah. C. A. Repenning and the writer collected fossils there from a section they measured in the W½ sec. 7 (incompletely surveyed), T. 14 S., R. 17 W., in May 1957 during a study of the upper Paleozoic stratigraphy of the Confusion Range, Utah, and adjacent areas (Gordon and others, 1957). The part of the measured section containing the top of the Pilot Shale and the *Goniatites*-bearing beds of the Chainman Shale is shown in figure 1.

The Joana Limestone of Early Mississippian age, which normally intervenes between the Pilot Shale and the overlying

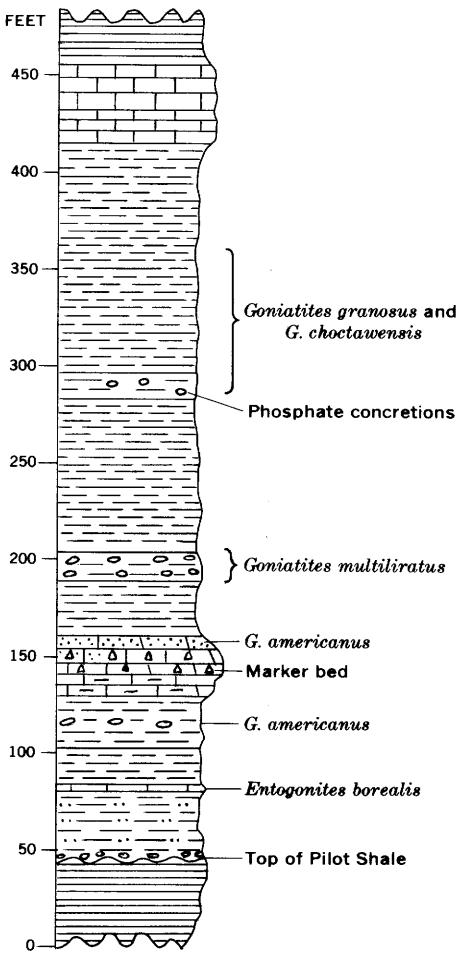

Figure 1.—Columnar section of the lower part of the Chainman Shale in the SE¼NW¼ and NE¼SW¼ sec. 7 (partly surveyed), T. 14 S., R. 17 W.,, on the northeast slope of Granite Mountain, Utah, showing the succession of goniatite-bearing beds.

Chainman Shale, is missing at Granite Mountain; the Chainman rests unconformably on the Pilot. Several hundred feet of silty shale with worm tracks, normally present between the top of the Joana Limestone and the *Goniatites*-bearing beds in Chainman sections to the south, also is absent. The lowest bed

of the Chainman Shale is a 1½-foot conglomeratic and sandy limestone containing numerous horn corals and crinoid columnals.

The goniatite-bearing beds begin with a 3-foot limestone containing the brachiopod *Rhipidomella* sp. and the cephalopod *Entogonites borealis* Gordon, 29 feet above the base of the Chainman. From the bottom of this limestone bed the next 250 feet stratigraphically is dominated by ammonoids of the *Goniatites americanus*, *G. multiliratus*, and *G. granosus* Zones, in ascending order (Gordon, 1970). *Entogonites borealis* is associated with *Goniatites americanus* n. sp., *Girtyoceras* n. sp., and *Dimorphoceras* n. sp. in a 2-foot zone of large calcareous concretions 42-44 feet above the base of the formation. (The primary types of *G. americanus* are from this bed.) *E. borealis* also occurs with *Goniatites americanus* n. sp., *Girtyoceras* n. sp., and *Prolecanites* sp. in a 5-foot bed of sandy limestone 78-83 feet above the base, immediately overlying a 12½-foot interval of gray-black chert and fine-grained limestone, known locally to geologists as the marker bed. Granite Mountain is the only place where beds carrying the *Goniatites americanus* fauna underlie and include the marker bed. Farther south in Utah, in the Confusion Range and Burbank Hills, the same marker bed is only 4 or 5 feet thick and invariably is found a few feet below the base of the *Goniatites americanus* Zone. The maximum thickness of this zone in the Granite Mountain area is approximately 55 feet.

About 30 feet of relatively barren dark-gray claystone intervenes between the top of the *G. americanus* Zone and 14 feet of similar claystone containing *Goniatites multiliratus* Gordon in layers of large concretions. Similarly, approximately 72 feet of relatively barren claystone is present between the top of the *G. multiliratus* Zone and the base of the *G. granosus* Zone. The *G. granosus* assemblage occurs typically in soft olive-colored shale with small scattered phosphatic concretions. The ammonoids are somewhat sideritic and weather out of the shale. Included in this assemblage are *Goniatites granosus* Portlock, *G. choctawensis* Shumard, and *Neoglyphioceras cloudi utahense* (Miller, Youngquist, and Neilsen). The fauna of this zone in the area near Cowboy Pass in the Confusion Range has been described by Miller, Youngquist, and Neilsen (1952). The fossils of the *Goniatites granosus* Zone become less abundant upward and die out approximately 80 feet stratigraphically above their first appearance in the Granite Mountain area.

In terms of the northwest European section, the *Goniatites americanus* Zone and *G. multiliratus* Zone are equivalent to the lower *Posidonia* (P_1) Zone. The *Goniatites granosus* Zone is equivalent to the upper *Posidonia* (P_2) Zone of the European Carboniferous section (Gordon, 1970).

DISTRIBUTION

The localities from which *Goniatites americanus* n. sp. is known are shown in figure 2. From northwest to southeast, they are located on the map as follows:

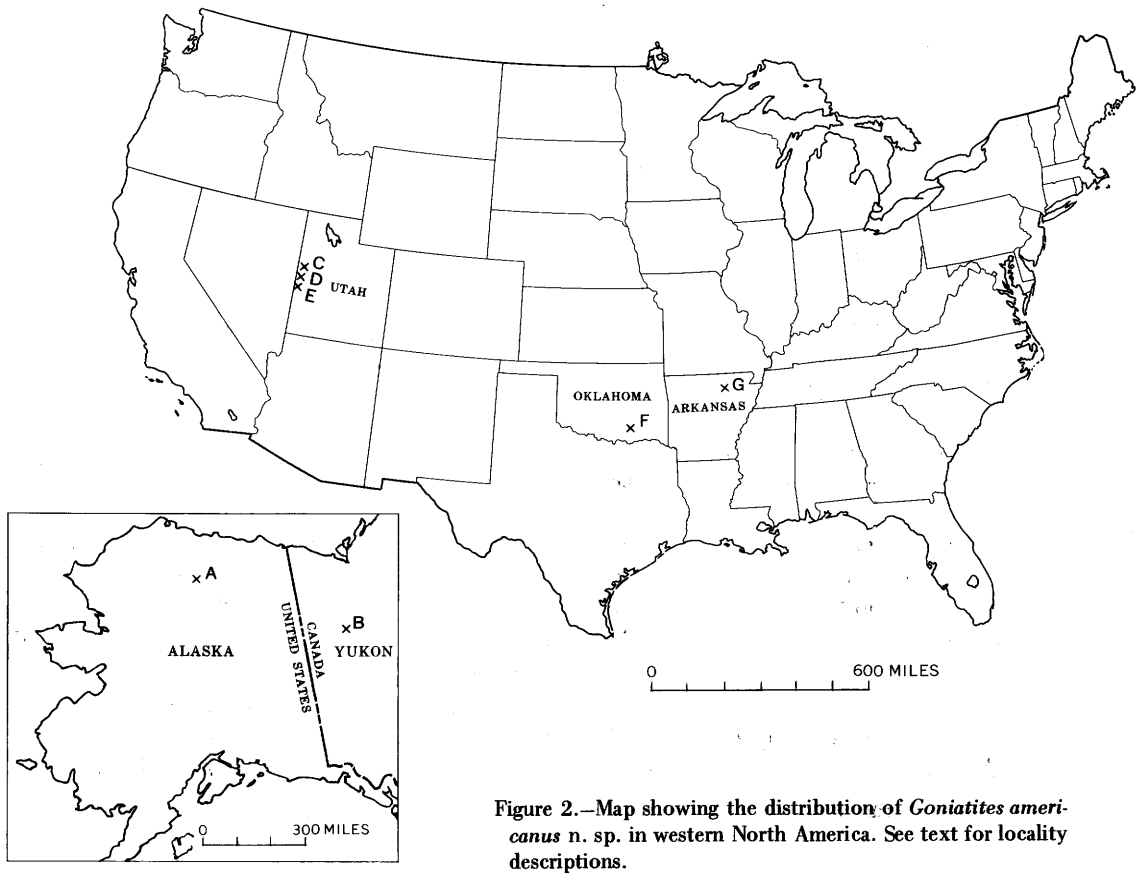

Figure 2.—Map showing the distribution of *Goniatites americanus* n. sp. in western North America. See text for locality descriptions.

A. Kiruktagiak River, north slope of Brooks Range, Alaska. Reported as *Goniatites crenistria* Phillips, wide form, at two localities about 3½ miles apart in the black chert and limestone member of the Alapah Limestone (Gordon, 1957, p. 7, 8, 42–45).

B. Upper Peel River, Yukon Territory, northwest Canada. Reported as *Goniatites crenistria* Phillips from dark silty limestone on the north bank of Peel River about 8 miles downstream from the mouth of Hart River (Sellers and Furnish, 1960, p. 1124–1126).

C. Granite Mountain, Juab County, Utah. Material described herein.

D. Confusion Range, Millard County, Utah. This species occurs in the lowest ammonoid zone in the Chainman Shale at several localities. The fauna from these localities is being studied.

E. Burbank Hills, Millard County, Utah. A southward extension of the lower part of the Chainman Shale contains this species at several localities.

F. Goose Creek, Pontotoc County, Okla. Specimens in the U.S. National Museum collection from the NE¼ sec. 26, T. 1 N., R. 7 E., show the typical ornamentation of this species. There are from the Caney Shale, 85 feet above the top of the Woodford Chert.

G. Moorefield, Independence County, Ark. Specimens from the hills just south of Moorefield have been reported by several authors. These fossils were discussed by the writer as *Goniatites* aff. *G. crenistria* Phillips. The stratigraphic position of these shells is roughly 30–40 feet below the top of the Moorefield Formation (Gordon, 1964, p. 15, 16, 187–189).

SYSTEMATIC PALEONTOLOGY

Phylum MOLLUSCA
Class CEPHALOPODA
Order AMMONOIDEA Zittel, 1884
Suborder GONIATITINA Hyatt, 1884
Superfamily GONIATITACEA de Haan, 1825
Family GONIATITIDAE de Haan, 1825
Subfamily GONIATITINAE de Haan, 1825
Genus GONIATITES de Haan, 1825

Goniatites americanus n. sp.

Figure 3, *a-p*

Glyphioceras incisum Hyatt. Smith, 1897 [part], p. 111–121, pl. 13, figs. 1, 2, 6–12; pl. 14, figs. 1–9; pl. 15, figs. 1–11 [not pl. 13, figs. 3–5].

Goniatites crenistria Phillips. Smith, 1903 [part], p. 68–76, pl. 14, figs. 1, 2, 7–12; pl. 15, figs. 1–9; pl. 16, figs. 1*a-j*; pl. 26, figs. 1–4 [not pl. 10, figs. 12–16; pl. 14, figs. 4–6; pl. 26, fig. 5]; Grabau and Shimer, 1910, p. 141, fig. 1393*f-h*; Girty, 1911, p. 99–101, pl. 15, figs. 8, 9; Gordon, 1957 [part], p. 42–45, pl. 5, figs. 1–8, 12–16 [not figs. 9–11], text fig. 17*A-D*; Sellers and Furnish, 1960, p. 1124–1126, pl. 141, figs. 1–5, text figs. 2*A, B*.

Goniatites choctawensis Shumard. Girty, 1911 [part], p. 97–99, pl. 15, figs. 7, 7*a* [not figs. 1–6].

Goniatites aff. *G. crenistria* Phillips. Gordon, 1964 [1965], p. 187–189, pl. 18, figs. 1–6, text figs. 44*A, B*, 46*A-C*.

Diagnosis.—*Goniatites* having globose shell in youth becoming subglobose at maturity, strongly involute; flanks gently rounded. Surface sculpture crenistriate; longitudinal lirae roughly 200 in number, on mature shells nearly reaching strength of transverse elements, giving finely cancellate appearance. Suture having mature ventral lobe indented to one-third its length, or slightly more, by median saddle.

Description.—Shell having well-rounded venter merging with gently rounded flanks that slope outward slightly toward umbilicus; umbilical shoulder strongly rounded; umbilical wall a little less rounded; umbilicus narrow, its diameter equaling approximately one-eighth to one-tenth diameter of shell.

Predominant surface sculpture on young shells consisting of fine transverse striae separated by wider interspaces. At diameters of 10–12 mm, striae beginning to appear crenulate and, with further growth, spaces between striae taking on aspect of flat transverse lamellae having crenulate adoral margins. Transverse growth lamellae shallowly sinuous, forming broad ventral and lateral sinuses alternating with ventrad bows on inner flanks and ventrolateral zones. Longitudinal lirae beginning to be visible at diameters between 16 and 18 mm, suppressed and flat on top with subequal interspaces, strongest in area of umbilical shoulder and adjacent inner flanks where minutely wavy; position of lirae coinciding with adoral points of crenulations; approximately 190 longitudinal lirae present between umbilici on holotype. On mature shells of 25 mm and more in diameter, longitudinal lirae becoming stronger until nearly equaling prominence of crenulate margins of transverse lamellae. Broad, shallow internal varices present within shell, three occurring on final volution of holotype; also locally on mature part of shell, internal molds show faint closely spaced transverse constrictions probably corresponding to transverse lamellae of outer surface of shell.

Mature external suture (fig. 3,*e*) consisting of ventral lobe of moderate width having diverging sides generally somewhat bulging in middle and constricted below and above bulge, terminating adapically in a pair of narrow acuminate prongs; median saddle occupying about one-third of length of ventral lobe. First lateral saddle narrowly rounded adorally; first lateral lobe slightly asymmetrical, having sigmoidal sides and a narrow acuminate termination; second lateral saddle curving broadly and asymmetrically across umbilical shoulder; umbilical lobe short, pointed, located near shoulder. Internal suture not seen.

Discussion.—This description is based on 16 specimens from a single collection. Measurements of six of them, given in table 1, show the range of variation in shape of this species. A rotund paratype (USNM 170620) shown in figure 3, *i-k, p*, retains the wide proportions common in young shells to a considerably larger size than normal in our specimens. Nevertheless, its surface sculpture (it has approximately 200 longitudinal lirae crossing the crenulate transverse lamellae)

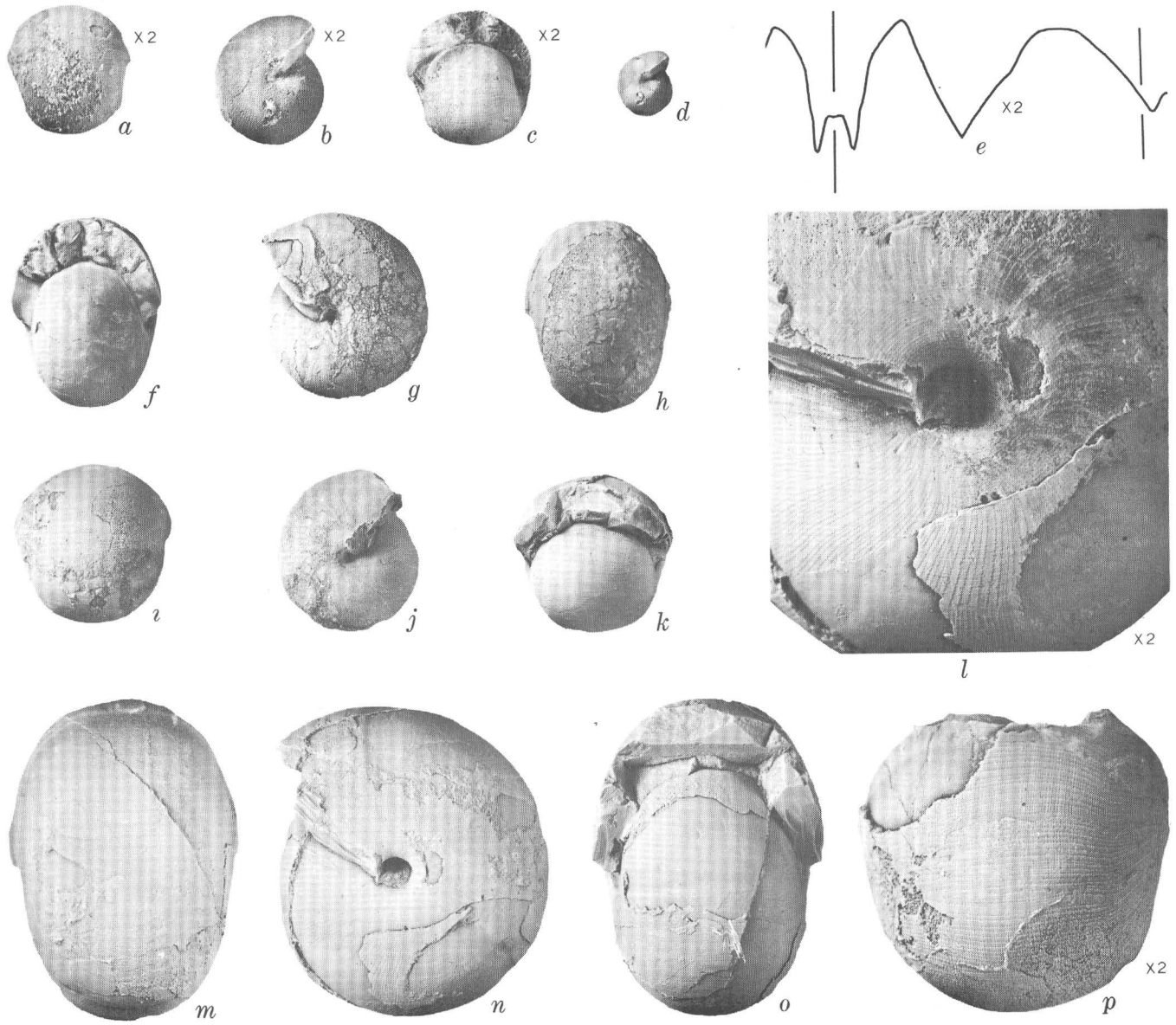

Figure 3.—*Goniatites americanus* n. sp. *a-d*, enlarged back, side, and front views, X 2, and side view of small paratype, USNM 170621; *e*, external suture of mature shell from another paratype, USNM 170617; *f-h*, front, side, and back views of typical paratype, USNM 170618; *i-k*, *p*, back, side, and front views and enlarged ventral view of rotund paratype, USNM 170620; *l-o*, enlarged side view, X 2, and back, side, and front views of holotype, USNM 170616. Unless otherwise indicated, views are natural size. All specimens from USGS locality 17010-PC, on northeast slope of Granite Mountain, Juab County, Utah.

indicates that it belongs in the same species as the typical narrower forms. Possibly this globose specimen is a sexual dimorph, but if so, its relative scarcity requires explanation. The largest specimen of the type lot, not included in the table of measurements because it is incomplete, is estimated to be slightly in excess of 70 mm in diameter, the entire final volution occupied by living chamber.

Although one of the distinguishing characters of this species is its relatively shallow median saddle in the ventral lobe, this character must be compared with that of other species at the same conch diameter because the median saddle of the ventral lobe deepens with growth. In specimens from 8 to 15 mm in diameter, the length of the median saddle is about one-fifth to one-fourth the length of the ventral lobe; at a 25-mm diameter the median saddle slightly exceeds one-fourth the length of the ventral lobe; and at a 34-mm diameter the median saddle has reached one-third the length of the ventral lobe. The writer has recorded (Gordon, 1957, p. 43, text fig. 17*A*) a specimen from northern Alaska in which, at a conch diameter of 41 mm, the median saddle is nearly two-fifths the length of the ventral lobe.

Goniatites americanus is rather easily distinguished from other species of the genus within the conterminous United States by its crenistriate growth lamellae, not present in

Table 1.—*Dimensions (in millimeters) and proportions of* Goniatites americanus *from Granite Mountain, Juab County, Utah*

USNM No.	170616	170617	170618	170620	170619	170621
Diameter of shell (D)	49.5	37.3	29.8	24.8	23.2	10.2
Height of last whorl (H)	26.0	18.5	15.1	12.0	13.0	5.5
Width of last whorl (W)	36.0	28.5	23.0	24.3	18.4	9.9
Diameter of umbilicus (U)	5.5	4.0	3.5	3.2	3.0	1.8
U/D	.11	.11	.12	.13	.13	.18
W/D	.73	.76	.77	.98	.79	.97
W/H	1.38	1.54	1.52	2.03	1.41	1.80

mature *Goniatites choctawensis* Shumard, *G. granosus* Portlock, *G. kentuckiensis* Miller, or *G. multiliratus* Gordon. It also differs from these slightly younger forms in having the ventral lobe of the suture a little less deeply indented by the median saddle.

Goniatites crenistria Phillips, which besides occurring at numerous European localities has been recorded in the Etivluk Valley, Alaska (Gordon, 1957, p. 42–45), is a narrower species that likewise develops crenistriate sculpture, but not the finely cancellate aspect of mature *G. americanus.*

Types.—Holotype USNM 170616, paratypes USNM 170617–170622 (15 specimens).

Occurrence.—Chainman Shale, lower part, USGS locality 17010–PC, on slopes of hill capped by marker ledge in the SE¼NW¼ sec. 7 (partly surveyed), T. 14 S., R. 17 W., on northeast slope of Granite Mountain, Juab County, Utah.

REFERENCES

Girty, G. H., 1911, The fauna of the Moorefield Shale of Arkansas: U.S. Geol. Survey Bull. 439, 148 p., 15 pls.

Gordon, Mackenzie, Jr., 1957, Mississippian cephalopods of northern and eastern Alaska: U.S. Geol. Survey Prof. Paper 283, 61 p., 6 pls., 26 text figs.

——1964, Carboniferous cephalopods of Arkansas: U.S. Geol. Survey Prof. Paper 460, 322 p., 32 pls., 96 text figs. 11 tables [1965].

——1970, Carboniferous ammonoid zones of the south-central and western United States: Congrès Internat. Stratigraphie Géologie Carbonifère, 6th, Sheffield, 1967, Compte rendu, v. 2, p. 817–826, 2 text figs.

Gordon, Mackenzie, Jr., Hose, R. K., and Repenning, C. A., 1957, Goniatites zones in the Chainman Shale equivalents (Mississippian), western Utah [abs.]: Geol. Soc. America Bull., v. 68, no. 12, pt. 2, p. 1737.

Grabau, A. W., and Shimer, H. W., 1910, Cephalopoda *in* North American index fossils; invertebrates; v. 2: New York, A. G. Seiler, p. 16–233, text figs. 1230–1516.

Haan, Guillielmus de, 1825, Monographiae ammoniteorum et goniatiteorum: Leiden, 168 p.

Hyatt, Alpheus, 1883-84 Genera of fossil cephalopods: Boston Soc. Nat. History Proc., v. 22, p. 253–338. (p. 253–272, 1883; p. 273–338, 1884).

Miller, A. K., Youngquist, Walter, and Nielsen, M. L., 1952, Mississippian cephalopods from western Utah: Jour. Paleontology, v. 26, no. 2, p 148–161, pls. 25, 26, 5 text figs.

Sellers, D. H. A., and Furnish, W. M., 1960, Mississippian ammonoids from northwestern Canada: Jour. Paleontology, v. 34, no. 6, p. 1124–1128, pl. 141, 3 text figs.

Smith, J. P., 1897, The development of *Glyphioceras* and the phylogeny of the glyphioceratidea: California Acad. Sci. Proc., ser. 3, Geology, v. 1, p. 105–128, pls. 13–15. Reprinted as Stanford Univ., Hopkins Seaside Lab., Contr. Biology, no. 13, same pagination and pls.

——1903, The Carboniferous ammonoids of America: U.S. Geol. Survey Mon. 42, 211 p., 29 pls.

Zittel, K. A. von, 1884, Handbuch der Palaeontologie: sect. 1, v. 2, 893 p., 1109 figs. (cephalopods, p. 329–522).

EOCENE (REFUGIAN) NANNOPLANKTON IN THE CHURCH CREEK FORMATION NEAR MONTEREY, CENTRAL CALIFORNIA

By EARL E. BRABB[1], DAVID BUKRY[2], and RICHARD L. PIERCE[1],
[1]Menlo Park, Calif., [2]La Jolla, Calif.

Abstract.—Nannoplankton from both the lower and upper parts of the Refugian Stage as represented in the Church Creek Formation near Monterey, Calif., are correlative with the youngest Eocene *Discoaster barbadiensis* zone. The Refugian Stage of the Pacific Coast Tertiary standard is therefore older than previously reported. Taxa reported for the first time in California strata include: *Chiasmolithus oamaruensis* (Deflandre), *Dictyococcites bisectus* (Hay, Mohler, and Wade), *Isthmolithus recurvus* (Deflandre), *Reticulofenestra umbilica* (Levin), and *Stradnerius dictyodus* (Deflandre) of Haq.

Several workers have attempted to correlate rocks of Tertiary age in California with those of standard sections in Europe (for example, see Berggren, 1969), but few had data for the Refugian Stage of Schenck and Kleinpell (1936). Irreconcilable differences of opinion about the correlation of this stage led Weaver and others (1944) to adopt the very broad series designation "Eo-Oligocene" as the West Coast standard for the lower (*Uvigerina cocoaensis*) zone and the term Oligocene Series for what was then an upper, unnamed zone of the Refugian. Kleinpell and Weaver (1963, fig. 2) considered the lower zone of the Refugian to be Eocene and the upper zone of the Refugian to be Oligocene. The practice of many California oil companies, however, has been to consider both zones of the Refugian Stage as synonymous with the Oligocene Series (see, for example, standard column in International Oil Scouts Association, 1968, pt. 1, p. 34).

Waters (1963) reported abundant benthonic and planktonic Foraminifera from Refugian strata in the Church Creek Formation about 25 miles southeast of Monterey (fig. 1) at its type locality, and we re-collected from Waters' measured sections in order to determine whether calcareous nannoplankton are associated with the Foraminifera. Fortunately, the rocks contain a fair nannoplankton assemblage that permits tentative correlation with Eocene sections in other areas of the world.

We gratefully acknowledge the assistance of Andrew L. Tarshis, University of California, Santa Cruz, who prepared some of the slides of our samples and determined that they contain nannoplankton.

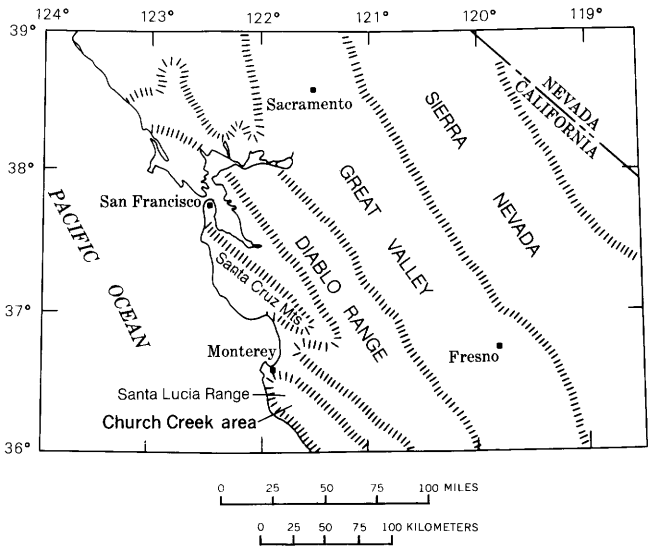

Figure 1.—Index map of central California, showing location of Church Creek area.

The name Church Creek beds was used informally by Reiche (1937, p. 144–146, map) for all Eocene and Oligocene sedimentary rocks in the Lucia quadrangle that rest depositionally on crystalline basement rocks and are truncated at the top by the Church Creek fault. Fiedler (1944) mapped the extension of these same sedimentary rocks in the adjoining Jamesburg quadrangle as the Vaqueros-Temblor Sandstone of Miocene age. Dickinson (1965, p. 36–39) subdivided the so-called Vaqueros-Temblor sequence in the Jamesburg and Lucia quadrangles into five formations of Paleocene, Eocene, and Oligocene age, and he restricted the name Church Creek to the youngest of these five. Dickinson's definition of the Church Creek Formation is herein adopted.

The samples collected are from the type locality (fig. 2) for the Church Creek Formation as used by Dickinson (1965), who described the basic geologic framework for the Church Creek area; section A-2 approximates his type section. The samples are tied to stratigraphic columns (fig. 3) measured by Waters (1963). All are from massive mudstone.

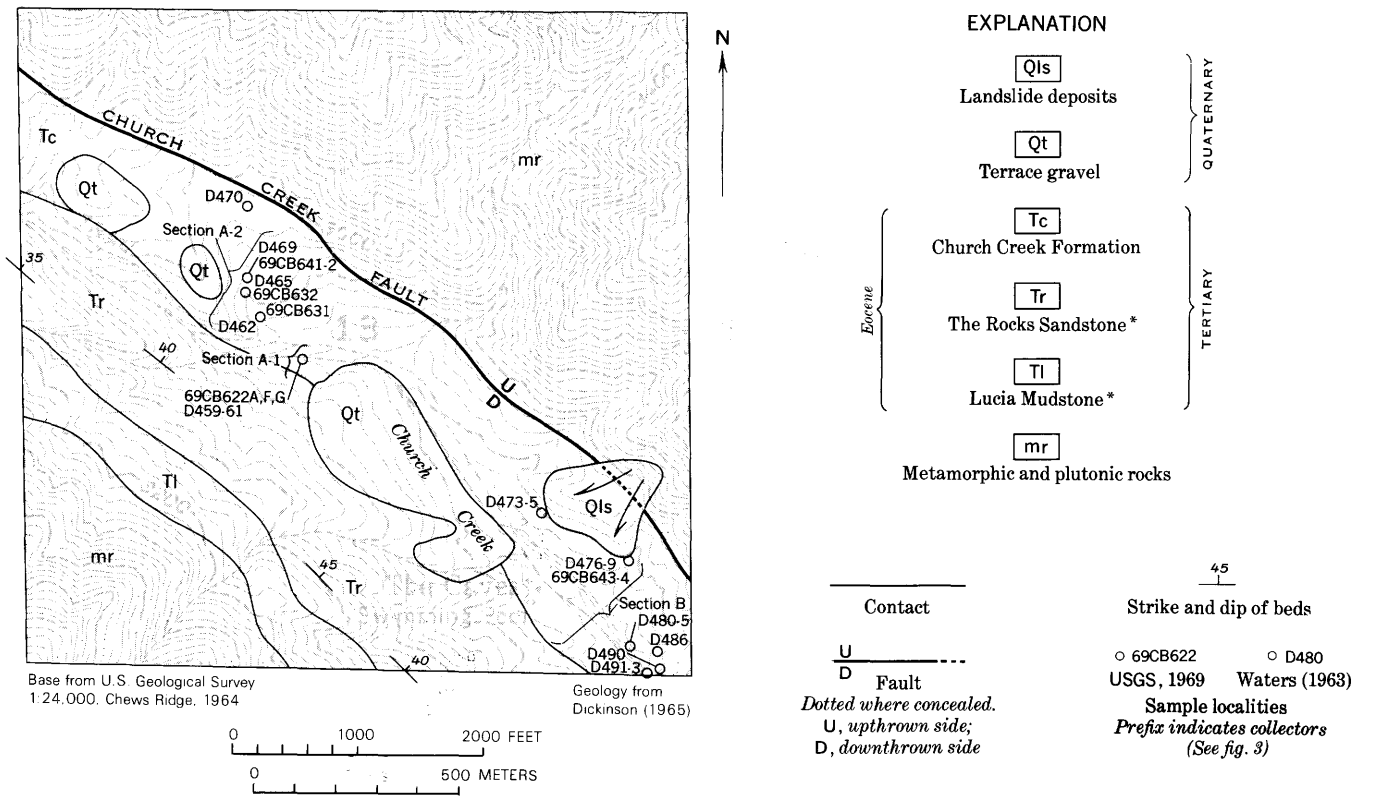

Figure 2.—Geological map of sec. 13, T. 19 S., R. 3 E., Church Creek area, California, showing location of fossil collections and measured sections of Waters (1963). *As used by Dickinson (1965).

The locations of Waters' samples on figures 2 and 3 are approximate because of difficulty in transferring the localities from a map at scale 1:1,200 with little cultural data. There is also some doubt about the relative stratigraphic position of samples he projected into the section at considerable distance from each other, such as samples D473-5 and D476-9 in section B. These difficulties are minor, however, and do not affect the basic conclusions of this report.

The biostratigraphic framework, based on benthonic foraminifers, is also from Waters (1963). He correlates the stratigraphically lowest faunas with the *Uvigerina cocoaensis* zone (lower Refugian) of Cushman and Simonson (1944), mainly on the abundance of *U. cocoaensis* and the absence of species characteristic of the upper Refugian. His younger faunas contain rare specimens of *Uvigerina vicksburgensis, U. gallowayi,* and *Cassidulina galvinensis* and abundant specimens of *Eponides kleinpelli*; he correlates these with the *Uvigerina vicksburgensis* zone (upper Refugian) of Kleinpell and Weaver (1963, p. 33). We were able to confirm the Refugian age on the basis of the joint occurrence of *Plectofrondicularia packardi packardi* and *Uvigerina cocoaensis* in samples 69CB622A, 69CB622F, 69CB631, and 69CB632, but we, like Waters, could not find any faunal assemblages that are definitely restricted to the lower Refugian *Uvigerina cocoaensis* zone.

Samples from section A-2 (fig. 3) are geographically close to, or at, Dickinson's samples SO (Standard Oil Co. of California) 7414, 7416, 7475, and 7470, which he considers to be of Refugian age (Dickinson, 1965, p. 38 and 43). Thus, all ages based on benthonic foraminifers are in agreement.

Nannoplankton from our samples are listed in table 1. The assemblage lacks many shallow-water indicator nannoplankton such as braarudosphaerids and rhabdolithids, which are common in coeval neritic deposits of the Gulf coast. Deposition at outer-shelf or slope depths is indicated. Some reworked material from early and middle Eocene rocks is present, but the overall assemblage correlates with that from the late Eocene Yazoo Clay of the Jackson Group. Taxa reported for the first time in California strata include: *Chiasmolithus oamaruensis, Dictyococcites bisectus, Isthmolithus recurvus, Reticulofenestra umbilica,* and *Stradnerius dictyodus* of Haq. These species are present in strata of late Eocene age from Germany (Haq, 1968), New Zealand (Stradner and Edwards, 1968), and Alabama (Levin and Joerger, 1967). The sparse occurrence of *Discoaster barbadiensis, D. tani tani* and *D. saipanensis* in the Church Creek assemblage confirms the late Eocene age of the assemblage and allows correlation with the youngest Eocene nannoplankton zone—*Discoaster barbadiensis* zone (see Bukry and Bramlette, 1970).

A late Eocene age for the upper part of the Refugian Stage near its type locality in southern California was also proposed by Lipps (1967, p. 996) on the basis of a few species of planktonic foraminifers. Lipps correlated the species with those from the upper Eocene *Globigerapsis semiinvoluta* zone

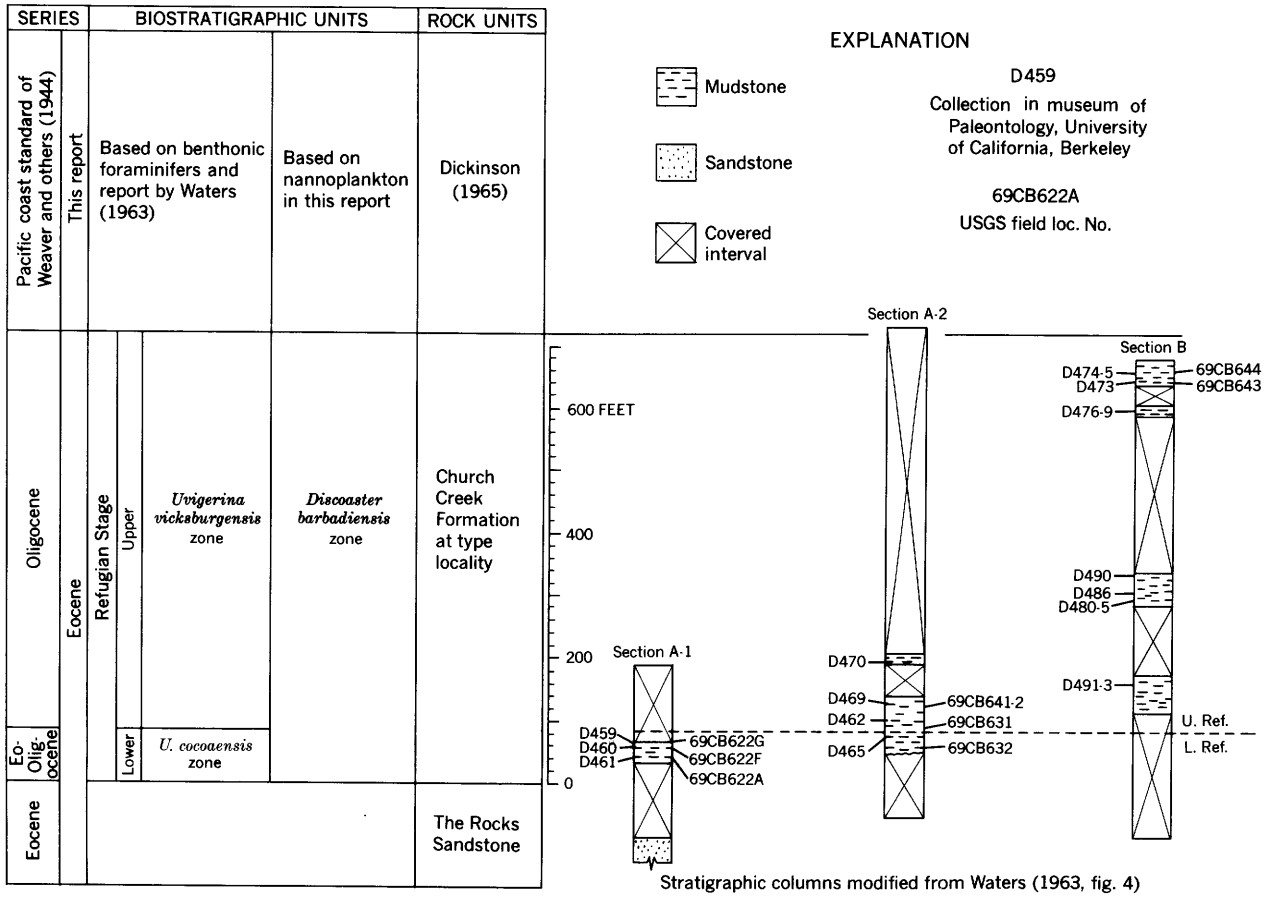

Figure 3.—Stratigraphic framework for the Church Creek area, California. Collections in Museum of Paleontology, University of California, Berkeley, collected by Waters (1963); other collections by Brabb and Pierce, 1969.

as defined by Bolli (1957) in Trinidad. The late Eocene age for the Refugian Stage based on nannoplankton is therefore in agreement with the age based on planktonic foraminifers.

REFERENCES

Berggren, W. A., 1969, Cenozoic chronostratigraphy, planktonic foraminiferal zonation and the radiometric time scale: Nature, v. 224, p. 1072–1075.

Bolli, H. M., 1957, Planktonic Foraminifera from the Eocene Navet and San Fernando Formations of Trinidad: U.S. Natl. Mus. Bull. 215, p. 155–172.

Bukry, David, and Bramlette, M. N., 1970, Coccolith age determinations, *in* Initial reports of the Deep Sea Drilling Project—v. 3, Leg 3 of cruises of *Glomar Challenger*, Dakar, Senegal, to Rio de Janeiro, Brazil, Dec. 1968 to Jan. 1969: Washington, D.C., U.S. Govt. Printing Office, p. 589–611, illus., tables.

Cushman, J. A., and Simonson, R. R., 1944, Foraminifera from the Tumey Formation, Fresno County, California: Jour. Paleontology, v. 18, p. 186–203.

Dickinson, W. R., 1965, Tertiary stratigraphy of the Church Creek area, Monterey County, California, *in* Short contributions to California geology: California Div. Mines and Geology Spec. Rept. 86, p. 25–44.

Fiedler, W. M., 1944, Geology of the Jamesburg quadrangle, Monterey County, California: California Jour. Mines and Geology, v. 40, no. 2, p. 177–250.

Haq, U. Z. B., 1968, Studies on upper Eocene calcareous nannoplankton from NW Germany: Stockholm Contr. Geology, v. 18, no. 2, p. 13–74.

International Oil Scouts Association, 1968, International oil and gas development: v. 38, pt. 1., 544 p.

Kleinpell, R. M., and Weaver, D. W., 1963, Oligocene biostratigraphy of the Santa Barbara embayment, California: California Univ. Pubs. Geol. Sci., v. 43, 250 p.

Levin, H. L., and Joerger, A. P., 1967, Calcareous nannoplankton from the Tertiary of Alabama: Micropaleontology, v. 13, p. 163–182.

Lipps, J. H., 1967, Planktonic Foraminifera, intercontinental correlation and age of California mid-Cenozoic microfaunal stages: Jour. Paleontology, v. 41, p. 994–999.

Reiche, Parry, 1937, Geology of the Lucia quadrangle, California: California Univ. Pubs. Geol. Sci., v. 24, p. 115–168.

Schenck, H. G., and Kleinpell, R. M., 1936, Refugian stage of Pacific coast Tertiary: Am. Assoc. Petroleum Geologists Bull., v. 20, no. 2, p. 215–225.

Stradner, Herbert and Edwards, A. R., 1968, Electron microscopic studies on upper Eocene coccoliths from the Oamaru Diatomite, New Zealand: Austria Geol. Bundesanst. Jahrb., Sonderb. no. 13, p. 1–66.

Waters, J. N., 1963, Oligocene Foraminifera from Church Creek, Santa Lucia Mountains, California: California Univ. (Berkeley), M.A. thesis, 102 p.

Weaver, C. E., and others, 1944, Correlation of the marine Cenozoic formations of western North America: Geol. Soc. America Bull., v. 55, no. 5, p. 569–598.

Table 1.—*Distribution of calcareous nannoplankton from the Church Creek Formation*

	USGS field loc. No.						
	69CB–622A	69CB–622F	69CB–622G	69CB–631	69CB–632	69CB–643	69CB–644
Chiasmolithus oamaruensis (Deflandre)	X	...	X	...	...	...	...
Coccolithus eopelagicus (Bramlette and Riedel)	X	X	...	X	X	...	X
C. fenestratus (Deflandre)	X	...	...	X	X	...	X
Cyclococcolithina formosa (Kamptner)	X	...	...	X	...	X	X
C. neogammation (Bramlette and Wilcoxon)	X	X	...	X	X	...	X
Dictyococcites bisectus (Hay, Mohler, and Wade)	X	X	X	X	X	X	X
Discoaster barbadiensis Tan	...	...	...	...	X	X	...
D. deflandrei Bramlette and Riedel	X	X	X	X	...	X	...
D. saipanensis Bramlette and Riedel	...	X	...	...	...	...	...
D. tani nodifer Bramlette and Riedel	...	X	...	...	...	X	...
D. tani tani Bramlette and Riedel	X	...	...	X	...	X	...
Discolithina sp. cf. *D. confossa* (Hay, Mohler, and Wade)	X	...	...	X	...	...	...
Helicopontosphaera compacta (Bramlette and Wilcoxon)	X	...	...	...	...	...	...
Isthmolithus recurvus Deflandre	X	X	X	X	X	X	X
Micrantholithus sp. cf. *M. crenulatus* (Bramlette and Sullivan)	...	...	...	...	...	X	...
Pontosphaera vadosa Hay, Mohler, and Wade	X	X	X	X	X	X	X
Reticulofenestra umbilica (Levin)	X	X	X	X	X	X	X
Sphenolithus predistentus Bramlette and Wilcoxon	X	...	...	...	...	...	...
Stradnerius dictyodus (Deflandre) of Haq	X	X	X	X	X	X	X
Zygrhablithus bijugatus (Deflandre)	X	X	...	X	...	...	...
Reworked taxa:							
Chiphragmalithus quadratus Bramlette and Sullivan	...	...	...	...	...	X	...
Discoaster lodoensis Bramlette and Riedel	...	X	...	X	...	X	X
Marthasterites tribrachiatus Bramlette and Riedel	...	...	...	...	...	...	X
Zygolithus dubius Deflandre	...	X	...	...	...	...	...

AN OVULIFEROUS CALLIPTEROID PLANT FROM THE HERMIT SHALE (LOWER PERMIAN) OF THE GRAND CANYON, ARIZONA

By SERGIUS H. MAMAY and ARTHUR D. WATT,
Washington, D.C.

Abstract.—Part of a penultimate division of a seed-bearing pteridosperm frond was found as an impression in the Hermit Shale (Lower Permian) of the Grand Canyon, Ariz. Each of its 20-odd pinnules is terminated by the impression of an approximately oval seed. The frond resembles both *Callipteris* and *Supaia*, but a definite generic identification cannot be made. This fossil is the first seed-bearing pteridosperm found in the Hermit Shale, and one of very few known in the Paleozoic of North America. The terminal seed position is interpreted as a primitive stage in pteridosperm morphology; along with the apparently anomalous high stratigraphic occurrence, it suggests that the specimen represents a conservative pteridosperm lineage in a phyletically complex alliance.

Paleobotanical investigations of the Permian have disclosed some noteworthy stages in the development of the pteridospermous seed habit; notable among these studies is Halle's (1929) work on fertile material from China. Specimens demonstrating the original organic connection of seeds or seedlike bodies to foliar organs are extremely rare, however, and the specimen described here is significant from that standpoint.

C. D. White's (1929) description of the flora of the Hermit Shale (Lower Permian) of the Grand Canyon, Ariz., remains the most comprehensive item of paleobotanical literature on the Permian in North America. The flora contained 32 named species of plants; most of those were presumed to be pteridosperms, although no convincing evidence of their fruiting habits was produced. A significant element among the supposed pteridosperms was the new genus *Supaia*, with nine named species. One of the specimens of *Supaia* illustrated by White (1929, pl. 34) contained a cordiform seed at the base of the rachis, but an organic connection with the frond could not be demonstrated satisfactorily; in all probability this superposition was only accidental.

Some years later, White (1934) published a short unillustrated note describing a specimen of *Supaia* with small winged pedicellate seeds, one attached to the rachis at the base of each pinnule. The specimen was reportedly found in the Supai Formation on the Apache Indian Reservation, Ariz., and was offered as conclusive proof of the pteridospermous nature of *Supaia*. White's article does not indicate a repository for the specimen, nor have we been able to locate a specimen fitting his *Supaia* description in the fossil plant collections of either the U.S. National Museum or the U.S. Geological Survey.

With the hope of uncovering evidence substantiating White's report or otherwise bearing on the reproductive habits of the Hermit Shale plants, Watt visited the Grand Canyon National Park Museum and obtained permission to examine the fossil-plant collection there. One seed-bearing fragment of a *Supaia*- or *Callipteris*-like frond was found; in the absence of White's specimen, this fragment is the only ovuliferous pteridophyll specimen known from the *Supaia* flora, and thus is worthy of description. The specimen was originally discovered in 1952 and therefore cannot be the one on which White's article was based. It was found in the Hermit Shale at Hermit Trail, Grand Canyon, by Mr. Frank Shaw, Ranger-Naturalist, and bears the Grand Canyon Museum catalogue number 3281.

Acknowledgments.—We are indebted to Mr. Merril D. Beal, Chief Park Naturalist, and Mr. Warren H. Hill, Acting Chief Park Naturalist, Grand Canyon National Park, for the loan of the specimen.

DESCRIPTION

The fossil is preserved as an impression on a small slab of typical Hermit Shale; the matrix is reddish brown and poorly bedded, and both surfaces of the specimen are crisscrossed by coarse filled mud cracks as much as 1 cm wide. The fossil contains no organic residue, but, nonetheless, it is clearly delimited on the matrix as a dark ferruginous stain with a slight amount of relief. It consists of the terminal portion of an ultimate rachis with parts of 21 pinnules attached (fig. 1); the tip of the frond fragment has been obliterated by a mud crack.

The rachis is stout and slightly bent, approximately 9 cm long and 2–3 mm wide. The pinnules are slightly falcate and virtually linear with scarcely any tapering from base to tip; including the terminal seeds, the pinnules range from 12 to 18 mm in length and reach maximum widths of 4 mm. The

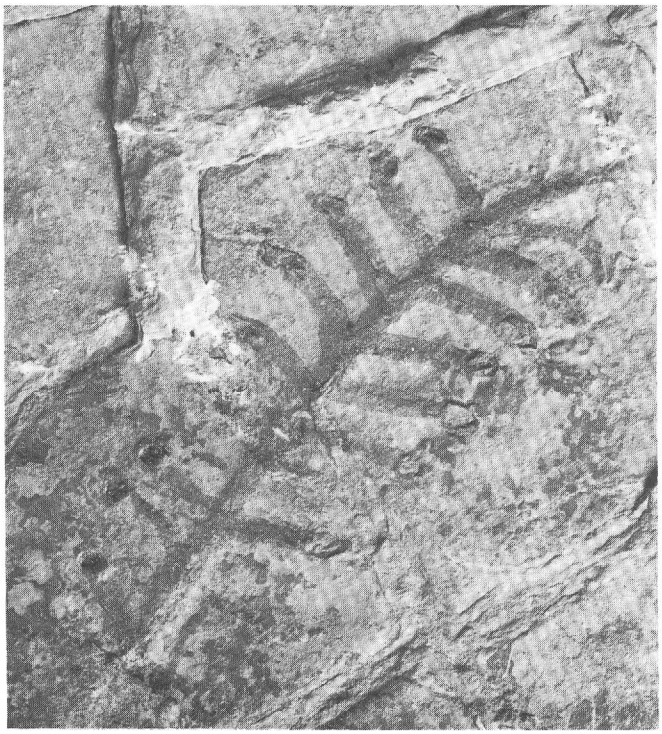

Figure 1.—Ovuliferous pteridosperm found in the Hermit Shale, Grand Canyon, Ariz. View is of the entire specimen, a penultimate frond division with narrow linear pinnules, each terminated by a seed impression. Grand Canyon Museum catalogue number 3281. Natural size.

Figure 2.—Upper left portion of specimen shown in figure 1, enlarged to show depth and shapes of seed impressions at tips of pinnules. × 3.

pinnules are spaced 2–6 mm apart and are oppositely to alternately inserted on the rachis; some of them have slightly decurrent bases. Except for indications of a fairly stout midvein in some pinnules, preservation is not sufficiently good to demonstrate the type of venation.

The major point of morphological interest in this specimen is that each complete pinnule is terminated by the impression of a large globose, ovoid, or pyriform body; the depth of these impressions relative to the very slight relief of the pinnules indicates that the terminal bodies were originally of considerably more substance than the foliar laminae (fig. 2). The bodies are as much as 7 mm long and 4 mm wide; thus some are significantly broader than the pinnules on which they are borne. The impressions of these terminal objects are irregularly wrinkled and show no distinctive structural features. These are clearly reproductive structures, and although their terminal positions at the tips of laminar divisions are reminiscent of those of the sporangia of some types of ferns, their large size discourages a sporangial interpretation. Thus, these bodies appear to be seeds. They are similar in position on the foliar lamina to the seeds of *Tinsleya* (Mamay, 1966), from the Lueders Limestone (Lower Permian) of Baylor County, Tex. The seeds of *Tinsleya*, however, show indications of having been enclosed by apically lobed cupular structures, a feature that is not apparent in the Hermit Shale specimen. The lack of any apical differentiation or other structural characteristics in the Hermit Shale specimen may be a function of poor preservation, preservation during an immature ontogenetic stage, or both. Accordingly, it is not possible to determine whether the seeds of the Hermit Shale specimen were platyspermic or radiospermic, or whether they had attained their full size by the time of burial.

IDENTITY OF THE FOLIAGE

Identification of the Hermit Shale specimen with a given genus of Paleozoic plants would be extremely important because of the light this identity would shed on the natural affinities of that genus. Such identification of this frond is unfortunately not possible because of the small size of the fragment and the lack of preservation of venation or other taxonomically critical foliar features. The overall attitude and shape of the pinnules suggest an alliance with the genus *Callipteris*; in their slight decurrence and long narrow shapes, the pinnules compare rather closely with those of plants identified in the Hermit Shale flora by White (1929, pl. 11, fig. 1; pl. 2, fig. 4) as *Callipteris conferta*. The incomplete nature of this specimen, however, prohibits a positive identification. The pinnae of *Callipteris* are characteristically accompanied at their bases by rachial or subsidiary pinnules; if such structures were present on this plant they are not observable in the fragment on hand because the base of the pinna is not preserved.

The occurrence of this specimen in the Hermit Shale invites comparison with *Supaia*, the dominant element in the Hermit

Shale flora. A suggestive resemblance exists between sterile foliar specimens illustrated by White (1929, pl. 17, fig. 1, 2) as *Supaia rigida* and the fertile specimen described here. A critical morphologic feature of the genus *Supaia* is its dichotomous method of division of the rachis and foliar blade. However, the incompleteness of the fertile fragment militates against a generic identification with *Supaia*. If this specimen was part of a dichotomously forked frond, that point cannot be established, and thus an affinity with *Supaia* must remain conjectural.

Comparisons with other sterile foliar forms are equally inconclusive. Perhaps sexual dimorphism existed in the plant considered here, sterile and fertile fronds having possibly considerable morphologic differences from each other. Such dimorphism could well be sufficient to cause confusion of this plant with others known only in the sterile form; indeed, only a slight degree of dimorphism would be necessary to confuse this fertile fragment with either *Callipteris* or *Supaia*. For this reason and those others already detailed, a generic name is not applied to the fertile specimen. Instead, the informal term "callipteroid" is used. This preference stems partly from the fact that pinnae of *Callipteris* and *Supaia* strongly resemble each other in some aspects, but primarily from the fact that a *Callipteris*-like plant (*Tinsleya*) is known to have borne seeds. Furthermore, if one accepts White's (1934) description of a seed-bearing *Supaia* as accurate, the differences between his specimen and the present one in regard to seed position and mode of attachment would appear to be too broad to permit inclusion of both specimens within the same genus; the seeds of White's material were reportedly rachial and pedicellate, whereas those of the specimen discussed here are terminal and sessile.

DISCUSSION

The specimen described here is not only the first demonstrably ovuliferous pteridosperm found in the Hermit Shale, but it is also one of very few examples of seed-bearing pteridospermous foliage known in the Paleozoic of North America or, indeed, the entire world. Thus, it is briefly discussed here in terms of possible relationships within the pteridosperm complex.

In considering the phyllospermous seed habit of the Paleozoic pteridosperms, various authors have emphasized the importance of seed positions and relative ages. Although evolutionary interpretations are generally presented guardedly, the implication is usually present that pteridosperm seed positions paralleled those of fern fructifications and, therefore, that the terminal seed position is primitive.

The Hermit Shale specimen bore its seeds terminally on pinnules which, if at all morphologically modified, were only slightly reduced; the pinnules were virtually as well developed as those of certain sterile associates in the Hermit Shale flora. Moreover, each pinnule bore a single seed of substantially the same size and position, so that confidence may be placed in this as a consistent feature. In terms of common interpretations of terminal fructifications, then, the Hermit Shale specimen would appear to occupy a morphologically primitive position among the seed ferns. But, compared with other Paleozoic forms in terms of chronologic-morphologic relationships, it occupies an anomalously high stratigraphic position (Zone 14 of Read and Mamay, 1964), which injects a certain amount of confusion into the consideration of trends in pteridospermous seed position.

Halle's (1929) widely quoted essay on the position of the seed in the pteridosperms demonstrated a series of fertile leaves indicative of "migration" of seed position during the Paleozoic, in which the oldest (Upper Carboniferous) forms bore seeds terminally on either reduced or normal pinnules, whereas 3 of 4 Permian forms bore their seeds surficially on normal foliar divisions. Through analogy with the ferns, those taxa with surficial seeds would logically be regarded as derived or advanced stages, an interpretation that acquires substantial support from the relevant chronologic facts.

It should be kept in mind that Halle's work was based on just 9 species, 8 from the Old World; it was inevitable, then, that subsequent discoveries would modify or complicate his interpretations. Since Halle's work was published, several other types of seed-bearing foliage have, in fact, been found in Paleozoic rocks (see Mamay, 1966, p. E9). With the discovery of such Pennsylvanian entities as *Spermopteris coriacea* (Cridland and Morris, 1960) and of seed-bearing specimens of *Lescuropteris moorei* (Darrah, 1968), it becomes apparent that the supposedly advanced surficial seed position on unmodified foliar organs had evolved significantly before the advent of Permian time.

Conversely, the Hermit Shale specimen is among the youngest known of seed-bearing leaf forms in the Paleozoic, yet its seeds were retained in the primitive terminal position. This apparent incongruity between morphologic simplicity and high stratigraphic occurrence might be taken by some to represent a diametric reversal of the trend in seed position suggested by Halle's presentation. However, we regard it as more plausible that the Hermit Shale specimen indicates the existence of a more conservative evolutionary lineage whose older components have not yet been recognized, and whose morphological modifications progressed at a much slower rate than those of other seed-fern lineages. Thus the Hermit Shale specimen serves to emphasize and contribute to a steadily growing accumulation of evidence for intricate phyletic diversity among the Paleozoic pteridosperms.

REFERENCES

Cridland, A. A., and Morris, J. E., 1960, *Spermopteris*, a new genus of pteridosperms from the Upper Pennsylvanian Series of Kansas: Am. Jour. Botany, v. 47, no. 10, p. 855-859.

Darrah, W. C., 1968, The pteridosperm genus *Lescuropteris*—Characteristics, distribution, and significance [abs]: Am. Jour.

Botany, v. 55, no. 6, pt. 2, p. 725.

Halle, T. G., 1929, Some seed-bearing pteridosperms from the Permian of China: Kgl. Svenska Vetenskapsakad. Handl., ser. 3, v. 6, no. 8, p. 1–24.

Mamay, S. H., 1966, *Tinsleya*, a new genus of seed-bearing callipterid plants from the Permian of north-central Texas: U.S. Geol. Survey Prof. Paper 523–E, 15 p.

Read, C. B., and Mamay, S. H., 1964, Upper Paleozoic floral zones and floral provinces of the United States: U.S. Geol. Survey Prof. Paper 454–K, 35 p., 19 pls.

White, C. D., 1929, Flora of the Hermit Shale, Grand Canyon, Arizona: Carnegie Inst. Washington Pub. 405, 221 p.

——1934, The seeds of *Supaia*, a Permian pteridosperm [abs.]: Science, new ser., v. 79, no. 2055, p. 462.

THE ORDOVICIAN-SILURIAN BOUNDARY IN THE YORK MOUNTAINS, WESTERN SEWARD PENINSULA, ALASKA

By C. L. SAINSBURY, J. T. DUTRO, JR.,
and MICHAEL CHURKIN, JR., Denver, Colo.,
Washington, D.C., Menlo Park, Calif.

Abstract.—Rocks of unquestionable Silurian age are rare on the Seward Peninsula. A biostratigraphic boundary between the Ordovician and the Silurian is recognized in a sequence of shelly fossil faunas near the top of a thick sequence of medium- to dark-gray dolomitic limestones. The rocks of Silurian age are light-brown fossiliferous limestones. Although the change from Ordovician to Silurian appears to be lithologically transitional, fossils suggest that rocks that contain a Middle Silurian fauna lie directly on rocks that contain a Late Ordovician fauna. The lithologic change to light-brown limestone is used to define a map unit of rocks of Silurian age; the gray limestones beneath this map unit are of Late Ordovician age except for a thin interval, not mappable lithologically, which also is of Silurian age.

Geologic mapping during 1966 in the York Mountains (fig. 1) resulted in recognition for the first time on the Seward Peninsula of a mappable boundary within a monotonous sequence of gray limestone which by fossils can be assigned to the Late Ordovician and to the Silurian (Sainsbury, 1969a). Many collections of fossils from this general area, which is structurally complex, were made in 1965 and 1966, and these indicated that most of the rocks range from Middle to Late Ordovician in age, but that upper light-brown limestone is of Silurian age (fig. 1). Fossils from the well-exposed transition were collected by Dutro and Churkin in July 1968 from 12 stratigraphic levels. This paper lists all the fauna collected prior to 1968, and it presents the stratigraphy and the sequence of fossils collected across the boundary. A geologic map of the area was published (Sainsbury, 1969a), but further large-scale mapping is recessed. Rocks of Silurian age have not been identified elsewhere. (See small-scale geologic map of the Teller 1:250,000 quadrangle, Sainsbury, 1970.) In view of current interest in the petroleum potential of northern Alaska, the intense structural complexity of the Seward Peninsula (Smith, 1910; Sainsbury, 1969a, b), and the paucity of Silurian rocks, the biostratigraphy at the locality herein described likely will be of some interest to petroleum geologists.

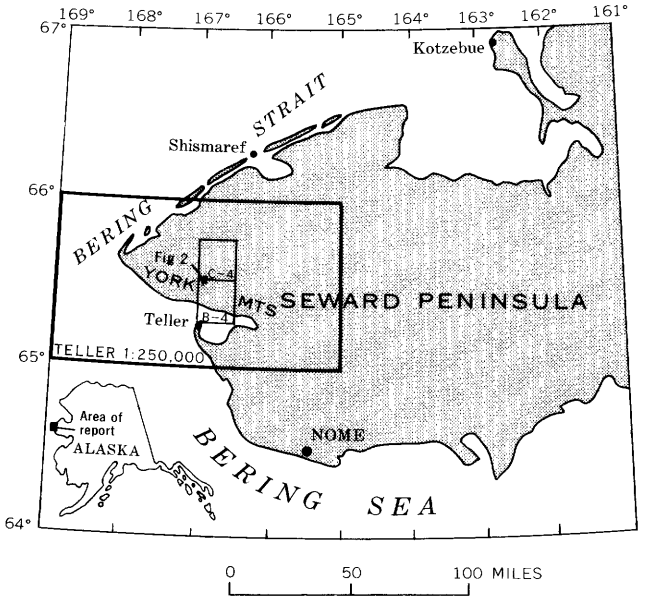

Figure 1.—Index map of the Seward Peninsula, showing areas of the Teller 1:250,000 quadrangle and the Teller B-4 and Teller C-4 quadrangles.

LOCATION

The rocks discussed herein crop out near the boundary of the Teller B-4 and C-4 quadrangles (fig. 2), at the east end of the main mass of the York Mountains. The contact between Ordovician and Silurian rocks is well exposed on a small hill 760 feet high between the Don River and its first large tributary which enters from the west at a point 9.3 miles by air from the mouth of the Don River. The mapped lithologic contact and the sites of critical fossil collections made by Sainsbury across the contact were marked in the field by rock cairns.

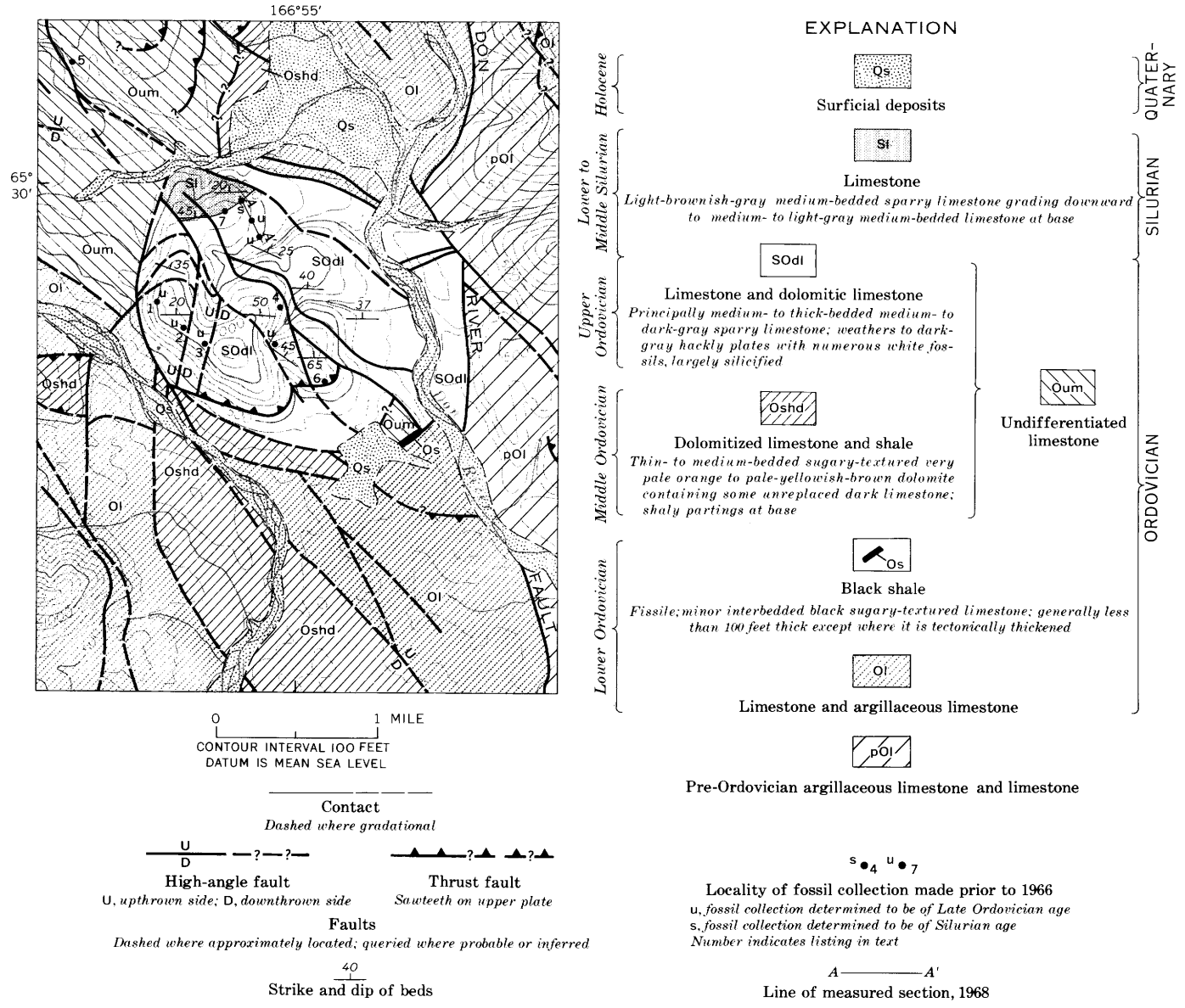

Figure 2.—Geologic map of the Don River area, showing fossil localities. Modified from Sainsbury (1969a). Base from U.S. Geological Survey Teller B-4 and Teller C-4 quadrangles, 1950; contour interval 100 feet.

GENERAL GEOLOGY

The general geology, stratigraphy, and structure of the York Mountains (just west of the area of fig. 2) were discussed in detail by Sainsbury (1969b). The geologic structure is dominated by thrust tectonics, inasmuch as rocks of the entire Seward Peninsula lie within the Collier thrust belt (Sainsbury, 1969c) and rocks of Precambrian and Paleozoic age are intimately intermixed in imbricate thrust sheets.

The geology of the immediate area of interest is shown in figure 2. Fossils of Late Ordovician age collected from this general area by earlier workers were summarized by Steidtmann and Cathcart (1922). As the locations of these old collections are not accurately known, only those collections made by the writers are discussed herein.

The Upper Ordovician and Silurian rocks crop out continuously over an area of about 4 square miles; they are bounded on all sides by faults, and are faulted within themselves. The Upper Ordovician rocks are mostly medium- to thick-bedded dark-gray limestone, finely crystalline, and with great numbers of fossils, many of which are silicified and weather into relief. The dark color and silicified fossils are diagnostic, and have allowed immediate recognition of equivalent rocks exposed in small windows in thrust sheets at other localities in the Teller 1:250,000 quadrangle. Dark chert occurs sporadically in the carbonates, commonly as nodules and small lentils a few inches in length, but discrete chert beds are lacking. Above thrust faults, and along normal faults cutting thrust plates, the dark limestones are extensively dolomitized; this dolomite is light tan to reddish tan. At the outer margins of the

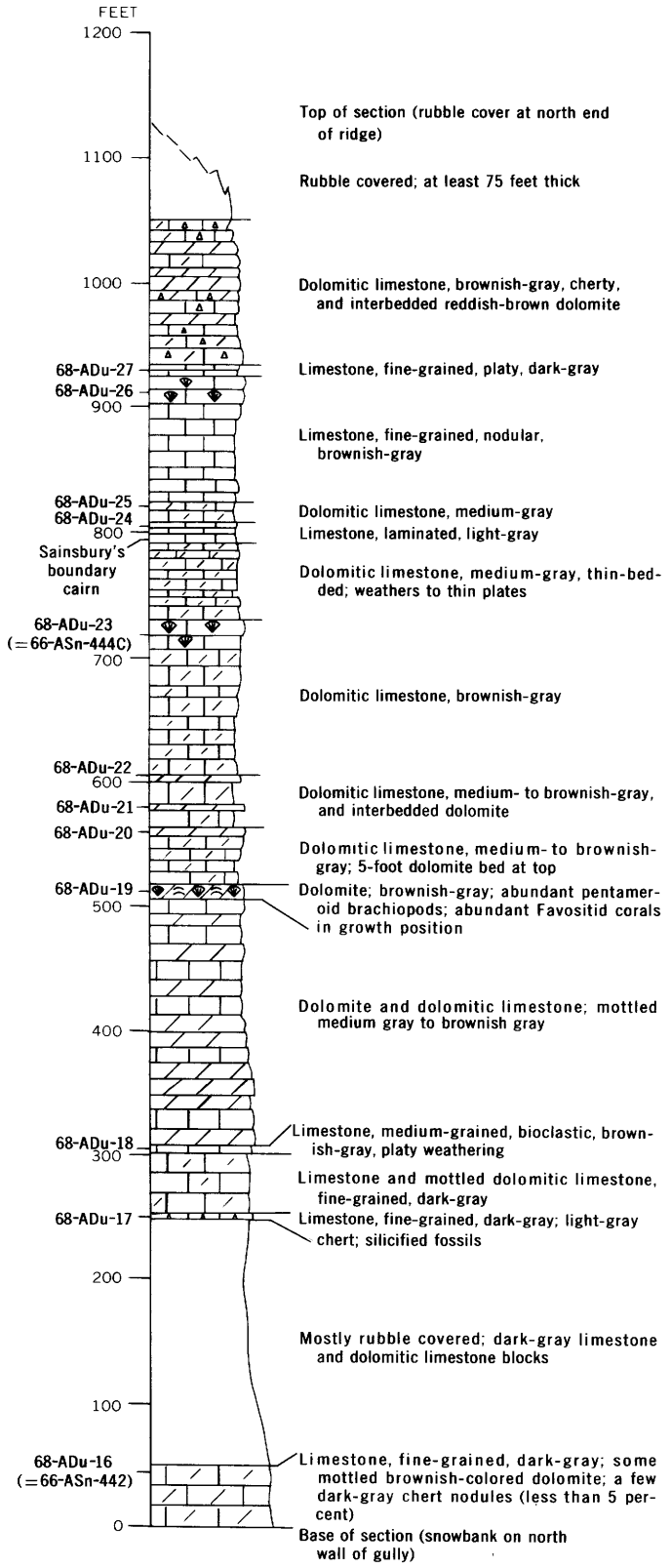

Figure 3.—Measured section of Ordovician and Silurian rocks. Hill 760, about 1 mile west of Don River; 65° 29′50″N., 166°56′W.; Teller B-4 quadrangle, Seward Peninsula, Alaska. 68–ADu–27, fossil collection number. Line of section shown on figure 2.

dolomitization, irregular mottling is characteristic; near faults, the limestone is completely replaced. Most of the dolomite exposed in the rocks discussed herein is considered by Sainsbury to be of tectonic origin, similar to that described by Spörli (1968) in the Helvetic nappes of central Switzerland.

Near the base of the Silurian rocks, the limestone changes abruptly upward from dark gray to light brownish gray, but dark-gray limestone reappears interbedded with light-brown limestone below the main lithologic change to light-brownish-gray limestone. The mappable lithologic change to light-brown limestone lies within the Silurian, and there is no evidence of an unconformity. In fact, the repetition of dark-gray and light-brown limestones suggests a transition indicative of rather continuous deposition, but fossils indicate a time hiatus.

A section was measured and systematically collected along a line trending southeast from the top of the hill at 760 feet down to an altitude of 500 feet (section A–A′, fig. 2). The measured section of beds is shown in figure 3.

FOSSILS AND AGE

The initial collection that yielded Silurian fossils was made in 1965 about 25 feet stratigraphically above the base of the light-brown Silurian limestone, where a stromatoporoidal zone is well developed (locality 4 on fig. 2). Over a thickness of some 4 feet, dark-brown stromatoporoids constitute some 35–50 percent of the rock, making a good stratigraphic marker. Other fossils are so numerous that the rock is virtually a biohermal limestone. Specimens of the types most numerous in the stromatoporoidal limestone were collected, and these are reported in the following list (W. A. Oliver, Jr., written commun., 1966-67) along with fauna of other collections made nearby. Corals were identified by W. A. Oliver, Jr., gastropods by E. L. Yochelson, pelecypods by John Pojeta, Jr., and trilobites by R. J. Ross, Jr.

Locality 4 (fig. 2) 65–ASn–79 (USGS 7593–SD)
Laminar stromatoporoid.
Massive stromatoporoid.
Alveolites sp.
Favosites sp.
Hexisma? sp.
Multisolenia sp. cf. *M. tortuosa* Fritz.
Parastriatopora sp.
Rugose corals (including *Cystiphyllum* sp.).
Age: Middle Silurian (W. A. Oliver, Jr.).

Locality 3 (fig. 2) 66–ASn–444C (USGS 7731–SD)
Halysites? sp.
Multisolenia sp.
Syringopora sp.
Cystiphyllum? sp.
Cyathophylloid coral, indeterminate.
Age: Certainly Silurian (W. A. Oliver, Jr.).

Locality 1 (fig. 2) 65–ASn–PG 4 (USGS 5513–CO)
Labechiid stromatoporoid.
Catenipora sp. cf. *C. robusta* (Wilson).
C. sp. a (cf. *C. jacovickii* of Duncan).

C. sp. b.
Favistina sp.
Cf. *Nyctopora* sp. a.
Age: Late Ordovician (W. A. Oliver, Jr.).

Locality 2 (fig. 2) 65–ASn–78 A (USGS 5446–CO)
Loxoplocus (Donaldiella) sp.
Straparollina sp.
Helicotoma "* * * it is a peculiar one. If not *Helicotoma* it is probably a new genus."
Age: "This fauna gives a superficial resemblance to later Middle Ordovician * * *." (E. L. Yochelson).

Locality 3 (fig. 2) 65–ASn–78 (USGS 5516–CO)
Massive stromatoporoid.
Calapoecia sp.
Catenipora sp. cf. *C. robusta* (Wilson).
C. sp. a?
Propora sp.
Horn coral, indeterminate.
Age: Late Ordovician (W. A. Oliver, Jr.).

Locality 4 (fig. 2) 65–ASn–64 (USGS 5515–CO)
Labechiid stromatoporoid.
Auloporoid? coral.
Catenipora sp. cf. *C. robusta* (Wilson).
C. sp. a (cf. *C. jacovickii* of Duncan).
Cf. *Nyctopora* sp. a.
Age: Late Ordovician (W. A. Oliver, Jr.).

Locality 5 (fig. 2) 65–ASn–85 (USGS 5517–CO)
Receptaculitid.
Labyrinthites? sp.
Reuschia sp.
Age: Late Ordovician (W. A. Oliver, Jr.).

Locality 6 (fig. 2) 65–ASn–278 (USGS 5518–CO)
Cystostroma sp.
Labechia sp.
Reuschia sp.
Age: Late Ordovician (W. A. Oliver, Jr.).

Locality 7 (fig. 2) 65–ASn–79 (USGS 7593–SD)
Laminar stromatoporoid.
Massive stromatoporoid.
Alveolites sp.
Favosites sp.
Hexisma? sp.
Multisolenia sp. cf. *M. tortuosa* Fritz.
Parastriatopora sp.
Rugose corals (not determined but includes *Cystiphyllum* sp.).
Age: Middle Silurian (W. A. Oliver, Jr.).

Fossil collections from the Don River area along the measured section (fig. 3) made by Dutro and Churkin in 1968 were studied as follows: corals and stromatoporoids by W. A. Oliver, Jr.; pelecypods by John Pojeta, Jr.; gastropods by E. L. Yochelson; ostracodes by J. M. Berdan; trilobites by R. J. Ross, Jr.; conodonts by John Huddle; and brachiopods by A. J. Boucot and J. T. Dutro, Jr. Collections are listed beginning with those at the top of the measured section.

68–ADu–27 (USGS 8345-SD)
Auloporoid corals, indeterminate.
Bryozoan?, indeterminate.
Atrypa sp.
Rhynchonelloid brachiopods, undetermined.

68–ADu–26 (USGS 8344–SD)
Horn corals, indeterminate
Favosites spp.

68–ADu–25 (USGS 8343–SD) = 65–ASn–79 (USGS 7593–SD)
Massive stromatoporoid, indeterminate.
Favosites sp.
Heliolites sp.
Alveolites sp.

68–ADu–24 (USGS 8342–SD)
Small horn corals, perhaps *Tabularia* sp. (identification by J. T. Dutro, Jr.).

68–ADu–23 (USGS 8341–SD) = 66–ASn–444C (USGS 7731–SD)
Massive stromatoporoid, undetermined.
Cystiphyllid coral, indeterminate.
Alveolites? sp.
Favosites spp.

68–ADu–22 (USGS 8340–SD)
Thamnopora? sp.
Halysites? sp.
Favosites sp.

68–ADu-21 (USGS 8339–SD)
Rugose horn coral indeterminate.
Halysites? sp.
Favosites sp.

68–ADu–20 (USGS 8338–SD)
Halysites? sp.
Favosites sp.
Pentamerus? sp.

68–ADu–19 (USGS 8337–SD)
Favosites spp.
Pentamerus sp.
Conchidium? sp.

68–ADu–18 (USGS D2036–CO)
Ostracodes (J. M. Berdan).
Aparchitella? sp.
Schmidtella sp., large.
Krausella sp., large.
Leperditellid, indeterminate.
Eurychilinid, indeterminate.
Smooth ostracodes, indeterminate.
Trilobites (R. J. Ross, Jr.).
Remipyga sp.
Monorakos n. sp.
Conodonts (John Huddle).
Panderodus sp.
Drepanodus suberectus (Branson and Mehl).
Brachiopods, indeterminate fragments.

68–ADu–17 (USGS 6747–CO).
Catenipora cf. *C. gracilis*
Horn corals, indeterminate.
Brachiopods, indeterminate.
Maclurites cf. *M. manitobensis* (Whiteaves).
Macluritacean operculum fragment.

68–ADu–16 (USGS 6746–CO) = 66–ASn–442 (USGS 6026–CO)
Catenipora spp. (two species).
Bighornia sp.
Favistina sp.
Tollina sp.
Maclurites cf. M. *manitobensis* (Whiteaves).
?Murchisonia (Hormotoma) sp. indeterminate.

On the basis of North American biostratigraphic assignments, the Silurian-Ordovician boundary falls somewhere between collections 68–ADu–18 and 19 (fig. 3). According to both J. M. Berdan and R. J. Ross, Jr. (written commun., 1969), the arthropods in 68–ADu–18 are of Ordovician (probably Late Ordovician) age. John Huddle stated (written commun., 1969) that the conodonts are of Middle or Late Ordovician age. The lowest pentamerids were collected 200 feet higher in the section; according to A. J. Boucot (written commun., 1969), these are either late Wenlockian (late Middle Silurian) or Ludlovian (Late Silurian) equivalents. There is no apparent unconformity in the sequence, and the alternation of lithologies suggests continuous deposition.

A few comments, based upon relations observed west of the Don River area (Sainsbury, 1969b), are pertinent to the age assignments discussed in the preceding paragraph. In that area a well-defined time-stratigraphic unit occurs at the Early Ordovician-Middle Ordovician time boundary; this unit is a thin black shale that has yielded numerous and diagnostic trilobites and graptolites of late Early Ordovician age (Ross, 1965, and written commun. in Sainsbury, 1969a). Above the shale, the Middle Ordovician rocks consist of medium- to thin-bedded dark-gray limestones with shaly partings, and, higher up, dark limestone with discoid bits of gray chert. (See Sainsbury, 1969b, p. 28–30 for a more detailed description.) These rocks are extensively dolomitized near thrust faults; they also weather to distinctly dusky brown slopes unlike any other limestone in this region, and they are fossiliferous. Because of their position immediately above the only shale so far recognized in the Ordovician, they are likely not misplaced, and their age of early Middle Ordovician is well established. Fossil collection USGS 5517–CO (fig. 2, loc. 5; p. C55, this report) is from these rocks; yet it is determined on the basis of corals to be of Late Ordovician age. Unfortunately, coral faunas have not been collected elsewhere near the shale, and comparative faunas are not available, but it seems possible that Ordovician coral faunas in this part of North America may appear to be younger than they actually are, relative to graptolites.

Three other collections were made several hundred yards south of the measured section, but are in areas separated by faults. These three collections listed below appear to correlate at about the level of 68–ADu–16 in the measured section. Their locations are not shown on figure 2.

68–ADu–28 (USGS 6748–CO)
Catenipora cf. *C. gracilis.*
Prisochiton sp.
"*Liospira*" aff. "*L.*" *mundula* Ulrich.
Trochonemella cf. *T. montrealensis* Okulitch.
Loxoplocus (Lophospira) cf. *L. (L.) burginensis* (Ulrich and Scofield).
Daidia cerithoides (Salter).
?Helicotoma n. sp.
Trochonema (Trochonema) n. sp.
Straparella circe Billings.
"*Straparella*" cf. "*S*" *eurydice* Billings.
Murchisonia (Hormotoma) sp. indeterminate.
Gastropod, undetermined.
Cephalopods, undetermined.

68–ADu–29 (USGS 6749–CO)
Favistina sp.
Catenipora cf. *C. gracilis.*
Calenipora sp.
Calapoecia sp.

68–ADu–30 (USGS 6750–CO)
Horn coral, undetermined.
Tabulate coral, undetermined.
Bryozoan, undetermined.
?Hebertella sp.
"*Liospira*" aff. "L." *mundula* Ulrich.
Liospira cf. *L. progne* (Billings).
Trochonemella cf. *T. montrealensis* Okulitch.
Daidia cerithoides (Salter).
Loxoplocus (Lophospira) sp. indeterminate.
Trochonema (Trochonema) n. sp.
?Murchisonia (Hormotoma) sp. indeterminate.
Straparella cf. *S. circe* Billings.
Gastropod, undetermined (2 kinds).
Ctenodont pelecypod fragment, indeterminate.
Curved flattened tube of unknown origin.

Concerning the age of 6749–CO, W. A. Oliver, Jr. (written commun., 1969), stated, "these corals, and those of collections 16 and 17 of the measured section, are of Late Ordovician age, probably representatives of the Bighorn-Red River coral fauna that seems to be so widespread in the Canadian and Arctic provinces."

Although the gastropod faunas come from beds slightly higher in the sequence, Yochelson was inclined to consider them as late Middle Ordovician correlatives. This difference of opinion may be more semantic than real.

The Ordovician age of D2036–CO seems to be well documented. R. J. Ross, Jr. (written commun., 1969), in discussing the two trilobites, stated: "One genus, *Remipyga*, is previously reported from Baffin Island and is like what the Russians identify as *Ceraurinus. Monorakos* is a Siberian Late Ordovician genus. The trilobites favor a Late Ordovician age for this collection."

In summing up a discussion of the ostracodes in D2036–CO, J. M. Berdan (written commun., 1969) stated: "Although the possibility of an Early Silurian age cannot be eliminated, the general aspect of the assemblage suggests an Ordovician age."

John Huddle considered the presence of *Drepanodus suberectus* as a clear indication of Middle or Late Ordovician age.

In summary, the Ordovician beds appear to be general correlatives of the Upper Ordovician Red River Formation of the Williston basin area and thus in terms of the standard

American sequence would be equivalent to beds high in the Trenton Limestone (Middle Ordovician) or Eden Stage (Upper Ordovician). A later Ordovician age for the ostracode-trilobite assemblage of D2036–CO is yet to be precisely determined. The oldest Silurian fossils seem, on the basis of the ages of corals, to be no older than Wenlockian, whereas the remainder of the Silurian sequence apparently would fall into the Late Silurian; the absence of Early Silurian, however, is not considered to be clearly established.

REFERENCES

Ross, R. J., Jr., 1965, Early Ordovician trilobites from the Seward Peninsula, Alaska: Jour. Paleontology, v. 39, no. 1, p. 17–20.

Sainsbury, C. L., 1969a, Geologic map of the Teller B-4 and southern part of the Teller C-4 quadrangles, western Seward Peninsula, Alaska: U.S. Geol. Survey Misc. Geol. Inv. Map I-572.

——1969b, Geology and ore deposits of the Central York Mountains, western Seward Peninsula, Alaska: U.S. Geol. Survey Bull. 1287, 101 p.

——1969c, The A. J. Collier thrust belt of the Seward Peninsula, Alaska: Geol. Soc. America Bull., v. 80, no. 12, p. 2595–2596.

——1971, Geologic map of the Teller 1:250,000 quadrangle, Alaska: U.S. Geol. Survey Misc. Geol. Inv. Map I-685. [In press]

Smith, P. S., 1910, Geology and mineral resources of the Solomon and Casadepaga quadrangles, Seward Peninsula, Alaska: U.S. Geol. Survey Bull. 433, 234 p.

Spörli, Bernhard, 1968, Syntectonic dolomitization in the Helvetic Nappes of Central Switzerland: Geol. Soc. America Bull., v. 79, no. 12, p. 1839–1846.

Steidtmann, Edward, and Cathcart, S. H., 1922, Geology of the York tin deposits, Alaska: U.S. Geol. Survey Bull. 733, 130 p.

CARBONATE CLASTS IN EPICLASTIC VOLCANIC ROCKS AND THEIR PALEOTECTONIC IMPLICATIONS, BLUE RANGE PRIMITIVE AREA, ARIZONA AND NEW MEXICO

By E. R. LANDIS, J. C. RATTÉ, and D. A. MYERS,
Denver, Colo.

Abstract.—Carbonate clasts constitute a large percentage of some conglomerate beds in the lower part of the exposed volcanic and epiclastic volcanic Tertiary rock sequence in the northern part of the Blue Range primitive area of Greenlee County, Ariz., and Catron County, N. Mex. The carbonate clasts are dominantly skeletal micritic and skeletal limestones probably deposited originally in a shelf environment; most of the carbonate rocks are of Des Moines age, though at least 20 percent are of Virgil age. Rocks of Missouri age may have been present in the sequence, but if so they probably were composed mostly of noncarbonate clastics. The clasts were probably derived from a nearby tectonically elevated sequence of rocks of Middle and Late Pennsylvanian age that directly overlay rocks of Precambrian age. Any such area is now hidden beneath the Tertiary rocks of the region.

The Blue Range primitive area in Greenlee County, Ariz., and Catron County, N. Mex., was investigated geologically at the same time that mineral surveys were made of areas under consideration for inclusion in the Wilderness System (Ratte' and others, 1969). The exposed rocks of the area were examined and mapped in reconnaissance at a scale of 1:62,500 both to determine the mineral resource potential of the area and to help understand the complex geologic history of this little-studied area. The carbonate clasts in the epiclastic volcanic rocks of the area yield information about the age and original distribution of Paleozoic rocks in parts of New Mexico and adjacent Arizona that are now largely covered by Tertiary volcanic rocks.

Earlier geologic work in the area consisted of reconnaissance geologic mapping of the New Mexico part of the area, at a scale of 1 inch to 2 miles, by Weber and Willard (1959), and geologic mapping of Greenlee and Graham Counties, Ariz., at a scale of 1 inch to 6 miles, by Wilson and Moore (1958). A study of the rocks of the Alpine-Nutrioso area a short distance north of the Blue Range primitive area made by Wrucke (1961) was of aid during the present investigation.

Fieldwork for the present investigation was done by Landis and Ratte'. Carbonate clasts that contained fossils were prepared by L. J. Vigil, and the fauna was examined and identified by D. A. Myers. Petrographic examination of the carbonate clasts was done by Landis, and the calcium-magnesium ratio determinations were made by R. F. Gantnier.

GEOLOGIC SETTING

The Blue Range primitive area is in the southwestern part of the White Mountain and Datil volcanic areas, and rocks exposed there are volcanic rocks or epiclastic volcanic rocks—sedimentary rocks composed largely of volcanic material. Table 1 shows the stratigraphic volcanic sequence in the Blue Range primitive area.

As indicated in table 1 the epiclastic volcanic rocks that form the basal part of the exposed rock sequence in the northern part of the Blue Range primitive area include some distinctive sandy conglomerates made up of as much as 70 percent or more nonvolcanic material. The nonvolcanic clasts are well rounded mostly subspherical pebbles, cobbles, and boulders as much as 2 feet in diameter, made up of a variety of carbonate rocks and distinctive reddish-gray gneissic biotitic granite and a variety of other resistant nonvolcanic lithic types. Many of the carbonates contain fusulinids, calcareous algae, and brachiopod and crinoid fragments. Carbonate clasts were collected at four localities—two (A, B) in the northern part of the primitive area; one (C) immediately adjacent to the northern boundary; and one (D) about one-half mile north of the area (fig. 1). That part of the epiclastic volcanic sequence that contains carbonate clasts is 116 feet thick (fig. 2) at locality C; the sequence was not measured at the other localities, because of poor exposures and structural complications.

A few miles northeast of the Blue Range primitive area Weber and Willard (1959) mapped rocks that contain carbonate clasts. R. H. Weber (written commun., 1970) stated that

> Conglomerates very similar to those described for the Blue Range area were found to be a prominent component of the volcanic sediment sequence along the eastern base of the San Francisco Mountains during reconnaissance mapping of the Reserve 30-minute quad. Well-rounded

U.S. GEOL. SURVEY PROF. PAPER 750-C, PAGES C58-C64

Table 1.—*Tertiary volcanic sequence in the Blue Range primitive area*

Rock unit	Approximate thickness (feet)	K-Ar isotope age (million years)
Gila Conglomerate . . . . . Includes some basaltic lava flows.	0–1,100	. . . . .
Erosional unconformity.		
Basaltic andesite	2,000	[1]23.3±0.7
Quartz latite and rhyolite (south half of area only) . . . . . Extrusive-intrusive dome complex; dikes of complex intrude lower flows of basaltic andesite, but complex appears to be older than most of basaltic andesite unit.	0–1,000	[2]23.4±0.7
Unconformity.		
Rhyolite tuff (north half of area only) . . . . . Welded rhyolite ash-flow tuff sheet interlayered with conglomerate, sandstone, andesitic lava flows, and other rhyolite and quartz latite ash-flow tuffs.	300–1,000	[3]24.9±0.7
Rhyolite of Red Mountain (south half of area only) . . . . . Welded rhyolite ash-flow tuffs, lava flows, and intrusive rhyolite.	0–1,000	. . . . .
Erosional unconformity.		
Pyroxene-hornblende andesite (south part of area)	2,000	[4]37.4±3.9
Epiclastic volcanic rocks (north part of area) . . . . . Includes some lava flows and non-volcanic conglomerate containing clasts of fossiliferous limestone and gneissic granite.	2,000	. . . . .

[1] Whole-rock age.
[2] Biotite age.
[3] Sanidine age.
[4] Hornblende age.

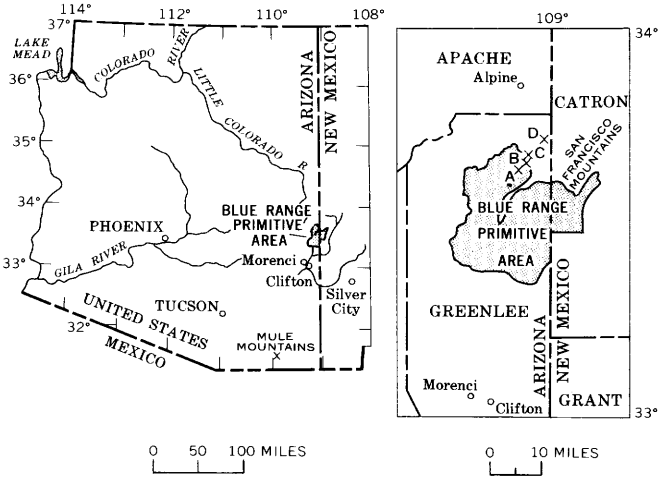

Figure 1.—Index map of the Blue Range primitive area, Arizona and New Mexico. A–D, carbonate clast localities.

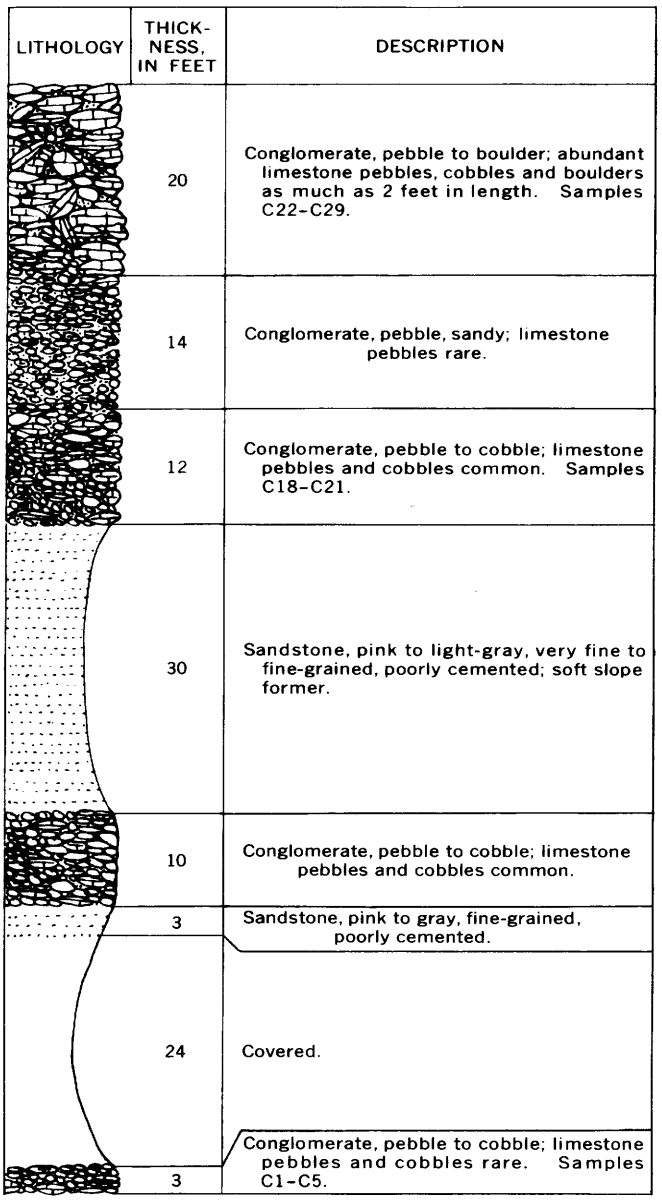

Figure 2.—Measured section at locality C, Red Bluff on the Red Hill Road, Blue quadrangle, Arizona.

pebbles and cobbles of limestone and coarse-grained gneissic red granite are locally abundant in this area. The limestones include crinoidal varieties.

No further information is available, but the limestone clasts Weber described may have had a geologic history comparable to the limestone clasts in conglomerates in the northern part of the Blue Range primitive area.

Figure 3 shows distribution of gross time-rock sequences at the beginning of the Tertiary. Because little direct information is available about pre-Tertiary rocks in and around the Blue Range primitive area, the map (fig. 3) is mostly inference and is highly generalized. The stratigraphic relations in the area are known well enough to allow the following general statement

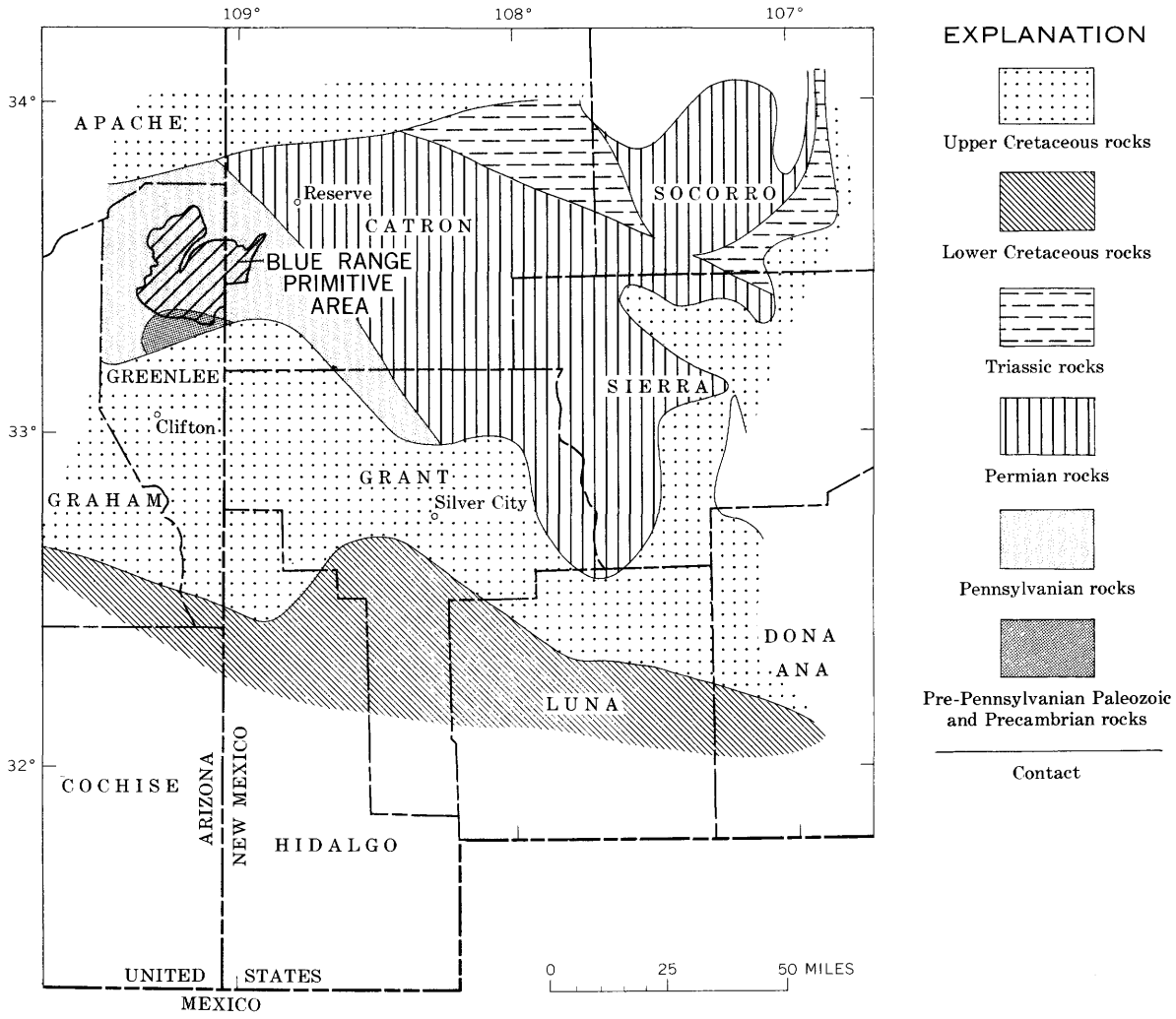

Figure 3.—Pre-Tertiary paleogeologic map of part of southwestern New Mexico and adjacent Arizona. Modified from Kottlowski (1962, 1963, 1965).

which is largely derived from Kottlowski (1962, 1963, and 1965) and Foster (1964):

1. Rocks of Paleozoic age probably ranged in thickness from a few feet to 2,000 feet (Kottlowski, 1965, fig. 2); they overlie a Precambrian sequence of undetermined thickness.
2. Rocks of Cambrian, Ordovician, Devonian, and Mississippian age are present south and southeast of the Blue Range primitive area near Clifton, Ariz., and near Silver City, N. Mex.
3. Rocks of these ages are not present in a well that was drilled about 35 miles north of the primitive area (Foster, 1964, p. 13, 14), but Kottlowski (1962, fig. 2) indicated that in some of the northern part of the Blue Range primitive area Paleozoic rocks of pre-Pennsylvanian age might be present.
4. Rocks of Pennsylvanian age may underlie part of the Blue Range area, where they may range in thickness from a few feet to 1,000 feet (Kottlowski, 1965, fig. 6).
5. If rocks of Permian age were deposited in the area, they were removed by subsequent erosion that accompanied the rise of the Burro uplift.

The Burro uplift is a positive feature of late Paleozoic and early Mesozoic age whose axis trends northwest through western Grant County, N. Mex., into Greenlee County, Ariz. It has a core of metamorphic and igneous rocks of Precambrian age (Foster, 1964, p. 4; Hewitt, 1959, p. 9–10) that was largely stripped of Paleozoic and lower Mesozoic rocks prior to the deposition of Cretaceous rocks. The northwest end of the core of the Burro uplift underlies the southern part of the Blue Range primitive area; and though direct evidence is lacking, rocks of Tertiary age probably directly overlie Precambrian rocks in an area of undetermined size. Rocks of Early Cretaceous age possibly were deposited over the Blue Range area, and it is nearly certain that Upper Cretaceous rocks covered the eroded edges of older rocks in the area. All the Cretaceous rocks were probably removed from the Blue Range area during an erosional interval that cannot be dated more

precisely than Late Cretaceous and(or) early Tertiary. In some nearby areas, such as the Clifton-Morenci area to the south (Lindgren, 1905, p. 94, 95), the period of erosion was preceded by igneous intrusion and intense faulting. It is possible, and indeed seems probable, that (1) the Blue Range primitive area shared this intrusive and tectonic history, and (2) the extrusive volcanic rocks and associated volcaniclastics that cover the older rocks were deposited on a surface of considerable local relief.

PETROGRAPHY AND FAUNA OF THE CARBONATE CLASTS

Samples of carbonate clasts were collected at each of the four localities, A, B, C, and D, shown on figure 1. A total of 41 samples were selected for thin-section examination, and 36 samples were submitted for determination of total carbonate content and calcium-magnesium molal ratio. The system of carbonate classification proposed by Leighton and Pendexter (1962) was followed in the petrographic descriptions, but not in designation of the rock name. For consistency in naming rocks of more than 50 percent carbonate compared with those of less, the descriptive terms in this report are given in order of decreasing amount; that is, a rock listed as limestone, micritic, skeletal, is a limestone with more than 50 percent micrite and less than 50 percent skeletal grains and in normal order would be written skeletal micritic limestone—Leighton and Pendexter (1962, p. 49) would call this same rock a micritic-skeletal limestone.

Examination of the carbonate clasts in thin section indicates that most of the clasts contain at least some skeletal material. Much of the fossil debris is virtually useless for age determination, but a considerable number of the clasts contain datable fusulinids. Table 2 lists the identified fusulinids and their age determinations.

The samples selected for petrographic study and fusulinid identification constitute a suite representative of the considerable variety of carbonate and calcareous rocks in the conglomerate beds. Table 3 presents a summary of petrographic and fusulinid data. Almost all the samples contain some calcareous skeletal grains and fragments. Fourteen of the 41 samples are classified as skeletal limestones and 21 of the 41 samples are classed as micritic limestones that contain some skeletal grains. Beside composing about half the clasts examined in thin section, skeletal micritic limestone makes up more than 50 percent of the clasts that contained fusulinids.

Only about half the samples selected for petrographic study contained fusulinids, but the whole sample suite is similar and most or all the samples probably come from a related suite of rocks of Pennsylvanian age. None of the samples appear to represent carbonate or calcareous rocks of any rock system other than Pennsylvanian.

Rocks of Pennsylvanian age crop out at three places near the Blue Range primitive area (fig. 4). The exposed Pennsylvanian rocks have been described as "Light-gray to medium-gray fossiliferous marine limestone, reddish-brown calcareous siltstone, and coarse arkose" (Weber and Willard, 1959). At another locality, Wrucke (1961, p. 6) stated that: [See p. C62]

Table 2.—*Fusulinids in carbonate clasts in epiclastic volcanic rocks, Blue Range primitive area, Arizona*
[Sample sites are shown on figure 1, this report]

Sample No.	Fusulinids	Age
A1	*Wedekindellina* cf. *W. henbesti* (Skinner).	Late early or early middle Des Moines.
	Beedeina aff. *B. cedarensis* (Ross and Sabins).	Late early or early middle Des Moines.
	Millerella sp	Late early or early middle Des Moines.
	Eoschubertella? sp	Late early or early middle Des Moines.
A2	*Wedekindellina ellipsoides* Dunbar and Henbest.	Probably middle Des Moines.
A3	*Wedekindellina* cf. *W. henbesti* (Skinner).	Early Des Moines.
	Beedeina cf. *B. arizonensis* (Ross and Sabins).	Early Des Moines.
A4	*Wedekindellina* aff. *W. euthysepta* (Henbest).	Early or middle Des Moines.
A5	*Wedekindellina* sp	Des Moines.
C1 (1st slide)	*Wedekindellina*? sp. indet	Des Moines.
	Beedeina sp. indet	Des Moines, early half.
C1 (2d slide)	*Wedekindellina* sp	Des Moines, early half.
	Beedeina sp	Des Moines, early half.
C4	*Beedeina* cf. *B. novamexicana* (Needham).	Late middle or early late Des Moines.
	Wedekindellina sp	Late middle or early late Des Moines.
C5	*Beedeina* sp. indet	Des Moines.
C18	*Beedeina* sp. indet	Des Moines.
C19	*Beedeina* sp., primitive form.	Probably early Des Moines.
	Wedekindellina cf. *W. henbesti* (Skinner).	Probably early Des Moines.
C20	Fusulinids indet. Possibly *Triticites.*	Probably post-Des Moines.
C23	*Wedekindellina* sp. indet	Des Moines, early half.
	Beedeina aff. *B. arizonensis*? (Ross and Sabins).	Des Moines, early half.
C24	*Beedeina* sp	Possibly late Des Moines form.
C25	*Beedeina* cf. *B. arizonensis* (Ross and Sabins).	Early Des Moines.
	Millerella sp	Early Des Moines.
	Eoschubertella? sp	Early Des Moines.
C27	*Beedeina* cf. *B. arizonensis* (Ross and Sabins).	Early Des Moines.
	A small fusulinid, either an immature form of above, or *Fusulinella* sp.	Early Des Moines.
C28	*Triticites* cf. *T. callosus* Dunbar and Henbest.	Probably late early Virgil.
C29	*Beedeina* sp. indet	Des Moines.
D1	*Triticites* aff. *T. bensonensis* Ross and Tyrrell.	Early middle Virgil.

Table 3.—*Summary of petrographic and fusulinid age data*

Rock type	Total number of thin sections	Total fusulinid age determinations	Number of samples classified by age										
			Des Moines	Des Moines, early	Des Moines, early half	Des Moines, early or middle	Des Moines, late early or early middle	Des Moines, middle	Des Moines, late middle or early late	Des Moines, late	Probably post-Des Moines	Virgil, late early	Virgil, early middle
Limestone, micritic, skeletal	20	13	3	3	1	2	....	1	1	....	.....	1	1
micritic, skeletal, clayey	1	....	....	....	....	....	....	....	....	....	.....	....	....
skeletal	3	1	....	....	....	....	....	....	....	1	.....	....	....
skeletal, micritic	8	2	....	....	....	....	1	....	....	....	1	....	....
skeletal, micritic,	1	1	....	....	....	....	....	....	....	....	.....	....	....
skeletal, dolomitic	1	....	....	....	....	....	....	....	....	....	.....	....	....
skeletal, silty, clayey	1	1	[1]1	....	....	....	....	....	....	....	.....	....	....
pelletal, skeletal	1	1	1	....	....	....	....	....	....	....	.....	....	....
oolitic, superficial	1	....	....	....	....	....	....	....	....	....	.....	....	....
Siltstone, clayey, sandy, limy, dolomitic	1	....	....	....	....	....	....	....	....	....	.....	....	....
clayey, dolomitic, calcitic	1	....	....	....	....	....	....	....	....	....	.....	....	....
clayey, limy	2	1	....	....	1	....	....	....	....	....	.....	....	....
Total number of thin sections	41	20	5	4	2	2	1	1	1	1	1	1	1

[1] Could be classified limy clayey siltstone.

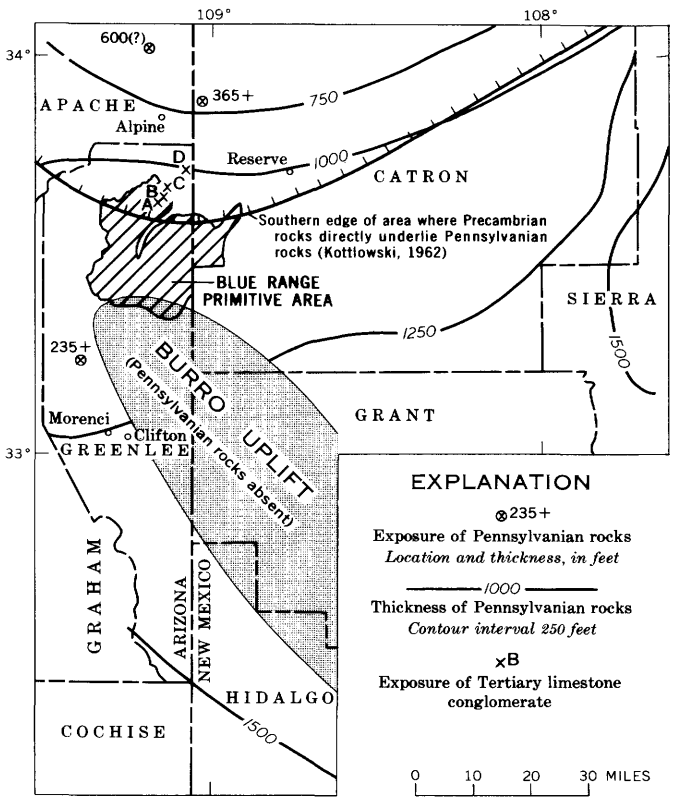

Figure 4.—Isopach map of Pennsylvanian rocks in southwestern New Mexico and adjacent Arizona. Modified from Kottlowski (1962; 1965, fig. 6) with additions. Published with permission, American Association of Petroleum Geologists.

Here the rock [limestone] is very light gray, medium grained to lithographic, and intensely brecciated. Local concentrations of brown argillaceous material emphasize the breccia fragments. A little opal also occurs between the fragments. Brown to maroon shale * * * appears to underlie the limestone * * *. * * * medium- to dark-gray commonly medium-grained brecciated limestone. * * * this limestone has small white chert nodules * * *.

Kottlowski (1960, p. 26-27) supplied a more detailed description of the rock reported on by Weber and Willard (1959) and stated that the commonest carbonate rocks are fossil-fragment calcarenite and algal micro-oolitic limestones. Though similarities in rock types are obvious, these descriptions cannot be compared in detail with the petrographic descriptions in table 3. The only comparative petrographic descriptions available are from rocks in the Naco Group of Pennsylvanian age in the Mule Mountains (fig. 1) of southern Arizona (Hayes and Landis, 1965). The limestone clasts of the Blue Range area are petrographically similar to carbonates of the lower member of the Horquilla Limestone, which is the oldest formation of the Naco Group in the Mule Mountains. The Horquilla is of Middle and Late Pennsylvanian age in southern Arizona, and the lower member of the Horquilla is of Middle Pennsylvanian age (Hayes and Landis, 1965, p. 31).

The rocks of Pennsylvanian age mapped by Weber and Willard (1959) were not assigned by them to any stratigraphic unit. Wrucke (1961) tentatively correlated the Pennsylvanian rocks exposed north of Alpine, Ariz., with the Naco Group of southern Arizona and recognized that some of the exposed rocks were also equivalent in age to part of the Supai Formation of central Arizona, which is mostly a red clastic

unit that contains subordinate amounts of limestone. In contrast, the Naco is largely limestone, so Wrucke assigned the exposed limestone to the Naco(?) Group. Both the exposures mapped in New Mexico by Weber and Willard (1959) and in Arizona by Wrucke (1961) seem to be in anomalous structural positions, and all may be xenoliths. Weber and Willard (1959) pointed out this possibility, and Wrucke (1961) discusses the possibility that the Tertiary volcanics were deposited on a surface with relief of as much as 1,100 feet and that the pre-Cenozoic bedrock was cut by faults with aggregate displacement of as much as 2,000 feet; or alternatively, that the exposed limestones are xenolithic blocks in the Tertiary volcanics.

Seventeen of the 20 samples that contained identifiable fusulinids represent rocks of Des Moines age; one sample is probably younger than Des Moines, and two are from rocks of Virgil age. Fusulinids only of Des Moines age have been reported (Kottlowski, 1960, p. 26) from the exposure mapped by Weber and Willard (1959). The rocks at the exposure in Arizona north of the Blue Range area reportedly contain fusulinids of Virgil age (Wrucke, 1961) and Missouri and Des Moines age (Kottlowski, 1960; Foster, 1964). Lokke (1962) reported fusulinids of early Des Moines and Virgil age from wells penetrating the Pennsylvanian rocks northwest of the Blue Range area. It is possible that the absence of fusulinids of Missouri age in the samples collected in the Blue Range area results from the northwestward lateral change of the Upper Pennsylvanian rocks from dominantly carbonate rocks to dominantly arenaceous and argillaceous clastics (Kottlowski, 1962, p. 352).

PALEOGEOLOGICAL CONSIDERATIONS AND CONCLUSIONS

Figure 4 is an isopach map modified from the map by Kottlowski (1965, fig. 6). The area where rocks of Pennsylvanian age are absent overlies the Burro uplift, a late Paleozoic to early Mesozoic tectonic feature. The core of the Burro uplift probably consists mostly of Precambrian igneous and metasedimentary rocks, overlain by isolated erosional remnants of, and possibly fringed by, a thin sequence of rocks of pre-Pennsylvanian age. After the removal of almost all previously deposited Paleozoic and lower Mesozoic sedimentary rocks, the Burro uplift was covered by Cretaceous rocks, which were subsequently removed prior to deposition of the Tertiary extrusive igneous rocks and associated volcaniclastic rocks. Though the northern boundary of the core of the Burro uplift is shown on figure 4 as a solid line, its actual placement is uncertain because all Mesozoic and older rocks are buried beneath the rocks of Tertiary age.

The hachured line shown in the northern part of figure 4, derived from Kottlowski (1962, fig. 2), represents the postulated southern boundary of an area in which rocks of Pennsylvanian age directly overlie rocks of Precambrian age. Foster (1964, pl. 1) shows a boundary representing the possible northern extent of pre-Pennsylvanian rocks in Catron County, N. Mex., which if extended into Arizona would be about 25 miles north of the Blue Range primitive area. Direct evidence regarding exact location of this boundary is very meager, and the line shown by Foster (1964, p. 4 and 15) is simply a straight line connecting two known points where rocks of pre-Pennsylvanian age are absent.

Studies of the distance of transport of carbonate clasts are particularly pertinent to the source of the limestone clasts in the Blue Range area. Such studies are relatively rare in the literature, as compared to studies of the more resistant rock types, but some information is available. Because of the solubility of limestone in most geomorphic and climatic environments, carbonate clasts are probably produced largely under conditions of high relief and rapid erosion (Pettijohn, 1957, p. 251–252). The applicability of laboratory studies to natural conditions is debatable, but abrasion-mill tests as cited by Pettijohn (1957, p. 535) do indicate that limestone clasts decrease in size (weight) very rapidly during simulated transportation. In a study of sediment transport on the east side of the Black Hills of South Dakota, Plumley (1948, figs. 18 and 19) showed that limestone fragments were very markedly rounded in short—10 miles or less—distances of transport and concluded that "A short distance of stream transport removes most of the soft-rock types by abrasion and breakage. In a distance of 30 miles in Rapid Creek the percentage of limestone plus sandstone pebbles 16–32 mm. is reduced from 26.2 percent to 2.6 percent." He further concluded that sandstone is less resistant to abrasion and breakage during stream transport than limestone and that "loss of the softer rocks by abrasion and breakage during stream transport is a function of rigor of transport and size and composition of associated particles" (Plumley, 1948, p. 575).

A consideration of the data, information, and ideas presented in this report has led us to formulate several conclusions about the buried pre-Tertiary rocks of the area and their geologic history.

The carbonate clasts and calcareous rock clasts in the pebble-and-boulder conglomerate in the lower part of the exposed Tertiary rock sequence in and adjacent to the northern part of the Blue Range primitive area were derived from a sequence of Pennsylvanian rocks that were preserved during pre-Tertiary erosional episodes. If the limestone conglomerate was derived from the fringe of the Burro uplift, or from a tectonically preserved area within the core of the Burro uplift, perhaps in a fault block, we should expect that some pre-Pennsylvanian carbonates might also be represented in the resulting limestone conglomerate. None of these carbonates seems to be pre-Pennsylvanian although Precambrian fragments are common. It seems much more probable that the limestone clasts were eroded from a nearby tectonically elevated block of Pennsylvanian rocks that directly overlie rocks of Precambrian age. The available information on the ease of destruction of carbonate rock during transport

indicates that the source of the limestone conglomerate was within 30 miles, and perhaps within no more than 10 miles, of the deposition site. This is further substantiated by the large size of some of the limestone boulders. These conclusions would support the postulated location of the area that Kottlowski (1962) indicated as having Pennsylvanian rocks that directly overlie Precambrian rocks.

Most of the rocks of Pennsylvanian age from which the limestone conglomerates were derived consist of skeletal micritic limestone and lesser quantities of varieties of skeletal limestone, both probably deposited in shelf environments. Most of the carbonate rocks are of Des Moines age, but some, perhaps as little as 20 percent, are of Virgil age. Rocks of Missouri age may be present in the area, but, if so, may consist largely of noncarbonate clastic rocks.

REFERENCES

Foster, R. W., 1964, Stratigraphy and petroleum possibilities of Catron County, New Mexico: New Mexico Bur. Mines and Mineral Resources Bull. 85, 55 p.

Hayes, P. T., and Landis, E. R., 1965, Paleozoic stratigraphy of the southern part of the Mule Mountains, Arizona: U.S. Geol. Survey Bull. 1201–F, 43 p.

Hewitt, C. H., 1959, Geology and mineral deposits of the northern Big Burro Mountains–Redrock area, Grant County, New Mexico: New Mexico Bur. Mines and Mineral Resources Bull. 60, 151 p.

Kottlowski, F. E., 1960, Summary of Pennsylvanian sections in southwestern New Mexico and southeastern Arizona: New Mexico Bur. Mines and Mineral Resources Bull. 66, 187 p.

——1962, Pennsylvanian rocks of southwestern New Mexico and southeastern Arizona, *in* Branson, C. C., ed., Pennsylvanian System in the United States–A symposium: Am. Assoc. Petroleum Geologists, p. 331–371.

——1963, Paleozoic and Mesozoic strata of southwestern and south-central New Mexico: New Mexico Bur. Mines and Mineral Resources Bull. 79, 100 p.

——1965, Sedimentary basins of south-central and southwestern New Mexico: Am. Assoc. Petroleum Geologists Bull., v. 49, no. 11, p. 2120–2139.

Leighton, M. W., and Pendexter, C., 1962, Carbonate rock types, *in* Classification of carbonate rocks–A symposium: Am. Assoc. Petroleum Geologists Mem. 1, p. 33–61.

Lindgren, Waldemar, 1905, The copper deposits of the Clifton-Morenci district, Arizona: U.S. Geol. Survey Prof. Paper 43, 375 p.

Lokke, D. H., 1962, Paleontological reconnaissance of subsurface Pennsylvanian in southern Apache and Navajo Counties, Arizona, *in* Guidebook of the Mogollon Rim region, east-central Arizona, 13th Field Conf., 1962: New Mexico Bur. Mines and Mineral Resources, p. 84–86.

Pettijohn, F. J., 1957, Sedimentary rocks: New York, Harper & Bros., 718 p.

Plumley, W. J., 1948, Black Hills terrace gravels: A study in sediment transport: Jour. Geology, v. 56, no. 6, p. 526–577.

Ratté, J. C., Landis, E. R., Gaskill, D. L., and Raabe, R. G., 1969, Mineral resources of the Blue Range primitive area, Greenlee County, Arizona, and Catron County, New Mexico, *with a section on* Aeromagnetic interpretation, *by* G. P. Eaton: U.S. Geol. Survey Bull. 1261–E, 91 p.

Weber, R. H., and Willard, M. E., 1959, Reconnaissance geologic map of Reserve thirty-minute quadrangle: New Mexico Bur. Mines and Mineral Resources Geol. Map 12.

Wilson, E. D., and Moore, R. T., 1958, Geologic map of Graham and Greenlee Counties, Arizona: Tucson, Arizona Bur. Mines.

Wrucke, C. T., 1961, Paleozoic and Cenozoic rocks in the Alpine-Nutrioso area, Apache County, Arizona: U.S. Geol. Survey Bull. 1121–H, 26 p.

CHEMICAL WEATHERING AND GLACIAL EROSION OF CRYSTALLINE ROCKS AND THE ORIGIN OF TILL

By TOMAS FEININGER, Quito, Ecuador

Abstract.—Preglacial rock weathering, considered of fundamental importance to glacial processes by some early workers, has been largely ignored or even specifically excluded by modern glacial geologists. This view is here held to be erroneous.

Prior to Pleistocene glaciation, a virtually uninterrupted mantle of weathered rock overlay crystalline rocks in all but perhaps the most polar regions of the Northern Hemisphere. Remnants of this mantle are numerous. Relationships between the topographic surface and the fresh rock surface at the base of the weathered mantle on crystalline rocks in Colombia, South America, are used to support the argument that the erosion of crystalline rocks by continental ice sheets is largely limited to the weathered rock mantle. Corroborative evidence is afforded by the following observations: (1) In areas of little local relief, thin till-bedrock topography of glaciated terrains is virtually identical with the fresh rock surface under the weathered rock mantle in nonglaciated terrains. (2) Topography of glaciated and nonglaciated areas of great local relief is very similar. (3) Glacial boulders were present as residual boulders in the weathered rock mantle prior to glaciation and are not evidence of glacial erosion of fresh rock.

Till on crystalline rocks is here considered to be practically an in situ deposit formed from the weathered rock mantle through flushing by subglacial water concurrent with mechanical churning and only local transport by the overriding ice sheet. Flushing will produce a mineralogically fresher and coarser grained material as it preferentially removes the finer sized fractions of the mantle which include the minerals of decomposition.

More than 70 years ago, after studying occurrences of chemically weathered rock in southeastern Canada, Robert Chalmers, of the Geological Survey of Canada, wrote (Chalmers, 1898, p. 280):

> During the glacial period this decayed rock furnished the principal portion of the material constituting the bowlder-clay.

Nearly 20 years later, after a long geological study of most of southern New England, B. K. Emerson (1917, p. 135) came to a similar conclusion:

> As the climate became more severe the thick water-soaked layer of rotted rock which had come to form the surface became frozen, and as the snow accumulation increased and became glacial ice, perhaps a mile thick over New England, the whole ultimately moved forward and the softened rock layer became the first and principal source of the till.

These are perhaps the only published statements on glacial erosion that ascribe a major role to preglacial rock weathering. More recently, glacial geologists have chosen to assign only a trivial role to, or to ignore or even specifically to exclude from consideration, the influence of preglacial rock weathering on glacial erosion or the formation of till.

The purpose of this report is to document the probably fundamental influence of preglacial rock weathering on glacial erosion and on the formation of till by continental ice sheets in areas of crystalline rocks. The restriction to crystalline rocks is invoked for the following reasons: (1) Most crystalline rocks, unlike most sedimentary rocks, are composed chiefly of minerals not in equilibrium with near-surface conditions. The decomposition of these rocks produces a heterogeneous mantle of weathered rock that can be related to glacial deposits by simple field inspection. (2) Considerably more information is available on the weathering of crystalline rocks than on the weathering of sedimentary rocks. (3) A mature stream-carved topography with a great range of local relief had been developed on immense areas of crystalline rocks in the Northern Hemisphere prior to Pleistocene glaciation. This is less true of the sedimentary rocks. For example, hundreds of thousands of square kilometers of nearly flat-lying sedimentary rocks in the interior northern United States and Canada, western U.S.S.R., Poland, Denmark, and the Baltic countries, had only negligible local topographic relief prior to glaciation. As will be shown, the influence of preglacial rock weathering on glacial erosion can be evaluated successfully only in areas where local relief is greater than in these regions.

Much of the present paper is based on a broad range of personal field observations, principally in Rhode Island and Connecticut during the mapping of glacial deposits and in nonglaciated areas of Colombia, South America. Quantitative data are provided by more than 140 boreholes in and through the weathered rock mantle in northern Colombia (fig. 1).

Acknowledgments.—Detailed topographic maps and logs of boreholes from two sites in Colombia were kindly made available to me by the engineering firm Integral, Ltda., Medellín, with the generous permission of Empresas Públicas de Medellín. Without the ample and patient cooperation of the staff of Integral, and especially Ing. Pablo Bravo, this study could not have been realized. I also wish to thank Clifford A.

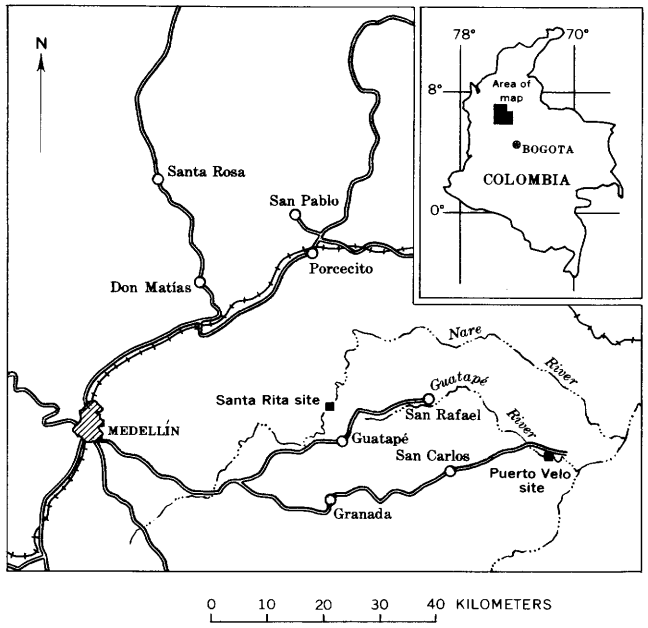

Figure 1.—Index map of localities in Colombia referred to in the text.

Kaye, U.S. Geological Survey, for continuing and enthusiastic encouragement.

CHEMICAL WEATHERING OF CRYSTALLINE ROCKS

General Statement

A humid temperate or tropical climate causes the chemical weathering of crystalline rocks at and near the earth's surface. This weathering comprises a series of complex and interrelated chemical reactions, such as hydration, oxidation, leaching, cation exchange, and solution, that act on rock-forming minerals. Many of these reactions are accompanied by volume increases that cause mechanical disaggregation. Weathering takes place in the vadose and phreatic zones, whose temperatures approximate the average annual air temperature at the site. The chemical reactions of weathering are started by downward-percolating water and are probably hastened by dissolved organic acids derived from the decay of vegetation. With time, a surficial weathered rock mantle that consists of decomposed rock as well as remnants of fresh rock is produced. The uppermost meter or two of this mantle is churned by colluvial processes, root action, windthrown trees, burrowing animals, and in temperate regions by frost. In areas of relatively little local relief (150 m or less), the texture and structure of the parent rock commonly is preserved in the weathered rock mantle below the churned layer. In areas of great local relief, however, much or all of the weathered rock mantle generally has been disturbed drastically by creep and landsliding.

The depth to which weathering will take place (the thickness of the weathered rock mantle) depends on such factors as time, climate, tectonic activity, topography, the rate of erosion, and the type of bedrock. On the stable Brazilian shield, for example, Branner (1896, p. 256–265) reported that the thickness of the weathered rock mantle on granite, gneiss, and schist ranged from 15 to 120 m. In the tectonically active Colombian Andes, drilling (discussed in detail below) revealed quartz diorite and similar rocks to be weathered to depths of more than 90 m, although the average is less. The ultimate depth of weathering may be that depth at which lithostatic pressure is sufficient to make the rock impermeable or so tight as to effectively arrest the circulation of water through it.

Weathering of Schistose and Gneissic Rocks

Such common foliated or laminated crystalline rocks as phyllite, schist, micaceous gneiss, gneissic igneous rocks, and layered or schistose amphibolite undergo a pervasive decomposition. The innumerable foliation planes and laminae of these rocks afford closely spaced conduits through which water circulates relatively easily and decomposes the rock in its entirety. Only near the base of the weathered rock mantle on these rock types are small remnants and rare residual boulders of fresh rock found.

Weathering of Massive Rocks

Relatively massive crystalline rocks such as weakly foliated or structureless igneous rocks, mica-poor gneiss and migmatite, and massive amphibolite undergo a unique decomposition (Wilhelmy, 1958). These rocks lack closely spaced foliation planes or laminae and are therefore not subject to pervasive decomposition. Instead, underground water acts on these rocks only along joints and fractures. Where these intersect, the specific surface is greater, and decomposition is more rapid (Chapman and Greenfield, 1949, p. 427). Thus, initially angular joint-bounded rock masses are reduced in size and made into subrounded or rounded boulders (fig. 2; for an earlier description, see Branner, 1896, p. 264–280). Many such residual boulders of felsic to intermediate igneous rocks are surrounded by mechanically separable concentric shells of partly decomposed rock a few centimeters thick. From the nuclear boulder outward, the rock of successive shells is increasingly decomposed and disaggregated (figs. 2, 3; Wilhelmy, 1958, figs. 10, 13, 74). The shells, or nuclear boulders of fresh rock where shells are absent, are abruptly succeeded by clayey saprolite (fig. 4).

The size and abundance of the residual boulders increase with depth in the weathered rock mantle. Primary control over these factors, however, is exercised by joint density. Rock that is closely jointed or intensely fractured will leave few boulders, all small, in the weathered rock mantle. Broadly jointed rock, on the other hand, will yield large boulders. Examples from

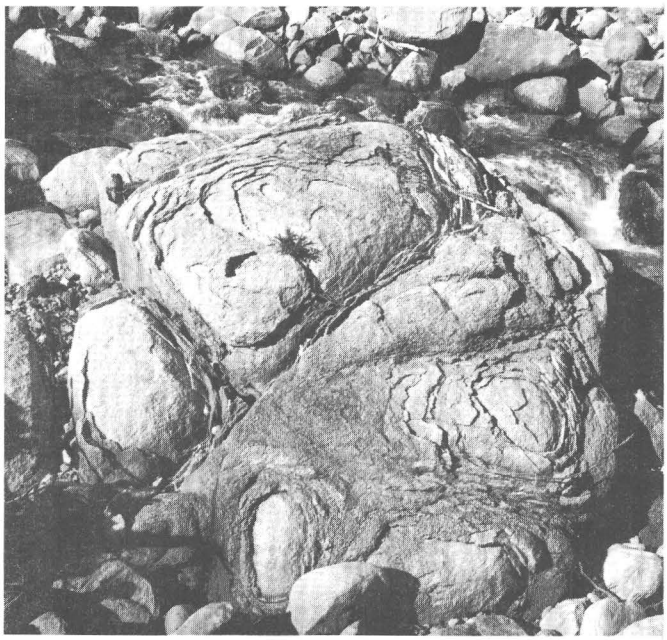

Figure 2.—Outcrop of massive quartz diorite. Four meters of overlying weathered rock mantle was removed by a flash flood in June 1967. Rounded masses of fresh rock are surrounded by shells of partly decomposed rock and bounded by joints. Revolver gives scale. Quebrada La Clara near Porcecito, 55 km airline northeast of Medellín, Colombia.

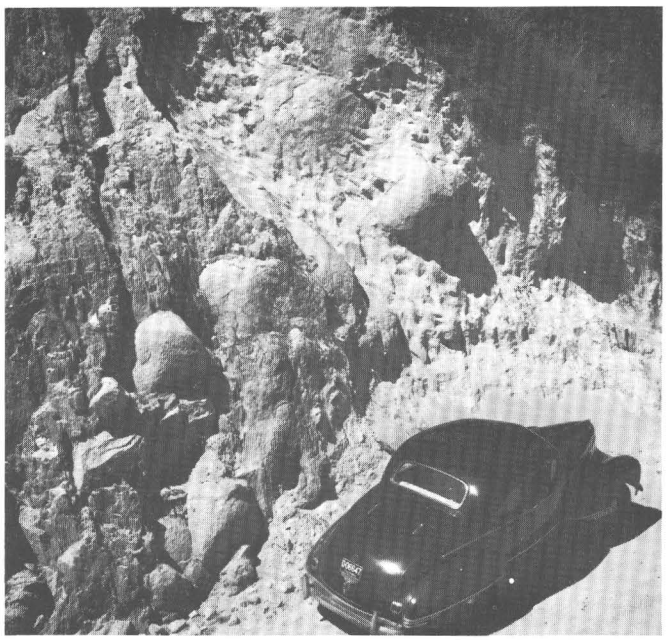

Figure 4.—Highly rounded residual boulders of fresh quartz diorite with weakly developed shells of partly decomposed rock in clayey saprolite. Cut in road between Porcecito and San Pablo, 50 km airline northeast of Medellín, Colombia.

Figure 3.—Outcrop of massive quartz diorite. Residual boulders of fresh rock in lenslike masses are surrounded by shells of partly decomposed rock. Structural control of decomposition is subhorizontal sheeting. Saprolite above uppermost lens perfectly preserves the texture of the quartz diorite. Note that some boulders are angular where they have parted along weakly developed joints subsequent to most of the weathering. Roadcut near Don Matías, 35 km airline northeast of Medellín, Colombia.

Colombia, as well as the worldwide examples figured by Wilhelmy (1958), show that most residual boulders of fresh rock have maximum dimensions between 0.5 and 6 m, although some exceptional boulders with long dimensions in excess of 20 m are found.

Because the rate of erosion of the weathered rock mantle commonly is greater than the rate at which chemical weathering can destroy the residual boulders beneath the ground surface, the boulders become exposed. Such surficial boulders are conspicuous features of many landscapes developed on massive crystalline rocks in humid climates (fig. 5; Wilhelmy, 1958, figs. 13, 16, 66, 67, 80). In Brazil, for example, the profusion of surficial boulders of granite and gneiss led Louis Agassiz more than a century ago to the erroneous conclusion that the area around Río de Janeiro had been glaciated (*in* Branner, 1896, p. 277).

Surficial residual boulders become concentrated in gullies and stream valleys chiefly because of creep and landsliding, but possibly also because they have been undermined by erosion and subsequently rolled downslope (Wilhelmy, 1958, p. 20; Botero A., 1963, p. 34–35).

Some Relationships Between Topography and the Fresh-Rock Surface

The relationship between the topographic surface and the fresh-rock surface that underlies the weathered rock mantle generally is known only where fresh rock crops out; here the two surfaces coincide. In humid temperate or tropical climates this occurrence is normally restricted to streambeds, although, in areas of great local relief, fresh rock may crop out on precipitous slopes as well.

Recently, an intensive program of borings was undertaken during construction of a series of hydroelectric projects in the Colombian Andes east of the city of Medellín. The results of these borings afford a nearly unique opportunity to assess qualitatively the relationship between the topographic and fresh-rock surfaces at two sites on crystalline rocks. Of 145 borings put down, 123 reached and cored several meters of fresh rock each.

The two sites bored are at Santa Rita (figs. 1, 6*A*, 6*B*), near the town of Guatapé, and at Puerto Velo (figs. 1, 7), near the town of San Carlos. Geologic, topographic, climatic, and borehole data for each site are summarized in table 1.

An unexpected discovery that resulted from the borings was that the transition from weathered to fresh rock, at what is here called the fresh rock surface, is surprisingly abrupt and in most borings can be picked within a meter or two. The identical observation was made by Thomas (1966, p. 177 and pl. 3) on the crystalline rocks of Nigeria. Rock just above the fresh rock surface at Santa Rita and Puerto Velo is described in the logs as stained, fractured, or fresh with numerous seams of clay. Core recovery in these materials ranged mostly from 40 to 75 percent. Rock at or below this surface is described as fresh, and core recovery was nearly everywhere more than 90 percent. Borings at the Santa Rita site were so closely spaced that it was possible to prepare a contour map of the fresh rock surface over an appreciable area (fig. 6*B*).

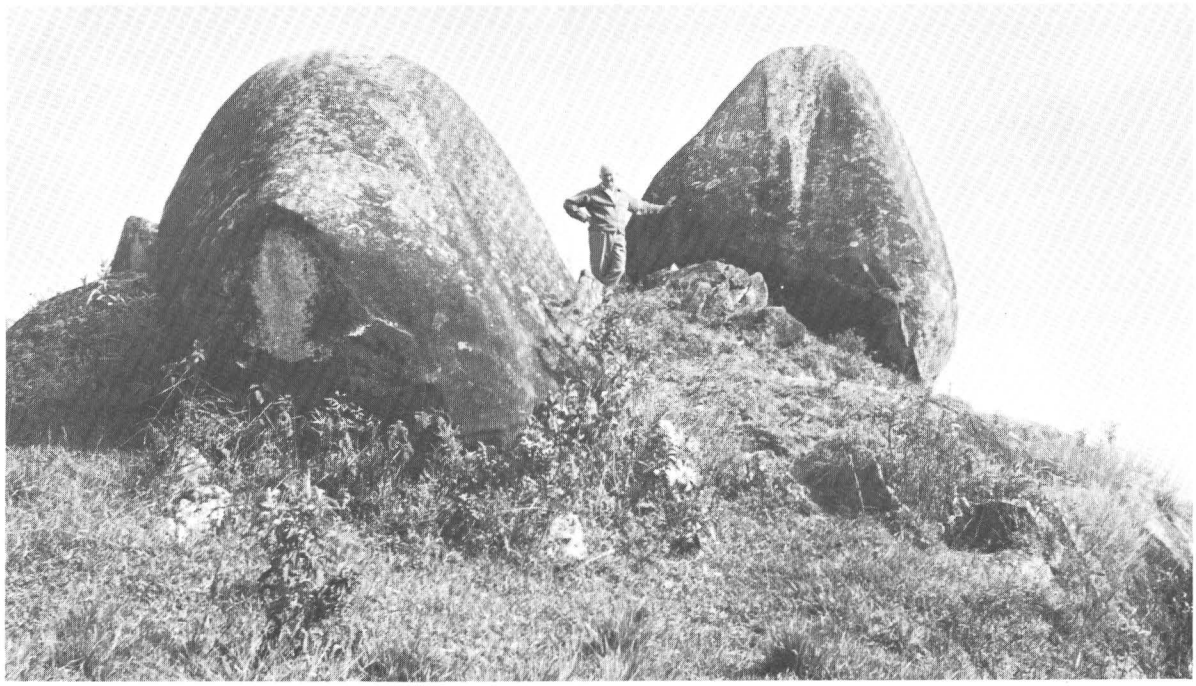

Figure 5.—Surficial residual boulders of fresh quartz diorite. South of Don Matías, 30 km airline northeast of Medellín, Colombia.

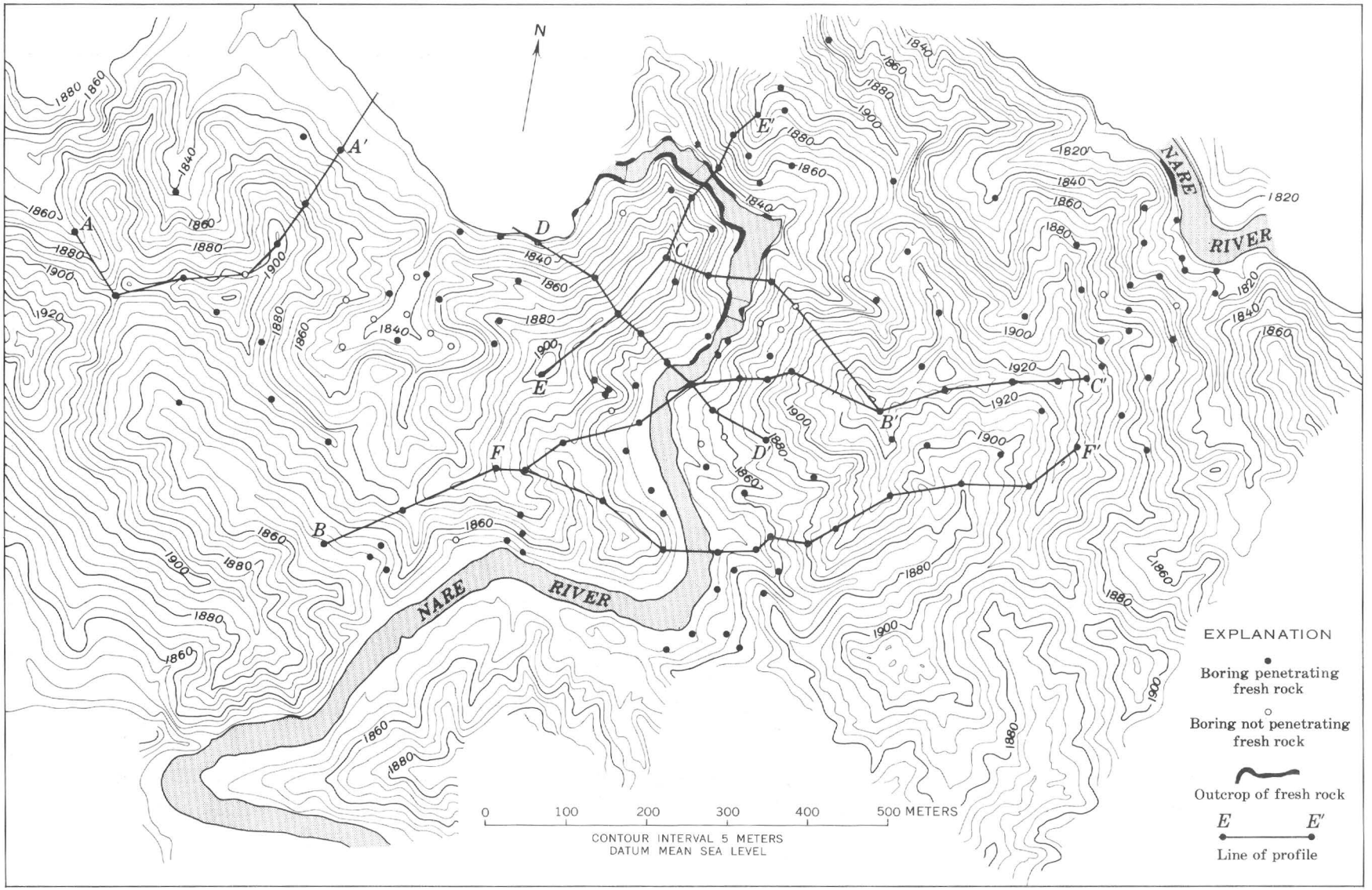

Base modified from a map made especially for Empresas Públicas de Medellín by the Instituto Geográfico "Agustin Codazzi," Bogotá, Colombia

Figure 6*A*.—Topography at the Santa Rita site, Colombia. Fresh rock surface and profiles are shown on figure 6*B*.


N
A
A′
B
B′
C
C′
D
D′
E
E′
F
F′
NARE RIVER
NARE RIVER
1800
1805
1810
1820
1830
1840
1850
1860
1880
1900
0 100 200 300 400 500 METERS
EXPLANATION
1840
Contours on fresh rock surface
Contour interval 5 meters; datum is mean sea level
Boring penetrating fresh rock
Boring not penetrating fresh rock
B B′
Line of profile

Figure 6*B*.

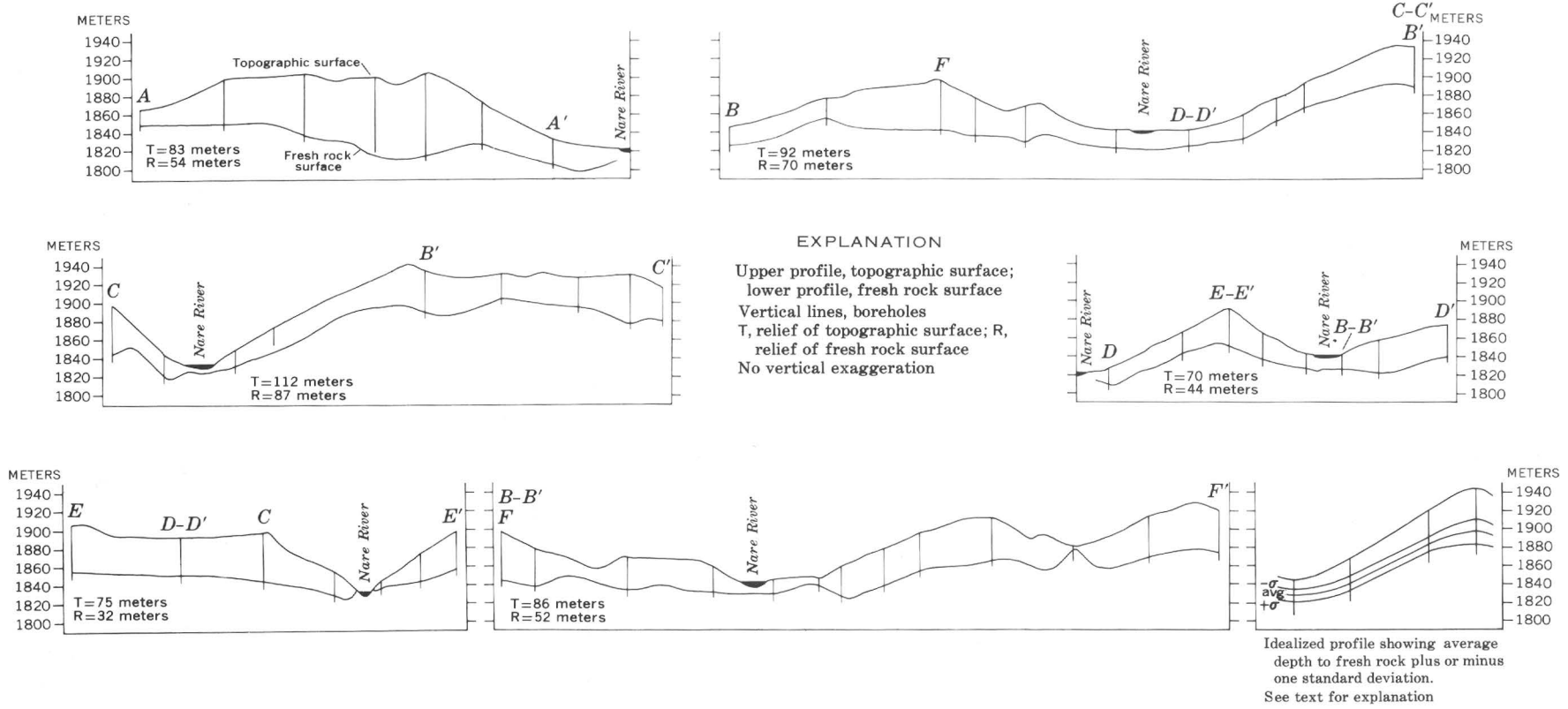

Figure 6*B*.—Fresh rock surface and profiles at the Santa Rita site, Colombia.

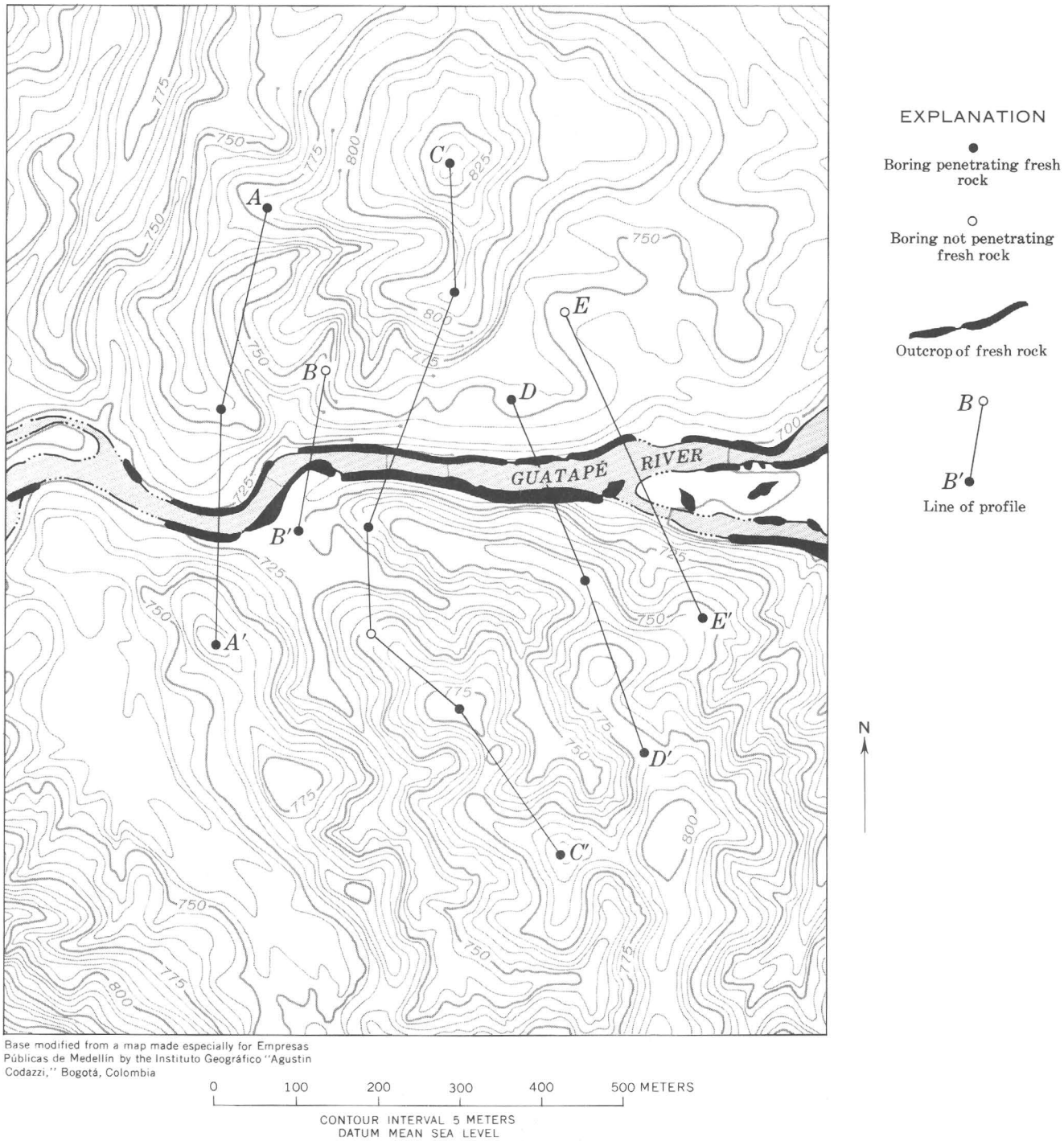

Figure 7.

On the following pages of this report, great weight will be given to the results of the borings, especially those at the Santa Rita site. The reader may rightly question the sagacity of this, as the sample is indeed small. However, in the absence of additional quantitative information, the relationships between topography and the fresh rock surface observed at the Santa Rita site are taken as broadly representative of such relationships elsewhere on crystalline rocks in humid climates for the following three reasons: (1) Information obtained from boreholes at the Puerto Velo site very closely duplicates that from the Santa Rita site, even though the two sites are underlain by somewhat different rock types and have quite dissimilar climates (table 1). (2) The relationships observed at the Santa Rita site are in accord with common simple field

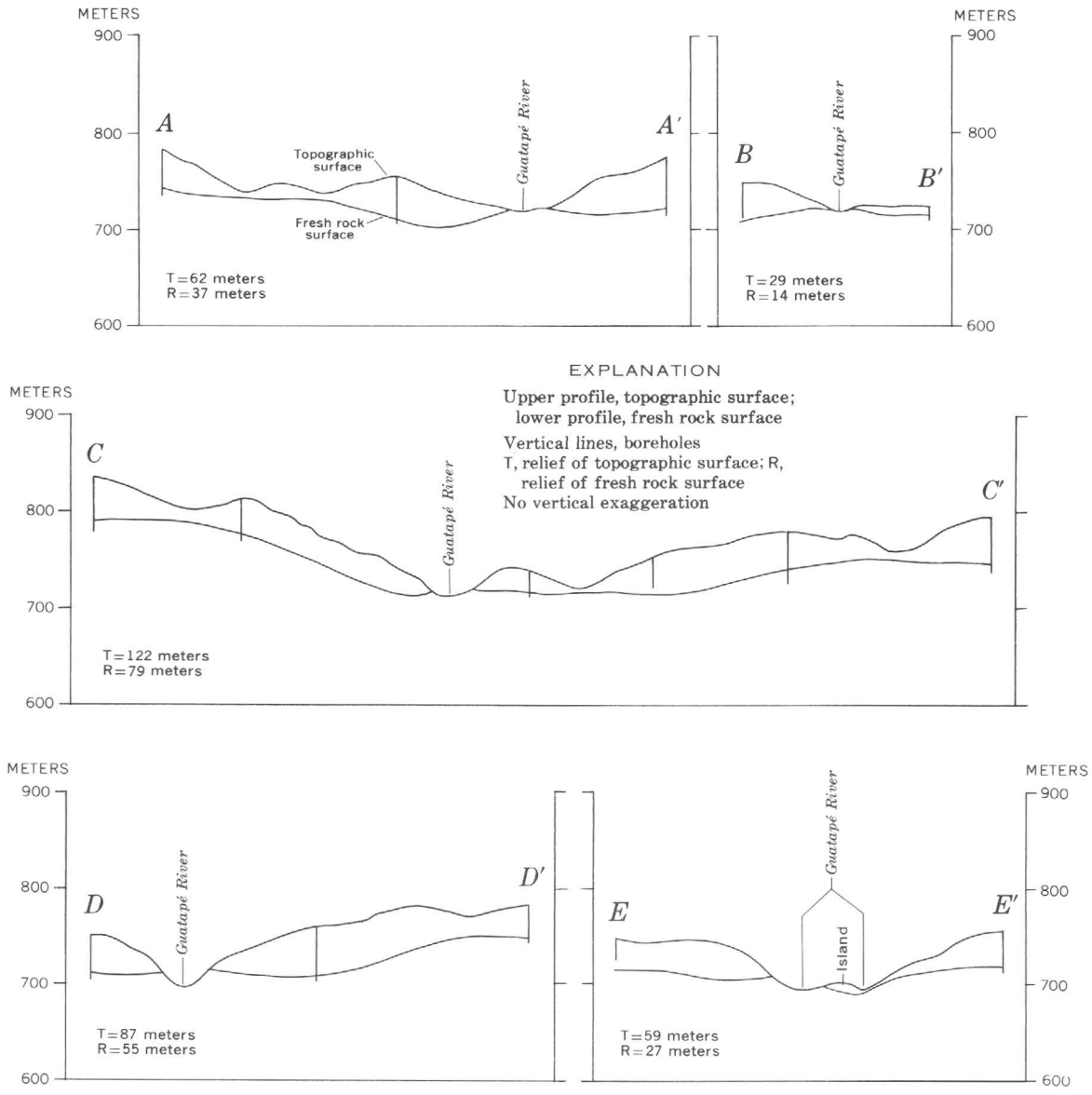

Figure 7.—Topography and profiles at the Puerto Velo site, Colombia.

observations, particularly that in the absence of rocks of unusual resistance to weathering and erosion, outcrops of fresh crystalline rocks in nonglaciated areas of little local relief under humid climates are normally restricted to streambeds. (3) Many of the apparent vagaries of erosion by continental ice sheets, a subject that will occupy the second half of this report, can be explained in a logical manner if crystalline rocks prior to Pleistocene glaciation were overlain by a weathered rock mantle similar to that studied at the Santa Rita site.

Thickness of the weathered rock mantle

Field observations referred to above suggest that the thickness of the weathered rock mantle is greater on hilltops or ridges, where outcrops of fresh rock are scarcest (fig. 8), than in valley bottoms, where fresh rock commonly crops out (fig. 9).

Quantitative information from borings at both the Santa Rita and Puerto Velo sites confirms this difference and, furthermore, shows that the vertical thickness of the weathered rock mantle decreases progressively and remarkably uniformly downslope from a maximum on hilltops and ridges to a minimum in valley bottoms (table 2). These data for the Santa Rita site are shown graphically (figs. 6*A*, 6*B*) with their respective standard deviations for each of the four topographic locations chosen in an idealized profile.

The reverse of the above relationship may occur in areas of great local relief, where mass wasting of the weathered rock mantle may locally fill valleys with thick colluvial deposits.

Table 1.—*Santa Rita and Puerto Velo sites east of Medellín, Colombia—Geologic, topographic, climatic, and borehole data*

	Santa Rita site	Puerto Velo site
Bedrock	Quartz diorite, hornblende diorite, inclusions of amphibolite.	Quartz diorite.
Mean elevation	1,890 m	750 m
Local relief	125 m	135 m
Mean annual air temperature.	[1]17°C	[1]27°C
Mean annual rainfall.	[2]495 cm	[1]250 cm
Number of borings	129	16
Number of borings to fresh rock.	110	13

[1] Estimated.
[2] Unpublished data, Empresas Públicas de Medellín.

Table 2.—*Average vertical thickness of the weathered rock mantle at the Santa Rita and Puerto Velo sites, east of Medellín, Colombia*

	Santa Rita site			Puerto Velo site	
Topographic location	Average vertical thickness (meters)	Standard deviation (meters)	Number of borings	Average vertical thickness (meters)	Number of borings
Hilltop and ridge	46	13.5	28	45	9
Upper half of slope	36	8.0	27	43	1
Lower half of slope	26	8.0	47	31	2
Valley bottom	17	7.5	27	10	1
All	31	14.0	129	40	13

Relief

A corollary of the preceding observations is that, in areas of little local relief, the relief of the fresh rock surface is generally considerably less than that of the topography on the overlying weathered rock mantle. For example, the relief of the fresh rock surface ranges from 43 to 78 percent of the relief of the topography along the 11 profiles drawn from borehole data at

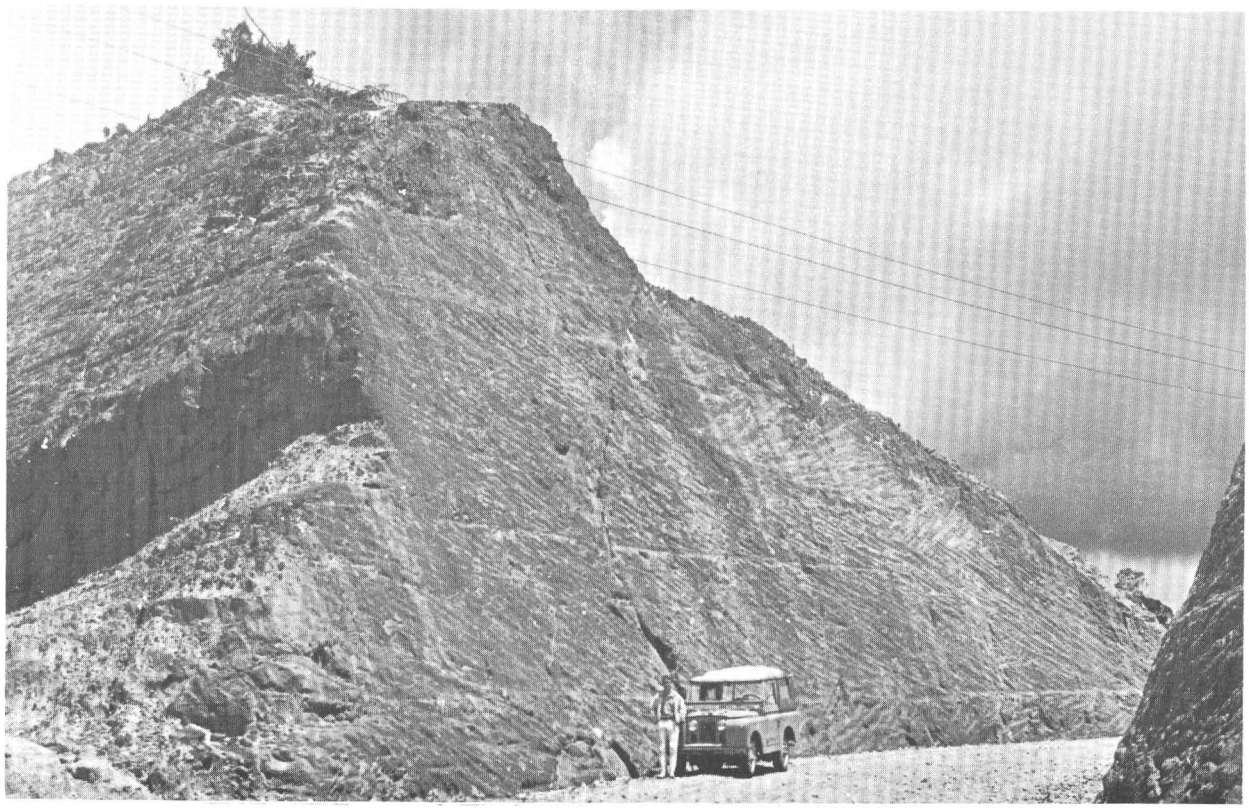

Figure 8.—Cut 12 m deep through a ridge on the access road to the Santa Rita site, Colombia. Quartz diorite bedrock is entirely decomposed.

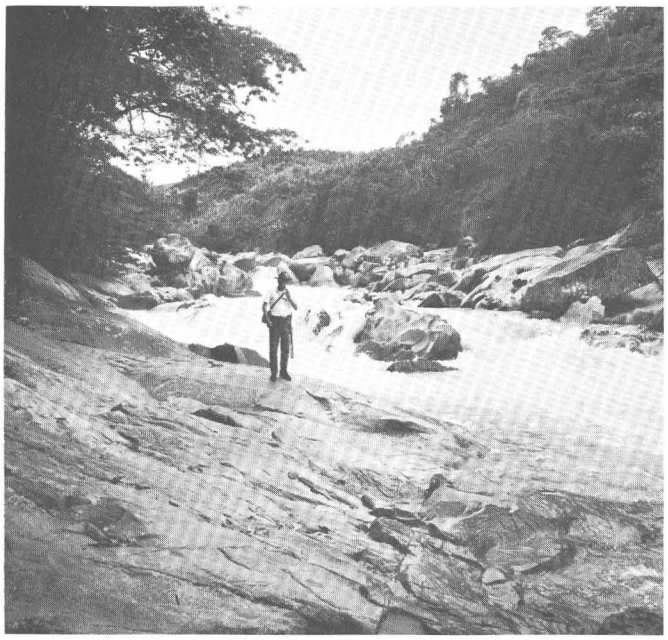

Figure 9.—Uninterrupted outcrops of fresh quartz diorite along both banks of the Guatapé River at the Puerto Velo site. Man stands on the south bank at the intersection of profile line $C–C'$ of figure 7.

the Santa Rita and Puerto Velo sites (figs. 6*A*, 6*B*, 7). Along three of the profiles (figs. 6*A* and 6*B*, $E–E'$; fig. 7, $B–B'$, $E–E'$) the relief of the fresh rock surface is less than half the relief of the overlying topography.

Slopes

In humid temperate or tropical climates, the range of slope angles is restricted by a combination of dynamic processes acting chiefly at or near the surface of the weathered rock mantle. These processes include erosion by sheet wash and gullying, mass wasting by creep and landsliding, and, in temperate climates, frost action. With time, these processes produce an equilibrium topography. For example, in areas of little to moderate local relief (100–300 m) underlain by rocks without unduly large contrasts of resistance to weathering and erosion, slopes steeper than a limiting value (usually about 35° or 40°) are unstable, and their angles will be reduced by creep and landsliding of the weathered rock mantle. On the other hand, long gentle slopes will be subject to gullying and thus be dissected to a complex of shorter and steeper slopes.

The dynamic processes that determine the form and steepness of slopes on the topographic surface do not affect the fresh rock surface, which develops under mechanically static conditions. Accordingly, slopes can form that are either steeper or more gentle than those of the overlying topographic surface. In general, owing to the greater depth of weathering on hilltops than in valley bottoms, slopes on the fresh rock surface will be more gentle than those on the overlying topography (see idealized profile on fig. 6*B*). This relationship is evident at the Santa Rita site through examination of figures 6*A* and 6*B*.

Closed depressions

Natural closed depressions in nonglaciated regions, unless they are products of volcanic action, faulting, differential solution of carbonate rocks, or mass wasting, are so rare as to command attention in the literature (LeGrand, 1952; Reed and others, 1963; Wright, 1964; Feininger, 1969). Once formed, most closed depressions are relatively quickly filled with sediments or vegetable matter.

On the other hand, the fresh rock surface, formed by in situ chemical weathering, could be expected to support numerous closed depressions. It is not surprising, therefore, to find no less than a half dozen closed depressions on the fresh rock surface in an area as small as the Santa Rita site (fig. 6*B*). Some of the depressions have closures greater than 10 m.

Valleys

Stream valleys obviously will be sharply reflected on the fresh rock surface in areas of great local relief where the thickness of the weathered rock mantle is small compared with the vertical distance between hilltops and valley bottoms. In areas of little to moderate local relief, however, stream valleys may be reflected on the fresh rock surface only weakly if at all. This difference is due in part to the appreciable thickness of the weathered rock mantle relative to topographic relief, but especially to the increasing depth of weathering from valley bottoms to hilltops described above. Figures 6*A* and 6*B* show that the well-defined valley of the Nare River at the Santa Rita site is only vaguely reflected on the fresh rock surface and that no vestige of its gradient is preserved. Cross sections through the Puerto Velo site (fig. 7) show how the valley of the Guatapé River similarly is reflected only feebly on the fresh rock surface.

Inversions of topography

I have made the following field observation on a variety of crystalline rock types in the Colombian Andes under humid climates with average annual temperatures ranging from less than 15°C to nearly 30°C. Where mule trails follow streams and are cut deeply into decomposed rock through long use, the floors of the trails are locally at lower elevations than the surfaces of fresh rock outcrops in the immediately adjacent streams. The difference in elevation may be as much as 3 m. Divides of weathered rock separate the streams from the trails and keep the trails from being flooded. At places where the floors of the trails are well above stream level, the users of the trails breach the divides to allow the runoff of rain water.

The Puerto Velo site offers an example. A small suspension bridge for pack animals crosses the Guatapé River coincident

with profile line $A-A'$ (fig. 7). Each tower of the bridge stands on fresh quartz diorite which crops out at the river's edge like that shown in figure 9. The trail to the bridge from the north is cut deeply into the weathered rock mantle, and, at the north tower, the floor of the trail—in thoroughly decomposed quartz diorite—is flush with the fresh rock surface on which the tower stands. It is clear that here the fresh rock surface is at a lower elevation than on the adjacent riverside outcrop, a view reinforced by a boring 125 m north of the north tower (fig. 7, profile $A-A'$).

On the basis of both borehole data and field observation, it can be shown that some reaches of stream valleys that have floors of fresh rock in areas of little local relief will be reflected on the underlying fresh rock surface as ridges. In other words, a complete inversion between the topographic and fresh rock surfaces is locally attained. Similar observations have been made by Thomas (1966, figs. 8, 10) on crystalline rocks in Nigeria.

Pre-Pleistocene Weathered Rock Mantle in the Glaciated Northern Hemisphere

Central to the theme of the present report is the contention that, by the onset of Pleistocene glaciation, a thick weathered rock mantle had developed on crystalline rocks in all but possibly the most polar regions of the Northern Hemisphere. Considerable evidence is available from eastern North America to support this contention.

Deep weathering of crystalline rocks in nonglaciated southeastern North America needs no documentation. A thick and virtually uninterrupted weathered rock mantle overlies fresh rock in the Piedmont and Blue Ridge provinces and makes detailed mapping there difficult. This mantle extends to the very limits of continental glaciation, where an abrupt change takes place. North of the glacial limit, weathered rock is the exception rather than the rule. It is most likely that a weathered rock mantle, much like if not identical with that to the south, extended an unknown distance north of the glacial limit before the Pleistocene glaciation. Most of this mantle has been either removed or reconstituted and is not preserved for our inspection.

Evidence from New England and southeastern Canada

Even though New England and southeastern Canada have been overridden repeatedly by continental ice sheets (Kaye, 1964a, b), patches of preglacial weathered rock mantle are so widely distributed that it becomes difficult if not impossible to deny the former presence of a universal weathered rock mantle of appreciable thickness in these areas, and by inference elsewhere in the glaciated Northern Hemisphere. The improbability that these occurrences are of interglacial origin must be stressed from the outset. Chemical weathering of crystalline rocks must be a slow process, though quantitative studies are wanting. Probably hundreds of thousands of years are required to weather such rocks to depths of much more than a meter. Outcrops of crystalline rocks in New England and elsewhere, exposed since deglaciation about 10,000 years ago, rarely show effects of chemical decay beyond a surficial rind a few centimeters thick stained with brown oxides of iron. Relatively porous and chemically reactive lower Pleistocene tills in the interior United States have been weathered to depths of only 3 or 4 m during interglacial stages that lasted perhaps as long as 100,000 years (Flint, 1957, p. 212–213). Accordingly, it is most unlikely that the occurrences of deeply weathered crystalline rocks and related evidence from glaciated areas (reviewed briefly below) are records of interglacial weathering. Rather, they are sparse but incontestable records of a period of preglacial weathering many millions of years long.

In eastern Canada, Chalmers (1898, p. 276) noted remnants of deeply weathered rocks in Quebec, New Brunswick, Nova Scotia, Prince Edward Island, and the Magdalen Islands. He concluded (1898, p. 280):

> The occurrence of such extensive sheets of decomposed sedentary rock [in situ weathered rock mantle] in the region under consideration, much denuded as it may seem to be, points to the former existence of a universal mantle of this material overspreading the country everywhere in Tertiary and preceding ages.

Goldthwait and Kruger (1938, p. 1187, 1190–1194) found that in New Hampshire about 1 out of every 1,000 outcrops is chemically weathered, in places to depths as great as 20 feet (6 m). In till they found oddly shaped boulders which they felt had been produced by a long period of preglacial weathering (Goldthwait and Kruger, 1938, p. 1194, 1197). They concluded (1938, p. 1196):

> * * * occurrences of rotted rock in and under the drift are rare, yet some are so deep as to call for long weathering before the last glaciation.

The strongest evidence of the former presence of a preglacial weathered rock mantle is found in Massachusetts. Here Kaye (1967a) reported what is probably the thickest known remnant of preglacially weathered rock recognized in eastern North America. It is found on phyllite at Boston, and in places it is more than 300 feet (91 m) thick. Kaye (1967a, p. C172) concluded:

> The bulk of the evidence indicates that the kaolinization was produced by very deep weathering. If this surmise is correct, then the kaolinized rock found today represents merely the roots of a once extensive and thick lateritic blanket that covered much, if not all, of the region.

In another paper, Kaye (1967b) described bauxite nodules in Kansan(?) drift on Martha's Vineyard. He interpreted the nodules as small samples of extensive areas of deeply weathered rock that existed to the northwest in New England prior to Pleistocene glaciation. Earlier, Tarr (1905, p. 166–168) described remnants of preglacially weathered granite on Cape Ann, 50 km northeast of Boston.

Extensive areas of granite gneiss in Rhode Island are overlain by a preglacial weathered rock mantle known locally as rottenstone. Many occurrences of rottenstone are shown on

published geologic maps of the U.S. Geological Survey's Geologic Quadrangle Map series. For example, in a single 7½-minute quadrangle astride the Rhode Island–Connecticut border, Schafer (1968) mapped no less than 39 exposures of "deeply disintegrated bedrock, weathered before last glaciation." One particularly well exposed occurrence near North Scituate in central Rhode Island has been described in detail by Birman (1952). The maximum thickness of the rottenstone at the site is unknown, but it exceeds 8 feet (2.4 m) (Birman, 1952, p. 722).

The brief review given above underlines the likelihood that a weathered rock mantle covered most, if not all, of New England and southeastern Canada prior to Pleistocene glaciation. Certainly the tectonic stability of the eastern North American Continent as well as its warm climate throughout the Tertiary would favor deep chemical weathering. The thickness of the preglacial weathered rock mantle cannot be measured directly, but as remnants 20 feet (6 m) thick are common even after repeated glaciations, and as at least one remnant exceeds 300 feet, an average thickness of more than 100 feet (more than 30 m) does not seem unreasonable.

GLACIAL EROSION OF CRYSTALLINE ROCKS

Statement of the Problem

Glacial erosion, particularly by continental ice sheets, has received surprisingly little attention from geologists. This is due in part to the difficult accessibility of existing continental ice sheets, and, of course, to the fact that the processes of glacial erosion take place at the bases of ice sheets, largely hidden from direct observation. Discussions of glacial erosion are therefore generally descriptive and qualitative.

Of the erosional features produced by continental ice sheets, only such small-scale features as the following on bedrock have been adequately studied: polished surfaces and striations, various crescentic markings, and quarried surfaces; and fluting on unconsolidated deposits (Flint, 1957, p. 56–66, 69–72). This is largely because most of these features are conspicuous in the field; in addition, they have been shown to be reliable indicators of the direction of ice-sheet movement and are therefore important guides to deciphering glacial geologic history.

Quantitative study of glacial erosion by continental ice sheets is hindered by the inapplicability of the law of uniformitarianism. The present is here not the key to the past because the first great ice sheets of the Pleistocene moved across a Northern Hemisphere landscape quite unlike that which is now exposed for study by geologists. It was a landscape covered nearly continuously by a mantle of weathered rock whose thickness varied greatly—from featheredges at outcrops in streambeds or on precipitous slopes in areas of great local relief, to tens or possibly even hundreds of meters on hilltops and ridges in areas of little local relief where the rate of erosion was slow. Today, only sporadic remnants of this mantle are preserved in glaciated areas, and, where it once overlay rocks now covered by ice, the mantle has long since been either removed or entirely reconstituted by that ice.

Erosion by Continental Ice Sheets

A view held by many geologists is that continental ice sheets have enormous erosive power and profoundly change landscapes by wholesale abrading and quarrying of fresh rock. This view is here challenged. Instead, I suggest that on crystalline terrains erosion of fresh rock by continental ice sheets is generally negligible. Modifications imposed on the preglacial landscape by ice sheets were largely limited to the weathered rock mantle that covered all but possibly the most polar regions of the Northern Hemisphere before the Pleistocene. Direct evidence to support this view is afforded by the largest and most active existing ice sheets, those of Greenland and Antarctica, which are transporting only negligible quantities of rock waste to their margins (Flint, 1957, p. 88). Other compelling although indirect evidence of the general ineffectiveness of continental ice sheets in eroding fresh crystalline rock, as well as the special circumstances under which ice sheets deeply erode fresh rock, are discussed below.

Areas of little local relief

The glacial geologist who has mapped in or is familiar with thin till-bedrock terrains in areas of little local relief, such as on the crystalline rocks of southern Sweden, the Canadian shield, or southern New England, must at once be struck by the similiarity between the topography of those regions and the fresh rock surface at the Santa Rita site (fig. 6*B*). Both are characterized by great ranges of slope angles and lengths. Valleys do not have uniform gradients, nor are they at grade with one another. The fresh rock surface at the Santa Rita site, if subaerially exposed, would be drained by a highly deranged network of nongraded streams typical of glaciated regions that have little local relief. The only fundamental difference between the fresh rock surface at Santa Rita and the topography of thin till-bedrock terrains of comparable local relief is the presence of numerous closed depressions at Santa Rita. However, thin till-bedrock terrains are characterized by areally extensive swamps and other postglacial deposits, many of which probably fill closed depressions on bedrock. Furthermore, borings in till commonly reveal closed depressions in the underlying bedrock floor (see for example, Crosby, 1945, p. 396–397).

These observations are consistent with the view that the highly modified topography of glaciated regions that have little local relief can be developed as the result of little if any glacial erosion of fresh rock. Simply the partial or complete removal, by a continental ice sheet, of the weathered mantle overlying fresh crystalline rock would be adequate to produce a landscape commonly considered the product of deep erosion of fresh rock by glacial ice.

Areas of great local relief

The greatest depths of chemical weathering probably rarely exceed 100 m. In areas of great local relief where erosion is relatively rapid, these depths are considerably less and are quantitatively small relative to vertical distances between hilltops and valley floors. Accordingly, if, as is here postulated, erosion of crystalline rocks by continental ice sheets is normally restricted to the weathered rock mantle, the topography of crystalline terrains of great local relief that have been overriden by ice sheets should differ but little from those that have not been glaciated. This indeed is the case. Excluding glaciofluvial deposits confined generally to the larger valleys of the glaciated terrains, the topography of glaciated and nonglaciated terrains of great local relief is virtually identical. These terrains can be distinguished from one another on topographic maps only with difficulty, if at all. To see this, it is only necessary to compare a topographic quadrangle map from the Green Mountains of Vermont, for example, with a map at the same scale from an area of similar local relief in the Blue Ridge or Great Smoky Mountains of Virginia or Tennessee. It is hard to reconcile this observation with the view that continental ice sheets deeply erode fresh crystalline rock.

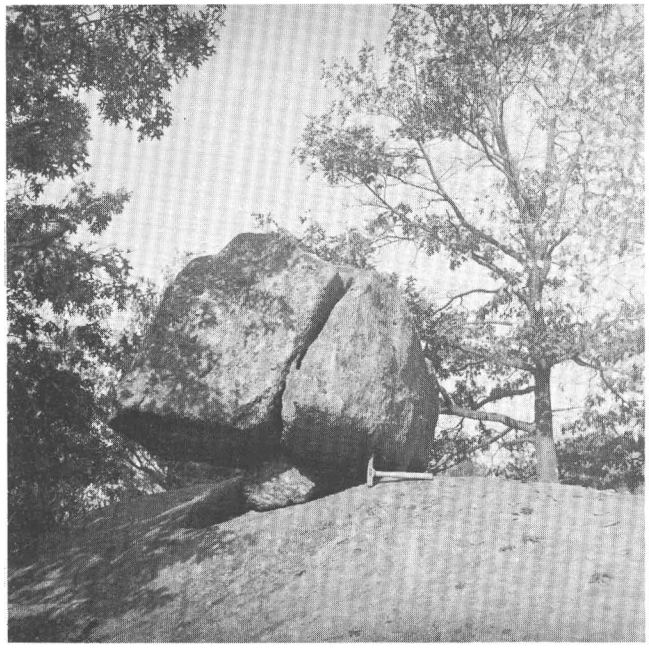

Figure 10.—Perched glacial boulder. Both boulder and bedrock are gneiss at Escoheag Hill (Feininger, 1965), a distinctive rock type that forms an isolated small pluton 5 km^2 in area. Hammer handle is 40 cm long. Escoheag Hill, 27 km north-northeast of Westerly, R.I. Compare with figures 4 and 5.

Glacial boulders

Although some glacial boulders have been transported tens or even hundreds of kilometers (Flint, 1957, p. 122–129), it is the common experience of glacial geologists to find that boulders in ordinary ground moraine generally have been derived from very local sources. Indeed, where boulders are perched on outcrops, boulder and outcrop commonly are of the same rock type (fig. 10). The short distance of transport of most glacial boulders in ground-moraine deposits suggests that these tills may have undergone less transportation than is generally conceded. This point will be examined further later in this report.

The commonly accepted origin of glacial boulders is that they have been quarried by moving ice from outcrops of fresh rock (Flint, 1957, p. 128). That some rock types (intrusive igneous rocks, mica-poor gneiss, and so forth) are more abundantly represented than others (schist, phyllite, and so forth) is attributed to the preferential attrition during transport of the latter rock types because of their relatively less mechanical resistance (Flint, 1957, p. 128).

Earlier it was shown that in all likelihood a thick mantle of weathered rock overlay crystalline rocks in most of the Northern Hemisphere prior to the Pleistocene. It was also shown, on the basis of the comprehensive study by Wilhelmy (1958) as well as personal field observations, that in humid climates the weathered rock mantle derived from such relatively massive crystalline rocks as intrusive igneous rocks and mica-poor gneiss contains a remarkable abundance of residual boulders of fresh rock. Conversely, schistose and gneissic crystalline rocks such as phyllite, schist, and others undergo a pervasive decomposition, and the weathered rock mantle derived from them contains few if any residual boulders of fresh rock. That the relative abundance of boulders of crystalline rock types derived by chemical weathering so closely mimics the relative abundance of rock types found as glacial boulders is here considered more than chance. Rather, it is held that although some glacial boulders may have been quarried from fresh rock, the overwhelming majority were available in and derived from the weathered rock mantle present at the onset of Pleistocene glaciation. The abundance of glacial boulders should therefore not be considered a measure of the amount of fresh rock eroded by an ice sheet. Rather, it is a rough measure of the thickness and boulder content of the preglacial weathered rock mantle.

It is commonly assumed that glacial boulders have undergone extensive attrition during subglacial or intraglacial transport (Flint, 1957, p. 128). The evidence to support this contention is that many glacial boulders are highly rounded (fig. 10), whereas joint-bounded glacially quarried blocks not subjected to attrition should be angular. However, this evidence loses its value if, as is here suggested, glacial boulders are chiefly reworked residual boulders from the preglacial weathered rock mantle. Most such boulders are rounded or subrounded (fig. 4; Wilhelmy, 1958, figs. 2, 10). Nonetheless, some residual boulders in the weathered rock mantle are subangular or even angular where they have parted along weakly developed joints after most of the chemical weathering has taken place (fig. 3). The presence of angular glacial

boulders, therefore, does not prove that glacial quarrying has occurred.

Deep glacial erosion of fresh rock

Mountain-valley or Alpine glaciers are able to erode large quantities of fresh rock. The spectacular cirques and U-shaped glacial valleys of the European Alps or the Canadian Rockies bear ample testimony to the efficiency of this erosion. Although continental ice sheets are here held incapable of eroding appreciable quantities of fresh crystalline rock, they may do so where they behave like Alpine glaciers. This will occur under two particular conditions.

The first is where axes of long, straight preglacial stream valleys parallel the direction of movement of a continental ice sheet (Flint, 1957, p. 83). Here the valleys effectively funnel a large volume of ice, which will move with greater freedom relative to adjacent ice on more random topography. Velocity of basal ice thus would be far higher in the valleys than on neighboring areas, and erosion of fresh rock, analogous to the erosion of fresh rock by Alpine glaciers, will result. Perhaps the two best known North American examples are in New York State: the Finger Lakes, in sedimentary rocks, and the Hudson River gorge, 50 km north of New York City, which is carved in granitic rock to a depth of nearly 1,000 feet (305 m) below sea level (Sanborn, 1950, p. 57–59).

The other condition under which a continental ice sheet can deeply erode fresh rock is where the ice sheet caps highlands and spills abruptly to much lower ground. The classic examples are the fiord terrains of Norway, East Greenland, and Chile. Here the ice, flowing off highlands that rise abruptly from the sea, preferentially followed initially small seaward-draining stream valleys, which funnelled relatively large volumes of ice under conditions similar to those outlined in the preceding paragraph.

THE ORIGIN OF TILL ON CRYSTALLINE ROCKS

Some of the conclusions drawn on the preceding pages have direct and important implications for the origin of till on crystalline rocks, and for that reason they are briefly reviewed here. It should be kept in mind, however, that what follows is conjectural and remains unproven. Nevertheless, the theory on the origin of till offered in the following paragraphs more adequately accounts for the morphology of glaciated crystalline-rock terrains and better explains the lithologic distribution and generally local transport of glacial boulders than do currently held theories. In addition, the proposed theory stresses a continuity rather than a hiatus between glaciated and nonglaciated country.

Till is generally considered to be produced chiefly through the abrasion and quarrying of fresh bedrock by glacial ice. For example, Flint (1957, p. 109–110) says:

> Drift, whether stratified or not, consists predominantly of rock material that was fresh and undecomposed before it was deposited. Minerals like the hornblendes, micas, and plagioclase feldspars, notably susceptible to chemical decay, are conspicuous in drift derived from rocks that contain these minerals. Most of the rock fragments in drift are mechanically broken or abraded. All this means that for the most part the glaciers were eating into fresh rock rather than the altered mantle. Chemical freshness characterizes the earlier glacial deposits as well as the later ones. The inference is plain that decomposed mantle did not contribute importantly to drift; the ice early got down below the weathered zone into the firmer rock beneath.

Or (Flint, 1957, p. 128):

> New England granites were glacially quarried along joints to produce boulders; boulders in transit were crushed and disaggregated into their component grains; this is the origin of much of the sand-size fraction in New England till.

If the erosive power of continental ice sheets is as limited as I have suggested, then the most likely source of till derived from crystalline rocks is not fresh bedrock, but the weathered rock mantle first encountered by the advancing ice sheets.

The principal argument mustered to support the contention that the preglacial weathered rock mantle did not figure in the formation of till is the mineralogic freshness of till materials (Flint, 1957, p. 128). Although, by definition, the weathered rock mantle on crystalline rocks consists in large part of thoroughly decomposed material, it also contains a surprising abundance of fresh rock and mineral matter, especially at depth near the fresh rock surface. The most obvious fresh material is in the residual boulders. The shells of partly decomposed rock that surround many of these boulders (figs. 2, 3), as well as weakly coherent grus that is common just above the fresh rock surface, are composed chiefly of fresh mineral grains. The hard-rock geologist who has had to resort to such materials for petrographic study knows that they are entirely suitable for thin sections. Their decomposition, which may appear profound owing to mechanical weakness, is largely restricted to incipient disaggregation caused by minor hydration and other changes along grain boundaries or mineral cleavages. These slightly altered surfaces bound virtually fresh unaltered mineral grains. Even near the surface and at little depth in the weathered rock mantle, panning of saprolite from most crystalline rocks reveals an abundance of sand-size quartz and, where present in the parent rock, such relatively resistant minerals as chlorite, muscovite, magnetite, the aluminosilicates, and many others. The volume of fresh mineral matter in the weathered rock mantle clearly is appreciable and probably ranges from 10 to more than 50 percent of the whole. It alone is an adequate source for all till on crystalline rocks.

Earlier in this report, the nearness of most glacial boulders to their source was cited as evidence that glacial transport is generally short. Even stronger evidence to support this view can be read from the tills themselves. Where the direction of movement carried a continental ice sheet from one terrain to another of markedly different rock type, the tills derived from each terrain are predominantly restricted to the areas of their corresponding source rocks. An outstanding example is afforded by the contrasting Triassic red sedimentary rocks of the Connecticut Valley and the older crystalline rocks of the

adjacent New England highlands. The tills on the Triassic rocks are a distinctive dark red, while those on the crystalline rocks are gray to olive. Even though ice movement was across the contact of the two rocks at most places, nowhere has the till derived from one rock type been carried much more than a kilometer onto the other rock type. Broadly speaking, tills are in situ deposits, and this fact strongly suggests that the basal ice of continental ice sheets is relatively slow moving and inactive.

Some glacial boulders have been carried truly heroic distances—tens or even hundreds of kilometers (Flint, 1957, p. 76–77)—and show that some material, contrary to the above examples, is far traveled. These remarkable boulders were probably lifted by thrusts within the ice (Shumskii, 1964, p. 325) to higher and faster moving levels of the ice sheet. Once they got above the relatively inactive basal ice, long transport was possible.

It has long been known that no sharp division exists between till and stratified drift deposited by glacial melt water. The two are end members of a continuous spectrum of deposits (Flint, 1957, p. 109). Water is an active agent in the formation of many rudely stratified and locally sorted tills and, as will be shown below, may be a paramount agent in the formation of nearly all tills on crystalline rocks. In this regard, it is significant that abundant water is available at the bases of both cold and temperate glaciers (Shumskii, 1964, p. 355).

Any process proposed to account for the origin of till produced by continental ice sheets on crystalline rocks must satisfy the following statements: (1) Glacial erosion of fresh bedrock is negligible. (2) The average thickness of till on crystalline rocks (Flint, 1957, table 7-A) is considerably less than the probable thickness of the preglacial weathered rock mantle, as deduced from the thickness of remnants of this mantle in glaciated areas and its thickness beyond the glacial limit. (3) Till is practically an in situ deposit that has been transported only locally relative to the enormous distances traversed by some of the ice in continental ice sheets. (4) Water is an important agent in the formation of many tills.

Perhaps the only mechanism that can satisfy the four statements listed is the subglacial flushing by water of the weathered rock mantle. Such flushing would be particularly effective on the weathered rock mantle derived from crystalline rocks. This mantle is a heterogeneous mixture of materials that range from clay to boulders. On the other hand, the mantle on the most abundant sedimentary rocks, shale and siltstone, is clayey, homogeneous, and probably not prone to appreciable flushing owing to its impermeability. Disturbance of the poorly sorted mantle on crystalline rocks by overriding ice would continuously expose the finer grained fractions to entrainment by subglacial water passing through interstices between coarser grained particles. Fractions coarser than a threshold value would be retained because of the general filtering action of the weathered rock mantle undergoing glacial reworking and flushing. The threshold size would vary from place to place depending upon the coarseness of grain and sorting of the weathered rock mantle. A high threshold value would lead to a sandy till, whereas a low one, where only extremely fine material could escape, would lead to a silty or clayey till. The net result of this proposed flushing mechanism would be a thinning of the weathered rock mantle and an increase in its average grain size. In addition, as the minerals of decomposition in the mantle are all in the size range of clay or fine silt, flushing will produce a material greatly enriched in fresh rock and mineral matter which is mostly sand sized or coarser. Also, the red-brown color of the weathered rock mantle will be weakened or eliminated by flushing, as this coloring is imparted nearly entirely by iron oxide-stained clay particles; being among the finest grained constituents of the mantle, they are the most easily removed. Later glacial lacustrine clay deposits are generally gray, not brown, because by the time of formation of these deposits at the close of the glacial cycle, the brown-stained easily removed clays have been largely eliminated by flushing.

Further evidence that a flushing mechanism is probably fundamentally important in the formation of till is afforded by the superposition of tills of different glaciations on crystalline rocks. For example, where two superposed tills occur in New England, the overlying younger till is generally described as loose and sandy with respect to the underlying older till. This condition is the reverse of that which would be expected if the younger till were the product of abrasion through mechanical reworking of the older. By such a mechanism, younger tills should be successively finer grained owing to progressive comminution of the older deposits. The progressive increase of average grain size of the younger tills, however, is well explained by the proposed flushing mechanism. With successive glacial advances, earlier tills are reflushed to produce yet coarser tills.

Glacial transport of the flushed and mechanically churned weathered rock mantle (till), excluding that thrust into higher and more freely moving levels of the ice sheets, is relatively ineffective. Although till under and in the basal parts of the ice sheet is carried in the direction of ice movement, the irregular contours of the fresh rock surface (fig. 6*B*) restrict transport of till to short distances. Most of the transport is limited to the movement of till from highs to valleys and depressions on the fresh rock surface, sites from which the till is subject to little if any further transport. This limited movement has obvious economic implications. Till itself, rather than merely its contained clasts, would be a suitable material to be sampled in geochemical prospecting for hidden ore bodies.

CONCLUSIONS

1. Prior to the Pleistocene a virtually continuous mantle of weathered rock of appreciable thickness overlay the crystalline rocks of all but possibly the most polar regions of the Northern Hemisphere.

2. Erosion of crystalline rocks by continental ice sheets is restricted largely to the weathered mantle. Deep erosion of

fresh rock occurs only under special topographic circumstances where ice is funnelled and assumes the characteristics of an Alpine glacier.

3. The topography of landscapes on crystalline rocks glaciated by continental ice sheets is therefore largely determined by the distribution and thickness of the preglacial weathered rock mantle, and not by the supposed vagaries of glacial erosion of fresh rock.

4. Most glacial boulders were present as residual boulders in the preglacial weathered rock mantle and are not products of glacial quarrying or plucking.

5. Till formed from crystalline rocks by continental ice sheets is practically an in situ deposit produced through flushing of the preglacial weathered rock mantle by subglacial water. Long glacial transport is restricted to materials lifted to higher levels in the ice sheet, where movement is more rapid than in the relatively inactive basal ice.

REFERENCES

Birman, J. H., 1952, Pleistocene clastic dikes in weathered granite-gneiss, Rhode Island: Am. Jour. Sci., v. 250, no. 10, p. 721–734.

Botero A., Gerardo, 1963, Contribución al conocimiento de la geología de la zona central de Antioquia: Medellín, Colombia, Facultad Nacional de Minas Anales, no. 57, 101 p.

Branner, J. C., 1896, Decomposition of rocks in Brazil: Geol. Soc. America Bull., v. 7, no. 2, p. 255–314.

Chalmers, Robert, 1898, The pre-glacial decay of rocks in eastern Canada: Am. Jour. Sci., 4th ser., v. 5, p. 273–282.

Chapman, R. W., and Greenfield, M. A., 1949, Spheroidal weathering of igneous rocks: Am. Jour. Sci., v. 247, no. 6, p. 407–429.

Crosby, I. B., 1945, Glacial erosion and the buried Wyoming valley of Pennsylvania: Geol. Soc. America Bull., v. 56, no. 4, p. 389–400.

Emerson, B. K., 1917, Geology of Massachusetts and Rhode Island: U.S. Geol. Survey Bull. 597, 289 p.

Feininger, Tomas, 1965, Bedrock geologic map of the Voluntown quadrangle, New London County, Connecticut, and Kent and Washington Counties, Rhode Island: U.S. Geol. Survey Geol. Quad. Map GQ–436.

——1969, Pseudokarst on quartz diorite, Colombia: Zeitschr. Geomorphologie, N. F., v. 13, no. 3, p. 287–296.

Flint, R. F., 1957, Glacial and Pleistocene geology: New York, John Wiley and Sons, 553 p.

Goldthwait, J. W., and Kruger, F. C., 1938, Weathered rock in and under the drift in New Hampshire: Geol. Soc. America Bull., v. 49, no. 8, p. 1183–1198.

Kaye, C. A., 1964a, Outline of Pleistocene geology of Martha's Vineyard, Massachusetts: U.S. Geol. Survey Prof. Paper 501-C, p. C134–C139.

——1964b, Illinoian and early Wisconsin moraines of Martha's Vineyard, Massachusetts: U.S. Geol. Survey Prof. Paper 501-C, p. C140–C143.

——1967a, Kaolinization of bedrock of the Boston, Massachusetts, area: U.S. Geol. Survey Prof. Paper 575-C, p. C165–C172.

——1967b, Fossiliferous bauxite in glacial drift, Martha's Vineyard, Massachusetts: Science, v. 157, no. 3792, p. 1035–1037.

LeGrand, H. E., 1952, Solution depressions in diorite in North Carolina: Am. Jour. Sci., v. 250, no. 8, p. 566–585.

Reed, J. C., Jr., Bryant, Bruce, and Hack, J. T., 1963, Origin of some intermittent ponds on quartzite ridges in western North Carolina: Geol. Soc. America Bull., v. 74, no. 9, p. 1183–1187.

Sanborn, J. F., 1950, Engineering geology in the design and construction of tunnels, *in* Paige, S. M., chm., Application of geology to engineering practice (Berkey Volume): New York, Geol. Soc. America, p. 45–81.

Schafer, J. P., 1968, Surficial geologic map of the Ashaway quadrangle, Connecticut-Rhode Island: U.S. Geol. Survey Geol. Quad. Map GQ–712.

Shumskii, P. A., 1964, Principles of structural glaciology—the petrography of fresh water ice as a method of glaciological investigation: New York, Dover Publications, 497 p.

Tarr, R. S., 1905, Some instances of moderate glacial erosion: Jour. Geology, v. 13, p. 160–173.

Thomas, M. F., 1966, Some geomorphological implications of deep weathering patterns in crystalline rocks in Nigeria: Inst. British Geographers Trans., v. 40, p. 173–193.

Wilhelmy, Herbert, 1958, Klimamorphologie der Massengesteine: Braunschweig, Georg Westermann Verlag, 283 p.

Wright, H. H., Jr., 1964, Origin of the lakes in the Chuska Mountains, northwestern New Mexico: Geol. Soc. America Bull., v. 75, no. 7, p. 589–598.

SEQUENCE OF GLACIATION IN THE MESABI-VERMILION IRON RANGE AREA, NORTHEASTERN MINNESOTA

By T. C. WINTER, St. Paul, Minn.

Work done in cooperation with the Minnesota Department of Iron Range Resources and Rehabilitation

Abstract.—Drift from three major ice advances exists in the Mesabi-Vermilion Iron Range area. The earliest ice lobe, which deposited dark-gray to dark-greenish and brownish-gray calcareous till, originated northwest of Minnesota but moved into the Iron Range area from the southwest. It was confined to the area south of the Giants Range and extended a few miles east of Aurora. The second major advance (Rainy lobe) deposited gray to yellow, red, orange, or brown bouldery noncalcareous till. The ice advanced from the northeast and extended into southern Minnesota, forming several drumlin fields in the Iron Range area. As it retreated many ice-contact and morainal features were formed. The third major advance, the St. Louis sublobe of the Des Moines lobe, was further divided into two sublobes in the Iron Range area. The larger of these deposited gray (brown where oxidized), silty, calcareous till in the western and north-central part of the area, the smaller deposited red clayey till in the south-central part. Glaciofluvial deposits are associated with the tills throughout the section.

During the Pleistocene, massive ice lobes moved into Minnesota from two ice centers in Canada. Most of the glacial deposits presently in the State were deposited by the most recent glaciation, the Wisconsin. Older drift occurs in the State, but it is deeply buried in most areas and its extent is largely unknown. The Iron Range area offered one of the few opportunities to study pre-Wisconsin drift, if present, because of extensive strip mining; and indeed the basal till unit might be pre-Wisconsin in age, although it could also be early Wisconsin.

Because glaciers moved into the State from two different directions, the history of the glacial events must be reconstructed from the resulting intermixed tills and complex geomorphic features. Much of the work since Leverett (1932) mapped the glacial deposits in the entire State has centered in east-central Minnesota (Schneider, 1961; Wright and Ruhe, 1965; Wright, Watts, and others, 1969), where the glacial history is particularly complex.

North of this area of concentrated study, recent unpublished work by the author and others, and a report by Cotter, Young, and Winter (1964) has aided in understanding the glacial deposits of northeastern Minnesota. This work has included examination of many open-pit mine exposures and hundreds of test-hole logs, description of the petrography of the major glacial units, and an interpretation of the regional stratigraphy of the entire glacial section in the Mesabi Iron Range area. The purpose of this paper is to outline the history of glaciation in the Iron Range area (fig. 1) as indicated by the petrography and stratigraphy of the glacial units.

GLACIAL DRIFT UNITS

Three major till units occur in the area; they are informally referred to as the basal till, bouldery till, and surficial till. The basal till is stratigraphically the lowest. It is a dark-gray to dark-greenish- and brownish-gray till and is sandy, silty, and calcareous. Pebbles are largely granitic and metamorphic rocks of local origin, but limestone, dolomite, shale, basalt, felsite, banded "Lake Superior" agate, and gabbro also occur. Clay-mineral content is largely illite.

The bouldery till (the middle till unit) is the thickest and most continuous of the three. It ranges in color from gray to yellow, red, orange, or brown. It consists of sand, silt, and abundant cobbles and boulders, and it is noncalcareous. Pebbles are largely granitic and metamorphic rocks of local origin, but the till also contains gabbro, basalt, and felsite in minor amounts. Montmorillonite is the most common clay mineral. Colored (yellow, red, orange, or brown) bouldery till below gray bouldery till may be a separate subunit, distinguished largely by particle size, but the overall characteristics are similar to the other bouldery till.

The surficial till is fairly extensive but thin, generally less than 25 feet thick. In the western and north-central parts of the area, this till is brown and silty, characterized by a light- to medium-brown sandy, silty, calcareous matrix. Pebbles are largely granitic and metamorphic rocks of local origin, but they include limestone, dolomite, shale, basalt, felsite, and gabbro. Clay-mineral content is largely mixed-layered montmorillonite and illite. In the south-central part of the area, the till is red and clayey, characterized by a red to reddish-brown clayey, silty, calcareous matrix. Pebble content is similar to that of brown silty till, but the red till includes slightly less limestone.

Glaciofluvial sediments occur between the major till units,

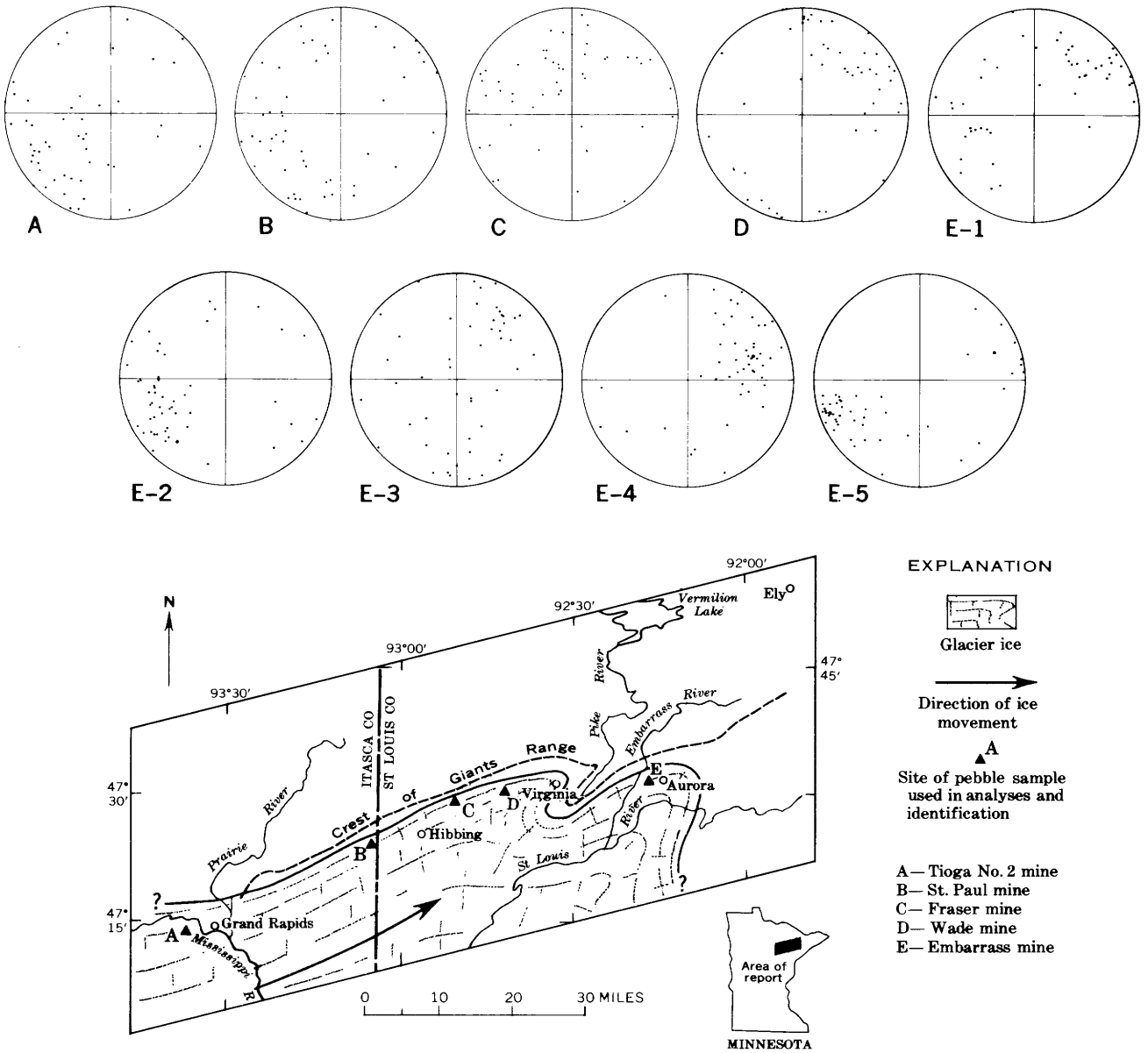

Figure 1.—Map showing extent of the ice lobe that deposited the basal till unit in northeast Minnesota. Pebbles show a general northeast-southwest orientation of long axes, as indicated by the pebble orientation diagrams (circles).

below the basal till, and above the surficial till. They vary greatly in areal extent, thickness, and particle-size distribution.

BEDROCK GEOLOGY

Bedrock of the area consists largely of granite and metamorphosed sedimentary and volcanic rocks, including iron formation. Limestone and shale in the glacial deposits must have been transported from Manitoba by glaciers, and basalt and felsite by glaciers moving from the northeast by way of the Lake Superior basin. Gabbro could have been derived from the highland northwest of Lake Superior by glaciers moving from the northeast. Glaciers moving out of the Lake Superior basin also could have picked up gabbro along the Lake Superior side of the highland.

SEQUENCE OF GLACIATION

The basal till provides the earliest record of glaciation in the area. The till is calcareous, indicating a northwestern source.

Pebble orientations were determined at several localities in the basal till. In the Embarrass mine near Aurora, five determinations were made to check local variations. The determinations from this mine (fig. 1, E) as well as one from the Wade mine (fig. 1, D) show a strong northeast-southwest orientation of long axes. The basal till in the St. Paul mine (fig. 1,B) and Tioga No. 2 mine (fig. 1,A) show a less distinct northeast-southwest pattern, and that from the Fraser mine (fig. 1,C) shows a very weak northwest-southeast pattern.

Pebble orientation and the general decrease in proportion of northwest indicator rocks from west to east across the Iron Range indicate that the basal till was deposited by an ice lobe that moved into the area from the west-northwest and extended eastward to just past Aurora (fig. 1). The ice lobe was probably confined to the area south of the Giants Range, which provided a topographic barrier presently 400 feet higher than the land to the south. The Giants Range is a low ridge of granitic hills oriented northeast-southwest that transects the area. The increasingly greater amount of sand in the till from west to east is probably due to the incorporation of preexisting sandy sediments lying immediately south of the Giants Range.

A physiographic record of this glacial episode is not present in the existing landscape. However, a subsurface record is found in the morainal area southwest of Grand Rapids, where the glacial section in the Tioga No. 2 mine and some deep test holes indicate that the drift consists largely of basal till.

It was thought in the early phases of fieldwork that the basal till might have been deposited by the Wadena lobe (Wright, 1962). Samples from Wadena County and the data presented by Arneman and Wright (1959) show little similarity in petrographic characteristics between the basal till and the Wadena till.

The age of the basal till is uncertain. A date of > 36,490 B.P. (years Before Present) (Y–250, Yale University Radiocarbon Laboratory) has been reported on wood from the Duncan-Douglas mine. The stratigraphic position of the sample is in question, but it is probably from outwash between the bouldery and basal tills. This would date the basal till as older than 36,490 years. According to Wright and Ruhe (1965) the Wadena lobe in the Hewitt phase was contemporaneous with the Rainy lobe, but the Rainy lobe subsequently advanced in the St. Croix phase to cover Wadena-lobe drumlins. The stratigraphic position of the basal till in the Iron Range area (below the bouldery till of the Rainy lobe) suggests that the basal till could represent a pre-Hewitt phase of the Wadena lobe, or a lobe older than the Wadena. If the Wadena lobe is middle-Wisconsin in age the basal till could be the same, or it could be early Wisconsin or even pre-Wisconsin in age.

The second episode of glacial activity is represented by the bouldery till. This till was deposited by the Rainy lobe, which moved into the area from the northeast, passing west of the highland that parallels the north shore of Lake Superior. The lobe moved southwest across the Canadian Shield and across the Giants Range (fig. 2*A*), so its drift has an extremely large percentage of granite cobbles and boulders. The Rainy lobe eroded the bedrock in its advance north of the Giants Range, as evinced by the lack of bouldery till in this area. South of the range it deposited its drift. The Giants Range may have had a significant effect on the ability of the ice to carry the load. Drumlins near Toimi in the southeastern corner of the area and those near Hibbing and Eveleth were formed during the advance of the Rainy lobe.

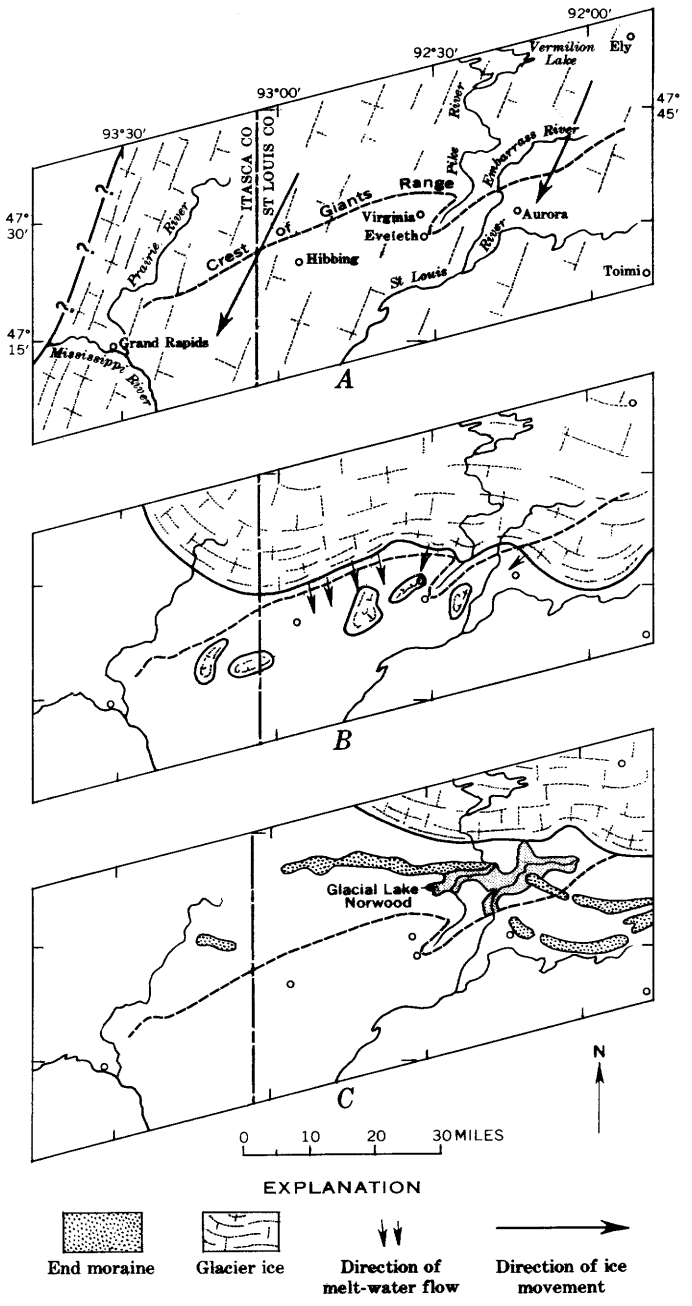

Figure 2.—Sequence of advance and retreat of Rainy lobe ice.

A. Advance of lobe, showing approximate western extent in the area.

B. Retreatal stage, showing the ice north of the Giants Range. Melt water poured through notches in the divide at this time and carried sediment that formed much of the ice-contact topography south of the Giants Range.

C. Retreatal stage, showing formation of the moraines in the northeastern part of the area and the formation of glacial Lake Norwood.

During the recession of the Rainy lobe, after the St. Croix phase (Wright and Ruhe, 1965), much of the basic present-day topography was formed. The large ice-crevasse filling near Calumet was probably formed parallel to the receding glacial

front at this time, as were the several moraines north of the Giants Range in the eastern part of the area, including the Vermilion moraine. Boulder pavements heading in notches in the Giants Range, such as the one northeast of Aurora, were probably formed by large volumes of melt water that passed through the notches when the Rainy lobe receded north of the Giants Range (fig. 2*B*). The large channel (Embarrass channel) where the Embarrass River transects the Giants Range northwest of Aurora could have been cut at this time, but it may also have been in existence previously. Numerous areas of ice-contact deposits south of the Giants Range were probably also formed as the ice receded from the region.

Glacial Lake Norwood (Winchell, 1901), an area presently drained by Pike and Embarrass Rivers, was formed about this time also (fig. 2*C*). The lake had an elevation at 1,450 feet. It drained by way of the Embarrass channel, which contains a terrace at 1,450 feet.

The age of the bouldery till is uncertain. A date of > 35,000 B.P. (W–500, U.S. Geol. Survey Radiocarbon Laboratory) was determined on wood from a drill hole near Hibbing. The wood was from glaciofluvial sediments overlying bouldery till. The sediments were probably deposited when the Rainy lobe was receding from the area. This date would make the advance (when the wood was probably incorporated into the ice) of the Rainy lobe much older than the minimum dates of retreat of the ice (14,000–16,000 years ago) discussed in Wright, Watts, and others (1969).

The third major phase of glacial activity is represented by the surficial tills (red clayey till and brown silty till). Two interpretations of their history have been proposed. It was believed for a number of years that the red clayey till was deposited by ice moving northwest into the Iron Range area from the Lake Superior basin near Duluth (Wright, 1955) and that the brown silty till was deposited by the St. Louis sublobe which moved into the area from the northwest. Two radiocarbon dates of 11,330±350 B.P. (W–827) and 11,100±400 B.P. (W–1140) from wood included in the red clayey till in the Mariska mine near Gilbert (between Aurora and Virginia) suggested that it was of Valders age. Subsequent work summarized by Wright and Ruhe (1965) and Wright, Watts, and others (1969) has resulted in a different interpretation of the history of the red clayey till. In particular, geomorphic interpretation now indicates that the red clayey till was deposited by the same ice lobe as the brown silty till, the difference in color and texture being due to the local incorporation of the red lake clay into the till as the ice lobe moved through the glacial Lake Upham I basin. The red lake clays are probably derived from red drift of the Highland moraine to the east.

On the basis of petrographic analysis the author supports the latter interpretation, with reservations. The calcareous matrix and the presence of limestone and shale in the red clayey till provide the strongest evidence that a northwest source is involved, although the color, particle-size distribution, and percentage of northwest indicator rocks in the red clayey till are significantly different from those in the brown silty till.

Pebbles in the surficial tills in most localities studied show either no predominant orientation or a weak northeast-southwest pattern (fig. 3). Pebbles in a sample of red clayey till near Aurora (fig. 3,M) and two others about 10 miles southwest of Hibbing (figs. 3,E and 3,F) exhibit a north-south orientation. The very weak orientation of pebbles in some of the samples suggests a general northeastward movement of ice, which is what would be expected for either of the two interpretations.

Pebble orientations do not provide much help in resolving details of the origin and history of the red clayey till. The geomorphic interpretation presented by Wright, Watts, and others (1969) must be regarded as the strongest argument for the red clayey till not being deposited by ice moving from the Lake Superior basin but, rather, being a part of St. Louis sublobe deposits. Petrographic analysis support this interpretation, although the difference in percentage of northwest indicator rocks between the two tills as well as the radiocarbon dates from the red clayey till in the Mariska mine leave the question not fully resolved. The following account of the most recent advance of glacial ice into the area assumes that the red clayey till and brown silty till were deposited by the same sublobe.

The St. Louis sublobe entered the area from the west-northwest and deposited brown silty till over the western part of the area. The Giants Range west of Hibbing and the topographically high area extending southwest from Hibbing to Goodland caused the sublobe to split. The part that moved eastward north of the Giants Range retained the character of the brown silty till. In this area the ice extended eastward as far as Sand Lake (north of Virginia) and to Pike Bay of Vermilion Lake (fig. 3). An eastern extent beyond Pike Bay to Ely is based on only a few inconclusive sample analyses and is therefore questionable. An area of questionable brown silty till occurs in the north-central part of the area. Roadcuts are very small and the material exposed, although similar in appearance to brown silty till, contains few pebbles at many places and may actually be glacial lake sediments.

The part of the St. Louis sublobe that was diverted southward around the topographic high in the Goodland area moved into the basin of glacial Lake Upham I. The ice presumably picked up red lake clays, which became thoroughly intermixed with the brown silty material to impart a distinctive color and texture to the material deposited as red clayey till.

Near the topographic high in the Goodland area the southern offshoot was diverted around the point of high ground and, near Goodland, the red clayey and brown silty tills are intermixed. Lenses of brown silty till are included in the red till in several other places, notably east of Hibbing. The southern offshoot of the St. Louis sublobe extended eastward to south of Aurora.

Throughout most of its extent, the surficial till is rather thin, usually 5 to 10 feet thick but as much as 40 feet thick

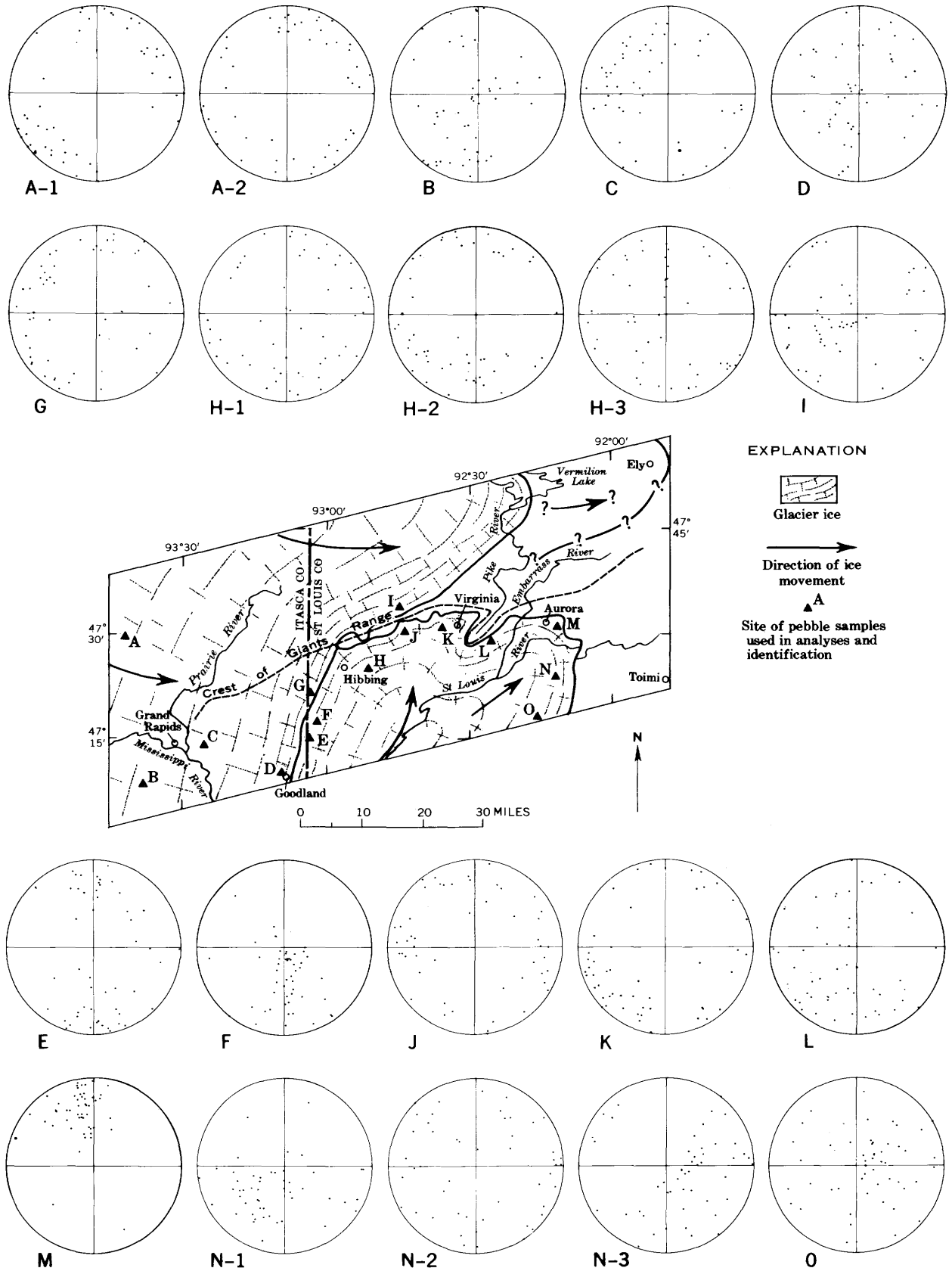

Figure 3.—Extent of the St. Louis sublobe of the Des Moines lobe ice. Pebbles in the red clayey till generally show either no predominant orientation or only a weak northeast-southwest orientation, as indicated by the pebble orientation diagrams (A–1 to O).

locally. It usually occurs as a thin mantle on preexisting topographic features and was not responsible for the formation of conspicuous topographic features. The exception to this is the morainal complex near the western edge of the area. Few large exposures exist in this area. A roadcut near Little Bowstring Lake (Fig. 3, loc. A), however, contains about 20 feet of brown silty till underlain by a few feet of dark gray to black silty till, which is merely the unoxidized brown silty till, according to petrographic analyses. This exposure suggests that most of the morainal complex was deposited by the St. Louis sublobe. However, the drift in the Tioga No. 2 mine southwest of Grand Rapids consists largely of basal till, suggesting the formation of the morainal complex during an earlier glaciation.

Analysis of the physiography indicates that the part of the morainal complex northwest of the Prairie River was deposited by the St. Louis sublobe (fig. 4). The position of outwash to the southeast of massive ice-contact areas, which in turn are southeast of the southwest-northeast morainal trend, is an excellent example of the geomorphic relationships that would be expected from a glacier lying northwest of the moraine. The trend of tunnel valleys and the large number of eskers oriented northwest-southeast also support this interpretation. It is concluded, therefore, that the morainal area southwest of Grand Rapids was formed largely at the time the basal till was being deposited, and the features northwest of the Prairie River were formed by the St. Louis sublobe.

After the retreat of the St. Louis sublobe much of the area was covered by glacial lakes. Glacial Lake Aitkin II (Wright and Ruhe, 1965) extended northward into the Grand Rapids area and deposited lacustrine sand (fig. 5).

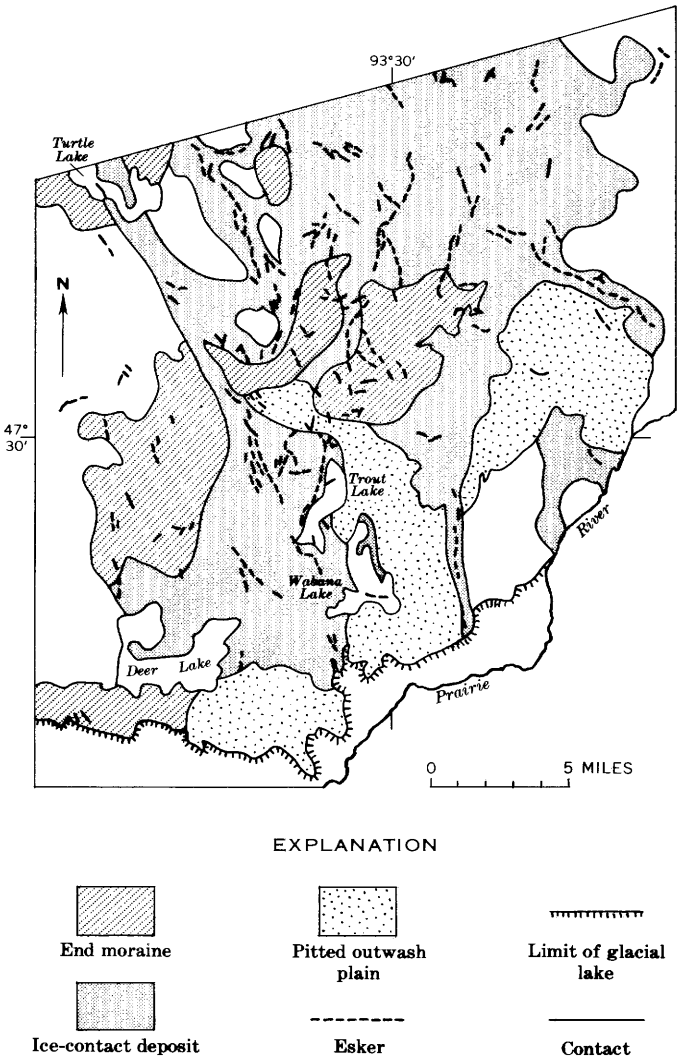

Figure 4.—Morainal complex northwest of the Prairie River, Minn., showing an excellent example of the relationship of moraine, ice-contact, outwash, and esker deposits. The edge of the ice would extend northeast-southwest along the southeast edge of the moraine. (See fig. 6*B* for area of map and inferred position of glacial ice).

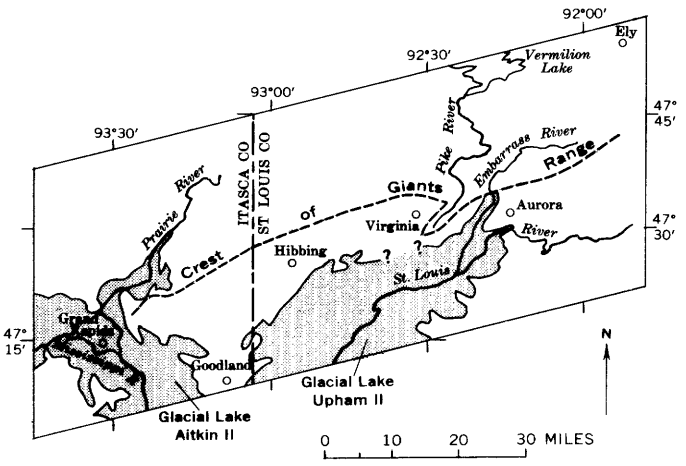

Figure 5.—Extent of glacial Lakes Aitkin II and Upham II.

Glacial Lake Upham II extended northeastward to near the southern end of the Embarrass channel near Aurora. The basin of this glacial lake is floored largely of sand, silt, and clay and contains many square miles of peatlands. Some of the sand was reworked by the wind, particularly south of Virginia.

A lake basin of unknown extent, not reported previously, exists in the north-central part of the area. Evidence for the lake includes shorelines, lake clays, lake-washed till plain, and lacustrine sand. More fieldwork is needed to define fully the extent and exact altitude of the lake. It was formed during the retreat of the St. Louis sublobe and probably represents an early, high stage of glacial Lake Agassiz. The lake had an altitude of about 1,420 feet. It probably drained southward at first down the Pike River valley, across a divide near Embarrass into the Embarrass River valley, through the Embarrass channel, and into the St. Louis River (fig. 6*A*). Then the ice retreated enough to open another southern outlet at a lower altitude, by way of the Prairie River into the Mississippi River (fig. 6*B*). Finally, after further ice recession to the north, glacial Lake Agassiz proper developed north of the area, and the Prairie River outlet was abandoned. The subsequent history of glacial Lake Agassiz has been discussed by a number of geologists, including Upham (1895), Johnston (1916),

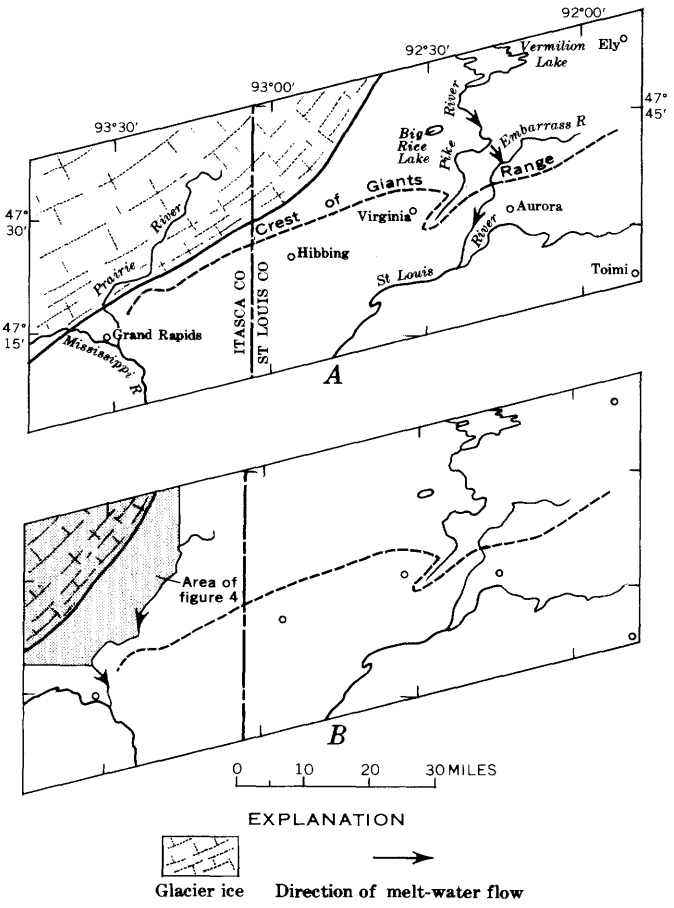

Figure 6.—Sequence of drainage of an unnamed glacial lake following retreat of the St. Louis sublobe from the north-central part of the area of report.

A. Upon retreat of the lobe north of the Giants Range, ponded lake waters west of Vermilion Lake and north of Big Rice Lake drained by way of the Pike and Embarrass Rivers to the St. Louis River.

B. Further retreat of the ice to northwest of the Prairie River opened the Prairie River as an outlet, and the higher eastern outlet was then abandoned.

Leverett (1932), Nikiforoff and others (1939), and Elson (1967).

REFERENCES

Arneman, H. F., and Wright, H. E., Jr., 1959, Petrography of some Minnesota tills: Jour. Sed. Petrology, v. 29, no. 4, p. 540–554.

Cotter, R. D., Young, H. L., and Winter, T. C., 1964, Preliminary surficial geologic map of the Mesabi-Vermilion Iron Range area, northeastern Minnesota: U.S. Geol. Survey Misc. Geol. Inv. Map I-403.

Elson, J. A., 1967, Geology of Glacial Lake Agassiz: p. 37–95 *in* W. J. Mayer-Oakes, ed., Life, land, and water—Proceedings of the 1966 conference on environmental studies of the Glacial Lake Agassiz region: Winnipeg, Univ. of Manitoba Press, 414 p.

Johnston, W. A., 1916, The genesis of Lake Agassiz; a confirmation: Jour. Geology, v. 24, no. 7, p. 625–638.

Leverett, Frank, 1932, Quaternary geology of Minnesota and parts of adjacent States: U.S. Geol. Survey Prof. Paper 161, 149 p.

Nikiforoff, C. C., and others, 1939, Soil survey (reconnaissance) of the Red River Valley area, Minnesota: U.S. Dept. Agriculture Ser. 1933, no. 25, 98 p.

Schneider, A. F., 1961, Pleistocene geology of the Randall region, central Minnesota: Minnesota Geol. Survey Bull. 40, 151 p.

Upham, Warren, 1895, The glacial Lake Agassiz: U.S. Geol. Survey Mon. 25, 658 p.

Winchell, N. H., 1901, Glacial lakes of Minnesota: Geol. Soc. America Bull., v. 12, p. 109–128.

Wright, H. E. Jr., 1955, Valders drift in Minnesota: Jour. Geology, v. 63, p. 403–411.

——1962, Role of the Wadena lobe in the Wisconsin glaciation of Minnesota: Geol. Soc. America Bull., v. 73, p. 73–100.

Wright, H. E., Jr., and Ruhe, R. V., 1965, Glaciation of Minnesota and Iowa, p. 29–41 *in* H. E. Wright, Jr., and D. G. Frey, eds., The Quaternary of the United States: Princeton, N.J., Princeton Univ. Press, 922 p.

Wright, H. E., Jr., and Watts, W. A., with contributions by Saskia Jelgersma, J. C. B. Waddington, Junko Ogawa, and T. C. Winter, 1969, Glacial and vegetational history of northeastern Minnesota: Minnesota Geol. Survey, Spec. Publ. Series, SP-11, 59 p.

DEVELOPMENT OF PILLOWS ON THE SUBMARINE EXTENSION OF RECENT LAVA FLOWS, MOUNT ETNA, SICILY

By JAMES G. MOORE; RENATO CRISTOFOLINI[1], and ANTONINO Lo GIUDICE[1], Menlo Park, Calif; Catania, Italy

Abstract.—Eleven scuba dives to the submarine extension of recent basalt lava flows erupted on the slopes of Mount Etna reveal that the surface features of the submarine part of the lava flows depend on the steepness of the slope of the bottom. Where bottom slope is gentle, the flow surface is hummocky but relatively smooth, and has elongate ridges and tumuli; where steep or cliffed, cylinderlike pillows, elongate downslope, drape the scarp and commonly bifurcate into smaller cylindrical or hemispherical pillows. The flows apparently propagate down the submarine slope by frontal development of pillows which dam the flow, cause it to thicken, and eventually to establish a steep front. Pillows fed through master channels near the top digitate and drape over the steep front of the advancing flow, thus forming a steeply inclined stack of foreset-bedded pillows. Because of these steep initial dips, indications of "top" and of thickness of ancient pillowed piles should be used with caution. Two features of Etnan flows may prove valuable in determining flow directions in ancient uplifted pillows: (1) blunt downslope termination of elongate pillows, and (2) division of elongate pillows into two or more smaller pillows in the downflow direction.

Mount Etna in eastern Sicily is the highest and one of the most active volcanoes in Europe. Its eastern flank slopes directly into the Ionian Sea (fig. 1), and many recent lava flows, including some of historic age, have flowed across this shoreline and have cooled below sea level. These lava flows offer an exceptional opportunity to compare the characteristics of young alkali basalt flows both above and below sea level. Consequently, 11 scuba dives ranging in depth from 8 to 24 m were made north of the city of Catania (fig. 1 and table 1) during the period of July 5–14, 1970. Four of the dives were to the lava flow of 1381; the others were to prehistoric flows. A total of 205 photographs and 9 samples were taken on the submarine extension of the Etnan lava flows. This report describes the preliminary results of that work. Antonino Lo Giudice, James G. Moore, and Laurent Stieltjes participated in the diving.

A study utilizing scuba-diving techniques has many limitations. The chief problem is that bottom time is short, and revisiting the same outcrop is difficult without elaborate preparation. This problem, coupled with limited visibility and freedom of movement and with the impossibility of discussion at the outcrop site, forces most of the interpretation to be based on photographs and samples.

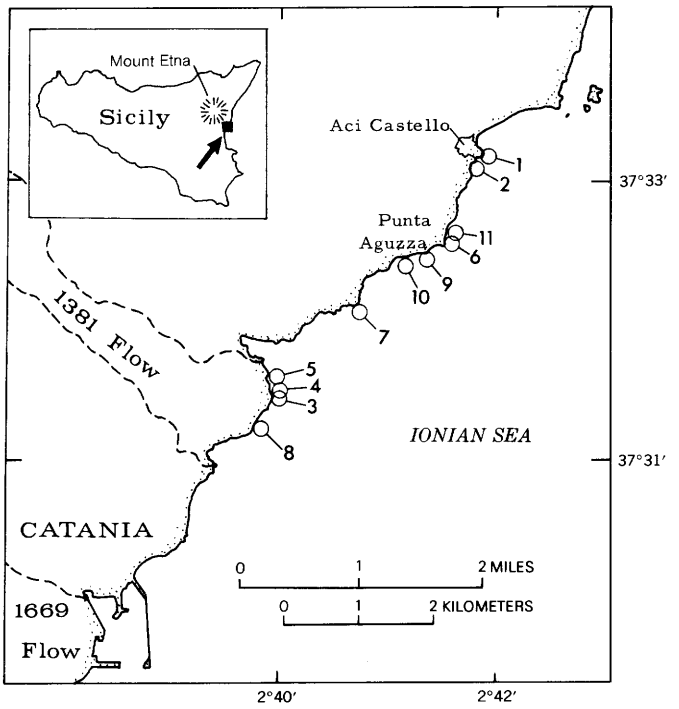

Figure 1.—Locations of scuba dives on Ionian seacoast northeast of Catania (compare with table 1). Inset map of Sicily shows relation of Mount Etna to map area (arrow). Longitude is relative to Rome meridian.

LAVA FLOW OF 1381

The lava flow of 1381 originated from a fissure on the south flank of Etna at an altitude of about 400 m. Its vent is the lowest in altitude of the historic eruptions of Mount Etna, and according to Rittmann (1964), this activity was not directly

[1]Universita Degli Studi, Catania, Italy.

Table 1. *Dives northeast of Catania, Sicily, July 1970*

[See fig. 1 for locations]

Dive locality	Depth (meters)	Remarks
1	20	The pillowed complex exposed on the wave-cut bench at Aci Castello is exposed in a steep scarp to a depth of 20 m with a gentle sandy slope at the base. Several pillows embedded in fragmental material were seen on the cliff face.
2	8–9	Coherent, rather smooth lava surface with sweeping flow structures. One lava tongue 40 cm wide drapes a small cliff composed of fragments of basalt. Tongue splits into two thin flow lobes.
3	13–16	Offshore from 1381 lava flow. Rather smooth to hummocky coherent lava surface. In places bulbous protrusions are common.
4	10	Offshore from 1381 flow. Rather smooth coherent lava surface with flow lobes and bulbous surfaces. Several dishlike depressions as much as 5–8 m in diameter in flow area between two lava pads. Some elongate pillows on scarps.
5	13–16	Offshore from 1381 flow. Irregular flow surface with several meters of local relief on elongate ridges, commonly with hackly fractured lava. Some elongate pillows droop over scarps. Broken flow lobes show "washboard" surfaces of incipient columnar joints 30–60 cm long with columns 2–4 cm in diameter.
6	16	Offshore from Punta Aguzza flow. Piles of elongate pillows hang over cliffs, commonly fork into 2 or more tongues. Excellent pahoehoe-festooned wrinkles on gentler slopes.
7	20	Between 1381 flow and Punta Aguzza flow. Rather flat and billowy coherent lava down to 6-m depth, then steep cliff to about 25 m. The scarp is largely covered with lava blocks.
8	24	Offshore from 1381 flow. Flow surface dominated by rounded ridges 3–5 m wide which plunge downslope. A rather regular and straight medial crack (about 60 cm wide and 60 cm deep) is present on the top of the ridge. Tumuli with cracked surfaces of striated lava surmount these ridges. Jagged blocks litter the bases of scarps.
9	24	Offshore from Punta Aguzza flow. Tongues of lava about 3 m wide bifurcate downslope and develop well-formed elongate pillows where they drape scarps. These pillows, elongate downslope, are inclined 45°–90°. Broken pillows litter bases of scarps.
10	16	Offshore from Punta Aguzza flow. Well-developed cylindrical and bolsterlike pillows (about 0.5–1 m in diameter) generally hang on steep slopes. One such pillow, 2.7 m long and 50 cm in diameter, drapes slopes ranging from 60° to 90°.
11	16	Offshore from Punta Aguzza flow. Hummocky lava surface with abundant interconnected, nearly spherical pillows and some elongate pillows hanging on steep slopes.

related to that of the main central crater. The lava flowed about 8 km, reached the sea 3 km northeast of Catania, and extended the shoreline seaward. Sciuto-Patti (1872) distinguished two different lava flows in the region mapped as the 1381 flow on figure 1. He designated the lower one, sampled and photographed in this study, as a lava flow of the 11th–13th century on the basis of a study of old chronicles; according to Sciuto-Patti, this flow could have originated from a higher, more northwesterly vent than the upper flow unit designated by him as 1381. Other authors (Grillo, 1954; Pichler, 1970) and the official geologic map (Travaglia, 1885), however, designate only one historic flow, that of 1381, in this region.

Near the seacoast the flow surface is rough and irregular, is covered with angular blocks, and would best be described as aa. However, in places small tongues and toes with characteristic smooth, ropy pahoehoe surfaces are present. Quarries in the flow show that the massive flow interior grades both up and down into blocky and clinkery material, and that some channels contain massive lava more than 10 m thick.

Below sea level, the flow surface is generally much smoother than on land, with gently undulating or bulbous and hummocky coherent lava surfaces prevailing (fig. 2*A*, *B*). In some places dishlike depressions 5–10 m in diameter and 1–2 m deep formed, apparently where lava drained away from under a solidified crust. In other places, round-topped ridges 3–5 m wide, commonly with a conspicuous medial crack as much as 60 cm wide, plunge steeply downslope and apparently mark large tubes that conducted lava into deeper water. These ridges are surmounted by tumuli which are made in part of jagged blocks bounded either by cooling fractures or by striated lava surfaces (fig. 2*D*). The cooling fractures commonly bound small, poorly developed columns 2–4 cm on a side and about 30 cm long. The striated lava surfaces were produced where still-plastic lava was either torn apart or scraped by jagged, more solid material.

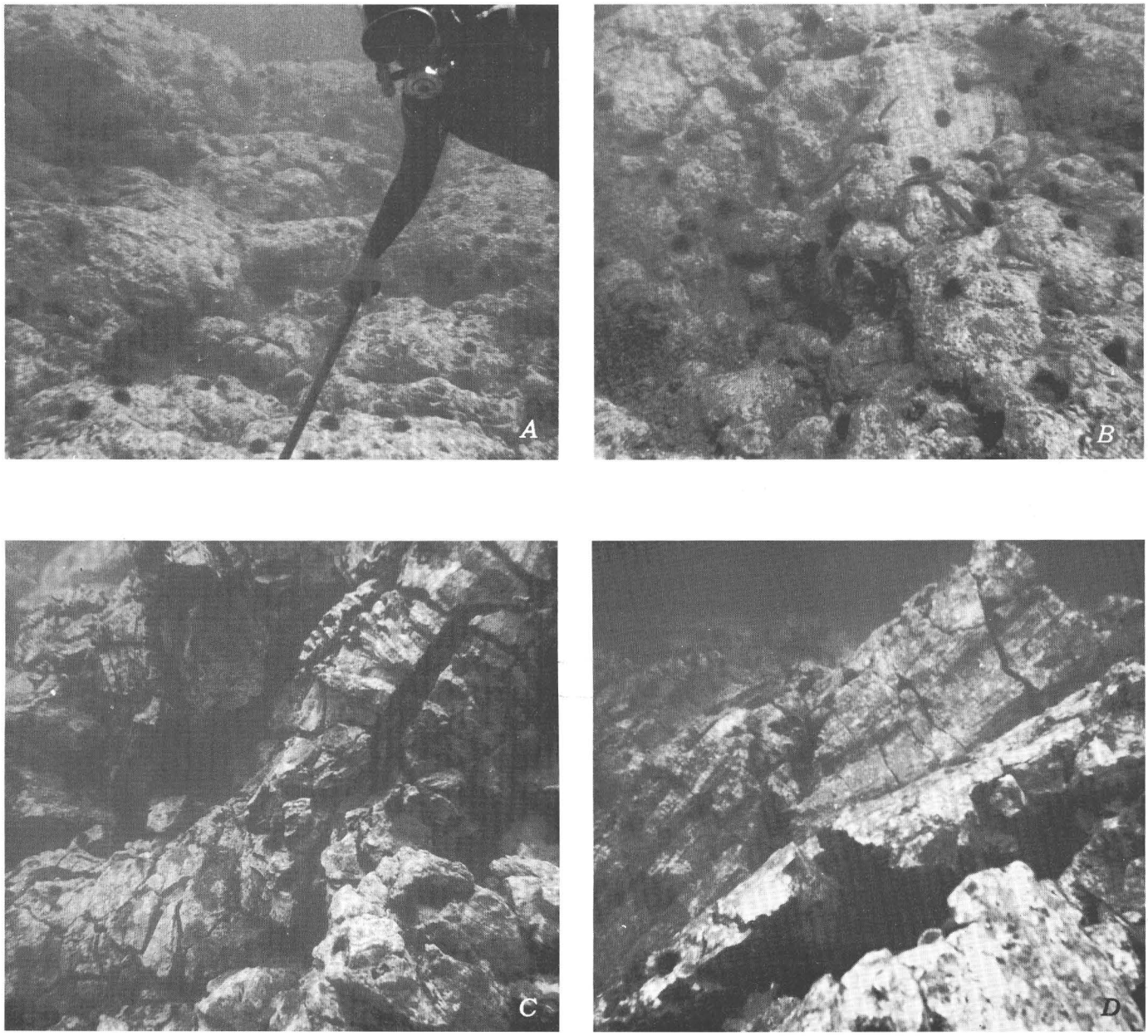

Figure 2.–Underwater views of the lava flow of 1381.

A, smooth, somewhat hummocky and bulbous surface of lava flow. Locality 3, depth 13 m.

B, smooth, coherent lava surface of flow, showing pillowlike bulbous protrusions flanking flow lobe on which hammer is resting. Hammerhead is 19 cm long, and dark sea urchins are about 8 cm in diameter. Locality 3, depth 15 m.

C, branching elongate pillow draping 60° scarp on flow. Note axial crack (about 15 cm wide) and columnar joints perpendicular to outer surface where pillow is broken open. Fragments of pillows litter base of scarp. Locality 5, depth 15 m.

D, crest of tumulus on flow, showing deep crack and striated lava surface. Sea urchins are about 8 cm in diameter. Locality 8, depth 24 m.

Pillow structures are not common or well developed on the parts of this flow that were explored in four dives, but some small budlike pillows occur on the margins of flow tongues (fig. 2*B*). In other places, flow tongues 1–1.5 m in diameter are noticeably cylindrical and bolsterlike. These elongate pillows typically drape steeper scarps (fig. 2*C*). Where broken, they characteristically show columnar joints bounding columns 2–3 cm wide perpendicular to the outer surface.

PUNTA AGUZZA FLOW

Punta Aguzza (Sharp Point) is formed by the feeding channel of a lava flow that flowed into the sea in prehistoric time. Soil

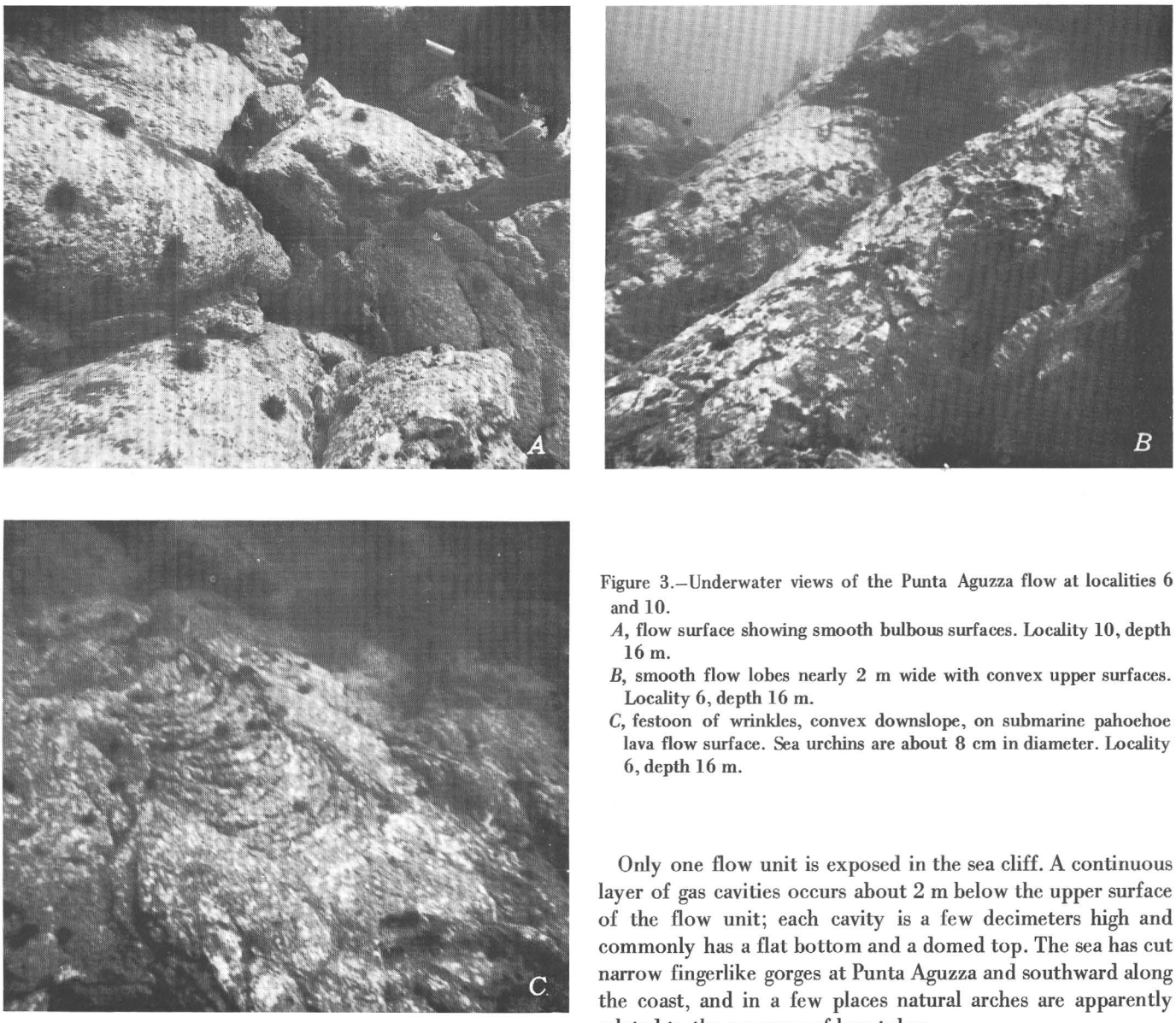

Figure 3.—Underwater views of the Punta Aguzza flow at localities 6 and 10.

A, flow surface showing smooth bulbous surfaces. Locality 10, depth 16 m.

B, smooth flow lobes nearly 2 m wide with convex upper surfaces. Locality 6, depth 16 m.

C, festoon of wrinkles, convex downslope, on submarine pahoehoe lava flow surface. Sea urchins are about 8 cm in diameter. Locality 6, depth 16 m.

and vegetation cover much of the original flow surface upslope and make it difficult to recognize the original flow boundaries or source of the flow on the slopes of Mount Etna. However, in a small area landward of the point the flow is clear of vegetation; there it has a dominantly pahoehoe surface with ropy structures and slightly domed smooth surfaces. Some small bulbous pahoehoe toes a few decimeters in width mark the edges of flow units.

A pronounced tumulus 10–20 m in diameter and 3–4 m high occurs at the edge of the sea cliff. The surface of the tumulus is rougher than the flow surface above sea level. Partly overturned slabs of crust are alined with one another and form diverging ridges several decimeters high and a few meters long. Several cracks about 1 m across and 2 m deep and with a V-shaped cross section are found near the edge of the sea cliff.

Only one flow unit is exposed in the sea cliff. A continuous layer of gas cavities occurs about 2 m below the upper surface of the flow unit; each cavity is a few decimeters high and commonly has a flat bottom and a domed top. The sea has cut narrow fingerlike gorges at Punta Aguzza and southward along the coast, and in a few places natural arches are apparently related to the presence of lava tubes.

South of Punta Aguzza, outcrops are much poorer because the sea cliff is absent and the shore is covered with large rounded boulders. Along a series of roadcuts near the coast, the upper flow (apparently the Punta Aguzza flow) appears to be thin (2–3 m thick).

The original flow surface is better preserved below sea level than on land and in general presents a smoother, more fluid appearance. On gentle slopes, flow units are generally broad and rather flat, with flow tongues averaging 3 m in width (fig. 3). Commonly, small bulbous buds protrude from the sides and tops of flow units. In one place, festoons of pahoehoe-type wrinkles, convex downslope, were observed (fig. 3*C*). These features, so characteristic of subaerial pahoehoe flows (Wentworth and Macdonald, 1953), can therefore also develop in subaqueously chilled lava flows.

However, on steeper slopes, from 30° to vertical, the most common features are cylindrical smooth-surfaced flow units,

here called elongate pillows (figs. 2*C*, 4, and 5). They average about 50 cm in diameter and are commonly 2–3 m long. The elongate pillows merge upslope into larger flow units (figs. 4*A*, *B*, *D*, and 5*B*), and they terminate downslope in hemispherical blunt ends (figs. 4*A*, *B*, *C*). Some of the elongate pillows divide downslope into two or three smaller tongues (figs. 4*B*, *C*, *D*, and 5*B*), and others are terminated by two or more bulbous pillowlike masses (figs. 4*A*, *C*). All the elongate pillows extend

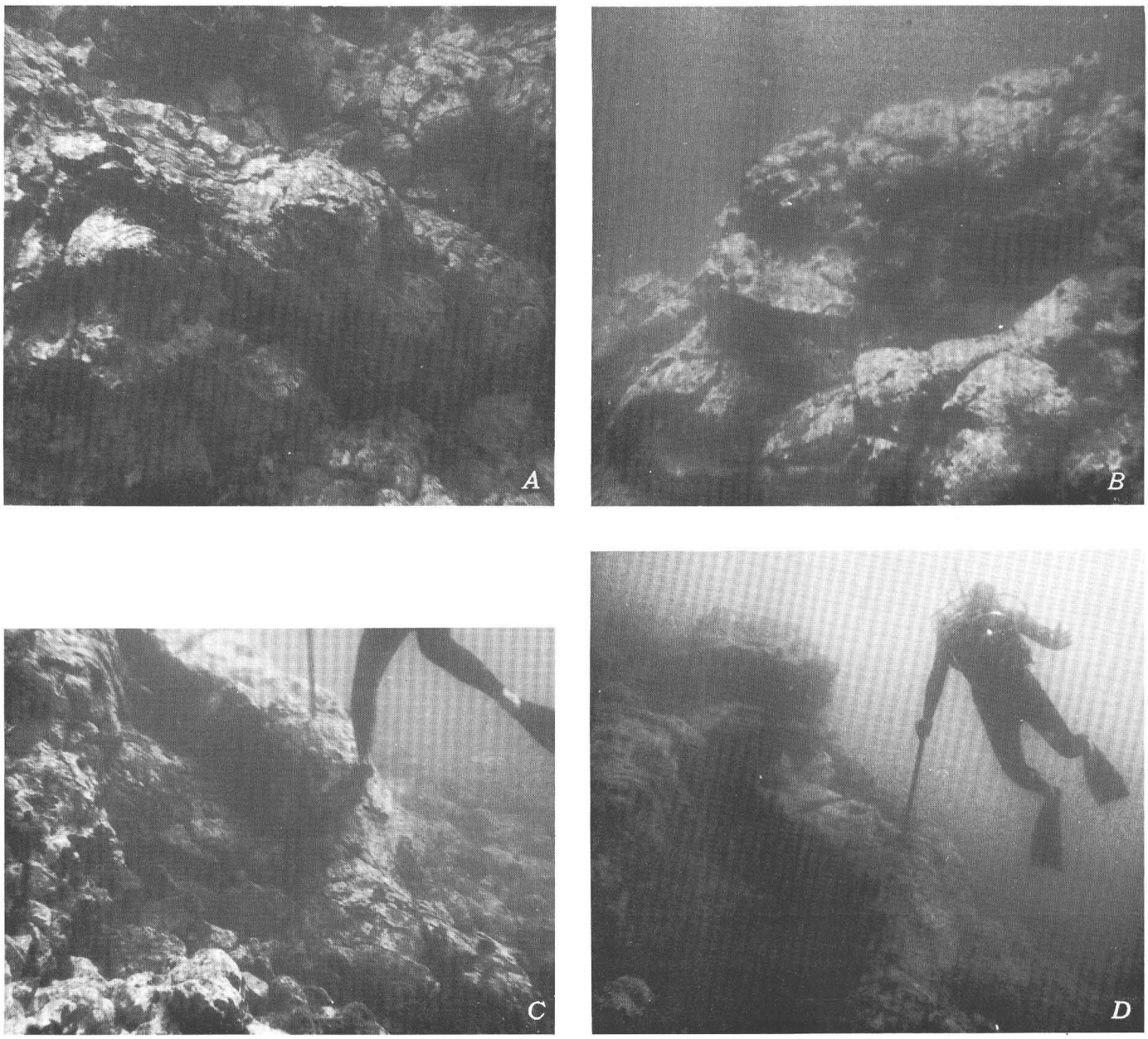

Figure 4.—Underwater views of the Punta Aguzza flow at localities 6 and 9.

A, cylindrical flow lobe which has divided into at least five nearly spherical pillows. Sea urchins are 6–8 cm in diameter. Locality 9, depth 24 m.

B, flow lobe showing division into several pillows, each of which is elongate downslope. Sea urchins are 6–8 cm in diameter, and truncated pillow on left is about 1 m in diameter. Locality 6, depth 16 m.

C, flow lobe or pillow, elongated downslope, which divides into three smaller lobes. Axes of small wrinkles are parallel with length. Locality 6, depth 16 m.

D, Flow lobe merging upslope into larger flow unit. The base of this lobe is shown in *B*.

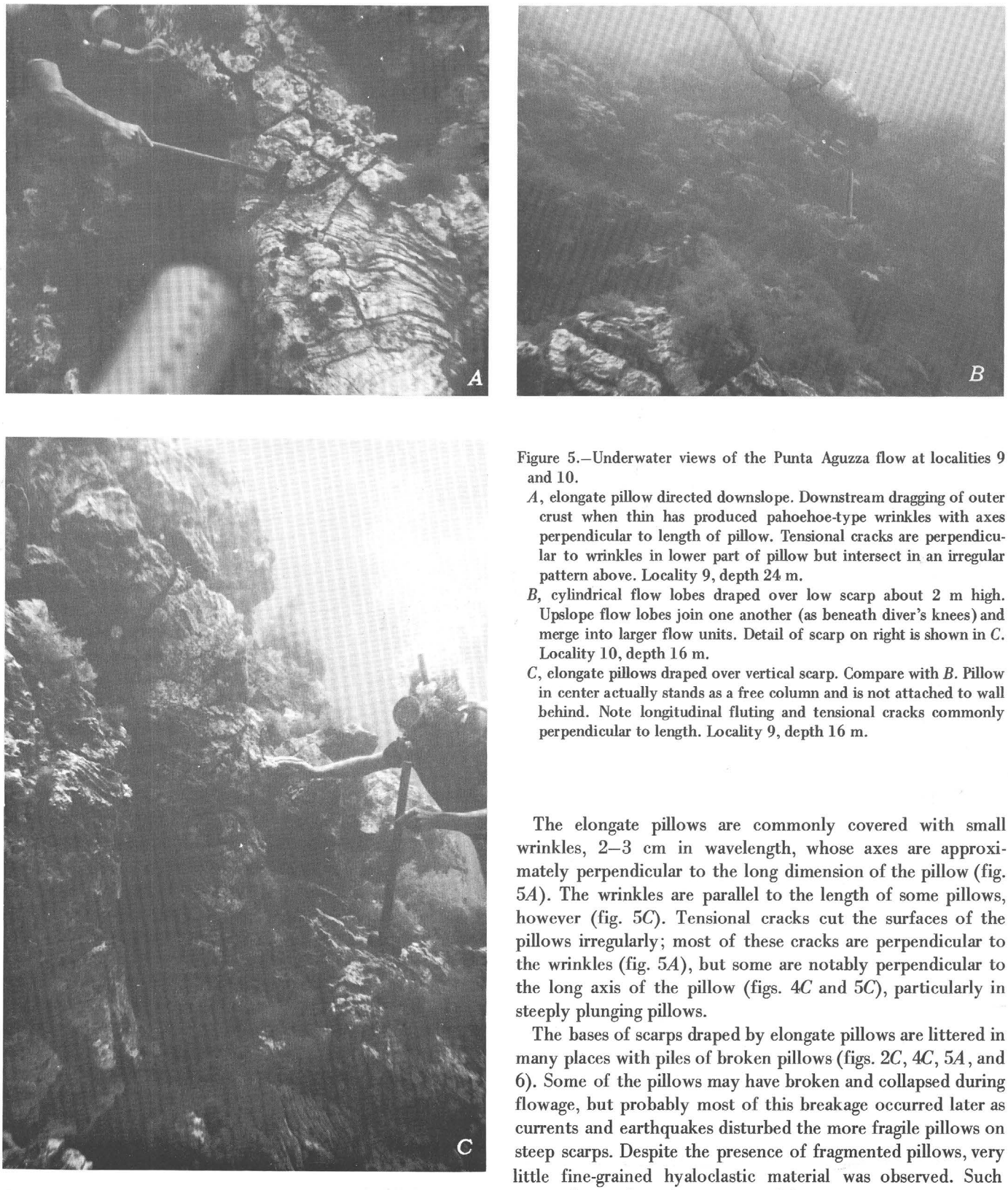

Figure 5.—Underwater views of the Punta Aguzza flow at localities 9 and 10.

A, elongate pillow directed downslope. Downstream dragging of outer crust when thin has produced pahoehoe-type wrinkles with axes perpendicular to length of pillow. Tensional cracks are perpendicular to wrinkles in lower part of pillow but intersect in an irregular pattern above. Locality 9, depth 24 m.

B, cylindrical flow lobes draped over low scarp about 2 m high. Upslope flow lobes join one another (as beneath diver's knees) and merge into larger flow units. Detail of scarp on right is shown in *C*. Locality 10, depth 16 m.

C, elongate pillows draped over vertical scarp. Compare with *B*. Pillow in center actually stands as a free column and is not attached to wall behind. Note longitudinal fluting and tensional cracks commonly perpendicular to length. Locality 9, depth 16 m.

downslope, though this direction is commonly slightly divergent because of local irregularities. No pillows were seen whose long axes are close to perpendicular to the downslope direction.

The elongate pillows are commonly covered with small wrinkles, 2–3 cm in wavelength, whose axes are approximately perpendicular to the long dimension of the pillow (fig. 5*A*). The wrinkles are parallel to the length of some pillows, however (fig. 5*C*). Tensional cracks cut the surfaces of the pillows irregularly; most of these cracks are perpendicular to the wrinkles (fig. 5*A*), but some are notably perpendicular to the long axis of the pillow (figs. 4*C* and 5*C*), particularly in steeply plunging pillows.

The bases of scarps draped by elongate pillows are littered in many places with piles of broken pillows (figs. 2*C*, 4*C*, 5*A*, and 6). Some of the pillows may have broken and collapsed during flowage, but probably most of this breakage occurred later as currents and earthquakes disturbed the more fragile pillows on steep scarps. Despite the presence of fragmented pillows, very little fine-grained hyaloclastic material was observed. Such material may have been removed by current action in some places, but where good sections are visible in submarine scarps, no sand- or gravel-size material is present, and elongate pillows side by side make up the entire exposure.

Figure 6.—Lower end of elongate pillow of fig. 5*A* is shown at left. Typical pillow fragments bounded by joint surfaces litter scarp. Locality 9, depth 24 m.

The long axes of elongate pillows are parallel to the flow direction, and the blunt terminations of the elongate pillows as well as their division into two or more smaller pillows are consistently in the downflow direction. These observations of the Etnan pillows may be of value in determining the flow direction of uplifted ancient pillowed complexes.

PETROLOGY

The basalts from the 1381 lava flow and from the Punta Aguzza flow are nearly identical petrographically. Both are very porphyritic and contain about 30 percent phenocrysts by volume, including plagioclase (20 percent), augite (4–9 percent), olivine (2–3 percent), and magnetite (about 0.5 percent).

Petrographically the basalt is similar to most of the recent Etnan lavas, particularly those with abundant plagioclase and augite phenocrysts (type 3 of Di Franco, 1930). It is typical of most, but not all, recent flows from the present main vent or from flank eruptions related to activity at the main vent.

Historic lavas from Mount Etna consist of from 46.5 to 50.0 percent SiO_2, 3.5 to 5.5 percent Na_2O, and 1.0 to 2.0 percent K_2O (Carapezza, 1962; Sturiale, 1968, 1970; Tanguy, 1966). Chemically these lavas from Etna are more similar to hawaiites than to alkali olivine basalt (Macdonald, 1968), differing from both chiefly by a higher alumina content (17.5 percent average versus 14.7–15.9) and by a lower titania content (1.8 percent average versus 3.0–3.4 percent) (Cristofolini, 1971).

In the basalts sampled in this study the largest phenocrysts, those of plagioclase, are elongate laths as much 2 mm long. The plagioclase shows oscillatory zoning and contains abundant inclusions of pale-brown glass where such glass is common in the matrix of chilled margins of pillows.

Augite occurs as prisms averaging 1.5 mm in length; it is pleochroic in shades of pale green and pale brown, and shows faint zoning, commonly oscillatory. Inclusions of magnetite, 0.2 mm in size or smaller, are common in augite phenocrysts.

Olivine phenocrysts are decidedly less abundant and are smaller than augite or plagioclase. The average 0.6 mm in greatest dimension and generally show good crystal form. Magnetite crystals are common within olivine crystals and also adhere to the margins of olivine phenocrysts.

Magnetite occurs as well-formed equidimensional octahedral crystals, the largest of which are approximately 0.3 mm. These microphenocrysts occur in sideromelane glass in the outermost quenched rim of pillows and hence were present in the melt at the time of quenching.

Fresh, pale-brown sideromelane is the chief groundmass material in the outer 1–2 cm of the submarine flow surfaces. However, these samples differ from pillows studied elsewhere (Moore, 1966) in that many microlites, principally plagioclase and augite, are enclosed by the sideromelane. Modal analysis under high-power magnification indicate that about one-fourth to one-third of the matrix is composed of microlites in the size range of 0.01–0.1 mm. Because these microlites are present out to the outermost quenched rim of pillows, they were present in the melt at the time of quenching. Therefore, the lava, although appearing to have been fluid, contained 48–53 percent solid material (including 30 percent phenocrysts) during the period of flow and quenching on the sea floor.

The outer rim of the pillows is covered with a thin layer of organic calcareous material 0.2–1.4 mm thick. Beneath this is a red-brown layer of palagonitized sideromelane. The total thickness of the palagonite layer, 120–220 microns, is about the same for submarine lava collected at all the localities. The palagonite, however, not only grows inward from the outer pillow surface but also grows outward from minute fractures which commonly surround the abundant microlites. Hence, the measured thickness of the palagonite do not represent the actual distance that water and other materials have diffused to effect the alteration, and the thicknesses cannot be compared with those of palagonite that coats unfractured, microlite-free sideromelane (Moore, 1966). The measure thicknesses of single palagonite layers around a microlite or diffused from a fracture range from 9 to 16 microns, but these measurements are approximate because of the complex interference of diffusion fronts from many surfaces.

PROPAGATION OF ETNAN SUBMARINE LAVA FLOWS

Generally the Etnan lava flows appear to have been more fluid and less fragmental below sea level than above. The submarine part of the 1381 flow is dominated by rather smooth flow surfaces, although in places ridgelike flows surmounted by tumuli with irregularly fractured and striated lava surfaces are common. Much of the underwater part of the

Punta Aguzza flow is composed of cylindrical, downslope-directed flow units which branch and divide and are smaller, smoother, and better developed on steep slopes. The rarity of fragmental top surfaces is probably primarily the result of rapid chilling of the top surface of the flow into a tough coherent crust so that continued flowage takes place beneath a crust that is physically fixed in place. In contrast, the fragmental surfaces of subaerial flows are largely developed by rafting of solid material on top of the flow where it is repeatedly broken into angular blocks.

Elongate pillows generally are better developed on the steepest parts of the flow, where the surfaces slope from 30° to 90°. The same relations were noted on the submarine extension of the 1801 Huehue flow in Hawaii (Moore, 1970). Apparently steeper slopes are conducive to development of elongate pillows. The steeper slope results in more rapid flowage, which causes the chilled outer skin of a newly forming lava tongue to be thinner than if flow were slower. This thinner outer skin is more easily stretched and broken, permitting the tongues to divide and bud into new pillows.

Because of this tendency for a flow lobe to digitate and produce elongate pillows on steep slopes, a submarine flow can advance by splitting into numerous pillow tongues which drape the steep front. In this manner, foreset-bedded pillows, analogous to foreset bedding in subaqueous basalt breccias, are produced (Fuller, 1931). Figure 7 is a schematic diagram showing the development of foreset-bedded pillows on a submarine lava flow moving down an irregular submarine slope with a steady supply of new lava. Where the sea floor steepens, the front of the flow ruptures, feeding a pillow which drapes the slope (fig. 7*A*). The pillow continues growing as long as the pressure of the lava feeding it is great enough to stretch its growing and strengthening crust. The crust is simultaneously thickening owing to cooling and thinning owing to stretching as a result of expansion of the pillow. As the pillow grows larger with a constant volume increase, thinning of the crust will decrease more rapidly than thickening because a given increment of volume increase will have less effect on the rate of surface area increase. Eventually the strength of the thickening crust will prevent further growth, and once growth ceases, the contained liquid lava becomes stagnant, thus allowing the crust to thicken so rapidly that it is impossible for the pillow to grow again. The first pillow acts as a barrier to the main flow lobe (fig. 7*B*) which inflates, lifts its roof, and eventually breaks out at a point above the first pillow where resistance is least. Pillows continue to grow at the flow front (figs. 7*C*, *D*), effectively damming the main lava flow and causing it to inflate and break out above the pillows and override them with new pillows. Each new pillow is capable of growing only about to the base of the scarp because growth and expansion require in part stretching due to gravity on the steep flow front. These pillows will, of course, branch laterally also, and some may break into fragments that accumulate at the base of the scarp; both these processes will also effectively dam the flow front. In this way the flow front is maintained at

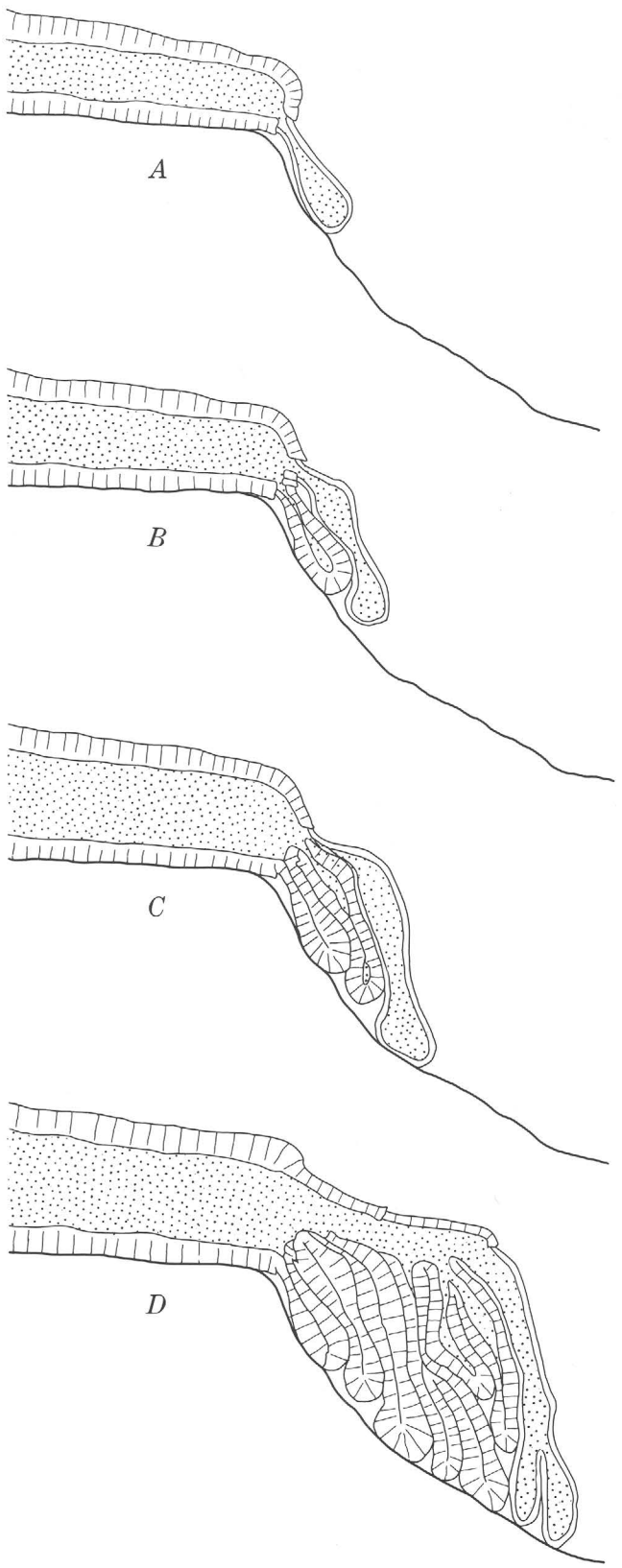

Figure 7.—Diagram showing propagation of a submarine lava flow moving down an irregular slope with a steady supply of new lava. Dotted pattern is liquid lava.

a steep angle of equilibrium, and a channel is propagated near the top of the growing pillow pile (fig. 7*D*). The ridges observed on the 1381 flow must mark near-surface lava tubes several meters in diameter which conduct lava to the digitating flow front. The channels do not solidify rapidly like the elongate pillows because they are generally larger and, more important, they contain flowing lava that continually supplies heat to retard growth of the crust. Continued delivery of lava causes the steep pillowed flow front to advance slowly downslope, thus pushing the original steep slope farther out to sea.

As shown in figure 7, each new pillow rests on the inclined stack of older ones but presents a free surface to water on its outer side. As a result, each pillow has a cuspate inner surface and a convex outer surface. A cross section of these elongate pillows would therefore show the characteristic differences between "top" and "bottom" surfaces so commonly described in ancient pillows (Compton, 1962; Jones, 1968). However, examination of figure 7 shows that the thickness of a pillowed flow, measured perpendicular to the long axes of the pillows, may be several times greater than the true stratigraphic thickness or the thickness of the feeding lava flow because of the steep initial dip

REFERENCES

Carapezza, Marcello, 1962, Caraterri petrochimici e litologici delle lave dell'Etna: Acta Geol. Alpina, v. 8. p. 181–248.

Compton, R. R., 1962, Manual of field geology: New York and London, John Wiley & Sons, Inc., 378 p.

Cristofolini, Renato, 1971, La distribuzione del titanio nelle vulcaniti etnee: Period. Mineralogia. [In press]

Di Franco, S., 1930, Ricerche petrografiche sulle lave dell'Etna: Accad. Gioenia Sci. Nat. Catania Atti, ser. 5, v. 17, Mem. 2, 120 p.

Fuller, R. E., 1931, The aqueous chilling of basaltic lava on the Columbia River plateau: Am. Jour. Sci., ser. 5, v. 21, no. 124, p. 281–300.

Grillo, M., 1954, Sistema eruttivo e colata lavica dell'Etna del 1381: Accad. Gioena Sci. Nat. Catania Boll., ser. 4, v. 2, fasc. 7, p. 405–419.

Jones, J. G., 1968, Pillow lava and pahoehoe: Jour. Geology, v. 76, no. 4, p. 485–488.

Macdonald, G. A., 1968, Composition and origin of Hawaiian lavas, *in* Coats, R. R., Hay, R. L., and Anderson, C. A., eds., Studies in volcanology—A memoir in honor of Howel Williams: Geol. Soc. America Mem. 116, p. 477–522.

Moore, J. G., 1966, Rate of palagonitization of submarine basalt adjacent to Hawaii, *in* Geological Survey Research 1966: U.S. Geol. Survey Prof. Paper 550-D, p. D163–D171.

———1970, Pillow lava in a historic lava flow from Hualalai volcano, Hawaii: Jour. Geology, v. 78, no. 2, p. 239–243.

Pichler, Hans, 1970, Volcanism in eastern Sicily and the Aeolian Islands, *in* Geology and history of Sicily: Petroleum Exploration Soc. Libya, Ann. Field Conf., 12th, p. 261–281.

Rittmann, Alfred, 1964, Vulkanismus and Tektonik des Aetna: Geol. Rundschau, v. 53, p. 788–800.

Sciuto-Patti, Carmelo, 1872, Carta geologica della cità di Catania e dintorni di essa: Accad. Gioenia Sci. Nat. Atti, ser. 3a, v. 7, p. 141–190.

Sturiale, Carmelo, 1968, A subterminal radial fissure eruption on Mt. Etna: Geol. Rundschau, v. 57, no. 3, p. 766–773.

———1970, La singolare eruzione dell'Etna del 1763 ("la Montagnola"): Soc. Italiana Mineralogia e Petrologia Rend., v. 26, fasc. 1, p. 313–351.

Tanguy, J. C., 1966, Les laves recentes de l'Etna: Soc. Geol. France Bull., ser. 7, v. 8, p. 201–217.

Travaglia, Riccardo, 1885, Geological map of Italy, Sheet 270, Catania: Comitato Geol. Roma, scale 1:100,000.

Wentworth, C. K., and Macdonald, G. A., 1953, Structures and forms of basaltic rocks in Hawaii: U.S. Geol. Survey Bull. 994, 98 p.

CLINOPTILOLITE-BEARING TUFF BEDS IN THE CREEDE FORMATION, SAN JUAN MOUNTAINS, COLORADO

By THOMAS A. STEVEN and RICHARD E. VAN LOENEN,
Denver, Colo.

Abstract.—Samples from three altered tuff beds in the Creede Formation near Creede, Colo., show that clinoptilolite is locally a major constituent, and in places is sufficiently abundant to be of economic interest. Considerable additional work will be required before the economic potential can be adequately assessed.

Samples of altered tuff beds from three localities in the Creede Formation near Creede, Colo. (fig. 1), indicate that the zeolite clinoptilolite is a major constituent and, locally at least, is sufficiently abundant to be of economic interest. These samples were taken in the summer of 1970 after earlier discussions with R. A. Sheppard, U.S. Geological Survey, suggested to us that the environment of deposition of the Creede Formation was similar to that in which other bedded zeolite deposits in the Western United States formed. Mr. Sheppard further helped in interpreting X-ray and analytical data from the samples, and his assistance throughout the investigation is gratefully acknowledged.

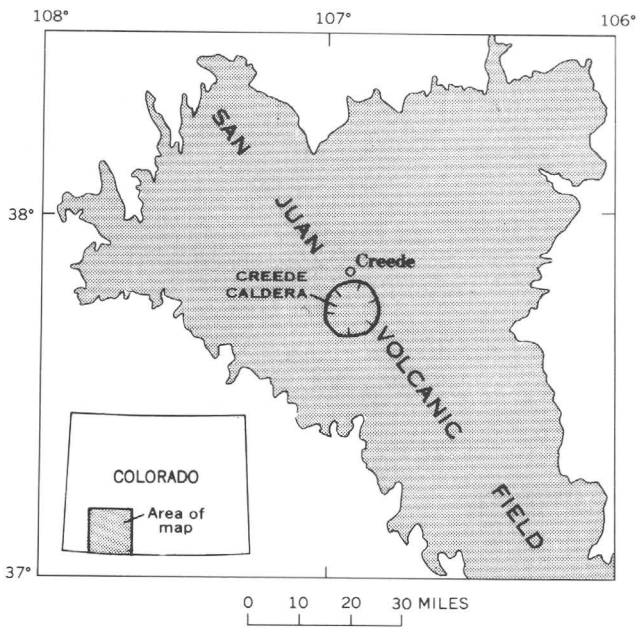

Figure 1.—Map of San Juan volcanic field, southwestern Colorado.

Many zeolites have the property of accumulating specific ions from solutions to which they are exposed, either by adsorption, by ion exchange, or by acting as molecular sieves. This property has found many practical applications, and the industrial use of zeolites is rapidly expanding. Clinoptilolite has the specific ability to trap ammonium ions (NH_4^+), and thus has considerable potential use in treating water polluted by sewage or agricultural effluents (Mercer, 1969). It adsorbs radioactive isotopes of cesium and strontium, and thus is effective in radioactive waste disposal (Brown, 1962); also, a process utilizing clinoptilolite has been developed which permits commercial separation of oxygen and nitrogen from the atmosphere (Minato and Utada, 1969, p. 132). Clinoptilolite is also used for absorbing noxious odors from the air, for removing moisture from gases, and as a soil conditioner and fertilizer extender in agriculture.

One of the altered tuff beds sampled (DS–429, fig. 3) was worked in the 1920's and 1930's as a source of bentonite; the clay produced was used as fuller's earth in purifying and decolorizing vegetable oils (Larsen, 1930, p. 108; Nutting, 1943, p. 151). Other zeolitic tuff beds were prospected during this period of activity, and the best exposures of these tuffs are in old pits and adits (DS–426, fig. 3).

Our sampling was preliminary, in that several different samples were taken at each of three localities; each locality was on a separate altered tuff unit. The purpose was to determine whether zeolites are present in any of these beds and, if so, in what types of materials. Many other altered tuff beds of the same general aspect are along the northern margin of the Creede caldera, but were not sampled.

GEOLOGY

The Creede Formation (figs. 2, 3) was deposited in a structural moat around the periphery of the Creede caldera in

U.S. GEOL. SURVEY PROF. PAPER 750-C, PAGES C98-C103

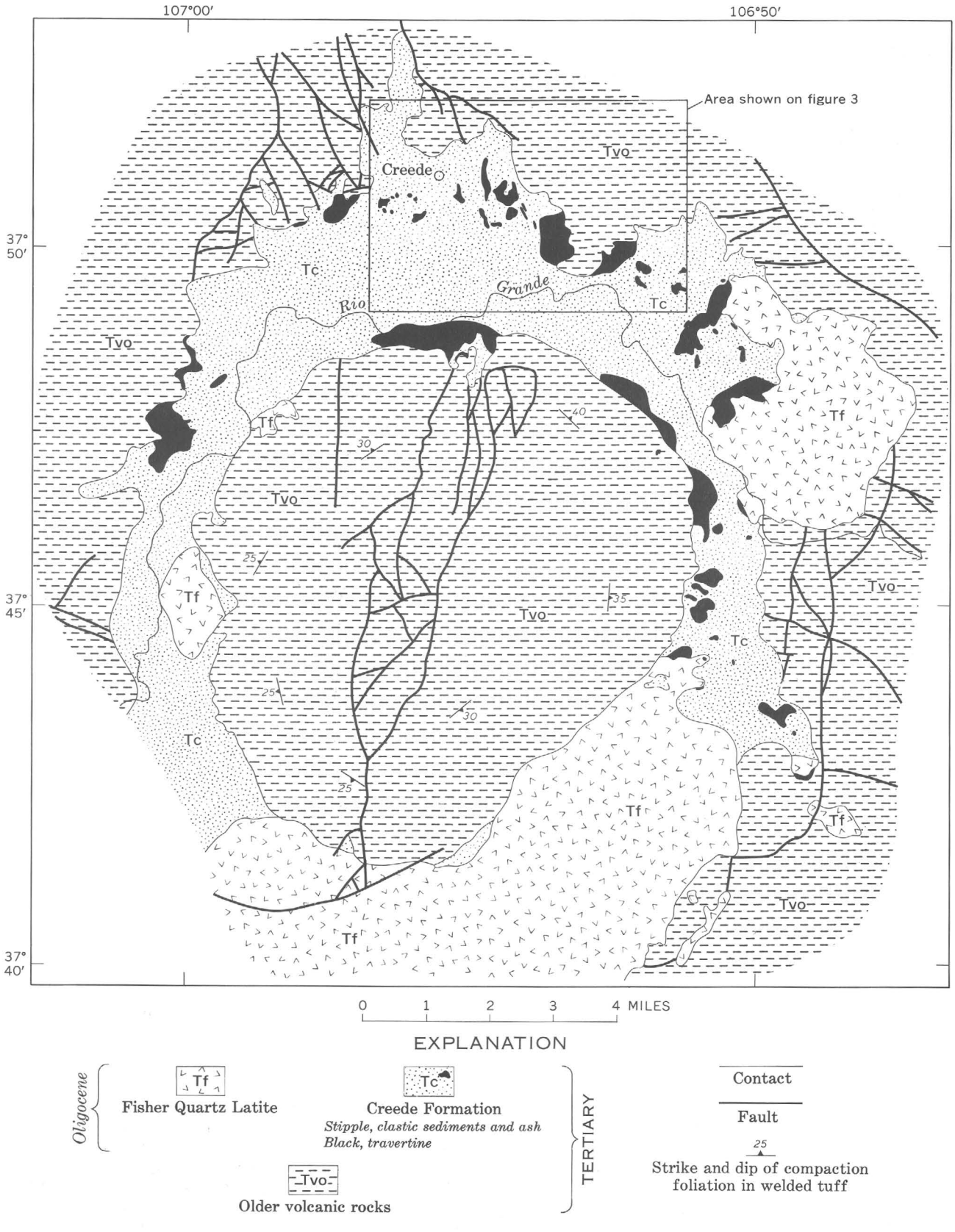

Figure 2.—Geologic map of the Creede caldera. From Steven and Friedman (1968, fig. 2).

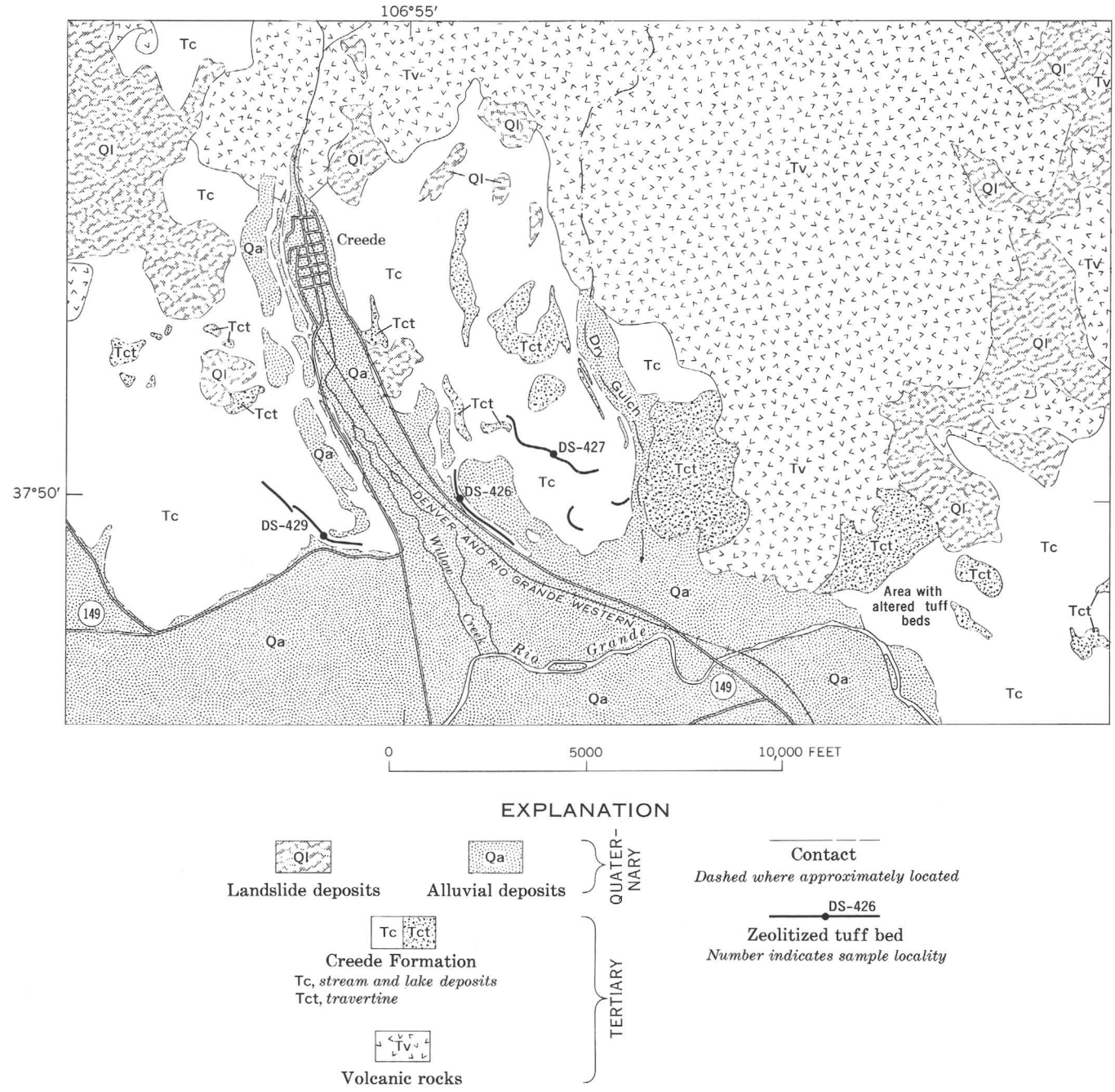

Figure 3.—Geologic map of the Creede area, San Juan Mountains, Colo., showing sample localities. Modified from Steven and Ratté (1965, pl. 1).

the central part of the San Juan volcanic field shortly after collapse and resurgent doming of the caldera core in late Oligocene time (Steven and Ratte', 1965; Steven and others, 1967). Details of caldera subsidence and postcaldera deposition of the Creede Formation have been given by Steven and Ratte' (1965) and Steven and Friedman (1968); the description given by Steven and Friedman (p. B30) is applicable to the present discussion, and is quoted in the following paragraphs:

The Creede Formation consists of several facies, whose distribution depends on local conditions of deposition and on proximity to sources of the different constituent materials. Primary igneous materials, largely ash, are abundant along the eastern margin of the caldera and increase southward toward their probable source in the Fisher Quartz Latite vent areas south of the caldera. Nonwelded ash-flow deposits form the largest bulk of this primary igneous material, although airfall ash is widespread and a few thin layers of welded tuff are present locally. Lava flows of Fisher Quartz Latite intertongue with the ashy deposits

of the Creede Formation and indicate that the Creede and the Fisher accumulated concurrently. Most of the Creede Formation along the northern and western margins of the caldera consists of reworked ashy sediments or of volcanic sands and gravels, and ranges from thin-bedded shallow-lake deposits to conglomeratic stream deposits. Most commonly the stream deposits are in tributary valleys in the outer wall of the caldera or they are interbedded with the lake-deposit facies opposite the mouths of such tributary valleys. Some layers of nearly pure bentonite representing ashfall deposits are interlayered with the reworked sedimentary deposits. The steep outer walls of the caldera commonly are mantled with a layer of talus-regolith which grades outward or intertongues laterally with stream or lake deposits toward the middle of the moatlike basin.

The travertine in the Creede Formation occurs in a wide variety of local deposits. Some was deposited by mineral springs that issued well above the level of concurrent sedimentation, and forms inclined sheetlike masses cementing talus or regolith deposits along the steep outer walls of the caldera. In places the lower ends of these tabular marginal masses split into a series of tongues that are interlayered with the clastic sedimentary beds and wedge out toward the center of the basin. In other places, masses of the travertine are completely surrounded by sedimentary rocks and commonly grade from a central mass of travertine, through a marginal zone of intertongued wedges of travertine and sedimentary beds, into normal stream or lake deposits with little or no travertine. Some of these masses show structures suggesting original travertine terrace form, but more commonly this is not apparent in present exposures. Some masses show local tubular openings that probably represent original spring orifices. Hard beds, ranging from sedimentary strata highly cemented with calcite to nearly pure limestone, occur in the Creede Formation in the vicinity of some of the irregular travertine masses, and probably resulted from carbonate deposition in shallow ponds fed by the mineral springs.

Of particular interest are the strata identified in the quotation as "layers of nearly pure bentonite representing ashfall deposits * * * " along the northern margin of the caldera, which are shown here to consist in part, and locally almost entirely, of clinoptilolite. These beds were deposited as glassy volcanic ash in shallow ponds along the northern margin of the caldera, at the side of the doughnut-shaped basin of deposition opposite from the probable sources of ash in the concurrently active Fisher Quartz Latite volcanoes. The ponds were shallow, as indicated by numerous mud cracks and ripple marks in the reworked ashy sediments nearby and by the abundant interlayered fluviatile deposits.

The zeolitic tuff units range in thickness from 0 to 20 feet and extend laterally from a few hundred feet to 4,000 feet or more. They are generally poorly exposed and are difficult to trace where they are a few feet or less thick. The thicker parts of the beds commonly are light-gray to white streaks across the relatively bare yellow clayey surfaces that characterize many of the steeper south-facing slopes underlain by the Creede Formation. As flatter slopes are generally grassy and the float consists mostly of relatively hard, somewhat silicified shale or sandstone, the soft zeolite tuff is difficult to follow.

Zeolitic tuff beds generally have formed during diagenesis by reaction of vitric volcanic ash with pore waters of varying salinities and alkalinities (Sheppard, 1970, p. 452–455). Ash deposited in lacustrine or marine environments seems especially subject to zeolitization. According to Mariner and Surdam (1970, p. 616), clinoptilolite and mordenite characterize fresh-water or marine deposits, whereas less siliceous zeolites commonly occur in saline alkaline lake deposits. No evidence was seen to indicate that the waters associated with the lacustrine facies of the Creede Formation were particularly saline.

ZEOLITIC TUFFS

The zeolitic tuff in the Creede Formation generally is a compact, white to gray earthy material with a characteristic conchoidal fracture. The surface texture ranges from smooth and chalky on extremely fine grained material to distinctly grainy on microgranular material. Details of original bedding can be discerned in places, but commonly the zeolitic alteration has obliterated the primary sedimentary textures and structures, and on cursory inspection the altered tuff appears massive. Small crystal fragments of pyrogenic phenocrysts, chiefly feldspar, quartz, and biotite, range in abundance from traces to as much as 20 percent or more of the tuff. Local irregular areas of harder opaline tuff have a greasy luster and are yellowish to greenish gray. Carbonized plant fragments are locally abundant in some tuff. Weathering slakes the zeolitic tuff to fine angular chips and chalky dust.

As seen in thin section, the clinoptilolite-rich tuffs have a well-preserved vitroclastic texture, in which the relict shards are mostly replaced by clinoptilolite. This texture is not well preserved in the opal-rich rocks. Vesicles are common throughout the tuffs; locally these are partially filled with very fine but well-crystallized clinoptilolite, and the core is either empty or filled with calcite. As discerned in X-ray diffractometer powder patterns, clinoptilolite also forms a major part of the very fine ($< 4\mu$) groundmass, where it is intermixed with opaline silica and (or) montmorillonite. The mean index of refraction of crystalline aggregates of clinoptilolite is 1.474–1.476.

The small fragments of pyrogenic phenocrysts mentioned above are unaltered and are dispersed uniformly throughout the zeolite-rich rocks that appear to have formed from single air falls, whereas they tend to be concentrated in layers in the zeolite-poor rocks that may represent reworked ash. Sanidine, plagioclase, and quartz occur as angular fragments as much as 0.2 mm in diameter; some biotite flakes are nearly 1 mm across.

Clinoptilolite is difficult to distinguish from a closely similar zeolite mineral, heulandite. However, the crystal structure of clinoptilolite is stable under thermal conditions (350°C), whereas heulandite heated above 230°C is transformed to "heulandite B" (Mumpton, 1960), a material with a partially collapsed crystal structure. Samples DS–426A and DS–427E were heated to 350°C for 4 hours and then scanned by X-ray diffraction. No apparent shift was noted for the 8.9–A (020) peak. Thus clinoptilolite is the only zeolite in these altered tuffs.

The approximate chemical composition of the zeolitic tuffs was determined by semiquantitative spectrographic analyses

(table 2). As can be seen from the analyses of the clinoptilolite-rich samples (DS–426A, B, from table 1), the alkali and calcium contents are approximately K=3 percent, Na=2–3 percent, and Ca=1.5 percent. This indicates that the Creede Formation clinoptilolite is relatively potassium rich compared with most clinoptilolites in which sodium is the dominant alkali (Sheppard and Gude, 1969, p. 13), but it is well within the range of other potassic clinoptilolites that have been described (Sheppard and others, 1965, p. 247; Sheppard and Gude, 1965, p. D45). Barium and strontium are consistently high (300–700 ppm) in all samples. The concentrations of these elements seem about the same whether the sample is mostly clinoptilolite (DS–426A–E; DS–427D, E), mostly opal (DS–427A), or mostly montmorillonite (DS–429B, C) (see table 1), and the two probably are in different mineral phases.

Table 1.–*Mineralogic composition (in parts of 10) of altered tuffs from the Creede Formation, Colorado, as estimated by X-ray diffraction*

[Tr., trace]

Sample No. DS– (fig. 3)	Clinoptilolite	Opal	Montmorillonite	Crystal fragments
426A	9	<1	...	1
426B	8	1	...	1
426C	7	2	...	1
426D	7	2	...	1
426E	6	3	...	1
427A	>1	6	Tr.	2
427B	4	>3	2	<1
427C	4	>2	>2	<1
427D	8	1	...	<1
427E	8	>1	...	<1
429A	4	>2	3	<1
429B	<1	3	7	<1
429C	<1	>2	6	1

The results of the sampling (table 1) show that the thickest high-grade zeolitic tuff came from locality DS–426, where samples A, B, C, and D contain 7–9 parts out of 10 clinoptilolite. At locality DS–427, samples D and E contain 8 parts out of 10 clinoptilolite, but the other samples are much lower in grade. Samples from the dump of the bentonite mine at locality DS–429 are irregular mixtures of clinoptilolite, montmorillonite, and opal. These results indicate that the mineralogy of the altered tuffs varies considerably from bed to bed and probably from place to place within individual beds. Considerable additional exploration and sampling will be necessary before the distribution of the higher grade clinoptilolite-bearing material can be determined or the economic potential of any of the deposits can be assessed.

DESCRIPTION OF SAMPLES

Several different samples were collected from each of the localities sampled in order to obtain some idea of the range in mineralogy within the altered tuff beds. Table 1 gives the mineralogic composition of the samples as determined by X-ray diffraction techniques.

Locality DS–426.–An old prospect adit into a massive white zeolitic tuff unit more than 10 feet thick. This bed crops out discontinuously along the low slopes 200–300 feet northeast of State Highway 149 and 400–500 feet northeast of the Denver and Rio Grande Western Railroad, 1–1½ miles southeast of Creede (fig. 3).

Sample A: Microgranular white tuff with clearly visible biotite flakes; collected from dump.

Sample B: Material similar to A collected from a massive tuff bed near the portal of the adit.

Sample C: Smooth-textured, even-grained chalky white tuff from dump.

Sample D: Bedded, very fine grained gray tuff from dump.

Sample E: Sack of fine chips of slaked zeolitic tuff from dump.

Locality DS–427.–A poorly exposed zeolitic tuff bed on the ridge between Willow Creek and Dry Gulch, about 1½ miles southeast of Creede. Grab samples were taken over a strike length of about 500 feet.

Sample A: White, thinly laminated fissile shale.

Samples B and C: Thin-bedded tuff with a greasy-gray luster.

Samples D and E: Massive earthy white tuff with clearly visible biotite flakes. Looks closely similar to the clinoptilolite-rich samples from DS–426.

Locality DS–429.–The abandoned bentonite mine about 1½ miles south of Creede. Workings are caved, and all samples were taken from the dump.

Sample A: From a large chunk of earthy massive gray tuff. The unslaked character of the material probably reflects the abundance of clinoptilolite and opal.

Sample B: Fragments of slaked gray tuff ½–1½ inches in diameter.

Sample C: Fine chips of slaked gray tuff; fragments mostly less than one-fourth inch in diameter.

REFERENCES

Brown, R. E., 1962, The use of clinoptilolite: Ore Bin, v. 24, no. 12, p. 193–197.

Larsen, E. S., Jr., 1930, Recent mining developments in the Creede district, Colorado: U.S. Geol. Survey Bull. 811–B, p. 89–112.

Mariner, R. H., and Surdam, R. C., 1970, Zeolitization of siliceous tuffs in saline alkaline lakes [abs.]: Geol. Soc. America Abs. with Programs, v. 2, pt. 7, p. 616–617.

Mercer, B. W., 1969, Clinoptilolite in water-pollution control: Ore Bin, v. 31, no. 11, p. 209–213.

Minato, Hideo, and Utada, Minoru, 1969, Zeolite, *in* The clays of Japan, 1969 Internat. Clay Conf.: Japan Geol. Survey, p. 121–134.

Mumpton, F. A., 1960, Clinoptilolite redefined: Am. Mineralogist, v. 45, nos. 3–4, p. 351–369.

Table 2.—*Semiquantitative spectrographic analyses of the altered tuffs from the Creede Formation, Colorado*

[Analyst: Leon A. Bradley. Results are to be identified with geometric brackets whose boundaries are 1.2, 0.83, 0.56, 0.38, 0.26, 0.18, 0.12, and so forth, but are reported arbitrarily as midpoints of these brackets; 1.0, 0.7, 0.5, 0.3, 0.2, 0.15, and 0.1, and so forth. The precision of a reported value is approximately plus or minus one bracket at 68-percent, or two brackets at 95-percent confidence. G, greater than 10 percent; N, not detected; L, detected but below limit of determination. Elements looked for but not detected: Ag, As, Au, Bi, Cd, Eu, Ge, Hf, In, Mo, P, Pd, Pr, Pt, Re, Sb, Sm, Sn, Ta, Te, Th, U, W, Zn]

Sample No. DS–.....	426A	426B	426C	426D	426E	427A	427B	427C	427D	427E	429A	429B	429C
Weight percent													
Fe	1.0	0.7	1.0	1.0	0.7	1.5	1.0	1.5	0.3	0.5	2.0	2.0	2.0
Mg	.5	.5	.5	.7	.5	.7	.7	.7	.3	.3	.7	1	1
Ca	1.5	1.5	1.5	1.5	1.5	1.5	1.5	2	2	1.5	1	1.5	1.5
Ti	.15	.1	.15	.1	.1	.2	.07	.07	.05	.07	.07	.1	.15
Si	G	G	G	G	G	G	G	G	G	G	G	G	G
Al	7	7	7	7	7	7	7	7	7	7	7	7	7
Na	3	2	1.5	3	1.5	1	.7	.5	.5	.5	.7	1.5	.7
K.	3	3	3	5	3	3	3	3	3	3	3	3	3
Parts per million													
B.	L	L	30	20	20	30	20	L	L	L	L	L	20
Ba	700	700	500	500	500	500	500	500	500	500	300	500	500
Be	3	2	3	2	3	3	3	3	1.5	2	1.5	1.5	2
Ce	N	N	N	300	N	N	N	N	N	N	N	N	N
Co	L	L	N	N	N	3	N	N	N	N	L	3	3
Cr	15	2	5	20	3	20	7	7	15	15	7	7	7
Cu	3	3	7	10	2	20	3	7	5	5	7	7	7
Ga	30	30	20	30	20	15	30	20	15	15	20	30	20
La	50	30	30	100	30	50	50	30	30	30	N	30	30
Li	L	L	L	L	L	50	70	70	L	L	L	150	100
Mn	150	150	100	150	150	200	150	100	30	30	150	300	300
Nb	10	L	10	10	10	10	10	10	10	15	L	L	L
Nd	N	N	N	150	N	N	N	N	N	N	N	N	N
Ni	10	N	N	15	N	15	L	L	7	7	L	L	L
Pb	30	30	30	30	20	15	15	15	15	20	20	30	30
Sc	7	5	7	5	L	10	5	5	L	L	5	5	5
Sr	700	700	500	500	500	500	700	700	700	700	500	500	300
V.	15	15	20	15	15	70	15	15	10	10	15	30	30
Y.	20	15	20	20	15	20	20	15	15	20	10	15	15
Yb	2	1.5	2	2	2	3	3	2	1.5	2	1	1.5	1.5
Zr	150	70	70	70	100	100	70	70	100	100	70	70	70

Nutting, P. G., 1943, Adsorbent clays, their distribution, properties, production, and uses: U.S. Geol. Survey Bull. 928–C, p. 127–221.

Sheppard, R. A., 1970, Zeolites in sedimentary deposits of the United States–a review, *in* Internat. Conf. on Molecular Sieve Zeolites, 2d: Washington, D.C., Am. Chem. Soc., p. 428–459.

Sheppard, R. A., and Gude, A. J., 3d, 1965, Zeolitic authigenesis of tuffs in the Ricardo Formation, Kern County, southern California, *in* Geological Survey Research 1965: U.S. Geol. Survey Prof. Paper 525–D, p. D44–D47.

——1969, Diagenesis of tuffs in the Barstow Formation, Mud Hills, San Bernardino County, California: U.S. Geol. Survey Prof. Paper 634, 35 p.

Sheppard, R. A., Gude, A. J., 3d, and Munson, E. L., 1965, Chemical composition of diagenetic zeolites from tuffaceous rocks of the Mojave Desert and vicinity, California: Am. Mineralogist, v. 50, nos. 1–2, p. 244–249.

Steven, T. A., and Friedman, Irving, 1968, The source of travertine in the Creede Formation, San Juan Mountains, Colorado, *in* Geological Survey Research 1968: U.S. Geol. Survey Prof. Paper 600–B, p. B29-B36.

Steven, T. A., Mehnert, H. H., and Obradovich, J. D., 1967, Age of volcanic activity in the San Juan Mountains, Colorado, *in* Geological Survey Research 1967: U.S. Geol. Survey Prof. Paper 575–D, p. D47–D55.

Steven, T. A., and Ratte', J. C., 1965, Geology and structural control of ore deposition in the Creede district, San Juan Mountains, Colorado: U.S. Geol. Survey Prof. Paper 487, 90 p.

CLAY MINERALS, LONGFELLOW MINE, SAN JUAN COUNTY, COLORADO

By ROBERT G. LUEDKE and JOHN W. HOSTERMAN,
Washington, D.C., Beltsville, Md.

Prepared in cooperation with the Colorado State Mining Industrial Development Board

Abstract.—A high-alumina montmorillonite-type clay mineral is found in association with pyrophyllite, dickite, and illite at the Longfellow mine in the San Juan Mountains, Colo. This mine is one of the chimney ore deposits in the highly fractured and locally solfatarically altered volcanic rocks in the Red Mountain mining district within the ring-fault zone of the Silverton cauldron. The variety and distribution of the clay minerals in the hydrothermal environment at the Longfellow mine suggest a crude zoning within the ore deposit. From the center of the ore body outward to the propylitically altered country rock, the zones on the basis of clay minerals are: (1) high-alumina montmorillonite; (2) high-alumina montmorillonite and pyrophyllite; (3) high-alumina montmorillonite, pyrophyllite, and dickite; (4) dickite and illite; and (5) illite and chlorite.

The Longfellow mine is just east of and near the crest of Red Mountain Pass (Ouray-San Juan County line) on U.S. Highway 550 (fig. 1). The deposit penetrated by this mine is fairly typical of chimney ore deposits of the Red Mountain mining district in the western San Juan Mountains of southwestern Colorado. Mine development started in the late 1940's or early 1950's and has continued intermittently to the present; the mine workings explore what are considered to be north and south ore bodies by means of a shaft and several short tunnels on the 150-foot level. In a shallow pit about 150 feet south of the shafthouse, a bulldozer cut has exposed mineralized ground which may, in part, be the near-surface expression of the south ore body. Geochemical samples collected from this pit were analyzed for both this preliminary study of clay minerals in rock alteration and a study of the nearby Uncompahgre primitive area (Fischer and others, 1968). Several samples collected from the mine workings in 1954 by C. T. Pierson, U.S. Geological Survey, were also examined.

W. S. Burbank (1950) has discussed some of the problems of solfataric alteration (hydrothermal) in shallow volcanic environments, particularly as related to the Red Mountain mining district of the San Juan region. He briefly mentioned (1950, p. 292) the associated clay minerals and stated a need for further study of them. This paper, therefore, presents preliminary data of our current study on the variety and distribution of the clay minerals in the Longfellow mine, which, in general, is representative of mines in the Red Mountain solfatarically altered area.

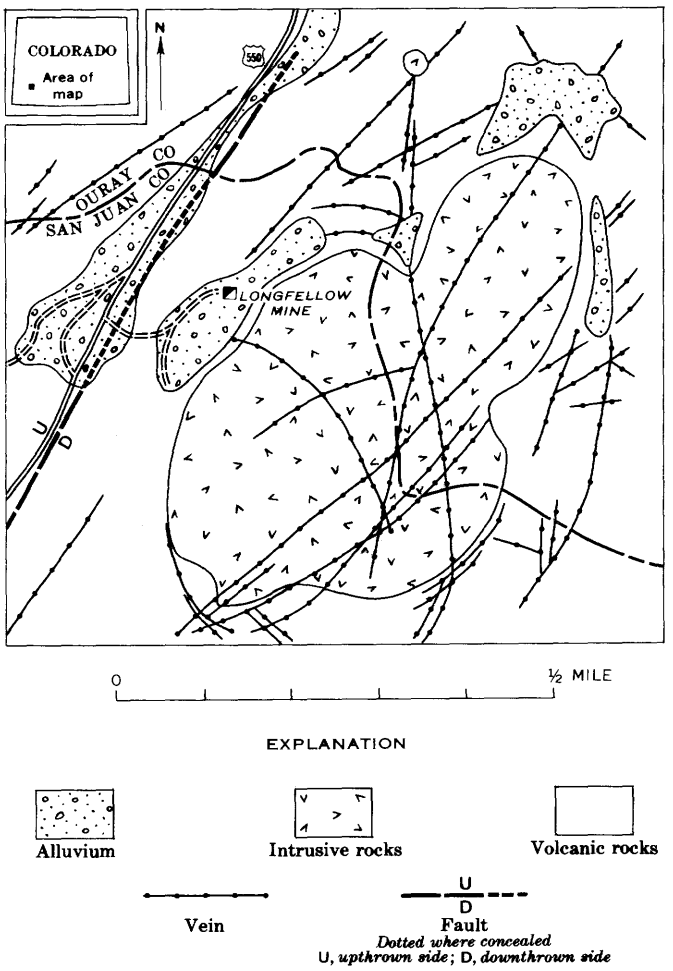

Figure 1.—Geologic map showing location of the Longfellow mine in volcanic rocks of southwestern Colorado.

U.S. GEOL. SURVEY PROF. PAPER 750-C, PAGES C104-C111

Acknowledgments.—Grateful acknowledgement for analytical laboratory assistance is extended to Laura Reichen for chemical analyses, to J. L. Harris and J. C. Hamilton for spectrographic analyses, and to E. J. Dwornik for electron microscopy. We wish to thank the owners of the Longfellow mine for permission to examine the property and to collect samples, and several colleagues of the U.S. Geological Survey, particularly Z. S. Altschuler, F. S. Fisher, and L. G. Schultz, for critical discussions and review. We are indebted to C. T. Pierson, U.S. Geological Survey, for use of his field notes and samples. Responsibility for interpretation of results as presented, however, is ours.

GEOLOGIC SETTING

The Longfellow mine is near the south end of a northeast-trending belt of altered and broken rocks about 3 miles long and half a mile wide. This belt, which contains most of the known chimney ore bodies in the Red Mountain area (Burbank, 1941; Burbank and Luedke, 1964), coincides with and is a segment of the structurally complex ring-fault zone on the west side of the Silverton cauldron (Luedke and Burbank, 1968; Burbank and Luedke, 1969); this cauldron is one of several principal eruptive source areas and volcano-tectonic subsidence structures within the San Juan volcanic field.

The country rock in the vicinity of the mine (fig. 1) consists of interbedded lava flows, flow breccias, and some tuffs of predominantly rhyodacitic to dacitic composition that have been extensively fractured and faulted into elongated and locally tilted blocks. Intruding this broken ground are circular to irregularly shaped composite quartz latitic and rhyolitic plugs of various sizes, which in part represent volcanic pipes. The ore deposits are vertical pipelike bodies or chimneys (fig. 2), commonly near the intrusive masses, and consist of massive sulfides with quartz and clay gangues.

The volcanic country rock in the area is everywhere altered to some extent and ranges from incipiently propylitized rock that has only a few minerals affected or new ones introduced away from the pipelike bodies to rock that is entirely decomposed to mostly quartz and clay minerals near the pipes. Where only slightly altered, the rock is hard, greenish gray, and moderately porphyritic, and contains plagioclase (mostly sodic andesine) and pyroxene phenocrysts in a dense aphanitic groundmass. Other interstitial materials include some biotite and apatite, and alteration products include chlorite, epidote, quartz, iron oxides, and carbonate and clay minerals. Where extensively altered, the yellow to red limonite-stained rock is a soft and crumbly to moderately hard granular mass. Pyrite varies in amount but is found throughout rocks of the area.

MINERALOGY

Mineralogical identifications of the clay minerals were made by X-ray diffraction methods using Cu$K\alpha_1$ (λ = 1.5405 A) radiation. Details of sample preparation are those described by Hosterman (1969, p. 6–7). In general, the samples were dispersed in deionized water, disaggregated ultrasonically, and, in several cases, size fractionated by centrifugal sedimentation. For X-ray diffraction, the clay fractions were mounted on porous tiles, a vacuum was used to extract the water through the tile, and the clay fractions were air dried at 100°C. A split of the dried clay fraction was pressed hydraulically into circular pellets, and some was made into stirred smear mounts.

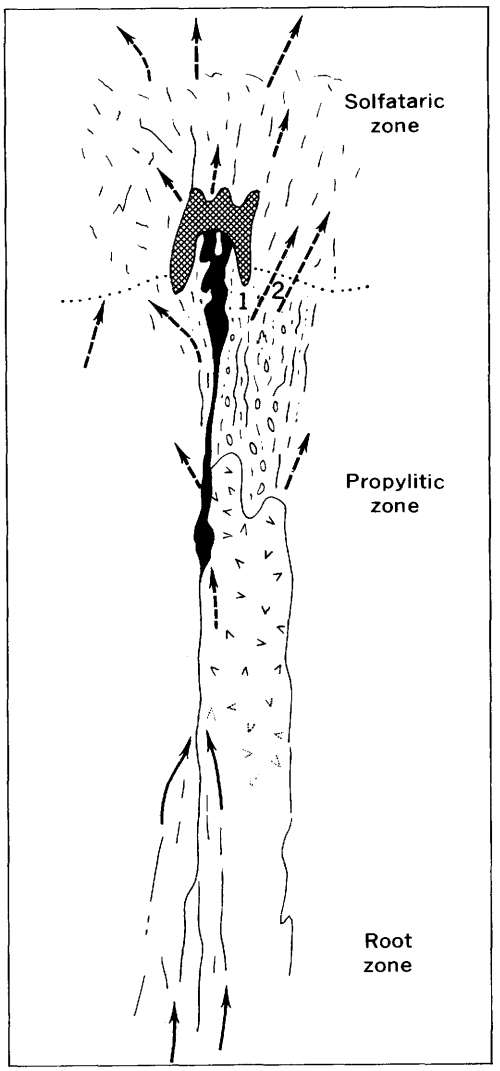

Figure 2.—Idealized chimney deposit of Silverton cauldron's solfatarically altered ring-fault zone (after Burbank and Luedke, 1961). Country rock was locally preheated by volcanic pipes before deposition of sulfide ore (black areas) under siliceous envelope of altered and mineralized rock (crosshatched). Solfataric zone is one of mixing with meteoric waters; propylitic zone is charged with carbon dioxide and other gases, under pressure, from deep-seated sources. Dashed arrows indicate general movements of gases; solid arrows, movements of solutions. Probable location of samples 1 and 2 in figure 3 is indicated.

Diffraction-pattern photographs were made of monomineral clays by use of the X-ray powder camera. All samples on tile were subsequently treated with ethylene glycol to check for expandable clay and heated to 300°C and 550°C to check for collapsible clay.

Within and near the mineralized ground of the Longfellow mine, the altered rock consists mostly of quartz, pyrite, and clay minerals, the principal subject of this paper. Quartz in the vugs and cavernous ground is crystalline, but elsewhere it is finely granular to dense. Pyrite likewise occurs in crystalline aggregates and as very fine granular to massive varieties. Very fine crystalline to massive enargite is locally intermixed with the pyrite. Other sulfide minerals found mainly within the ore bodies, but also sparingly through the altered rock, are chalcopyrite, sphalerite, galena, and silver-bearing sulfosalts. Gangue minerals, in addition to quartz and clay minerals, consist of fluorite, barite, and zunyite in very minor amounts.

The clay-mineral assemblage in the solfataric zone contains high-alumina montmorillonite, dickite, and pyrophyllite. The minerals in the propylitic zone are illite and chlorite. A discussion of the chemical and mineralogical properties of these minerals, their spatial relationships, and their probable hydrothermal origin follows.

Table 1.—*Chemical analyses of high-alumina montmorillonite, beidellite, and rectorite, in weight percent*

	Sample			
	1	2	3	4
SiO_2	45.19	47.28	45.32	54.11
Al_2O_3	36.29	20.27	27.84	40.38
Fe_2O_3	.76	8.68	.80	.15
CaO	.78	2.75	2.76	.52
MgO	.40	.70	.16	.78
Na_2O	3.95	.97	.10	3.87
K_2O	1.34	Trace	.12	.29
H_2O+	6.61	19.72	22.64	.....
H_2O-	4.18			
TiO_2	.12	.....	.....	.01
MnO	.06	.....	.....	.....
BaO	.06	.....	.....	.....
SO_3	.39	.....	.....	.....
S	.01	.....	.....	.....
Cl	.08	.....	.....	.....
F	.16	.....	.....	.....
Total	100.38	100.37	99.74	100.11
Less O	.09			
	100.29			

1. Lab. No. W171762. Field No. Long 3B. High-alumina montmorillonite from Longfellow mine, San Juan County, Colo. Chemical analysis by Laura Reichen; fluorine determined by S. M. Berthold. Analysis corrected for presence of sodium hexametaphosphate. Specific gravity: 2.38.
2. Beidellite from Beidell Creek, Saguache County, Colo. (Larsen and Wherry, 1917, p. 213).
3. Beidellite from Black Jack mine, Owyhee County, Idaho (Shannon, 1922, p. 4).
4. Rectorite from Fort Sandeman district, Baluchistan, Pakistan (Kodama, 1966, p. 1036).

High-alumina montmorillonite

The calculated chemical formula of high-alumina montmorillonite from the Longfellow mine is

$$[Al_{2.11}Fe_{0.04}Mg_{0.04}][Al_{0.86}Si_{3.14}]O_{10}[OH]_2x_{0.33}.$$

This formula corresponds in general to the theoretical structural formula for the montmorillonite group and is based upon the chemical analysis shown in table 1 and calculated using the method described by Ross and Hendricks (1945, p. 41–42). This analysis is one of a pure mineral in which no impurities were observed by X-ray diffraction and electron microscopy. As indicated in the chemical formula, almost one Al^{+3} ion replaces every fourth Si^{+4} ion in the tetrahedral sheet, and very few Al^{+3} ions are replaced by Mg^{+2} and Fe^{+2} ions in the octahedral sheet. The exchangeable cations of Ca, Na, and K are represented by x in the formula; x has an average value of 0.33, according to Ross and Hendricks (1945, p. 41). Their average value was used, as the cation exchange capacities were not determined for our mineral.

Very minor amounts of some trace elements may be accommodated in the octahedral sites (Deer and others, 1962, p. 230), but it is not possible to account for the relatively high concentrations of the few trace elements in the high-alumina montmorillonite (table 2). The conspicuous amounts of copper, lead, and zinc indicate close association with mineralized rock. Spectrographic analyses by J. C. Hamilton (written commun., Jan. 20, 1956) of clay samples collected by C. T. Pierson from the 150-foot level of the mine detected, in addition to most of the elements in table 2, trace amounts of Bi, Cs, Co, La, Nd, Ag, and Sn.

X-ray powder data show mainly the basal (00*l*) reflections because of the preferred orientation of the particles and the 060 reflection of d = 1.4849 A, which is used to indicate that this montmorillonite is a dioctahedral layered silicate mineral. The diffraction traces (fig. 3) show the basal (00l) spacing of this high-alumina montmorillonite to be about 24 A with water present and to range from 20 A, when the water molecules are removed upon heating to 300°C, to 27 A, when the clay is saturated by ethylene glycol.

The differential thermal analysis curve (fig. 4) of the high-alumina montmorillonite was made from an untreated pure mineral that had been maintained prior to heating in an atmosphere of 50-percent relative humidity. The endothermic peak at 100°C is due to moisture in the sample. The shoulder on this endothermic peak at 150°C, we suspect, may be due to Al^{+3} ions in the cation position. The broad endothermal peak

Table 2.—*Semiquantitative spectrographic analysis, in parts per million, of high-alumina montmorillonite, Longfellow mine, Colorado*

[J. L. Harris, analyst; lab. No. W171763. Elements looked for but not detected: Ag, As, Au, Be, Bi, Cd, Ce, Co, Eu, Ge, Hf, In, La, Li, Mo, Nb, Pd, Pt, Re, Sb, Sn, Ta, Te, Th, Tl, U, W]

B	50	Sc	20
Cr	30	Sr	200
Cu	500	V	150
Ga	20	Y	20
Ni	70	Yb	2
Pb	1,000	Zn	2,000
		Zr	70

at about 550°C is due to dehydroxylation and is in good agreement with data given by Greene-Kelly (1957, p. 148). The high-temperature endothermic peak obtained at about 975°C probably represents complete destruction of the crystal lattice.

Figure 5*A* shows the morphology of the high-alumina montmorillonite in an electron photomicrograph. The wispy, otherwise nondescript, character is typical of montmorillonite minerals. E. J. Dwornik (written commun., June 23, 1969) described the observed fraction as an extremely thin filmy phase similar in habit to the Mg-montmorillonite, saponite. The almost negligible amount of MgO in the chemical analysis (table 1), however, eliminates consideration of a Mg-montmorillonite phase.

Optical determinations of the high-alumina montmorillonite in thin section showed a pale-brown, almost amorphous-appearing material of moderate to low birefringence. Minute flakes of montmorillonite removed from a tile sample appeared in index oils as irregularly shaped masses, and in plain light they were colorless to very pale brown. Acute bisectrix figures indicated a biaxial negative mineral with a low $2V$ value estimated at 5°–15°.

The chemistry, X-ray diffraction traces, differential thermal analysis, and morphology (as seen in the electron microscope) of high-alumina montmorillonite suggest similarities to and differences from both beidellite and rectorite. Beidellite, a high-allumina montmorillonite from Beidell Creek, Saguache County, Colo., was first named and described by Larsen and Wherry (1917, 1925). This mineral was questioned and discredited by many mineralogists. Weir and Greene-Kelly (1962) redefined it, using a sample from the Black Jack mine, Idaho, as a dioctahedral montmorillonite that contains very little magnesium and iron. They recommended that the term "aluminian montmorillonite" be dropped and that the name "beidellite" be adopted for the aluminum-rich magnesium- and iron-poor dioctahedral end member of the montmorillonite-beidellite mineral series.

Rectorite, a so-called mixed-layer clay mineral from Garland County, Ark., was first named and described by Brackett and Williams (1891). This mineral has been shown by Brown and Weir (1963) to be the same as allevardite from Allevard, France; the former name had priority. The name "rectorite" has been applied to mixed mineral pairs of pyrophyllite layers or pyrophyllite and vermiculite layers (Bradley, 1950), micalike layers (Brindley, 1956), micalike and montmorillonitelike layers (Brown and Weir, 1963), and paragonitelike and montmorillonite-beidellitelike layers (Kodama, 1966).

The low magnesia and iron and high alumina contents (table 1) relate the Longfellow high-alumina montmorillonite chemically to both beidellite and rectorite. The moderately high weight percentage of Na_2O also suggests a comparison with, particularly, rectorite. The low weight percentage of K_2O is too low to compare with even the reduced amount considered necessary for mixed-layer illite and montmorillonite, or for a true mica (Hower and Mowatt, 1966).

The basal (001) reflection of 24 A for the high-alumina montmorillonite is high compared with 15 A for beidellite, but does compare with the 24 A for rectorite. The peaks are sharp in the X-ray diffraction traces (fig. 3), however, and show no separate and intermediate peaks (or submultiples of these) of either the single or combined basal spacings of the constituent clay minerals on the many diffraction traces examined; this factor is suggestive of a single mineral. This mineral responds to glycolation (expansion to 27 A) and heating to 300°C and 550°C (collapse to 20 A) in a manner typical of a montmorillonite group mineral without any interference by a nonswelling clay mineral that would be expected in mixed layering.

The wispy morphology of the high-alumina montmorillonite in figure 5*A* has no resemblance to the lath-shaped grains of a mixed-layer montmorillonite-mica phase shown by Velde (1969, fig. 2). Likewise, it does not resemble the ribbonlike rectorite described in Brown and Weir (1963, pl. 1B).

In most other respects, the Longfellow high-alumina montmorillonite seems to be and behaves as an excellent representative of the montmorillonite group. X-ray data as well as electron microscopy, already pointed out, support this conclusion. Comparison of approximate values of interlayer spacing d_{001} for montmorillonite (15 A) with dickite (7 A), pyrophyllite (9 A), and illite (10 A) gives approximate combined reflections of 22 A, 24 A, and 25 A, respectively. Thus, if this presently considered monomineralic clay mineral on further analytical work is found to be a mixed-layer clay, we would expect it to be composed of montmorillonite and pyrophyllite. However, this mineral might be a polymorph of beidellite composed of two 10-A layers and only one water layer, thus totaling 24 A. This conclusion is somewhat supported by the low amount of interlayer water (H_2O-) indicated in the chemical analysis. As no cogent evidence has been found to eliminate the possibility of a clay mineral with a high basal spacing forming naturally, and as the described mineral from the Longfellow mine does not correspond exactly to the definition of beidellite established by Weir and Greene-Kelly (1962, p. 145), we have used the name "high-alumina montmorillonite" provisionally, pending continuing field and laboratory studies at the Longfellow and neighboring mines.

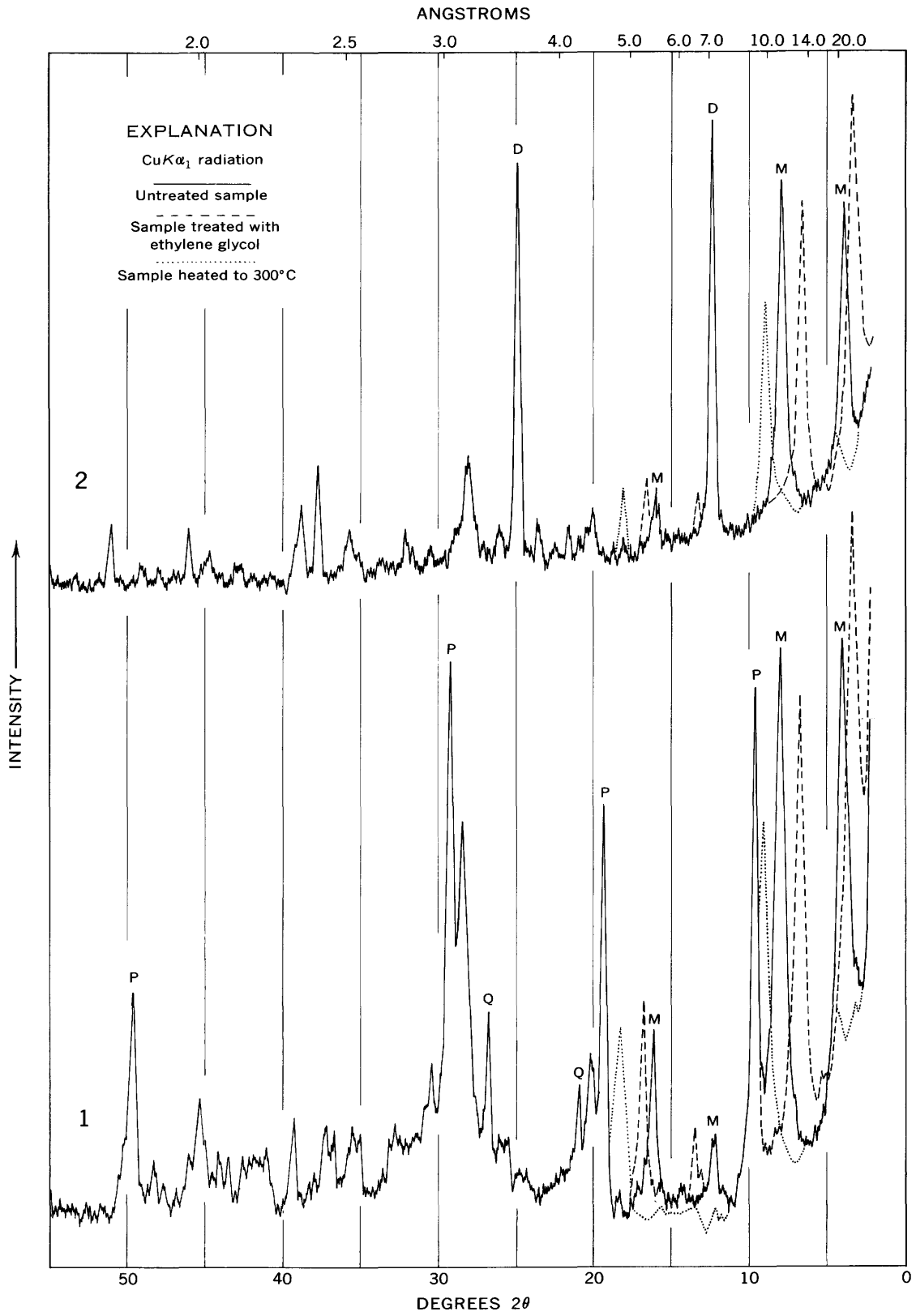

Figure 3.—X-ray diffractometer traces of clay samples from the Longfellow mine, San Juan County, Colo. 1, montmorillonite (M), pyrophyllite (P), and quartz (Q); 2, montmorillonite (M) and dickite (D).

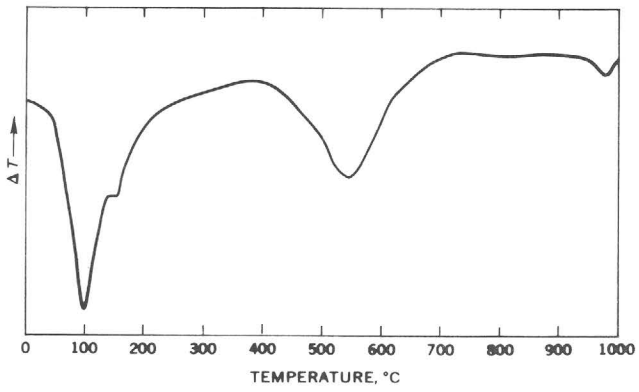

Figure 4.—Differential thermal analysis curve of high-alumina montmorillonite from the Longfellow mine, San Juan County, Colo.

Pyrophyllite

Pyrophyllite has a structural formula of $Al_2Si_4O_{10}[OH]_2$ and a theoretical composition of 66.7 percent SiO_2, 28.3 percent Al_2O_3, and 5.0 percent H_2O; it has the highest Si:Al ratio of the four aluminum silicate minerals discussed herein. X-ray diffraction patterns (fig. 3) have sharp peaks instead of scattered fuzzy peaks, thus suggesting a certain degree of order in the crystal structure. The basal (00*l*) spacing of pyrophyllite is not affected by heating or other treatment.

Electron photomicrographs show flakes of pyrophyllite associated with filmy montmorillonite (fig. 5*B*) and micaceous flakes of pyrophyllite only (fig. 5*C*). The pyrophyllite is readily identifiable because of its characteristic electron diffraction pattern (E. J. Dwornik, written commun., June 23, 1969).

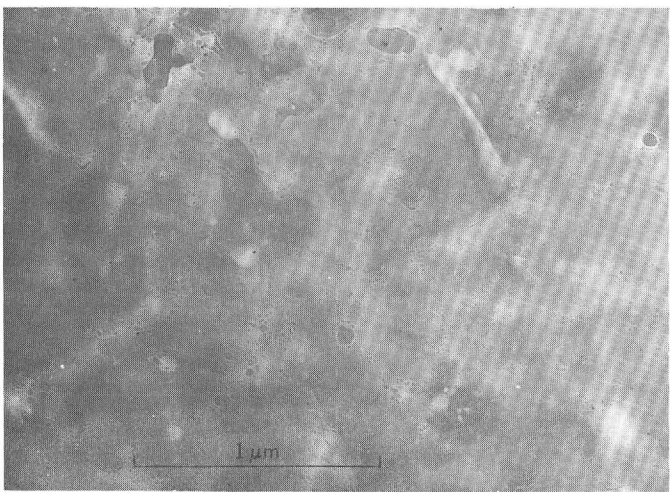

A

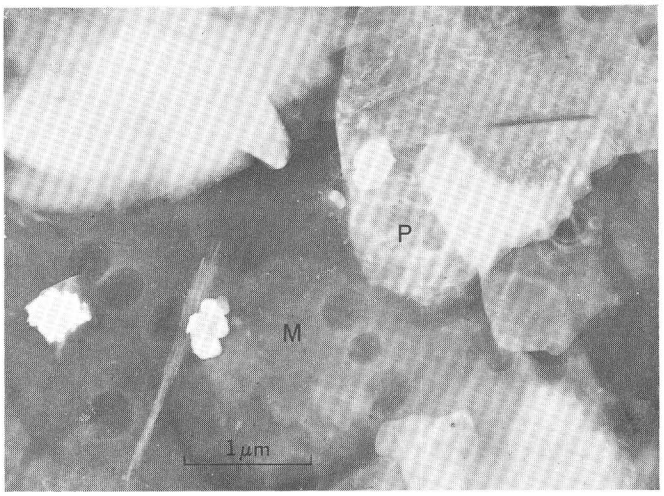

B

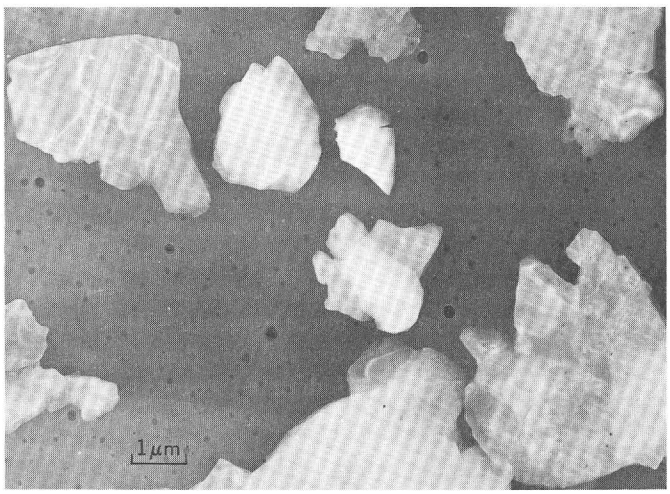

C

Figure 5.—Electron-microscope photographs of clay minerals. Photographs by E. J. Dwornik, U.S. Geological Survey.
A. High-alumina montmorillonite, Longfellow mine, San Juan County, Colo.
B. High-alumina montmorillonite (M) and pyrophyllite (P), Longfellow mine, San Juan County, Colo.
C. Pyrophyllite, Longfellow mine, San Juan County, Colo.

The pyrophyllite in hand specimen appeared and felt greasy and was generally white under surface stains. It was found both as small vein and pod fillings and in massive nondistinctive form. In thin section, it appeared as moderately highly birefringent minute crystalline flakes in veinlets, as rims on some grains, and as a filling in interstices. In several of the sections, skeletal outlines of feldspar now completely replaced by pyrophyllite were observed.

Dickite

Dickite, a member of the kaolinite group, has a structural formula of $Al_4Si_4O_{10}[OH]_8$ and a theoretical composition of 46.54 percent SiO_2, 39.50 percent Al_2O_3, and 13.96 percent H_2O. The basal (00*l*) spacing of the dickite unit cell is 7.15 A (fig. 3). The dickite is white to light gray, massive appearing, and moderately soft. It occurs principally as small pod and cavity fillings and locally encrustations about ore minerals. As seen in thin section, the dickite occurs as single and clustered irregular pseudohexagonal crystals with low birefringence.

Illite

Two polymorphs (M*d* and 2M) of illite are found at the Longfellow mine. The 2M polymorph is associated with pyrophyllite in samples from the 150-foot level of the mine. In thin section, this illite appears as very fine crystalline flakes with moderately high birefringence. The M*d* (disordered) illite polymorph is from the surface pit and occurs with quartz and pyrite in what appear to be crude beds or layers. This illite, and undoubtedly some pyrophyllite, is the sericite or hydromica noted in earlier literature describing alteration products in the Red Mountains area.

DISCUSSION

The clay minerals at the Longfellow mine occur in close association with the ore body in a crude zonal relationship and undoubtedly formed as alteration products under hydrothermal conditions. However, in the uppermost near-surface parts, some of the illite may have resulted from weathering.

Five clay zones seem to exist at the Longfellow mine from the center of the chimney deposit out to and including the surrounding country rock. At the center of the body, generally with sulfide-ore minerals, is high-alumina montmorillonite. The rock here is converted to fine-textured and dense cavernous aggregates of quartz, clay, and minor accessory minerals. However, the quartz or some other silica polymorph is not intimately mixed with clays, as determined by X-ray diffraction. High-alumina montmorillonite and pyrophyllite occur within the next or second zone. These two clay minerals plus dickite characterize the third zone; the dickite is replaced by pyrophyllite, apparently one at the expense of the other, according to the reaction: kaolinite (dickite) + quartz = pyrophyllite + water (steam). The fourth and fifth zones outward, respectively, consist of dickite, illite (2M polymorph), and quartz, and of illite, quartz, and chlorite of the surrounding propylitically altered country rock. Pyrophyllite would not be expected to exist with the illite-chlorite assemblage in the fourth and fifth zones (Velde, 1968, p. 15). Presumably overlying the above-described zones at the Longfellow mine and peripheral to the siliceous cap (fig. 2) is a final zone that consists mainly of illite (M*d* polymorph) and quartz; the origin of this zone is problematical. The exact nature of the zonal boundaries, whether sharp or gradational, the thicknesses of the zones, and their continuity in plan and depth are unknown at this time.

The clay minerals discussed are an integral part of the result of intense and complex alteration processes in the Red Mountain part of the Silverton cauldron, site of the Longfellow mine. These alteration processes, discussed more fully by Burbank and Luedke (1969), are related in part to late-volcanic to postvolcanic and premineralization degassing of the region. The gaseous materials, predominately CO_2, pervasively invaded the locally heated rocks; reactions between the rocks and altering fluids resulted in widespread propylitization of the volcanic rocks. Continued attack by CO_2-laden fluids, plus the introduction of sulfur gases and the mixing with meteoric waters in the near-surface environment, caused intensive solfataric alteration locally in the cauldron's ring-fault zone. The solfataric activity leached the country rock along intersecting fractures and fissures and created irregular open channels and cavernous ground that for the most part subsequently were filled with sulfide ores and products of rock decomposition. Under optimum temperature and pressure conditions, excess silica derived in the central part of the channelway through rock decomposition was carried upward to be concentrated and precipitated as a nearly impervious layer. This siliceous cap or envelope impeded movement of sulfide-bearing solutions, thereby resulting in deposition of ore to form ore bodies of vertical pipelike or chimney shape (fig. 2).

Burbank (1941, 1950) and Burbank and Luedke (1969) discussed the problems related to the formation of the chimney ore deposits in the light of available field and laboratory evidence. The possible temperature and pressure ranges can only be surmised by examining the known stability fields of pyrophyllite and kaolinite (dickite). The experimental results of numerous investigators, summarized by Kerrick (1968), give the upper stability limit of pyrophyllite as ranging from about 400°C at 1,000 bars to 580°C at 2,000 bars. Pyrophyllite was observed to form from mica at about 350°C and 1,000 bars and from kaolinite and quartz at about 380°C and 1,000 bars in some experiments by Hemley and Jones (1964). Subsequently, Reed and Hemley (1966, p. C164) stated that the latter reaction takes place at 300°C and 1,000 bars partial water pressure when allowed to run for a long period of time. The true upper stability limit for kaolinite (and possibly dickite) is thought by Reed and Hemley (1966, p.

C164) probably to be lower than the limits indicated in earlier published experimental work. The highest temperature of stability for montmorillonite and beidellite (Deer and others, 1962, p. 238) is 480°C at 1,000 bars, and the lowest is about 255°C at 1,000 bars. The stability fields of the clay minerals mentioned, however, are probably dependent not only on the temperature and pressure conditions, but also upon the pH of the altering solutions and the parent rock composition (Norton, 1941, p. 17; Hemley and Jones, 1964, p. 564; Velde, 1969, p. 367).

REFERENCES

Brackett, R. N., and Williams, J. F., 1891, Newtonite and rectorite—two new minerals of the kaolinite group: Am. Jour. Sci., 3d ser., v. 42, p. 11–21.

Bradley, W. F., 1950, The alternating layer sequence of rectorite: Am. Mineralogist, v. 35, p. 590–595.

Brindley, G. W., 1956, Allevardite, a swelling double-layer mica mineral: Am. Mineralogist, v. 41, p. 91–103.

Brown, G., and Weir, A. H., 1963, The identity of rectorite and allevardite, *in* International Clay Conference, Stockholm, 1963, Proc., v. 1: New York, Macmillan Co., p. 27–35.

Burbank, W. S., 1941, Structural control of ore deposition in the Red Mountain, Sneffels, and Telluride districts of the San Juan Mountains, Colorado: Colorado Sci. Soc. Proc., v. 14, no. 5, p. 141–261.

——1950, Problems of wall-rock alteration in shallow volcanic environments, *in* Van Tuyl, F. M., and Kuhn, T. H., Applied geology, a symposium: Colorado School Mines Quart., v. 45, no. 1B, p. 287–319.

Burbank, W. S., and Luedke, R. G., 1961, Origin and evolution of ore and gangue-forming solutions, Silverton caldera, San Juan Mountains, Colorado: U.S. Geol. Survey Prof. Paper 424–C, p. C7–C11.

——1964, Geology of the Ironton quadrangle, Colorado: U.S. Geol. Survey Geol. Quad. Map GQ–291.

——1969, Geology and ore deposits of the Eureka and adjoining districts, San Juan Mountains, Colorado: U.S. Geol. Survey Prof. Paper 535, 73 p.

Deer, W. A., Howie, R. A., and Zussman, J., 1962, Rock-forming minerals—v. 3, Sheet silicates: New York, John Wiley and Sons, 270 p.

Fischer, R. P., Luedke, R. G., Sheridan, M. J., and Raabe, R. G., 1968, Mineral resources of the Uncompahgre primitive area, Colorado: U.S. Geol. Survey Bull. 1261-C, 91 p.

Greene-Kelly, R. G., 1957, The montmorillonite minerals (smectites), *in* Mackenzie, R. C., ed., The differential thermal investigation of clays: London, Mineralog. Soc. (Clay Minerals Group), p. 140–164.

Hemley, J. J., and Jones, W. R., 1964, Chemical aspects of hydrothermal alteration with emphasis on hydrogen metasomatism: Econ. Geology, v. 59, no. 4, p. 538–567.

Hosterman, J. W., 1969, Clay deposits of Spokane County, Washington: U.S. Geol. Survey Bull. 1270, 96 p.

Hower, John, and Mowatt, T. C., 1966, The mineralogy of illites and mixed-layer illite/montmorillonite: Am. Mineralogist, v. 51, nos. 5–6, p. 825–854.

Kerrick, D. M., 1968, Experiments on the upper stability limit of pyrophyllite at 1.8 kb and 3.9 kb water pressure: Am. Jour. Sci., v. 266, no. 3, p. 204–214.

Kodama, Hideomi, 1966, The nature of the component layers in rectorite: Am. Mineralogist, v. 51, no. 7, p. 1035–1055.

Larsen, E. S., and Wherry, E. T., 1917, Leverrierite from Colorado: Washington Acad. Sci. Jour., v. 7, p. 208–217.

——1925, Beidellite, a new mineral name: Washington Acad. Sci. Jour., v. 15, no. 21, p. 465–466.

Luedke, R. G., and Burbank, W. S., 1968, Volcanism and cauldron development in the western San Juan Mountains, Colorado: Colorado School Mines Quart., v. 63, no. 3, p. 175–208.

Norton, F. H., 1941, Hydrothermal formation of clay minerals in the laboratory, pt. 2: Am. Mineralogist, v. 26, no. 1, p. 1–17.

Reed, B. L., and Hemley, J. J., 1966, Occurrence of pyrophyllite in the Kekiktuk Conglomerate, Brooks Range, northeastern Alaska: U.S. Geol. Survey Prof. Paper 550-C, p. C162–C166.

Ross, C. S., and Hendricks, S. B., 1945, Minerals of the montmorillonite group, their origin and relation to soils and clays: U.S. Geol. Survey Prof. Paper 205-B, p. 23–79.

Shannon, E. V., 1922, Notes on the mineralogy of three gouge clays from precious-metal veins: U.S. Natl. Mus. Proc., v. 62, art. 15, 11 p.

Velde, Bruce, 1968, The effect of chemical reduction on the stability of pyrophyllite and kaolinite in pelitic rocks: Jour. Sed. Petrology, v. 38, no. 1, p. 13–16.

——1969, The compositional join muscovite-pyrophyllite at moderate pressures and temperatures: Soc. Française Minéralogie et Cristallographie Bull., v. 92, p. 360–368.

Weir, A. H., and Greene-Kelly, R. G., 1962, Beidellite: Am. Mineralogist, v. 47, nos. 1–2, p. 137–146.

ACCESSORY EPIDOTE FROM HYBRID GRANITOID ROCKS OF THE MOUNT WHEELER MINE AREA, NEVADA

By DONALD E. LEE, ROBERT E. MAYS, RICHARD E. VAN LOENEN;
and HARRY J. ROSE, JR., Denver, Colo.; Washington, D.C.

Abstract.—Chemical data and physical properties are listed for 18 accessory epidotes recovered from hybrid granitoid rocks exposed north of the Mount Wheeler mine, White Pine County, Nev. The environment of these epidotes is well known from a detailed field and laboratory study that included chemical, spectrographic, normative, and modal analyses of the rocks from which they were separated. Amounts of epidote present in these hybrid rocks range from zero to 2 percent, depending upon rock chemistry, but apparently chemical composition of the epidote is rather consistent from one rock type (granodiorite) to another (quartz monzonite). The Fe^{3+}:($Al+Fe^{3+}$) ratio of epidote from one of the more mafic rocks is 0.27. X-ray fluorescence analysis (total iron as Fe_2O_3), indices of refraction, and unit-cell parameters indicate a similar Fe^{3+}:($Al+Fe^{3+}$) ratio for three other epidotes from more felsic rocks. There is only slight correlation between rock chemistry and the minor-element contents of these constituent epidotes.

Granitoid rocks of Jurassic age (Lee and others, 1968) crop out a few miles north of the Mount Wheeler mine in the southern part of the Snake Range, about 50 miles southeast of Ely, Nev. These rocks range in composition from granodiorite with a CaO content of more than 4.5 percent to quartz monzonite with a CaO content of about 0.5 percent, and a detailed field and laboratory study (Lee and Van Loenen, 1971) has shown that this range in composition is related to magmatic assimilation of such chemically diverse host rocks as limestone and quartzite. The change from high to low CaO values is rather systematic over a horizontal distance of about 3 miles, and other major elements and most minor elements tend to vary either directly or inversely with CaO, much as one would expect in a series of differentiates. Amounts of essential and accessory minerals respond to the major-element chemistry of these hybrid rocks, and epidote provides a good example of this response (Lee and Dodge, 1964). Epidote is absent in the most felsic rocks, begins to appear where CaO content of the rock is about 1.2 percent, and amounts to as much as 2 percent of the most mafic rocks.

This paper presents, in table 1, minor-element analyses for 20 accessory epidotes—18 from the hybrid rocks just mentioned, one from a Tertiary aplite, and one from a lamprophyre dike crosscutting the hybrid rocks. We also list unit-cell parameters for 16 of these epidotes and major-element data and optics for 5. The locations, major- and minor-element analyses, norms, and modes of the rocks from which these constituent epidotes were recovered are given by Lee and Van Loenen (1971). A given sample number refers both to the whole rock and to each mineral fraction recovered from that rock.

The epidote in these rocks tends to be associated with biotite and with other accessory minerals present in the rock. It tends especially to be intergrown with allanite. Typical intergrowths (epidote 38–MW–61, table 1) are illustrated in the report by Lee and Bastron (1962).

EPIDOTE ANALYSES AND PHYSICAL PROPERTIES

After the preliminary mineral concentration by Lee and Dodge (1964), the epidote concentrates were ground to -150 mesh (about 100 microns) and washed in tapwater to remove material smaller than about 40 microns. All these epidotes coexist with allanite, so it was necessary to use Clerici solution, in the final purification of these epidotes, to remove the allanite. After centrifuging in Clerici solution each epidote fraction was subjected to ultrasonic vibration in distilled water for about an hour. The effectiveness of this cleaning is indicated by the fact that thallium was not detected during subsequent spectrographic work. (Lower limit of detection for thallium is 0.005 weight percent.)

During the purification process, epidotes 16–MW–60, 8–DL–61, and 43–DL–61 were found to have a specific gravity of 3.45±0.01; epidote 151–MW–61 had a specific gravity of 3.43±0.01. (There is a straight-line plot between the specific gravity and refractive index of Clerici solution.) Each of the other epidotes in table 1 was found to have a specific gravity greater than 3.32 and less than 3.49, but was not centrifuged in any liquid with a specific gravity between 3.32 and 3.49.

Cell parameters and refractive indices are listed in table 1.

Major elements

Epidote 43–DL–61 was analyzed by wet chemistry, and the analysis (table 1) was recalculated to the structural formula (table 2) on the basis of 13 (O,OH), using the computer program described by Jackson, Stevens, and Bowen (1967). Results of the recalculation are in good agreement with the ideal formula $Ca_2(Fe^{3+}, Al_3 Si_3O_{12}(OH)$. When the Fe^{3+}:$(Al+Fe^{3+})$ ratio (0.27) is considered, the data for this epidote are consistent with the results obtained by Seki (1959), who has related unit-cell parameters and optical properties of epidotes to their Fe^{3+}:$(Al+Fe^{3+})$ ratios. The compositions (total iron as Fe_2O_3) and physical properties of samples 190–DL–62, 40A–MW–60, and 40B–MW–60 are similar to those of 43–DL–61. Moreover, excepting 119–MW–60 from a Tertiary (Lee and others, 1970) aplite phase, the unit-cell parameters of all epidotes in table 1 are similar to those of the epidotes for which major-element data are listed; this indicates similarity of composition, despite the large range of composition of rocks from which these constituent epidotes are recovered (Lee and Van Loenen, 1971).

No discrete grains of impurity were observed in the final epidote fractions, but when viewed in oil with a refractive index near that of epidote most epidote grains are seen to contain tiny inclusions. Almost all these inclusions are colorless and have a low birefringence and a refractive index much less than that of epidote. Most of them appear to be quartz, which might account for the slightly high silicon content in the structural formula of 43–DL–61 (table 2).

As noted above, epidote 119–MW–60 is from a mass of Tertiary aplite. The relatively low iron content of this mineral probably relates to the low iron content of the aplite itself (Lee and Van Loenen, 1971).

Minor elements

There is only slight correlation between rock chemistry and the minor-element contents of these constituent epidotes. Thus beryllium, germanium, and tin tend to be present in larger amounts in epidotes from the more felsic rocks. The minor-element contents of the sphenes coexisting with these epidotes also show a relative lack of response to whole-rock chemistry (Lee and others, 1969). On the other hand, coexisting allanites and monazites (Lee and Bastron, 1967) and zircons (Lee and others, 1968) show remarkable correlation between their minor-element contents and the major-element chemistry of the rocks from which they were recovered.

These epidotes contain much smaller amounts of the rare-earth elements than do the coexisting sphenes and zircons, although allanite (an epidote structure containing as much as 23 percent of rare-earth oxides) also is part of these accessory mineral assemblages. Strontium is concentrated in these epidotes.

REFERENCES

Evans, H. T., Jr., Appleman, D. E., and Handwerker, D. S., 1963, The least squares refinement of crystal unit cells with powder diffraction data by an automatic computer indexing method [abs.]: Am. Crystallog. Assoc. Program and Abs. 1963 Ann. Mtg., p. 42–43.

Jackson, E. D., Stevens, R. E., and Bowen, R. W., 1967, A computer-based procedure for deriving mineral formulas from mineral analyses *in* Geological Survey Research 1967: U.S. Geol. Survey Prof. Paper 575–C, p. C23–C31.

Lee, D. E., and Bastron, Harry, 1962, Allanite from the Mount Wheeler area, White Pine County, Nevada: Am. Mineralogist, v. 47, nos. 11–12, p. 1327–1331.

———1967, Fractionation of rare-earth elements in allanite and monazite as related to geology of the Mt. Wheeler mine area, Nevada: Geochim. et Cosmochim. Acta, v. 31, no. 3, p. 339–356.

Lee, D. E., and Dodge, F. C. W., 1964, Accessory minerals in some granitic rocks in California and Nevada as a function of calcium content: Am. Mineralogist, v. 49, nos. 11–12, p. 1660–1669.

Lee, D. E., Marvin, R. F., Stern, T. W., and Peterman, Z. E., 1970, Modification of potassium-argon ages by Tertiary thrusting in the Snake Range, White Pine County, Nevada *in* Geological Survey Research 1970: U.S. Geol. Survey Prof. Paper 700–D, p. D92–D102.

Lee, D. E., Mays, R. E., Van Loenen, R. E., and Rose, H. J., Jr., 1969, Accessory sphene from hybrid rocks of the Mount Wheeler mine area, Nevada *in* Geological Survey Research 1969: U.S. Geol. Survey Prof. Paper 650–B, p. B41–B46.

Lee, D. E., Stern, T. W., Mays, R. E., and Van Loenen, R. E., 1968, Accessory zircon from granitoid rocks of the Mount Wheeler mine area, Nevada *in* Geological Survey Research 1968: U.S. Geol. Survey Prof. Paper 600–D, p. D197–D203.

Lee, D. E., and Van Loenen, R. E., 1971, Hybrid granitoid rocks of the southern Snake Range, Nevada: U.S. Geol. Survey Prof. Paper 668. [In press]

Seki, Yôtarô, 1959, Relation between chemical composition and lattice constants of epidote: Am. Mineralogist, v. 44, nos. 7–8, p. 720–730.

Table 1.—*Analytical data and physical properties for accessory*

[Samples arranged in order of increasing CaO content of rock. CaO analyses by Paul Elmore, Samuel Botts, H. Smith, and Gillison Chloe. Cell program developed by Evans, Appleman, and Handwerker (1963). The internal standard was CaF_2. Indices of refraction determined in sodium analyses of other epidotes by Harry J. Rose, Jr., using X-ray fluorescence. Semiquantitative spectrographic analyses by Robert E. Mays. Results arbitrarily as midpoints of these brackets: 1, 0.7, 0.5, 0.3, 0.2, 0.15, and 0.1, respectively. The precision of a reported value is approximately

	Sample No.	119–MW–60[1]	205–MW–61	147–MW–61	151–MW–61	190–DL–62	71–MW–60	14–MW–60	8–DL–61	40A–MW–60	
	CaO in rock (weight percent)	0.63	1.4	1.5	1.8	2.0	2.1	2.2	2.3	2.4	
	Cell parameters										
1	a (±0.002 A)	8.870	8.881	.....	8.891	8.891	8.897	8.894	8.897	8.893	1
2	b (±0.002 A)	5.620	5.620	.....	5.634	5.633	5.632	5.633	5.633	5.631	2
3	c (±0.004 A)	10.151	10.149	.....	10.157	10.159	10.161	10.165	10.167	10.164	3
4	Volume (±0.2 A^3)	457.0	457.6	.....	459.7	459.6	459.8	460.1	460.2	459.7	4
5	β (±2′)	115°27′	115°24′	.....	115°22′	115°24′	115°26′	115°24′	115°26′	115°25′	5
	Indices of refraction										
6	α (±0.003)	1.721	.....	.....	.....	1.727	.....	.....	.....	1.728	6
7	β (±0.003)	1.740	.....	.....	.....	1.752	.....	.....	.....	1.752	7
8	γ (±0.003)	1.754	.....	.....	.....	1.768	.....	.....	.....	1.769	8
	Major elements (weight percent)										
9	SiO_2	38.0	.....	.....	.....	39.1	.....	.....	.....	38.3	9
10	Al_2O_3	26.3	.....	.....	.....	22.2	.....	.....	.....	21.9	10
11	Fe_2O_3	10.6	.....	.....	.....	12.4	.....	.....	.....	12.9	11
12	FeO[4]	.....	.....	.....	.....	.....	.....	.....	.....	.....	12
13	MgO	.....	.....	.....	.....	.....	.....	.....	.....	.....	13
14	CaO	24.7	.....	.....	.....	23.5	.....	.....	.....	22.9	14
15	Na_2O	.....	.....	.....	.....	.....	.....	.....	.....	.....	15
16	K_2O	.10	.....	.....	.....	.10	.....	.....	.....	.12	16
17	H_2O+	.....	.....	.....	.....	.....	.....	.....	.....	.....	17
18	TiO_2	.63	.....	.....	.....	2.34	.....	.....	.....	1.32	18
19	MnO	.48	.....	.....	.....	.31	.....	.....	.....	.44	19
20											20
	Semiquantitative spectrographic analyses (weight percent)										
21	Mg	0.007	0.015	0.02	0.02	0.02	0.015	0.01	0.015	0.015	21
22	Na	.....	.1	.05	.....	.07	.07	.05	.07	.1	22
23	Ba	.....	.0007	.002	.0015	.002	.0015	.0015	.0015	.002	23
24	Be	.0005	.0003	.....	.....	.....	.....	.....	.....	.....	24
25	Ce	.05	.....	.1	.....	.1	.....	.....	.....	.....	25
26	Co	.....	.....	.....	.....	.....	.....	.....	.....	.....	26
27	Cr	.....	.....	.005	.005	.003	.005	.005	.005	.005	27
28	Cu	.0005	.0003	.0007	.0005	.0005	.0005	.0003	.0003	.0005	28
29	Ga	.02	.01	.007	.007	.007	.007	.007	.007	.007	29
30	Ge	.007	.002	.....	.....	.....	.....	.....	.....	.....	30
31	La	.02	.01	.03	.....	.03	.02	.....	.005	.....	31
32	Nb	.007	.....	.005	.005	.007	.005	.....	.002	.003	32
33	Ni	.....	.....	.0007	.0005	.0007	.....	.0005	.....	.....	33
34	Pb	.01	.02	.015	.015	.01	.015	.015	.02	.015	34
35	Sc	.015	.01	.02	.02	.02	.02	.015	.02	.015	35
36	Sn	.02	.005	.005	.005	.007	.005	.....	.....	.....	36
37	Sr	.1	.1	.3	.3	.3	.3	.3	.3	.3	37
38	V	.007	.015	.03	.03	.05	.03	.03	.05	.03	38
39	Y	.03	.015	.02	.015	.1	.015	.....	.....	.0015	39
40	Yb	.002	.001	.002	.001	.005	.001	.....	.....	.0003	40
41	Zr	.007	.007	.007	.007	.....	.01	.007	.007	.007	41

[1]Epidote from aplite. [2]Epidote from lamprophyre. [3]Epidote from xenolith. [4]Total iron as Fe_2O_3.

epidotes from the Mount Wheeler mine area, Nevada

parameters were obtained by least-squares refinement of powder diffractometer data by R. E. Van Loenen, using a self-indexing computer light by the immersion method. Major-element analysis of epidote 43–DL–61 by wet chemistry, Elaine L. Munson, analyst. Major-element are based on their identity with geometric brackets whose boundaries are 1.2, 0.83, 0.56, 0.38, 0.26, 0.18, 0.12, and so forth, and are reported plus–or–minus one bracket at 68–percent, or two brackets at 95–percent confidence]

	31–DL–61	38–MW–61	150–MW–61[2]	25–DL–61	152–MW–61	40B–MW–60[3]	126–MW–61[3]	43–DL–61	27–DL–61[3]	16–MW–60	98–DL–62[3]	
	2.4	2.5	2.8	3.1	3.2	3.5	3.5	3.9	4.1	4.3	4.5	
						Cell parameters						
1	.....	8.896	8.886	8.890	8.890	8.892	.....	8.897	.....	8.894	8.890	1
2	.....	5.635	5.624	5.624	5.632	5.635	.....	5.629	.....	5.633	5.635	2
3	.....	10.156	10.152	10.154	10.153	10.171	.....	10.161	.....	10.157	10.154	3
4	.....	459.9	458.3	458.7	459.4	460.2	.....	459.6	.....	459.7	459.5	4
5	.....	115°23′	115°25′	115°24′	115°21′	115°25′	.....	115°26′	.....	115°23′	115°24′	5
						Indices of refraction						
6	.....	.....	.....	.....	.....	1.728	.....	1.728	.....	.....	.....	6
7	.....	.....	.....	.....	.....	1.753	.....	1.751	.....	.....	.....	7
8	.....	.....	.....	.....	.....	1.771	.....	1.769	.....	.....	.....	8
						Major elements (weight percent)						
9	.....	.....	.....	.....	.....	38.0	.....	38.71	.....	.....	.....	9
10	.....	.....	.....	.....	.....	23.2	.....	22.36	.....	.....	.....	10
11	.....	.....	.....	.....	.....	13.1	.....	13.20	.....	.....	.....	11
12	.....	.....	.....	.....	.....	[4]	.....	.30	.....	.....	.....	12
13	.....	.....	.....	.....	.....	.....	.....	.07	.....	.....	.....	13
14	.....	.....	.....	.....	.....	22.9	.....	22.75	.....	.....	.....	14
15	.....	.....	.....	.....	.....	....	.....	.10	.....	.....	.....	15
16	.....	.....	.....	.....	.....	.08	.....	.03	.....	.....	.....	16
17	.....	.....	.....	.....	.....	.....	.....	1.82	.....	.....	.....	17
18	.....	.....	.....	.....	.....	2.72	.....	.64	.....	.....	.....	18
19	.....	.....	.....	.....	.....	.42	.....	.25	.....	.....	.....	19
20							Total	100.23				20
						Semiquantitative spectrographic analyses (weight percent)						
21	0.03	0.015	0.03	0.015	0.02	0.015	0.03	0.02	0.03	0.015	0.03	21
22	.03	.07	.1	.07	.07	.1	.05	.07	.07	.07	.....	22
23	.0015	.0015	.005	.0015	.002	.0015	.0015	.0015	.0015	.0015	.0015	23
24	.....	.....	.....	.....	.....	.....	.....	.....	.....	.....	.....	24
25	.1	.....	.15	.....	.05	.....	.15	.....	.07	.....	.1	25
26	.....	.....	.0007	.....	.....	.....	.....	.....	.....	.....	.....	26
27	.007	.005	.02	.01	.007	.....	.0015	.01	.03	.01	.0005	27
28	.0007	.0007	.0015	.0003	.0005	.0002	.003	.0007	.0005	.0007	.001	28
29	.007	.007	.007	.007	.007	.007	.007	.007	.007	.007	.007	29
30	.....	.....	.....	.....	.....	.....	.....	.....	.....	.....	.....	30
31	.05	.01	.07	.007	.03	.....	.1	.....	.03	.....	.03	31
32	.....	.003	.001	.002	.....	.....	.002	.....	.....	.....	.....	32
33	.....	.....	.....	.....	.....	.....	.....	.....	.0005	.0003	.....	33
34	.015	.02	.015	.01	.02	.015	.01	.015	.015	.015	.01	34
35	.03	.015	.01	.015	.015	.015	.02	.02	.02	.015	.03	35
36	.....	.....	.....	.....	.....	.....	.005	.....	.....	.002	.003	36
37	.3	.3	.2	.3	.3	.3	.1	.3	.3	.2	.2	37
38	.05	.05	.03	.05	.05	.05	.05	.05	.05	.05	.05	38
39	.005	.002	.005	.005	.....	.002	.01	.005	.02	.003	.005	39
40	.0005	.0003	.0005	.0005	.....	.0003	.0007	.0005	.0015	.0003	.0005	40
41	.01	.007	.01	.007	.007	.....	.003	.002	.....	.005	.....	41

Table 2.—*Structural formula, optical properties, and other properties of epidote 43–DL–61*

[Analysis, refractive indices, and unit-cell parameters given in table 1]

Number of ions, on basis of 13(O,OH)		
Si	3.07	3.07
Al	....	
Al	2.09	2.92
Fe^{3+}	.79	
Ti	.04	
Fe^{2+}	.02	2.00
Mg	.01	
Mn	.02	
Ca	1.93	
Na	.02	
OH	.96	0.96

Optical and other properties	
Specific gravity observed	3.45±0.01
Density calculated	3.450±0.002 g/cm^3
Cell volume measured	4.59.6±0.2 A^3
Cell volume calculated	459.6 A^3
Estimated $2V$	75° (−)
Dispersion	V > R moderate.
α	Colorless.
β	Light yellow green.
γ	Yellow green.

SUMMARY OF MINERALOGIC AND LITHOLOGIC CHARACTERISTICS OF TERTIARY SEDIMENTARY ROCKS IN THE MIDDLE ROCKY MOUNTAINS AND THE NORTHERN GREAT PLAINS

By N. M. DENSON and W. A. CHISHOLM[1],
Denver, Colo., Placentia, Calif.

Abstract.—Regional mapping in the middle Rocky Mountains and northern Great Plains and the related study of nonopaque heavy minerals indicate that the Tertiary sedimentary rocks comprise six major lithogenetic units. These units, established by faunal and floral succession and by potassium-argon age determinations, as well as by the characteristic heavy-mineral assemblages from the very fine grained sand fractions, are summarized as: (1) Paleocene rocks, containing mostly tourmaline and pinkish-violet zircon; (2) lower Eocene rocks containing mostly epidote, blue-green hornblende, and garnet; (3) upper Eocene rocks, characterized by two rock facies containing two distinct volcanic assemblages—the first containing abundant green-brown hornblende and augite, the second containing abundant euhedral colorless zircon; (4) Oligocene rocks containing about equal amounts of volcanic and plutonic minerals—the volcanically derived heavy-mineral assemblage generally containing $>$ 40 percent green-brown hornblende and $<$ 15 percent augite; (5) lower Miocene rocks, mostly volcanic, containing 20-40 percent augite and 20-60 percent green-brown hornblende; and (6) upper Miocene and Pliocene sequence containing a highly variable mixture of heavy minerals of plutonic and (or) volcanic origin. Study of 3,000 heavy-mineral separates from 200 stratigraphic sections reveals that the characteristic assemblages substantially aid Tertiary correlation and assist in interpreting some major regional tectonic events.

Since the early part of the 20th century the stratigraphy of continental Tertiary rocks in the middle Rocky Mountains and northern Great Plains has, with few exceptions, attracted little interest from investigators and appraisers of the nation's mineral resources. This general disinterest persisted largely because these rocks blanket and thus obscure the underlying Mesozoic, Paleozoic, and Precambrian rocks in which mineral exploration has been the most rewarding. In many areas the early geologists could distinguish few lithologic differences in the poorly consolidated sandstone, siltstone, claystone, and conglomerate which make up most of the Tertiary sequence. Today, however, because of the discovery of commercially significant occurrences of uranium and gas in the Tertiary rocks of the intermontane basin areas of central Wyoming, exploration geologists are intensively studying rocks that only a few years ago were considered as uninteresting overburden.

Since 1959, the senior author has been engaged in a regional study of the Tertiary sedimentary rocks in parts of western North Dakota and South Dakota, eastern Montana, northern Colorado, western Nebraska, and the eastern two-thirds of Wyoming. Approximately 3,000 samples collected from 200 measured sections were studied by the junior author. The general area studied is shown on figure 1.

The study of the variety and characteristics of the nonopaque heavy minerals was undertaken to: (1) determine whether the heavy-mineral assemblages were useful in correlating formations in one area with those of another, (2) aid in identifying the source rocks, and (3) establish, within broad limits, whether certain minerals reflect specific periods of Tertiary volcanism and tectonism. Although the results of the study show that the use of only a few samples generally is not adequate to establish the identity of any rock unit, they also show that a series of 10 or more samples taken across an interval of at least 200 feet contains a nonopaque heavy-mineral assemblage distinctive enough to identify the rock unit. Furthermore, the study reveals that some of the Tertiary units possess heavy-mineral assemblages that are consistently and predominantly of volcanic origin, whereas other units possess assemblages chiefly of plutonic origin. These results indicate also that the heavy minerals reflect specific periods of volcanism and tectonism, some of which appear to have regional significance.

This report presents the principal similarities and differences of the major lithogenetic units of the Tertiary Period and summarizes the pertinent field and laboratory data bearing on the geologic history of the middle Rocky Mountains-Great Plains region. In preparing this summary, the authors have assembled a substantial amount of new information and have integrated this with information previously published in reports by Denson and Bergendahl (1961), Denson and Gill

[1] Union Oil Company of California.

Figure 1.—Map showing sample localities (dots) of Tertiary rocks collected for heavy-mineral analysis. Patterned areas, basins; G, Gas Hills; R, Rattlesnake Hills.

(1965), Denson and Richmond (1965), Sato and Denson (1967), Denson (1969a and 1969b), Denson and Pipiringos (1969), and Izett, Denson, and Obradovich (1970).

Acknowledgments.—The authors are indebted to R. F. Gantnier, M. W. Green, Elizabeth B. Ternes, T. D. Hessin, and D. E. Schieck for making size analyses and preparing more than 3,000 heavy-mineral slides. T. D. Hessin and P. M. Banks assisted with field mapping and helped with sample collecting. Several colleagues supplied suites of samples of Tertiary rocks from measured sections in Colorado, Wyoming, and North Dakota: A. F. Bateman, C. S. V. Barclay, W. C. Culbertson, J. R. Donnell, E. N. Harshman, G. H. Horn, G. A. Izett, G. N. Pipiringos, M. W. Reynolds, H. W. Roehler, E. M. Schell, and K. S. Soward. Mineral identifications and counts were made by W. A. Chisholm and Yoshiaki Sato. Interpretation of field and laboratory data was the responsibility of the senior author.

PRINCIPAL SUBDIVISIONS OF THE TERTIARY

Sedimentary rocks of widely diverse origins of the report area are assigned to the Tertiary, which spans about 63 m.y. (million years) (Funnell, 1964). Areal mapping integrated with the results of the petrographic study of nonopaque heavy-mineral samples from measured sections indicates that, in the middle Rocky Mountains-northern Great Plains region, the Tertiary System is made up of six major rock units, each having diagnostic lithologic and mineralogic characteristics that can be observed and mapped over great areas (table 1). The six major rock units and their stratigraphic equivalents herein recognized are (1) the Fort Union Formation of Paleocene age, (2) the Wasatch Formation of early Eocene age, (3) the Bridger Formation of late Eocene age, (4) the White River Formation of Oligocene age, (5) the Arikaree Formation of early Miocene age, and (6) the Ogallala Formation of late Miocene and Pliocene ages. Locally, these formations are subdivided into members, which can be mapped.

The age of each of the six major subdivisions of the Tertiary has been established by fauna and flora, and at many localities by potassium-argon age determinations on tuffs (Damon, 1970; Evernden and others, 1961, 1964; Funnell, 1964; Izett and others, 1970; Kulp, 1961). Publications describing the geology and listing some of the diagnostic faunas and floras are listed in the reports by Sato and Denson (1967, p. C54) and Denson and Pipiringos (1969, p. 17–18).

The lithologic and mineralogic criteria for subdividing the Tertiary rocks in central and eastern Wyoming make it clear that the Eocene rocks can, in general, be divided into two, and at most localities into only two, parts—a lower predominantly detrital part and an upper predominantly volcanic part (Denson and Pipiringos, 1969; Roehler, 1970). The lower detrital part consists of the Wasatch, Green River, Battle Spring, and Wind River Formations—the upper volcanic part consists of the Bridger, Continental Peak of Nace (1939), Uinta, and Wagon Bed Formations. A study of the lithologic and mineralogic characteristics of the lower Eocene formations shows that these formations have much in common and can be distinguished readily in most areas from the overlying upper Eocene sequences and the underlying Paleocene sequences.

Sato and Denson (1967) have described a twofold division of the Miocene and Pliocene rocks in parts of the middle Rocky Mountains and northern Great Plains: a lower predominantly volcanic part of early Miocene age (Gering Sandstone through Marsland Formation—see Lewis, 1969), and an upper predominantly detrital part of late Miocene and Pliocene age (Sheep Creek Formation through Blancan provincial age of Wood and others, 1941). The lower unit consists of the Arikaree and the lower parts of the Browns Park and the Troublesome Formations. The upper unit consists of the Flaxville, Ogallala, North Park, South Pass, Dry Union, and Wagontongue (of Stark and others, 1949) Formations, and the upper parts of the Browns Park and Troublesome Formations.

Inasmuch as major mineralogic and lithologic differences are not apparent within either the Oligocene or the Paleocene Series, a subdivision of these rocks is not feasible.

PHYSICAL CHARACTERISTICS

The lithologic and mineralogic characteristics of the major Tertiary rock units of the middle Rocky Mountains and the northern Great Plains are given in detail in table 1. These differences are summarized here.

The Tertiary rocks from the six major units differ markedly in average grain-size distribution, carbonate content, and percentage of total heavy minerals in the very fine grained size fraction.

The Paleocene and Oligocene rocks are very fine grained and are similar in that they contain one of the lowest percentages of heavy minerals of any of the Tertiary rocks studied. (See table 1.)

The lower Miocene rocks are generally well sorted and moderately calcareous, and, except for the hornblende-rich facies of the upper Eocene rocks, contain the highest percentage of heavy minerals of all the Tertiary rocks studied.

The lower Eocene rocks, like the upper Miocene and Pliocene rocks, are mostly poorly sorted moderately calcareous sandstones that have intermediate contents of very fine grained heavy minerals.

Lenticular beds of volcanic ash, bentonite, and limestone occur locally in nearly all the Tertiary formations. Conglomerate and coarse-grained sandstone occur as channel-fill and fanlike deposits throughout the sequence but are the most common in the upper Miocene and Pliocene sequence.

The physical characteristics of the Tertiary rocks, by themselves, are of limited value for correlating rock units in one area with those in another, but are helpful when used as supporting data with the mineral identification of the heavy-mineral concentrates.

HEAVY-MINERAL STUDIES

Most of the samples for heavy-mineral studies were collected by the authors and their colleagues at arbitrary stratigraphic

Table 1.—*Lithologic and heavy-mineral characteristics of six major units of*

[Heavy-mineral characteristics are based on identification of 3,000 slides (100 grain counts per slide). In general, the percentages of minerals listed excluded in the sampling. Brackets indicate that the diagnostic heavy-mineral assemblage may be made up of any combination of the minerals conform to subdivisions of the Eocene used by other geologists of the U.S. Geological Survey. Radiometric ages are from potassium-argon age bl-gr, blue-green]

Series	Radiometric age (m.y.)	Unit	Formations	Diagnostic nonopaque heavy-mineral assemblage (percent)[1]	Average percentage of total heavy minerals in sand fraction[2]
Pliocene	2–3	6	Flaxville, Ogallala, North Park, South Pass, Dry Union, Troublesome (upper part), Browns Park (upper part), and Wagontongue (of Stark and others, 1949) Formations. These units are generally considered to be late Miocene and (or) Pliocene in age. To the authors' knowledge, these units have yielded fossils no older than late Miocene.	Plutonic Garnet . . . . . } 40–80 Epidote . . . . . } Hornblende (bl-gr) . } And (or) volcanic Hornblende (gr-br) . } Hypersthene . . . . . } >50 Augite . . . . . } Locally flood amounts of hornblende (gr-br), hypersthene, and augite.[3]	≈1.1
Miocene, Upper	12				
	18		MAJOR UNCONFORMITY		
Miocene, Lower		5	Browns Park (lower part), Troublesome (lowermost part), and Arikaree Formations. In Nebraska, the Arikaree is locally a group which includes the Gering, Monroe Creek, and Harrison Sandstones. The overlying Marsland Formation (Lugn, 1939) is included in the Arikaree Group by Wilson (1960), Sato and Denson (1967), Izett (1968), and Denson (1969b).	Volcanic . . . . . >75 Augite . . . . . 20–40 Hornblende (gr-br) . 20–60	≈1.5
	26		DISCONFORMITY		
Oligocene		4	White River Formation; in Nebraska and North and South Dakota, the White River is locally a group which includes the Chadron and Brule Formations. Antero Formation of Stark and others (1949) in South Park, Colo.	Volcanic and plutonic Augite . . . . . <15 Hornblende (gr-br) . >40 Hornblende (bl-gr) . } Epidote . . . . . } Zircon . . . . . } >30 Garnet . . . . . } Sphene . . . . . } Biotite (gr-br) . . . . } Hypersthene rare or absent in Oligocene and underlying Tertiary rocks.[4]	≈0.3
	37–38		MAJOR UNCONFORMITY		
Eocene, Upper		3	*Facies A and B:* time equivalents (not a stratigraphic succession).	Volcanic (first significant appearance of red-brown hornblende—absent or rare in underlying Tertiary rocks).	
			Facies A: Uinta and Bridger Formations in Green River and Washakie Basins. Continental Peak Formation of Nace (1939) and Bridger Formation in Great Divide Basin. (See fig. 1.)	*Facies A:* Augite . . . . . } Hornblende (gr-br) . } >50	≈3.0
			Facies B: Wagon Bed Formation in Wind River and Shirley Basins.	*Facies B:* Zircon (euhedral, colorless) >50	≈0.3
	49				
Eocene, Lower		2	Battle Spring, Wasatch, Wind River, and Green River Formations in Wyoming and northwestern Colorado. Golden Valley Formation in southwestern North Dakota.	Plutonic[5] Epidote . . . . . } Hornblende (bl-gr) . } >50 Garnet . . . . . }	≈1.0
	53–54		MAJOR UNCONFORMITY		
Paleocene		1	Fort Union Formation (includes the Tullock, Lebo, and Tongue River Members in eastern Wyoming). Middle Park Formation (upper part) in northern Colorado.	Plutonic[6] Tourmaline . . . . . } Zircon (rounded, pinkish-violet) . . . . } >50	≈0.2
	65		MAJOR UNCONFORMITY		

[1] Total nonopaque minerals = 100 percent.
[2] Includes both opaque and nonopaque fractions.
[3] In central Wyoming, unit 6 can readily be distinguished in hand specimen by the ubiquitous glass shards in calcareous, sandy, or siliceous beds.
[4] Rocks assigned to the lowermost part of the White River Foundation in some areas in the Powder River and Denver Basins are lithologically and mineralogically similar to the Wagon Bed Formation.
[5] In Williston Basin, chloritoid is a diagnostic heavy mineral in addition to epidote and hornblende (bl-gr).
[6] In Williston Basin, garnet, zircon, and tourmaline generally constitute at least 55 percent of the total heavy-mineral assemblages. Many samples contain other metamorphic minerals. In some of the intermontane basin areas, garnet is locally a common heavy-mineral constituent.

the Tertiary in the middle Rocky Mountains and the northern Great Plains

are representative of those in 10 or more samples taken across an interval of at least 200 feet. Channel sandstones and conglomerates were listed. In some assemblages only one mineral may predominate. The terms upper and lower Eocene as used in this report are informal and may not determinations on tuff (Damon, 1970; Evernden and others, 1961, 1964; Funnell, 1964; Izett and others, 1970; Kulp, 1961). gr-br, green-brown;

Source of nonopaque heavy minerals	Lithologies, thicknesses, and origin
Highly variable mixture derived from plutonic and volcanic rocks. Significantly more minerals from volcanic sources in areas to the west.	Notable lithologic dissimilarity from area to area. Extreme heterogeneity of composition and sorting both laterally and vertically. Unit composed of poorly cemented calcareous claystone, siltstone, sandstone, and conglomerate of fluviatile origin. Thin lenticular beds of algallike limestone suggest local areas of lacustrine deposition. Blue-gray rhyolitic ash beds as much as 30 feet thick in intermontane basin areas. Stringers, nodules, and concretionary masses of black to milky-gray chert near base. Lenticular hard dense lithographic limestone as much as 50 feet thick locally at contact with underlying lower Miocene. Rocks are porous and permeable. Thicknesses range from 0 to 2,500 feet.
Largely from volcanic sources; only minor amounts from Precambrian rocks. Significantly uniform in composition over large areas. Variations in grain-size distribution and total percentage of heavy minerals suggest a westerly source.	Predominantly windblown buff to tan fine- to medium-grained poorly bedded sandstone with abundant tiny grains of bluish-gray magnetite. Generally highly altered chalky-white ash as much as 6 feet thick common near the base. Thin lenticular poorly cemented chalky-gray basal conglomerate present locally with relatively high contents of augite. Good sorting, laterally persistent lithology, and the general absence of coarse detritus and of locally derived debris are outstanding characteristics. Very fine grained fraction, constituting 60–70 percent of the sandstone, contains a relatively large percentage of heavy minerals. Masses of glassy amorphous secondary chert from devitrification of volcanic ash common near the base. Gem varieties of agate present locally in Granite Mountains area of Wyoming. A relatively poor aquifer. Carbonate content about 15 percent. Average thickness about 1,000 feet.
About equal amounts from volcanic and plutonic sources. More volcanic minerals to the west.	Siltstone, claystone, and conglomerate, pink to gray; thin beds of fresh-water limestone and relatively thick beds of altered chalky-white ash. Ash beds in lower half rich in biotite, but contain few other heavy minerals. The upper half is generally eolian except in the Shirley Basin-Granite Mountains area and locally along the eastern flank of the Laramie Mountains where it is highly conglomeratic and predominantly of fluviatile origin; the lower half is generally of fluviatile origin. The conglomerates in the upper part of the Oligocene, in contrast to those at the base of the lower Miocene, are pink or reddish brown and have relatively low contents of augite. Channel sandstones and conglomerates are good aquifers. Carbonate content about 20 percent. Sand fraction contains about the lowest percentage of heavy minerals of any of the Tertiary rocks studied. Average thickness about 850 feet.
Largely volcanic with minor amounts from Precambrian rocks.	*Facies A:* Bentonitic medium- to coarse-grained sandstone, claystone, and siltstone rich in airborne volcanic materials. Contains about the highest percentage of heavy minerals in the sand fraction of any of the Tertiary rocks studied. Fluviatile and lacustrine, containing major eruptive eolian constituents. Probable source area Absaroka volcanic field, northwestern Wyoming. Interfingers with the underlying lacustrine Laney Shale Member of the Green River Formation in the Green River and Washakie Basins. Average thickness about 3,500 feet. *Facies B:* Siliceous bentonitic mudstone, claystone, sandstone, and altered yellowish-green, pale-olive, and dark-greenish-gray tuff. Poorly sorted arkose and boulder conglomerate occur locally in upper and lower parts. Largely fluviatile with major amounts of volcanic constituents. Carbonate content generally less than 5 percent. One of the most impervious units in the Tertiary sequence. Areal distribution suggests Rattlesnake Hills as probable source area. Average thickness about 300 feet.
Mostly first-cycle minerals from Precambrian plutonic and metamorphic rocks.	
Multicycle minerals largely from Mesozoic and Paleozoic rocks. Locally, minor sources from Precambrian rocks.	Very fine grained sandstone and quartzite (ganister), containing varying amounts of admixed silt, clay, and coal of fluviatile and paludal origin. In general, these rocks are finer grained, better sorted, and darker in overall appearance than the overlying Eocene rocks. Percentage of heavy minerals in the sand fraction very low. In some areas the Paleocene rocks contain much coarse debris, particularly near the mountain fronts. This debris is generally composed of pebbles of chert, quartzite, sandstone, and limestone derived largely from Mesozoic and Paleozoic rocks. Average thickness about 2,000 feet.

intervals of about 20 feet in measured sections. Lenses or thin beds of texturally different material within thick, otherwise homogeneous beds were not sampled. Only the very fine grained (0.062–0.125 mm) sand fraction from these samples were studied, because this fraction generally contains the greatest variety and quantity of nonopaque heavy minerals and is in general considered to be representative of the mineral constituents in any given sample. The percentage of each constituent was established by counting 100 grains or more per sample after the magnetic opaque minerals had been removed.

The nonopaque heavy minerals from volcanic ash from middle and upper Tertiary rocks in the basin areas of central and eastern Wyoming were also studied and were compared with the heavy minerals from grab samples collected from terrace deposits of streams draining only the Precambrian terrane in seven major mountain uplifts in the middle Rocky Mountains. Sato and Denson (1967) and Denson and Pipiringos (1969) described techniques of study and interpretations placed on these heavy-mineral analyses. The results show that in a sedimentary sequence derived largely from a plutonic and metamorphic terrane the most common nonopaque heavy minerals are blue-green hornblende, garnet, epidote, zircon, tourmaline, and gray-green biotite; whereas in a sedimentary sequence derived largely from a volcanic terrane the nonopaque heavy minerals most common are green-brown hornblende and red oxyhornblende, augite, hypersthene, and red-brown biotite.

HEAVY-MINERAL CHARACTERISTICS OF THE SIX MAJOR LITHOLOGIC SUBDIVISIONS

Paleocene (unit 1)

The dominant heavy minerals in samples from the Paleocene Fort Union Formation (and equivalents) (table 1) are tourmaline and the pinkish-violet plutonic variety of zircon. These minerals generally make up more than 50 percent of the heavy-mineral concentrates and were derived primarily from the reworking of the marine Mesozoic and Paleozoic rocks as they were stripped from the crests of the major mountain ranges during the Late Cretaceous to early Eocene Laramide orogeny. In some of the intermontane basin areas, garnet is a common heavy-mineral constituent.

Perhaps other nonopaque heavy minerals were at one time constituents of the Paleocene rocks but were removed by surface weathering or more rarely by intrastratal solutions subsequent to deformation of the sediments. Both the very low percentage of heavy minerals and the abundance of limonitic concentrations and iron-cemented sandstone throughout the Paleocene sequence seem to support this interpretation. The nonopaque heavy-mineral assemblages from the Upper Cretaceous Lance Formation are so similar to those from the Paleocene Fort Union Formation that they cannot be differentiated reliably on the basis of percentages of contained mineral species. This similarity also may be the result of surface weathering or intrastratal solution.

The Fort Union Formation is correlative, in part, with the Middle Park Formation in Middle Park, northern Colorado, and the Denver Formation in the Denver Basin, eastern Colorado. In both areas the Paleozoic and lower Mesozoic rocks had been removed by erosion by Late Cretaceous Lance time, and as a result the Precambrian crystalline rocks contributed significantly to the Paleocene sediments. The heavy-mineral concentrates from the Paleocene rocks in these areas, therefore, are atypical and quite unlike those in other areas where the Precambrian was not exposed until early Eocene. The concentrates commonly contain appreciable amounts of blue-green hornblende, epidote, and other plutonic and metamorphic minerals, which characterize the overlying lower Eocene sequence.

In the Williston Basin many of the sandstones in the Fort Union Formation are characterized by heavy minerals—garnet, sphene, kyanite, staurolite, and andalusite.

Lower Eocene (unit 2)

The nonopaque heavy minerals from the very fine grained sand fraction in representative samples collected from the lower Eocene Wasatch, Battle Spring, Green River, and Wind River Formations are characterized by the abundance of one of the minerals—blue-green hornblende, epidote, or garnet—or any combination of the three (table 1). Their abundances are in marked contrast to the relatively low percentages in the overlying upper Eocene rocks and in the underlying Paleocene formations. These minerals are largely the product of erosion of Precambrian rocks. In the Williston Basin, chloritoid, in addition to epidote and blue-green hornblende, is a diagnostic heavy mineral in the lower Eocene Golden Valley Formation. This mineral is an erosion product of a metamorphic terrane, probably Precambrian, and similarly reflects a marked change in the provenance of sediment deposition at the beginning of the Eocene. Not only are the percentages of the various heavy-mineral species different in most of the samples of lower Eocene rocks from those in the underlying Paleocene, but the abundance of heavy minerals in the lower Eocene is generally three times that in the underlying Paleocene. These differences further suggest a change in source of sediment at the beginning of the Eocene.

There are exceptions to the above generalizations. For example, the heavy-mineral concentrates from the lower Eocene Wasatch Formation at some localities in the vicinity of the Uinta Mountains contain exceptionally high percentages of zircon and tourmaline more like those in the Fort Union Formation than those generally found in the Wasatch. This high concentration reflects the fact that the Precambrian quartzites, sandstones, and shales of the Uinta Mountain Group contributed substantially to those lower Eocene sediments. These Precambrian rocks, unlike those in most areas,

yield heavy-mineral concentrates made up almost entirely of zircon and tourmaline. The Wasatch Formation, derived locally from these source rocks, therefore, cannot be differentiated on the basis of heavy-mineral species from the underlying Paleocene Fort Union Formation.

Similarly, in some areas by the end of Paleocene time, the Paleozoic and Mesozoic rocks blanketing the Precambrian possibly had not been completely removed, and during the early stages of Eocene deposition the Paleozoic and Mesozoic rocks possibly were continuing to contribute major amounts of sediment. In these areas it would be difficult, if not impossible, to distinguish the lower Eocene rocks from the underlying Paleocene rocks by means of heavy minerals.

Upper Eocene (unit 3)

The abundance of the volcanic assemblage (green-brown hornblende, augite, and the colorless euhedral variety of zircon) in the very fine sand fraction in representative samples of upper Eocene rocks in central Wyoming contrasts markedly with the relatively low percentages of these minerals in the underlying lower Eocene rocks (Johannsen, 1914; Denson and Pipiringos, 1969).

Differences from place to place in the character of the volcanic assemblage in the upper Eocene rocks are attributed to the source areas that supplied the volcanic materials. The green-brown hornblende and augite assemblage is believed to have come from the vicinity of the Absaroka volcanic field in northwestern Wyoming, whereas the zircon assemblage, because of its local areal distribution in the Granite Mountains–Shirley Basin area, is believed to have been derived largely from volcanoes in the vicinity of the Rattlesnake Hills in central Wyoming.

Oligocene (unit 4)

The nonopaque heavy-mineral assemblage from the Oligocene White River Formation is characterized by the relatively low percentage of augite (generally less than 15 percent) and the relatively high percentages of green-brown hornblende (generally more than 40 percent). During Oligocene time, the Precambrian rocks in the major mountain ranges were eroded, and they contributed significant amounts of detritus to the White River Formation and its equivalents. The nonopaque heavy-mineral assemblage from Oligocene rocks thus contains about equal amounts of plutonic and volcanic minerals. In the lowermost part of the White River Formation at some localities in the Shirley Basin and the Granite Mountains areas 50–150 feet of reddish-brown and green siltstone and claystone is largely detrital and contains a very low percentage of volcanic materials. In most areas, however, the lowermost part of the White River Formation directly above the basal conglomerate is highly tuffaceous, and the heavy-mineral concentrates from it contain large percentages of volcanic minerals.

Lower Miocene (unit 5)

The lower Miocene rocks in the middle Rocky Mountains and northern Great Plains region (Arikaree Formation and its correlatives) are highly tuffaceous and contain a diagnostic assemblage of nonopaque heavy minerals of volcanic origin (green-brown hornblende, and augite). The heavy-mineral assemblage is characterized by the fairly uniform abundance of augite which makes up 20–40 percent of the assemblage—a concentration fairly constant throughout a stratigraphic interval of at least 1,000 feet. Tiny grains of characteristic bluish-gray magnetite are generally abundant. Hypersthene is a minor volcanic constituent in some of the heavy-mineral concentrates. The very low percentage of plutonic heavy minerals in the Arikaree Formation (generally less than 25 percent) may indicate that by the end of Oligocene time most of the mountains were reduced to low relief or were blanketed by lower and middle Tertiary sediments, either of which conditions would have prevented those mountains from contributing significantly to the lower Miocene deposits. In general, the mineral grains of both the light and the heavy fractions from these rocks are angular to subangular, suggesting little reworking.

Upper Miocene and Pliocene (unit 6)

The heavy-mineral assemblage from the upper Miocene and Pliocene rocks (Ogallala Formation and equivalents) is largely locally derived and has only minor volcanic constituents which probably have been derived for the most part from the reworking of older Tertiary rocks (Denson, 1969b). Most of the assemblage is characterized by an abundance of blue-green hornblende, garnet, epidote, and zircon. Locally, particularly in some of the intermontane areas to the west, very large amounts of hypersthene, augite, and hornblende (green brown and reddish brown) characterize the heavy-mineral assemblage of the upper Miocene and Pliocene. In general, the widely distributed heavy minerals derived from plutonic rocks are well rounded, and were transported by water from their source area to their present sites of deposition.

PRINCIPAL FINDINGS

Sampling and petrographic study of the nonopaque heavy minerals from 200 measured sections carried on in conjunction with regional surface and subsurface mapping of the Tertiary rocks suggest individually or jointly the following:

1. Rocks of Paleocene age in Wyoming are characterized by the abundance of reworked tourmaline and zircon and were derived largely from the erosion of Paleozoic and Mesozoic rocks. Although, locally, some constituents of the Paleocene rocks were derived from Precambrian rocks, the amount contributed by crystalline sources is extremely small compared to that from sedimentary sources. The upper and lower limits of the Paleocene Series in the Rocky Mountains and

Great Plains region are at some localities indefinitely known; however, at most localities unconformities and conspicuous lithologic differences are observable at these boundaries. The faunas and floras of the Paleocene are clearly seen to be distinguishably different from those of the overlying Eocene and the underlying Cretaceous. Around most of the Tertiary basins the Paleocene rocks overlie the pre-Tertiary rocks with marked angular discordance, but near the basin centers they are probably conformable or are separated by only a slight unconformity from the underlying fluviatile rocks of the Upper Cretaceous Lance Formation or its equivalents. Near some basin margins the magnitude of the angular discordance between the Fort Union and older formations can be clearly demonstrated by electric, sonic, and gamma-ray logs and by well cuttings from oil and gas tests (Denson and Pipiringos, 1969, fig. 7). However, in many places the magnitude of this unconformity has been inadequately evaluated because of poor exposures and the paucity of surface and subsurface data. It is certain, however, that the unconformity at the base of the Paleocene surpasses in degree the angular discordance at the base of the Eocene, which many workers have described and have mapped in detail over wide areas (Love, 1952, 1954; Pipiringos, 1961; Roehler, 1961; Rich, 1962; Sharp and others, 1964; Soister, 1967; Tourtelot, 1953; Van Houten, 1964; Zeller, 1957; Harshman, 1968; Denson and Harshman, 1969).

2. Rocks of early Eocene age are composed mostly of first-cycle sediments derived largely from the Precambrian cores of the mountains. The abrupt appearance of blue-green hornblende and epidote, ubiquitous constituents of some plutonic and metamorphic rocks, indicates a roughly simultaneous uncovering of the Precambrian sequence in widely separated uplifts in early Eocene time. At most places, the lower Eocene rocks overlie the Paleocene rocks with marked angular discordance. The contact generally is marked by lithologic, faunal, floral, and mineralogic changes that can be mapped with assurance over wide areas. At most places the lower Eocene rocks are coarser grained, more poorly sorted, and are lighter in overall appearance than those of Paleocene age. Although in some areas a particular coal bed may coincide with the Paleocene-Eocene boundary, a distinct lithologic and mineralogic break is a more reliable criterion in selecting the contact.

3. In late Eocene time an influx of a different group of nonopaque heavy minerals over thousands of square miles suggests a widespread volcanic activity in and adjacent to the middle Rocky Mountains. The important changes in the heavy-mineral suites were the abrupt increase in the volcanic variety of zircon and the first appearance and relative abundance of augite and green-brown hornblende. The upper Eocene sequence at most places rests with apparent conformity on, or interfingers with, the underlying lower Eocene. The upper Eocene rocks are rich in airborne volcanic materials now represented by bentonite; at many places they constitute the most impervious sequence in the Tertiary rock column. The local removal of this highly bentonitic rock sequence along channels that were cut early in Oligocene time is believed by the authors to have influenced significantly the occurrence of commercial deposits of uranium in some of the basin areas of central Wyoming. The Shirley Basin and Gas Hills uranium deposits, for example, appear to be spatially related to those areas where the upper Eocene rocks were removed before the deposition of the Oligocene White River Formation. In these areas, mineralizing ground-water solutions had easy access through channels that directed the concentrated flow of the solutions into the underlying host rocks of the lower Eocene Wind River Formation.

4. Volcanism continued throughout most of the Oligocene Epoch. Heavy minerals were contributed in about equal amounts from distant volcanic sources and locally from the Precambrian cores of the mountains. The Oligocene rocks rest with marked angular discordance on rocks as old as Precambrian. Thick beds of light-gray coarse-grained arkosic sandstone exposed mainly near the base of the White River Formation in some areas and a thick sequence of reddish-brown conglomerate in the upper part of the White River in other areas indicate uplift of the major mountain areas at the beginning of and near the close of Oligocene time.

5. In early Miocene time volcanism reached its peak. The very fine grained nonopaque heavy-mineral suites in rocks of this age are 75 percent or more of volcanic origin. Pyroxene is much more abundant than in the underlying White River Formation, and its abrupt increase in abundance also denotes an abrupt increase in volcanic activity at the beginning of Miocene time. The general paucity of plutonic and metamorphic minerals in the Arikaree Formation and its equivalents suggests that by this time the Precambrian rocks were virtually buried by pre-Miocene sediments. A westerly source for the lower Miocene sediments is suggested by the higher percentage of volcanic minerals in heavy-mineral concentrates and the generally coarser grain size of the samples from the western part of the region. At most places the lower Miocene rocks rest with only minor disconformity on upper Oligocene rocks.

6. In late Miocene and early Pliocene time, tectonism and uplift of regional significance, perhaps second only to that of the Late Cretaceous to early Eocene Laramide orogeny, profoundly affected the middle Rocky Mountain and northern Great Plains region. As a consequence, the sediments deposited during this time show extreme heterogeneity of composition and sorting, both laterally and vertically. In some areas, rhyolitic ash beds as much as 30 feet thick indicate that uplift and tectonism were locally accompanied by volcanism. Locally, the rocks associated with these ash beds contain very large amounts of pyroxene and volcanic varieties of amphibole. In general, however, the upper Miocene and Pliocene rocks are characterized by a very high percentage of heavy minerals of plutonic and metamorphic derivation (60–70 percent), whereas the underlying lower Miocene rocks contain 25 percent or less. The noticeably less uniform distribution of sand-size fractions, as well as the greater frequency of

conglomerate and coarse-grained sandstone throughout this part of the Tertiary sequence, substantiates a late Miocene and Pliocene period of crustal instability. This period of late Tertiary uplift had its inception approximately 18 m.y. ago and is believed to have activated the system through which most of the uranium ore in the intermontane basin areas of Wyoming and adjacent areas was first emplaced.

7. Collapse of many parts of mountain ranges occurred near the close of the Pliocene. Displacements of as much as 2,000 to 3,000 feet were largely along Laramide faults, but were in directions opposite to Laramide movements. These late Pliocene collapse features, generally down on the mountainward side, are common throughout parts of the Granite Mountains (Stephens, 1964; Van Houten, 1964; Carey, 1954; Rich, 1962), the Wind River Range (Nace, 1939; Zeller and Stephens, 1969), Laramie Mountains (McGrew, 1963), Hartville uplift (Denson and Botinelly, 1949), and Saratoga Valley (Montagne, 1953). These collapse structures have allowed the preservation of a magnificent sequence of Tertiary rocks in some places, which otherwise might long ago have been removed by erosion.

8. Data on the distribution and thickness of Tertiary strata obtained at the surface and subsurface indicate that the major streams and main drainage framework in central and eastern Wyoming were in existence at the close of the Eocene and persist today with only minor modifications. The Sweetwater and Platte Rivers, for example, follow routes today not far from the main canyons they followed in late Eocene time in traversing the Wind River Range, the Granite Mountains, and the Hartville uplift. Most of the field evidence gathered during this study seems to favor an interpretation that stream piracy, reversals of drainage, and superposition of streams from a middle and late Tertiary cover occur only locally and that the present-day erosion is largely exhuming an ancient antecedent drainage pattern that was well established by the close of the Eocene.

REFERENCES

Carey, B. D., Jr., 1954, A brief sketch of the geology of the Rattlesnake Hills, *in* Wyoming Geol. Assoc. Guidebook 9th Ann. Field Conf., 1954: p. 32–34, 1 pl.

Damon, P. E., 1970, Correlation and chronology of ore deposits and volcanic rocks: U.S. Atomic Energy Comm. Research Div. Ann. Prog. Rept. COO–689–130, Contract AT(11–1)–689.

Denson, N. M., 1969a, New evidence on age relationships of possible Eocene rocks in southwestern North Dakota, *in* Geological Survey Research 1969: U.S. Geol. Survey Prof. Paper 650-B, p. B63–B65.

——1969b, Distribution of nonopaque heavy minerals in Miocene and Pliocene rocks of central Wyoming and parts of adjacent States, *in* Geological Survey Research 1969: U.S. Geol. Survey Prof. Paper 650-C, p. C25–C32.

Denson, N. M., and Bergendahl, M. H., 1961, Middle and upper Tertiary rocks of southeastern Wyoming and adjoining areas: Art. 209 *in* U.S. Geol. Survey Prof. Paper 424-C, p. C168–C172.

Denson, N. M., and Botinelly, Theodore, 1949, Geology of the Hartville uplift, eastern Wyoming: U.S. Geol. Survey Oil and Gas Inv. Prelim. Map 102, 2 sheets.

Denson, N. M., and Gill, J. R., 1965, Uranium-bearing lignite and carbonaceous shale in the southwestern part of the Williston basin—A regional study, *with a section on* Heavy minerals, by W. A. Chisholm: U.S. Geol. Survey Prof. Paper 463, 75 p.

Denson, N. M., and Harshman, E. N., 1969, Map showing areal distribution of Tertiary rocks, Bates Hole-Shirley basin area, south-central Wyoming: U.S. Geol. Survey Misc. Geol. Inv. Map I-570.

Denson, N. M., and Pipiringos, G. N., 1969, Stratigraphic implications of heavy-mineral studies of Paleocene and Eocene rocks of Wyoming, *in* Wyoming Geol. Assoc. Guidebook 21st Ann. Field Conf., 1969: p. 9–18.

Denson, N. M., and Richmond, G. M., 1965, Relation of Tertiary drainage changes to uplift and collapse of a mountain arch, *in* Internat. Assoc. Quaternary Research (INQUA) Guidebook Field Conf. E, Northern and Middle Rocky Mountains, 1965: p. 23–25.

Evernden, J. F., Curtis, G. H., Obradovich, John, and Kistler, R. W., 1961, On the evaluation of glauconite and illite for dating sedimentary rocks by the potassium-argon method: Geochim. et Cosmochim. Acta, v. 23, nos. 1–2, p. 78–99.

Evernden, J. F., Savage, D. E., Curtis, G. H., and James, G. T., 1964, Potassium-argon dates and the Cenozoic mammalian chronology of North America: Am. Jour. Sci., v. 262, no. 2, p. 145–198.

Funnell, B. M., 1964, The Tertiary period, *in* Harland, W. B., Smith, A. G., and Wilcock, Bruce, eds., The Phanerozoic time-scale—A symposium dedicated to Professor Arthur Holmes: Geol. Soc. London Quart. Jour., v. 120 S, p. 179–191.

Harshman, E. N., 1968, Geologic map of the Shirley basin area, Albany, Carbon, Converse, and Natrona Counties, Wyoming: U.S. Geol. Survey Misc. Geol. Inv. Map I-539.

Izett, G. A., 1968, Geology of the Hot Sulphur Springs quadrangle, Grand County, Colorado: U.S. Geol. Survey Prof. Paper 586, 79 p.

Izett, G. A., Denson, N. M., and Obradovich, J. D., 1970, Isotope age of the lower part of the Browns Park Formation, northwest Colorado, *in* Geological Survey Research 1970: U.S. Geol. Survey Prof. Paper 700-C, p. C150–C152.

Johannsen, Albert, 1914, Petrographic analysis of the Bridger, Washakie, and other Eocene formations of the Rocky Mountains, with introductory note by W. D. Matthews: Am. Mus. Nat. History Bull., v. 33, p. 209–222.

Kulp, J. L., 1961, Geologic time scale: Science, v. 133, no. 3459, p. 1105–1114.

Lewis, G. E., 1969, Large fossil mammals and mylagaulid rodents from the Troublesome Formation (Miocene) of Colorado, *in* Geological Survey Research 1969: U.S. Geol. Survey Prof. Paper 650-B, p. B53–B56.

Love, J. D., 1952, Preliminary report on uranium deposits in the Pumpkin Buttes area, Powder River Basin, Wyoming: U.S. Geol. Survey Circ. 176, 37 p.

——1954, Preliminary report on uranium in the Gas Hills area, Fremont and Natrona Counties, Wyoming: U.S. Geol. Survey Circ. 352, 11 p.

Lugn, A. L., 1939, Classification of the Tertiary system in Nebraska: Geol. Soc. America Bull., v. 50, no. 8, p. 1245–1276, 1 pl.

McGrew, L. W., 1963, Geology of the Fort Laramie area, Platte and Goshen Counties, Wyoming: U.S. Geol. Survey Bull. 1141-F, 39 p.

Montagne, J. M. de la, 1953, Late Tertiary normal faults along the east flank of the Park Range, Wyoming and Colorado, *in* Wyoming Geol. Assoc. Guidebook 8th Ann. Field Conf., Laramie Basin and North Park, 1953: p. 103–105.

Nace, R. L., 1939, Geology of the northwest part of the Red Desert, Sweetwater and Fremont Counties, Wyoming: Wyoming Geol. Survey Bull. 27, 51 p., 1 pl.

Pipiringos, G. N., 1961, Uranium-bearing coal in the central part of the Great Divide Basin: U.S. Geol. Survey Bull. 1099-A, 104 p. [1962].

Rich, E. I., 1962, Reconnaissance geology of Hiland-Clarkson Hill area, Natrona County, Wyoming: U.S. Geol. Survey Bull. 1107-G, p. 447–540.

Roehler, H. W., 1961, The late Cretaceous-Tertiary boundary in the Rock Springs uplift, Sweetwater County, Wyoming, *in* Symposium on late Cretaceous rocks, Wyoming and adjacent areas, Wyoming Geol. Assoc. 16th Ann. Field Conf., 1961: p. 96–100.

——1970, Nonopaque heavy minerals from sandstone of Eocene age in the Washakie Basin, Wyoming, *in* Geological Survey Research 1970: U.S. Geol. Survey Prof. Paper 700-D, p. D181–D187.

Sato, Yoshiaki, and Denson, N. M., 1967, Volcanism and tectonism as reflected by the distribution of nonopaque heavy minerals in some Tertiary rocks of Wyoming and adjacent States, *in* Geological Survey Research 1967: U.S. Geol. Survey Prof. Paper 575-C, p. C42–C54.

Sharp, W. N., McKay, E. J., McKeown, F. A., and White, A. M., 1964, Geology and uranium deposits of the Pumpkin Buttes area of the Powder River Basin, Wyoming: U.S. Geol. Survey Bull. 1107-H, p. 541–638.

Soister, P. E., 1967, Geology of the Puddle Springs quadrangle, Fremont County, Wyoming: U.S. Geol. Survey Bull. 1242-C, 36 p.

Stark, J. T., Johnson, J. H., Behre, C. H., Jr., Powers, W. E., Howland, A. L., Gould, D. B., and others, 1949, Geology and origin of South Park, Colorado: Geol. Soc. America Mem. 33, 188 p., 22 figs., 18 pls.

Stephens, J. G., 1964, Geology and uranium deposits at Crooks Gap, Fremont County, Wyoming, *with a section on* Gravity and seismic studies in the Crooks Gap area, by D. L. Healy: U.S. Geol. Survey Bull. 1147-F, 82 p.

Tourtelot, H. A., 1953, Geology of the Badwater area, central Wyoming: U.S. Geol. Survey Oil and Gas Inv. Map OM-124, 2 sheets.

Van Houten, F. B., 1964, Tertiary geology of the Beaver Rim area, Fremont and Natrona Counties, Wyoming: U.S. Geol. Survey Bull. 1164, 99 p. [1965].

Wilson, R. W., 1960, Early Miocene rodents and insectivores from northeastern Colorado: Kansas Univ. Paleont. Contr. [24], Vertebrata art. 7, 92 p.

Wood, H. E., 2d, Chaney, R. W., Clark, John, Colbert, E. H., Jepsen, G. L., Reeside, J. B., Jr., and Stork, Chester, 1941, Nomenclature and correlation of the North American continental Tertiary: Geol. Soc. America Bull., v. 52, no. 1, p. 1–48.

Zeller, H. D., 1957, The Gas Hills uranium district and some probable controls for ore deposition, *in* Wyoming Geol. Assoc. Guidebook 12th Ann. Field Conf., Southwest Wind River Basin, 1957: p. 156–160.

Zeller, H. D., and Stephens, E. V., 1969, Geology of the Oregon Buttes area, Sweetwater, Sublette, and Fremont Counties, southwestern Wyoming: U.S. Geol. Survey Bull. 1256, 60 p.

AGE OF THE IGNEOUS ROCKS ASSOCIATED WITH ORE DEPOSITS, CORTEZ-BUCKHORN AREA, NEVADA

By JOHN D. WELLS, JAMES E. ELLIOTT,
and JOHN D. OBRADOVICH, Denver, Colo.

Abstract.—In the Cortez-Buckhorn area, Nevada, three ages of igneous activity are distinguished: (1) the plutonic intrusion of the Mill Canyon stock and associated dikes in Jurassic time (150 m.y.), (2) the hypabyssal intrusion of quartz porphyry dikes and extrusion of welded tuff (Caetano Tuff) during Oligocene time (33–35 m.y.), and (3) the hypabyssal intrusion of feeder diabase dikes and the extrusion of basaltic andesite lava during Miocene time (16.3 m.y.) followed by intrusion of rhyolite plugs and extrusion of rhyolite lava, also in the Miocene (15.3 m.y.). Rocks representing these episodes, correlated on the basis of similar age and petrography, are present in the mountain ranges nearby. Ore deposits in the area are spatially associated with the igneous bodies. Those associated with Tertiary rocks consist of simple sulfides and gold, whereas those associated with Jurassic rocks contain sulfosalts as well. The deposits are younger than the Jurassic Mill Canyon stock and at least as young as the Miocene rhyolite. Mineral deposits associated with the youngest rock may be nearly the same age and genetically related to it.

The rocks of the Cortez-Buckhorn area, Nevada (fig. 1), most recently described by Gilluly and Masursky (1965), include Paleozoic sedimentary rocks of the upper and lower plates of the Roberts Mountains thrust, Jurassic intrusives, Tertiary sedimentary, intrusive, and extrusive rocks, and Quaternary alluvial and colluvial deposits (fig. 2). Steep faults of post-Oligocene age cross the area. The north boundary of the Caetano Tuff is the Copper fault, where several thousand feet of vertical movement has occurred. The Cortez fault has an offset of about 3,000 feet with the west side down, and the Crescent fault, which bounds the Cortez Mountains on the northeast, has a maximum offset of about 10,000 feet (Gilluly and Masursky, 1965).

In this report we are concerned primarily with the igneous events and metallization. Radiometric dates and geologic observations reported here are intended to establish the ages of rocks that previously have not been determined radiometrically and to clarify the ambiguities in correlation and age that remained after work of Gilluly and Masursky (1965). The ages of the various mineral deposits associated with the igneous rocks will be discussed because of their significance, even though data to establish the time of mineralization are not available except within broad limits.

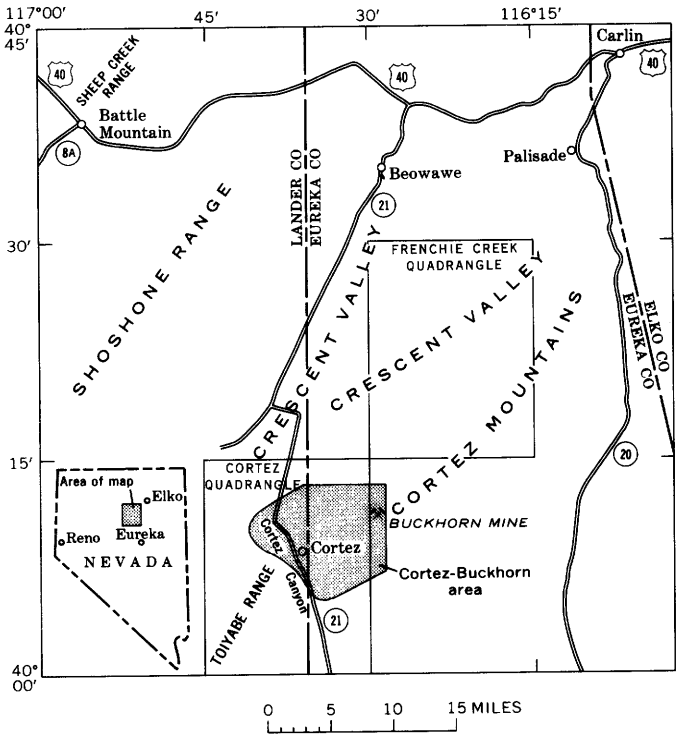

Figure. 1.—Index map showing location of the Cortez-Buckhorn area, Nevada. Base from U.S. Geological Survey, Winnemucca quadrangle, 1:250,000, 1962.

The periods of igneous activity are (1) the intrusion of the Mill Canyon stock and associated dikes during the Mesozoic (most likely the Jurassic), (2) the hypabyssal intrusion of quartz porphyry dikes and extrusion of welded tuff (Caetano Tuff) during the Oligocene, and (3) the extrusion of basaltic andesite flows and the intrusion of feeder diabase dikes, followed by the intrusion of rhyolite plugs and extrusion of rhyolite lava flows, all within the late Miocene.

The Cortez mining district at the southern end of the Cortez Mountains has yielded about $14 million in ore since the

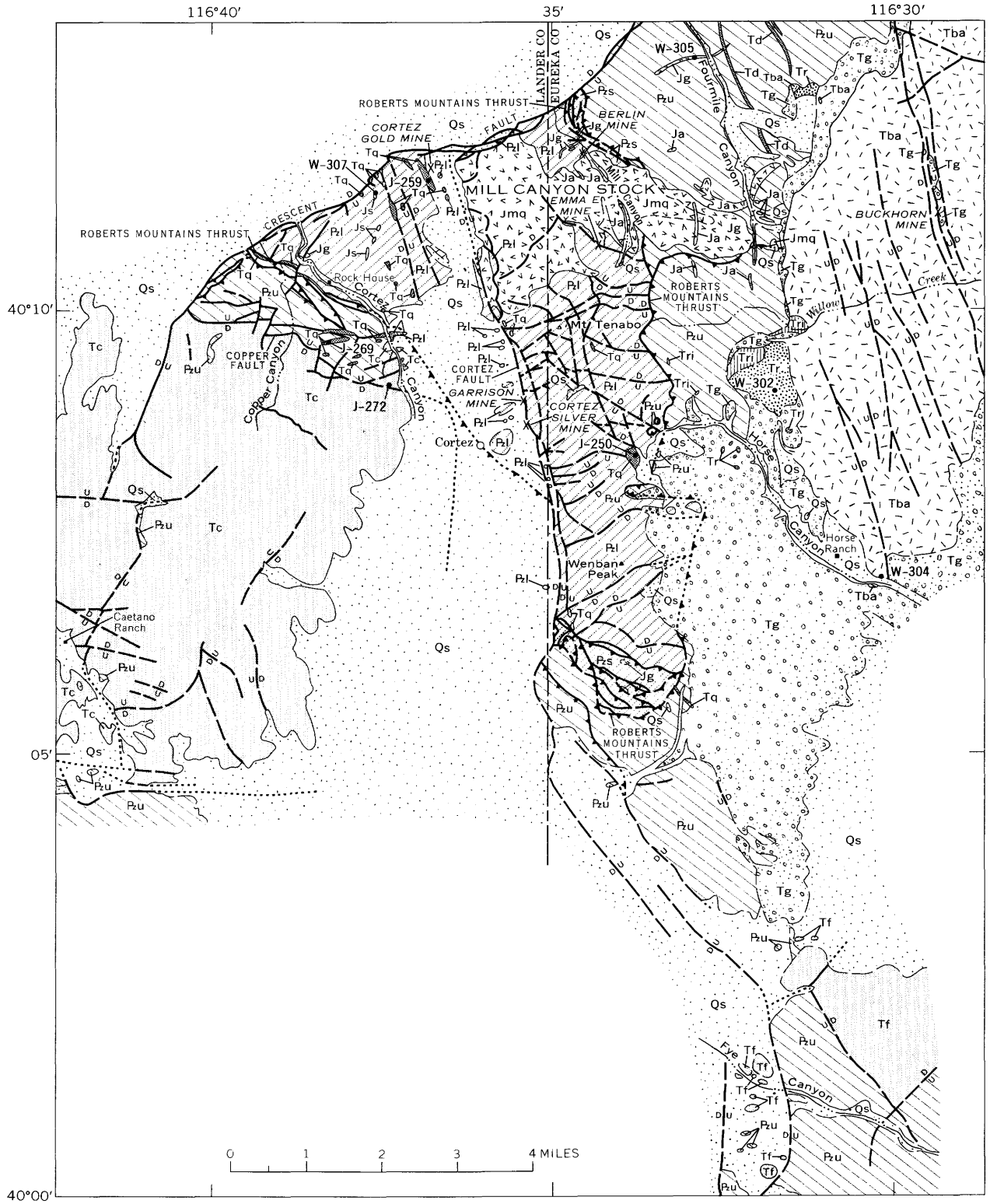
116°40′
35′
116°30′
40°10′
05′
40°00′
LANDER CO
EUREKA CO
ROBERTS MOUNTAINS THRUST
CRESCENT FAULT
CORTEZ GOLD MINE
BERLIN MINE
MILL CANYON STOCK
EMMA EL MINE
BUCKHORN MINE
ROBERTS MOUNTAINS THRUST
Rock House Canyon
COPPER FAULT
Copper Canyon
CORTEZ FAULT
GARRISON MINE
CORTEZ SILVER MINE
Cortez
Mt Tenabo
ROBERTS MOUNTAINS THRUST
Fourmile Canyon
Willow Creek
Horse Canyon
Horse Ranch
Wenban Peak
Caetano Ranch
ROBERTS MOUNTAINS THRUST
Frye Canyon
W-305
W-307
J-259
J-269
J-272
J-250
W-302
W-304
Qs
Tc
Pzu
Pzl
Pzs
Jg
Ja
Jmq
Js
Tq
Td
Tr
Tri
Tg
Tba
Tf
0 1 2 3 4 MILES

Figure 2.

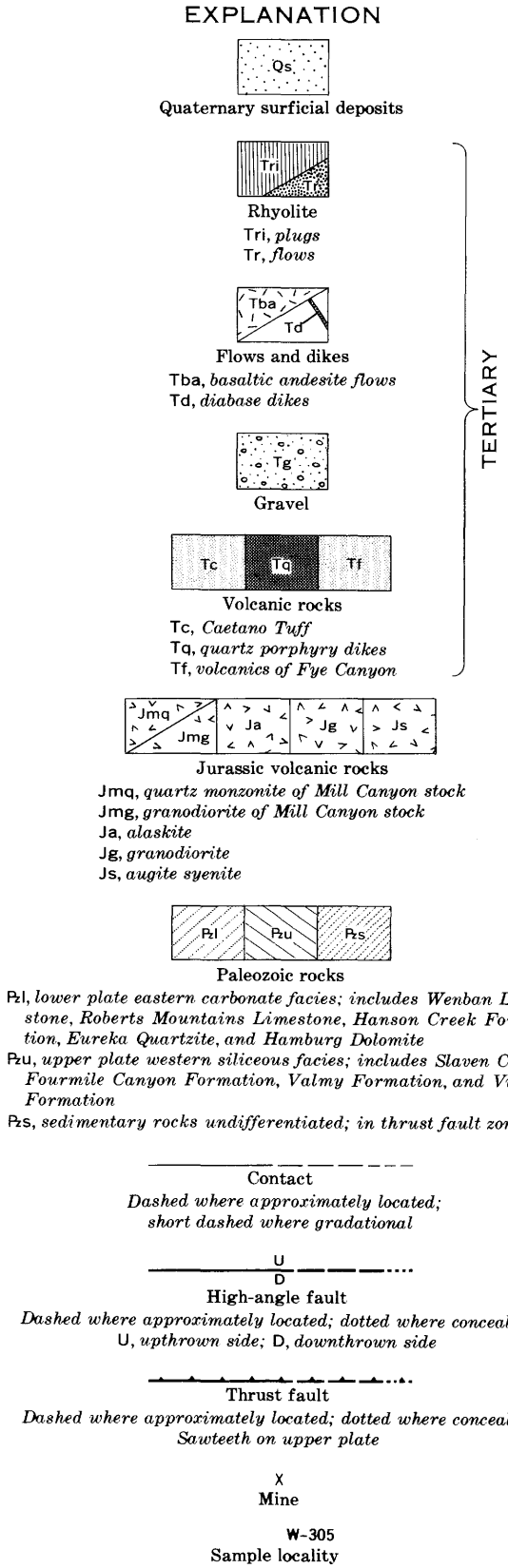

Figure 2.—Geologic map of the Cortez-Buckhorn area, Nevada, showing sample localities. Geology generalized and modified by Wells and Elliott from Gilluly and Masursky (1965) and Masursky (unpub. data).

discovery of the lode in the Cortez silver mine in 1863 (Emmons, 1910). Revenues have been primarily from silver, but significant amounts of gold, copper, lead, and zinc have been produced. Most of this production came from the Cortez silver mine and the mines in Mill Canyon (fig. 2). The Buckhorn district has produced about $1.1 million of gold and silver ore (Roberts and others, 1967). The recently developed Cortez gold mine has a reserve of 3.4 million tons valued at $34.5 million (Wells and others, 1969).

All the mineral deposits in the Cortez-Buckhorn area occur in or near igneous rocks. The ore mineral suites are simple sulfides or simple sulfides plus sulfosalts, and the sedimentary host rocks are lower plate carbonates and upper plate siliceous rocks. The igneous rocks near the mineralized area all show some effects of hydrothermal alteration and commonly are mineralized.

We thank the many mine and claim owners for permitting access to their lands and generally facilitating our work.

JURASSIC IGNEOUS ROCKS

Mill Canyon stock

The Mill Canyon stock (fig. 2), whose greatest exposed dimensions are about 4 by 1½ miles, occupies most of the north slope of the Cortez Mountains west of Mill Canyon and extends eastward as a narrower body to the head of Fourmile Canyon. It is exposed through a vertical distance of nearly 3,000 feet. Small plugs composed of rock types which are similar to those in the Mill Canyon stock occur in the head of Fourmile Canyon.

The Mill Canyon stock is a composite body consisting predominantly of granitoid biotite quartz monzonite, with a granodiorite border zone in the eastern part. Alaskite porphyry dikes and irregular masses occur in the stock and extend into the country rock; Gilluly and Masursky (1965) considered these to be simply a somewhat younger facies of the stock. Granodiorite porphyry dikes (not mapped by Gilluly and Masursky) are present in widely scattered areas, but although some are as close as a quarter of a mile, none are known to cut the Mill Canyon stock.

The Jurassic Mill Canyon stock and the associated bodies have metamorphosed their wallrocks. Scapolite (meionite) is common and widespread in the lower plate carbonate units in the contact aureole. Locally, irregular bodies of tactite containing garnet, idocrase, epidote, and diopside were developed. Limestone units were silicified and bleached, and marble and tremolitic hornfels were formed near the stock (Gilluly and Masursky, 1965). Metamorphic effects have not been noted in the upper plate chert and shale units except near the stock where the Fourmile Canyon Formation has been baked to dense hornfels.

The quartz monzonite is a gray medium-grained (1–4 mm) granitoid rock with a salt-and-pepper appearance. A representative specimen consists of approximately 27 percent quartz,

18 percent microcline, 40 percent plagioclase, and 15 percent biotite. The rock weathers tan or light brown.

Rocks of the granodioritic border zone are slightly porphyritic, and similar in color but finer grained than those of the central part of the stock. In a typical specimen the groundmass is fine grained (0.25–0.5 mm) and the phenocrysts, making up about 8 percent of the rock, are fine to medium grained (0.5–2 mm) and consist of about 3 percent plagioclase, 4 percent biotite, and trace amounts of hornblende. The whole rock consists of approximately 20 percent quartz, 11 percent microcline, 60 percent plagioclase, 9 percent biotite, and trace amounts of hornblende This rock also weathers tan or light brown.

Dikes

Dikes considered Jurassic in age are alaskite, granodiorite, and augite syenite.

The alaskite is a very light gray porphyry with quartz and feldspar phenocrysts as much as 4 mm long and biotite phenocrysts as much as 1 mm long set in a fine-grained (0.05–0.1 mm) groundmass. The groundmass constitutes 60 to 80 percent of the rock. Phenocrysts of plagioclase aggregate approximately 10 to 20 percent; perthitic microcline 5 to 10 percent; quartz, trace to 7 percent; and biotite, trace to 5 percent of the rock. The whole rock consists typically of approximately 20 percent quartz, 45 percent microcline, 30 percent plagioclase, 5 percent biotite, and trace amounts of hornblende. The rock weathers reddish brown.

The granodiorite porphyry dikes are typically medium gray to pinkish gray, with a fine-grained (0.05–1.0 mm) groundmass that constitutes from 80 to 90 percent of the rock; phenocrysts, which are generally less than 3 mm in size, consist of approximately 3 to 10 percent hornblende, 2 to 5 percent biotite, trace to 1 percent quartz, trace to 2 percent plagioclase, and trace to 1.5 percent pyrite. The composition of the typical whole rock is approximately 3 percent quartz, 76 percent feldspar, 11 percent hornblende, 8 percent biotite, and 2 percent pyrite. Locally the rock has a medium-grained groundmass (2–3 mm) with only a few phenocrysts; this rock consists of approximately 8 percent quartz and 30 percent each of plagioclase, biotite, and hornblende. Strong alteration effects are common and consist of hornblende altered to chlorite, biotite to chlorite, and muscovite and feldspar to sericite. The oxidation of pyrite gives a reddish-brown color to the rock in outcrop.

The augite syenite described by Gilluly and Masursky (1965, p. 72–73) occurs as dikes of mixed contaminated igneous rock and inclusions of reconstituted carbonate wallrock; less contaminated parts were recognized as being similar to the quartz monzonite of the Mill Canyon stock. Gilluly and Masursky stated that the rock contains abundant calcite and alkali feldspar (some of the feldspar has micrographic intergrowths with quartz), major amounts of augite, and small amounts of hornblende, quartz, and labradorite.

Age of the Mill Canyon stock and associated dikes

From contact relations the age of the Mill Canyon stock can be bracketed only as being younger than the Roberts Mountains thrust which it cuts, that is, post-Early Mississippian, and older than the late Cenozoic age of the basaltic andesite which caps the cuesta to the east. Geologic criteria for distinguishing the ages of the many dikes are almost entirely lacking. Dikes with noteworthy contact aureoles have been classified by Gilluly and Masursky (1965) as belonging to the same epoch as the Mill Canyon stock, which has a definite contact aureole. Those lacking aureoles were classed as Tertiary. Even though this criterion for classifying dikes has some evidence favoring it, it led Gilluly and Masursky to identify the Jurassic granodiorite porphyry dike shown (fig. 2) in lower Fourmile Canyon as Tertiary quartz porphyry.

Three published K-Ar (potassium-argon) age determinations on biotite from the Mill Canyon stock indicate that this igneous body is at least of latest Jurassic age. These determinations are as follows:

A. 150±3 m.y. (million years). Age determined by Armstrong (1970b).
B. 147 m.y., Armstrong (1963); also tabulated by Schilling (1965, p. 37). Age determined at the University of California at Berkeley.
C. 151 m.y. Gilluly and Masursky (1965). Age determined by G.H. Curtis at the University of California at Berkeley.

Efforts to obtain unaltered hornblende mineral concentrates from samples of the Mill Canyon stock were not successful. We were successful, however, in obtaining a suitable hornblende concentrate from the augite syenite, which in its less contaminated part was recognized to be petrographically similar to the quartz monzonite of the Mill Canyon stock. A K-Ar age for this sample (W-307, table 1) is 150±5 m.y. The maximum ages determined on the three biotites and the hornblende age are the same within analytical uncertainty and probably represent the time of emplacement of the Mill Canyon stock (fig. 3).

The granodiorite porphyry dikes show some alteration at all exposures visited; for this reason satisfactory minerals for K-Ar dating were not obtained. However, C. W. Naeser, of the U.S. Geological Survey (written commun., 1969), dated, by the fission-track method, apatite (sample W-305, fig. 3) from a granodiorite porphyry dike located on the ridge between Fourmile Canyon and Mill Canyon, lat 40°12.8′ N., long 116°32.9′ W. The analytical data are as follows:

Spontaneous track density: 3.64×10^5 tracks/cm^2 (765 tracks)
Induced track density: 2.42×10^5 tracks/cm^2 (508 tracks)
Age: 134±14 m.y.

Naeser considered this to be a minimum age for the rock. Accordingly, the granodiorite porphyry may be considered to be the same age as the Mill Canyon stock and simply a phase of this intrusive sequence. The granodiorite porphyry dikes may be the earliest phase of this Jurassic period of igneous activity, inasmuch as mafic minerals are more abundant in

Table 1.—*Potassium-argon dating of igneous rocks in the Cortez-Buckhorn area, Nevada*

[Data by J. D. Obradovich]

Sample No.	Mineral	K_2O (percent)	Radiogenic Ar^{40} (moles/g $\times 10^{-10}$)	Radiogenic argon (percent)	Age (m.y.)
W-307	Hornblende	0.539	1.24	89.9	150±5
J-250	Biotite	8.56	4.39	81.0	34.4±1.2
	Sanidine	10.62	5.42	96.0	34.3±1.1
J-259	Biotite	8.25	4.17	82.2	33.9±1.1
	Sanidine	12.34	6.42	94.9	35.0±1.2
J-269	Biotite	8.39	4.37	85.3	35.0±1.0
	Sanidine	10.52	5.40	91.6	34.5±1.1
J-272	Biotite	8.37	4.29	80.3	34.4±1.1
	Sanidine	11.85	5.76	93.8	32.6±1.0
Average of 8 ages					34.3
W-304	Plagioclase	.295	.0713	18.8	16.3±0.9
W-302	Sanidine	10.10	2.28	91.7	15.3±0.4

Sample description and locality:

W-307, Augite syenite (contaminated quartz monzonite) 4,700 feet northeast of the mouth of Cortez Canyon; lat 40°11.30′ N., long 116°37.60′ W.

J-250, Quartz porphyry plug 7,500 feet north of Wenban Peak; lat 40°8.40′ N., long 116°33.77′ W.

J-259, Quartz porphyry dike at the Cortez mine; lat 40°11.44′N., long 116°36.82′ W.

J-269, Quartz porphyry dike 4,000 feet south of Rock House; lat 40°9.66′ N., long 116°36.82′ W.

J-272, Caetano Tuff, welded tuff, 7,500 feet northwest of Cortez; lat 40°09.15′ N., long 116°37.40′ W.

W-304, Basaltic andesite 3,500 feet southeast of Horse Ranch; lat 40°12.83′ N., long 116°32.94′ W.

W-302, Rhyolite flow on the divide north of Horse Canyon 12,350 feet northwest of Horse Ranch; lat 40°09.12′ N., long 116°31.75′ W.

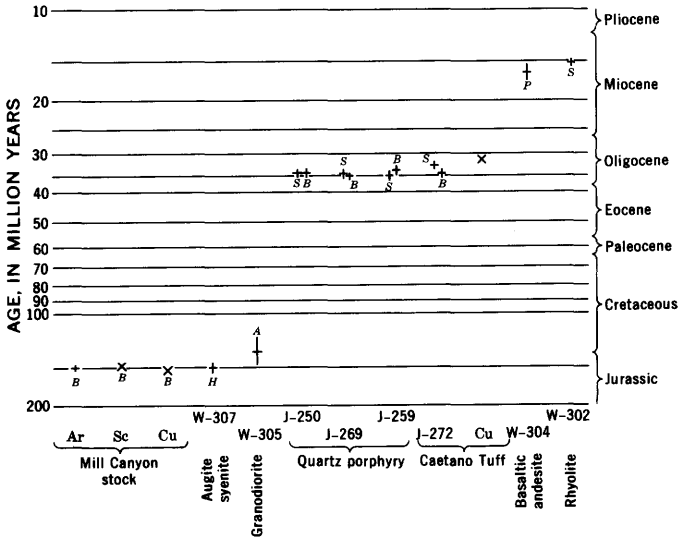

Figure 3.—Age of igneous rocks in the Cortez-Buckhorn area, Nevada, determined on biotite (*B*), sanidine (*S*), hornblende (*H*), apatite (*A*), and plagioclase (*P*). Horizontal bar of symbol is reported value, vertical bar is analytical error; x, value with analytical error not reported. Sources of data: Ar, Armstrong (1970b); Sc, Schilling (1965); Cu, G. H. Curtis (Gilluly and Masursky, 1965); sample numbers prefixed by W or J, this report.

them than in the Mill Canyon stock and none of these dikes are known to cut the stock.

About 6 miles to the northeast of the Mill Canyon stock a group of rocks that are petrographically similar to those of the stock occur in the Frenchie Creek quadrangle. These rocks have been designated by Muffler (1964) as Cretaceous(?), but K-Ar ages on a biotite sample and a hornblende sample from the intrusive complex in the quadrangle have been determined (Armstrong, 1970b) as 153±3 and 143±3 m.y., respectively. These data indicate that Mill Canyon stock and the Frenchie Creek intrusives (not to be confused with the Frenchie Creek Rhyolite of the Pony Trail Group) constitute a complex intrusive center that extends about 20 miles along the Cortez Mountains. The Pony Trail Group, composed of volcanic and sedimentary rocks in the Frenchie Creek area, is considered to be of Mesozoic (probably Jurassic) age and related to the intrusive complex in the Frenchie Creek quadrangle, although a Triassic age cannot be ruled out (Muffler, 1964). These rocks may be as much as 10,000 feet thick and may extend to Palisade (Roberts and others, 1967) about 20 miles northeast of the intrusive complex. No volcanics of this age are known in the Cortez-Buckhorn area.

The only other Jurassic igneous body nearby (about 45 miles southeast of Cortez) is the Whistler Mountain stock, a two-mica leucoadamellite (quartz monzonite), dated by Armstrong (1970b) as 152±3 m.y.

TERTIARY IGNEOUS ROCKS

Caetano Tuff

The Caetano Tuff (fig. 2) is exposed in the northern end of the Toiyabe Range. This unit is about 8,000 feet thick and consists mostly of rhyolitic welded tuff with minor amounts of water-laid andesitic tuff and black vitrophyre. Lenses of conglomerate and sandstone derived from nearby Paleozoic sedimentary rocks are present (Gilluly and Masursky, 1965; Masursky, 1960).

The Caetano Tuff consists of phenocrysts of pink to smoky quartz, sanidine, biotite, plagioclase, and lithic fragments in a pinkish-gray to purple-gray matrix of welded glass shards. Parts of the unit are vitric and black. Flow structure is everywhere present, and most phenocrysts are broken or bent. The matrix generally constitutes 55 to 65 percent of the rock; quartz phenocrysts form approximately 15 to 20 percent, sanidine makes up 5 to 20 percent, plagioclase, 5 to 10 percent, and biotite, trace to 2 percent of the rock.

Paleontologic evidence as to the age of the Caetano Tuff has been obtained from the interbedded water-laid tuffs. These beds have yielded pollen that has been assigned an age of Miocene or older by E. B. Leopold (Gilluly and Masursky, 1965, p. 77). A 31.5-m.y. K-Ar age determination on biotite from the Caetano Tuff reported by Gilluly and Masursky and the additional radiometric data in the present article confirm the age assignment of Oligocene.

Biotite and sanidine from another sample of the Caetano Tuff both have been dated (sample J-272), and ages of 34.4±1.1 m.y. and 32.6±1.0 m.y. have been obtained. Armstrong (1970a) reported two K-Ar age determinations for the Caetano Tuff. The first age—30.6 m.y.—was determined on chloritized biotite from a sample collected just south of the upper plate of the Roberts Mountains thrust and roughly half a mile east of the Crescent fault. The second age—31.2 m.y.—was determined on a whole-rock sample taken about 1 mile east of the Caetano Ranch 5 miles southwest of Cortez. McKee and Silberman (1970) reported ages of 31 m.y. for Caetano(?) Tuff in the Shoshone Range and 33.5 m.y. for three separate welded tuffs designated Caetano(?) in the vicinity of Battle Mountain, in the northern Fish Creek Mountains (20 miles southwest of Battle Mountain), and in the east-central flank of the Toiyabe Range.

Quartz porphyry dikes

Gilluly and Masursky (1965), in describing the dikes associated with the Mill Canyon stock, mentioned that they were unable to find unambiguous criteria for distinguishing the dikes associated with that intrusive from those probably related to the Caetano Tuff. However, they related the Tertiary quartz porphyry dikes to the Caetano Tuff by their chemical similarity and by their orientation parallel to the Cortez fault. The general light color, greater abundance of phenocrysts, absence of hornblende, and presence of sanidine serve to distinguish these dikes from the Jurassic granodiorite porphyry.

The quartz porphyry dikes cut both upper and lower plate sedimentary rocks and were injected along the plane of the Roberts Mountains thrust (fig. 2). The dikes commonly have glassy chilled margins and have had little if any contact effect on the wallrock except locally where jasperoid has formed by silicification of carbonate rocks.

The quartz porphry dikes are mostly very light gray to pinkish gray and consist of euhedral quartz, sanidine, plagioclase, and biotite phenocrysts in a fine-grained (less than 0.5 mm) crystalline to glassy groundmass; the glassy rocks are very dark green to black, particularly along chilled borders. Flow structure is common, and lithic fragments are present. The groundmass generally constitutes from 85 to 95 percent of the rock; quartz phenocrysts constitute approximately 1 to 6 percent, plagioclase, 1 to 3.5 percent, sanidine, trace to 6 percent, and biotite, trace to 2 percent of the rock. The rock weathers pink to tan; the plagioclase may weather pink or may be altered to clay and removed, leaving a pitted surface.

K-Ar age determinations were made on biotite-sanidine mineral pairs from three quartz porphyry samples. The ages (table 1) show a very narrow range and average 34.5 m.y. These results clearly substantiate the assumption of Gilluly and Masursky (1965) that the quartz porphyry dikes and the Caetano Tuff are related to a single igneous episode.

These quartz porphyry dikes may not represent the first middle Tertiary igneous activity in this region; older ages have been obtained by radiometric methods on igneous rocks in nearby areas. In the southeast corner of the Cortez quadrangle, in Fye Canyon about 10 miles southeast of Cortez, volcanic rocks, chiefly flow-banded and autobrecciated rhyolite, cover 1 square mile. Chemically these rocks are closely similar to those of the Caetano Tuff but are higher in silica and perhaps slightly higher in combined alkalis. However, difference in provenance for the two does not seem indicated. No tuff has been recognized among these rocks, nor are any lava flows known in the Caetano Tuff. These volcanics extend for several miles south and east of the Cortez quadrangle. Three K-Ar age determinations have been made on samples of the volcanics of Fye Canyon. A K-Ar analysis on biotite by G. H. Curtis yielded on age of 36.8 m.y. (Gilluly and Masursky, 1965). Armstrong (1970a) reported two K-Ar age determinations based on whole-rock samples of 30.9 m.y. However, these results, being from whole-rock samples, can be considered as only minimum values.

Silberman, Wrucke, and Armbrustmacher (1969) and McKee and Silberman (1970) reported K-Ar age determinations on biotite, sanidine, and hornblende from igneous rocks on the east side of the Shoshone Range about 12 miles north of Cortez; the ages were 37.3 m.y. for porphyritic granodiorite and 34.8 m.y. for rhyolite porphyry dikes. The dikes are equivalent in age to the quartz porphyry dikes near Cortez and to the Caetano Tuff. The granodiorite stock may represent an earlier phase of igneous activity within the Oligocene. K-Ar age determinations on similar rocks from other parts of the Shoshone Range give values ranging from 34 to 38 m.y. (McKee and Silberman, 1970).

Basaltic andesite

Basaltic andesite flows cover the east flank of the Cortez Mountains (fig. 2), forming a cuesta, and were considered by Gilluly and Masursky (1965) to be the faulted extension of a comparable group of flows that form the dip slope on the east flank of the Shoshone Range across Crescent Valley to the northeast. The flows dip 3°—16° E. and attain maximum thickness of about 350 feet in the Cortez-Buckhorn area. The flows rest mostly on Tertiary gravel, but locally they rest directly on Paleozoic bedrock. Northwest-trending dolerite dikes east of Fourmile Canyon are believed to represent feeders to the flows (Gilluly and Masursky, 1965). These flows are part of a series that occurs along a zone 5 to 10 miles wide

and extends at least 125 miles, from just north of the city of Battle Mountain southeastward nearly to Eureka.

The basaltic andesite ranges from dense to vesicular and is black with irregular patches of green. A few plagioclase phenocrysts as much as 3 mm long, smaller grains of pyroxene, and magnetite are visible in hand specimen. The plagioclase and pyroxene are present in nearly equal quantities and constitute approximately 95 percent of the rock. The vesicles are filled with chalcedony. The rock weathers a rusty brown.

The basaltic andesite has been considered to be Pliocene by Gilluly and Masursky (1965, p. 83–84) on the basis of structural, stratigraphic, and paleontologic evidence.

A K-Ar age determination on a plagioclase concentrate (W-304) from a sample of basaltic andesite collected southeast of Horse Ranch yielded an age of 16.3±0.9 m.y. An identical value of 16.3 m.y. was obtained by McKee and Silberman (1970) for a whole-rock sample of basaltic andesite collected some 4 miles northeast of Granite Mountain on the east flank of the northern Shoshone Range.

These identical age determinations confirm Gilluly and Masursky's assertion that the two isolated bodies of basaltic andesite are simply faulted extensions of one another. However, these K-Ar ages support a late Miocene age for the andesites, not the middle or late Pliocene age that had been previously inferred (Gilluly and Masursky, 1965, p. 84).

Rhyolite

In the headwater interfluve of Willow Creek and Horse Canyon near the margin of the basaltic andesite, rhyolite plugs intrude and flows overlie the basaltic andesite; the rhyolite is clearly younger and is, therefore, the youngest igneous rock in the Cortez-Buckhorn area (fig. 2).

Gilluly and Masursky (1965, p. 85) believed that the plugs probably represent only slightly dissected domes because the rocks show both very pronounced flow structures parallel to the borders and streaking in the direction of dip. The rock is lithoidal and highly vesicular, very fine grained (approximately 0.05 mm), porous, light gray to brownish gray to pale lavender. A few phenocrysts (less than 3 percent), which generally range in size from 0.5 to 1 mm, and lithic fragments are present. The phenocrysts are smoky quartz, plagioclase, and sanidine in about equal proportions are sparse biotite flakes. The vesicles are partially filled with cristobalite, small clear quartz crystals, topaz, or fluorite, and combinations of these. The trace-element suite in this rock shows unusually high concentrations of Sn (20 ppm), Be (10 ppm), Nb (30 ppm), Y (70 ppm), and Pb (70 ppm). These high values, together with the presence of numerous vesicles, cristobalite, and smoky quartz, and the paucity of phenocrysts, serve to distinguish this rock from the quartz porphyry and granodiorite porphyry dikes in which the concentrations of these elements are considerably lower.

A K-Ar age determination on sanidine from the rhyolite yielded an age of 15.3±0.4 m.y. (W-302, table 1 and fig. 3). Armstrong (1970a) reported an age of 14.5±0.5 m.y. on a whole-rock sample of the flow just to the north of the plug. The closeness of the ages for the basaltic andesite and rhyolite suggests an episode of bimodal magmatism.

Rhyolite of late Miocene age is scattered throughout Nevada and adjacent States (Armstrong and others, 1969) but is not abundant in the region around the Cortez-Buckhorn area. Armstrong (1970a) reported an age of 15.0±0.1 m.y. for a whole-rock sample of rhyolite collected near Palisade, about 40 miles northeast of Cortez, whereas McKee and Silberman (1970) reported ages of 13.8 and 13.9 m.y. on sanidine from rhyolite in the Sheep Creek Range about 55 miles northwest of Cortez.

A small body southwest of the main mass of Horse Canyon was considered to be part of the young rhyolite by Gilluly and Masursky (1965). However, the rock is petrographically similar to the quartz porphyry dikes, and K-Ar age determinations of 34.4 and 34.3 m.y. (J-250, table 1 and fig. 3) on biotite and sanidine confirm this petrographic identity.

AGE OF ORE DEPOSITS

The most significant mines and prospects in the report area are the Cortez silver mine, the Cortez gold mine, the Buckhorn mine, and those in Mill Canyon, in Copper Canyon, and in Horse Canyon.

The mineral deposits in Mill Canyon occur in fissure veins and as replacement bodies in the Jurassic Mill Canyon stock and the adjacent Devonian Wenban Limestone. Veins trend generally north and northeast. These deposits contain pyrite, arsenopyrite, sphalerite, galena, boulangerite, bournonite, argentian tetrahedrite, chalcopyrite, pyrargyrite-proustite, gold, stibnite, and owyheeite. Vanderburg (1938, p. 27) noted that argentite and stephanite occur also.

In the vicinity of the Cortez silver mine both Tertiary quartz porphyry dikes and Jurassic granodiorite porphyry dikes are present. Most of the ore at the mine occurs in west-northwest-trending veins and manto deposits in the Cambrian Hamburg Dolomite. The ore mineral suite is similar to that in Mill Canyon, but the ores have lower gold and copper contents than those in Mill Canyon.

The ore at the Cortez gold mine is a disseminated deposit in Roberts Mountains Limestone that has been bleached, leached of carbonates, and silicified adjacent to altered Oligocene quartz porphyry dikes (Wells and others, 1969). The ore zone trends northwesterly, and the known gold occurs as very fine grains in oxidized altered sediments. The deposit is terminated on its northwest end by the Crescent fault and has been offset about 3,000 feet vertically relative to the Mill Canyon area and Cortez silver deposit by the Cortez fault. Metals other than gold occur in very small amounts. Very small quantities of Pb (<10 ppm), Zn (<200 ppm), Cu (<30 ppm), Ag (<0.5 ppm), As (<2,000 ppm), Sb (<50 ppm), W (<100 ppm), and Hg (<5 ppm) are present. In the ore zone, iron oxide pseudomorphs

after sulfides remain. Presumably the original minerals were simple sulfides, probably mostly iron sulfide.

In the Copper Canyon vicinity a mineralized zone has been explored for several years, but only small amounts of ore have been mined. Strong geochemical anomalies in copper, lead, and zinc occur. Primary sulfides are pyrite, sphalerite, chalcopyrite, galena, pyrrhotite, and marcasite. Mineralized northwest-trending fracture zones occur in the upper plate siliceous rocks and Oligocene quartz porphyry; clay-alteration effects are common in both rock units.

The gold-silver veins at the Buckhorn mine cut the Miocene basaltic andesite and are controlled by faults associated with a north-northwest-trending horst in which Tertiary sedimentary deposits underlying the flows are exposed. Clay alteration of both igneous and sedimentary rocks has been extreme. The primary minerals are mostly pyrite and marcasite. Much of the production has been from the upper, oxidized parts of the sulfide zones.

Mineralized area in Horse Canyon northwest of Horse Ranch consists of small amounts of cinnabar and gold in poorly defined zones in upper plate siliceous rocks. Miocene rhyolite dikes are present in this mineralized area. The dikes and wallrock were hydrothermally bleached and somewhat altered to clay.

From the foregoing discussion certain conclusions concerning the chronology of mineralization can be reached; these are summarized in table 2. Obviously the latest episode of significant mineralization is indicated by the veins emplaced along fault zones cutting the Miocene basaltic andesite. The source of the ore-forming fluids might be the Miocene rhyolites, for there is some indication of this in Horse Canyon. None of the major rhyolite plugs crop out within about 2 miles of the Buckhorn mine, but, as the alinement of the plugs between Horse Canyon and Willow Creek is toward the mine, they might project under it.

The mineralization of the Cortez gold mine and zones in the Copper Canyon vicinity occurred contemporaneously with or later than emplacement of the Oligocene quartz porphyry dikes. The mineralized areas are spatially associated with the Oligocene dikes. Neither Miocene nor Jurassic igneous units are exposed in the immediate vicinity of the mineralized areas. However, Jurassic rocks crop out southwest of the Cortez gold mine, and a faulted westward extension of the Jurassic Mill Canyon stock possibly occurs at depth under the mine.

Mineralized rocks at the Cortez silver mine and in Mill Canyon show an obvious spatial relationship to the Mill Canyon stock and the granodiorite porphyry dikes. Further, the mineralization in Mill Canyon and the Cortez silver mine differed from that at the Cortez gold mine and Buckhorn mine both in mineralogy and in kind and relative amounts of metals present.

The foregoing evidence is not conclusive and does not allow an unequivocal determination of the age of mineralization for each of the deposits; nevertheless, spatial relationship and differences in ore mineralogy seem to indicate three periods of mineralization that correlate with the three periods of igneous activity—Jurassic, Oligocene, and Miocene. On this basis the most significant contributors regionally would be the Oligocene igneous rocks because they are widespread, whereas both Jurassic and Miocene igneous rocks are only locally present. An alternate and possibly more reasonable interpretation would be that all the deposits were formed at one time, probably in the Miocene or later, and that the mineralogic variations reflect the influence of the various host rocks and (or) the depth of emplacement below the surface.

Table 2.—*Characteristic metals, geologic relation to igneous rocks, and inferred age of mineral deposits in the Cortez-Buckhorn area, Nevada*

Ore deposit	Characteristic metals	Relation to igneous rock	Inferred age
Mill Canyon	Cu, Ag, Pb, Zn, Au, and so forth.	In veins cutting Jurassic Mill Canyon stock and replacement deposits adjacent to stock.	Post-Jurassic.
Cortez silver	Cu, Ag, Pb, Zu, Au, and so forth.	Veins and replacement deposits in Cambrian rocks, near Tertiary and Jurassic dikes.	Do.
Cortez gold	Au	Altered Roberts Mountains Limestone, along altered Oligocene dikes.	Post-Oligocene.
Copper Canyon	Cu, Pb, Zn	Mineralized fractures in upper plate siliceous rocks and Oligocene quartz porphyry.	Do.
Buckhorn mine	Au, Ag	Veins cutting Miocene basaltic andesite.	Post-Miocene basaltic andesite.
Horse Canyon	Hg, Au	Zones in upper plate siliceous rocks near altered Miocene dikes.	Miocene(?).

CONCLUSIONS

In the Cortez-Buckhorn area, Nevada, three ages of igneous rocks are distinguished: (1) the intrusion of the Mill Canyon stock and associated dikes in the Jurassic (150 m.y. ago), (2) the hypabyssal intrusion of quartz porphyry dikes and extrusion of welded tuff (Caetano Tuff) during the Oligocene (33–35 m.y. ago), and (3) the intrusion of feeder diabase dikes and extrusion of basaltic andesite lava, followed by intrusion of rhyolite plugs and extrusion of rhyolite lava, in the late Miocene (15–16 m.y. ago).

All mineralized rocks are correlated spatially with igneous intrusives and are known to be no older than Jurassic (150 m.y.). Mineralization at the Cortez gold mine and Copper Canyon is known to be no older than Oligocene (33–35 m.y.), and that at Buckhorn and Horse Canyon is known to be no older than Miocene (15–16 m.y.). However, all mineralization may be as young as or younger than the Miocene. Mineralization almost certainly accompanied the Miocene igneous activity and may also have accompanied the Oligocene and Jurassic activity.

REFERENCES

Armstrong, R. L., 1963, Geochronology and geology of the eastern Great Basin in Nevada and Utah: Yale Univ. unpub. Ph. D. thesis, 202 p.

——1970a, Geochronology of Tertiary igneous rocks, eastern Basin and Range province, western Utah, eastern Nevada, and vicinity, U.S.A.: Geochim. et Cosmochim. Acta, v. 34, no. 2, p. 203–232.

——1970b, K-Ar data using neutron activation for Ar analysis–Comparison with isotope dilution Ar analyses: Geochim. et Cosmochim. Acta, v. 34, no. 2, p. 233–236.

Armstrong, R. L., Ekren, E.B., McKee, E. H., and Noble, D. C., 1969, Space-time relations of Cenozoic silicic volcanism in the Great Basin of the western United States: Am. Jour. Sci., v. 267, no. 4, p. 478–490.

Emmons, W. H., 1910, A reconnaissance of some mining camps in Elko, Lander, and Eureka Counties, Nevada: U.S. Geol. Survey Bull. 408, 130 p.

Gilluly, James, and Masursky, Harold, 1965, Geology of the Cortez quadrangle, Nevada, *with a section on* Gravity and aeromagnetic surveys, by D. R. Mabey: U.S. Geol. Survey Bull. 1175, 117 p.

Masursky, Harold, 1960, Welded tuffs in the northern Toiyabe Range, Nevada: Art. 129 *in* U.S. Geol. Survey Prof. Paper 400-B, p. B281–B283.

McKee, E. H., and Silberman, M. L., 1970, Geochronology of Tertiary igneous rocks in central Nevada: Geol. Soc. America Bull., v. 81, no. 8, p. 2317–2327.

Muffler, L. J. P. 1964, Geology of the Frenchie Creek quadrangle, north-central Nevada: U.S. Geol. Survey Bull. 1179, 99 p. [1965].

Roberts, R. J., Montgomery, K. M., and Lehner, R. E., 1967, Geology and mineral resources of Eureka County, Nevada: Nevada Bur. Mines Bull. 64, 152 p.

Schilling, J. H., 1965, Isotopic age determinations of Nevada rocks: Nevada Bur. Mines Rept. 10, 79 p.

Silberman, M. L., Wrucke, C. T., and Armbrustmacher, T. J., 1969, Age of mineralization and intrusive relations at Tenabo, northern Shoshone Range, Lander County, Nevada: Geol. Soc. America Abs. with Programs for 1969, pt. 3, p. 62.

Vanderburg, W. O., 1938, Reconnaissance of mining districts in Eureka County, Nevada: U.S. Bur. Mines Inf. Circ. 7022, 66 p.

Wells, J. D., Stoiser, L. R., and Elliott, J. E., 1969, Geology and geochemistry of the Cortez gold deposit, Nevada: Econ. Geology, v. 64, no. 5, p. 526–537.

GEOCHEMICAL PROSPECTING FOR THORIUM VEINS BY STREAM-SEDIMENT SAMPLING, LEMHI PASS QUADRANGLE, IDAHO AND MONTANA

By MORTIMER H. STAATZ, CARL M. BUNKER,
and CHARLES A. BUSH, Denver, Colo.

Abstract.—In an area that contains many thorium veins, samples of stream sediment were collected to determine whether the thorium content of the samples would aid in locating these veins. The thorium content of most of these samples ranges from 6 to 20 ppm. The wide range of thorium values is due in part to the relatively low thorium values of samples collected from streams that drain areas underlain by Challis Volcanics in contrast to higher thorium values in samples collected from streams that drain areas underlain by rocks of the Belt Supergroup in which all the known thorium veins were found. Thorium values of four samples that were collected a short distance downstream from mine dumps on thorium veins are clearly above all background values. A comparison of the thorium content of other samples along some streams shows small increases in the thorium content of some samples collected close to and downstream from thorium veins.

Most of the known thorium veins in the Lemhi Pass quadrangle, Idaho and Montana, have been delineated with the aid of either a Geiger or scintillation counter, both of which measure the radiation emitted by thorium. A thorium vein cannot be detected with either a scintillation or Geiger counter, however, if the vein is overlain by more than several inches of soil that does not contain residual pieces from the vein. Although many thorium veins have been located in the Lemhi Pass area by radiation counters, other veins cannot be found by this method owing to thick residual soils or glacial till. Here veins or parts of veins have been located by making deep bulldozer cuts, at random or along continuations of known veins. The present geochemical study is an effort to find a quicker and more economical method of locating covered thorium veins.

Geochemical prospecting methods have been used in many places to define areas anomalously high in copper, lead, zinc, cobalt, and molybdenum. Deposits hidden under many feet of soil can commonly be detected by the small amounts of these metals that are leached out of them and carried down the neighboring streams. Analyses of the stream sediments, panned heavy-mineral concentrates, or the water itself may indicate that anomalous amounts of a particular metal exist somewhere in the stream's drainage basin. If thorium could be traced by a similar method, it might be possible to locate thorium veins under thick overburden, which completely masks any anomalous radiation.

The Lemhi Pass quadrangle is the part of the Lemhi Pass thorium district that contains the district's largest and most concentrated thorium veins. Stream-sediment sampling was chosen as the most likely method of locating covered thorium veins. This method was chosen over water sampling because metal concentrations tend to accumulate in the sediments and, although small, they are easier to detect than the much smaller amounts in the water. The use of panned heavy-mineral concentrates in this area was not feasible for the analytical methods available to us—gamma-ray spectrometry and spectrography. Less than half an ounce of heavy minerals can be concentrated per pan of sand collected from these streams, and material is required in much greater amount for gamma-ray spectrometry and in higher thorium content for spectrography.

METHODS OF SAMPLING AND ANALYSIS

A total of 67 stream-sediment samples was collected from several places along the larger streams and at the mouths of tributaries entering these streams. The samples consisted mainly of silt and mud, and commonly contained a large amount of organic material. The samples were air dried and sieved, and the minus 20-mesh fraction, which ranged from about 45 to 200 grams, was analyzed for thorium on a gamma-ray spectrometer. The spectrometer system includes a 400-channel pulse-height analyzer and four 5-inch-diameter by 4-inch-thick NaI (Tl) crystal detectors, each viewed by a 5-inch-diameter photomultiplier tube. The signal output from each detector is routed to a 100-channel group in the analyzer, where the pulses are electronically sorted and stored in a memory circuit. The accumulated spectra are interpreted through a computer program using a linear least-squares

U.S. GEOL. SURVEY PROF. PAPER 750-C, PAGES C136-C140

method, which compares the spectrum from each sample with thorium standards and thereby calculates the concentration of thorium in each sample.

The thorium content of each sample is shown on figure 1. The reported thorium value on these relatively small samples could vary as much as 10 percent from the actual thorium content.

THORIUM BACKGROUND VALUES

In an area containings thorium deposits, stream sediments can contain thorium contributed both from the veins and from the generally small amounts present throughout the country rocks. Hence, to determine the amount of vein-derived thorium in a stream sediment some knowledge of the background thorium (that which is derived from the country rock) is necessary. Background thorium can be determined (1) for the entire area, (2) for individual rock types within an area, or (3) for individual drainage basins within a particular rock type.

A composite background of all rocks within the Lemhi Pass quadrangle was obtained by plotting a histogram of the number of samples versus thorium content (fig. 2). Of the 67 samples, 61 are grouped together in a block (fig. 2) with a thorium content of 6–18 ppm. Two other adjacent samples with a thorium content of 18–20 ppm might also be considered a part of this block. The wide spread in these background values suggests an uneven distribution of the thorium.

Several country rocks with different thorium backgrounds can be one of the causes of broad variations in background values. The three principal rock units in the Lemhi Pass quadrangle (fig. 1) are (1) Precambrian Belt Supergroup, which consists of fine-grained micaceous quartzite and siltite, (2) Tertiary Challis Volcanics, which consists of rhyodacite and basalt flows with interbedded rhyolitic tuffs, and (3) Quaternary glacial deposits, which consist principally of quartzite from the Belt Supergroup but which near the Challis have some volcanic fragments.

Most of the samples taken in the Lemhi Pass quadrangle were from streams that cross only rocks of the Belt Supergroup, but some samples are from streams that cross (1) glacial deposits, (2) Challis Volcanics, or (3) both Challis and Belt rocks. Table 1 gives the range and the average thorium content of all stream sediment samples collected in the Lemhi Pass quadrangle, and of samples collected in streams draining the various rock types. The average thorium content of the samples from streams that drain only the Belt rocks is substantially higher than that of samples from streams that drain the other rock types, as shown in figures 3 and 4. Four of the samples (those above 20 ppm thorium) collected from streams draining the Belt rocks, however, have a thorium content that is above the range of possible background values. If these samples are not included in the average, then the average thorium content of samples collected from streams draining Belt rocks is 11.9 ppm. Even without the obviously anomalous samples, the thorium content of samples from streams draining only Belt rocks is noticeably higher than the thorium content from samples collected in streams draining areas underlain by the other three rock types, and this higher content is probably in part due to detrital thorium minerals from thorium veins within the Belt rocks. However, thorium veins have not been found in all areas of Belt rocks, and above-average thorium values of samples from streams draining these areas may be due to a higher background of some of the Belt rocks.

Local thorium anomalies may be difficult to distinguish if they fall within the broad range of the general background values (figs. 2, 3). A more meaningful interpretation can commonly be made by comparison of thorium analyses from a single drainage system. For example, the range in thorium content of 12 samples in the drainage of upper Bear Creek (fig. 1) is 7.5–16.3 ppm. The 10 samples which contain 7.5–11.6 ppm thorium can be arbitrarily classed as a background group for this basin, and the two samples which contain 16.1 and 16.3 ppm thorium, and which lie distinctly above this group, are anomalous.

ANOMALOUS THORIUM VALUES

The range in thorium content (6.0–37.3 ppm) of the stream sediment samples in the Lemhi Pass quadrangle is small, and the highest analysis is only 3.1 times that of the average (11.9 ppm) for the background group (fig. 3) of samples from streams that drain only rocks of the Belt Supergroup. Hence, even in an area that contains numerous high-grade thorium veins, anomalies are relatively weak. Furthermore, only four values are greater than those of the overall background group of analyses (figs. 2 and 3), and by this standard would be considered anomalous. All four samples were collected fairly close to thorium veins which had substantial dumps. The sample with the highest thorium content (37.3 ppm) was collected on a northwest-trending branch of Copper Queen Creek, 0.4 mile below where this stream crosses the toe of the dump from the lowest adit on the Wonder vein (fig. 1). A sample that contained 32.0 ppm thorium was collected on Flume Creek below the Lucky Horseshoe vein. Here a series of bulldozer cuts has scattered vein material down a steep hillside, making it readily movable by slope wash. A stream sample collected 0.25 mile above this sample contained 14.4 ppm thorium, and one collected 0.7 mile below it contained only 12.9 ppm. A sample that yielded 24.5 ppm thorium was collected on a northeast-trending branch of Copper Queen Creek, 1 mile below the Cago 12 vein. One large bulldozer cut, which extends 0.2 mile along this vein, and a series of smaller cuts furnish an abundant supply of material to the stream below. A sample containing 22.1 ppm thorium was collected on Agency Creek just above the mouth of Copper Queen Creek. Two-tenths of a mile above this sample locality, Agency

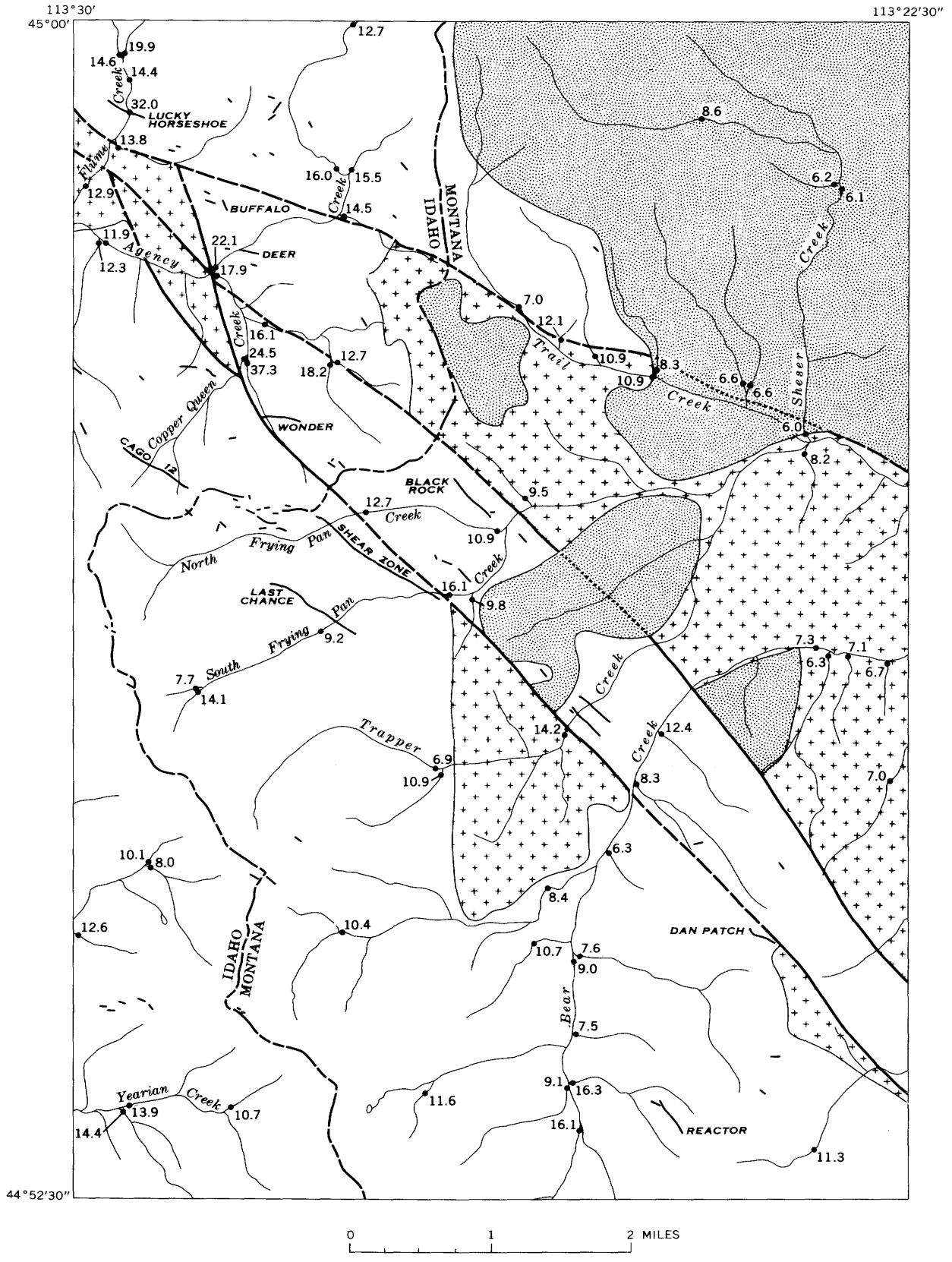
113°30'
113°22'30"
45°00'
44°52'30"
LUCKY HORSESHOE
BUFFALO
DEER
WONDER
BLACK ROCK
LAST CHANCE
DAN PATCH
REACTOR
MONTANA
IDAHO
IDAHO
MONTANA
Flume Creek
Agency Creek
Copper Queen
CAGO 12
North Frying Pan SHEAR ZONE
South Frying Pan
Trapper Creek
Yearian Creek
Bear Creek
Trail Creek
Sheep Creek
0 1 2 MILES

Figure 1.

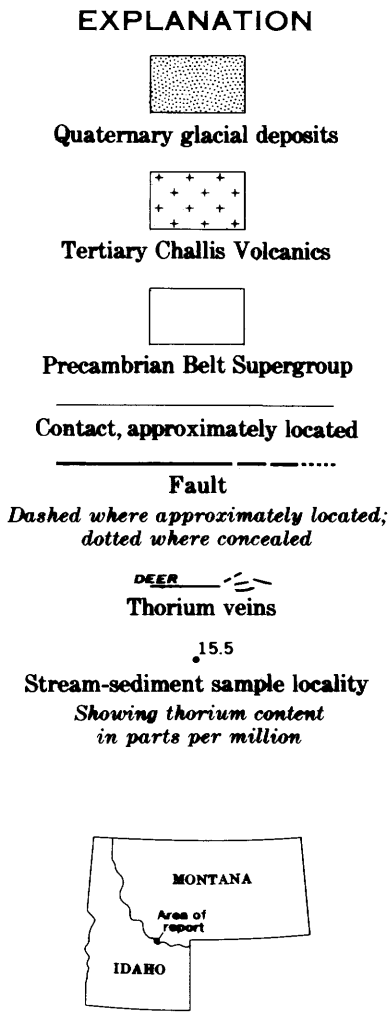

Figure 1.—Generalized geologic map showing the thorium content of stream-sediment samples and the thorium veins in the Lemhi Pass quadrangle, Idaho and Montana.

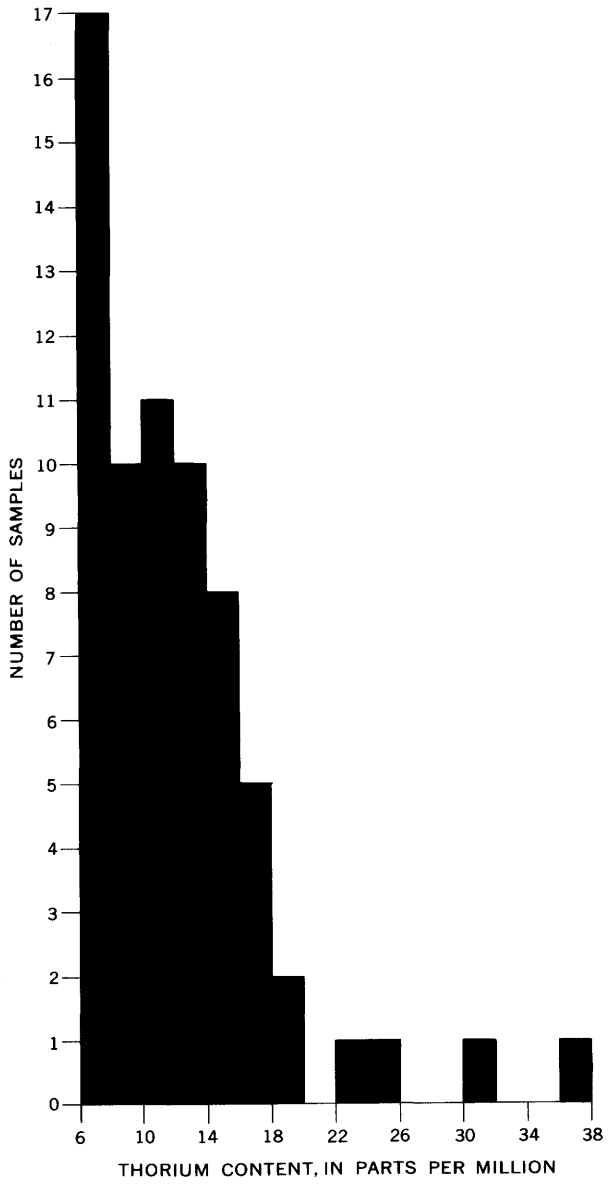

Figure 2.—Histogram of thorium content of all samples collected from streams in the Lemhi Pass quadrangle.

Creek crosses the toe of a dump on one of the veins on the Deer property.

The small number of well-defined anomalies is rather disappointing, as several seemingly normal samples were taken on streams that drain areas known to contain thorium veins. Some of these samples that were collected close to and downstream from a large thorium vein, however, contain more thorium than is normal for the drainages in which they were collected. South Frying Pan Creek (fig. 1) is crossed by two large veins, the Shear Zone and the Last Chance. Five samples collected on this stream and its tributaries contained 7.7–16.1 ppm thorium. The sample that contained 16.1 ppm thorium was collected just downstream from where the Shear Zone is projected across the creek and about 0.7 mile below where the Last Chance vein crossed the creek. A sample taken 0.3 mile above the Last Chance vein yielded 9.2 ppm thorium. Similarly a sample collected at the mouth of a small west-flowing tributary of Bear Creek that drains the ridge on which the two Reactor veins are exposed by several trenches contained 16.3 ppm thorium, and a sample taken on Bear Creek just above this tributary had 9.1 ppm.

Other small local increases in thorium content cannot be readily correlated to known thorium veins and may possibly represent thorium from concealed veins. One such example is in the northwest corner of the quadrangle (fig. 1), in the upper part of Flume Creek, where samples from the two branches of the creek have yielded 14.6 and 19.9 ppm thorium. Another example occurs near the south edge of the quadrangle in the

Table 1.—*Thorium content of stream-sediment samples in the Lemhi Pass quadrangle, Idaho and Montana*

Source of samples	Number of samples	Thorium content (ppm) Range	Average
Belt Supergroup	49	6.3–37.3	13.3
Challis Volcanics	6	6.3–9.5	7.5
Both Belt and Challis rocks	5	7.3–14.2	10.8
Glacial deposits	7	6.0–8.6	6.9
Total	67	6.0–37.3	11.9

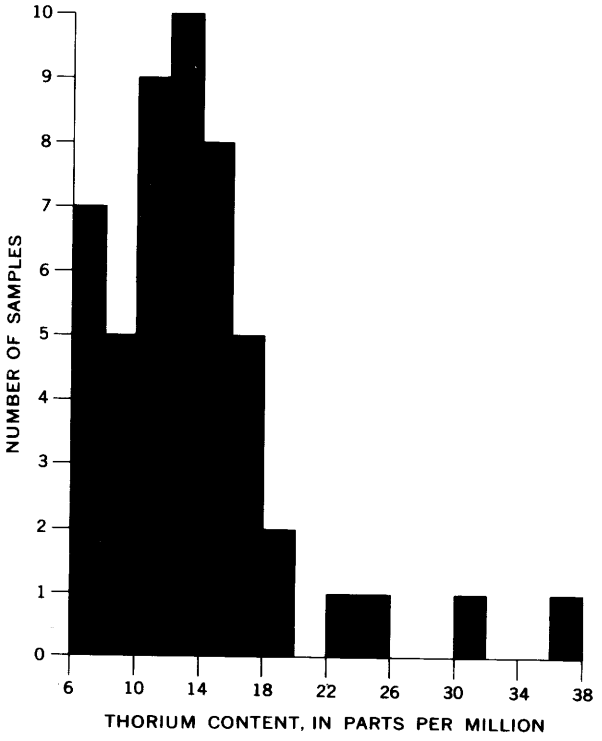

Figure 3.—Histogram of thorium content of samples collected from streams that drain areas underlain only by rocks of the Belt Supergroup in the Lemhi Pass quadrangle.

headwaters of Bear Creek, where a sample contained 16.1 ppm thorium. Such small increases in thorium suggest the addition of thorium to the stream from some source other than the country rock, and may represent thorium contributed to the streams from concealed veins.

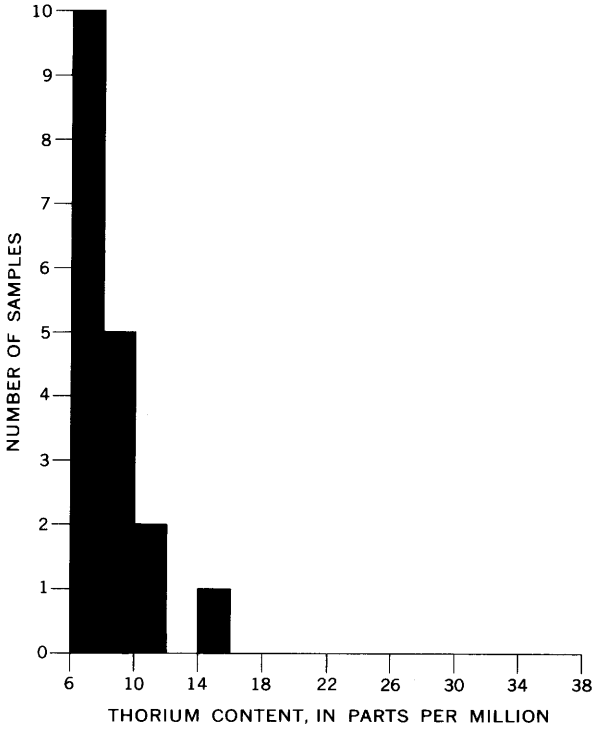

Figure 4.—Histogram of thorium content of samples collected from streams that drain areas underlain by glacial deposits, by Challis Volcanics, and by both the Challis Volcanics and rocks of the Belt Supergroup in the Lemhi Pass quadrangle.

CONCLUSIONS

The results obtained in geochemical prospecting for thorium from veins by collecting stream-sediment samples are disappointing. The thorium from poorly exposed veins does not tend to collect in the sediments, and the most anomalous sample collected in an area with a high concentration of veins was only three times the average background. The only samples that were clearly above average background values came from streams that were a short distance below well-exposed veins; in two of the samples the stream actually ran across the toe of a mine dump on these veins. Thorium veins which have workings on ridges or which are covered by alluvium where they cross the streams furnish only small amounts of thorium to the stream sediments. Minor differences in thorium content of samples along an individual stream indicated, in some places, the parts of the stream drainage that are more favorable for finding thorium veins.

GEOCHEMICAL EXPLORATION OF THE MONTE ALTO COPPER DEPOSIT, BAHIA, BRAZIL

By RICHARD W. LEWIS, JR., ANTONIO LUIS SAMPAIO de ALMEIDA[1], ANTONIO GERMANO GOMES PINTO[1], CARLOS PIRES FERREIRA[1], FLÁVIO JUAREZ TÁVORA[1], and FRANCISCO BATISTA DUARTE[1], Rio de Janeiro, Brazil

Work done in cooperation with the Departamento Nacional da Produção Mineral, under the auspices of the Agency for International Development, U.S. Department of State

Abstract.—Geochemical studies of four copper-bearing shear zones that cut schists and quartzites at Monte Alto in southern Bahia State reveal two low anomalies that warrant further investigation and two more possible mineralized zones. Statistical analyses of the results indicate that the uppermost A_1 soil horizon should not be used for geochemical sampling and that the B_2 soil horizon at depths of 15–25 cm is an adequate indicator of mineralization. The safe threshold value for anomalous amounts of copper indicative of mineralization is estimated to be 125 ppm. Frequency distribution of plant species along sampling traverses shows a coincidence of plant assemblage and copper content; three plant species merit further investigation as indicators or accumulators of copper from the soil.

The Monte Alto copper deposit is in the southern part of the State of Bahia, Brazil, about 30 km north of Vitória da Conquista and 950 km north of Rio de Janeiro (fig. 1).

This investigation was part of a training program for the Departamento Nacional da Produção Mineral in geochemical prospecting and the use of a truck-mounted geochemical laboratory. The results presented herein are a condensed version of the subsequent statistical exercise on the data, which are typical of copper mineralization in the semiarid region of northeast Brazil.

GEOLOGY AND MINERALIZATION

Monte Alto is in a belt of undifferentiated Precambrian phyllite, schist, quartzite, and migmatite that is intruded by granite and diorite, and which rests unconformably on the Precambrian Gneissic Complex and discordantly underlies the Precambrian Minas Group (Maack, 1963). The area investigated is underlain by quartz-mica schist containing intercalated

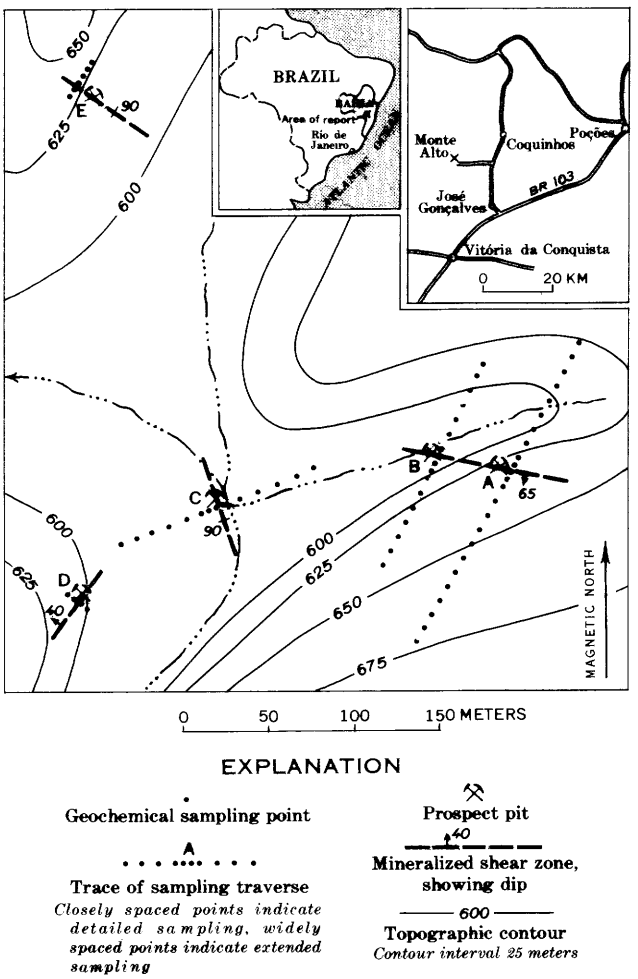

Figure 1.—Sketch map showing area of geochemical sampling at Monte Alto, Bahia, Brazil.

[1]Departamento Nacional da Produção Mineral, Rio de Janeiro, Brazil.

quartzite, metamorphosed arkose, and bands of granitic gneiss. Regionally the rocks trend northwest and dip moderately to the southwest. In the immediate area of this investigation, however, the rocks are intensely folded; the schistosity and banding range in strike from northwest to northeast and in dip from 65° SW. to 40° NW.

The mineralization consists of secondary copper minerals, principally malachite with some brochantite and a little chrysocolla, concentrated along four shear zones (fig. 1). These shear zones contain 1–4 m of fractured, sericitized, and chloritized rock with seams and lenses of quartz. Copper minerals are disseminated in quartz and sheared rock.

CLIMATE, SOILS, AND VEGETATION

The climate of the area is semiarid and tropical, having a single rainfall maximum during the summer months, December to March. Rainfall ranges from 350 to more than 2,000 mm per year and averages about 800 mm per year. More than 80 percent of the total annual precipitation falls during the summer months. All smaller streams are intermittent and on the average carry water only 2–3 months of the year.

The soils in the area studied are moderately stony and silty to sandy in texture. Organic content is generally low. Iron oxides predominate over clay minerals in the finer fractions, commonly giving the soil a characteristic reddish color. This is especially true of soils overlying rocks such as mica schist that contain moderate amounts of mafic minerals. Soil thickness ranges from a few tens of centimeters on the steeper slopes to more than 150 cm along or near valley bottoms. On hilltops and slopes the color and texture of soils vary in accordance with composition of bedrock, indicating that at least part of the soil material has been derived directly from subjacent rock.

The vegetation of the region is transitional between what Luetzelburg (1923) termed brushy caatinga (Siccideserta) and woody caatinga (Durifruticeta). The brushy caatinga that dominates the hilltops and slopes is characteristic of the vegetation of areas having a semiarid climate in which the moderate annual precipitation (500 to 1,000 mm) is concentrated in a 3- to 4-month period. This vegetation is predominantly xerophytic and highly adapted to taking full advantage of a short rainy season and tolerating long dry spells. It typically consists of open to moderately thick brushy ground cover, dominated by plants of the mallow (Malvaceae) and spurge (Euphorbiaceae) families, along with isolated trees and wooded thickets whose individuals belong principally to the leguminous (Leguminosae) and cashew (Anacardiaceae) families. Characteristic of this area, but not found in drier regions of caatinga, is the arborescent cactus *Pereskia bahiensis*, locally called quiabento (Braga, 1953). Other types of cactus and varieties of terrestial bromelids, common to the drier regions in northeast Brazil, are scarce in this area.

The woody caatinga is confined to the valley bottoms, where soils are deeper and ground moisture more abundant. This vegetation consists of moderately thin trunked (15–30 cm in diameter) trees of medium height (10–20 m) and a dense and commonly spiny underbrush. Vines and climbing plants are abundant in places. Trees and bushes of the leguminous family predominate.

GEOCHEMICAL INVESTIGATIONS

Three hundred and seventeen soil samples were taken along five sample lines traversing the four mineralized shear zones (fig. 1). Surface samples were collected at 1-m intervals for 20 m along the five sample lines. Sampling along traverses A, B, and C was extended an additional 50–100 m at each end and was done at 10-m intervals. At each sample point the A_1 and B_2 soil horizons were sampled and a count of the vegetation made. Material from the A_1 soil horizon was collected at depths of 5–15 cm, and the B_2 horizon was sampled at depths of 15–25 cm. Plant counts were made in a 50- by 50-cm area around the sample points spaced at 1-m intervals and in a 2- by 2-m area around points spaced at 10 m. Furthermore, at prospect pit C, three vertical soil profiles were sampled at 10-cm intervals from the surface to depths of 100–150 cm.

Standard analytical procedures for the determination of copper by the biquinoline method, as described by Ward and others (1963), were used. Chemical analyses were made only of soil samples; none of the plant material collected was analyzed.

The concentrations of copper in soils of the A_1 and B_2 soil horizons along detailed and extended sampling traverses are shown in figure 2. These graphs show that on the average the copper values were higher in the B_2 soil horizon than in the A_1. This increase in copper content with depth is also shown in the vertical sampling profiles in figure 3. The C horizon and deeper parts of the B_2 horizon in these vertical profiles gave copper values slightly higher than values found at easily sampled depths of 15–20 cm; therefore they better define the presence of mineralization. It is believed, however, that the anomalies found at the shallower depths of the B_2 soil horizon are clear enough that the extra work and time required for sampling at greater depths are not necessary.

The best anomalies of copper were found in traverses D and E, in which values ranged from 100 to 350 ppm of Cu. These values are high enough to warrant further investigation, especially as these traverses contain sectors having at least 250 ppm of Cu over a length of 4 m or more.

The low values of copper in traverses A and B were surprising, because A had the best surface showing of copper minerals. Thus, concentration of copper minerals is evidently more restricted than originally thought.

Attention should be called to possible mineralized fractures other than those recognized in the field. These are indicated by (1) a high anomaly in traverse D (fig. 2) 8 m southeast of the fracture exposed in the prospect pit and (2) a moderate anomaly in traverse A (fig. 2) 95 m south of the principal fracture sampled.

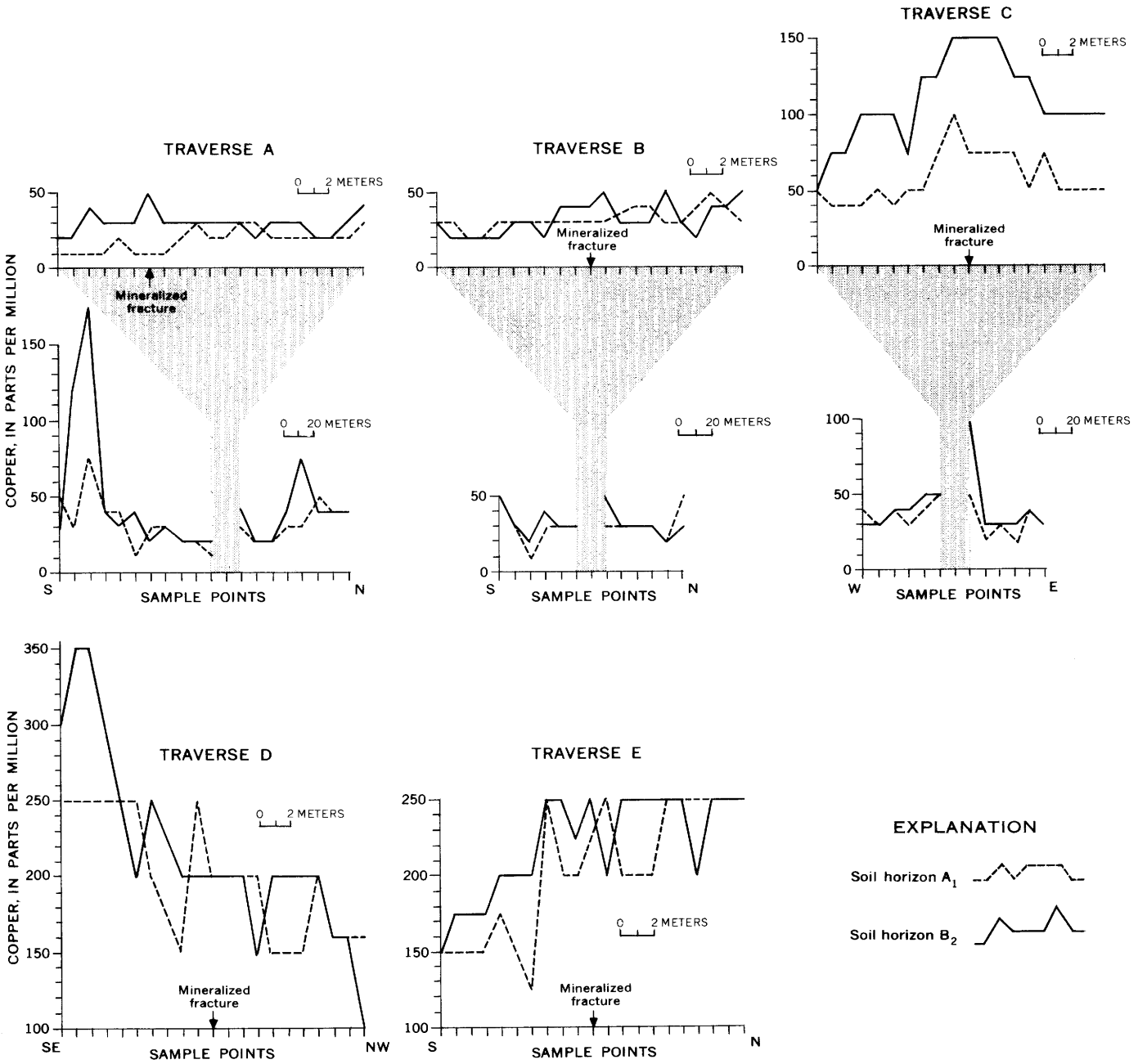

Figure 2.—Concentration of copper in soils over mineralized fractures, Monte Alto, Bahia, Brazil.

The distribution of copper values at Monte Alto is shown in figure 4. Sampling at 10-m intervals along traverses A, B, and C, which involved 46 samples for each soil horizon, shows a unimodal distribution typical of a background population.

The histograms of copper values found in detailed sampling traverses represent 102 sample points and show bimodal distributions typical of background plus anomaly populations. The frequencies of interpolated copper values (such as 125, 175, and 225 ppm) which are not integer multiples of the standards used are low and are probably not representative of true copper distribution.

Because copper determinations were made by visual comparison with prepared standards, the above-mentioned inconsistencies are believed to be caused by the difficulty of interpolating intermediate values under field conditions. Thus, interpolated values are considered to be below the precision obtainable in the field and should not be used for critical evaluation of the data.

In order to predict a safe threshold value for copper concentrations indicative of mineralization, the data were plotted on probability graph paper, with cumulative percentage frequencies against the logarithm of copper values in parts

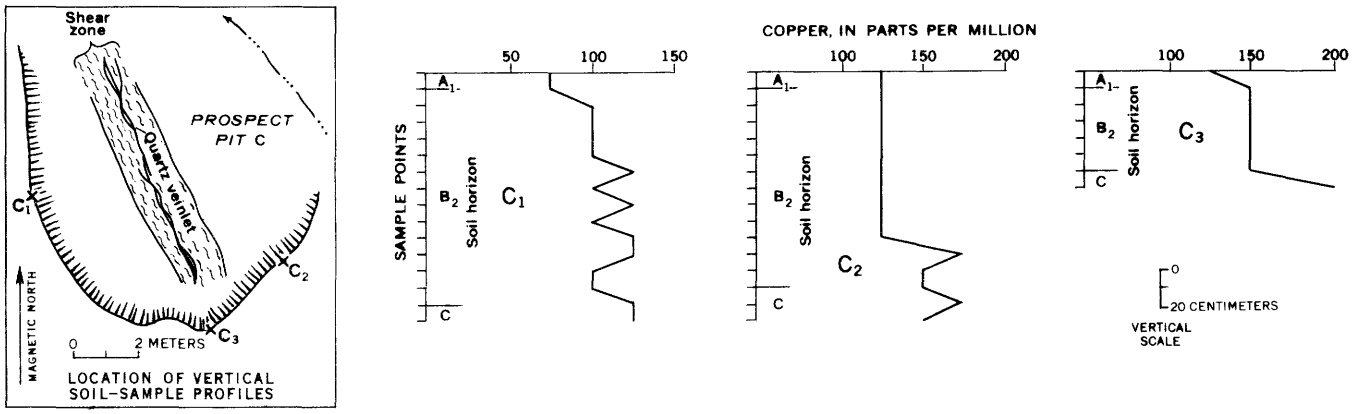

Figure 3.—Concentration of copper in three vertical soil profiles at prospect pit C, Monte Alto, Bahia, Brazil.

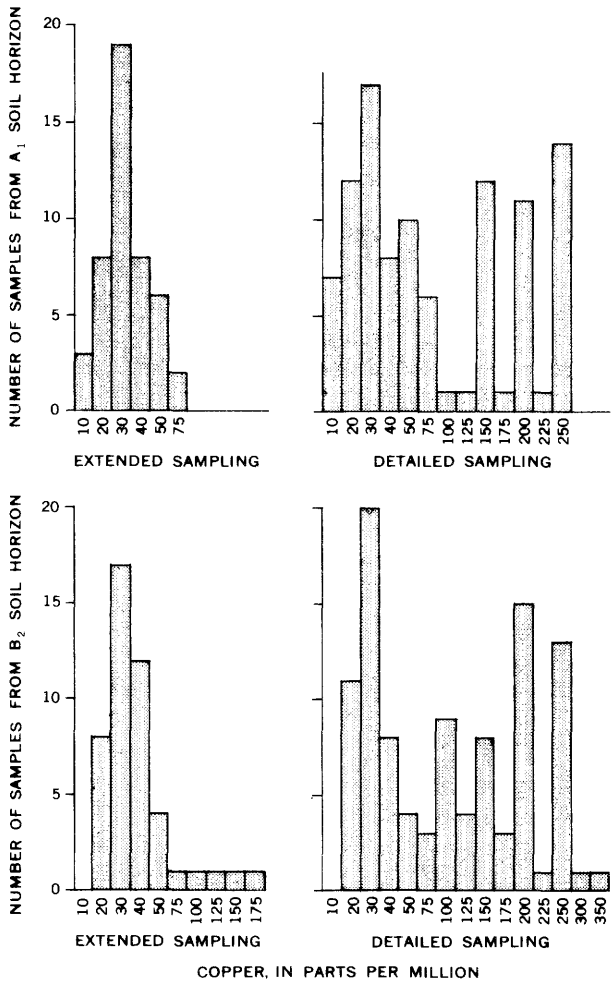

Figure 4.—Distribution of copper in A_1 and B_2 soil horizons along traverses A, B, and C, Monte Alto, Bahia, Brazil.

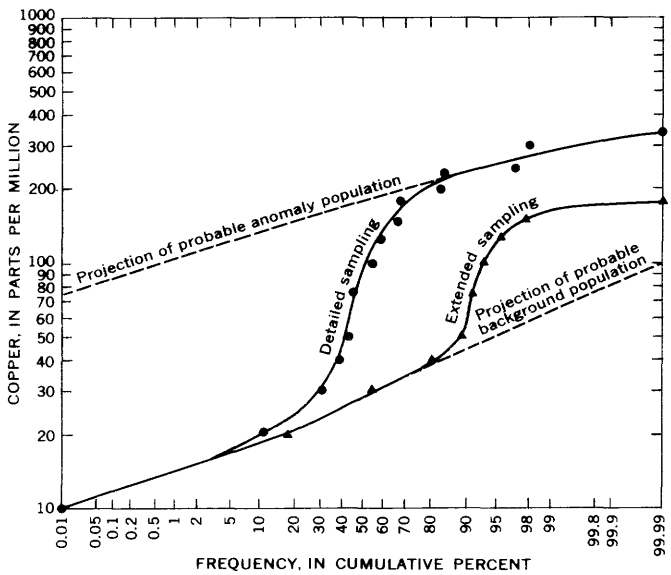

Figure 5.—Cumulative frequency curves for concentrations of copper in the B_2 soil horizon along detailed and extended sampling traverses, Monte Alto, Bahia, Brazil.

per million (fig. 5). Both curves are S-shaped (like most others of this type), suggesting the presence of three families of data, each represented by a near straight-line segment of the curve (Tennant and White, 1959). These three families of data are interpreted as representing background values, anomalous values, and a hybrid set of values from the background, anomalous, and possibly other groups. Thus, a projection of the upper straight-line segment (believed to represent anomalous values) of these curves gives a quick, graphic estimate of the lower limit of anomalous values, and a similar projection of the lower curve segment gives an upper limit of expected values belonging to the background (see fig. 5). Admittedly, this type of solution is overly simplified, but if it is assumed that the data represent a statistically adequate coverage of the range of variables that affect the distribution of copper in the soils of the area, then grouping of copper values into three distinct populations is valid.

The cumulative percentage frequency graph for samples from the A_1 soil horizon did not show well-defined S-shaped curves, which suggests poor definition of anomalous values and

Table 1.—*Statistical parameters of geochemical sampling for copper at Monte Alto, Bahia, Brazil*

Type of sampling	Soil horizon	Number of samples	Copper (parts per million)				
			Arithmetic mean	Geometric mean	Mode	Median	Range
Extended	A_1	46	34	31	30	30	10–75
	B_2	46	43	37	30	30	20–175
Detailed	A_1	101	101	64	30/250	50	10–250
	B_2	102	119	82	30/200	100	20–350

indicates the inadvisability of using this horizon for geochemical prospecting in this region.

The graph for copper values in the B_2 soil horizon did show well-defined S-shaped curves, from which a lower limit of anomalous values and an upper limit of background values can be extrapolated. The lower limit of anomalous values estimated from these curves was 75 ppm of Cu, and the upper limit of background values was 100 ppm (fig 5). We can conclude that although copper values indicative of mineralization may start at 75 ppm, a safe threshold value is 125 ppm. The validity of this extrapolation was checked by taking the geometric mean of a typical background sampling profile (extended sampling along traverse A, less the highest value of 175 ppm) and adding two and three standard deviations for this population to the mean value. This yielded a probable threshold of 83 ppm of Cu and a safe threshold of 108 ppm.

Table 1 shows common statistical values for the sampling at Monte Alto. The extended sampling profiles can be considered equivalent to background value, whereas the detailed profiles include both background and anomalous values of copper.

The botanical survey made along detailed sampling traverses revealed a positive correlation between the presence and abundance of certain plant species and high copper values in the soil (fig. 6). Of the 25 plant species observed, 9 were found only at points having 175 ppm or more of Cu in the B_2 horizon; of these, 3 species—guabiraba (*Eugenia* sp.), velame preto (*Croton mortibensis*), and araçá' (*Psidium araçá'*)—were particularly abundant and may be indicator plants.

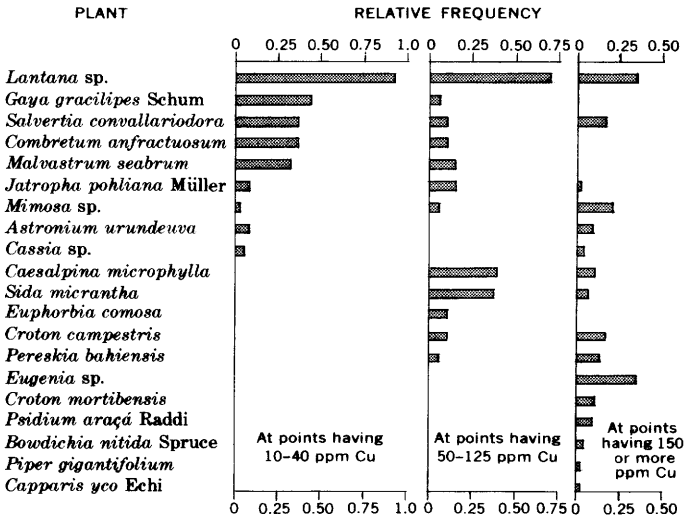

Figure 6.—Relative frequencies of plant species in relation to copper content of B_2 soil horizon along detailed sampling traverses, Monte Alto, Bahia, Brazil.

CONCLUSIONS

The following conclusions can be drawn from this preliminary study:

1. Soil samples for geochemical prospecting for copper in this region should be taken from the B_2 soil horizon and not the A_1 horizon.

2. Analytical results obtained in the field by methods of visual comparison with standards should be reported in integer multiples of the standards, as precision of visual interpolation between whole-number values is too poor.

3. Samples having more than 75 ppm of Cu may be indicative of copper mineralization, but 125 ppm is a safer threshold value.

4. Three plant species—velame preto (*Croton mortibensis*), araçá', (*Psidium araçá'*), and guabiraba (*Eugenia* sp.)—may favor high copper content in the soil and should be investigated as possible indicator plants.

5. From the economic point of view, this area should be investigated in more detail; in particular, the anomalies at prospects D and E warrant more study.

REFERENCES

Braga, Renato, 1953, Plantas do Nordeste, especialmente do Ceará: Ceará Univ., Biblioteca de Divulgação e Cultura, Estudos e Ensaios Pub., no. 2, ser. 1, 523 p.

Luetzelburg, Phillip von, 1923, Estudo botânico do Nordeste: Brazil Inspetoria Federal de Obras Contra Secas Pub., no. 57, ser. 1, pt. A, v. 3, 283 p.

Maack, Reinhard, 1963, Geologia e geografia da bacia hidrográfica do Rio de Contas, no Estado da Bahia: Paraná Univ., Instituto de Geografia Bol. no. 5, 54 p., 3 maps.

Tennant, C. B., and White, M. L., 1959, Distribution of some geochemical data: Econ. Geology, v. 54, no. 7, p. 1281–1290.

Ward, F. N., Lakin, N. W., Canney, F. C., and others, 1963, Analytical methods used in geochemical exploration by the U.S. Geological Survey: U.S. Geol. Survey Bull. 1152, 100 p.

A DEVICE FOR MEASURING DOWN-HOLE PRESSURES AND FOR SAMPLING FLUIDS IN GEOTHERMAL WELLS

By ROBERT O. FOURNIER and ALFRED H. TRUESDELL,
Menlo Park, Calif.

Abstract.—Long flexible stainless-steel tubes can be used to measure down-hole pressures in geothermal wells by balancing gas pressure in the tube against the hydrostatic pressure external to the tube. If water will flow naturally from a well (wells with positive wellhead pressure) water samples may be collected from any desired depth by allowing water to flow up through the steel tube (provided boiling does not occur during ascent).

The pressure at any given depth within a well is equal to the weight of the overlying column of fluid plus the gage pressure measured at the wellhead plus the atmospheric pressure. Where water or brine completely fills a well, the pressure at any given depth can be calculated, provided depth-temperature data is available to allow a correction to be made for changing densities of the liquid. However, in geothermal wells, mixtures of water and steam commonly are present and calculated down-hole pressures, extrapolated from conditions at the wellhead, may be greatly in error.

Long small-diameter flexible stainless-steel tubes have been utilized to measure pressures and collect fluid samples in research holes drilled in hot-spring areas of Yellowstone National Park, Wyo. Thus far, two sizes of tubes have been used: (1) 0.093 inch OD, 0.069 inch ID, 1,200 feet long, and (2) 0.064 inch OD, 0.040 inch ID, 748 feet long.

A schematic diagram of the equipment used for measuring down-hole pressures is shown in figure 1. The flexible tubing, *b*, is wound upon a reel, *a*, from which it is lowered into a well through suitable fittings. The bottom of the tube is fitted with a check valve, *k*, that prevents water or gas in the hole from entering the tube, but allows gas in the tube to escape when the internal pressure exceeds the fluid or gas pressure outside the tube by an amount sufficient to overcome force of the spring holding the valve closed (see figure 2 for detail). Before permanently attaching the fittings to secure the check valve, the tube is fed through a plug, *r*, and packing gland, *s*, as shown in figure 3.

In practice, the tube is placed over a sheave, *t*, the end of the tube and its fittings are inserted into the short length of pipe, *i*, that serves as a pressure chamber above the main gate valve, *h*, and the plug, *r*, and packing gland, *s*, are installed on the top of the pipe. The gate valve, *h*, is then opened, and the tube is lowered to the bottom of the hole. A cylinder of nitrogen gas, *g*, is then attached to the apparatus, and increments of this gas, or other inert gas, are fed into the tube. Each increment of newly added gas causes a pressure surge that is monitored by precision gage, *c*. After each addition of gas, the pressure in the apparatus is allowed to equalize, as determined by a steady reading on gage *c*. When the same steady pressure is attained after successive addition of more gas from cylinder, *g*, the gas pressure in the long tube is balanced by the pressure external to the tube at the depth of check valve, *k*. Simultaneously, the wellhead pressure is measured with another gage, *u*. The valve, *d*, at the top of the tube, mounted on the reel, is then closed, and the connection, *e*, to the gas cylinder, *g*, is removed so that the reel may be turned and the tube slowly withdrawn in stages. As the lower end of the tube is raised, gas leaks through the check valve, *k*, in response to diminished external pressure, and the pressures are measured with the gage, *c*. The bottom end of the tube must remain stationary for a few minutes at each measuring point to allow for a new pressure equalization as indicated by no further change in the gage readings.

The pressure inside the tube must be corrected for the pressure equivalent of the spring load on the check valve to obtain the pressure external to the tube. In our measurement, this required subtracting 0.25 psi from the indicated gage reading. Corrections for the weight of gas in the tubing are trivial, amounting to less than 0.41 psi for a 1,200-foot tube filled with nitrogen gas at 300 psi at 150°C. Our pressure measurements for any one depth in a well were reproducible to ±0.5 psi.

Pressure versus depth data can be plotted as measurements are made, allowing identification and detailed study of anomalies. Pressure and temperature versus depth curves for two holes drilled in Yellowstone Park are shown in figures 4 and 5. The hydrostatic pressure curve for water everywhere just at boiling, with only liquid water filling the well to the ground surface (corrected for changes in water density as

U.S. GEOL. SURVEY PROF. PAPER 750-C, PAGES C146-C150

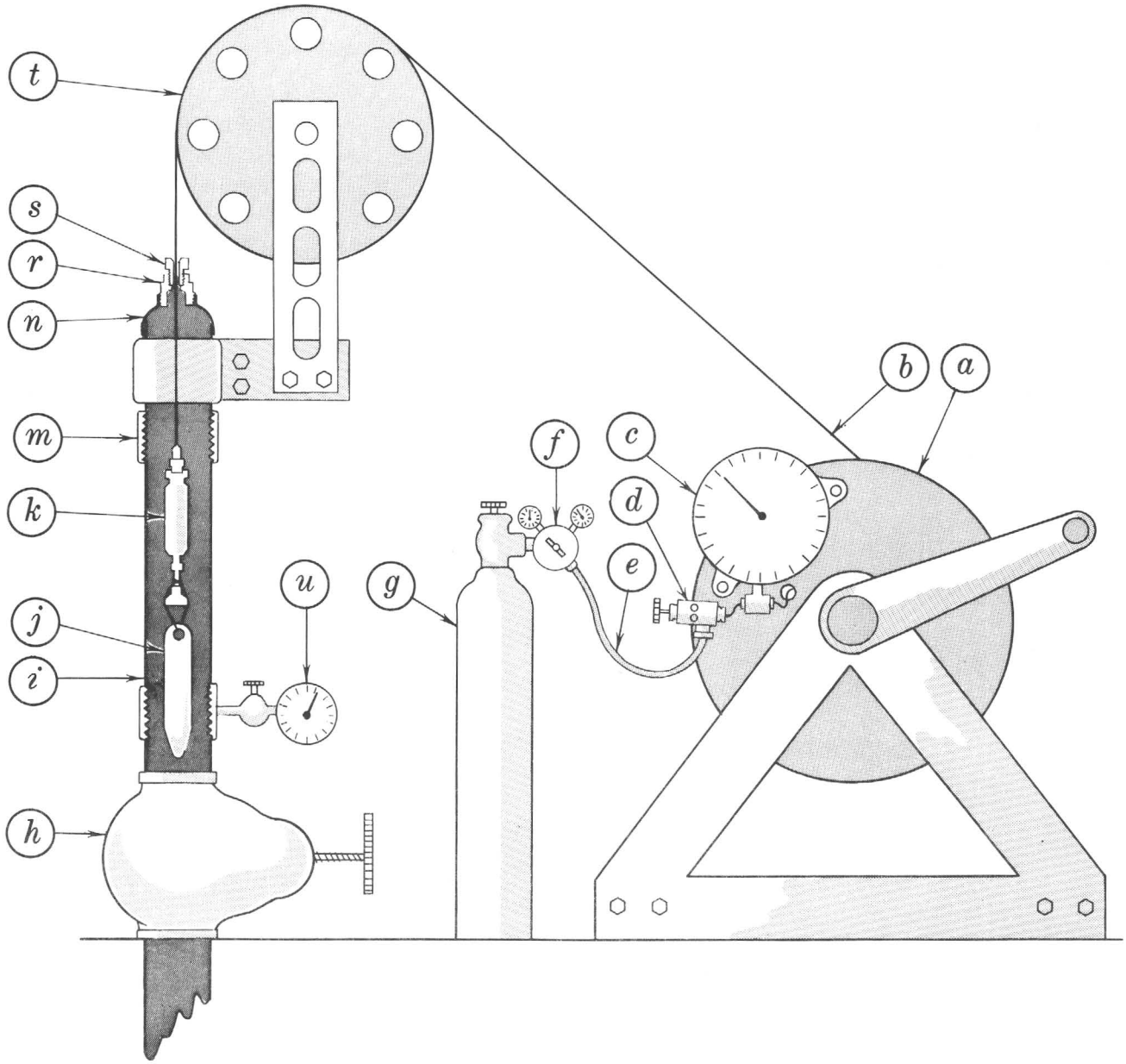

Figure 1.—Equipment for measuring down-hole pressures: *a*, reel with flexible stainless-steel tube, *b*, wound upon it; *c*, precision pressure gage; *d*, high-pressure valve; *e*, flexible high-pressure connecting tubing; *f*, gas-regulating valve; *g*, cylinder of nitrogen gas; *h*, gate valve; *i*, short length of pipe; *j*, 5-pound lead weight; *k*, check valve; *m*, coupling that serves as support ring for sheave; *n*, reducer; *r*, plug; *s*, packing gland; *t*, sheave with automatic counter to tally the number of revolutions; *u*, pressure gage for wellhead pressures.

temperature changes with depth), is shown for reference. This will be referred to here as the "normal" hydrostatic pressure curve for boiling conditions. The well depicted in figure 4 had a wellhead pressure of 102 psig (pounds per square inch, gage) and, at the bottom of the hole, a pressure of 359 psig, which is 94 psi above the "normal" hydrostatic pressure. The slope of the pressure versus depth curve shows that water alone fills the hole below about -275 feet, and water plus a small amount of steam plus gas is present above -275 feet. Water at about 194°C moves up from the bottom of the hole with little temperature change until the pressure becomes low enough for boiling to start at a depth of about -275 feet. From -275 feet to the bottom of the casing at -120 feet, temperatures in the hole follow a boiling-point curve[1] appropriate for the pressures.

[1] This temperature profile was measured a year prior to the pressure profile. At that time the wellhead pressure was only 80 psig. The pressure in the hole has increased with time. In the cased part of the well, conductive heat loss maintained temperatures below boiling.

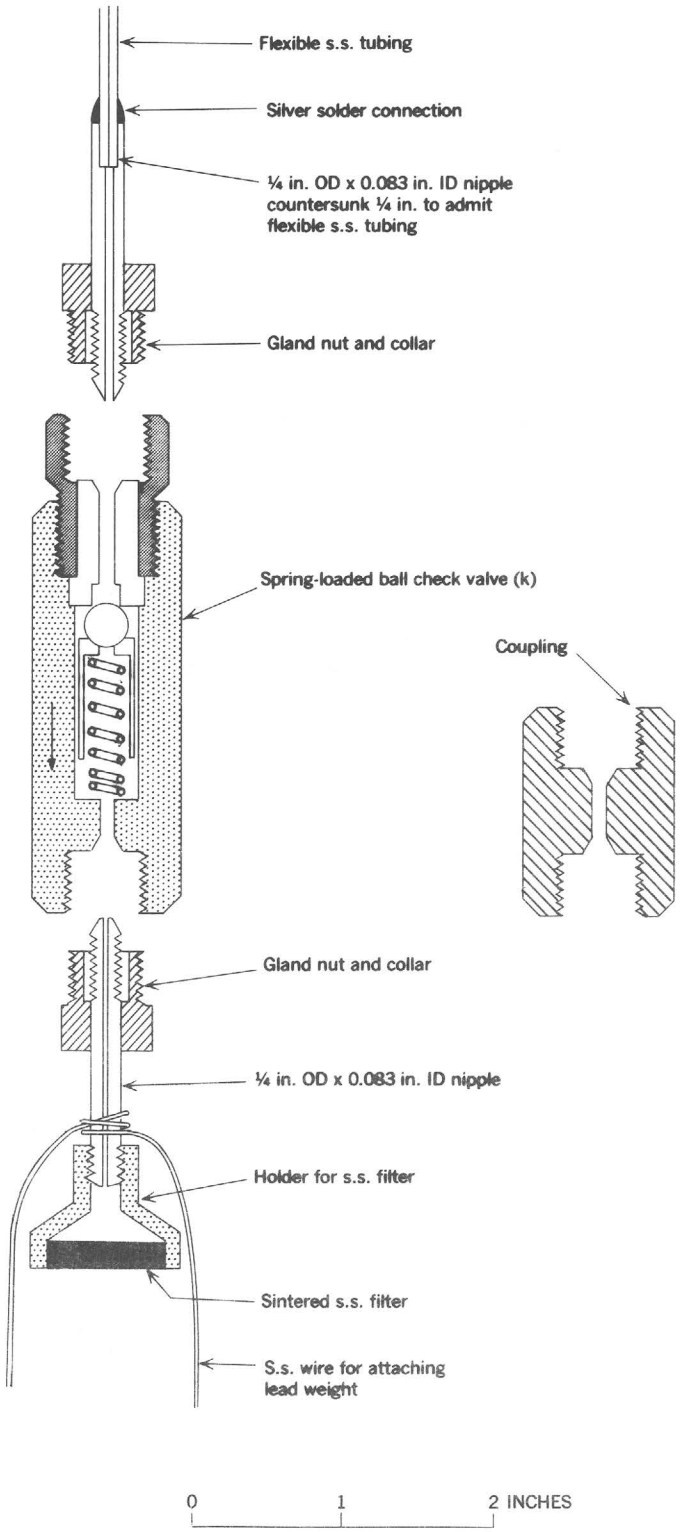

Figure 2.—Detail of check-valve assembly and holder for stainless-steel filter.

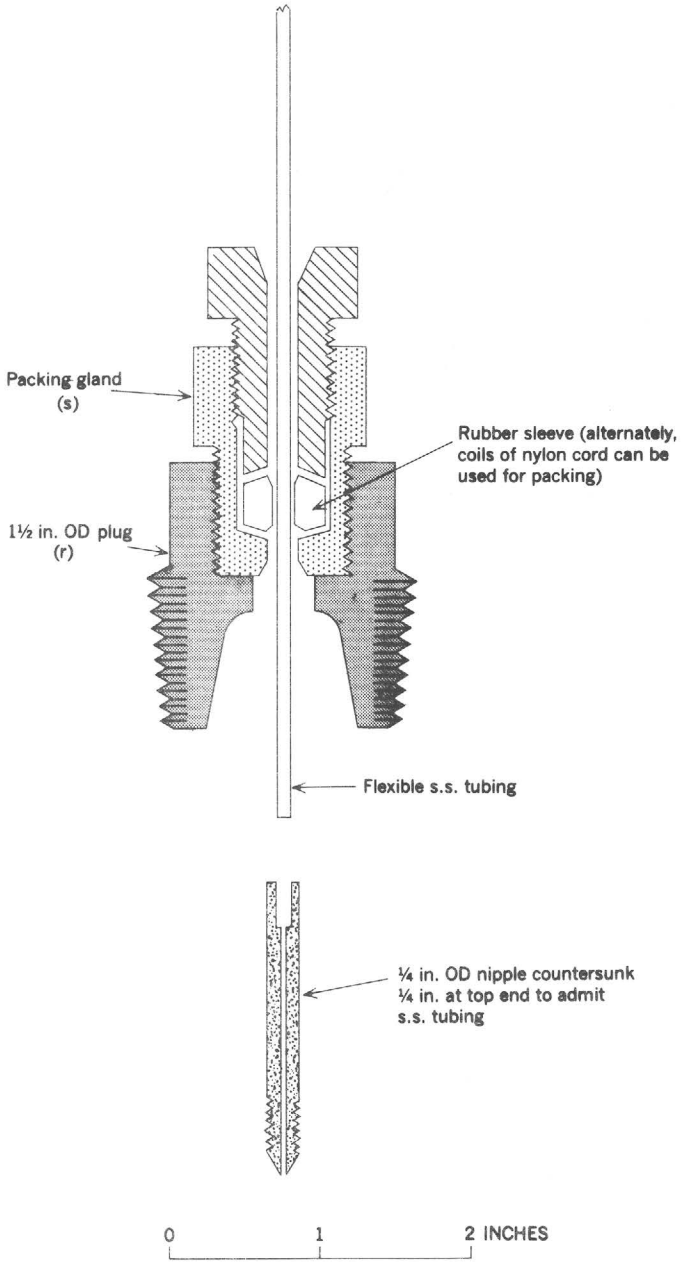

Figure 3.—Detail of plug and packing-gland assembly.

Steam or steam and water together enter well Y9 from a fissure zone extending from about -195 to -210 feet (see figure 5). A steam-water interface exists at -195 feet. From there down, water fills the hole. The bottom-hole pressure is 357 psig, which is 51 psi in excess of the "normal" pressure. The excess pressure at about -200 feet, where the steam enters, also is just 51 psi above the "normal" hydrostatic pressure for boiling conditions.

Where subsurface water pressure is in excess of "normal" hydrostatic pressure, the stainless steel tube can be utilized to obtain fluid samples. The check valve at the bottom of the tube is removed and replaced with a coupling so that water may flow up the tube through a disk of porous, sintered stainless steel that filters the fluid at the point of collection (see figure 2). Before lowering the tube into a well for sampling, the valve (*d*, fig. 1) at the top end of the tube is

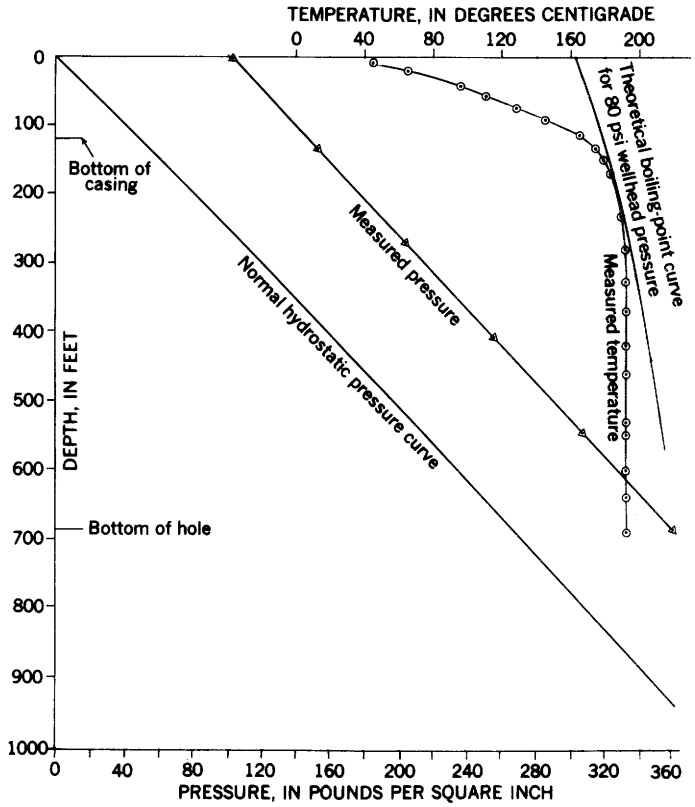

Figure 4.—Pressure and temperature versus depth in the Y4 drill hole, Nez Perce patrol cabin, Lower Geyser Basin, in Yellowstone National Park. Pressure measurements made on September 17, 1969. Temperature measurements taken by D. E. White, June 14, 1968. The theoretical boiling-point curve for a wellhead pressure of 80 psig (pounds per square inch, gage) is shown for reference.

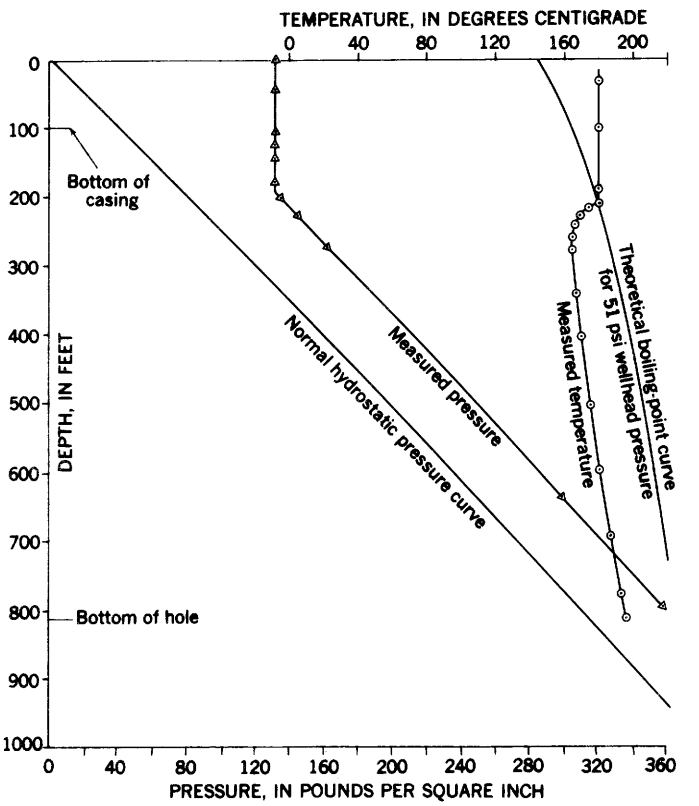

Figure 5.—Pressure and temperature versus depth in the Y9 drill hole at Norris Geyser Basin in Yellowstone National Park. Pressure measurements made on September 13, 1969. Temperature measurements taken by D. E. White, June 10, 1968. The theoretical boiling-point curve for a wellhead pressure of 51 psig (pounds per square inch, gage) is shown for reference.

opened. Water then rises in the tube as the tube is slowly lowered into the well through the packing gland. If the top valve, *d*, is not opened until the tube reaches the desired point of collection, air pressure in the tube may decrease so quickly that water rising in the tube may flash to steam, allowing constituents originally dissolved in the water to precipitate on the inside walls of the tube.

The excess tubing wound around the reel serves as an excellent cooling coil, and the temperature of the emerging water is close to air temperature. Before starting the final collection, a volume of water equivalent to the internal volume of the tubing is first collected and discarded. It has been found convenient to collect a water sample through a 100-ml-capacity gas-collection tube, with stopcocks at each end, attached to the stainless-steel tube by means of thick-walled sulfur-free rubber tubing. The times taken to first fill the tube with water (exit port up) and then displace the water with noncondensed gas (exit port down) may be used to calculate the ratio of water to noncondensed gas, and at the same time a gas sample can be collected for analysis. If possible, the above procedure should be repeated several times in order to purge air from the gas tube. Depending on the magnitude of the excess subsurface pressure, approximately 1 to 4 hours are required to collect 1,000 ml of water through the 0.069-inch ID tube.

The water- and gas-sample collection method is ideally suited for drill holes where temperature and pressure conditions, as shown in figure 4, are such that liquid water fills the hole. However, the method does not work under pressure-temperature conditions such as are illustrated in figure 5. Water in the upper part of this hole is so hot that it will evaporate in the tube, leaving its dissolved residue behind as a precipitate on the tube walls.

Stainless-steel tubes longer than the ones described here may be obtained on special order from several manufacturers. Alternatively, many shorter tubes may be fastened together. In order to allow free movement through the packing gland, the tubes should be fastened in such a manner that the outside diameter will not be increased at the joints. This may be done by inserting a short length of smaller diameter tube inside the

main tube where the joint is to be made and then silver-soldering the connection together. If it is impractical to maintain a constant diameter at the joints, a special stuffing box can be constructed to open or close as necessary to allow for passage of the joints. This might be done by using two separate sets of packing shoes with an intermediate chamber.

In order to avoid endangering nearby trees and vegetation, the research holes drilled in Yellowstone Park have not been tested under production conditions. However, the pressure-measuring procedure described here should be capable of measuring down-hole pressures during production tests of geothermal wells. Such measurements may be of value in determining depths to producing zones. Measurements of pressure gradients allow calculation of average fluid densities and enthalpies of fluids in the two-phase region, provided that the partial pressures of other gases are low.

A DEVICE FOR COLLECTING DOWN-HOLE WATER AND GAS SAMPLES IN GEOTHERMAL WELLS

By ROBERT O. FOURNIER and JOSEPH C. MORGENSTERN,
Menlo Park, Calif.

Abstract.—A sampling device with an internal volume of about 500 ml has been designed to collect liquid and gas samples in wells where both steam and water are present at temperatures up to about 280°C. A long flexible stainless steel tube serves as the support cable. The sample device is lowered in the open position and fluid flows through it during its descent. Closure is accomplished by nitrogen gas pressure applied from the surface through the flexible tube to a piston and plunger within the sample chamber. Continued application of nitrogen gas pressure during withdrawal of the device prevents leakage caused by changing conditions of temperature and pressure. The sampling device has been used successfully to collect water and gas samples from research holes drilled in hot-springs areas of Yellowstone National Park, Wyo.

A variety of sampling devices have been used to obtain down-hole water samples from given depths within wells and drilled holes. Closure mechanisms have included electrically operated valves and spring-loaded valves actuated by preset timing devices or by "messengers" sent down the supporting cable. Most sampling devices that work well at low temperatures are ineffective in geothermal wells where boiling conditions are encountered. A sampling device that is closed and sealed deep in a geothermal well may leak owing to differential contraction of materials as the device is cooled during withdrawal. Leakages occur because pressures within sampling devices generally differ from external pressures as the devices are pulled from geothermal wells. Where the temperature is abnormally high in the upper part of a well, pressure within the sample chamber may become very high relative to the external pressure, with the result that gas and water leak from the sample chamber. In contrast, where deep temperatures are very high and shallow temperatures are low, cooling and contraction of the liquid sample and condensation of steam as the container is raised may cause a partial vacuum to form so that unwanted water from shallow depths is sucked into the sample chamber.

The sample device described here has an internal volume of about 500 ml and is designed to collect liquid and gas samples where both steam and water are present. Closure is accomplished by nitrogen gas pressure applied from the surface to a piston and plunger within the sample chamber. Continued application of this gas pressure during withdrawal of the device prevents leakage caused by changing conditions of temperature and pressure. The piston prevents mixing of the nitrogen "closure gas" with water and gas trapped in the sample chamber.

FABRICATION

A working drawing of the sampling device is shown in figure 1. All materials are stainless steel, except for one Teflon O-ring, two Viton O-rings, and parts *g* and *m* which are Teflon. The circular plate, *r*, can be manufactured from brass, aluminum, or other metal. The main body of the sampling device, parts *a* and *b*, is fabricated from 2-inch OD stainless-steel pipe. The connecting rod, part *d*, is fabricated from ½-inch OD pipe. The holes drilled along the length of *d* permit escape of air and mixing of water inside *d* with water in the main sample chamber. The number and spacing of these holes is not critical. Alternatively, a solid rod may be substituted for the ½-inch pipe, thus increasing strength and eliminating all possibility of insufficient mixing of water within *d* with water in the main sample chamber. However, a solid connecting rod would increase the weight of the device and decrease the size of the fluid sample obtained.

The internal diameter of the threaded section of part *b* above the ⅛-inch groove should be about 0.01 inch greater than the internal diameter of part *b* above the shoulder and below the ⅛-inch groove in order to facilitate the removal of gasket *g* and part *h*. The design for the closure at the bottom of part *a* is identical with that at the top of part *b*, except for the differences indicated in parts *h* and *o*.

The dimensions of the sample device that we fabricated are shown in figure 1. Larger samplers may be constructed to fulfill specific needs. If different dimensions are used, care should be exercised to insure that the connecting rod, *d*, is the proper length to allow the piston (parts *j* and *k*) to close the exit ports when the plunger, *m*, is seated in part *o*. In the closed position the Teflon O-ring rests below the exit port

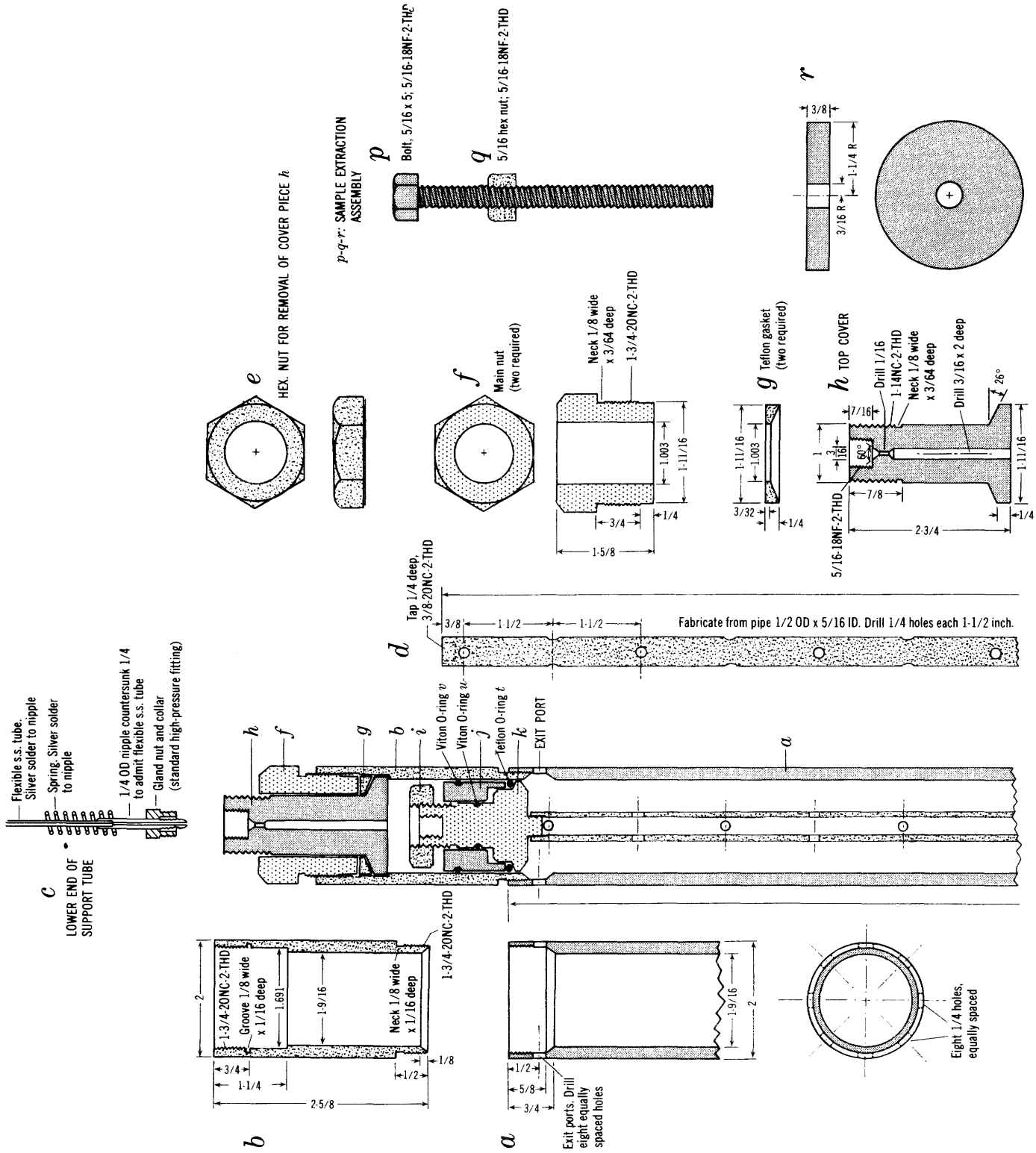
p-q-r: SAMPLE EXTRACTION ASSEMBLY
p Bolt, 5/16 x 5; 5/16-18NF-2-THD
q 5/16 hex nut; 5/16-18NF-2-THD
r
3/8
1-1/4 R
3/16 R
e HEX. NUT FOR REMOVAL OF COVER PIECE h
f Main nut (two required)
Neck 1/8 wide x 3/64 deep
1-3/4-20NC-2-THD
1.003
1-11/16
3/4
1/4
1-5/8
g Teflon gasket (two required)
1-11/16
1.003
3/32
1/4
h TOP COVER
Drill 1/16
1-14NC-2-THD
Neck 1/8 wide x 3/64 deep
Drill 3/16 x 2 deep
26°
7/16
1
3/16
90°
7/8
2-3/4
5/16-18NF-2-THD
d
Tap 1/4 deep, 3/8-20NC-2-THD
3/8
1-1/2
1-1/2
Fabricate from pipe 1/2 OD x 5/16 ID. Drill 1/4 holes each 1-1/2 inch.
c LOWER END OF SUPPORT TUBE
Flexible s.s. tube. Silver solder to nipple
Spring. Silver solder to nipple
1/4 OD nipple countersunk 1/4 to admit flexible s.s. tube
Gland nut and collar (standard high-pressure fitting)
h
f
g
b
i
Viton O-ring v
Viton O-ring u
j
Teflon O-ring t
k
EXIT PORT
a
b
2
1-3/4-20NC-2-THD
Groove 1/8 wide x 1/16 deep
1.691
1-9/16
Neck 1/8 wide x 1/16 deep
1-3/4-20NC-2-THD
3/4
1-1/4
1/2
1/8
2-5/8
a
1-9/16
2
1/2
5/8
3/4
Exit ports. Drill eight equally spaced holes
Eight 1/4 holes, equally spaced

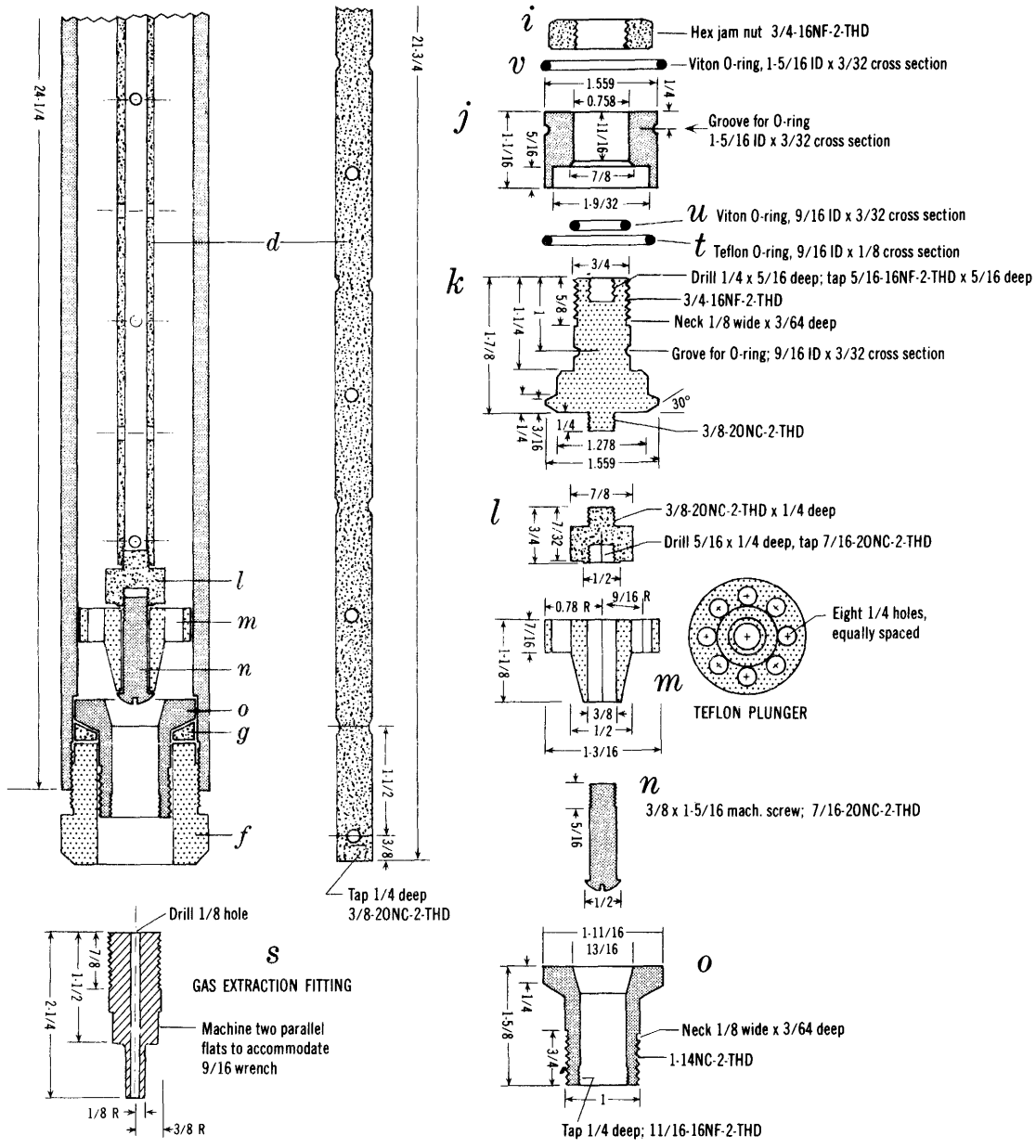

Figure 1.—Working drawing of device for collecting down-hole samples of water and gas in geothermal wells. All dimensions in inches.

groove, and the upper Viton O-ring rests above that groove. The exit port groove is formed by parts *a* and *b* when they are attached together. This groove is necessary to prevent damage to the Teflon O-ring as it moves past the exit ports.

SAMPLING PROCEDURE

The sample device is assembled as follows: The bottom cover, part *o*, Teflon gasket *g* (one of two), and main nut *f* (one of two) are assembled into the bottom of the main body, *a*, and tightened in place with the aid of a pipe wrench and adjustable wrench. The connecting rod, plunger, and part of the piston, parts *d*, *k*, *l*, *m* and *n*, are assembled finger tight. The piston is completed by placing the Teflon O-ring, *t*, $^{9}/_{16}$-inch ID Viton O-ring, *u*, and part *j* on part *k*. Jamnut *i* is then screwed tightly on to *k* so that the Teflon O-ring is slightly deformed. The $1^{5}/_{16}$-inch ID Viton O-ring, *v*, is then placed on part *j* and the piston and plunger assembly is inserted into part *a*. Part *b* is then attached to part *a* and, using the bolt *p*, the piston assembly is drawn up onto *b* until part *k* is clear of the eight ¼-inch exit ports. Bolt *p* is removed, and pieces *h*, *g*, and *f* are assembled into *b* and tightened in place with wrenches. Nut *e* is used only to extract parts *g* and *h* from part *b* after a fluid sample has been collected. The sample device is then attached to a long flexible stainless-steel tube (assembly *c*) that serves as a support cable and is ready to be used. The spring shown in assembly *c* prevents undue bending of the flexible tube at the point of connection with the nipple.

The flexible stainless-steel tube and other supporting equipment are described elsewhere (Fournier and Truesdell, 1971) (p. C146–C150, this chapter). In brief, the flexible steel tube is wound upon a reel, and a valve and pressure gage are attached to the upper end of the tube and also mounted on the reel. The flexible steel tube is placed over a sheave or pully at the top of the geothermal bore or well, and the attached sampling apparatus is placed in a pressure chamber mounted above the main valve of the well. The flexible tubing passes through a packing gland at the top of the pressure chamber. The main valve is opened and the apparatus is lowered to the desired depth, as indicated by a counter on the sheave.

As the sampler is lowered, water flows into it through the large opening at the bottom (part *o*), up through the eight holes in the Teflon plunger, part *m*, and out the eight exit ports just below the piston, *k*. As the sampler is lowered, the valve at the surface end of the flexible steel tube should be at the open position so that heated air in the small chamber of *b* will not reach pressures large enough to close the sampler prematurely. However, premature closure is very unlikely in wells filled with water because hydrostatic pressure holds the piston in an open position.

When it is desired to close and seal the sample apparatus, a cylinder of nitrogen gas[1] is connected to the upper end of the flexible steel tube. A nitrogen gas pressure of 10–20 atmospheres in excess of the calculated hydrostatic pressure for the sample depth is then applied to the top of the piston through the flexible steel tube. This forces the piston down and seats the Teflon plunger, *m*, in part *o*, sealing the bottom of the sample chamber. Simultaneously, the Teflon O-ring held between parts *j* and *k* is moved to a position below the exit ports and effectively seals the upper end of the sample chamber. An important aspect of the design of the piston assembly is that part *j* is free to move and exert continued pressure upon the Teflon O-ring after parts *m* and *k* have come to rest. Thus, a very tight seal is formed at the upper end of the chamber after the lower seal is formed and after the Teflon O-ring slides past the exit-port groove. Before detaching the gas cylinder, the valve at the top end of the flexible tube is closed so that nitrogen gas pressure is maintained in the chamber of part *b* while the sampler is removed from the well. Thus, tight seals are maintained in spite of changing conditions of temperature and pressure.

Upon removal from a hot well, the sampler is cooled, and any residual steam is condensed by suspending the sampler in a specially fabricated deep cylindrical container of water. The sample apparatus is then dried, the nitrogen gas pressure is released by opening the valve at the upper end of the flexible steel tube, and the tube, assembly *c*, is disconnected. The release of externally applied gas pressure does not open the device because equal internal pressure is exerted down on part *m* and up on part *k*. To extract the fluid sample from the container, the top cover piece, *h*, must first be removed. Using a pipe wrench and adjustable wrench, the top main nut, *f*, is unscrewed about five or six revolutions. Then nut *e* is attached to part *h* and tightened against the main nut, *f*. This pulls part *h* and gasket *g* out of the sealed position in *b* so that further unscrewing of the main nut, *f*, removes the entire closure assembly. Nut *q* and plate *r* are then placed high up on bolt *p* and the end of bolt *p* is screwed into the top of part *k* (still within part *b*). The bottom end of the sample apparatus is placed over a bottle or beaker and, while holding bolt *p* steady with one wrench, nut *q* is turned with a second wrench so that it moves down bolt *p* and against plate *r*. This pulls the piston assembly and plunger *m* upward and opens the bottom of the container so that the liquid sample may run out.

To collect a gas sample or to exclude air from the system, fitting *s* is first attached to part *o* before pulling open the device. Teflon tape is used on the threads of fitting *s* to secure a gas-tight seal. A hose, a 3-way valve, and an appropriate container are attached to fitting *s*, and these are evacuated or filled with an inert gas before opening the sampling apparatus. Note that the bottom seal of the sample device, at *m*–*o*, opens before the top seal so that there is no contamination of air leaking into the container at the top exit ports. If both liquid and gas are present in the sample chamber after cooling, a portion of the gas may be sampled by turning the apparatus upside down before opening the chamber. The gas may then be extracted into a syringe or other evacuated chamber or

[1] We used nitrogen gas because it is inert, relatively inexpensive, and easy to obtain. Other gases could be used in place of nitrogen to close the sampler.

allowed to mix with a given amount of inert "carrier" gas. The bottom of the sampler is then lowered and the liquid portion allowed to drain from the chamber.

We have found that the Teflon plunger, *m*, works well in repeated usage, even after undergoing considerable permanent deformation. However, spare Teflon parts should be kept available and used frequently. New O-rings should be installed after each run where subsurface temperatures in excess of 200°C are encountered.

APPLICATION

The sampling device has been used successfully to collect down-hole water and gas samples from research holes drilled by the U.S. Geological Survey in hot-spring areas of Yellowstone National Park (White and others, 1968). The deepest and hottest sample was collected at a depth of 1,088 feet and temperature of 240°C in the Y12 drill hole at Norris Geyser Basin. Other samples were obtained from cooler holes, but under more adverse conditions. In one hole, Y9 at Norris Geyser Basin, a sample of liquid water was collected from beneath a region of superheated steam that filled the top of the hole. When the sampling apparatus was removed from the hole, the temperature of the water sample filling the container was 180°C. In spite of an internal pressure of about 10 atm within the sample apparatus and only 1 atm pressure external to it, no leakage occurred. In another well, Y7 at Biscuit Basin, dirty water was encountered and a few sand-sized grains became caught between the Teflon plunger, *m*, and part *o* when gas pressure was applied to close the container. The Teflon flowed around the sand grains and made a perfect seal in spite of the impurities.

The sample device can be used at temperatures up to about 280°C. Above this temperature the Teflon becomes very soft, and it melts at about 300°. Substitution of other materials for the Teflon may extend the temperature range of application. For instance, copper or other easily deformable metal may be used for gaskets *g* and plunger *m*. Substitution of other materials for the O-rings presents a more difficult problem, but new plastics and silicon rubbers just appearing on the commercial market may be usable at temperatures about 280°C.

REFERENCES

Fournier, R. O., and Truesdell, A. H., 1971, A device for measuring down-hole pressures and sampling fluids from geothermal wells, *in* Geological Survey Research 1971: U.S. Geol. Survey Prof. Paper 750-C, p. C146–C150.

White, D. E., Muffler, L. J. P., Truesdell, A. H., and Fournier, R. O., 1968, Preliminary results of research drilling in Yellowstone thermal areas [abs.]: Am. Geophys. Union, Trans., v. 49, p. 358.

MICROEARTHQUAKES NEAR LASSEN PEAK, CALIFORNIA

By JOHN D. UNGER and JOHN M. COAKLEY,
Menlo Park, Calif.

Abstract.—A network of eight portable seismographs set up around Lassen Peak, Calif., for about 2 weeks during the summer of 1969 recorded about 25 earthquakes well enough to permit calculation of hypocenters. The only clustering of epicenters was near Brokeoff Mountain. There were no concentrations of epicenters near either Lassen Peak or Chaos Crags.

Lassen Peak, 80 km east of Redding, Calif., is the only volcano in the Cascade chain to have a well-documented historic eruption. Pyroclastic eruptions occurred intermittently from 1914 to 1917, and in 1915 lava appeared in the summit crater and spilled over the west and northeast rims (Williams, 1928). In conjunction with the program to monitor microearthquakes at Mount Rainier, Wash., during the summers of 1968 and 1969 (Unger and Decker, 1970), and in the interest of the U.S. Geological Survey's concern in the seismicity and potential geologic hazards of the Cascade volcanoes (Crandell and Mullineaux, 1967, 1969), the U.S. Geological Survey set up a network of portable seismographs around Lassen Peak during the summer of 1969 to monitor the seismic activity of this volcanically active region.

From August 13 to August 26, 1969, eight portable seismographs were in operation around Lassen Peak volcano (fig. 1). These vertical-component seismographs (Eaton, 1967; Unger and Decker, 1970) are battery-powered, high-gain units with a 6-decibel-per-octave increase in magnification with increasing frequency in the bandpass from 0.5 to 17 hertz and a magnification at 17 hertz of about 5×10^6 using the attenuation level normally set in the field. The amplified seismic signal is frequency modulated and recorded on magnetic tape.

During the 13-day recording interval, 29 events were recorded at three or more seismographs, an average of 2.2 events per day. This average is close to the 1.2 events per day recorded by a single high-gain portable smoked-paper seismograph operated during an 89-hour interval at Manzanita Lake (Decker and Harlow, 1970).

Hypocenters of the events recorded on the Lassen Peak network were calculated by using P and S arrivals and a crustal velocity model of horizontal layers over a half space (Eaton, 1966) as input to a computer program (Eaton, 1969). Figure 1 shows the epicenters of those events near Lassen Peak. Clustering is not observed around the two regions that have shown the most recent volcanic activity, Lassen Peak and Chaos Crags (Crandell and Mullineaux, 1969). The only concentration of epicenters occurs around the region roughly defined by the now volcanically inactive Brokeoff Mountain region. Brokeoff Mountain is the western rim of a caldera formed by the collapse of ancient Mount Tehama, a large stratovolcano that collapsed about the time Lassen Peak was

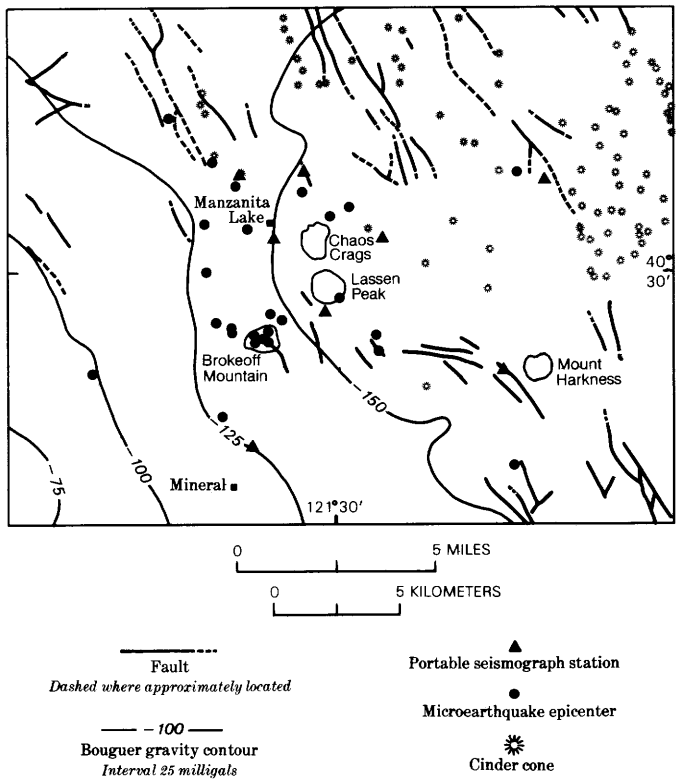

Figure 1.—Portable seismograph stations and microearthquake epicenters on a simplified geologic map (after Lydon and others, 1960) of faults and cinder cones, Lassen Peak area, California; 25-milligal Bouguer gravity contours after Pakiser (1964).

U.S. GEOL. SURVEY PROF. PAPER 750-C, PAGES C156-C157

formed. The floors and walls of the now eroded caldera contain many normal faults, along which are many hot springs and other hydrothermal features (Williams, 1932). Five of the nine microearthquakes in this cluster occurred in a small swarm on August 20. The remaining epicenters are in a poorly defined north-northwest-trending zone passing through Lassen Peak. Most of the epicenters described lie in a zone of steep gravity gradients (Pakiser, 1964). Although it is possible that the zone of sharp lithologic contrasts and structural change indicated by the steep gradient may influence the location of the microearthquakes, the exact nature of this influence is not clear. This zone also contains normal faults and some areas of hot springs and steam vents. A group of epicenters not shown in figure 1 and about 35 km south of Lassen Peak may be blasts, as these events all occurred during normal working hours, all have compressional first motions, and some are accompanied by what appears to be an air blast when observed on the nearby portable seismograph records.

The magnitudes of the microearthquakes shown in figure 1 range from -0.9 to 1.9 (Richter scale). The distribution is similar to the range of magnitudes of the microearthquakes around Mount Rainier, -1.0 to 1.2 (Unger and Decker, 1970).

One must be cautious in extrapolating the above results because the recording interval was extremely brief. Since the early 1930's, there have been various semipermanent seismographs at Manzanita Lake, Mount Harkness, and Mineral recording for rather long periods of time. Records from these seismographs show periods of several months when the seismicity of the Lassen Peak region increased markedly (see, for example, Robinson and Byerly, 1948). This seismicity is in the form of local earthquake swarms during which the frequency of occurrence of local events is two to three orders of magnitude greater than those normally observed. The instruments that recorded the swarms have sensitivities at least a factor of 10 less than the sensitivities of portable seismographs described. These swarmlike, high-seismicity periods typically seem to occur every 10 to 20 years (Swartzlow, 1937; Robinson and Byerly, 1948). With this picture of local seismicity in mind, it appears that the portable instruments were recording in the Lassen region during one of the normal intervals. The seismic activity reported here may not have any spatial relation to the swarm-type activity. We plan to reoccupy the Lassen Peak network when a new episode of earthquake swarms occurs.

REFERENCES

Crandell, D. R., and Mullineaux, D. R., 1967, Volcanic hazards at Mount Rainier, Washington: U.S. Geol. Survey Bull. 1238, 26 p.

——1969, Preliminary appraisal of potential geologic hazards near Manzanita Lake, Lassen Volcano National Park, California: U.S. Geol. Survey open-file report, 18 p.

Decker, R. W., and Harlow, David, 1970, Microearthquakes at Cascade Volcanoes: Am. Geophys. Union Trans., v. 51, p. 351.

Eaton, J. P., 1966, Crustal structure in northern and central California from seismic evidence in geology of northern California, *in* Bailey, E. H., ed., Geology of Northern California: California Div. Mines and Geology Bull. 190, p. 419–426.

——1967, Instrumental seismic studies, *in* Brown, R. D., Jr., and others, The Parkfield-Cholame, California earthquakes of June-August 1966—Surface geologic effects, water-resources aspects, and preliminary seismic data: U.S. Geol. Survey Prof. Paper 579, p. 57–65.

——1969, HYPOLAYR, a computer program for determining hypocenters of local earthquakes in an earth consisting of uniform flat layers over half-space: U.S. Geol. Survey open-file report, 155 p.

Lydon, P. A., Gay, T. E., Jr., and Jennings, C. W., 1960, Geologic map of California, Westwood sheet, Olaf P. Jenkins edition: California Div. Mines, scale 1:250,000.

Pakiser, L. C., 1964, Gravity, volcanism, and crustal structure in the southern Cascade Range, California: Geol. Soc. America Bull., v. 75, no. 7, p. 611–620.

Robinson, H. B., and Byerly, Perry, 1948, Earthquake swarm in Lassen Volcano National Park: Seismol. Soc. America Bull., v. 38, no. 3, p. 179–193.

Swartzlow, C. R., 1937, Recent seismic disturbances in Lassen Volcanic National Park: Seismol. Soc. America Bull., v. 27, no. 1, p. 35–39.

Unger, J. D., and Decker, R. W., 1970, The microearthquake activity of Mount Rainier, Washington: Seismol. Soc. America Bull., v. 60, no. 6, p. 2023–2036.

Williams, Howel, 1928, A recent volcanic eruption near Lassen Peak, California: California Univ. Dept. Geology Bull., v. 17, no. 7, p. 241–263.

——1932, Geology of the Lassen Volcanic National Park, California: California Univ. Pubs. Geol. Sci. Bull., v. 21, no. 8, p. 195–385.

HAWAIIAN SEISMIC EVENTS DURING 1969

By ROBERT Y. KOYANAGI and ELLIOT T. ENDO,
Hawaiian Volcano Observatory, Hawaii,
Menlo Park, Calif.

Abstract.—During 1969 the Hawaiian Volcano Observatory seismic net recorded 673 earthquakes of magnitudes 2.0 to 5.0 beneath Hawaii. Of this total, 119 were reported felt; 5 throughout the entire island of Hawaii. The overall pattern of seismicity remained the same as for recent years; the highest concentrations of earthquakes were in the volcanically active areas of southeastern Hawaii.

During 1969, the Hawaiian Volcano Observatory seismic net recorded 673 earthquakes of magnitude 2.0 to 5.0 (Richter scale) beneath Hawaii. Of these, 119 were felt; 5 throughout the entire island. Seismic activity during 1969, as in recent years, was concentrated beneath the southeastern part of the Hawaiian Ridge. This summary of seismic phenomena is the eighth compiled jointly by the U.S. Geological Survey's Hawaiian Volcano Observatory and National Center for Earthquake Research, Menlo Park, Calif. Earlier reports were by Koyanagi (1964, 1968, 1969a, b, c), Koyanagi and Endo (1965), and Koyanagi and Okamura (1966).

Earthquake hypocenters were calculated on the U.S. Geological Survey IBM 360/65 computer by means of the program HYPOLAYR (Eaton, 1969). Determinations of hypocenters were based on crustal model B of Eaton (1962), a layered model, and primarily on P-wave arrival times. S-wave arrival times were used to fix the origin times of some events that originated outside the seismic net. Arrival times were read to the nearest 0.05 second on the Develocorder film system (telemetered network) and to the nearest 0.1 second on the standard paper recorders. Of the 4,000 local events picked for study during 1969, 2,432 had epicenters with standard errors of less than 2.5 km in the latitude and longitude. The standard error in depth depends strongly on the number of stations available for the solution and on their location with respect to the epicenter. The error in depth is commonly comparable to that in epicenter position, but it can be much larger for unfavorably located epicenters. Earthquakes that occur at moderate distances outside the network have larger standard errors and have not been included in the plot of hypocenter and epicenter. Magnitudes were calculated from records from several types of short-period seismographs, which have been related empirically to the standard Wood-Anderson seismograph at Hilo.

The distribution of well-located earthquakes larger than, or equal to, magnitude 2.0 in the vicinity of the island of Hawaii, southeasternmost in the Hawaiian archipelago (fig. 1), is shown for each quarter of the year (fig. 2). Events that occurred outside the map boundaries are listed in table 1.

The zone of concentrated seismic activity around the summit of Kilauea volcano is shown in detail in figures 3, 4,

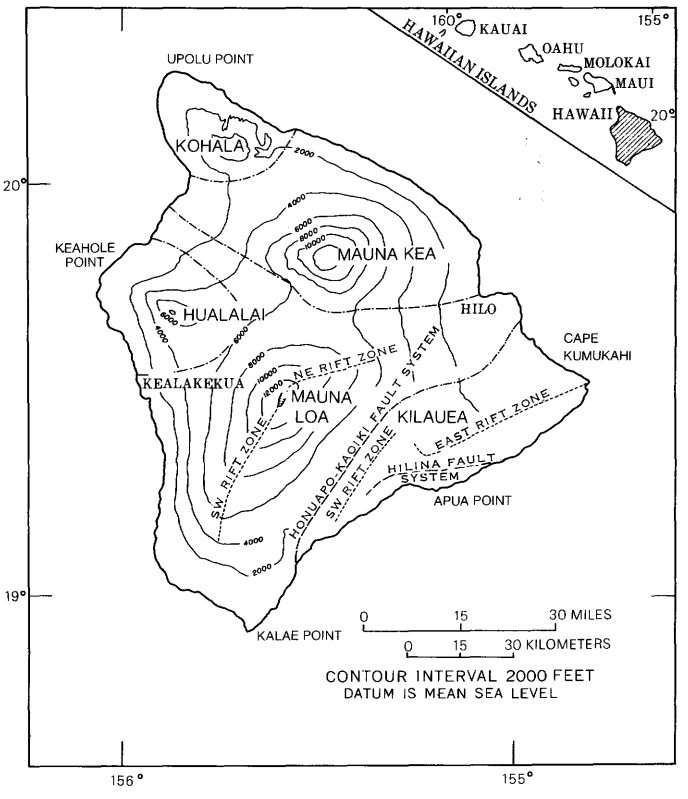

Figure 1.—Map of the island of Hawaii, showing the five volcanoes and their principal structural features. Dot-and-dash lines are boundaries of volcanic systems.

U.S. GEOL. SURVEY PROF. PAPER 750-C, PAGES C158-C164

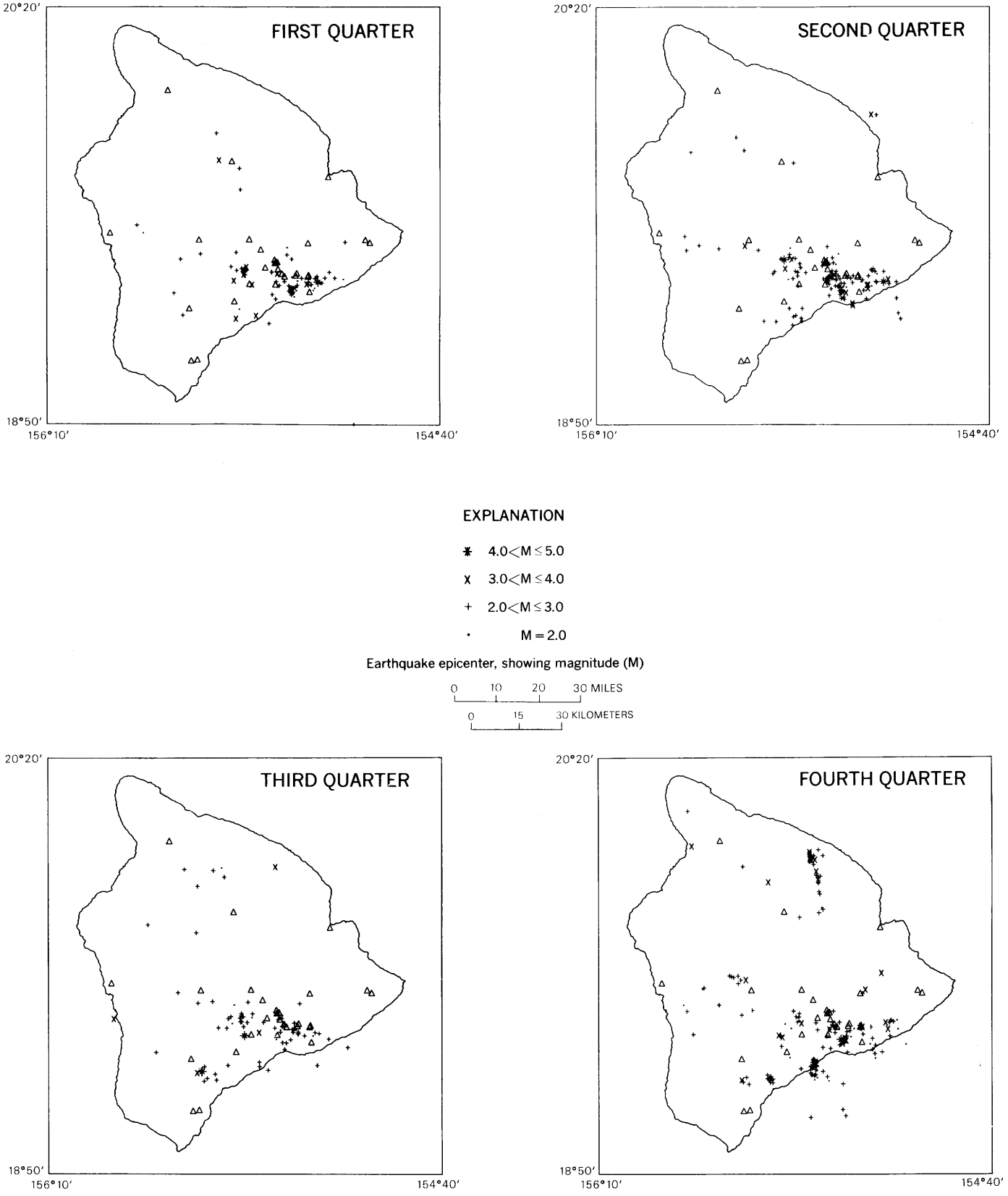

Figure 2.—Epicenters of earthquakes beneath or near the island of Hawaii during 1969. Earthquakes with magnitudes smaller than 2.0 or with standard errors of 2.5 km or greater in latitude or longitude are not included. Seismometer locations are indicated by open triangles.

Table 1.—*Earthquakes of magnitude 2.0 or larger located off the quarterly epicenter maps*

Date (1969)	Time[1]	Magnitude	Depth (kilometers)	Epicenter coordinates	
				North latitude	West longitude
January	1 . . . . . 02–47–27.8	4.2	13	20°06′	157°52′
	28 . . . . . 10–44–19.1	2.0	13	20°52′	155°05′
February	3 . . . . . 01–15–47.3	2.9	13	19°37′	156°28′
	4 . . . . . 21–15–23.1	2.5	13	18°35′	156°01′
	10 . . . . . 10–55–08.0	2.5	31	20°10′	156°22′
	22 . . . . . 12–24–23.5	3.5	13	19°30′	156°20′
March	6 . . . . . 04–54–26.4	2.4	13	20°44′	156°06′
	13 . . . . . 00–21–32.7	2.8	13	19°19′	156°22′
	24 . . . . . 20–51–14.0	2.8	3	19°39′	156°22′
April	9 . . . . . 07–30–56.1	4.2	13	20°59′	155°43′
May	7 . . . . . 04–35–59.0	4.5	13	20°50′	155°21′
	7 . . . . . 04–48–33.5	2.2	13	20°50′	155°21′
	19 . . . . . 02–20–03.0	2.9	10	20°43.1′	155°33.1′
	22 . . . . . 05–25–08.5	2.6	59	20°23.7′	156°17.3′
	24 . . . . . 05–49–33.9	3.0	10	19°19.0′	156°34.7′
	28 . . . . . 20–20–12.9	2.9	10	20°06.3′	156°49.9′
	31 . . . . . 21–12–19.7	2.2	56	19°04.4′	154°41.1′
June	10 . . . . . 23–20–58.3	3.1	[2]67?	18°49.8′	155°41.6′
	21 . . . . . 03–48–24.0	3.3	8	20°26′	156°50′
	26 . . . . . 15–24–58.4	3.1	10	20°29.9′	155°27.1′
	30 . . . . . 08–57–51.1	3.2	8	20°36′	154°54′
July	15 . . . . . 17–54–14.5	3.3	13	18°28′	156°48′
August	14 . . . . . 12–27–20.0	2.5	10	19°05.0′	156°43.4′
	30 . . . . . 14–27–11.3	2.9	10	19°38.3′	156°28.3′
September	2 . . . . . 05–06–22.0	3.3	10	19°34.9	156°23.3′
	19 . . . . . 08–24–34.6	3.0	[2]83?	19°42.0′	156°11.3′
October	3 . . . . . 19–25–56.2	2.8	22	18°49.0′	155°23.1′
	12 . . . . . 15–28–11.0	2.4	10	20°49.3	156°04.6′
November	5 . . . . . 16–51–07.0	2.8	34	19°32.9′	156°18.8′
	16 . . . . . 07–06–37.2	2.2	10	20°17.0′	156°14.8′
	17 . . . . . 23–05–17.0	2.9	10	19°36.8′	156°31.6′
	24 . . . . . 09–44–09.1	2.7	45	19°43.4′	156°10.9′
	30 . . . . . 21–11–14.0	3.9	10	20 3/4°	162°
December	9 . . . . . 17–09–43.0	2.6	10	19°01.3′	154°43.3′
	17 . . . . . 19–42–25.3	3.1	13	19°03′	156°48′
	24 . . . . . 19–34–12.0	2.9	13	20°45′	154°54′

[1] Hawaiian standard time in hours, minutes, and seconds.
[2] Depth determinations for earthquakes deeper than 60 km are questionable.

and 5. Seismograph stations and the principal structural features of the region are illustrated in figure 3; all well-located earthquakes for the entire year are plotted on the same scale in figure 4; and all events in a 16-km-wide swath of concentrated activity trending south-southwestward through the Kilauea caldera are projected onto a cross section (A–A', fig 3) in figure 5.

CHRONOLOGY OF SEISMIC ACTIVITY DURING 1969

The year 1969 showed an increase in the level of seismic activity as compared with 1968, and was characterized by frequent discontinuous volcanic eruptions from the upper east rift zone of Kilauea. Swarms of small earthquakes associated with eruptions normally were confined to the outbreak area and to the area just south of the caldera that subsided during the eruptions. Such swarms generally were only a few kilometers deep. Between eruptive episodes, earthquakes were scattered over large areas adjacent to the eruptive centers and tended to occur at depths of about 10 km. Earthquakes associated with eruptions did not appear to exhibit the normal range in magnitude.

The flank eruption of February 22–28, 1969, and the flank eruption that started on May 24, 1969, and continued to the end of the year were characterized by sharp deflation of the summit, many shallow earthquakes, and continuous tremor. During both eruptions, phases of vigorous lava outpouring and strong tremor alternated with periods of degassing and weak tremor. The relation between the various types of seismic

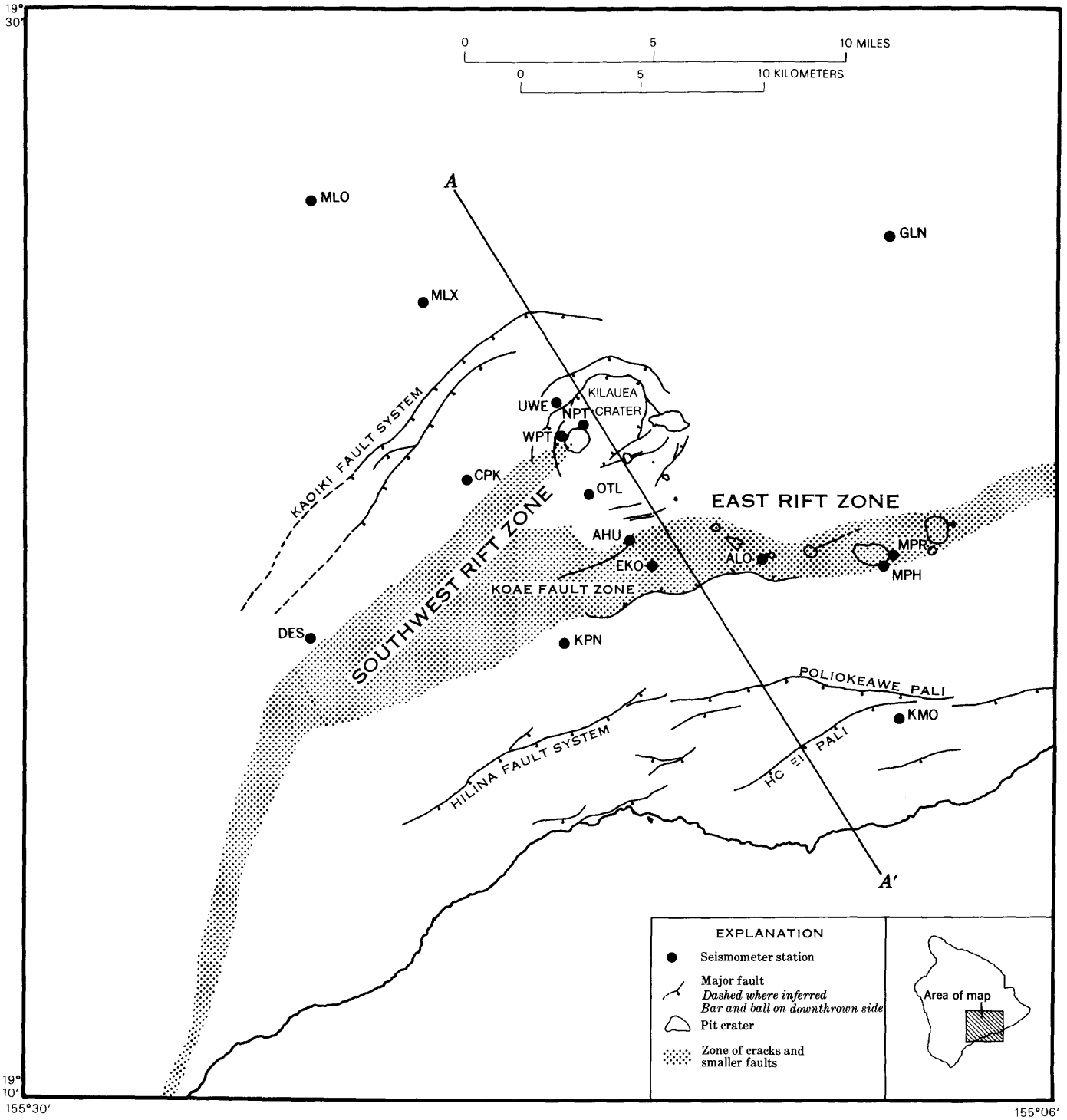

Figure 3.—Map of Kilauea summit region, showing geologic structures, seismometer locations, and cross section line A–A'. Geologic structures are after Stearns and Macdonald (1945), Peterson (1967), and Walker (1969).

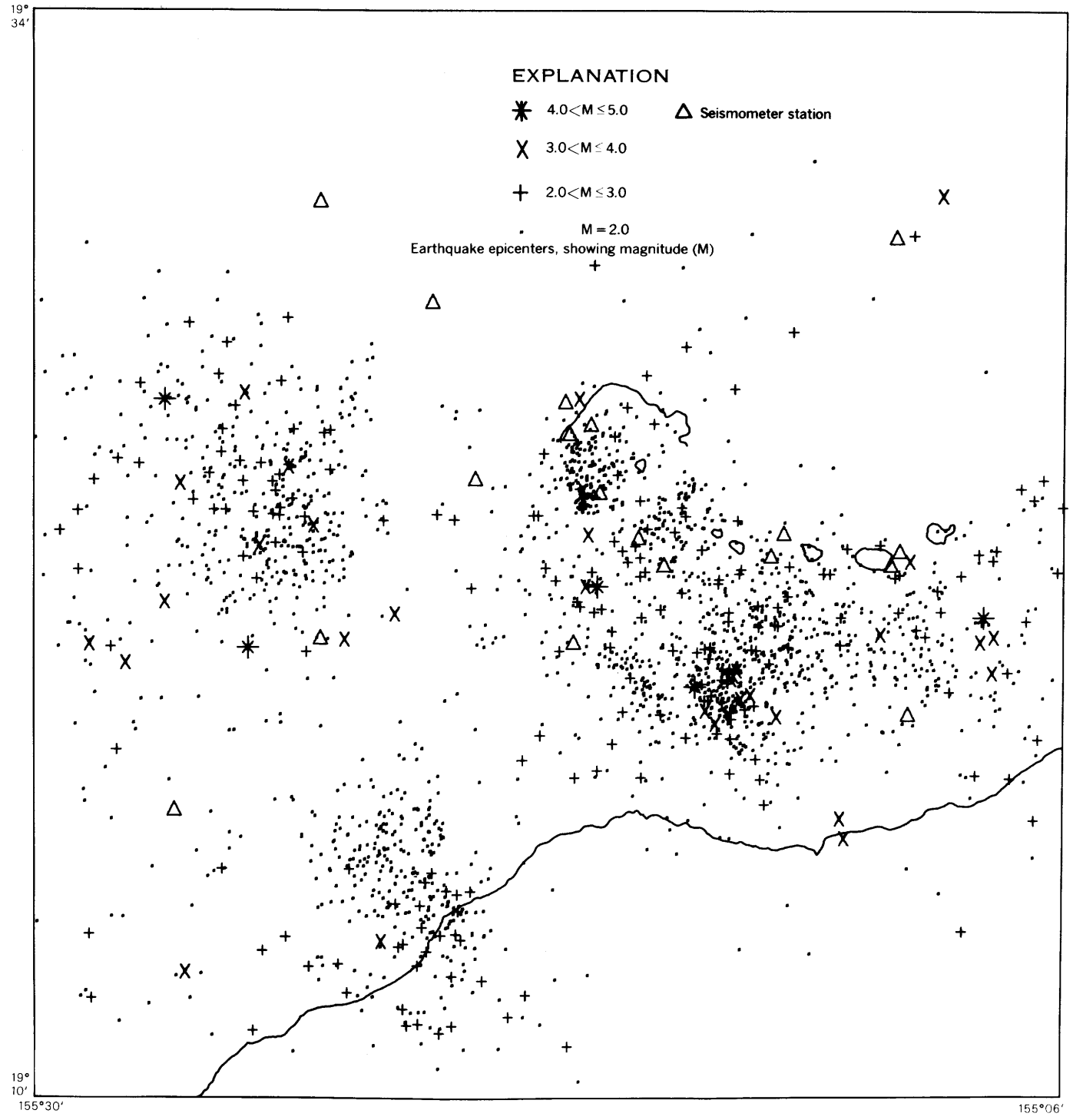

Figure 4.—Epicenters of earthquakes beneath the central part of Kilauea volcano and the adjacent southeast flank of Mauna Loa. All well-located epicenters with standard errors less than 2.5 km in latitude and longitude are included.

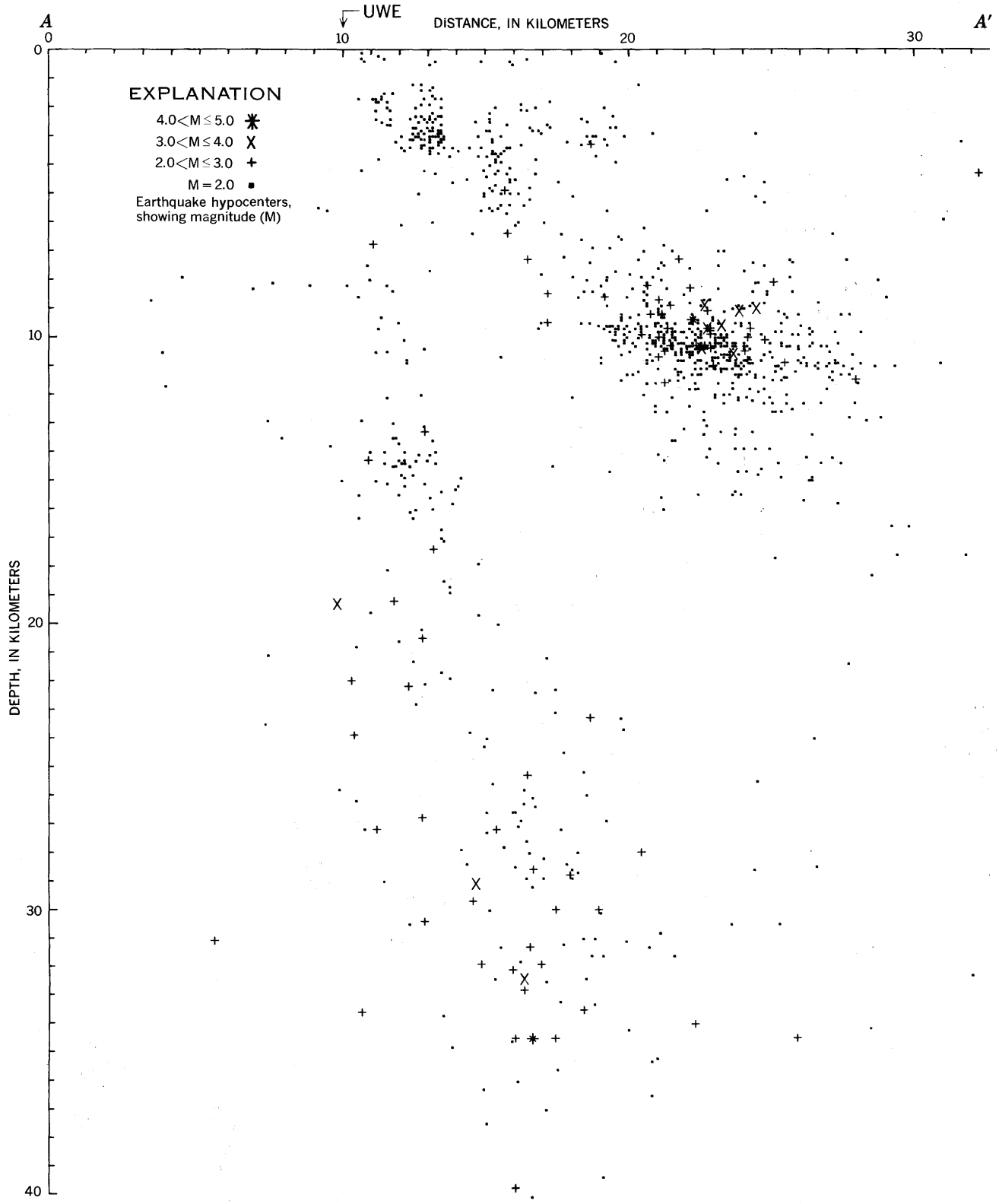

Figure 5.—Cross section along line A–A' produced by projecting all events within 8 km of the vertical plane through A–A' onto that plane. The sources of some of the families of earthquakes mentioned in the Hawaiian Volcano Observatory Quarterly Summaries can be identified on this cross section. Shallow caldera earthquakes are concentrated at depths of less than 5 km between 10 and 15 km along the profile, upper east rift, Koae, and Poliokeawe earthquakes are concentrated at depths near 10 km between 17 and 30 km along the profile, and 30-km south-summit earthquakes are distributed through the depth range 20 to 40 km between 10 and 23 km along the profile.

activity recorded and the style of the corresponding eruptive activity can be summarized as follows:

Initial phase of eruption	*Between phases of eruption*	*Secondary phases of eruption*
Summit deflation, shallow rift quakes, shallow caldera quakes. Lava fountains and strong tremor.	Summit inflation, weak tremor, "long-period" caldera quakes. Continued summit inflation, weak tremor near eruptive fissure, shallow caldera quakes.	Summit deflation, occasional shallow rift quakes, lava fountains, moderate tremor.

During the first half of the year, Kilauea earthquake activity was relatively high. Shallow caldera quakes averaged nearly 100 per day, and earthquakes beneath the southeast and southwest flanks of the volcano occurred at a rate of several tens per day. About two dozen of these were large enough to be felt. The largest earthquake of the year in Hawaii had a magnitude of 5.0 and was felt over the entire island. It originated about 20 km southeast of Kilauea caldera at 15:33[1] on May 9.

During the second half of the year, the frequency of Kilauea earthquakes remained at a moderate level. In addition to the flurries of small summit and southeast flank quakes that appeared to be associated with the activity of the erupting volcano, there were moderate concentrations of seismic activity in several other areas.

Late in September, activity picked up along the lower part of Kilauea's zone, about 20 km southwest of the summit. Between September 28 and October 16, 868 quakes were recorded; 310 occurred during the peak of activity on October 7–8. By November, seismicity about the southwest rift had declined considerably, and the center of activity shifted to the Mauna Kea region.

On the morning of November 5, residents along the northeast coast of the island reported that 14 earthquakes were felt. These earthquakes were the largest of a group that originated beneath the eastern flank of Mauna Kea at depths of 5 to 20 km. During the most intense period of activity, November 5–7, 30 earthquakes of magnitude 2.0 to 3.7 were recorded on the observatory seismographs. A smaller burst followed on November 10–11, and relative quiescence resumed thereafter. Only occasional shocks from this region were recorded during the rest of the year.

The number of deep quakes beneath the southeast flank of Mauna Loa increased during the second half of the year. These quakes originated at depths of 20–50 km and were characterized by relatively long periods (0.5 to 1.0 second) of their predominant waves.

SUMMARY

The seismic activity during 1969, as in recent years, was concentrated beneath the southeastern part of the Hawaiian Ridge. Seventy-three percent of the quakes with magnitudes 2.0 to 5.0 were centered beneath active Kilauea and Mauna Loa volcanoes. Secondary centers were found beneath the flanks of Mauna Kea and off the west coast of the island of Hawaii. Focal depths were generally shallow, 0 to 10 km; the deep quakes were mostly from depths of 20 to 40 km beneath the south-summit area of Kilauea.

In 1969, 119 earthquakes were felt by residents of the island of Hawaii, 5 of the larger ones with magnitudes 3.7 to 5.0 islandwide. In the following table, the 673 events of magnitude 2.0 to 5.0 determined for the year are grouped to show their distribution according to magnitude and depth:

Magnitude	Depth (km)							
	<10	10–19	20–29	30–39	40–49	50–59	60–69	70–128
2.0–2.4	195	119	19	34	4	1	...	2?
2.5–2.9	103	59	11	14	6	3	1?	1?
3.0–3.4	25	23	1	2	2	...	2?	1?
3.5–3.9	12	12	1	5	1			
4.0–4.4	3	5	...	2				
4.5–4.9	1	1	...	1				
5.0	...	1						

NOTE.—Depth determinations for earthquakes deeper than 60 km are questionable.

REFERENCES

Eaton, J. P., 1962, Crustal structure and volcanism in Hawaii, *in* The crust of the Pacific Basin: Am. Geophys. Union Mon. 6, p. 13–29.

——1969, HYPOLAYR, a computer program for determining hypocenters of local earthquakes in an earth consisting of uniform flat layers over a half space: U.S. Geol. Survey open-file report, 106 p.

Koyanagi, R. Y., 1964, Hawaiian seismic events during 1962, *in* Geological Survey Research 1964: U.S. Geol. Survey Prof. Paper 475–D, p. D112–D117.

——1968, Hawaiian seismic events during 1965, *in* Geological Survey Research 1968: U.S. Geol. Survey Prof. Paper 600–B, p. B95–B98.

——1969a, Hawaiian seismic events during 1966, *in* Geological Survey Research 1969: U.S. Geol. Survey Prof. Paper 650–B, p. B113–B116.

——1969b, Hawaiian seismic events during 1967, *in* Geological Survey Research 1969: U.S. Geol. Survey Prof. Paper 650–C, p. C79–C82.

——1969c, Hawaiian seismic events during 1968, *in* Geological Survey Research 1969: U.S. Geol. Survey Prof. Paper 650–D, p. D168–D171.

Koyanagi, R. Y., and Endo, E. T., 1965, Hawaiian seismic events during 1963, *in* Geological Survey Research 1965: U.S. Geol. Survey Prof. Paper 525–B, p. B13–B16.

Koyanagi, R. Y., and Okamura, A. T., 1966, Hawaiian seismic events during 1964, *in* Geological Survey Research 1966: U.S. Geol. Survey Prof. Paper 550–C, p. C129–C132.

Peterson, D. W., 1967, Geologic map of the Kilauea Crater quadrangle, Hawaii: U.S. Geol. Survey Geol. Quad. Map GQ–667, scale 1:24,000.

Stearns, H. T., and Macdonald, G. A., 1945, Geologic and topographic map of the island of Hawaii, county of Hawaii: U.S. Geological Survey.

Walker, G. W., 1969, Geologic map of the Kau Desert quadrangle, Hawaii: U.S. Geol. Survey Geol. Quad. Map GQ–827, scale 1:24,000.

[1] All times are noted in Hawaiian standard time.

MAGNETIC AND RESISTIVITY STUDIES OF GOLD DEPOSITS IN THE TETON NATIONAL FOREST, TETON COUNTY, WYOMING

By LENNART A. ANDERSON, Denver, Colo.

Abstract.—Magnetic and resistivity surveys were made in Teton National Forest, Teton County, Wyo., in known placer areas as determined by geochemical surveys for gold. In the surveyed areas adjoining Buffalo Fork and smaller tributaries of the Snake River, the magnetic method successfully delineated zones of magnetic mineral concentrations. Resistivity soundings were useful in determining thickness of gravel sections. Magnetic susceptibility measurements on soil samples proved useful in discriminating between magnetic anomalies that result from concentrations of magnetic minerals at the surface and anomalies that result from concentrations at depth.

The magnetic and resistivity surveys which were made at four locations in the Teton National Forest, Teton County, Wyo. (fig. 1), were prompted by the following factors: successful use of these methods in locating gold in other areas (see, for example, Joesting, 1941, and Jakosky and Wilson, 1933), increased sensitivity of present-day magnetometers, modern techniques of interpreting resistivity data, and renewed interest in the gold potential of this area stimulated by the work of Antweiler and Love (1967).

The geophysical work was undertaken to outline the distribution of magnetic minerals within gravel beds and to determine the thickness of these beds by the resistivity method where the magnetic data indicated magnetic mineral concentrations (magnetite). No attempt was made to outline the total magnetite distribution along any one stream or gravel deposit, but each area was sufficiently sampled to show that magnetite zones can be delineated. In areas where magnetic anomalies were obtained, soil samples were collected and analyzed for gold content and magnetic susceptibility. The magnetic susceptibility data were particularly useful in determining whether a magnetic anomaly was caused by magnetic material at the surface or at depth. The locations were selected on the basis of anomalously high gold values determined by geochemical exploration methods (Antweiler and Love, 1967).

METHODS AND INSTRUMENTATION

The magnetic surveys were made with a proton-precession magnetometer that measures the absolute value of the total magnetic field of the earth. The reading accuracy of the instrument was within ±10 gammas. A 50-foot spacing was generally used in magnetic profiling, but smaller spacings were used in areas of large magnetic gradients. All magnetic data were corrected for diurnal variations and instrument drift.

The resistivity surveys were made using the Schlumberger electrode configuration in which the electrode spacing (AB/2) was recorded in meters. In most soundings a spacing (AB/2) of 170 meters (≈ 500 ft) would have been adequate to resolve the thickness of the gravel deposits, but to determine something of the nature of the bedrock, the spacings were extended to a minimum of 250 m (≈ 800 ft) in all the soundings.

The electrical sounding curves were interpreted using an album of three-layer Schlumberger theoretical curves (Orellana and Mooney, 1966) in conjunction with the auxiliary point diagrams (Kalenov, 1957; Keller and Frischknecht, 1966; Orellana and Mooney, 1966; and Zohdy, 1965). The geoelectric section at each sounding station, obtained on the basis of the interpretation of each sounding curve, was then modeled by means of a large-scale computer to approximate the curve described by the field data as a means of verifying the original interpretation. In the final interpretation, the geoelectric section at each sounding site was correlated with lithologic units on the basis of known geology, valley configuration, and the general resistivity ranges and thicknesses of the rock types in the area of interest.

GEOLOGIC SETTING

Except for near-surface variations, the stratigraphic section is virtually the same in each of the four survey locations (fig. 1).

1. The Turpin Meadow location (*A*) is covered with recent alluvial deposits that rest on the Harebell Formation of Late Cretaceous age. The Harebell is a thick succession of sandstone, conglomerate, claystone, and shale that was deposited in a fresh-water environment and, as suggested by Love (1956b), it is more than 4,000 feet thick in the vicinity of Buffalo Fork.

2. The Buffalo Fork-Blackrock Creek location (*B*) is similar in geologic environment to Turpin Meadow.

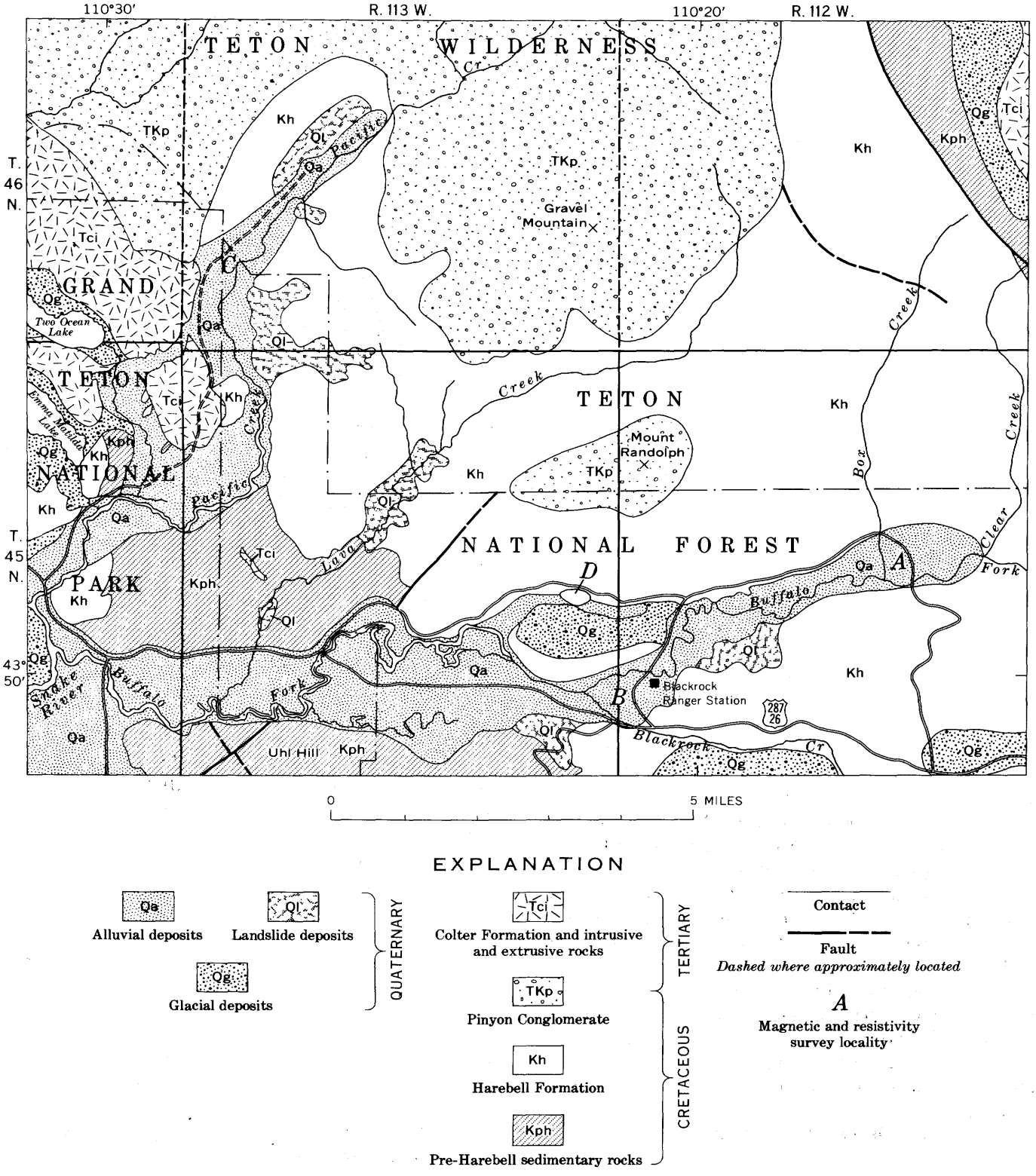

Figure 1.—Map showing location and generalized geology of areas of magnetic and resistivity surveys in Teton National Forest, Wyo. Survey localities: *A*, Turpin Meadow; *B*, Buffalo Fork-Blackrock Creek; *C*, Pacific Creek; *D*, Tracy Lake. Geology generalized from Love (1956a).

3. At the Pacific Creek location (*C*), the creek flows through an alluvial valley where the bedrock is again the Harebell Formation.

4. The Tracy Lake location (*D*), a dry lakebed, is composed of recent alluvial deposits that rest on Quaternary glacial sand and gravel overlying the Harebell Formation.

GEOPHYSICAL SURVEYS

As Joesting (1941) pointed out, many problems are involved in recognizing magnetic anomalies that result from magnetite in placer deposits. Placer anomalies are generally small, and many are obscured or distorted by variables such as bedrock anomalies, irregular bedrock surfaces, and nonuniform distributions of magnetic minerals within the stream gravels. Bedrock anomalies in the areas surveyed, however, are not considered to be a problem: as shown by a large number of magnetic readings that were made over exposures of the Harebell Formation—the local source of placer gold (Antweiler and Love, 1967) and magnetite (J. C. Antweiler, oral commun., 1968)—magnetite within the bedrock is not sufficiently concentrated to produce anomalies of significant size.

The other vaiables, of course, do impose a limit on the diagnostic qualities of the magnetic data presented here for the four survey locations, and, therefore, the data were used primarily as an indicator of magnetic mineral concentrations within the unconsolidated stream deposits.

AREAS INVESTIGATED

Turpin Meadow

At the Turpin Meadow location (fig. 2), four magnetic profiles were initially obtained: two (T and M) across the meadow in a southeast direction and two (A and B) oriented north-south across the stream deposits north of the present-day Buffalo Fork channel. The data obtained from this preliminary effort indicated that the magnetic mineral concentrations are located mainly within the more recent sand and gravel deposits of Buffalo Fork. Therefore, 17 additional magnetic profiles were obtained at irregular intervals, about 300-400 feet apart, in a north-south pattern on both banks of the river. The magnetic data obtained were contoured on a 20-gamma interval (fig. 2). The contour representing a total field intensity of 57,000 gammas is labeled 1,000, and deviations from this value are scaled accordingly.

The contoured total magnetic field data (fig. 2) effectively delineate the zones of magnetic mineral concentrations. Twenty-seven soil samples were collected from areas of high and low magnetic intensity along the traverses north of the river. The magnetic susceptibility determinations made on these samples indicate that the magnetic contours that are alined with the riverbank represent recent deposits of magnetite. At distances greater than 150 feet from the riverbank, the sample magnetic susceptibilities cannot be correlated with the observed magnetic field intensity, indicating that the fluctuations in the field measurements are caused by magnetic sources at depth.

Two vertical electrical soundings (VES-1 and VES-2), located as shown in figure 2, were made in the Turpin Meadow area. The sounding curves, interpreted geoelectric sections, and probable corresponding lithologies are shown in figure 3.

Interpretation of the VES-1 sounding indicates that the stream deposits can be divided into three distinct geoelectric layers that are progressively less resistive with depth, suggestive of variations in water content and differences in the amount of clay and other fine-grained materials within the stream gravels. The depth to the bedrock surface (layer 4) is 83 m (270 ft). Layer 4 is only assumed to be the Harebell Formation, however, in that there are no water wells in the surveyed area sufficiently deep to assist in the interpretation of the resistivity data.

A sufficient number of data points were obtained for sounding VES-1 to indicate a change in the resistivity at a depth of 230 m (750 ft). If the Harebell Formation is 4,000 feet thick along the Buffalo Fork, as suggested by Love (1956b), then the resistivity change must represent a variation in the lithology within the formation.

At the site of VES-2, on Turpin Meadow proper, the nature of the upper layer is shown to be substantially different from that observed at the VES-1 site. The ground surface at VES-2 is smooth and suggestive of an ancient lakebed. The surface layer is identified as silt and is interpreted from the sounding data to be 7.5 m (25 ft) thick. The top of the bedrock (Harebell Formation) is at a depth of 53 m (175 ft) and is covered by a sand, clay, and gravel section about 45 m (150 ft) thick that is similar in resistivity to the sand, clay, and gravel section detected at the VES-1 site.

The combined data obtained in the Turpin Meadow area indicate that the bulk of the magnetic minerals lie within the old stream gravel near the existing stream channel. Soil sampling was particularly useful as a means for discriminating between anomalies due to recent magnetite deposition and more meaningful anomalies due to magnetite concentrations at depth. The VES-1 sounding curve indicates that bedrock is 83 m (270 ft) beneath the surface in the vicinity of the main stream channel. If this depth figure is valid, then possibly heavy-mineral concentrations in this area are well beyond the reach of any known dredge.

Buffalo Fork-Blackrock Creek

Six magnetic profiles were obtained across the alluvium-covered area bounded by Buffalo Fork and Blackrock Creek (fig. 1, loc. *B*). The contoured data (fig. 4) indicate that the zone of greatest heavy-mineral concentration is centered between the stream channels, but, unlike Turpin Meadow, there is no evidence of recent magnetite deposition along the banks of Buffalo Fork in this area.

Gold values of 34 soil samples are plotted along the various traverses in figure 4. These data demonstrate a random gold

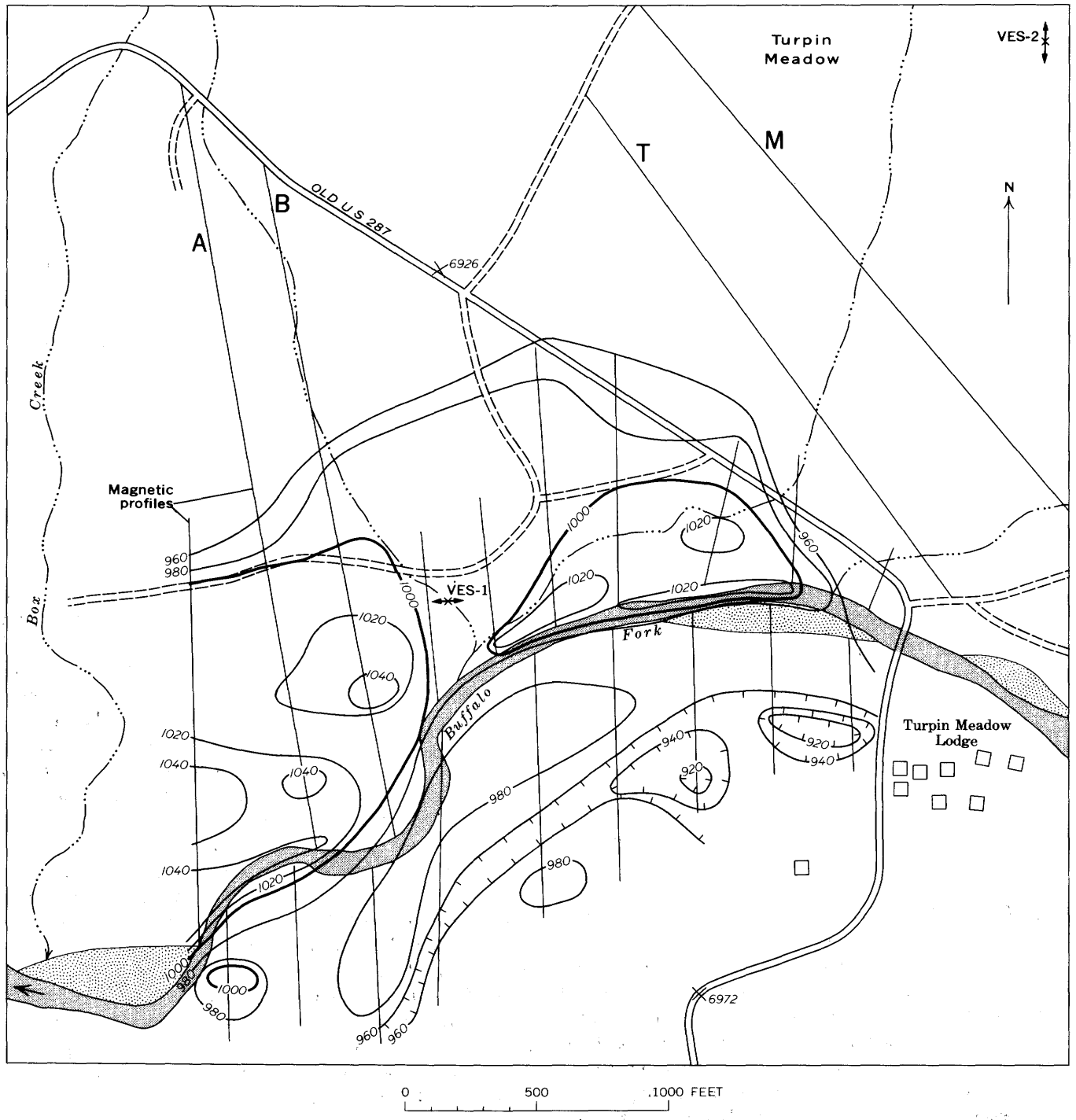

Figure 2.–Map of the Turpin Meadow survey site (fig. 1, loc. *A*), showing magnetic traverses and contoured total magnetic field data (interval 20 gammas). Level of reference, 56,000 gammas. VES, resistivity sounding location.

distribution incidental to the heavy-mineral distribution near bedrock. The magnetic susceptibilities of the soil samples (not shown on fig. 4) are uniformly low and do not correlate with the magnetic field data; therefore, it is assumed that the high magnetic values measured in the field are caused by magnetic minerals at depth.

The resistivity sounding obtained at the site marked "VES" in figure 4, the interpreted geoelectric section, and probable corresponding lithologies are shown in figure 5.

With the exception of the near-surface layers, the geoelectric section is very similar to that measured at the Turpin Meadow site. The third layer is equivalent to the lower alluvial section

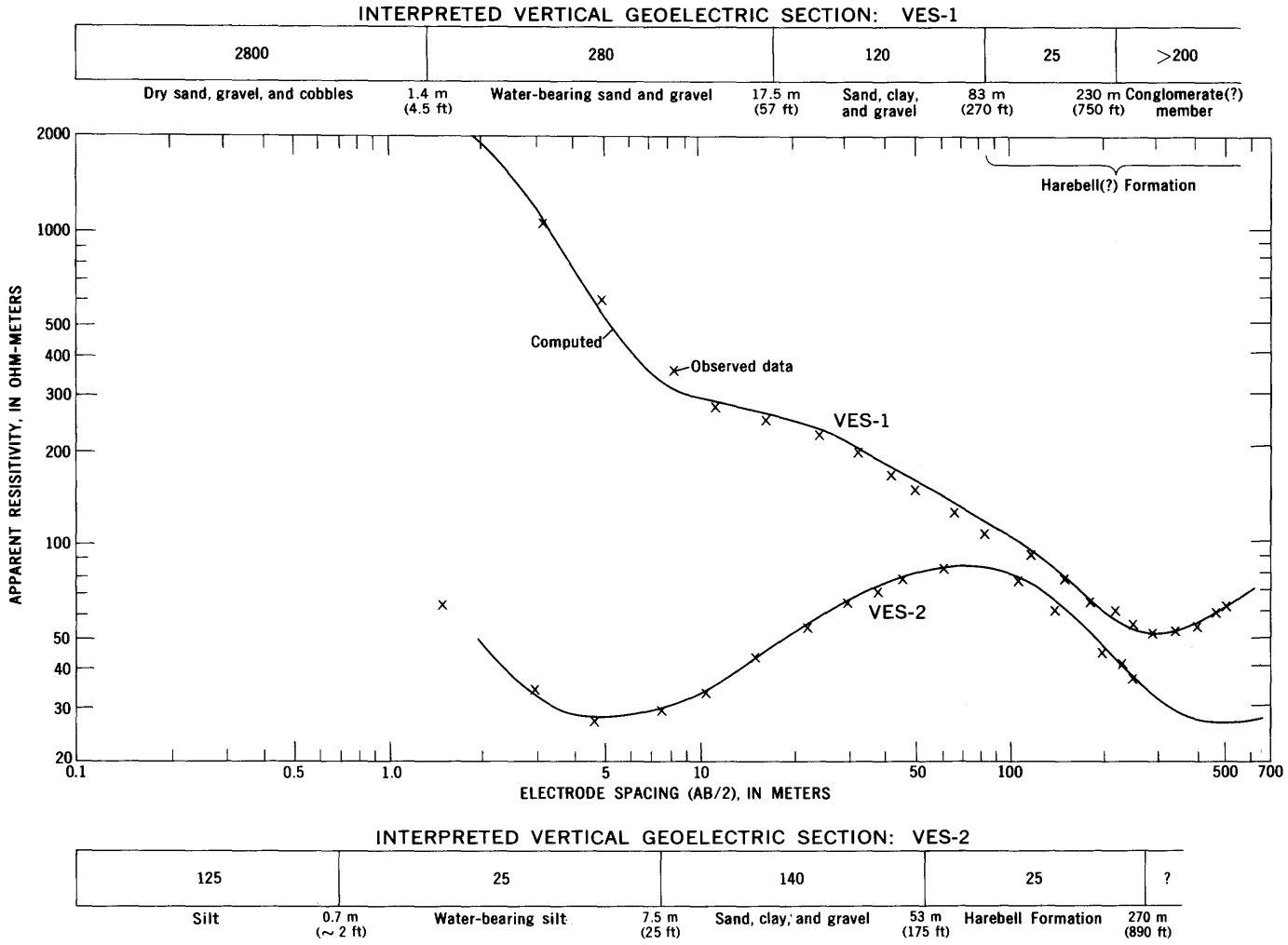

Figure 3.—Vertical electrical sounding curves VES-1 and VES-2 obtained at the Turpin Meadow survey location (fig. 1, loc. *A*). Columns indicate geoelectric section and corresponding lithology. Numbers in column are true resistivity values in ohm-meters.

at Turpin Meadow described as sand, clay, and gravel, and what is assumed to be the Harebell Formation (15 ohm-m) forms the bedrock at a depth of 43 m (130 ft). As noted at Turpin Meadow, there is a probable change in the lithology within the Harebell Formation, the lower interval having a higher resistivity than the uppermost member.

In summary, the magnetic surveys delineate a zone of heavy-mineral concentration within the alluvium between the two present stream channels. Soil sampling indicates that recent deposits of "black sand" are not responsible for the observed magnetic variations. The resistivity sounding data suggest that the alluvial section extends to a depth of 130 feet, the probable depth at which the bulk of the placer minerals occur.

Pacific Creek

The Pacific Creek site (fig. 1, loc. *C*) is a wedge-shaped plot of land bounded on the west by Grand Teton National Park and on the north and east by the Teton Wilderness. The valley through which the creek flows is narrow and is strewn with large quartzite cobbles which made resistivity measurements difficult because of poor electrode contact and lateral inhomogeneities in the geoelectric section.

The northernmost traverse of the magnetic traverses shown on figure 6 was placed approximately 1,100 feet south of the wilderness boundary to avoid a complex of ranch facilities. Six magnetic profiles were obtained along traverses spaced about 200 feet apart. The magnetic data, contoured on a 20-gamma interval (fig. 6), delineate the zones of high magnetic mineral concentrations within the valley fill. These concentrations occur as isolated accumulations of magnetic minerals, the largest of which are located at depth within ancient stream channels.

At the Pacific Creek site, 32 soil samples were collected, of which 16 had a measurable gold content ranging from 10 to 950 ppb. Neither the values of gold nor magnetic susceptibility determined for the soil samples is coincident with the

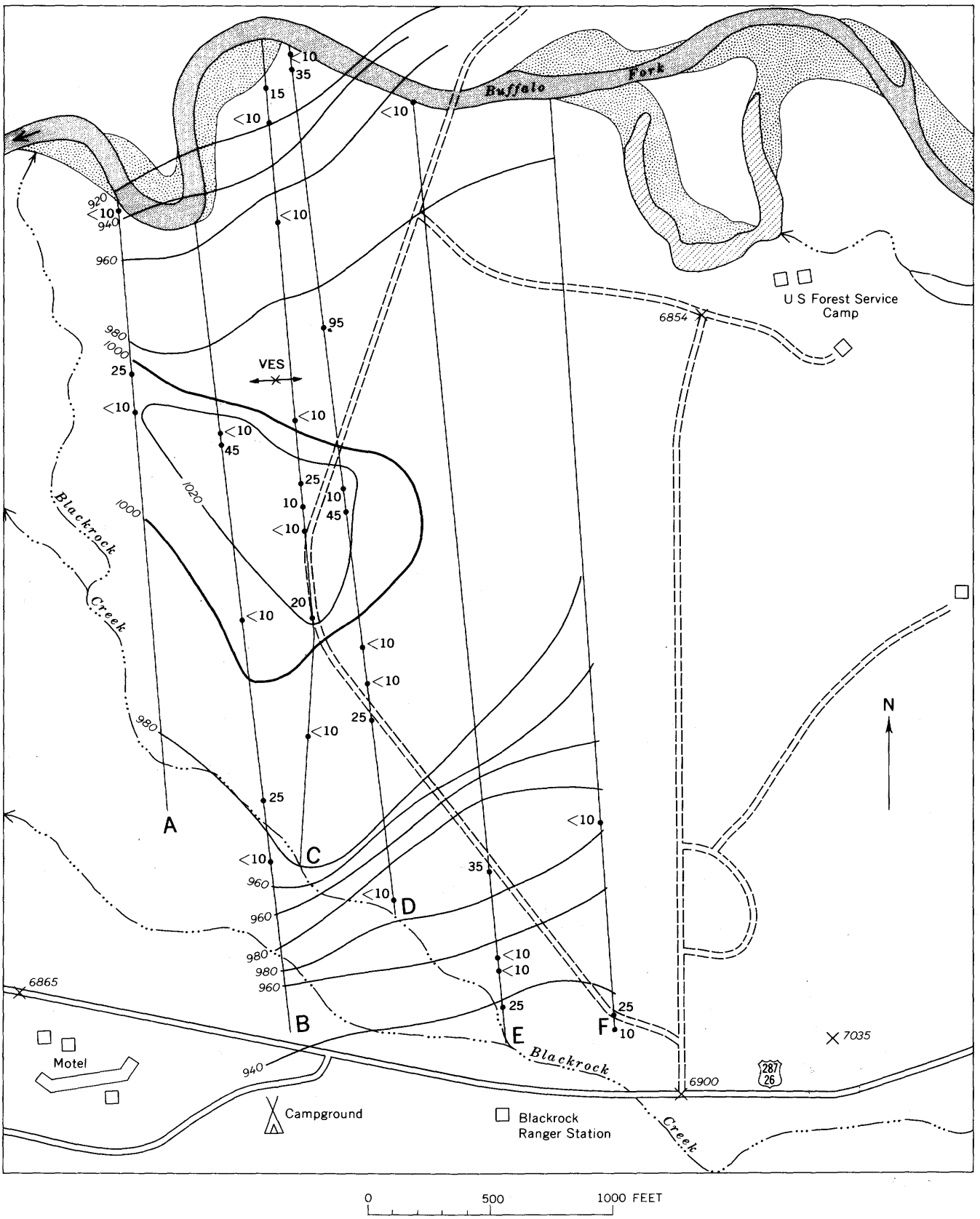

Figure 4.—Map of the Buffalo Fork-Blackrock Creek survey site (fig. 1, loc. *B*), showing magnetic traverses (A–F) and contoured total magnetic field data (interval 20 gammas). Level of reference, 56,000 gammas. VES, resistivity sounding location. Solid dot, collection point for soil sample, showing associated gold value in parts per billion.

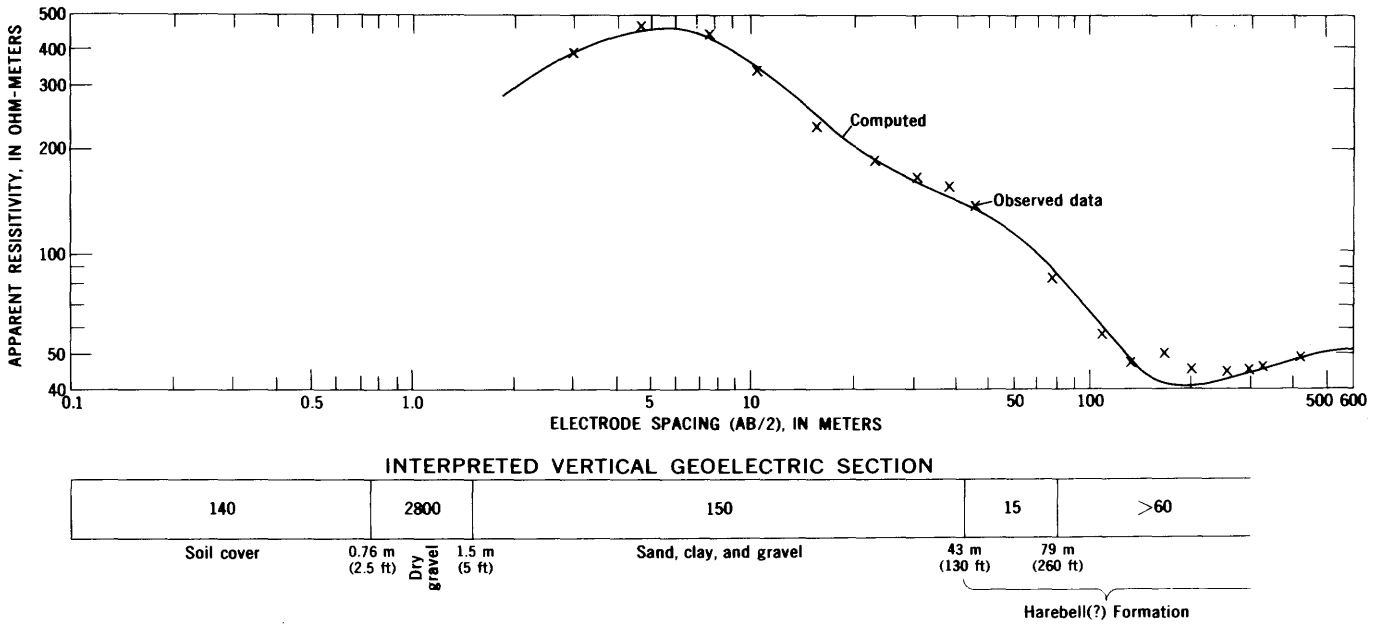

Figure 5.—Vertical electrical sounding curve obtained at the Buffalo Fork-Blackrock Creek survey location (fig. 1, loc. *B*). Column indicates geoelectric section and corresponding lithology. Numbers in column are true resistivity values in ohm-meters.

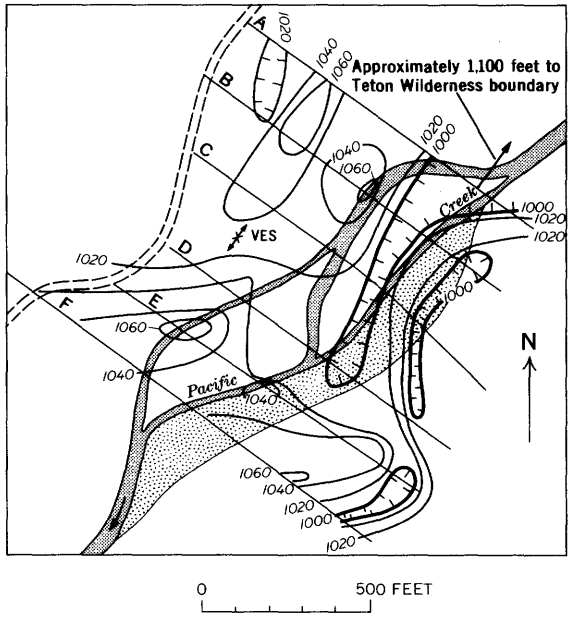

Figure 6.—Map of the Pacific Creek survey site (fig. 1, loc. *C*), showing magnetic traverses (A–F) and contoured total magnetic field data (interval 20 gammas). Level of reference, 56,000 gammas. VES, resistivity sounding location.

magnetic anomalies, indicating that the sources causing the anomalies are at depth; nor is there correspondence between the gold values and magnetic susceptibility.

As previously stated, the abundance of quartzite cobbles covering the valley floor made the resistivity measurements difficult, especially along the south end of the current spread where adequate contact with the ground was not easily achieved. The location labeled "VES" on figure 6 is the center point of the most acceptable sounding obtained in this area, the results of which are shown on figure 7. The scatter of data points required a certain degree of smoothing before an interpretation could be attempted. The maximum part of the curve described by the data points obtained at small electrode spacings is too sharp to be attributed to horizontal layering (Alfano, 1959). To overcome the limitation imposed by the near-surface inhomogeneity in the resistivity, the upper layers were lumped into a single layer and an interpretive section was established which could be verified by computer modeling. The geoelectric section and probable lithology at the Pacific Creek sounding site are also shown on figure 7.

If the 10-ohm-m layer is a claystone or clay-rich sandstone upper member of the Harebell Formation, then the bedrock surface is at a depth of 44.5 m (146 ft).

The data obtained at the Pacific Creek site suggest a wide distribution of magnetic minerals within the surveyed section of the valley. The amplitudes of the magnetic anomalies are sufficiently high to indicate sizable concentrations of magnetic minerals at depth. This fact coupled with the relatively large number of soil samples indicating gold values makes the Pacific Creek site interesting in terms of potential gold yield.

Tracy Lake

Eleven magnetic profiles were obtained at varying intervals across the dry lakebed called Tracy Lake (fig. 1, loc. *D*). The

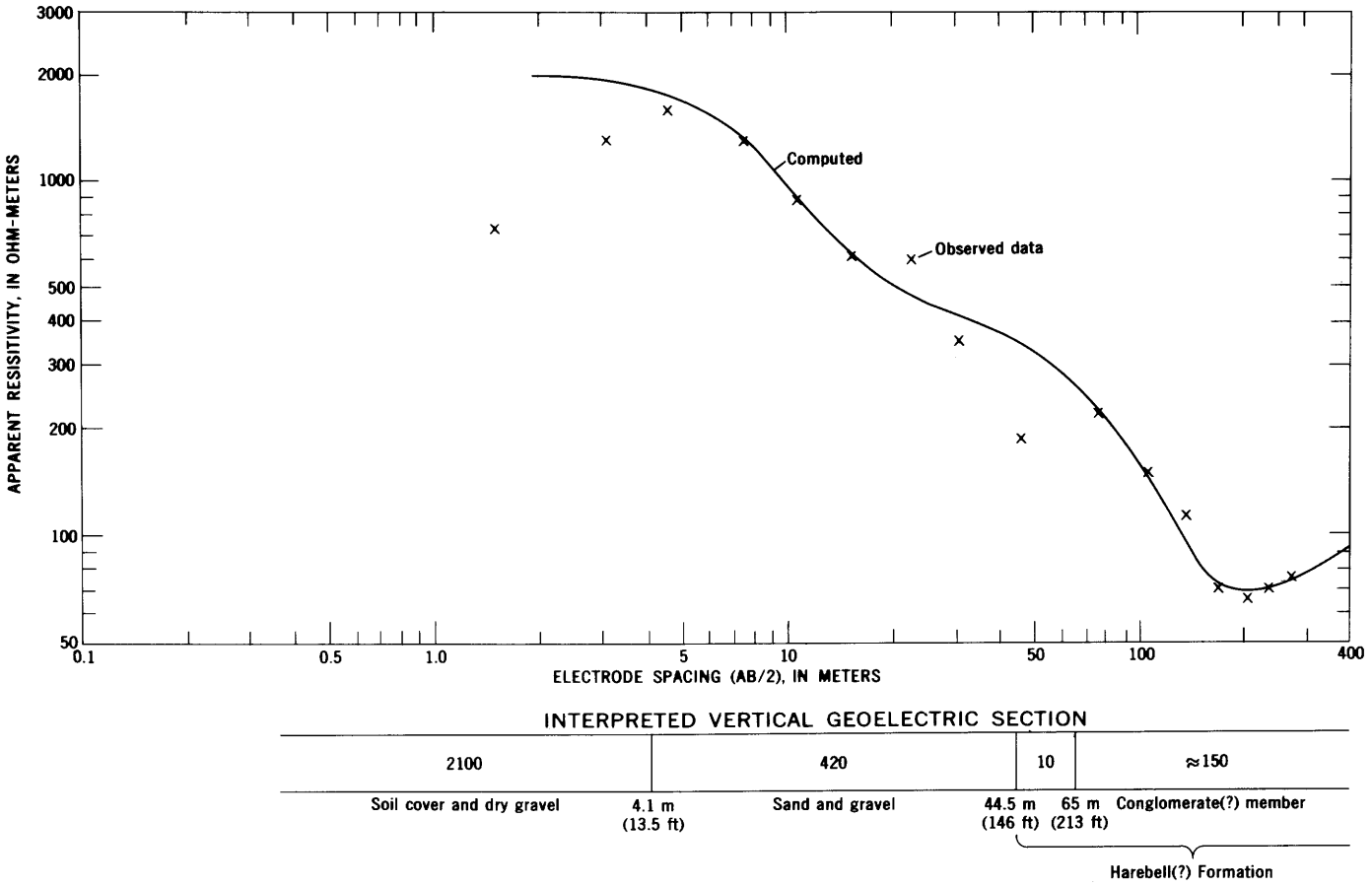

Figure 7.—Vertical electrical sounding obtained at the Pacific Creek survey location (fig. 1, loc. *C*). Column indicates geoelectric section and corresponding lithology. Numbers in column are true resistivity values in ohm-meters.

survey failed to detect any magnetic minerals concentrated in a stream placer; however, it did detect a noteworthy magnetic feature near the center of the lake.

The anomaly over the magnetic body (fig. 8) suggests that the feature is not deeply buried and is dikelike in form. To test this observation a theoretical magnetic body was constructed using a two-dimensional magnetic profile computer program to approximate the principal observed magnetic profile. A model that generates a profile similar to the observed profile is also shown in figure 8. The theoretical magnetic body is 40 feet wide, dips 60° S., and extends to an infinite depth. The magnetic susceptibility contrast (K) was chosen to be 1.65×10^{-3} emu. A physical counterpart to the model structure may be a basic plutonic dike whose top lies within 35 feet of the lakebed surface.

The surface material of the lakebed is a hard dry crust only a few inches thick underlain by a wet gelatinous mud. In contrast, the surface over the apex of the magnetic anomaly is slightly elevated and littered with cobbles, which condition suggests that the dike was intruded subsequent to the

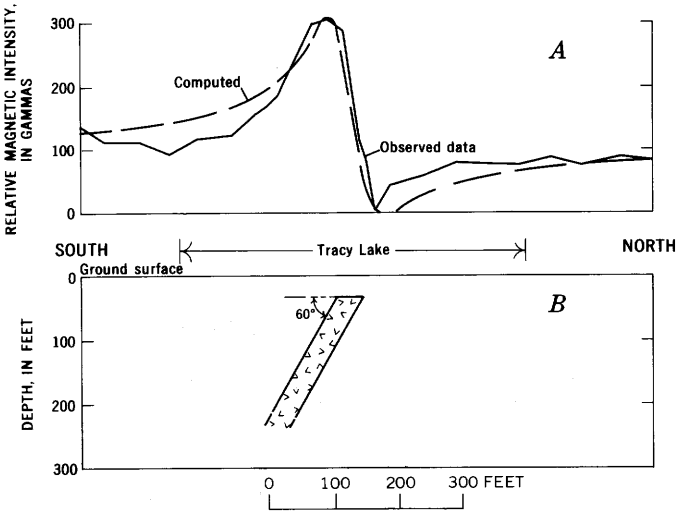

Figure 8.—Measured and computed magnetic profiles (A) over an assumed dike of infinite depth extent (B) at the Tracy Lake survey location (fig. 1, loc. *D*). Station interval, 100 feet.

deposition of the glacial till. A resistivity sounding made over the lake indicates a glacial till and gravel thickness of 42.5 m (140 ft).

SUMMARY AND CONCLUSION

Several areas within the Teton National Forest, selected on the basis of gold determinations, were investigated by magnetic surveys in an attempt to locate heavy-mineral concentrations in stream-deposited sand and gravel. Resistivity soundings were also made, where warranted by the magnetic data, to determine the thickness of the gravel beds.

In the northeast quadrant of the Teton National Forest, along the Buffalo Fork and smaller tributaries of the Snake River, the magnetic method worked well in delineating zones of magnetic mineral accumulation. The gold and magnetic susceptibility values obtained from near-surface soil samples did not correlate with the observed magnetic field data and therefore were not representative of the heavy-mineral concentrations located at depth. Soil analyses, however, did prove useful in separating magnetic anomalies caused by surface contamination from those caused by magnetic minerals at depth.

The resistivity sounding method proved useful in determining the thickness of gravel deposits. Resistivity data coupled with magnetic profiles and sufficient drill-hole data may provide an economical means by which gold placer deposits can be evaluated in terms of distribution of the heavy-metal concentrations and possible yield.

REFERENCES

Alfano, L., 1959, Introduction to the interpretation of resistivity measurements for complicated structural conditions: Geophys. Prosp., v. 7, no. 3, p. 311–366.

Antweiler, J. C., and Love, J. D., 1967, Gold-bearing sedimentary rocks in northwest Wyoming–A preliminary report: U.S. Geol. Survey Circ. 541, 12 p.

Jakosky, J. J., and Wilson, C. H., 1933, Geophysical studies in placer and water-supply problems: Am. Inst. Mining and Metall. Engineers Tech. Pub. 515, 18 p.

Joesting, H. R., 1941, Magnetometer and direct-current resistivity studies in Alaska: Am. Inst. Mining and Metall. Engineers Tech. Pub. 1284, 20 p.

Kalenov, E. N., 1957, Interpretation of vertical electrical sounding curves [in Russian]: Moscow, Gostoptekhizdat, 471 p.

Keller, G. V., and Frischknecht, F. C., 1966, Electrical methods in geophysical prospecting: London, Pergamon Press, 517 p.

Love, J. D., compiler, 1956a, Geologic map of Teton County, Wyoming *in* Wyoming Geol. Assoc. Guidebook 11th Ann. Field Conf., 1956: In pocket.

——1956b, Cretaceous and Tertiary stratigraphy of the Jackson Hole area, northwestern Wyoming *in* Wyoming Geol. Assoc. Guidebook 11th Ann. Field Conf., 1956: p. 75–94

Orellana, Ernesto, and Mooney, H. M., 1966, Master tables and curves for vertical electrical sounding over layered structures: Madrid, Interciencia, 150 p., 66 tables.

Zohdy, A. A. R., 1965, The auxiliary point method of electrical sounding interpretation, and its relationship to the Dar Zarrouk parameters: Geophysics, v. 30, no. 4, p. 644–660.

RESET DIRECTION OF REMANENT MAGNETIZATION FOR UPPER CAMBRIAN RHYODACITIC WELDED TUFF, PENSACOLA MOUNTAINS, ANTARCTICA

By MYRL E. BECK, JR.[1], and DWIGHT L. SCHMIDT,
Bellingham, Wash., Denver, Colo.

Abstract.—Four magnetically stable samples of rhyodacitic welded tuff from the Upper Cambrian Gambacorta Formation of the Pensacola Mountains, Antarctica, give a paleomagnetic pole position near 52° S., 112° W. This pole lies about 35° from the pole of the Jurassic Dufek intrusion of the northern Pensacola Mountains and lies less than 20° from the cluster of poles for the widely tested Jurassic dolerite samples from the Transantarctic Mountains. In contrast, the rhyodacite pole lies about 90° from the Late Cambrian and Ordovician poles for crystalline rocks of the Sør Rondane Mountains and Lutzow-Holm Bay areas of East Antarctica. The rhyodacite probably was remagnetized during a major early Mesozoic orogeny that is well developed in the Pensacola Mountains; the accompanying regional thermal event is marked by weak chlorite-zone metamorphism and a reset K–Ar date on biotite from Upper Cambrian granite.

During the 1965–66 field season in the Pensacola Mountains, Antarctica (fig. 1), gabbroic rocks of the stratiform Dufek intrusion were collected for a paleomagnetic study (Beck and others, 1968). At the same time a few oriented samples were collected from other igneous and sedimentary rock units in the Pensacola Mountains to test their natural remanent magnetization. Of 10 oriented samples from the Hawkes Rhyodacite Member of the Gambacorta Formation, four have a stable remanent magnetization that gives a pole position near 53° S., 112° W. Although the four stable magnetization directions are closely grouped, the sampling is too scant to yield a truly reliable pole; the remoteness of the field area, however, precludes further collection at the present time.

Acknowledgments.—Willis H. Nelson aided in the collection of oriented field specimens. Daniel Stinnett and William Huff made the remanent magnetism determinations. This work is part of a U.S. Geological Survey geologic study of the Pensacola Mountains for the U.S. Antarctic Research Program and is financed by the National Science Foundation. Field logistic support was given by the U.S. Navy Operation Deep Freeze and by the U.S. Army Helicopter Detachment, Antarctica.

[1] Western Washington State College.

GAMBACORTA FORMATION

The Gambacorta Formation is a thick complex volcanic pile of felsic flows and pyroclastic rocks of Late Cambrian age (Schmidt and others, 1965; Schmidt and Ford, 1969). The formation thickens to more than 1,500 m in the southeastern Neptune Range in the vicinity of its eruptive center. Part of the eruptive center is a circular volcanic caldera about 25 km across which is bounded by concentric border faults and filled by more than 1,000 m of an intracaldera phase of rhyodacitic welded tuff of the Hawkes Rhyodacite Member of the Gambacorta Formation (Schmidt, 1969). An indistinct flow foliation in the caldera rock strikes subparallel to the caldera walls and dips less than 36° toward the center. Gravity data at 5-mile spacing show a 10-mgal gravity low over the caldera area (Behrendt and others, 1966; J. C. Behrendt, written commun., 1968). Away from the caldera an outflow phase of the rhyodacite is a distinctive, relatively thin ignimbrite that retains a thickness of more than 70 m at a distance of 40 km.

The Gambacorta Formation and older rocks of the Pensacola Mountains in general were intensely deformed during a major Cambrian-Ordovician orogeny. Subsequently, middle and upper Paleozoic sandstones and siltstones, more than 3,000 m thick, were deposited above the folded Gambacorta Formation. These younger Paleozoic rocks were in turn deformed during the early Mesozoic Weddell orogeny (Ford, 1970). Significantly, however, the Hawkes Rhyodacite Member in the caldera and the overlying sedimentary rocks in the vicinity of the caldera have not been greatly deformed despite strong sinuous folding of the middle and upper Paleozoic sedimentary rocks just west of the caldera in the central Neptune Range. The sedimentary rocks near and above the caldera are flat lying with maximum dips of about 10°.

The Hawkes Rhyodacite Member and associated rocks have been slightly to moderately altered thermally in the chlorite zone of regional metamorphism; the characteristic dark green of the rhyodacite is outwardly indicative of low-grade altera-

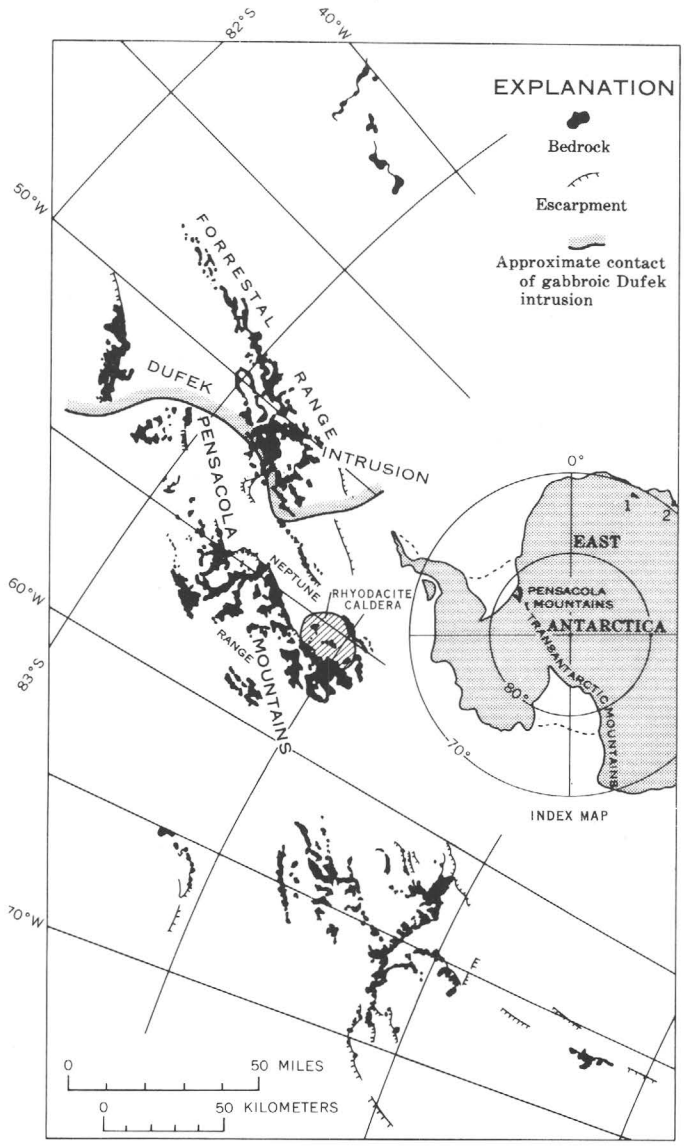

Figure 1.—Index map of Antarctica and the Pensacola Mountains, showing the location of the volcanic caldera of the Upper Cambrian rhyodacite in the Neptune Range. Localities in East Antarctica: *1*, Sør Rondane Mountains; *2*, Lutzow-Holm Bay area.

tion. Plagioclase phenocrysts are partly altered to sericite with or without epidote, calcite, and chlorite; primary mafic phenocrysts of biotite, hornblende, and sparse augite are commonly altered to chlorite, epidote, and calcite, and the groundmass is a finely recrystallized mosaic of quartz, altered feldspar, sericite, and minor chlorite. The overlying middle and upper Paleozoic sedimentary rocks are similarly metamorphosed; but, because these are chiefly quartzose sandstones, the alteration is not as obvious. The rhyodacite was thermally metamorphosed during the Cambrian-Ordovician orogeny and again less strongly altered thermally during the early Mesozoic Weddell orogeny (Ford, 1970).

Twelve whole-rock Rb-Sr determinations of the Gambacorta volcanic rocks indicate a 500±10-m.y. (million year) isochron age (Gunter Faure, written commun., 1969). Four of these age determinations were made on the Hawkes samples that were used during the present study. The rhyodacite is thus of latest Cambrian age. The Gambacorta Formation is bracketed by Middle Cambrian (A. R. Palmer, written commun., 1964) and Middle Devonian (Schopf, 1968, p. 176) fossil ages.

Four of the paleomagnetic samples were also analyzed chemically (table 1). Chemical and petrographic study indicates that the Hawkes, as part of the Gambacorta Formation, is comagmatic with the granite of the Median Snowfield which occurs about 40 km north of the rhyodacite caldera. A whole-rock Rb-Sr analysis of this granite indicates an age of 510±30 m.y. (Z. E. Peterman, written commun., 1964). The only available K-Ar date for these rocks, a biotite age of 265±13 m.y. for the granite (R. F. Marvin, written commun., 1964), suggests reheating and argon loss during Permian or later time.

MAGNETIZATION

The 10 oriented samples used in this study (table 1) came from widely separated localities within the caldera and represent the intracaldera phase of the Hawkes Rhyodacite Member. Steep-sided outcrops with a maximum relief of 1,000 m assure excellent exposure of fresh rock. Directions of natural remanent magnetization of cylindrical specimens cut from the oriented samples were measured on a spinner magnetometer described by Phillips and Kuckes (1967). Initial directions were scattered over much of the upper hemisphere of an equal area stereographic projection (fig. 2). To remove the secondary magnetization suspected to have contributed most of this scatter, the specimens were magnetically cleaned by the alternating field demagnetization method (As, 1967; As and Zijderveld, 1958) in peak fields of as much as 400 oe (oersteds). Four samples responded well to this treatment, reaching stable end points (points at which the vector of remanent magnetization ceased to change direction with further demagnetization) in fields ranging from 100 to 300 oe. The remaining six samples did not reach stable end points, and in addition showed demagnetization curves suggesting varying degrees of magnetic instability; these six samples were excluded from further analysis. Figure 3 shows the four stable samples after magnetic cleaning, and table 1 lists directions of remanent magnetization before and after magnetic cleaning.

Directions of magnetization given in table 1 and plotted on figures 2 and 3 were determined for each specimen in its present-day orientation in outcrop. The four stable samples plotted in figure 3 have a Fisher precision parameter, k (Fisher, 1953) of 62.3 (table 2). If, however, these same samples are rotated to bring their respective field flow foliations to horizontal, the scatter of the magnetization directions is greatly increased (k decreases to 18.2). This increase indicates that the observed natural remanent magnetization was established after the foliation was set. This is as would be expected, if the magnetization was reset during the

Table 1.—*Directions of remanent magnetization and partial results of chemical analyses for samples of Upper Cambrian rhyodacite, Pensacola Mountains, Antarctica*

[Varying degrees of magnetic instability (U), and lack of stable end points, precluded analyses of six samples]

Sample No.	Location		Chemical analyses[1] (percent)		Directions of remanent magnetization[2]				$\widetilde{H}$[4]
					Before magnetic cleaning		After magnetic cleaning[3]		
	Lat (°S.)	Long (°W.)	Fe_2O_3	Fe	*D*	*I*	*D*	*I*	
1	83.98	54.65	....	....	281.0	−56.0	....	....	U
2	83.95	54.45	....	....	19.0	−20.5	....	....	U
3	83.96	54.53	....	....	225.0	−64.0	....	....	U
4	84.00	54.82	....	....	73.5	−82.0	136.5	−69.0	300
5	84.00	54.70	0.94	1.15	154.5	−76.0	....	....	U
6	84.05	55.02	1.82	.61	141.0	−81.0	134.0	−83.0	100
7	84.05	55.02	1.31	1.24	229.5	−66.0	....	....	U
8	83.92	56.17	....	....	326.0	−43.0	103.5	−64.5	200
9	83.92	56.05	....	....	80.0	−26.0	104.0	−66.0	300
10	83.92	56.00	.85	2.20	.5	−55.0	....	....	U

[1] Iron analyses by E. E. Engleman.
[2] *D*, declination; *I*, inclination.
[3] As (1967), As and Zijderveld (1958).
[4] $\widetilde{H}$, peak value of optimum alternating field used for magnetic cleaning, in oersteds. U, unstable.

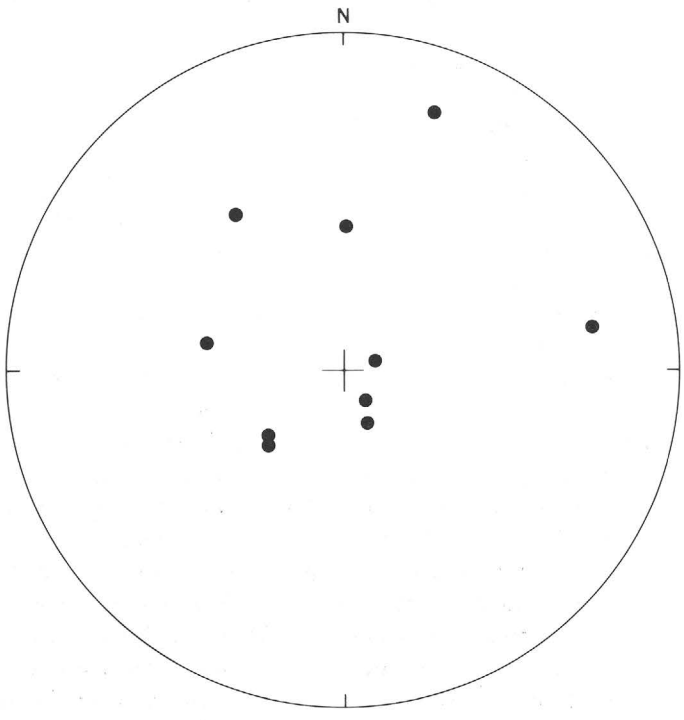

Figure 2.—Equal-area upper-hemisphere plot of directions of natural remanent magnetization for 10 samples of Hawkes Rhyodacite Member of the Gambacorta Formation, Neptune Range, Antarctica.

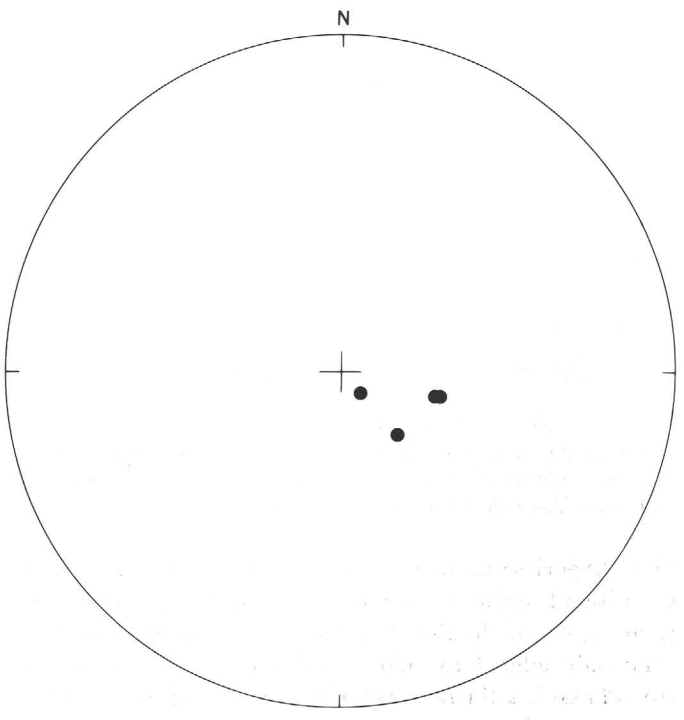

Figure 3.—Equal-area upper-hemisphere plot of directions of remanent magnetization for stable samples of Hawkes Rhyodacite Member, after magnetic cleaning.

early Mesozoic orogeny during which the Hawkes Rhyodacite Member in the caldera was not more than slightly deformed.

The rejection of more than half the samples for magnetic instability is surprising because all samples are texturally and petrographically similar and were collected from an apparently uniform rock unit. Four samples were chemically and spectrographically analyzed, and all four are chemically similar except for their Fe_2O_3:FeO ratio. Magnetically stable sample 6 has an Fe_2O_3:FeO ratio of 3:1, whereas the three unstable samples have Fe_2O_3:FeO ratios of 1:1 to 1:3 (table 1). These data are

presented as a point of interest only and do not now suggest a solution to the stability problem. Undoubtedly the iron-oxide ratios and the magnetic stability are complexly related to heterogeneous oxidation during primary cooling as has been studied for basalt (Watkins and Haggerty, 1967; Strangway and others, 1968). Later remagnetization of the Hawkes Rhyodacite Member may have further complicated the magnetic stability of the samples.

INTERPRETATION

The tight grouping of directions of remanent magnetization of stable samples after magnetic cleaning is at a substantial angle to the direction of the present geomagnetic field, suggesting that the rhyodacite records a former direction of the earth's magnetic field. However, as only four samples are suitable for paleomagnetic analysis, the magnetization direction is poorly defined. The pole position calculated from these data (table 2 and fig. 4) therefore indicates only approximately a former position of the south geographic pole with respect to Antarctica.

Table 2.—*Average direction of remanent magnetization and location of the virtual geomagnetic pole, on the basis of data of table 1*

D	I	α_{95}	δ	k	Lat	Long
115.5	−71.55	11.7	8.9	62.3	112.5° W.	53.0° S.

Explanation:

D, I; average declination and inclination of the four stable samples of table 1, after magnetic cleaning.

α_{95}, radius of circle of confidence at the 95-percent probability level (Fisher, 1953).

δ, angular standard deviation (Wilson, 1959).

k, estimate of precision parameter (Fisher, 1953).

Lat, Long; latitude and longitude of virtual geomagnetic pole (Irving, 1964).

The age of the stable remanent magnetization of the Hawkes Rhyodacite Member is probably early Mesozoic as shown by the fact that the calculated pole position falls within 20° of poles for the Jurassic Ferrar dolerites (poles 9.37, 9.38, 9.42, 9.56 of Irving, 1964). The rhyodacite pole lies about 40° from the pole of the Jurassic Dufek gabbroic intrusion (Beck and others, 1968). On the other hand, poles for the Lower Ordovician granitic rocks from the Sør Rondane Mountains (Zijderveld, 1968) and Upper Cambrian gneisses from Lutzow-Holm Bay and Ongul Island (Nagata and Yama-ai, 1961; Zijderveld, 1968) lie near southern Africa, some 90° from the Hawkes Rhyodacite Member pole. Although it is possible to account for this arrangement of poles in terms of apparent polar wandering, it seems more likely that the Hawkes samples have been remagnetized during the early Mesozoic.

The weak chlorite-zone regional metamorphism of middle and upper Paleozoic sedimentary rocks in the Neptune Range

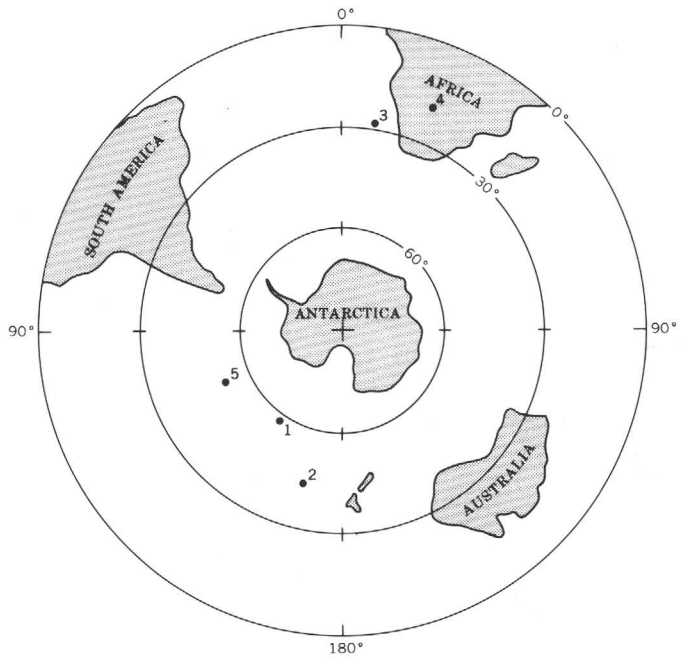

Figure 4.—Paleozoic and Mesozoic paleomagnetic poles for Antarctica. 1, Ferrar dolerites (four tightly grouped poles here represented by Bull and others, 1962); 2, Dufek intrusion (Beck and others, 1968); 3, Sør Rondane granitic rocks (Zijderveld, 1968); 4, Lutzow-Holm Bay and Ongul Island gneisses (Nagata and Yama-ai, 1961); 5, Hawkes Rhyodacite Member, Gambacorta Formation (present report).

during the Weddell orogeny means that the Hawkes was similarly altered thermally during the early Mesozoic in addition to its stronger chlorite-zone metamorphism during the Cambrian-Ordovician orogeny. The reset Permian K–Ar date on biotite from the Upper Cambrian granite of Median Snowfield in the Neptune Range further supports a thermal event during the late Paleozoic or early Mesozoic. Ford (1970) has defined an early Mesozoic age for the Weddell orogeny, and therefore this age is accepted as the time of the thermal event.

Theoretically, the Hawkes Rhyodacite Member samples may have acquired their remanence when the polarity of the earth's geomagnetic field was reversed, but this leads to unlikely general conclusions about Antarctica. Only remagnetization in a magnetic field roughly parallel to the field known to have prevailed in Antarctica during the Jurassic is capable of accounting for all the observations.

It seems likely, therefore, that the rocks of the Neptune Range in general have been regionally reheated during the early Mesozoic and that the Hawkes specifically has been reheated to a temperature sufficient to have given it a new stable remanent magnetization. The temperature required for remagnetization should depend upon the magnetization process and composition of the magnetic minerals and could be as low as a few hundred degrees centigrade.

REFERENCES

As, J. A., 1967, The a.c. demagnetization technique, p. 221–223 *in* Collinson, D. W., Creer, K. M., and Runcorn, S. K., eds., Methods in palaeomagnetism: Amsterdam, Elsevier Publishing Co., 609 p.

As, J. A., and Zijderveld, J. D. A., 1958, Magnetic cleaning of rocks in palaeomagnetic research: Geophys. Jour., v. 1, no. 4, p. 308–319.

Beck, M. E., Jr., Ford, A. B., and Boyd, W. W., Jr., 1968, Palaeomagnetism of a stratiform intrusion in the Pensacola Mountains, Antarctica: Nature, v. 217, no. 5128, p. 534–535.

Behrendt, J. C., Meister, Laurent, and Henderson, J. R., 1966, Airborne geophysical study in the Pensacola Mountains of Antarctica: Science, v. 153, no. 3742, p. 1373–1376.

Bull, C., Irving, E., and Willis, I., 1962, Further palaeomagnetic results from South Victoria Land, Antarctica: Geophys. Jour., v. 6, no. 3, p. 320–336.

Fisher, R. A., 1953, Dispersion on a sphere: Royal Soc. [London] Proc., ser. A, v. 217, no. 1130, p. 295–305.

Ford, A. B., 1970, The Weddell orogeny—early Mesozoic deformation at the Weddell Sea margin of the Transantarctic Mountains *in* SCAR-IUGS symposium on Antarctic geology and solid earth geophysics, Oslo, August 6–15, 1970 [abs.]: p. 73.

Irving, E., 1964, Paleomagnetism and its application to geological and geophysical problems: New York, John Wiley & Sons, Inc., 399 p.

Nagata, T., and Yama-ai, M., 1961, Palaeomagnetic studies on rocks on the coast of Lutzow-Holm Bay: Antarctic Rec., v. 11, p. 945–947.

Phillips, J. D., and Kuckes, A. F., 1967, A spinner magnetometer: Jour. Geophys. Research, v. 72, no. 8, p. 2209–2212.

Schmidt, D. L., 1969, Precambrian and lower Paleozoic igneous rocks, Pensacola Mountains, Antarctica: Antarctic Jour. U.S., v. 4, no. 5, p. 203–204.

Schmidt, D. L., and Ford, A. B., 1969, Geology of the Pensacola and Thiel Mountains, pl. V *in* Bushnell, V. C., and Craddock, Campbell, eds., Geologic maps of Antarctica: Am. Geog. Soc. Antarctic Map Folio Ser., Folio 12.

Schmidt, D. L., Williams, P. L., Nelson, W. H., and Ege, J. R., 1965, Upper Precambrian and Paleozoic stratigraphy and structure of the Neptune Range, Antarctica, *in* Geological Survey Research 1965: U.S. Geol. Survey Prof. Paper 525–D, p. D112–D119.

Schopf, J. M., 1968, Studies in Antarctic paleobotany: Antarctic Jour. U.S., v. 3, no. 5, p. 176–177.

Strangway, D. W., Larson, E. E., and Goldstein, M., 1968, A possible cause of high magnetic stability in volcanic rocks: Jour. Geophys. Research, v. 73, no. 12, p. 3787–3795.

Watkins, N. D., and Haggerty, S. E., 1967, Primary oxidation variation and petrogenesis in a single lava: Contr. Mineralogy and Petrology, v. 15, no. 3, p. 251–271.

Wilson, R. L., 1959, Remanent magnetism of late secondary and early Tertiary British rocks: Philos. Mag., ser. 8, v. 4, p. 750–755.

Zijderveld, J. D. A., 1968, Natural remanent magnetizations of some intrusive rocks from the Sør Rondane Mountains, Queen Maud Land, Antarctica: Jour. Geophys. Research, v. 73, no. 12, p. 3773–3785.

CHEMICAL AND SPECTROGRAPHIC ANALYSES OF LUNAR SAMPLES FROM APOLLO 12 MISSION

By C. S. ANNELL, M. K. CARRON, R. P. CHRISTIAN, FRANK CUTTITTA, E. J. DWORNIK, A. W. HELZ, D. T. LIGON, JR., and H. J. ROSE, JR., Washington, D. C.

Abstract.—Seven samples of lunar material returned by the Apollo 12 mission were analyzed by semimicro chemical, X-ray fluorescence, and optical emission spectrographic methods for their major-, minor-, and trace-element content. The Apollo 12 materials are notably lower in TiO_2 content (≈ 3 percent) than are the Apollo 11 igneous rocks (≈ 9–14 percent). Trace-element variations between igneous rock samples from Apollo 12 reflect their greater diversity in texture and modal mineralogy.

Seven lunar samples collected at the Ocean of Storms by the Apollo 12 mission were analyzed. Five of the samples were analyzed for major and 45 trace elements by a combination of semimicro chemical, X-ray fluorescence, and d-c arc emission spectrographic techniques. The methods have been previously described (Annell and Helz, 1970a, b; Rose and others, 1970a, b) for the Apollo 11 lunar materials. A related study of six additional lunar samples—two of igneous rock and four of lunar fines—was also made by the authors and is reported in a companion paper (Rose and others, 1971) (C182–C184, this chapter).

The small quantities allocated for two samples (12009,42 and 12035,15) were sufficient only for the emission spectrographic analysis of the trace-element abundances, and no major-element data could be generated for these two samples. For the spectrographic analyses, samples were ground to a fine powder in an agate mortar and an aliquot of the ground material was mixed with graphite prior to arcing. The analytical data are given in tables 1 and 2.

The mineral and rock classifications (table 2) were made by the Lunar Receiving Laboratory of the National Aeronautics and Space Administration, in Houston, Tex. The one sample of fines (12070,89) is reported to contain meteoritic material (Lunar Sample Preliminary Examination Team, 1970). This can account for some of the differences in composition of the igneous rock samples, as noted also for the fines and breccias from Apollo 11 (Lunar Sample Analysis Planning Team, 1970): (1) the Zn and Ni have higher concentrations in the fines, as in the Apollo 11 samples, and (2) the alkalies K, Rb, and Li are more concentrated in the fines, along with Ba and the rare earths La, Y, and Yb.

Table 1.—*Major- and minor-element composition of some Apollo 12 lunar samples, in weight percent*

Constituent	12020,42	12021,97	12038,28	12070,89	12075,18
SiO_2	44.6	46.5	47.1	45.8	44.8
Al_2O_3	8.00	10.5	12.8	12.9	7.87
Fe_2O_3	.00	.00	.00	.00	.00
FeO	20.7	19.4	17.4	16.3	20.7
MgO	14.4	7.48	6.80	10.2	14.4
CaO	8.53	11.3	11.4	10.5	8.53
Na_2O	.23	.30	.64	.50	.23
K_2O	.06	.06	.07	.25	.07
H_2O	.00	.00	.00	.00	.00
TiO_2	2.56	3.51	3.17	2.83	2.55
P_2O_5	.08	.09	.17	.33	.08
MnO	.27	.27	.24	.22	.27
Cr_2O_3	.60	.41	.31	.44	.60
Total	100.03	99.82	100.10	100.27	100.10
Total Fe as Fe_2O_3	23.0	21.5	19.4	18.1	23.0
Total reducing capacity.	20.7	20.0	17.7	17.9	20.7
ΔRC	.0	.6	.3	1.6	.0

NOTES:
Δ RC—total reducing capacity measured for the lunar samples less the reducing capacity attributable to the FeO content of the lunar samples.
See table 2 for description of samples.

Table 3 shows the average major-element concentrations in the igneous rocks and the breccias and fines from Apollo 11 and 12. Compared with the Apollo 11 lunar materials, the Apollo 12 samples are characterized by higher SiO_2 and lower

Table 2.—*Trace-element abundances of some Apollo 12 lunar samples, in parts per million*

Element	12009,42	12020,42	12021,97	12035,15	12038,28	12070,89	12075,18
Zn	4	<4	4.3	<4	<4	8	<4
Cu	14	9.0	13	6.5	10	12	8.5
Ga	5.0	4.8	4.7	4.2	5.9	4.9	4.8
Rb	1.4	1.4	1.2	1.2	<1	6.2	1.4
Li	6.4	5.7	8.1	5.8	8.5	17	5.7
Mn	2,120	2,150	2,150	2,140	1,850	1,650	2,020
Cr	4,390	4,330	2,850	4,540	2,210	3,060	4,000
Co	59	64	38	71	34	52	69
Ni	62	77	16	101	6.7	222	72
Ba	71	61	71	51	142	423	58
Sr	75	65	84	65	158	123	59
V	166	155	130	204	126	121	158
Be	1.4	1.4	1.5	1.6	<1	3.3	N.D.
Nb	<10	13	11	<10	12	29	16
Sc	44	39	51	42	50	42	37
La	<20	<20	<20	N.D.	<20	40	<20
Y	42	37	53	36	71	145	38
Zr	114	119	133	88	186	498	95
Yb	5.3	5.1	5.4	4.7	6.3	14	5.1

NOTES:

1. The following elements were looked for but not detected (N.D.) in the analyzed samples:
   If present, they would be in concentrations below the amount (in parts per million) indicated in parentheses. Ag (0.2), As (4), Au (0.2), B (10), Bi (1), Cd (8), Ce (100), Cs (1), Ge (1), Hf (20), Hg (8), In (1), Mo (2), Nd (100), P (2,000), Pb (1), Pt (3), Re (30), Sb (100), Sn (10), Ta (100), Te (300), Th (100), Tl (1), U (500), W (200).
2. Lunar Receiving Laboratory (LRL) classification for the allocated Apollo 12 samples:
   12009,42—porphyritic olivine (feldspar) basalt (selected sample).
   12020,42—olivine basalt (selected sample).
   12021,97—pigeonite dolerite, pegmatite (selected sample).
   12035,15—troctolite (documented sample).
   12038,28—basalt (documented sample).
   12070,89—fines (contingency sample).
   12075,18—olivine basalt (contingency sample).

TiO_2 content. The MgO average is higher and range greater (7 to 14 percent) for the Apollo 12 samples than for the Apollo 11 samples (6 to 8 percent).

In table 4 a comparison is made of the average concentrations of trace elements in the corresponding types of lunar samples returned on the Apollo 11 and 12 missions. Although no generalizations can be made from such limited sampling, the report by the Lunar Sample Preliminary Examination Team (1970), from a much larger sampling, indicates a wide range in texture and mode for the crystalline rocks. These rocks consist primarily of pyroxene, olivine, plagioclase, ilmenite, and glasses in varying proportions. The basalt, 12038, was described by the Lunar Sample Preliminary Examination Team (1970) as being compositionally similar to eucrites. The relatively higher Ca content of the basalt is accompanied by higher Ba, Sr, Y, and Zr and lower Cr and Ni than the other three basalts analyzed. The Lunar Sample Preliminary Examination Team (1970) reported a higher pyroxene-olivine ratio in sample 12021, whereas the other gabbro (troctolite), 12035, shows higher concentrations of Ba, Sr, Y, Zr, and Cu and lower Co and Ni than does the pigeonite dolerite, reflecting their differences in mineralogic composition.

In conclusion, igneous rock and fines from Apollo 12 were lower in titanium, reflecting a lower ilmenite content, as compared with the Apollo 11 returned lunar samples. The trace-element contents of the Apollo 12 lunar fines show higher concentrations of Zn, Ni, Ba, Sr, Be, Nb, rare earths, and Zr than the Apollo 12 igneous rocks (table 2). This can be attributed in some measure to the presence of meteoritic material in the fines, and to other lunar debris scattered by meteoritic impact on material of a differentiated nature.

This research was undertaken on behalf of the National Aeronautics and Space Administration under contract No. 9-170021, order No. T-74398.

Table 3.—*Comparison of average major- and minor-element concentrations of some Apollo 11 and 12 lunar samples, in weight percent*

Constituent	Basalts		Gabbros		Breccias and fines	
	Apollo 11 (1)	Apollo 12 (3)	Apollo 11 (8)	Apollo 12 (1)	Apollo 11 (4)	Apollo 12 (1)
SiO_2 . . .	40.1	45.5	40.2	46.5	41.8	45.8
Al_2O_3. . .	8.60	9.56	10.4	10.5	13.1	12.9
FeO . . .	18.9	19.6	18.4	19.4	15.9	16.3
MgO . . .	7.74	11.9	7.02	7.48	7.7	10.2
CaO . . .	10.7	.49	11.3	11.3	11.8	10.5
Na_2O . . .	.46	.37	.43	.30	.45	.50
K_2O . . .	.30	.07	.14	.06	.16	.25
H_2O- . . .	.00	.00	.00	.00	.00	.00
TiO_2 . . .	12.2	2.76	11.3	3.51	8.49	2.83
P_2O_5 . . .	< .2	< .2	< .2	< .2	< .2	.33
MnO . . .	.25	.26	.27	.27	.22	.22
Cr_2O_3. . .	.37	.50	.28	.41	.32	.44
Total. . .	99.62	100.01	99.74	99.73	99.94	100.27
Total Fe as Fe_2O_3.	21.0	21.8	20.4	21.5	18.6	18.1

NOTES:
Number of samples included in averages are shown in parentheses at head of column.
Data for Apollo 11 from Rose and others (1970a, b, c).

REFERENCES

Annell, C. S., and Helz, A. W., 1970a, Emission spectrographic determination of trace elements in lunar samples: Science, v. 167, no. 3918, p. 521–523.

——1970b, Emission spectrographic determination of trace elements in lunar samples from Apollo 11, *in* Levinson, A. A., ed., Proceedings of the Apollo 11 Lunar Science Conference, Houston, Texas, January 5–8, 1970, v. 2, Chemical and isotope analyses: New York, Pergamon Press, p. 991–994.

Lunar Sample Analysis Planning Team, 1970, Summary of Apollo 11 Lunar Science Conference: Science, v. 167, no. 3918, p. 449–451.

Lunar Sample Preliminary Examination Team, 1970, Preliminary examination of lunar samples from Apollo 12: Science, v. 167, no. 3923, p. 1325–1339.

Rose, H. J., Jr., Cuttitta, Frank, Annell, C.S., Carron, M. K., Christian, R. P., Dwornik, E. J., Helz, A. W., and Ligon, D. T., Jr., 1971, Semimicro analysis of Apollo 12 lunar samples, *in* Geological Survey Research 1971: U.S. Geol. Survey Prof. Paper 750-C, p. C182–C184.

Rose, H. J., Jr., Cuttitta, Frank, Dwornik, E. J., Carron, M. K., Christian, R. P., Lindsay, J. R., Ligon, D. T., Jr., and Larson, R. R., 1970a, Semimicro chemical and X-ray fluorescence analysis of lunar samples: Science, v. 167, no. 3918, p. 520–521.

——1970b, Semimicro X-ray fluorescence analysis of lunar samples, *in* Levinson, A. A., ed., Proceedings of the Apollo 11 Lunar Science Conference, Houston, Texas, January 5–8, 1970, v. 2, Chemical and isotope analyses: New York, Pergamon Press, p. 1493–1497.

——1970c, Errata and addenda: Geochim. et Cosmochim. Acta, v. 34, p. 1367.

Table 4.—*Comparison of average trace-element concentrations of some Apollo 11 and 12 lunar samples, in parts per million*

[N.D., looked for but not detected]

Element	Basalts		Gabbros		Breccia	Fines	
	Apollo 11 (4)	Apollo 12 (4)	Apollo 11 (1)	Apollo 12 (2)	Apollo 11 (7)	Apollo 11 (1)	Apollo 12 (1)
Zn	N.D.	<4	N.D.	4	24	19	8
Cu	9	10	7	10	15	10	12
Ga	5	5	5	4.5	5	3.8	4.9
Rb	5	1	1	1.2	3	2.7	6.2
Li	17	7	9	7.0	12	11	17
Mn	2,250	2,035	2,580	2,145	1,870	1,960	1,650
Cr	2,870	3,730	1,860	3,695	2,460	1,740	3,060
Co	31	57	15	55	32	24	52
Ni	7	54	3	59	202	185	222
Ba	440	83	160	61	250	210	423
Sr	135	90	150	75	130	130	123
V	73	151	82	167	60	50	121
Be	3.1	1	1.5	1.6	2.0	1.6	3.3
Nb	24	12	21	10	23	18	29
Sc	97	43	94	47	68	56	42
La	26	<20	15	<20	19	16	40
Y	162	47	113	45	102	81	145
Yb	21	5.5	14	5.1	13	10	14
Zr	594	129	380	111	400	273	498

NOTES:
Number of samples included in averages are shown in parentheses at head of column.
Data for Apollo 11 from Annell and Helz (1970a, b).

SEMIMICRO ANALYSIS OF APOLLO 12 LUNAR SAMPLES

By H. J. ROSE, JR., FRANK CUTTITTA, C. S. ANNELL,
M. K. CARRON, R. P. CHRISTIAN, E. J. DWORNIK, A. W. HELZ,
and D. T. LIGON, JR., Washington, D.C.

Abstract.—The major-, minor-, and trace-element composition of two igneous rocks and four fines was determined by combined semimicro chemical, X-ray fluorescence, and spectrographic methods. The samples collected by the Apollo 12 mission at the Ocean of Storms have a higher refractory-element content and lower volatile-element content than comparable terrestrial rocks.

We have determined the composition of two igneous rocks and four samples of fines from the lunar regolith collected by the Apollo 12 mission at the Ocean of Storms (Lunar Sample Preliminary Examination Team, 1970). The igneous rocks have similar mineral assemblages but different proportions of pyroxene, olivine, plagioclase, and ilmenite. Sample 12018,34 was received as two small rock fragments, and sample 12021,78 was received as pulverized material. The particle size of three of the samples of lunar regolith was less than 1 mm, and the fourth consisted of particles 1 to 2 mm in size.

The data presented in this report were obtained by a combination of semimicro analytical techniques: X-ray fluorescence, atomic absorption, flame photometry, wet chemical (titrimetry and spectrophotometry), and optical spectroscopy. Major elements were determined by X-ray and chemical methods (Rose and others, 1970a, b). Trace elements were determined by d-c arc spectrographic methods (Annell and Helz, 1970a, b). A related study of seven additional lunar samples was made by the authors and is reported in a companion paper (Annell and others, 1971) (p. C179–C181, this chapter).

The major-element analyses are given in table 1. As with the Apollo 11 samples (Rose and others, 1970a, b), there are notable differences between the igneous rocks and lunar fines in the Apollo 12 samples. The Al_2O_3, Na_2O, K_2O, and P_2O_5 values are higher in the lunar fines, whereas FeO and MnO are higher in the igneous rocks.

The two igneous rocks analyzed show minor but significant variation in chemical composition, particularly in MgO (table 1). This variation reflects a higher content of mafic minerals. The total reducing capacity of Apollo 11 samples from Tranquillity Base was considerably higher than the determined values for FeO (Rose and others, 1970a, b). This excessive reducing capacity suggests the presence of other reduced species such as metallic Fe or Ti(III). Although the reducing capacity and TiO_2 values are much lower in the Apollo 12 than in the Apollo 11 samples, the exact reason for these relationships is unknown.

The results of trace-element analyses are given in table 2. The two lunar igneous rocks are different from the lunar fines and have higher Mn and V contents and a higher Cr/Ni ratio. The Cr, Co, and Ni contents of rock 12018,34 are significantly higher than those in rock 12021,78. Compared with the igneous rock samples, the lunar fines are characterized by higher concentrations of Rb, Li, Ni, Ba, Sr, Be, Nb, La, Y, Yb, and Zr. Sample 12033,59 is considerably different from the other three analyzed lunar fines as shown by higher content of Rb, Li, Ba, Sr, La, Y, Yb, and Zr, and a higher Cr/Ni ratio and by lower contents of Co, Ni, and Zn. This sample (12033) has been tentatively considered by the Lunar Sample Preliminary Examination Team (1970) to be a crystal-vitric ash with similarities to terrestrial volcanic ash.

Several critical elemental ratios also distinguish the igneous rocks from the lunar fines as given in table 3. The Fe/Ni ratios for the two igneous rocks are much higher (1,900 and 11,000) than the ratios of 500–800 in the fines. The Rb/Sr, Ni/Co, and Ba/V ratios are lower in the rocks when compared with the fines.

In summary, the Apollo 12 lunar materials have the same nonterrestrial compositional character as the Apollo 11 samples, being low in volatile-element and high in refractory-element concentrations.

This research was undertaken on behalf of the National Aeronautics and Space Administration under contract No. 8-078049, order No. T-75447.

REFERENCES

Annell, C. S., Carron, M. K., Christian, R. P., Cuttitta, Frank, Dwornik, E. J., Helz, A. W., Ligon, D. T., Jr., and Rose, H. J., Jr., 1971, Chemical and spectrographic analyses of lunar samples from Apollo 12 mission, *in* Geological Survey Research 1971: U. S. Geol. Survey Prof. Paper 750-C, p. C179–C181.

U.S. GEOL. SURVEY PROF. PAPER 750-C, PAGES C182–C184

Table 1.—*Chemical composition of some Apollo 12 lunar materials, in weight percent*

Constituent	Rocks		Fines			
	12018,34	12021,78	12033,59	12042,40	12070,90	12070,143b
SiO_2	43.6	46.7	47.2	45.7	45.7	46.0
Al_2O_3	8.28	11.1	14.3	13.0	13.0	12.7
FeO	20.6	19.1	14.2	16.2	16.4	16.4
MgO	15.1	7.38	9.28	10.4	10.5	9.56
CaO	8.54	11.5	10.6	10.6	10.4	10.6
Na_2O	.26	.30	.66	.54	.48	.47
K_2O	.04	.05$_2$	.41	.25	.23	.23
H_2O^-	.10	.05	.00	.00	.00	.00
TiO_2	2.60	3.45	2.48	2.71	2.78	2.82
P_2O_5	.07$_0$	.08$_8$	.52	.33	.32	.32
MnO	.28	.27	.19	.24	.23	.22
Cr_2O_3	.69	.38	.32	.39	.42	.43
Total	100.16	100.37	100.16	100.36	100.46	99.75
Total Fe as Fe_2O_3	22.9	21.2	15.8	18.0	18.2	18.2
Total reducing capacity as FeO.	20.7	19.2	14.5	17.8	17.9	17.9
ΔRC	.1	.1	.3	1.6	1.5	1.5

NOTES:

1. ΔRC—total reducing capacity measured for the lunar materials less the reducing capacity attributable to their FeO content.
2. Lunar Receiving Laboratory (LRL) classification for the allocated returned Apollo 12 samples:
   12018,34—olivine dolerite (selected sample).
   12021,78—pigeonite dolerite, pegmatite (selected sample).
   12033,59—fines (documented sample), <1 mm.
   12042,40—fines (documented sample), <1 mm.
   12070,90—fines (contingency sample), <1 mm.
   12070,143b—fines (contingency sample), 1–2 mm.

Table 2.—*Trace-element abundances in Apollo 12 lunar materials determined by optical emission spectroscopy, in parts per million*

Element	Rocks		Fines			
	12018,34	12021,78	12033,59	12042,40	12070,90	12070,143b
Zn	N.D.	4.0	<4	7.5	7.6	8.2
Cu	8.1	14	8.7	10	14	11
Ga	5.0	5.4	5.2	4.4	4.8	5.0
Rb	1.2	1.4	10.3	5.5	5.2	5.9
Li	6.0	6.6	23	16	15	15
Mn	2,000	2,160	1,430	1,620	1,670	1,540
Cr	4,600	3,180	2,960	2,930	3,220	2,430
Co	70	36	36	52	49	49
Ni	84	13	137	235	215	150
Ba	67	88	667	445	420	430
Sr	58	73	137	110	115	125
V	158	147	106	108	110	114
Be	1.6	1.9	8.0	6.8	4.3	3.2
Nb	<10	16	38	26	29	30
Sc	42	48	38	38	38	44
La	N.D.	N.D.	61	48	46	39
Y	37	48	190	128	133	142
Yb	5.4	5.7	20	14	14	12
Zr	99	112	645	482	462	410

NOTES:

1. Elements are listed in approximate order of decreasing volatility in the d-c arc.
2. The following elements were looked for but not detected (N.D.) in the analyzed samples:
   If present, they would be in concentrations below those indicated in parentheses. Ag (0.2), As (4), Au (0.2), B (10), Bi (1), Cd (8), Ce (100), Cs (1), Ge (1), Hf (20), Hg (8), In (1), Mo (2), Nd (100), P (2,000), Pb (1), Pt (3), Re (30), Sb (100), Sn (10), Ta (100), Te (300), Th (100), Tl (1), U (500), and W (200).
3. See table 1 for description of samples.

Table 3.—*Significant elemental ratios of the Apollo 12 lunar samples*

Sample	Fe/Ni	Rb/Sr	Ni/Co	Cr/V	Cr/Ni	Ba/V
12018,34	1,908	0.021	1.2	29.1	55	0.42
12021,78	11,415	.019	.36	21.6	245	.60
12033,59	807	.075	3.81	27.9	22	6.3
12042,40	536	.050	4.52	27.2	13	4.1
12070,90	596	.045	4.39	29.3	15	3.8
12070,143b . .	794	.047	3.98	21.8	16	4.0

Annell, C. S., and Helz, A. W., 1970a, Emission spectrographic determination of trace elements in lunar samples: Science, v. 167, no. 3918, p. 521–523.

——1970b, Emission spectrographic determination of trace elements in lunar samples from Apollo 11, *in* Levinson, A. A., ed., Proceedings of the Apollo 11 Lunar Science Conference, Houston, Texas, January 5–8, 1970, v. 2, Chemical and isotope analyses: New York, Pergamon Press, p. 991–994.

Lunar Sample Preliminary Examination Team, 1970, Preliminary examination of lunar samples from Apollo 12: Science, v. 167, no. 3923, p. 1325–1339.

Rose, H. J., Jr., Cuttitta, Frank, Dwornik, E. J., Carron, M. K., Christian, R. P., Lindsay, J. R., Ligon, D. T., and Larson, R. R., 1970a, Semimicro chemical and X-ray fluorescence analysis of lunar samples: Science, v. 167, no. 3918, p. 520–521.

——1970b, Semimicro X-ray fluorescence analysis of lunar samples, *in* Levinson, A. A., ed., Proceedings of the Apollo 11 Lunar Science Conference, Houston, Texas, January 5–8, 1970 v. 2, Chemical and isotope analyses: New York, Pergamon Press, p. 1493–1497.

PLANT NUTRIENTS AND THE ESTUARY MECHANISM IN THE DUWAMISH RIVER ESTUARY, SEATTLE, WASHINGTON

By L. J. TILLEY and W. A. DAWSON, Tacoma, Wash.

Prepared in cooperation with the Municipality of Metropolitan Seattle (Metro)

Abstract.—The Duwamish River estuary traps plant nutrients in the water of its salt wedge. Analyses of input and output of nutrient concentrations in the estuary show a nearly twofold increase in concentrations of nutrients in the salt wedge. The increase consists of nutrients transferred from the outflowing river water in amounts which barely affect river-water concentrations

Estuaries are traps which accumulate solids borne in suspension by their river inputs. Many estuaries confine sea water in subsurface salt wedges, and they can act as entrapments for plant-nutrient salts. Data illustrating these phenomena, which require consideration when one evaluates the effects of manmade nutrient inputs to an estuary, are presented in this paper.

The U.S. Geological Survey and the Municipality of Metropolitan Seattle (Metro) are engaged in a long-term comprehensive study of the influence of waste disposal upon the water quality of the Duwamish River estuary. Study of the effects of changes in waste-disposal practices began in 1964. In 1965, Metro constructed the large Renton Sewage Treatment Plant, 21 river kilometers above the mouth of the estuary (fig. 1). Discharge of treatment-plant effluent was 38,000 m^3/day (cubic meters per day) in 1965 and has increased each year, but the ultimate plant-design capacity of 545,000 m^3/day will not be reached for some years. Industrial wastes and sewage that entered downstream from the treatment plant are being diverted from the river, the estuary, and Elliott Bay to an interceptor trunkline sewer which, when completed, will take them to a second plant for primary treatment and final disposal at a depth of 230 feet in Puget Sound.

The Renton Sewage Treatment Plant employs the high-rate activated-sludge process followed by secondary sedimentation and by chlorination. The plant is efficient, for it removes 92–98 percent of the biochemical oxygen demand, but, as is usual with the activated-sludge process, the effluent contains most of the incoming plant-nutrient salts and is particularly high in ammonium ion.

The Duwamish River estuary is two layered from its mouth to a point halfway upstream to its confluence with the Green River at river kilometer 18.3. The upper layer of the estuary is mixed salt and fresh water, and the lower layer is mostly unmixed salt water. The seaward end has tides that reach an extreme range of 4 meters. The upstream end of the estuary receives fresh-water inflow from the Green River averaging 2,200 m^3/min (3,160,000 m^3/day). (The Black River which formerly joined the Green River at river kilometer 18.3 was completely diverted in 1915, leaving the Green River as the sole source of fresh water for the Duwamish.) Maximum recorded Green River inflow is 20,000 m^3/min (28,800,000 m^3/day), and minimum flow is 400 m^3/min (576,000 m^3/day). This fresh-water inflow is but one of two water inputs to the estuary. Because the upper layer has a net transport seaward and consists of mixed fresh and salt water, there must necessarily be a net inward flow of salt water beneath to replace the salt water lost by way of the upper layer. Figure 2 is a schematic longitudinal profile of the estuary. The pathways of the two water inputs are traced by arrows.

PROCEDURES AND METHODS

As pointed out by Ketchum (1967, p. 329), estuaries can be fertilized from three principal sources: (1) the submerged countercurrent or salt wedge, fed by sea water which has been below the sea surface and hence is enriched in nutrients; (2) man-introduced nutrients supplied either directly into the estuary or to the river input; and (3) the natural river water itself, enriched by nutrients leached from the soil. The nutrient-sampling program, which lasted from March 1967 to July 1968 and which yielded the data interpreted here, was designed to evaluate the input from these three sources. The area covered by the program extends from a station 1.9 km upstream from the mouth to a point above the Renton Sewage Treatment Plant outfall, at river kilometer 21.1, well above any salt water in the estuary. Each day of sampling resulted in nine samples being collected at six places, monthly in winter and weekly in summer. Locations of the sampling points are listed in table 1 and are shown by their identifying letters in figures 1 and 2.

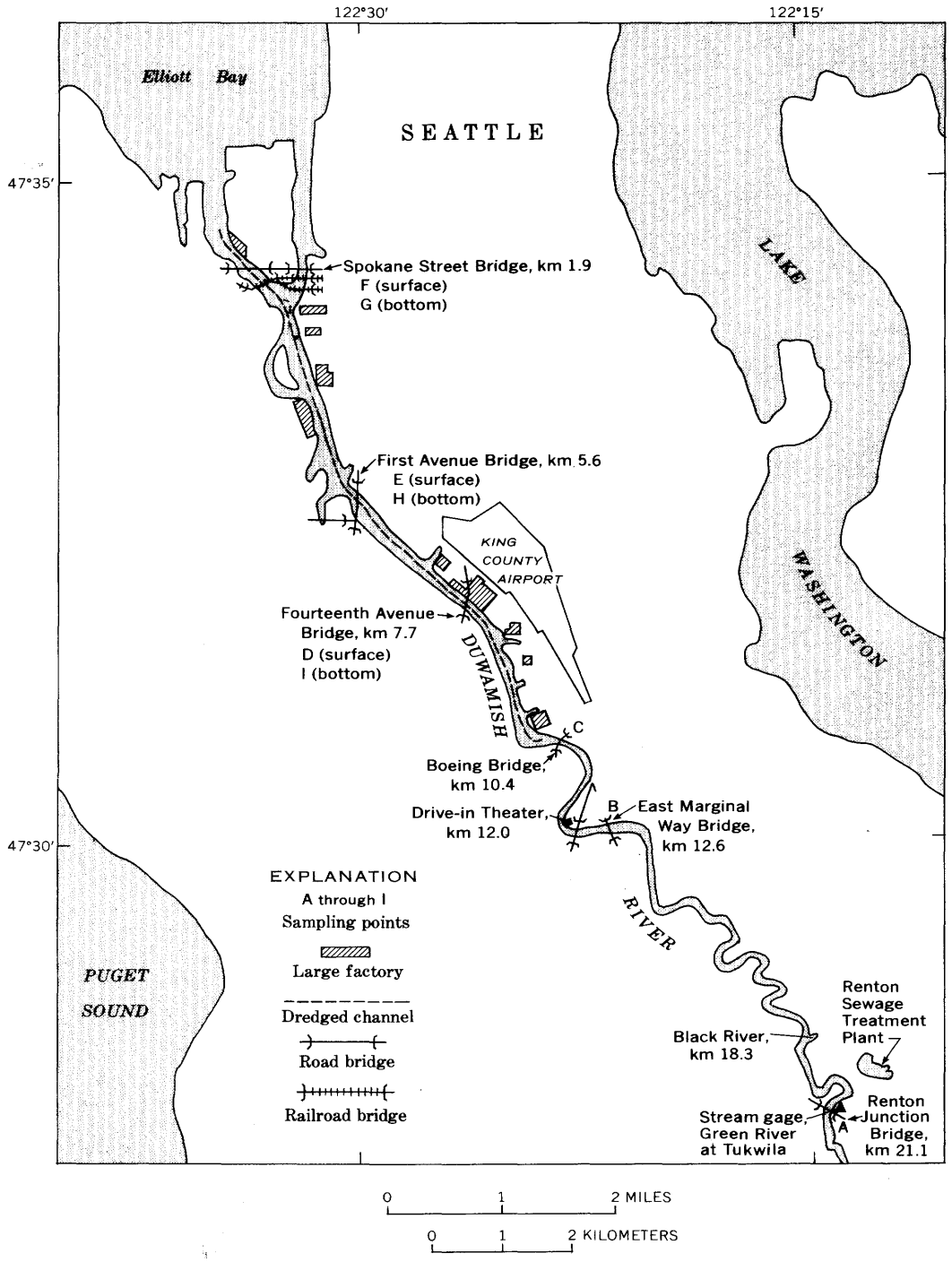

Figure 1.—Duwamish River estuary, Seattle, Wash., showing sampling points.

Sampling procedures were in general the same as those of Welch (1969, p. A7). Separate notes (W. A. Dawson, written commun., 1969) cover details of collection and handling of samples where our procedures differed from those of Welch. It was not possible to perform the standard analyses for plant nutrients in all their generally recognized forms. The samples were analyzed for total phosphate, soluble phosphate (Strickland and Parsons, 1965, p. 44), particulate phosphate, and ammonium ion (American Public Health Association, 1965, p. 193). The analyses were performed by personnel in the Metro Water Quality Laboratory, Seattle.

Points G and A account for two of the three principal sources of fertilization. Point G represents the submerged countercurrent source (the salt wedge), point A represents the inflowing fresh-water source, and point B serves as an indirect measure of the increment added by the Renton Sewage

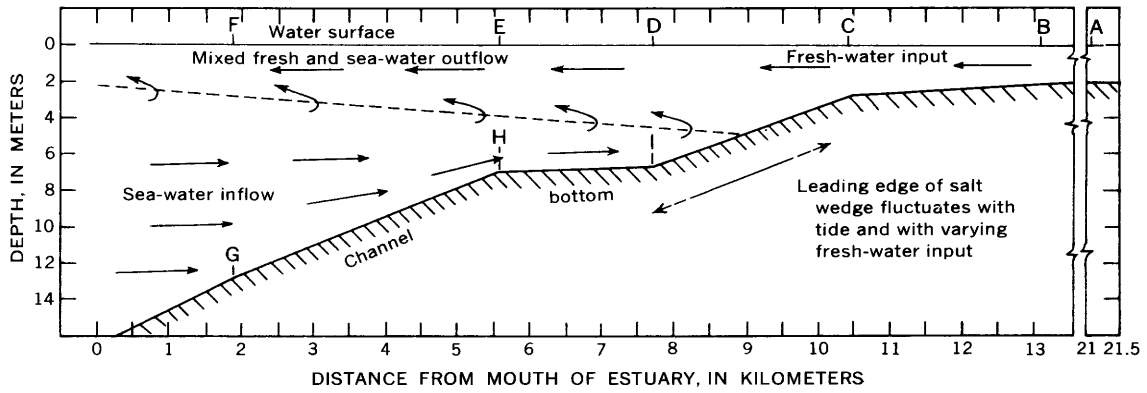

Figure 2.—Schematic longitudinal section of Duwamish River estuary, showing pathways of water movement (arrows) and location of sampling points (A–I).

Table 1.—*Description of plant-nutrient sampling points in the Duwamish River estuary, Seattle, Wash.*

Sampling point	Distance upstream (river km)	Sampling depth	Location name	Metro location identifier
A	21.1	1 m below surface	Renton Junction Bridge	311S
B	12.6	. . .do. . .	East Marginal Way Bridge	309S
C	10.4	. . .do. . .	Boeing Bridge	308S
D	7.7	. . .do. . .	14th Avenue Bridge	307S
E	5.6	. . .do. . .	First Avenue Bridge	306S
F	1.9	. . .do. . .	Spokane Street Bridge	305S
G	1.9	1 m above bottom	Spokane Street Bridge	305B
H	5.6	. . .do. . .	First Avenue Bridge	306B
I	7.7	. . .do. . .	14th Avenue Bridge	307B

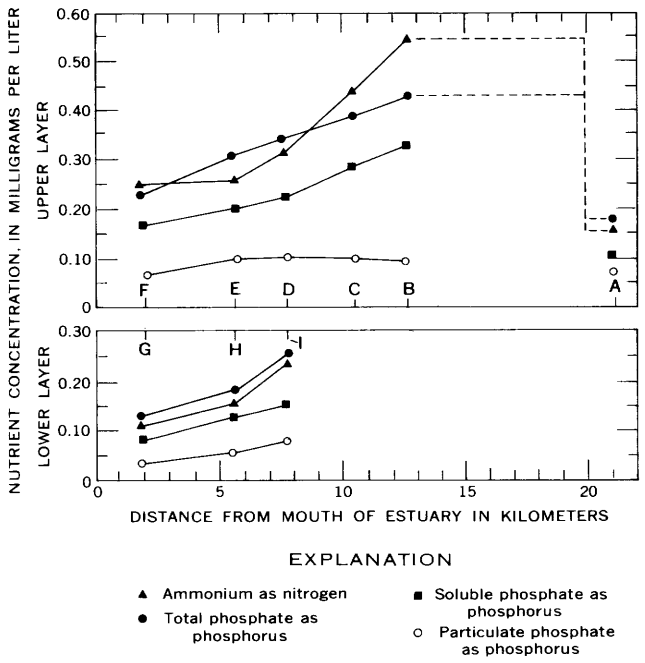

Figure 3.—Mean nutrient concentrations along the Duwamish and lower Green Rivers and in the salt wedge at sampling points A through I. (Dashed where inferred to be contribution from treatment plant; see text.)

Treatment Plant. There was no one location suitable for measuring the contribution of all the remaining outfalls, which are scattered, but the effluent discharge from the Renton plant is the largest single nutrient source: the highest mean concentrations were at point B, below which is a continuous decline (fig. 3, table 2, and Welch, 1969, p. 27) in spite of the numerous outfalls in the lower estuary.

RESULTS

Figure 4 shows how riverflow affects nutrient concentration in the upper Duwamish River (points A and B). Total phosphate is used as an example; concentrations of other nutrients are affected in a similar manner. Lack of comparable water-flow data for the salt-water part of the system precluded such a calculation for points C through F and G through I. The plots for points A and B indicate nearly constant nutrient loads from Green River and the Renton Sewage Treatment Plant, except during very high riverflows. At such times nutrient load jumps higher probably because of scour of organic matter from both the riverbed and from trunkline sewers (fig. 4).

The mean values for nutrient concentrations in table 2 are not time weighted, but they are otherwise comparable to those of Welch (1969, p. A24), who described the distribution of nutrient concentrations in the upper layer only, using data he gathered from 1964 to 1967. The writers' more recent upper-layer mean values for concentrations are in overall

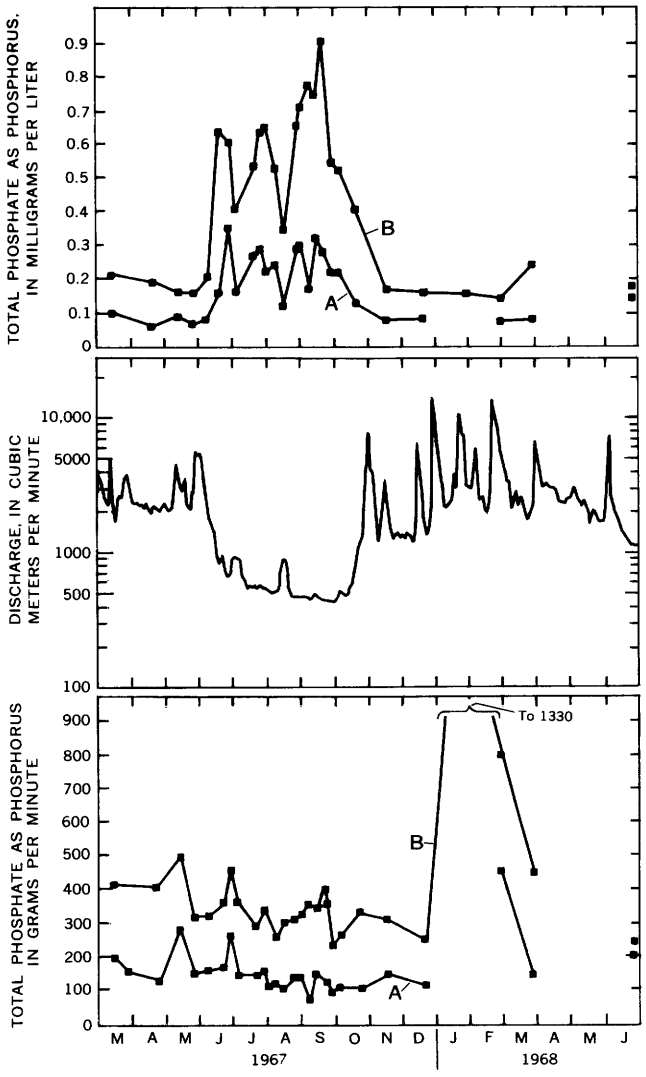

Figure 4.—Phosphate concentrations at sampling points A and B (top), discharge of Green River at Tukwila (center), and amounts of phosphate passing sampling points A and B (bottom).

agreement with his, and so are the conclusions that (1) all concentrations increase between points A and B (fig. 3); (2) all concentrations decrease from point B to point F; (3) concentrations tend to increase with a decrease in fresh-water inflow (fig. 4); (4) the increased concentrations do not, therefore, necessarily indicate higher nutrient load; and (5) total phosphate and ammonium being discharged by the Renton Sewage Treatment Plant account for the nutrient increases between points A and B, on a discharge-weighted basis.

In addition to continuing the previous upper-layer sampling program, the present study has been expanded to sample nutrients in the salt wedge. This expanded program enabled the writers to compare nutrient inputs and to assess the possible effects on the estuary in a manner not available to Welch. The first finding from the expanded sampling was that the nutrient concentrations in the salt wedge increased upstream from the mouth of the estuary (table 2 and figure 3, points G–I). There are two possible explanations for this. First, since the river water has higher nutrient concentrations than does the incoming salt-wedge water, dilution of the salt water by the fresh water could raise salt-wedge nutrient concentrations. However, by the time the salt-wedge water reaches point I (river km 7.7) it has acquired only 7.5 percent river water (table 3). In order that this small increment of river water double the nutrient concentrations in the salt wedge between points G and I, the river water at point B would have to contain about 12 times the nutrient concentration of the incoming wedge water at point G. In reality the river water has only about 4 times as much nutrient material, specifically, 3.5 times as much total phosphate; 4.0, soluble phosphate; 3.3, particulate phosphate; and 4.9, ammonium.

The second possible explanation is that the nutrients in the overlying fresh water somehow leave the fresh water and sink into the salt wedge beneath. This pathway is open to particulate nutrients, and one can readily assume that the nutrient-bearing particle load of the upper layer will lose a fraction to the salt wedge by settling out as the upper layer

Table 2.—*Nutrient concentration and salinity at sampling points on the Duwamish and lower Green Rivers, March 1967–July 1968*

[Number of samples taken at each sampling point is 24. $\bar{x}$, mean; s, standard deviation]

Sampling point	Phosphate–phosphorus (mg/l)						Ammonium nitrogen (mg/l)		Salinity (ppt)	
	Total		Soluble		Particulate					
	$\bar{x}$	s	$\bar{x}$	s	$\bar{x}$	s	$\bar{x}$	s	$\bar{x}$	s
A	0.19	0.089	0.11	0.055	0.08	0.071	0.16	0.055	0.0	0.0
B	.46	.23	.36	.20	.10	.055	.59	.30	.9	1.7
C	.41	.19	.30	.14	.11	.071	.48	.34	3.2	4.9
D	.36	.14	.24	.13	.11	.055	.33	.23	7.1	13.5
E	.29	.10	.20	.077	.09	.055	.26	.12	10.5	6.3
F	.24	.099	.17	.073	.07	.033	.26	.15	17.0	9.1
G	.13	.063	.09	.054	.03	.026	.12	.29	28.0	.675
H	.19	.11	.12	.055	.07	.077	.16	.071	27.6	1.29
I	.24	.10	.15	.071	.09	.055	.24	.18	26.9	1.39

moves past on its way seaward. The increase in the concentration of dissolved nutrients in the salt wedge is harder to account for, since material in solution cannot be transferred from one solvent to another without mixing the solvents. A less direct pathway can be assumed, however. Dissolved nutrients can leave the water of the upper layer if (1) they are transferred to the particulate phase by phytoplankton growth in the upper layer of the estuary; (2) some of the plankton produced in the upper layer sinks into the wedge; and (3) some of what sinks into the wedge, decomposes there, and releases its nutrients into solution.

The reality of the gradients was verified with analysis of variance tests showing that, for ammonium, total phosphate, and soluble phosphate, there is one chance in two hundred of the gradients shown in figure 3 being the result of random fluctuation. For particulate phosphates in the wedge the chance of the gradient being merely random fluctuation increases to one in a hundred. However, the lack of a gradient in particulate phosphates in the upper layer was also verified by the same test. We did not attempt to estimate the probability that all the gradients in figure 3 would decline in the same direction as a result of random fluctuation; we believe that it is low.

A direct test of the hypothesis that nutrients are transferred downward from the overlying mixed layer of the estuary to the salt wedge beneath possibly could be made by comparing the decrease of discharge-weighted nutrient load borne by the upper layer with the increase of discharge-weighted nutrient load borne by the salt wedge. However, such a test must await improved data on the turnover times of both upper-layer and salt-wedge waters.

In the absence of the data on turnover times, a simple test was devised to see whether the decline in nutrient concentration in the river water outruns the decline to be expected on the basis of dilution with sea water. The sources of a given liter of water at points C through F were derived by the following argument: The travel path for fresh water is A-B-C-D-E-F (fig. 2). Enroute, the salinity of the upper-layer water increases as it entrains and is mixed with water from the salt wedge beneath. Note, in table 2, the continuous gain in salinity from point B to point F (and the small decline in salinity from G to I). Following the order shown by the arrows in figure 2, the waters from points C through F were resolved into two-component mixtures, using the algebra of simple mixtures and the sample salinity values shown in table 2. The calculated compositions of the waters at these points are listed in table 3. Point C, which is shown in figure 2 as being upstream from the tip of the salt wedge, receives increments of salty water on floodtide excursions.

Because the nutrient concentration of each component was known, the nutrient concentration to be expected in each mixture could be calculated. For each nutrient listed there were 24 sets of samples, each set comprising those samples collected the same day. It was planned to compare the average expected nutrient concentration in the upper layer, calculated on the basis of dilution of fresh water by salt water, with the average measured concentration. A meaningful comparison of values was not expected from within any single set of nutrient samples, but it was expected that the mean values for each sampling point would yield a useful comparison. Nevertheless, the nutrient values to be expected by dilution alone were calculated for the individual sample sets in order to compute the variance of the samples. A statistical test of the significance of the difference between "calculated" and "measured," making use of this sample variance, was chosen. The statistical "sample" for this test became those measurements of a single nutrient made the same day and used in a dilution calculation. Means of the 24 individual calculations are listed in the first column of table 4. The second column of this table contains the means of the corresponding 24 measured values. The third column lists the means of the individual differences, not merely the difference between a calculated value and a measured value.

Table 3.—*Mean salinity, percentage composition, and calculated makeup of mixed waters at upper-layer sampling points*

Sampling point	River kilometer	Mean salinity, ‰ ppt	Salt water (percent)	Fresh water (percent)	Makeup of water, assuming other sampling point sources (percent)
A	21.1	0.0	0.0	100.0	
B	12.6	.9	6.8	93.2	
C	10.4	3.2	11.4	88.6	90.8 B and 9.2.I
D	7.7	7.1	27.5	72.5	83.5 C and 16.5 I
E	5.6	10.5	37.5	62.5	82.8 D and 17.2 I
F	1.9	17.0	60.7	39.3	61.9 E and 38.1 H
G	1.9	28.0	100.0	0.0	
H	5.6	27.6	98.5	1.5	
I	7.7	26.9	92.5	7.5	

We chose the test with the form

$$t = \frac{\bar{d}-0}{s/\sqrt{N}},$$

where

t = 2.069 or more signifies that the difference between observed and calculated values is significant at the 0.95 probability level when there are 23 (N-1) degrees of freedom,

$\bar{d}$ = mean difference, observed and calculated,

s = standard deviation of the "samples," and

N = number of samples.

The t values and their interpretation are given in table 4. We concluded that the decline in concentration of nutrients

Table 4.—*Mean differences between the nutrient concentrations measured and the concentrations calculated on the assumption that salt water dilutes fresh water*

[Value of t and significance of difference at 0.05 level ($t_{0.95}(23) = \pm 2.069$). Each mean calculated value is the mean of 24 individual calculations derived from groups of 9 samples collected the same day paired with individual sample values of that day. Mean differences are means of individual measured-calculated differences]

Sampling point	Mean (mg/l)			t value	Significant difference
	Calculated	Measured	Difference		
Total phosphate–phosphorus					
C	0.42	0.41	0.004	0.39	No
D	.37	.36	.015	.64	No
E	.33	.29	.040	3.13	Yes
F	.26	.24	.022	1.00	No
Soluble phosphate–phosphorus					
C	0.30	0.30	0.016	0.75	No
D	.28	.24	.042	2.47	Yes
E	.22	.20	.021	1.79	No
F	.16	.17	-.008	-.62	No
Particulate phosphate–phosphorus					
C	0.10	0.11	-0.016	-0.14	No
D	.11	.11	-.006	-.47	No
E	.11	.09	.025	1.62	No
F	.10	.07	.038	2.64	Yes
Ammonium nitrogen					
C	0.51	0.48	0.030	0.56	No
D	.44	.33	.104	2.87	Yes
E	.32	.26	.064	2.50	Yes
F	.23	.26	-.031	.12	No

moving downstream in the upper layer of the estuary can be accounted for by dilution alone in 11 of the 16 possible places for which the dilution effect was calculated.

The distribution of the five significant differences had no obvious pattern with respect either to position on the estuary or type of nutrient. Not unexpectedly, the significant differences are the large ones, and in support of our view of the upper layer as the source for the increase in salt-wedge nutrients, all the significant differences are positive. That is, where a significant difference occurs, smaller concentrations than those expected from dilution are found in the upper layer.

DISCUSSION

Two pathways or mechanisms can transfer nutrients out of the upper layer into the salt wedge: a direct one for particulate nutrients and the indirect one outlined in the previous section, for dissolved nutrients. A third pathway could account at least in part for the downstream decline in ammonium concentrations. Nitrification—the biochemical oxidation of ammonium to nitrite and nitrate—in the upper-layer water enroute downstream would show up as a decline in ammonium concentration. However, the best available estimates of travel-time (or residence time) are in hours (not days or weeks) for upper-layer water (J. D. Stoner, written commun., 1969). In this amount of time no more than 15 or 20 percent of the upper-layer decline is likely to be accounted for by this pathway. In the salt wedge the upstream increase in ammonium concentration might be accounted for with a corresponding denitrification argument, except that denitrification is an anaerobic process and the salt wedge is not anoxic.

Hutchinson (1957, p. 852–861) observes that ammonium does not seem to behave as a free ion but rather as though it is sorbed to particles in suspension, such as silt or clay. The reach of greatest silt fallout probably lies between C and D, where the estuary widens and deepens abruptly. Here the mean velocity of the river drops as its cross section increases, resulting in a corresponding loss of suspended load. Here also, Welch (1969, p. A44–A45, fig. 18) located the reach with the highest biochemical oxygen demand and the lowest dissolved oxygen in the bottom waters.

To make a quantitative comparison of the three pathways along which ammonium can decrease in the lower estuary, ammonium, nitrite, and nitrate must be measured at several points both in the upper layer and at depth within a time interval small enough to allow synoptic sampling. Salinity must be measured at the same time and equivalent coverage of the phosphorus compounds is highly desirable. Samplings like

this should be repeated at intervals, and the whole sampling process must be accompanied by estimates of residence time, both for upper-layer water and salt-wedge water. The lack of concurrent data on residence-time variation would preclude any comparison of loss from the upper layer with gain in the salt wedge, especially within any short series of synoptic samplings. The residence time of the salt-wedge water is not the same as that of the overlying water, nor is the ratio between the two times likely to be constant.

With the requisite information on how residence times vary, the three ammonium-decline pathways could receive a quantitative comparison—after dilution and loss to the wedge have been accounted for, any remaining decline could be ascribed to nitrification. A comparison of corresponding changes within the overall phosphate budget could serve both as a cross-check on settling-loss calculation and, by means of nitrogen-phosphorus ratios, as an additional source of new information about the estuarine ecosystem.

Because time as a factor is measured, such an expanded sampling program would amount to a study of the time course of nitrification. Full-scale tests of the results of laboratory-scale studies of this process are not readily available.

As the human management of natural bodies of water becomes more prevalent, studies like the one just outlined will provide information essential to the managers. In contrast, the present note represents only what can be accomplished in the absence of a nutrient budget—namely an indication of what processes are operative, without any analysis of rates of travel along the various pathways.

Phosphate and ammonium determinations are ordinarily carried out to microgram amounts per liter, but the concentration differences under discussion here are of the order of 0.01 mg/l or 10 μg/l—quantities by no means trivial. The evidence presented here for nutrient trapping in an estuary both by a physical mechanism and by a biological mechanism involves substantial quantities of plant nutrients.

The patterns of nutrient concentrations would not have been noticed without a clear understanding of the circulation in the estuary, gained from other phases of this study (Dawson and Tilley, unpub. data). Conversely, the nutrient patterns serve as an independent verification of the circulation paths and, as more of these data become available, may also provide additional insight into the residence times of waters in various parts of the estuary.

REFERENCES

American Public Health Association, 1965, Standard methods for the examination of water and wastewater [12th ed.]: New York, Am. Public Health Assoc., Inc., 769 p.

Hutchinson, G. E., 1957, A treatise on limnology, v. 1: New York, John Wiley & Sons, p. 852–861.

Ketchum, B. H., 1967, Phytoplankton nutrients in estuaries, *in* Estuaries, edited by George H. Lauff: Washington, Am. Assoc. Adv. Sci. Pub. 83, p. 329–335.

Strickland, J. D. H., and Parsons, T. R., 1965, A manual of sea water analysis [2d ed., revised]: Fisheries Research Board Canada, 203 p.

Welch, E. B., 1969, Factors initiating phytoplankton blooms and resulting effects on dissolved oxygen in Duwamish River estuary Seattle, Washington: U.S. Geol. Survey Water-Supply Paper 1873-A, 62 p.

DATA RELAY SYSTEM SPECIFICATIONS FOR EARTH RESOURCES TECHNOLOGY SATELLITE IMAGE INTERPRETATION

By JAMES F. DANIEL, St. Louis, Mo.

Work done in cooperation with the National Aeronautics and Space Administration

Abstract.—The first Earth Resources Technology Satellite (ERTS) for the Earth Resources Observation Systems (EROS) program is scheduled for launch in early 1972. Included among the experiments to be conducted with this satellite is the relay of ground-sensor data (primarily stream-gage height and quality parameters) in a near real-time mode. The goals of the experiment are to (1) provide ground truth to aid in interpretation of the imagery obtained from onboard sensors and (2) establish the feasibility of real-time data relay to the satellite for aid in river basin management.

Experiments with the Data Collection System (DCS) of the Earth Resources Technology Satellites (ERTS) have been developed to stress ERTS applications in the Earth Resources Observation Systems (EROS) program. To date (December 1970), the active pursuit of this policy has resulted in the design of eight specific experiments requiring a total of 98 DCS ground-data platforms (electronic package containing a transmitter and antenna). Of these eight experiments, six are intended to make use of DCS data as an aid in image interpretation, whereas two will make use of the capability to relay data from remote locations. Preliminary discussions regarding additional experiments indicate a need for at least 150 DCS platforms within the EROS program for ERTS experimentation. Results from the experiments will be used to assess the DCS suitability for satellites providing online, real-time, data relay capability.

The rationale of the total DCS network of ground platforms and the relationship of each experiment to that rationale will be discussed herein. Technical details of the DCS capability (Daniel, 1970) will not be discussed.

DESIGN GOALS

One of the key elements in determining ERTS performance requirements was, and is, the capability of satellite sensors to monitor change in terrestrial features. Changes occur in important features in all disciplines which will make use of ERTS data, but the time frame of change varies from a few minutes or hours for water features to geologic time for some land features. The concept of time rate of change is also important to the DCS. Ground data planned for relay in each of the experiments are applicable to one or more of several goals tentatively grouped into the two broad categories of interpretation aids and real-time uses.

Interpretation aids

Ground-sensed parameters which fulfill goals basically categorized as interpretation aids are those which furnish quantitative information regarding:

1. Conditions within an image or image set (solar radiation, air temperature, wind, and so forth).
2. Changes in successive images (water levels, precipitation, and so forth).
3. Image features (areal extension of point-collected water-quality data).
4. Applicability of images to the problem or experiment (water levels are high, low, median, and so forth).

Categories 1 and 4 require the collection of background data concurrent with imagery in order to fully satisfy requests for imagery representing specific climatic or hydrologic conditions.

All four of these categories have application to image interpretation whether there is a functioning DCS or not. A report on Apollo 9 photography (Powell and others, 1970) is an example of the use of ground data to help interpret imagery. All hydrologic data within the photographed area for the time of overflight, as well as all historical data for the area, were used to formulate a conceptual working model of the geohydrologic system in that area. This use of ERTS–A data will be typical and significant, but the model can be constructed within a leisurely paced time frame. When interpretation of the imagery must proceed in real time, the DCS is required in order to shorten the data collection process, and a conceptual or mathematical model of the system being studied must already be in existence. The criteria for experiments with the DCS related to interpretation are: (1) relayed

parameters must relate to one or more of the four stated categories; (2) a working model of the image area must be in existence; and (3) interpretation must be done in near real time (hours or a very few days).

Real-time uses

The other advantages of the DCS which include ground-sensed parameters usable in real time are:

1. Ground sensors may be located where they cannot be physically reached in a reasonable time frame (mountainous or estuarine environments).
2. Data may be used by management units for operational decision making (hydroelectric power development, municipal water supplies, and so forth).
3. Data are the basis for standing requests for imagery collection and (or) precision processing for specific climatic or hydrologic conditions (ERTS data management).
4. Ground sensors are useful in determining proper exposure or probability of successful exposure of satellite sensors (net or total radiation in ERTS spectral bands; oceanic turbidity near shore for effect on bottom detail).

The last advantage specifically relates to satellite sensor management, little of which may be done with ERTS–A (excluding tape recorder usage). However, experimentation with these sensors on ERTS–A will allow development of techniques for managing forthcoming operational satellites.

These four uses are intrinsically time related and hence require a real-time data relay system. The sole criterion for experiments with the DCS related to real-time uses is that the DCS (exclusive of satellite cost) be an economical method of data collection at the present time.

Very few management requirements for data can be satisfied with the once-every-12-hour capability of ERTS–A for data collection. Most users will eventually require an online capability. Therefore, the performance of the DCS in all the experiments will be used to determine the applicability of an ERTS relay system to the economic alternative of a series of orbiting satellites, geosynchronous satellites, or combination of the two. Each of these alternatives would supply an online data relay capability.

PLANNED EXPERIMENTS

There are, to date, eight planned DCS experiments for ERTS, each of which satisfies one or more of the design goals. These experiments represent the major disciplines of hydrology, geology, and geography and will be discussed in the order of listing in table 1.

Delaware River basin

This experiment is in effect a microcosm of the entire DCS rationale. The primary purpose is to obtain near real-time data from water-quality monitors and water-level monitors in the basin, to correlate the values with near real-time imagery (as obtained), and to use this information in the management decision processes of the Delaware River Basin Commission. Data from the platforms will also be used during the time between image overflights as input to management decisions. The experiment will focus primarily on the following questions: Is bulk-processed imagery satisfactory for management purposes, or is precision-processed imagery required? What logistical problems arise in supplying either type of imagery in real time? How are decisions modified with real-time imagery and real-time data? The experiment will add two dimensions to current operations: (1) The dimension of near real time (12 hours), and (2) the areal extension of point-collected water-quality data. This experiment is described in more detail by Paulson (1971) (p. C196–C201, this chapter).

Regional ecological test sites

Central Arizona, South Dakota, and Lake Ontario (numbers 2–4 in table 1) are regional test sites for ERTS that will have a few platforms for image interpretation purposes. Because there will be intensive ground-truth collection programs at these sites during image orbits, there is a need to be able to assess the ground conditions prior to the overflight. By use of data relayed from key sites in the test area, a decision can be made regarding whether conditions warrant a large, manned effort in the area during image overflights. Therefore, the investment of a small amount of money in platforms has a potential benefit of saving several times that amount by reducing unnecessary ground-truth collection as well as providing ground truth at key locations.

San Juan Mountains, Colo.

The DCS will provide near real-time data in this mountainous Colorado region for use in assessing the efficiency of the atmospherics research being conducted there. Climatic extremes will provide a good operational test of the DCS platforms in a hostile environment, and the test will produce more up-to-date data than are presently available. Image analysis assessing snow moisture conditions on an areal basis will also be aided.

Volcano monitoring

Experiments 6 and 7 will both be conducted on volcanoes in the Cascade Range, Wash., and in Central America, but in general these experiments will not be using the same platforms. One set of platforms will be located at optimum sites for measuring the number of seismic events and tilt, while the other set will be located at optimum sites for measuring subsurface temperature. These two experiments will utilize the capability of the DCS to relay data from remote locations, with the short-term goal of adding to the knowledge of

Table 1.—*EROS Data Collection System networks for ERTS experimentation*

Experiment location	Discipline	Purpose	Parameters	Number of platforms
1. Delaware River basin, Pennsylvania and New Jersey.	Hydrology	Water management.	Water quality. Stream stage. Reservoir stage. Ground-water stage.	20 ERTS–A
2. Central Arizona	. . .do. . .	Arid hydrology.	Precipitation. Solar radiation. Air temperature.	2 ERTS–A 4 ERTS–B 6 total
3. South Dakota	. . .do. . .	Snow and ice, shallow aquifers.	Ground-water stage. Air temperature. Solar radiation.	2 ERTS–A 4 ERTS–B 6 total
4. Lake Ontario, New York and Canada.	. . .do. . .	Prototype ocean, circulation.	Water quality. Current velocity and direction. Solar radiation.	2 ERTS–A 4 ERTS–B 6 total
5. San Juan Mountains, Colo.	. . .do. . .	Atmospherics modification.	Precipitation. Snow (water equivalent). Wind. Stream stage. Rime ice.	12 ERTS–A
6. Cascade Range, Wash.; Central America.	Geology	Volcano monitoring.	Seismic events. Tilt.	10 ERTS–A 20 ERTS–B 30 total
7. . . .Do. . .	. . .do. . .	. . .do. . .	Temperature.	5 ERTS–A 5 ERTS–B 10 total
8. Baltimore, Md.	Geography	Image evaluation.	Solar radiation.	8 ERTS–A
				98 total

eruptive processes and the long-term goal of eruption prediction at these and other volcanoes.

Baltimore, Md.

The Geographic Applications Program will relay data from eight platforms in the Baltimore, Md., area for two primary purposes. The first is to provide an intensively instrumented solar radiation test site to determine methods of image processing to adjust for atmospheric attenuation conditions. Results from this site will be used to develop methods of extrapolating solar radiation data from a single monitor to larger areas. Successful experimentation would mean that recorded solar radiation data from several agencies' ongoing programs (for example, the National Weather Service's network of ground stations) could be used for image processing control in many other parts of the country. The second purpose is to develop criteria for management of satellite sensors in order to operate those sensors only under acceptable conditions, as indicated by real-time solar radiation data.

RELATIONSHIP TO AIRCRAFT PROGRAM

For several of the experiments relating to image interpretation, aircraft imagery in the ERTS spectral bands is required in order to complete the local DCS networks. As aircraft data are obtained, the local networks of ground sensors (in some cases these number in the hundreds) will be analyzed to determine which types of sensors and how many of each type are desirable for DCS instrumentation. After this preliminary analysis, the final choice of sites will be made. During the actual experiments, aircraft flights are needed at some sites during ERTS image overflights for integrated ground, air, and space data collection. Therefore, many of these experiments will be included in the aircraft program.

SUMMARY

The EROS program plans experiments with the DCS requiring 98 ground platforms, but indications are that this number will shortly be increased to 150. Uses of the DCS can be basically categorized as interpretation aids or as near real-time data collection. Although only the Delaware River basin experiment embraces nearly all of the possible reasons for using the DCS, each of the other experiments relates in a particular manner to the total rationale.

REFERENCES

Daniel, J. F., 1970, Satellite (ERTS–A) network of ground data sensors–A user-oriented experiment: Natl. Symposium on Data and Instrumentation for Water Quality Management Proc., Univ. of Wisconsin, July 1970, p. 166–175.

Paulson, R. W., 1971, The role of remotely sensed and relayed data in the Delaware River basin, *in* Geological Survey Research 1971: U.S. Geol. Survey Prof. Paper 750–C, p. C196–C201.

Powell, W. J., Copeland, C. W., and Drahouzal, J. A., 1970, Delineation of linear features and application to reservoir engineering using Apollo 9 multispectral photography: Alabama Geol. Survey Inf. Ser. 41, 37 p.

THE ROLE OF REMOTELY SENSED AND RELAYED DATA IN THE DELAWARE RIVER BASIN

By RICHARD W. PAULSON, Harrisburg, Pa.

Work done in cooperation with the National Aeronautics and Space Administration

Abstract.—The U.S. Geological Survey operates a system of hydrologic stations in the Delaware River basin that provides data to water-resources agencies in the basin. Data from 20 stations will be radiotelemetered from the basin to the Earth Resources Technology Satellite—A (which will be launched in 1972) and related to a ground acquisition site. The data will be sent by landline teletype from the acquisition site to the Geological Survey's Current Records Center in Philadelphia for dissemination to water-resources agencies. The existing time lag of 2 weeks to 2 months between data collection and dissemination can be reduced to 12 hours.

For several years the U.S. Geological Survey has operated a system of water-quality monitoring stations in the Delaware River basin that provides riverine and estuarine water-quality data to water-resources agencies in the basin. This report is a discussion of the planned integration of the existing monitoring and data-processing systems with a data-relay experiment proposed for the Earth Resources Technology Satellite (ERTS), the first one (ERTS–A) of which will be launched in 1972. A description of the data-relay system of the ERTS program and how the Delaware River basin experiment fits into the system is given by Daniel (1971) (p. C192–C195, this chapter). The experiment is designed to use ERTS–A as a data-relay link for a maximum of 20 hydrologic stations in the basin, including stream gaging, reservoir level, ground-water level, and water-quality monitoring stations. This experiemnt has the potential for reducing the timelag between data collection and dissemination to less than 12 hours. At present there is a significant lag between the time the data are recorded at a monitoring site and the time the water-resources agencies receive the data. The timelag exists because most of the instruments operate in remote locations without telemetry, and the data records are removed manually, generally at a weekly frequency. For most water-quality monitoring, the data do not reach water-resources agencies for a period of 2 weeks to 2 months.

WATER-RESOURCES MANAGEMENT IN THE DELAWARE RIVER BASIN

Several governmental agencies are concerned with the daily status of the quality and quantity of surface and ground waters in the Delaware River basin. The chief water-resources agency in the basin is the Delaware River Basin Commission (DRBC), which was authorized by the Delaware River Basin Compact, Public Law 87-328. This compact, whose signatory parties are the U.S. Government and the States of Delaware, New Jersey, New York, and Pennsylvania, became public law in 1961. It requires the DRBC to develop, adopt, and maintain a comprehensive plan for the orderly development of the basin's water resources. The basin commissioners, who are the governors of the four States and a Presidential appointee (currently the Secretary of the Interior), have a permanent staff that is charged with the management of the water resources of the basin. Projects and areas of research for the plan include water supply, flood protection, stream quality, recreation, fish and wildlife, pollution abatement, and regionalization of waste treatment.

As a Federal-State compact, the DRBC is a uniquely authorized regulatory agency that has adopted a plan for managing the water resources of the Delaware River basin, including pollution abatement in the Delaware River estuary. The pollution abatement plan is expected to produce a measurable improvement in water quality in the next several years at a cost of several hundred million dollars. The water-quality monitoring program of the Geological Survey is one of several sources of data for the commission.

For many years the city of Philadelphia has been interested in the water resources of the Delaware River basin and the water quality of the Delaware River estuary. Since 1946 the city's water department, which uses the estuary as a major water-supply source, has spent "... nearly $300 million to expand and modernize its wastewater system. About $100 million of this has gone into facilities that directly protect the

rivers . . . ." (City of Philadelphia, 1970). In participating in the DRBC's pollution abatement plan, Philadelphia ". . . will expand its water pollution control plants and replace many of the older tributary sewers" at a cost that ". . . . may exceed $200 million in the next decade . . . ." (City of Philadelphia, 1970). The water department has supported the operation of the water-quality monitoring system to ". . . warn of industrial spills, temperature rises, salt-water influx, sewage problems, . . . other forms of pollution . . . [and to provide] data for long-range prediction of river conditions." (City of Philadelphia, 1970).

A third agency concerned with the daily status of water resources in the basin is the U.S. Geological Survey's Office of the Delaware River Master. The River Master is charged with implementing a decree of the U.S. Supreme Court, which resolved a conflict of water-supply need. On a daily basis, and in accordance with the decree, the River Master prescribes releases of water from New York City reservoirs in the Delaware River basin to maintain the required level of streamflow and monitors withdrawals from the reservoirs for New York City's water supply.

State health and natural-resource agencies, municipalities, and Federal agencies, including the Army Corps of Engineers and the Federal Water Quality Administration, also have need for water-resources information in the basin.

DELAWARE RIVER BASIN WATER-QUALITY MONITORING AND DATA-PROCESSING SYSTEMS

The Geological Survey's water-quality monitoring system is composed of continuously operating instruments that record dissolved-oxygen concentration, temperature, specific conductance at 25°C, and pH at 11 sites in the basin (see fig. 1). The system, which is cooperatively supported by the Geological Survey, the Philadelphia Water Department, the Delaware River Basin Commission, the Delaware Geological Survey, and other local, State, and Federal agencies, provides water-resources agencies with data on stream quality in the major rivers of the basin in addition to the Delaware River estuary and Delaware Bay.

Many of the monitors operate in remote locations where seasonal ranges in temperature and humidity are large, where sediment, algae, and other debris in the water adversely affect sensors and water-sample transfer systems, where ice and wave motion can damage sensors in the stream, and where vandalism contributes to equipment failure. For example, two of the stations frequently operate for long periods of time between servicing visits because they are on islands in the Delaware River estuary and Delaware Bay and are very difficult to service, especially during the winter months when high winds and ice make conditions very hazardous. A continuing effort is made to protect the instruments from environmental hazards, and field calibration checks are run on the instruments at every opportunity. Nevertheless, although monitors work well

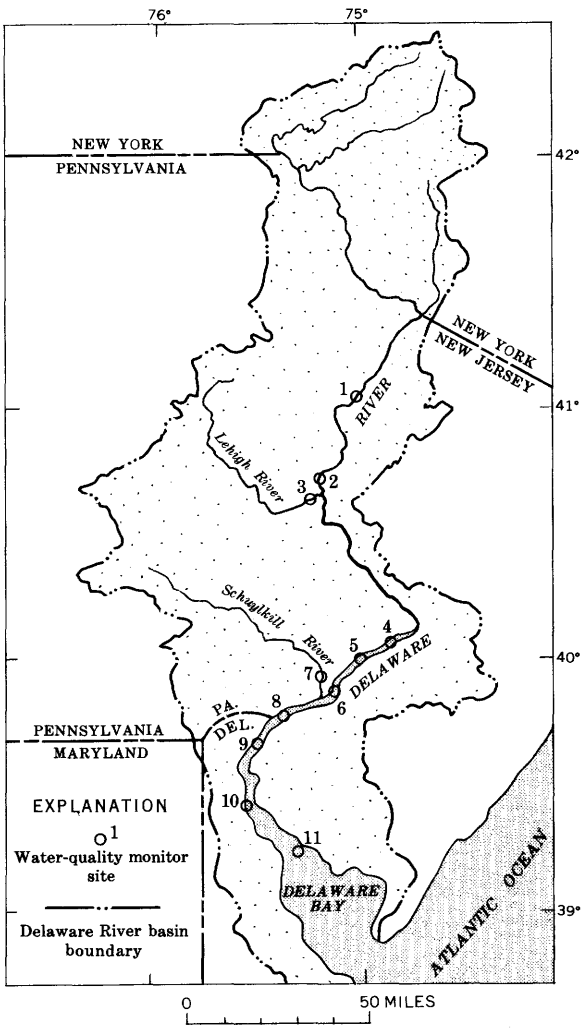

Water-quality monitor sites:

1. Delaware River near East Stroudsburg, Pa.
2. Delaware River at Easton, Pa.
3. Lehigh River at Easton, Pa.
4. Delaware River at Bristol, Pa.
5. Delaware River at Torresdale, Philadelphia, Pa.
6. Delaware River at Benjamin Franklin Bridge
7. Schuylkill River at Philadelphia, Pa.
8. Delaware River at Chester, Pa.
9. Delaware River at Delaware Memorial Bridge
10. Delaware River at Reedy Island Jetty, Del.
11. Delaware River at Ship John Shoal Lighthouse

Figure 1.—Location of U.S. Geological Survey water-quality monitor sites in the Delaware River basin.

most of the time, they do fail occasionally. As will be discussed subsequently, data must be continuously screened for equipment failures, some of which cannot be detected in the field.

The value of the large mass of water-quality data presently being collected is diminished because of the timelag between data collection and dissemination. In recognition of this, efforts are made to disseminate some of these data more rapidly. The monitoring station at the Benjamin Franklin Bridge (Pier 11 North) is in one of the most heavily polluted

reaches of the estuary and is near the Geological Survey's Current Records Center (CRC) office. This station is serviced daily, and preliminary water-quality data are released via teletype (fig. 2) to several agencies. A summary of water-resources conditions is also recorded each day, and agencies can telephone directly for information. These releases provide the DRBC with data from a key estuary station. A second key station is at Reedy Island Jetty, Del., where the quality of the water is better than that in the more upstream Philadelphia-Chester reach of the estuary. This station also is valuable because it is in the salt-water intrusion zone of the estuary and because a large nuclear electric generating station, potentially capable of altering the thermal regime of the estuary, is being constructed near the station. In response to the key role of the station, the DRBC has requested that the Geological Survey install landline telemetry from the Reedy Island monitor to the CRC during fiscal year 1971. Upon installation of telemetry, the daily release shown in figure 2 will be expanded to include these data.

In addition to the daily teletype summaries of data from the Benjamin Franklin Bridge station, preliminary weekly and monthly summaries also are released for data not yet completely through the CRC processing system.

AN APPROACH TO PROCESSING SATELLITE–RELAYED HYDROLOGIC DATA

It is expected that a maximum of 20 hydrologic sites in the basin will be instrumented with radiotelemetry at the time of launch of ERTS–A. The 20 sites will include most, or all, of the water-quality monitors in figure 1, plus key stream-gaging stations and reservoir and ground-water level stations. Data from these sites will provide water-resources management agencies with indices of water quality, streamflow, reservoir levels, and ground-water levels. The radiotelemetry will provide a redundant communications link with at least one station, because by March 1972 the Reedy Island monitor will have landline telemetry. The landline telemetry will help to provide a sound basis for measuring the utility and accuracy of three modes of operation: (1) no telemetry, (2) conventional landline telemetry, and (3) satellite-relayed telemetry.

Radiotelemetry instrumentation, which is still under development, will be designed to broadcast a brief data message from each station once every 90 or 120 seconds. Although the data will be telemetered continually, data will be relayed only when the satellite is simultaneously in view of both the radio transmitter at the station and a receiving station, called an acquisition site. The acquisition site for data relayed from the Delaware River basin is at the National Aeronautics and Space Administration's (NASA) Goddard Space Flight Center in Greenbelt, Md. Figure 3 gives the four or more periods of time during the daily passes of the satellite over the basin when a hydrologic station and the acquisition site are both in view of ERTS. A data message is broadcast every 90 or 120 seconds; so, there will be 4–7 data messages sent during a 10-minute period of mutual visibility every 12 hours. Seventeen days are represented in figure 3 because the orbital pattern is repeated at a 17-day frequency.

The NASA Goddard acquisition site will have a very high probability of receiving satellite-relayed data from each of the Delaware basin stations at least once every 12 hours. These data will be processed and relayed by NASA to the CRC on the Bell System teletype network, which is the system the CRC uses for data dissemination. After the CRC receives data from a water-resources station the data will be screened before dissemination.

The screening process for data from a particular station, while highly speculative at present, will probably include a comparison of the data with data recently received from that station. This comparison will be made for estuary stations at least because the day-to-day changes of water-quality conditions usually are small. On the other hand, as daily changes in stage can be large at stream-gaging stations (especially during periods of heavy rainfall), such a comparison alone would not be valid for them.

It also will be useful to compare the data with summaries of recent historical data at a station. Summaries for Delaware estuary stations are becoming available as a result of a recent

```
FM:  US GEO SURVEY PH

TO:  GEO SURVEY TNT, GEO SURVEY HBG, WB-TNT, WB-HBG, DRBC

SUBJ:  DAILY WATER QUALITY OF DELAWARE ESTUARY AT
       BEN FRANKLIN BRIDGE (PIER 11 NORTH) PHILA PA
DATE   D.O.(MG/L)      TEMP.(F)      SPEC.COND.(MICROMHOS)      PH
1/20   10.7 - 8.6      37 - 34       328 - 300                  7.1 - 6.9
1/21*  10.6 - 8.4      36 - 35       329 - 309                  7.1 - 6.9
* PROVISIONAL MAX AND MIN VALUES (MIDNIGHT - 8AM)
END/CRC

GEO SURVEY-PH
```

Figure 2.—A daily teletype release of Delaware River estuary water-quality data.

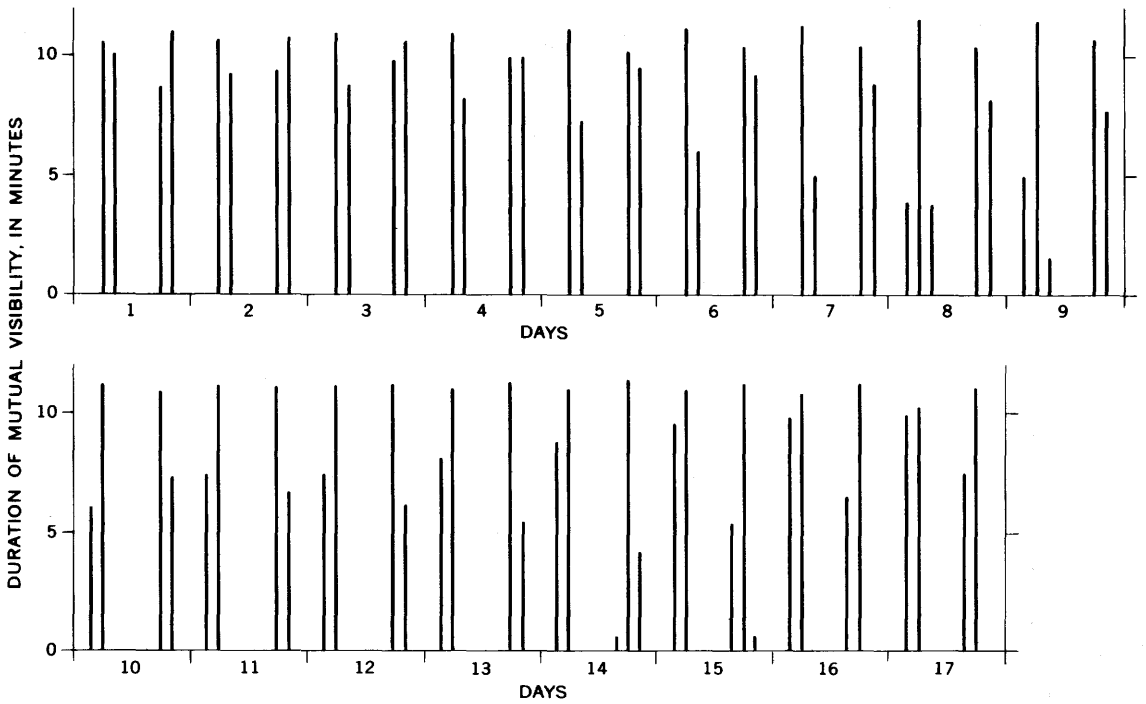

Figure 3.—Estimated periods of mutual visibility of a Delaware River basin hydrologic station and the National Aeronautics and Space Administration's Goddard Space Flight Center from a typical orbital pattern of the Earth Resources Technology Satellite.

CRC effort to provide water-resources agencies with comparisons of recent water-quality conditions and the new DRBC stream-quality objectives. Figure 4 is an example of a computer-generated summary for dissolved-oxygen concentration.

The dissolved-oxygen concentration summary (Merk, 1970) presented in figure 4 has time as the ordinate, or vertical coordinate. The water year (October 1–September 30) is broken down down into 122 periods of 3 days each. The abscissa or horizontal coordinate is dissolved-oxygen concentration, from 0 to 15 mg/l (milligrams per liter). The period October 1, 1964–September 30, 1969, or water years 1965–69, is summarized on the graph. The summary indicates the maximum and minimum concentrations recorded for each 3-day period during the 5 years, plus statistical information on the distribution of the 15 daily means. The DRBC stream-quality objectives are also plotted to provide a comparison of these data with the objectives of the DRBC pollution abatement program. Thus, dissolved-oxygen data received from this station can be referenced to this graph to determine whether or not the data are in the range of variation recently experienced. Of course, the graph will have to be updated as water-quality conditions improve in the estuary.

When the CRC receives satellite-relayed data they will be screened against the hydrologic range and variability of historical station data before being released. Criteria may have to be established to flag data when the hydrologic condition is extreme or outside the range of a permissible level established by water-resource management officials. Flagging of the data may be provided as a service to management officials.

CONCLUSION

Frequently, water-resources management agencies have difficulty taking action against unfavorable water-resource conditions because of lack of data or knowledge of the condition and the lack of means to affect a change. The result may be a persistent undesirable condition, such as pollution; or, as in the early 1960's during the Northeast drought, an imperiled water supply in part of the Delaware River basin. Difficulty may also be met in coping with short-term natural disasters such as the severe flooding, and concomitant loss of life and property, that occurred in August 1955 when two hurricanes swept across the Delaware River basin.

In meeting its obligation under the Delaware River Basin Compact, the DRBC has created a comprehensive plan to develop the water resources of the basin. The plan will provide the DRBC with the means of safeguarding the basin's water resources. In order to implement the comprehensive plan, the DRBC has encouraged and directly supported the system of hydrologic stations maintained by the Geological Survey in the basin and has supported the installation of telemetry at key locations. Thus, progress is being made to overcome some of the limitations that prevent water-resources officials from managing the basin's water resources.

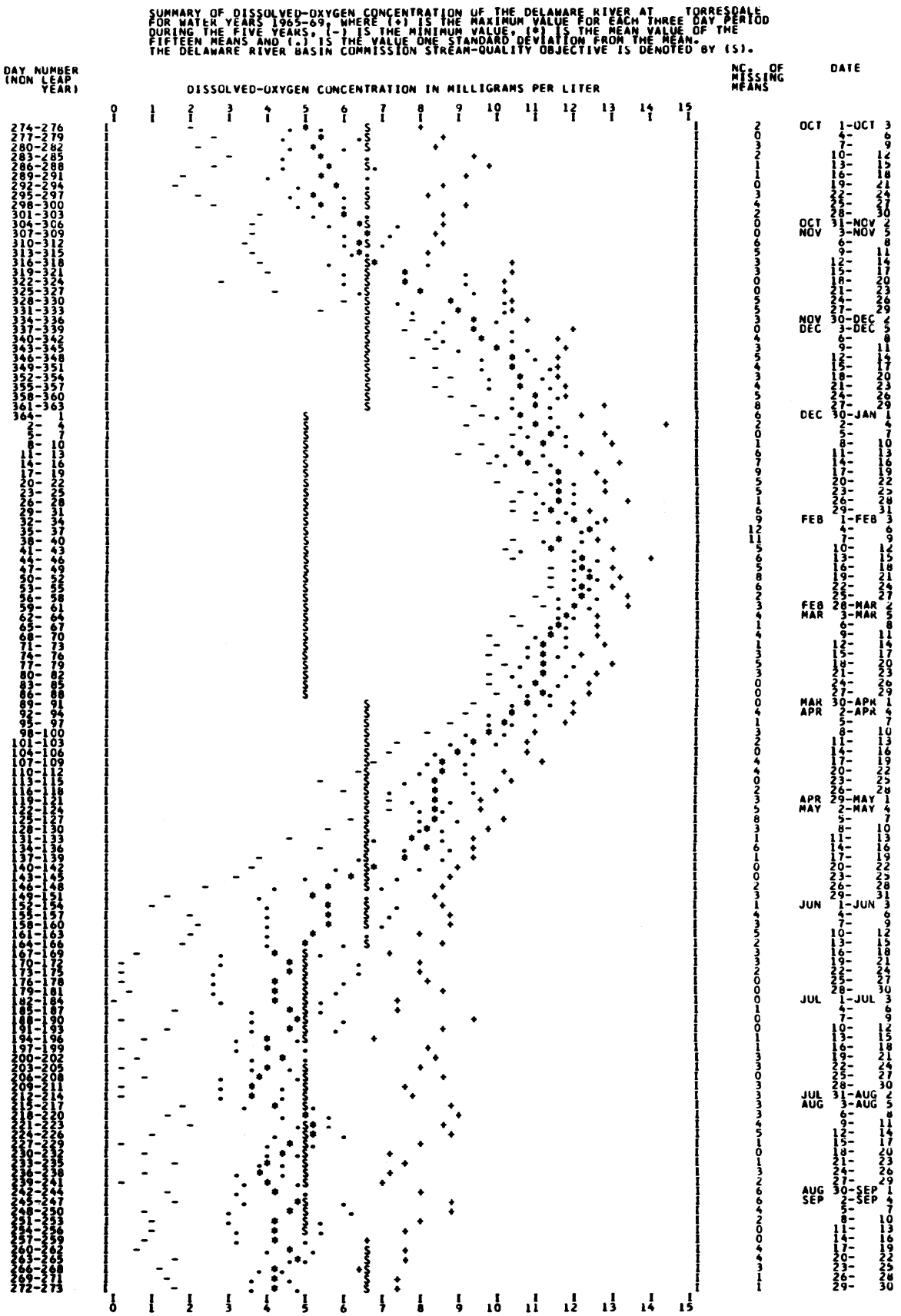

Figure 4.—Computer summary of dissolved-oxygen concentration data for the Delaware River at Torresdale, Philadelphia, Pa. (site 5, fig. 1).

The satellite data relay experiment discussed herein will determine whether satellite-relay data will be adequate to meet the data needs for responsible river basin management. It should provide the basis for determining whether or not data collected once every 12 hours from a tidal estuary are sufficient to meet these needs when the large ranges of particular parameters are weighed against time of collection within a tidal cycle. For some parameters, such a collection frequency may not be adequate, while for others it may.

The experiment will also provide impetus to develop an operational system of real-time data processing and dissemination to handle the large quantity of data that will be obtained from the stations in the basin. A library of the characteristics of hydrologic conditions at each site will be developed as reference material for screening the data as they enter the CRC. Where possible, digital-computer techniques for data summarization and screening will be developed. Human intervention in the system will probably be necessary to maintain quality control on the data.

Finally, as water-resources agencies develop the means for managing river basins, the results of this experiment will demonstrate the relative merits of satellite relay of data versus conventional means of data telemetry and will provide a basis for the development of operational satellite relay of hydrologic data.

REFERENCES

City of Philadelphia Water Department, 1970, Clean streams for Philadelphia, the city's $500 million river cleanup: Philadelphia, Pa., 36 p.

Daniel, J. F., 1971, Data relay system specifications for Earth Resources Technology Satellite image interpretation, *in* Geological Survey Research 1971: U.S. Geol. Survey Prof. Paper 750-C, p. C192–C195.

Merk, C. F., 1970, A graphical summary of dissolved oxygen data for the Delaware River estuary for water years 1965–69: U.S. Geol. Survey open-file report, 15 p.

CARBONATE EQUILIBRIA DISTRIBUTION AND ITS RELATION TO AN AREA OF HIGH GROUND-WATER YIELD IN NORTHWEST OHIO

By STANLEY E. NORRIS and RICHARD E. FIDLER,
Columbus, Ohio

Work done in cooperation with the Ohio Department of Natural Resources, Division of Water

Abstract.—The distribution of areas in northwest Ohio in which the ground water is most undersaturated with respect to calcium carbonate coincides closely with a regionally extensive strip of highly productive strata termed the high-yield area. Supported by the distribution pattern of selected chemical constituents in the ground water, the carbonate saturation data indicate that the high-yield area is the principal area of recharge to the limestone and dolomite aquifer. In achieving better understanding of this important aquifer system, the study will promote more effective development of Ohio's ground-water resources. The study demonstrates the applicability of a geochemical method developed in Florida to another limestone region.

In a previous paper (Norris and Fidler, 1971), the authors described the occurrence of ground water in limestone and dolomite aquifers in a 20-county study area in northwest Ohio. They showed that wells of highest yield, defined as those with specific capacities greater than 5 gallons per minute per foot of drawdown, are largely confined to a long striplike area that winds for many miles along the flanks of the Cincinnati arch, a generally north-south-trending regional anticline. A hypothesis, based in part on caliper-log data, was presented to show that the high-yield area is the result of ground-water solution acting over long intervals in the geologic past on a structurally controlled, and periodically emergent, peninsulalike landmass. The effects of solution are now largely restricted to the peripheral area of the original landmass as a result of subsequent erosion and removal of the beds that formerly made up its higher central part.

The northwest Ohio investigation was based on a drilling and aquifer test program in which the Division of Water, Ohio Department of Natural Resources, in cooperation with the U.S. Geological Survey, drilled and test pumped approximately 80 wells ranging in depth from about 200 feet to more than 400 feet.

Shortly after completion of the first part of the investigation, a special study of ground-water quality characteristics in northwest Ohio was made to determine whether the chemical properties of the ground water, especially carbonate saturation data and the distribution of selected chemical constituents, could provide further useful knowledge of the hydrologic system. Questions of primary interest were the location of principal recharge areas and the effects of the high-yield area on the system. The study was based on the work of Back (1963), Hanshaw, Back, and Rubin (1965), and Back and Hanshaw (1970), who investigated the geochemistry of ground water in the principal limestone aquifer in central Florida and developed the theory and field methods after which the northwest Ohio investigation was closely patterned. The authors are grateful for the help and advice of William Back, who visited the area and advised them on the theory and field techniques of analysis.

The investigation shows that the limestone and dolomite aquifers are principal components of a regional geochemical system, the characteristics of which confirm the hydrologic importance of the high-yield area.

THEORY AND METHODS

Back (1963) showed that in Florida the chemical character of the ground water is largely determined by the pattern of circulation within a limestone aquifer. He delineated recharge and discharge areas based on the distribution of selected chemical constituents in the ground water and the departure of the water from equilibrium with respect to calcite. Water in a recharge area, typically undersaturated with respect to calcium carbonate, was shown (Back and Hanshaw, 1970) to have been in contact with the aquifer a relatively short time. Such water is still dissolving limestone. As the water moves from the recharge area through the aquifer towards an area of natural discharge, its contact time with the limestone increases, and it becomes increasingly saturated, and eventually supersaturated, with respect to calcium carbonate minerals. Ultimately, the water may precipitate carbonate minerals,

U.S. GEOL. SURVEY PROF. PAPER 750-C, PAGES C202-C206

especially in areas of natural discharge where release of dissolved gases commonly occurs. One would expect, therefore, barring long-term changes in the flow system, that limestone aquifers would be of highest permeability in recharge areas where ground water is dissolving calcium carbonate (thereby enlarging fissures and other openings in the rocks) and of progressively lower permeability in areas downgradient from the recharge areas, where the water is dissolving less and less material or where perhaps it is precipitating material and reducing the size of whatever openings remain from earlier hydrologic regimens.

The concept developed in Florida appeared to offer much promise as applied to northwest Ohio, especially for determining aquifer recharge characteristics. The principal question was whether recharge occurred uniformly throughout the study area or whether water entered the aquifer chiefly in favored areas, such as through stream channels or in areas of thin glacial drift or high permeability. Knowing where and how the aquifer is chiefly replenished is highly important in understanding the hydrogeologic system in northwest Ohio and is essential to a comprehensive plan of water management for optimum water use.

Although interpretation of calcium carbonate saturation data is relatively straightforward, collection of samples and analysis of the data involve closely controlled conditions and highly exacting field procedures. As soon as water is withdrawn from a well, its chemical properties start to change as it typically begins to lose dissolved gases. These changes may be vastly speeded up if the temperature of the water is allowed to change appreciably.

The chemical equations used to determine the departure of the ground water from equilibrium with calcite and other solid phases are given by Back (1963). For acceptable accuracy, the pH and bicarbonate concentrations must be determined in the field. Required also in the equations are concentrations of other chemical constituents, obtained from standard laboratory analyses. Except for the calcium ion concentration, which was determined in the laboratory from an acidified sample collected when the field titrations were made, the concentrations of the other chemical constituents were obtained from standard analyses of water samples which had been collected from the wells when they were test pumped. The wells were test pumped shortly after they were drilled, in most instances several months before the field determinations were made. It was not practical to determine the significance of any differences in the chemical character of the ground water that may have occurred between the two times of sampling or because of the differences in methods of sampling.

Barnes (1964, p. 1–5) has described the procedures and instrumentation required to obtain representative and accurate values of pH and alkalinity in the field. In the northwest Ohio investigation, values of pH, bicarbonate, and specific conductance were determined within about 15 minutes after the sample had been collected from the well. The analytical apparatus was set up in a lightweight van, and the determinations were made at the well site. Most of the test wells are conveniently located alongside roads and were easily accessible. The wells were without pumps, and the 12-inch-diameter casings were covered with welded plates, into each of which was screwed a 4-inch-diameter access plug. The plugs were removed, and the wells were sampled by means of a thief-type sampler, holding a little more than a liter, which was lowered to the desired position below water level and closed by allowing a weight to slide down the retaining line. The water level in the wells ranged from a little above the ground surface in a few flowing wells to about 50 feet below the surface. In most wells the range was from about 10 to 20 feet below the surface. For consistency, each sample was taken at a depth approximately 100 feet below the water level in the well. Typically at this depth the sampler was several tens of feet below the casing, in the open hole part of the well. In rare instances where a well was cased to or below the preferred depth, the sample was taken at a lower depth to ensure that it came from the uncased part of the well where circulation of ground water was assumed to be more active.

AQUIFER CIRCULATORY SYSTEM

The principal aquifer in northwest Ohio is composed of hydraulically interconnected beds of Silurian-age limestone and dolomite, generally ranging in thickness from 200 to 500 feet. These carbonate rocks, exposed locally at the surface in quarries or the beds of shallow streams, underlie the generally flat and relatively featureless terrain beneath a thin covering of lacustrine clay or glacial till. Of prime hydrologic importance is the high-yield area (fig. 1), a sinuous band of highly permeable strata, 7 to 18 miles wide, believed to have resulted from ground-water solution in the geologic past of an early, relatively restricted landmass. Wells in the high-yield area typically pass through cracks and other openings in the rocks, and caliper-log data indicate that the rocks in the high-yield area contain more such openings than do the rocks outside this area. The high-yield area, as shown here, is based on the distribution of test wells having specific capacities greater than 5 gallons per minute per foot of drawdown (Norris and Fidler, 1971). The boundaries, based on scattered data, are approximate.

Regional flow of ground water in northwest Ohio is controlled by a generally uniform potentiometric surface (fig. 1) which slopes, as does the land surface, north and northeast toward Lake Erie, the chief area of natural ground-water discharge. By coincidence, the direction of ground-water flow is generally the same as the direction of dip, as indicated by the large arrows on figure 1, but the regional dip of the strata generally exceeds the slope of the potentiometric surface. For example, in the western part of the study area the regional dip is north 15–20 feet per mile, and the slope of the potentiometric surface is about 5 feet per mile. The shape of this surface is not notably modified by the high-yield area. The potentiometric high in the southern part of the study area

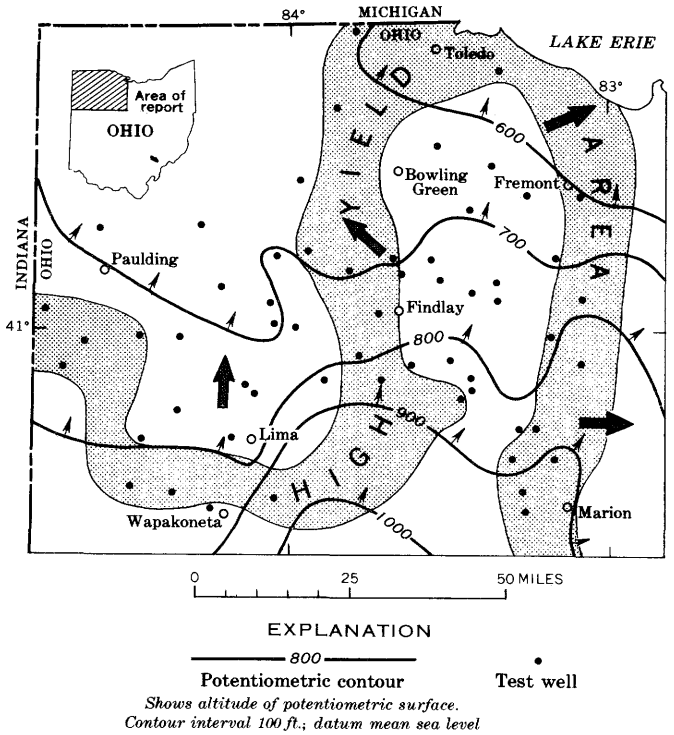

Figure 1.—Contours on the potentiometric surface in northwest Ohio, based on water levels in State-drilled test wells. Small arrows drawn perpendicular to potentiometric contours indicate direction of ground-water flow; large arrows indicate direction of dip of the consolidated rocks.

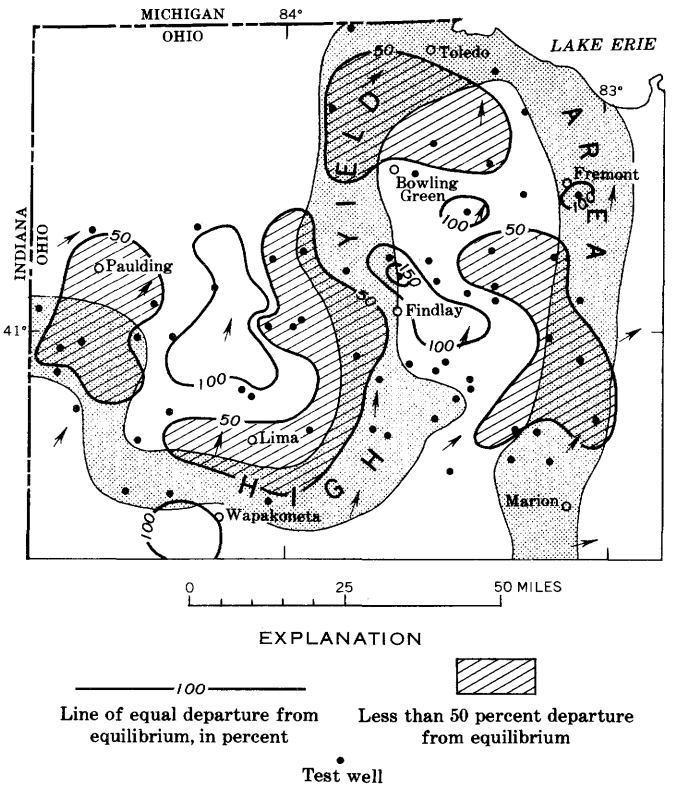

Figure 2.—Saturation of ground water in northwest Ohio with respect to calcium carbonate. Arrows indicate direction of ground-water movement.

conforms to a region of generally higher terrain, centering about 15 miles south of the study area.

CHEMICAL CHARACTERISTICS OF THE GROUND WATER

In the Florida investigation, it was shown that ground water is typically undersaturated in areas of major recharge and increases in saturation away from recharge areas. Figure 2 shows the departure of ground water from equilibrium with respect to calcite in northwest Ohio. Ground water in most of the study area is undersaturated; however, the water is most undersaturated in areas within, or on the periphery of, the high-yield area. The relationship is emphasized on figure 2 by the shading of areas in which the saturation of the ground water is less than 50 percent. The distribution of the shaded areas conforms fairly closely with the configuration of the high-yield area. As the boundaries of each of these areas are generalized, the actual degree of conformity may be even closer than shown here. The distribution of the most undersaturated areas may be a better guide, locally, to the availability of large ground-water supplies than is the indicated position of the high-yield area. It seems safe to say that the undersaturation of the ground water in locations within or contiguous to the high-yield area is strongly indicative that this area is the major area of recharge to the carbonate-rock aquifers in northwest Ohio.

Figures 3, 4, 5, and 6 show the distribution of selected chemical constituents in the ground water in northwest Ohio. Figure 3 shows the calcium concentration in the ground water, which generally ranges from 100 to 400 mg/l (milligrams per liter). The area of low calcium concentration (hatched) conforms reasonably well to the position of the high-yield area, but not as closely as do the areas of most undersaturated ground water.

The bicarbonate concentration in the ground water, shown in figure 4, generally ranges from 100 to 500 mg/l. The bicarbonate distribution conforms poorly with the calcium distribution, except that areas of low bicarbonate concentration coincide in a general way with areas of high calcium concentration. Areas of low bicarbonate do not relate significantly to the high-yield area, though they do coincide locally in the western and northern parts of the study area. Neither does the bicarbonate distribution bear an obvious relationship to the potentiometric surface. This lack of correlation is unlike conditions in Florida, where Back (1963) reported that the bicarbonate concentration decreases in the direction of ground-water movement. Figure 5 shows the distribution of specific-conductance values determined in the field. As expected, areas of low specific conductance coincide closely with areas of low calcium concentration (fig. 3).

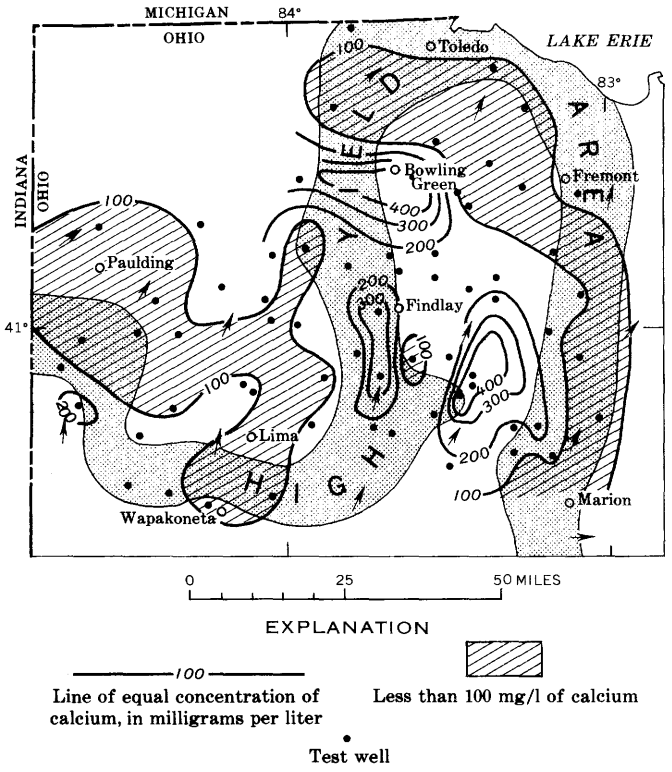

Figure 3.—Calcium concentration in the ground water, northwest Ohio. Arrows indicate direction of ground-water movement.

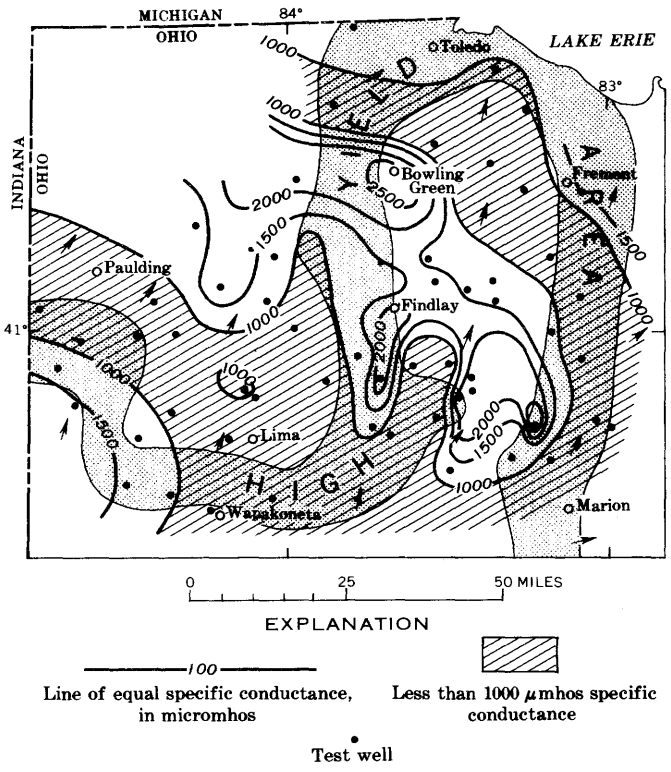

Figure 5.—Specific conductance of the ground water, northwest Ohio. Arrows indicate direction of ground-water movement.

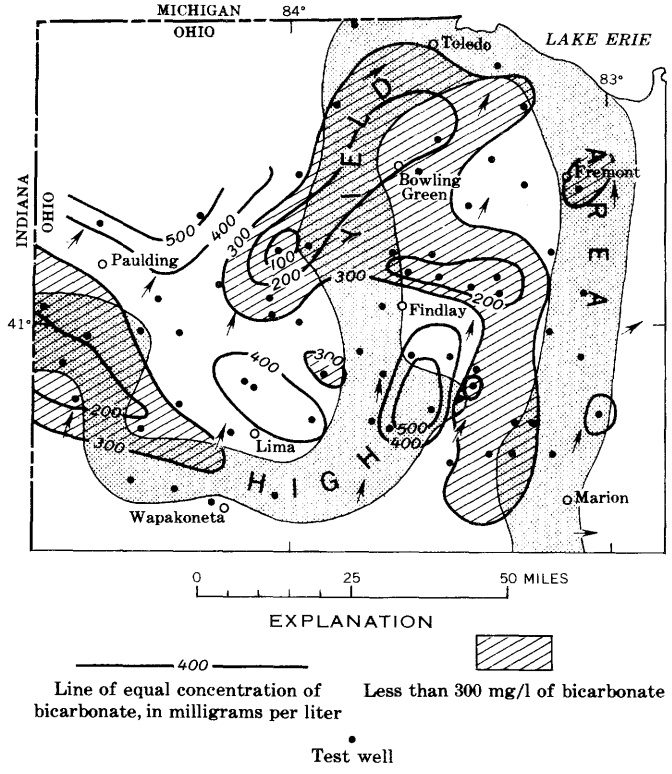

Figure 4.—Bicarbonate concentration in the ground water, northwest Ohio. Arrows indicate direction of ground-water movement.

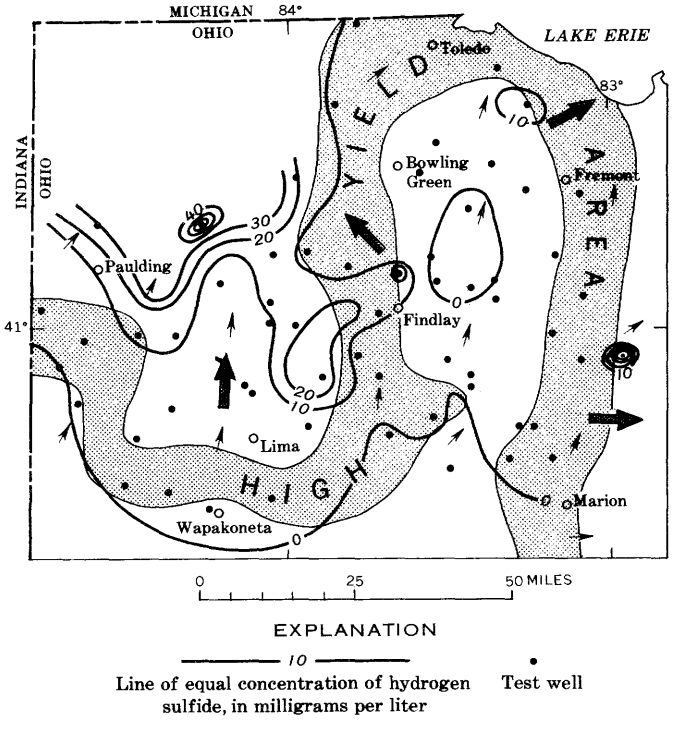

Figure 6.—Hydrogen sulfide concentration in the ground water, northwest Ohio. Large arrows indicate regional dip; small arrows indicate direction of ground-water movement.

Figure 6 shows the distribution of hydrogen sulfide (H_2S) in the ground water of northwest Ohio, based on laboratory analyses of samples collected when the test wells were pumped. The samples were treated in the field by the addition of zinc acetate to preserve the H_2S content. Comparison of the H_2S distribution (fig. 6) with the map of the potentiometric surface (fig. 1) shows that the H_2S concentration generally increases downdip, away from the high-yield area and in the direction of ground-water movement. This tendency is additional evidence that the high-yield area is a principal area of recharge. The H_2S content increases downgradient primarily because residence time in the aquifer increases as water moves away from the recharge area and circulates to greater depths.

The H_2S distribution shown in figure 6 must be viewed with some qualification, as it is not unusual for the concentration locally to vary with the depth of the well. Typically, the H_2S content increases with depth, and the water from a shallow domestic well in a given area might not be as high in H_2S as the value indicated by figure 6, which is based on analyses of samples from relatively deep test wells. In contrast, a few wells were observed during the test-drilling program in which the H_2S content of the water decreased with depth, and the water quality improved as the wells were deepened.

CONCLUSIONS

Maps of northwest Ohio showing the departure of the ground water from equilibrium with respect to calcite, and the distribution of selected chemical constituents in the ground water, indicate that the high-yield area is the major area of recharge to the limestone and dolomite aquifers. Solution by ground water is occurring in the high-yield area now, as in the geologic past. The water is actively removing material and enlarging fissures and other openings in the rocks through which it moves. The chemical data thus confirm the high-yield area as an extensive zone of high permeability, which underscores the importance of this area as a potential source of large ground-water supply.

Although modified to some extent by local conditions and other variable factors such as well depth, the chemical constituents in water from wells that substantially penetrate the aquifers show consistent patterns of distribution. Thus, the chemical characteristics of the ground water are generally predictable on an areal basis, meaning that wells can be selectively located, perhaps to avoid the undesirable effects of certain unwanted constituents, or for other reasons. Because of water-treatment costs, such an option is of obvious economic benefit and can be highly important to those seeking to develop ground-water supplies in northwest Ohio.

Use of carbonate saturation data to better define the hydrologic system in northwest Ohio demonstrates the applicability of a geochemical method developed in Florida to other limestone regions. Studies of the geochemistry of ground water can yield important knowledge of geologic processes and the effect of these processes on the hydrologic environment and can promote more effective use of aquifers and greater economy in the development of ground-water supplies.

REFERENCES

Back, William, 1963, Preliminary results of a study of calcium carbonate saturation of ground water in central Florida: Internat. Assoc. Sci. Hydrology Pub., v. 8, p. 43–51.

Back, William, and Hanshaw, B. B., 1970, Comparison of chemical hydrogeology of the carbonate Peninsulas of Florida and Yucatan: Jour. Hydrology, v. 10, no. 4, p. 330–368.

Barnes, Ivan, 1964, Field measurement of alkalinity and pH: U.S. Geol. Survey Water-Supply Paper 1535–H, p. H1–H17.

Hanshaw, B. B., Back, William, and Rubin, Meyer, 1965, Carbonate equilibria and radiocarbon distribution related to ground-water flow in the Floridan limestone aquifer, U.S.A.: Internat. Assoc. Sci. Hydrology Pub., v. 13, p. 601–614.

Norris, S. E., and Fidler, R. E., 1971, Availability of ground water from limestone and dolomite aquifers in northwest Ohio and its relation to geologic structure, *in* Geological Survey Research 1971: U.S. Geol. Survey Prof. Paper 750–B, p. B229–B235.

A METHOD FOR ESTIMATING EFFECTIVE POROSITY IN A RUBBLE CHIMNEY FORMED BY AN UNDERGROUND NUCLEAR EXPLOSION

By M. S. GARBER, Denver, Colo.

Work done in cooperation with the U.S. Atomic Energy Commission

Abstract.—Explosion of a nuclear device underground at the Nevada Test Site produced a rubble chimney which was completely dewatered at the time of its formation and required a period of about 5 years for infill to the preexplosion water level. Numerous pumping tests conducted during the period of infill of the chimney disclosed that pumping often caused an interruption in the rise of water level in the chimney. A method was devised for estimating the effective porosity of the chimney in selected zones by comparing the volume of water removed during a pumping test with the observed interruption in water-level rise resulting from infill. The porosity of the rubble chimney, determined by this method is between 1.5 and 7.9 percent.

The Bilby nuclear explosion took place on September 13, 1963, at a depth of about 2,300 feet beneath Yucca Flat, Nevada Test Site. The nuclear device, which had a reported yield of about 200 kilotons (TNT equivalent), was emplaced in saturated zeolitized tuff at a depth of about 732 feet below the water table.

The nuclear explosion created a nearly spherical cavity with an average radius of about 275 feet. Sphericity may have been distorted slightly by the presence of dense sedimentary rocks several hundred feet below the shot point. The roof of this cavity collapsed within 31 minutes after the explosion. As collapse progressed upward, it created a rubble chimney that extended to the surface and formed an irregularly shaped subsidence crater with a maximum depth of 81 feet and a radius of about 800 feet (Houser, 1970, p. 30).

The effect of the nuclear explosion on the aquifer relates principally to the distribution of pressure in the surrounding rocks. In general, at the time of cavity formation, the rocks surrounding a nuclear explosion are compressed and pore space, therefore, is slightly reduced. Above the cavity, unsupported rocks shift downward, filling the cavity and chimney with rubble. The net result of the compression and collapse produces a hydraulic sink above the explosion point, and a circular ridge is produced in the potentiometric surface in the vicinity of the rubble chimney, with the vertical axis of the explosion point as its center. Water from the ridge drains outward toward the surrounding part of the aquifer and inward to the rubble chimney (Piper and Stead, 1965, p. 49). As chimney filling proceeds, the ridge dissipates, and a cone of depression in the potentiometric surface then extends outward from the chimney. The configurations of the potentiometric surface are shown diagrammatically in figure 1.

The rate of inflow to the chimney and the time required for filling to the preexplosion level depends upon four principal factors—transmissivity of the contributing aquifer(s), chimney height and radius, porosity of the chimney, and difference between the water level in the chimney and the level of the potentiometric surface before the explosion. The infill curve for the Bilby chimney is shown in figure 2.

Five pumping tests, utilizing the reentry well, were run during various stages of chimney infill. In pumping tests 3, 4, and 5, the rise of water in the chimney was interrupted. This interruption delayed infill and offset the infill curve (fig. 3). The vertical component of this offset defines the height of a cylinder having a radius equal to that of the chimney that would have been filled under nonpumping conditions. The effective porosity of the chimney can be estimated by comparing the volume of pumped water with the volume of the described cylinder. The following equation illustrates the comparison:

$$\theta = \frac{V_w}{\pi r^2_{ch}\, h} \times 100,$$

where θ = porosity, in percent,
V_w = volume of pumped water, in cubic feet,
r_{ch} = radius of chimney, in feet, and
h = vertical displacement of infill curve, in feet.

This approximate equation is based on the assumption that the permeability in the chimney is several orders of magnitude higher than the permeability in the surrounding rock, and the

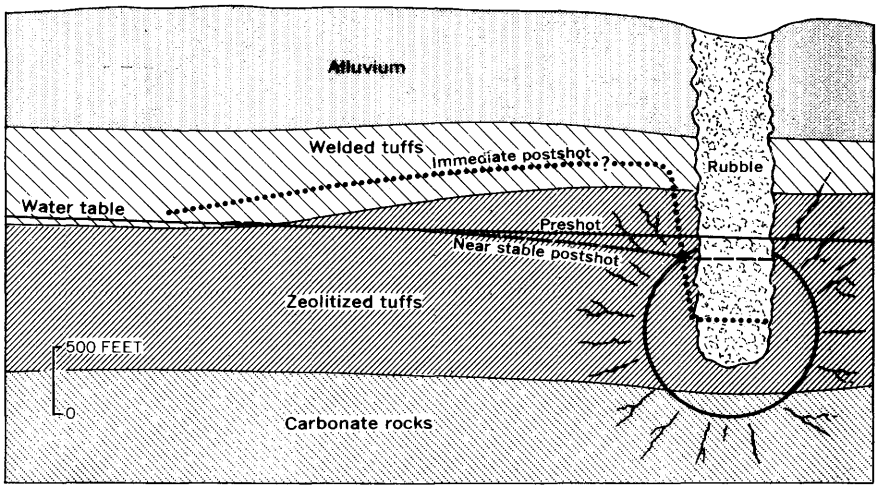

Figure 1.—Reaction of water table to the Bilby event, Nevada Test Site. After Houser (1968, p. 28).

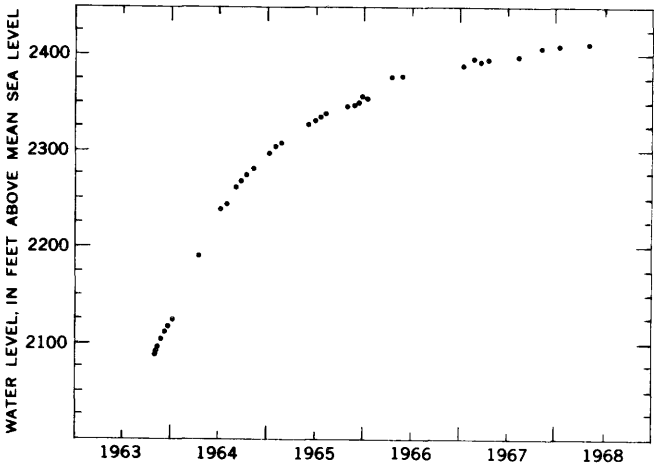

Figure 2.—Rubble-chimney infill curve after the Bilby event, Nevada Test Site.

pumping rate is sufficiently high so as to dewater the chimney before significant infill occurs from the surrounding rock.

Pumping tests in the reentry well were run at separate inflow zones. The lower inflow zone was at a depth of about 1,930 feet below land surface, and the upper zone was from 1,680 to 1,730 feet. Tests 1, 2, and 3 were made with only the lower zone open to the well bore. A packer was then installed to seal off the lower zone, and the upper zone was perforated. Tests 4 and 5 were made with only the upper zone open to the well bore. Effects of these tests on infill of the rubble chimney are shown in figure 3. Data from tests 1 and 2 are not included in this report, because pumping was of insufficient time or quantity to produce a measurable offset of the chimney-infill curve.

The material making up the chimney rubble in these zones probably fell a distance of about 400 feet. The unpublished log of a well located near the rubble chimney suggests that the lower inflow zone of the reentry well in the Bilby rubble chimney consists of fragments of zeolitized tuff. The upper inflow zone probably consists of fragments of poorly indurated bedded tuff.

Determination of the chimney's effective porosity from the data shown in figure 3 depends upon the radius of the chimney. Calculated values of porosity for each test (chimney radii of 250, 275, and 300 feet) are presented in the following table:

Radius of chimney (feet)	*Effective porosity (percent)*		
	Test 3	*Test 4*	*Test 5*
300	5.5	2.3	1.5
275	6.5	2.8	1.7
250	7.9	3.3	2.1

The calculated values of the chimney's effective porosity are considerably greater than the calculated or measured effective porosities in undisturbed rock in this area. Effective porosity in zeolitized tuff, for example, is estimated as less than 1 percent and perhaps as low as 0.1 percent. Thus, the data indicate a certain amount of bulking in the rubble chimney. The higher value of effective porosity in the lower zone relative to that in the upper zone probably relates to the bulking properties of the rocks making up the chimney rubble in these zones. Bulking depends principally on the physical properties of the rock and the amount of overburden. Accordingly, the friable bedded tuff in the upper zone is probably less resistant to overburden pressure than the material in the lower zone; therefore, it bulks less.

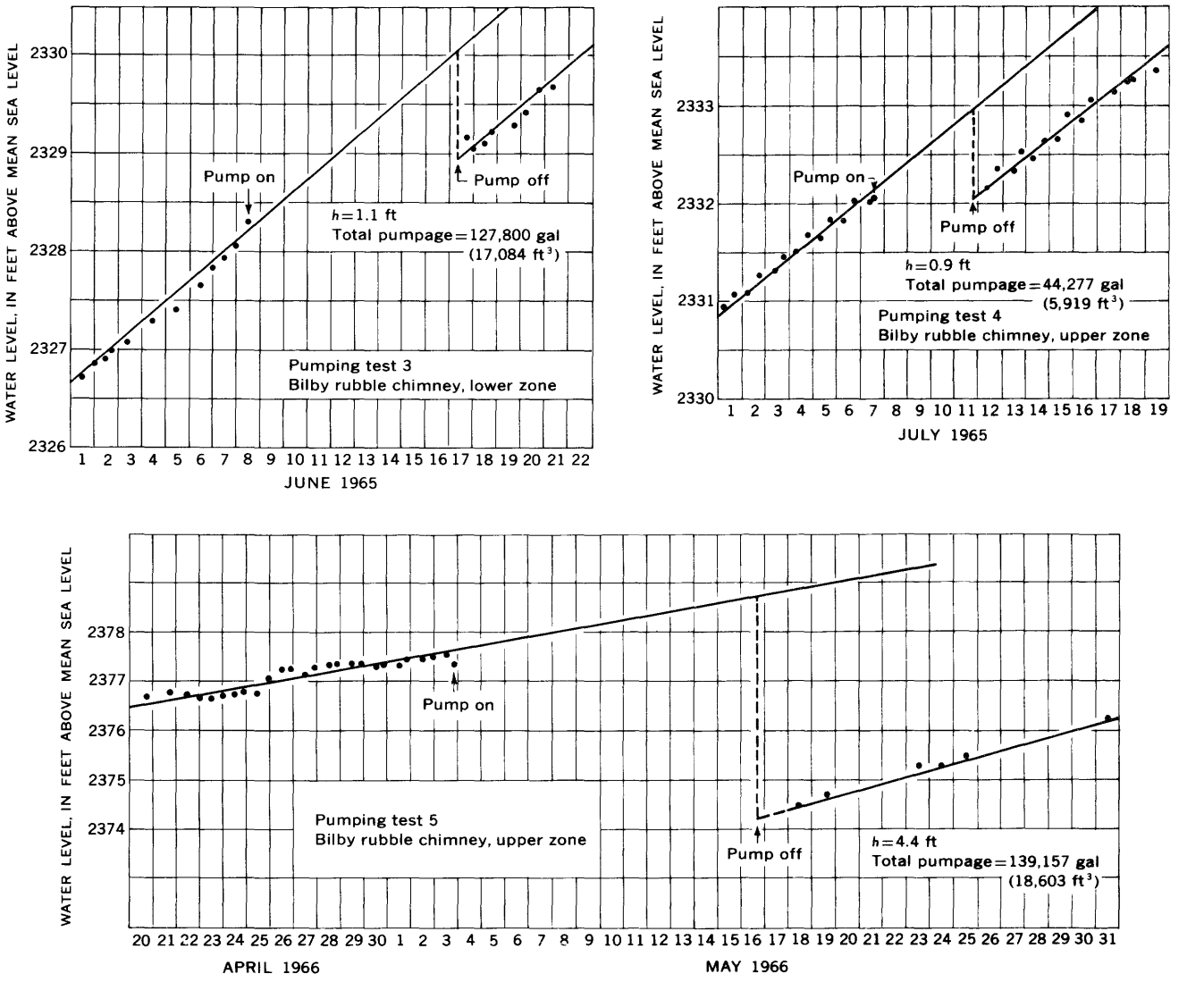

Figure 3.—Offset of rubble-chimney infill curve as a result of pumping. Bilby event, Nevada Test Site.

REFERENCES

Houser, F. N., 1968, Application of geology to underground nuclear testing, Nevada Test Site, *in* Nevada Test Site: Geol. Soc. America Mem. 110, p. 21–33.

——1970, A summary of information and ideas regarding sinks and collapse, Nevada Test Site: Natl. Tech. Inf. Service, USGS–474–41, 123 p.

Piper, A. M., and Stead, F. W., 1965, Potential applications of nuclear explosions in development and management of water resources—Principles: U.S. Geol. Survey TEI–857, 128 p.

DETERGENTS IN THE STREAMFLOW OF SUFFOLK COUNTY, LONG ISLAND, NEW YORK

By PHILIP COHEN, D. E. VAUPEL, and N. E. McCLYMONDS,
Mineola, N.Y.

Work done in cooperation with the Suffolk County Water Authority and the Suffolk County Department of Health

Abstract.—In 1962–69, the average MBAS (methylene-blue active substance) content of 46 streams in Suffolk County, Long Island, N.Y., was, on a yearly basis, approximately inversely related to the amount of streamflow. This relation partly reflected (1) the close similarity between the quality of the shallow ground water and the quality of the streamflow, coupled with the dilution effect of recharge from precipitation on the quality of the shallow ground water, (2) areal differences in the MBAS content of the shallow ground water and the effects of these differences on the quality of the streamflow as the headwaters of the streams shifted in response to the 1962–66 drought, and (3) the substitution of LAS (linear alkylsulfonate) for ABS (alkylbenzenesulfonate) in 1965. The average MBAS content and load of the streams in 1962 were virtually the same as in 1969. However, during the same period the average chloride content and load of the streams increased.

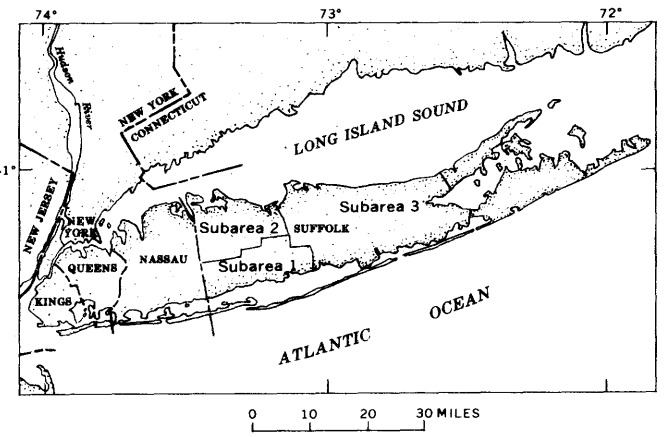

Figure 1.—Index map of Long Island, N.Y., showing subareas described in this report.

The entire fresh public-water supply of Suffolk County, Long Island, N.Y. (fig. 1), which serves a population of more than 1 million people, is derived from the ground-water reservoir underlying the county. Moreover, about 95 percent of the domestic and industrial sewage in the county is discharged into the ground through cesspools, septic tanks, and disposal basins (Nassau-Suffolk Research Task Group, 1969, p. 3–8). As a result, the ground water of Suffolk County, especially in the shallow, highly permeable, and productive water-table aquifer, is slowly becoming contaminated with numerous constituents of sewage origin.

The purpose of this paper is to report on the occurrence of certain synthetic-detergent compounds found in the streamflow of Suffolk County, and on changes in the content and load of these compounds in the period 1962–69. Inasmuch as 90 percent or more of the streamflow is derived from the water-table aquifer (Pluhowski and Kantrowitz, 1964, p. 35), the chemical quality of the streamflow is closely representative of the chemical quality of ground water in the water-table aquifer, and the quality of the streamflow thereby provides considerable insight into the nature and extent of pollution in that aquifer.

The chemical constituents of principal concern in this report are the surfactants ABS (alkylbenzenesulfonate) and LAS (linear alkylsulfonate). The two compounds commonly are collectively termed MBAS (methylene-blue active substance) because they cannot be distinguished from one another by the methylene-blue laboratory test (American Public Health Association, and others, 1965, p. 297).

The MBAS content of most of the streamflow in Suffolk County in 1970 did not exceed the recommended limit of 0.5 mg/l (milligrams per liter) for drinking water established by the U.S. Public Health Service (1962, p. 7). However, the presence of MBAS is an indication of pollution of sewage origin, and is of marked concern to public officials and others in Suffolk County.

The MBAS data considered in this report were obtained from 46 streams in Suffolk County; 11 are equipped with

continuous-record streamflow stations, and the remainder are equipped with partial-record streamflow stations. Insofar as possible, the samples were obtained at the streamflow stations which, in most places, were located immediately upstream from the points where the streams become estuaries. Practically all the samples were obtained at times when base flow (streamflow derived from the ground-water reservoir) comprised virtually the total flows of the streams. The MBAS and chloride analyses were made in the laboratory of the Suffolk County Water Authority under the supervision of Mr. A. A. Guerrera.

MBAS CONTENT OF THE WATER

The MBAS content of streamflow in Suffolk County from 1962 to 1969 is shown in figure 2. The data in figure 2 are grouped according to three subareas (fig. 1)—subarea 1 which includes the towns of Babylon and Islip, subarea 2 which includes the towns of Smithtown and Huntington, and subarea 3 which includes the towns of Brookhaven, Riverhead, and the western part of the town of Southampton. The graphs in figure 2 show that the average MBAS content of the streamflow was highest in subarea 1 and lowest in subarea 3, which suggests that the shallow ground water in subarea 1 had the highest MBAS content and that in subarea 3 had the lowest MBAS content. These observations and inferences largely reflect the fact that the population density (table 1) and the associated degree of contamination of the shallow ground water with domestic waste water was greatest in subarea 1 and least in subarea 3.

Monthly average flows (the average streamflow for the months in which the samples were obtained) and yearly average flows for the 11 principal streams equipped with continuous streamflow recorders are shown in figure 3. Also shown are the average MBAS and the average chloride contents of the 46 streams in the county.

On a short-term basis, the relation between the amount of streamflow and the average MBAS content was poor. However, on a yearly basis, the average MBAS content seems to have been approximately inversely related to the amount of streamflow. The long-term decrease in streamflow from 1962 to 1966 closely paralleled and was caused by a decline in ground-water levels associated with a severe drought (Cohen and others, 1969). Therefore, the yearly inverse relation between the amount of streamflow and the average MBAS content is inferred to have been caused at least partly by changes in the amount of ground-water recharge from precipitation and associated changes in the resulting degree of dilution of the contaminated shallow ground water by MBAS-free natural recharge.

The postulated close relation between the detergent content of the shallow ground water and that of the streamflow is partly confirmed by data from several shallow observation wells in Suffolk County (Perlmutter and Guerrera, 1970, pl. 2). Long-term and seasonal fluctuations in the MBAS content of water from those wells closely paralleled the fluctuations observed in the MBAS content of the streamflow. Moreover, the largest fluctuations were noted in the shallowest wells, thereby supporting the premise that dilution related to natural recharge from precipitation was at least to some extent

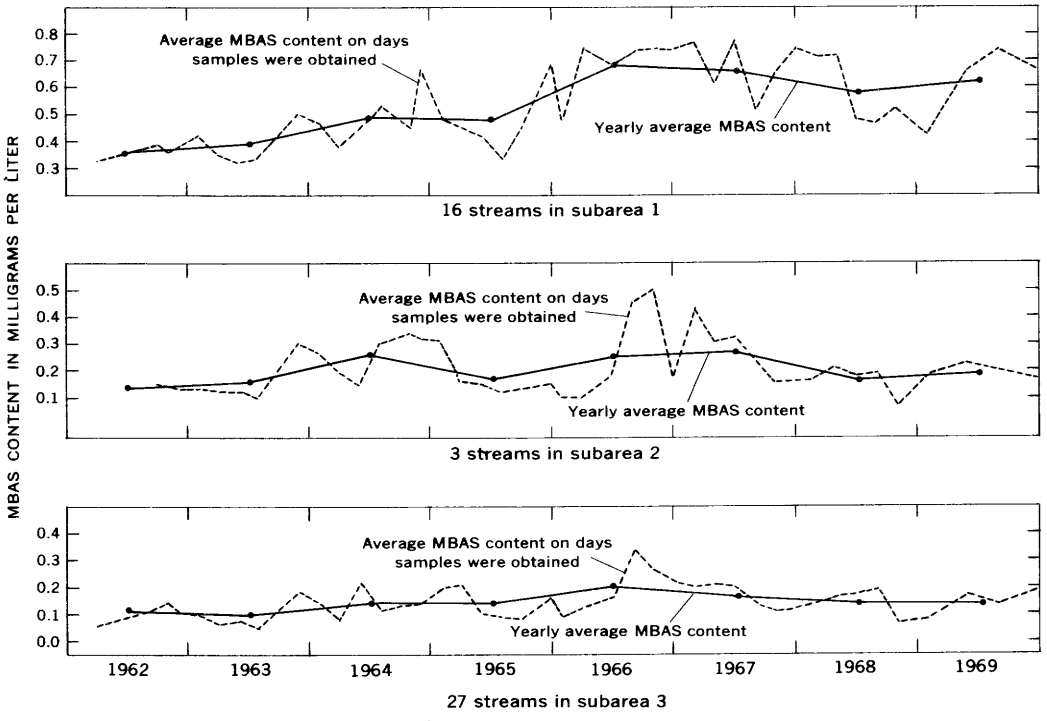

Figure 2.—MBAS (methylene-blue active substance) content of streamflow in Suffolk County, N.Y.

Table 1.—*Population and population densities for three subareas in Suffolk County, Long Island, N.Y.*

[Population data from the Long Island Lighting Co.]

Subareas	1962		1969	
	Population	Population density (people per sq mi)	Population	Population density (people per sq mi)
1. Towns of Babylon and Islip.	359,000	2,300	471,000	3,100
2. Towns of Smithtown and Huntington.	208,000	1,400	297,000	2,000
3. Towns of Brookhaven, Riverhead, and the western part of the town of Southampton.	159,000	400	245,000	620
Total	726,000	.....	1,013,000	.....

responsible for changes in the MBAS content of the shallow ground water.

The inverse relation between the yearly average MBAS content and the yearly average streamflow also may partly have been indirectly related to areal variations in the MBAS content of the shallow ground water. N. M. Perlmutter (written commun., 1970) found that the MBAS content of the shallow ground water in adjacent Nassau County decreases inland seemingly as a function of the increasing depth to the water table. If the same situation exists in Suffolk County, then as the water table fluctuates, the headwaters of the streams (the points at which the streams begin to flow) shift landward or seaward and the flows increase or decrease, resulting in changes in the average MBAS content of the streamflow. For example, when ground-water levels rise, the headwaters of the streams shift landward, streamflow increases, the streams intercept ground water having a lower MBAS content, and the average MBAS content of the streamflow decreases.

Another factor which should be considered in evaluating changes in MBAS content during the study period is that, beginning in about mid-1965, LAS replaced ABS in household detergents (Perlmutter and Guererra, 1970, p. 4). This change was made mainly because LAS reportedly is more biodegradable than ABS in an aerobic environment. Accordingly, some of the observed yearly decrease in the average MBAS

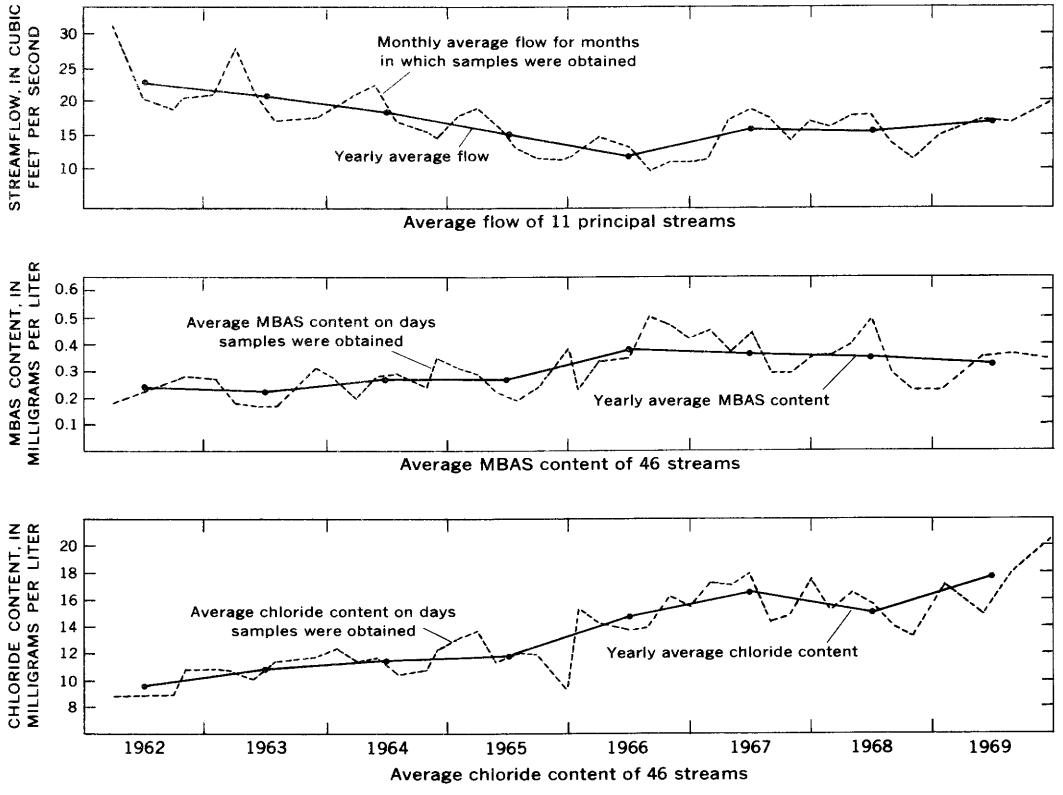

Figure 3.—Relation between streamflow, MBAS content, and chloride content of streams in Suffolk County, N.Y.

content of the streamflow, beginning in about 1966, might be related to the substitution of LAS for ABS in household detergents.

Finally, some of the increase in MBAS content in the streamflow of Suffolk County from 1962 to 1966 probably was caused by increased contamination of the shallow ground water associated with increased population and related increased waste disposal.

CHLORIDE CONTENT OF THE WATER

Where the water is not directly or indirectly contaminated with sea water, much of the chloride in the shallow ground water and, therefore, in the streamflow of Long Island in excess of 5 mg/l is derived from sewage or other sources of pollutants (Perlmutter and Guererra, 1970, p. 16–18). Accordingly, chloride data obtained at the same time as the MBAS data help provide additional insight into the changes in MBAS content of the streamflow in Suffolk County.

As shown in figure 3, the average chloride content of the streamflow increased markedly during the drought. However, it did not begin to decrease until 1968 (about 2 years after the drought ended), and it again increased (to a record high for the period of record) in 1969. The increase in chloride content from 1962 to 1966 probably partly resulted from decreased recharge associated with the drought. However, part of the increase during those years and the increases in 1967 and 1969 probably were associated with increased contamination of the shallow ground water with domestic wastes, with salt used for road deicing, and with chloride derived from other minor sources.

Streamflow data and the computed MBAS and chloride loads (concentrations multiplied by the rates of flow for the 11 continuous-record stations) are shown in figure 4. The short-term load data, as might be expected, seem to have been related fairly closely to the short-term streamflow data; when the flows increased the loads increased and, conversely, when the flows decreased the loads decreased. The yearly MBAS loads seem to have been virtually unrelated to the yearly flows, but the yearly chloride loads seem to have been roughly related to the yearly flows. The yearly average MBAS load was virtually the same in 1969 as it was in 1962. However, the yearly average chloride load increased from 7 tons per day in 1962 to about 9 tons per day in 1969.

CONCLUSIONS

The average MBAS content of all streams sampled in Suffolk County increased very slightly (by about 0.05 mg/l), and the MBAS load of the 11 principal streams remained virtually

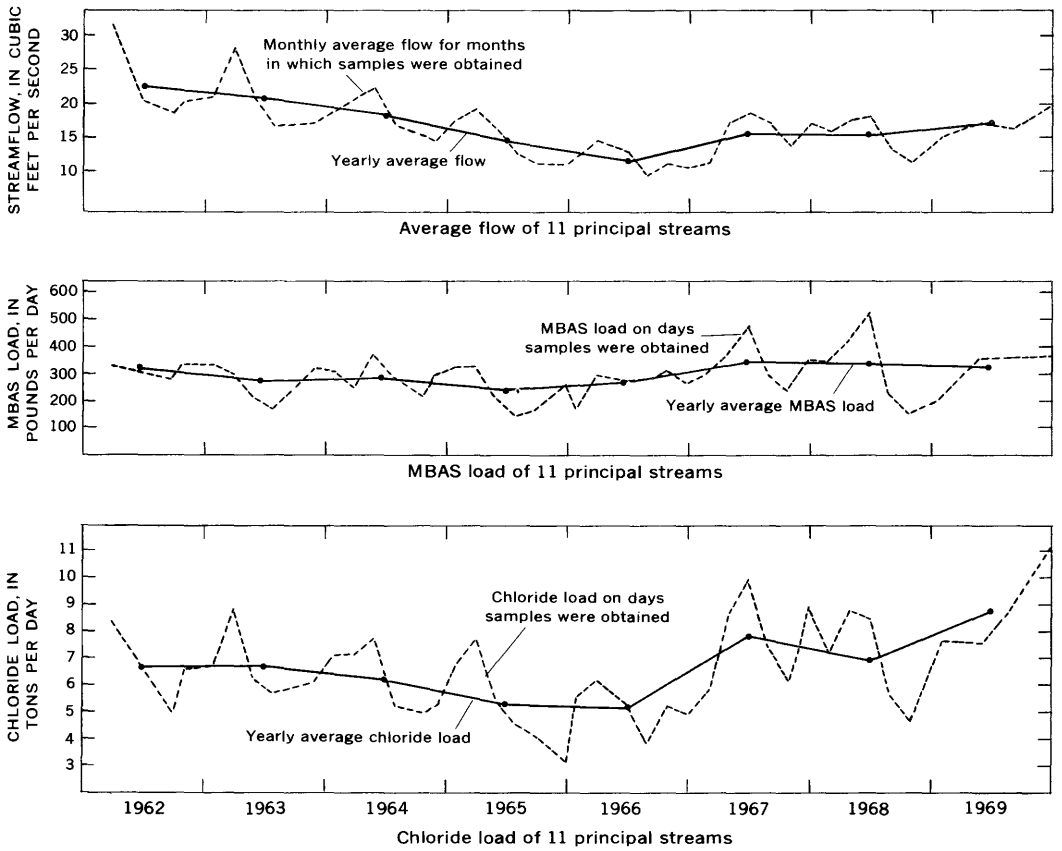

Figure 4.—Relation between streamflow, MBAS load, and chloride load of streams in Suffolk County, N.Y.

unchanged from 1962 to 1969. However, the average chloride content of all streams sampled increased from about 10 mg/l to 18 mg/l, and the average chloride load of 11 principal streams increased significantly during the same period. The overall increase in chloride content and load is attributed mainly to increased contamination of the ground water. The negligible net change in MBAS content and load from 1962 to 1969 probably reflected a combination of (1) the fairly close yearly inverse relation between MBAS content and ground-water recharge from precipitation, (2) areal differences in the MBAS content of the ground water and the effects thereof on the MBAS content of the streamflow, and (3) the substitution of LAS for ABS in 1965. However, insufficient data are available to assess the relative significance of these and possibly other unknown factors with respect to the MBAS contents and loads of the streams in Suffolk County.

Plans have been developed, and initial efforts presently are underway to construct widespread sanitary-sewer facilities in Suffolk County. When these facilities are completed and fully operational, the source of virtually all the MBAS contamination in the ground and surface water of Suffolk County will be eliminated. Shortly thereafter, the MBAS content of both the ground and surface water and the load of MBAS in Long Island's streams probably will begin to decrease. The time required to fully flush the MBAS from the ground-water reservoir is uncertain, but it may be on the order of several decades or more.

REFERENCES

American Public Health Association, and others, 1965, Standard methods for the examination of water and waste water, 12th ed.: New York, Am. Pub. Health Assoc. Inc., 626 p.

Cohen, Philip, Franke, O. L., and McClymonds, N. E., 1969, Hydrologic effects of the 1962–66 drought on Long Island, New York: U.S. Geol. Survey Water-Supply Paper 1879–F, p. F1–F18.

Nassau-Suffolk Research Task Group, 1969, The Long Island ground water pollution study: New York State Dept. Health, 395 p.

Perlmutter, N. M., and Guerrera, A. A., 1970, Detergents and associated contaminants in ground water at three public-supply well fields in southwestern Suffolk County, Long Island, New York: U.S. Geol. Survey Water-Supply Paper 2001–B, p. B1–B22.

Pluhowski, E. J., and Kantrowitz, I. H., 1964, Hydrology of the Babylon-Islip area, Suffolk County, Long Island, New York: U.S. Geol. Survey Water-Supply Paper 1768, 119 p.

U.S. Public Health Service, 1962, Drinking water standards: Public Health Service Pub. No. 956, 61 p.

NITRATE AND ORTHOPHOSPHATE IN SEVERAL NEBRASKA STREAMS

By R. A. ENGBERG, Lincoln, Nebr.

Abstract.—Analytical data for sampling sites on 11 streams indicate mean concentrations of nitrate ranging from 0.6 to 6.1 mg/l (milligrams per liter) and mean concentrations of orthophosphate ranging from 0.35 to 2.0 mg l. Weighted by water discharge, average concentrations of nitrate and orthophosphate in all 11 streams were 2.1 mg/l and 0.81 mg/l, respectively. Concentrations of nitrate and orthophosphate do not correlate with total dissolved-solids content of the water nor with water discharge. However, nitrate concentrations show some correlation with population density, cattle density, and percentage of drainage area planted to corn.

Nitrogen and phosphorus are among the many essential nutrients required to sustain growth of algae and other plants in an aquatic environment. Thus, water bodies that are overly rich in nitrogen and phosphorus may become sites for excessive production of organic matter. If a stream becomes choked with vegetation it is more subject to flooding and provides a less suitable environment for desirable fish and other animal life. Furthermore, water taken from such a stream generally requires more treatment to make it usable for most purposes. For these reasons, information on concentrations of nutrient elements in stream water is of economic significance.

Nitrogen may occur in streams as dissolved nitrogen gas, organic nitrogen, ammonia, nitrite, and nitrate. Dissolved nitrogen gas is relatively inert chemically and in most instances can be disregarded as an important source of nitrogen available for algae and other water plants. Organic nitrogen and ammonia may be of highly variable concentrations in stream water that contains decomposing wastes but in time they generally are converted to nitrate by biological activity. Nitrite is very unstable and is seldom found in significant amounts in streamflow. Nitrate, the most common form of nitrogen, may be present in relatively high concentrations in streams draining predominantly agricultural areas. Sources of such nitrate include human and animal wastes, fertilizers, nitrogen fixed in soils by biological activity, rainfall, and ground-water inflow.

Phosphorus in streams generally occurs in the form of soluble orthophosphate. Many of the more complex forms of phosphorus are unstable in water and, according to an American Water Works Association Task Group on Nutrients in Water (1970), are slowly hydrolyzed to orthophosphate. Orthophosphate derived from solution of phosphate ores, human and animal wastes, detergents, and fertilizer may enter streams in either overland runoff or ground-water seepage. The orthophosphate values used in this report represent only the orthophosphate in solution.

This report presents data on nitrogen and phosphorus in 11 streams in Nebraska. The relation of concentrations to various basin characteristics and environmental factors is explored. As discharge data were available for each sampling site, mean loads, in pounds per acre per year, could be computed and comparisons made from them.

AREAS OF STUDY

Figure 1 shows the location of all the sampling sites and the extent of area drained at each. A variety of terrains and land-use practices are represented by the 11 drainage areas. For examples, the area above site 1 consists of sand dunes stabilized by vegetation and is used almost exclusively as rangeland; the area above site 3 consists of loess-mantled hills of glacial drift and is used mostly for growing nonirrigated grains and as pasture for cattle; the area above site 5 consists of glacial drift hills, and land use is similar to that in the area above site 3; and the area above site 9 consists of loess on sandy gravel, is nearly flat to gently rolling, and is used mostly for growing irrigated grains. The drainage areas also differ widely in the proportion of streamflow contributed by ground-water seepage and by overland runoff. At site 1, for example, nearly all streamflow is derived from ground-water seepage, whereas at site 3 streamflow is derived largely from overland runoff. Descriptions of the 11 drainage areas are given in table 1 together with areal extent, length of streamflow record, and mean water discharge for the period of record.

The values given for extent of area drained need to be qualified. Each represents the approximate maximum area from which, according to topographic divides, overland runoff could be derived if weather and soil conditions were such that the entire area produced overland runoff. However, where sand is the surface material or shallow closed basins are a feature of the terrain, production of overland runoff under

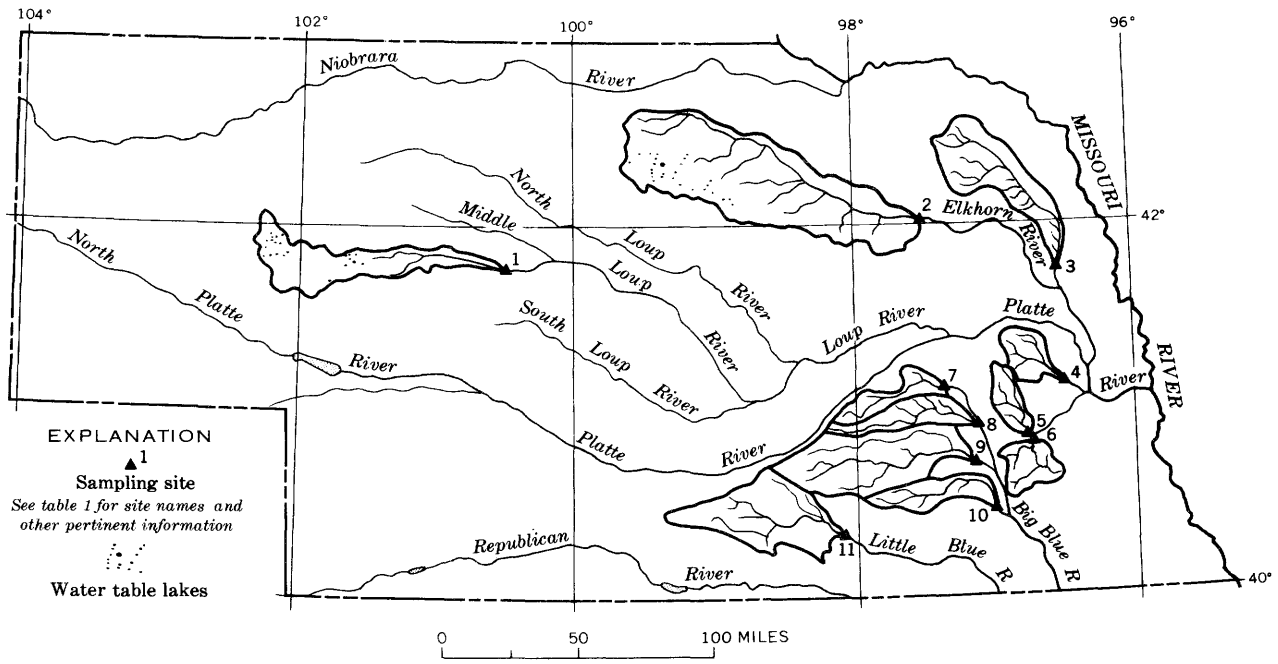

Figure 1.—Map of Nebraska, showing sampling sites (numbered) and drainage area (outlined) above each site.

Table 1.—*Areal extent, period of record, mean discharge, and drainage-area characteristics for 11 sampling sites shown in figure 1*

[Except as noted, values for drainage area and mean water discharge are from U.S. Geol. Survey (1970)]

Sampling site	Site name	Extent of area drained (square miles)	Length of water discharge record (years)	Mean water discharge for period of record (cubic feet per second)	Description of drainage area
1	Dismal River near Thedford.	960	2	192	Sand dunes and interdune flats. Nearly continuous grass cover; much naturally subirrigated wild hay in areas of shallow water table. Virtually no cultivated land. Cattle on open range. Several water-table lakes. Most streamflow derived from ground-water seepage.
2	Elkhorn River near Norfolk.	2,790	24	527	Sand dunes, interdune sandy flats, and extensive sand plain in upper two-thirds of drainage area; loess plain in lower third. Nearly continuous grass cover on dunes and in interdune valleys. Much naturally subirrigated wild hay and alfalfa in areas of shallow water table; considerable cultivated land, mostly planted to corn. Cattle on open range on sand dunes and in dry interdune valleys. Several water-table lakes. Some ground water used for irrigation. In upper two-thirds of drainage area, the larger part of streamflow is derived from ground-water seepage; in lower one-third the larger part of additional streamflow is derived from overland runoff.
3	Logan Creek near Uehling.	1,030	28	181	Loess-mantled hills of glacial till. Almost wholly cropland and pasture. Corn is principal crop; considerable feeding of livestock. Small use of water for irrigation. Streamflow derived mostly from overland runoff.
4	Wahoo Creek at Ithaca.	272	20	81.9	Loess-mantled hills of glacial till and loess-mantled deposits of sandy gravel. Almost wholly cropland and pasture. Some feeding of livestock. Corn is principal crop. Some ground water used for irrigation. Overland runoff generally constitutes the greater part of streamflow.

Table 1.—*Areal extent, period of record, mean discharge, and drainage-area characteristics for 11 sampling sites shown in figure 1*—Continued

[Except as noted, values for drainage area and mean water discharge are from U.S. Geol. Survey (1970)]

Sampling site	Site name	Extent of area drained (square miles)	Length of water discharge record (years)	Mean water discharge for period of record (cubic feet per second)	Description of drainage area
5	Oak Creek at Lincoln.	[1]260	19	[2]67	Rolling hills of glacial till. Mostly cropland and pasture, but some residential and industrial land use in lower part of drainage area. Sorghum, wheat, and corn are principal crops. Lower reach of stream in dredged channel. Streamflow altered by storage in flood-control and recreation reservoir and by numerous stock ponds on small tributaries; considerable contour terracing. Almost no water used for irrigation.
6	Salt Creek at South Street in Lincoln.	[1]310	19	[2]79	Same as for site 5 except streamflow altered by storage in several flood-control and recreation reservoirs.
7	Big Blue River at Surprise.	345	5	39.8	Loess on deposits of sandy gravel or glacial till. Considerable nearly level upland having some undrained depressions. Mostly cropland and pasture. Corn is principal crop; sorghum and wheat also important. Some cattle feeding. Considerable ground water used for irrigation of corn in upland part of drainage area. Nearly all streamflow derived from overland runoff.
8	Lincoln Creek near Seward.	466	16	49.9	Loess on deposits of sandy gravel. Considerable nearly level upland having some undrained depressions. Almost wholly cropland; corn is principal crop; sorghum and wheat also important. Much ground water used for irrigation of corn. Considerable cattle feeding. About three-fourths of streamflow derived from overland runoff.
9	West Fork Big Blue River near Dorchester.	1,206	11	193	Same as for site 8 except for some streamflow used for irrigation. Population density higher than in any of other drainage areas.
10	Turkey Creek near Wilber.	460	10	87.6	Mostly loess on deposits of sandy gravel; some loess on glacial till. Mostly gently rolling but some nearly level upland having a few undrained depressions. Almost wholly cropland or pasture. Corn is the principal crop in upper part of drainage area where much ground water is used for irrigation. Nearly all streamflow derived from overland runoff.
11	Little Blue River near Deweese.	979	16	159	Loess on deposits of sandy gravel. Partly nearly level upland having several undrained depressions; partly gently rolling. Almost wholly cropland or pasture. Wheat, corn, and sorghum are principal crops. Considerable ground water used for irrigation. About half of streamflow is derived from overland runoff.

[1] Author's estimate.
[2] Estimated from records of nearby station.

usual climatic conditions may be from a smaller area than that indicated. In many years, less than 5 percent of the indicated drainage area above sampling site 1 and no more than about 65 percent of that above sampling site 2 provides overland runoff. In each of the other drainage areas some overland runoff is impounded in stock ponds, and in the drainage areas above sites 7 to 11 some overland runoff is held in natural depressions on the undissected upland surface.

In general, topographic basins coincide approximately with ground-water basins. However, as is true of topographic basins, parts of ground-water basins may not consistently contribute to streamflow. Probably a significantly large part of the ground-water basin above sampling site 1 and a smaller part of the ground-water basin above sampling site 2 discharge to the atmosphere through evapotranspiration and so generally do not contribute to streamflow.

Because the drainage areas, as given, are maximum values, some of the computed mean loads of nitrogen and phosphorus, which are expressed in pounds per acre per year, are smaller than they would be if the number of acres contributing to streamflow were known precisely and had been used in the computation. As all parts of each drainage area may at some time contribute to streamflow either by overland runoff or ground-water seepage, the maximum value for drainage area was used in determining mean load.

RESULTS

Mean concentrations of nitrate in milligrams per liter (mg/l) and mean nitrate loads in pounds per acre per year are given in table 2 for each of the 11 sampling sites. The lowest mean concentration observed was 0.6 mg/l in Oak Creek at Lincoln, and the highest was 6.1 mg/l in the Big Blue River at Surprise. The Little Blue River near DeWeese and the Dismal River near Thedford were alike in having the lowest nitrate load, 0.4 pound per acre per year; Wahoo Creek near Ithaca had the highest load, 3.7 pounds per acre per year.

Table 2.—*Mean concentrations of nitrate for sampling period and mean loads of nitrate for period of water-discharge record*

Sampling site	Site name	Number of samples	Length of sampling period (years)	Mean concentration (milligrams per liter)	Mean load (pounds per acre per year)
1. . .	Dismal River near Thedford.	25	2	0.7	0.4
2. . .	Elkhorn River near Norfolk.	41	3	1.5	.9
3. . .	Logan Creek near Uehling.	16	2	3.7	2.0
4. . .	Wahoo Creek at Ithaca.	24	2	4.0	3.7
5. . .	Oak Creek at Lincoln.	14	2	.6	.5
6. . .	Salt Creek at South Street in Lincoln.	14	2	.9	.7
7. . .	Big Blue River at Surprise.	34	3	6.1	2.2
8. . .	Lincoln Creek near Seward.	40	3	4.1	1.4
9. . .	West Fork Big Blue River near Dorchester.	50	3	5.0	2.5
10. . .	Turkey Creek near Wilber.	70	5	2.3	1.3
11. . .	Little Blue River near Deweese.	39	3	.9	.4

Table 3 shows mean concentrations and loads of orthophosphate observed at the same sampling sites. The lowest mean concentration, 0.35 mg/l, and the lowest orthophosphate load, 0.28 pound per acre per year, were for Oak Creek at Lincoln, and the highest mean concentration and highest mean load, 2.0 mg/l and 0.98 pound per acre per year, respectively, were for West Fork Big Blue River near Dorchester.

Mean concentrations of nitrate and orthophosphate, as shown for each sampling site, represent an arithmetic average of all results for that site. Computations of mean loads are based on these mean concentrations and the average discharge for the period of discharge record at the site.

The periods of sampling ranged from 2 to 5 years, whereas the periods of discharge record ranged from 2 to 27 years. For a few sites the average discharge for the period of sampling was almost the same as the average discharge for the period of record, and at 9 of the 11 sites the mean discharges for the two periods differed by less than 20 percent. It is assumed from this close agreement that basing load calculations on average discharge for the period of record is valid even though the period of sampling is shorter than that of discharge measurement. Values for mean concentration and mean load, as given in tables 2 and 3, should be regarded as representative of conditions during the period of study but not necessarily as reliable for making projections into the future.

INTERPRETATION OF RESULTS

Regression analyses of nitrate concentrations on specific conductance and on water discharge (K. A. Mac Kichan, unpublished data for three sampling sites in eastern Nebraska) indicate neither positive nor negative correlation between concentration of nitrate and total dissolved-solids content as measured by specific conductance or between concentration of nitrate and water discharge. In other words, nitrate concentrations appear to be independent of both the dissolved-solids content of the water and the rate of discharge. Of the three sites for which regression analyses were made, two—Turkey Creek at Wilber and Lincoln Creek near Seward—are among the 11 at which data were collected for this report. Although the third—Big Blue River at Barneston—is not one of the 11, it does include in its drainage area 4 of the 11 sampling sites and is thought, therefore, to be representative. It is inferred that a similar lack of correlation would be indicated by regression analyses of data for the 9 sampling sites not included among the 3 for which such analyses have already been made.

Regression analyses for orthophosphate at the same three locations indicate results similar to those for nitrate concentrations. No correlation between orthophosphate concentrations and total dissolved-solids content or between orthophosphate concentrations and water discharge could be demonstrated.

Graphs of nitrate and orthophosphate concentrations plotted against water discharge were prepared for those sites for which regression analyses had not been made. The graph

Table 3.—*Mean concentrations of orthophosphate for sampling period and mean load of orthophosphate for period of water-discharge record*

Sampling site	Site name	Number of samples	Length of sampling period (years)	Mean concentration (milligrams per liter)	Mean load (pounds per acre per year)
1.	Dismal River near Thedford.	23	2	0.57	0.35
2.	Elkhorn River near Norfolk.	34	3	.72	.42
3.	Logan Creek near Uehling.	14	2	.84	.45
4.	Wahoo Creek at Ithaca.	22	2	.96	.89
5.	Oak Creek at Lincoln.	14	2	.35	.28
6.	Salt Creek at South Street in Lincoln.	14	2	.51	.40
7.	Big Blue River at Surprise.	26	3	.86	.30
8.	Lincoln Creek near Seward.	35	3	1.1	.38
9.	West Fork Big Blue River near Dorchester.	44	3	2.0	.98
10.	Turkey Creek near Wilber.	40	5	1.1	.64
11.	Little Blue River near Deweese.	37	3	.86	.43

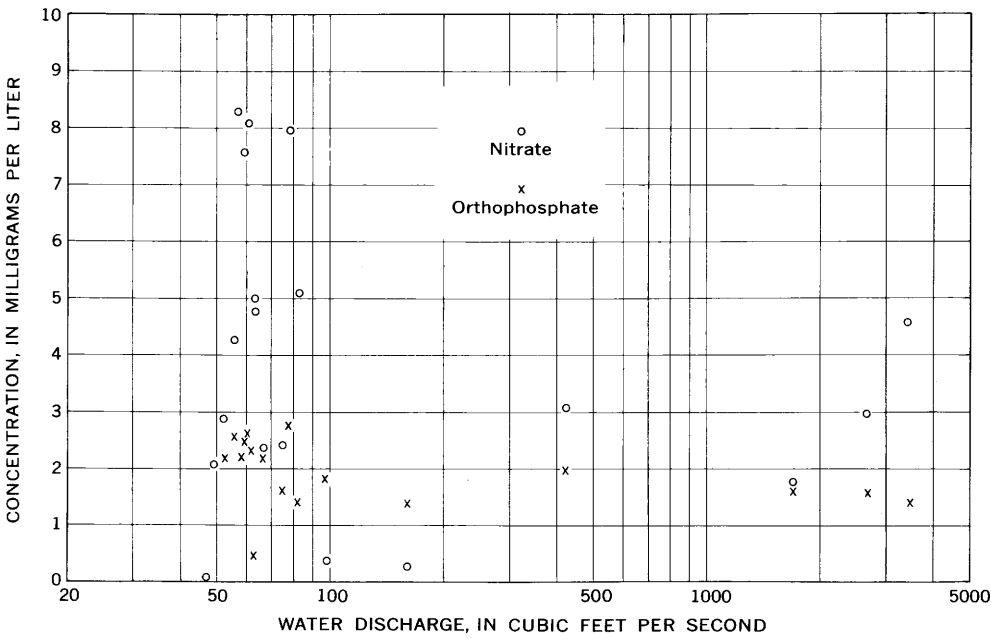

Figure 2.—Relation of nitrate and orthophosphate concentration to water discharge, West Fork Big Blue River near Dorchester, Nebr. Samples collected during 1968 water year.

for West Fork Big Blue River near Dorchester, typical of all the plots obtained, is shown in figure 2. No curve can be drawn to the values for nitrate as they have a wide range independent of water discharge, and a curve drawn to the orthophosphate values would have a slope of near zero, indicating little variation of phosphate concentration with great variation of water discharge. For either nitrate or orthophosphate, therefore, use of the mean concentration to calculate mean load should be valid.

Mean concentrations of nitrate and orthophosphate are similarly independent of both total dissolved-solids content and water discharge. However, as nitrate and orthophosphate do not occur naturally in near-surface rocks in Nebraska, the source and concentration of these constituents in streamflow must be related to other factors that characterize the drainage areas. Data on three likely sources of nitrate and orthophosphate—population density, cattle density, and percentage of drainage area planted to corn—each of which differs considerably from one drainage area to another, are given in table 4. No large urban areas exist in any of the basins; population densities range from less than 1 person to as many as 36 per square mile. Cattle raising and marketing, which amounted to 73 percent of total livestock receipts for 1968 in Nebraska, is representative of the livestock business in the State. Corn amounted to 44 percent of all crop market receipts for 1968 in Nebraska and, in 9 of the 11 drainage areas under consideration, ranked first, second, or third in importance with respect to acreage under cultivation.

Mean concentrations of nitrate at each of the 11 sampling sites were plotted against population density, cattle density, and percentage of drainage area planted to corn. (See fig. 3.) Although the scatter of points indicates a less-than-perfect correlation, the tendency toward alinement does indicate a positive relationship between nitrate and all three environmental factors, particularly cattle density and percentage of drainage area planted to corn. At each of the 4 sites where the mean concentration of nitrate was less than 1.0 mg/l, the value for each of the three environmental factors is relatively low, and at the 4 sites where the mean concentration of nitrate was 4.0 mg/l or larger, the value for at least one of the environmental factors is relatively high.

Undoubtedly, cattle concentrated in feedlots that are close to drainage courses contribute more nitrate to streamflow than do cattle grazing in pastures or on the range. In those drainage areas where the cattle density is high, a large percentage of the cattle is likely to be in feedlots. For example, in the drainage

Table 4.—*Population and population density, cattle density, and extent of corn planting in drainage areas*

Sample site	Site name	Population[1]		Number of cattle per square mile[2]	Extent of corn planting	
		Number of persons	Number of persons per square mile		Number of square miles	Percent of drainage area
1	Dismal River near Thedford.	750	0.8	50	0.9	0.1
2	Elkhorn River near Norfolk.	23,320	8.4	80	285	10
3	Logan Creek near Uehling.	24,070	33	166	261	25
4	Wahoo Creek at Ithaca.	9,380	34	120	93	34
5	Oak Creek at Lincoln.	4,140	16	72	30	12
6	Salt Creek at South Street in Lincoln.	8,440	27	71	16	5
7	Big Blue River at Surprise.	5,895	17	115	92	27
8	Lincoln Creek near Seward.	8,690	20	154	164	37
9	West Fork Big Blue River near Dorchester.	43,100	36	110	390	32
10	Turkey Creek near Wilber.	6,430	14	105	93	20
11	Little Blue River near Deweese.	11,330	12	77	146	15

[1] Based on 1960 census.
[2] Nebraska Dept. Agriculture (1970).

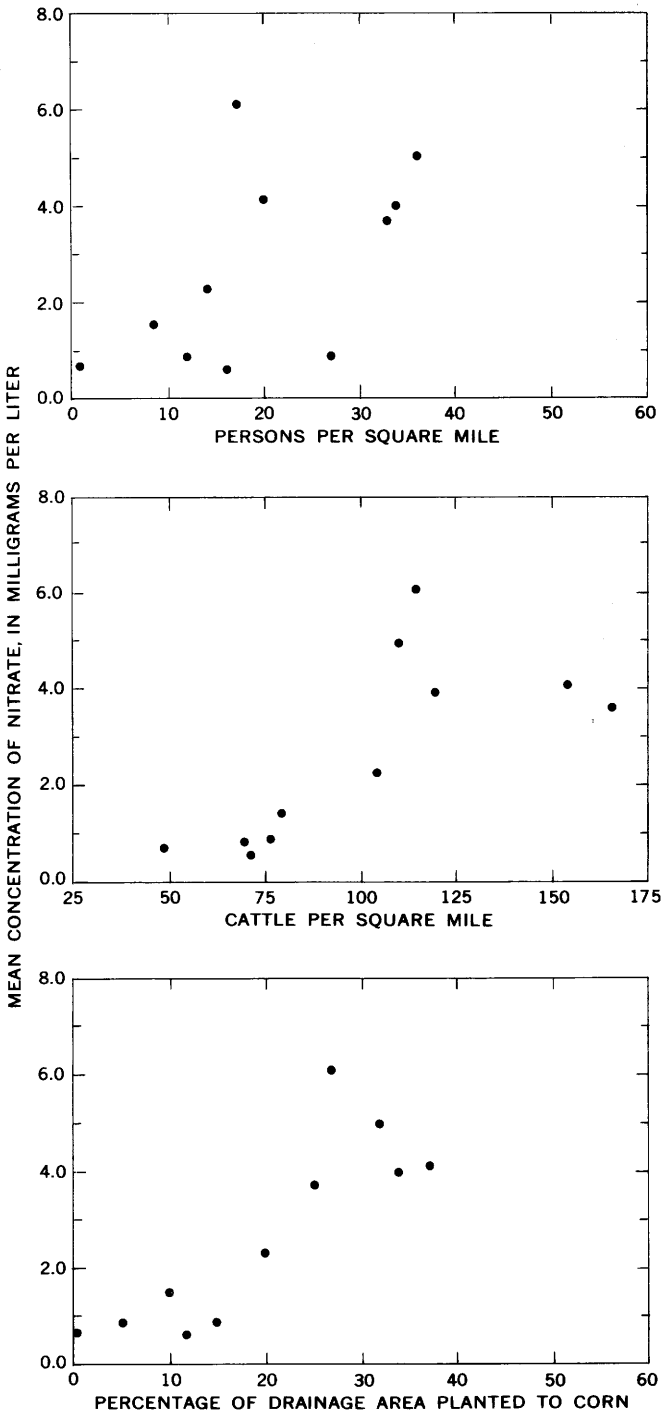

Figure 3.—Relation of nitrate concentration at 11 stream sampling sites in Nebraska to population density, cattle density, and percentage of drainage area planted to corn.

area of Wahoo Creek at Ithaca, as many as 80 percent of the cattle are feeder cattle. Possibly, weighting cattle density by the ratio of cattle in near-stream feedlots to cattle not in near-stream feedlots would improve the correlation of mean nitrate concentration with cattle density.

The positive correlation of mean nitrate concentration to percentage of drainage area planted to corn probably reflects, to some degree, the amount of fertilizer used on that crop. It probably also reflects the extent of irrigation in the drainage area, as return flow from irrigated fields provides a medium for transport of nitrate from the fields to drainage courses. During the irrigation season, return flow probably constitutes a large part of the discharge at the four sampling sites having the highest percentage of land planted to corn. Generally speaking, large corn acreages are indicative of highly productive soils, and such soils provide another source of nitrogen. Again, weighting of the values for percentage of land in corn by the other factors mentioned would enhance the correlation between mean nitrate and extent of corn plantings.

In figure 4, mean concentrations of orthophosphate at the 11 sites are plotted against the same sources as for nitrate. None of the graphs indicate a well-defined relationship,

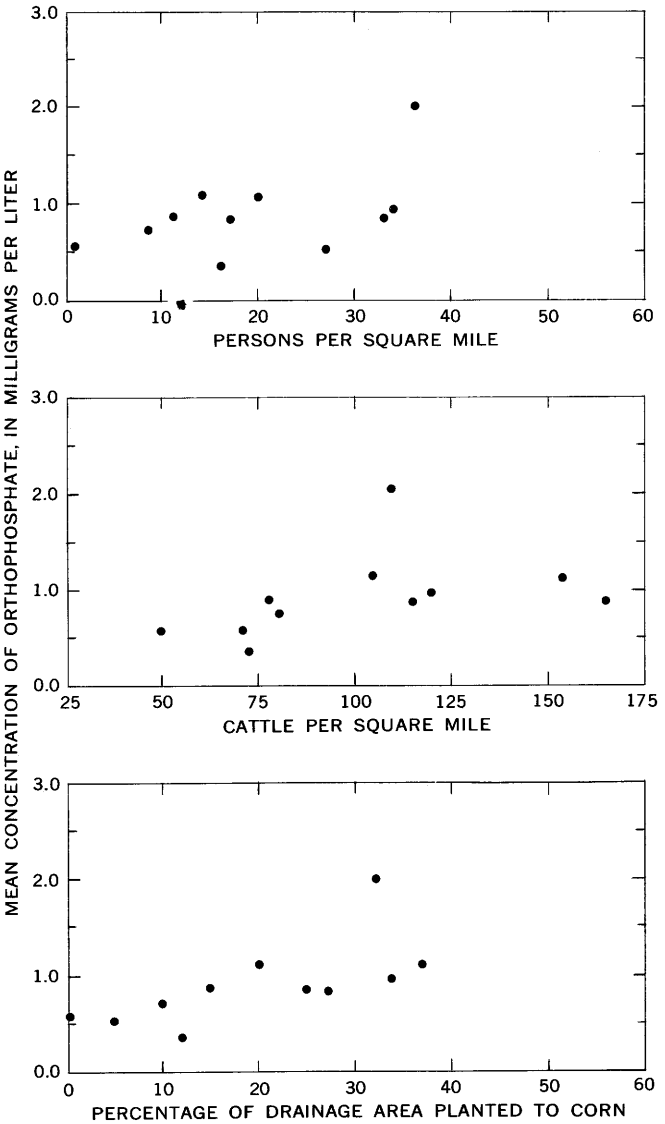

Figure 4.—Relation of orthophosphate concentration at 11 stream sampling sites in Nebraska to population density, cattle density, and percentage of drainage area planted to corn.

probably owing to the physical and chemical characteristics of orthophosphate in soil and water. Orthophosphate is readily adsorbed to soil particles and is less readily available for solution of either infiltrating water or overland runoff. Moreover, small amounts of orthophosphate can be adsorbed to suspended sediment in streams, and as the values given in this report represent dissolved orthophosphate, the adsorbed orthophosphate is not included in the measured values.

The American Water Works Association Task Group 2610 P (1967) estimated that the 450,000 billion gallons of water annually discharged by streams draining the United States contains about 5 billion pounds of nitrogen, which is equivalent to an average concentration of 1.35 mg/l. The same task group also indicated that 1.8–3 billion pounds of nitrogen per year reaches streams in the form of nitrate. If the average is assumed to be 2.5 billion pounds of nitrogen, then the mean concentration of nitrate as nitrate in streamflow would be 2.7 mg/l. At 5 of the 11 sampling sites on Nebraska streams, the mean concentration of nitrate was greater than the 2.7 mg/l concentration calculated from the task-group data, and at the others it was less. A discharge-weighted average concentration of nitrate for all 11 sampling sites was 2.1 mg/l, or a little less than the national average.

The American Water Works Association Task Group 2610 P similarly estimated that annual stream discharge from the United States contains about 1 billion pounds, or 0.27 mg/l, of phosphorus. As more than 90 percent of the phosphorus reaching streams probably is in the form of orthophosphate, the national average concentration of phosphorus estimated by the task group would be equivalent to about 0.83 mg/l orthophosphate. At 7 of the 11 sampling sites in Nebraska, the mean concentration of orthophosphate exceeded the national average and at 4 it was less. A discharge-weighted average for all 11 sampling sites is 0.81 mg/l, again slightly less than the national average.

REFERENCES

American Water Works Association Task Group 2610P, 1967, Sources of nitrogen and phosphorus in water supplies: Am. Water Works Assoc. Jour., v. 59, no. 3, p. 344–366.

—— 1970, Chemistry of nitrogen and phosphorus in water: Am. Water Works Assoc. Jour., v. 62, no. 2, p. 127–140.

Nebraska Department of Agriculture, 1970, Nebraska agricultural statistics annual report 1968: Lincoln, Nebr., State-Federal Div. Agr. Statistics, 168 p.

U.S. Geological Survey, 1970, Water resources data for Nebraska, 1969, pt. 1, Surface-water records: Lincoln, Nebr., U.S. Geol. Survey, 218 p.

OCCURRENCE OF PHOSPHORUS AND NITROGEN IN SALT CREEK AT LINCOLN, NEBRASKA

By R. A. ENGBERG and T. O. RENSCHLER,
Lincoln, Nebr.

Abstract.—Concentrations of phosphorus and nitrogen in Salt Creek increase markedly in the 6-mile reach of the creek within the city of Lincoln, Nebr. Most of the increase is due to inflow from the Lincoln sewage-treatment plant and from storm-sewer and other urban runoff entering the reach. The city contributes average amounts of 0.94 ton phosphorus and 1.8 tons nitrogen per day to the stream, indicating annual per capita contributions of phosphorus and nitrogen of 4.5 and 8.7 pounds per year, respectively.

This paper gives the results of a study made between October 1967 and February 1969 to determine the increase in phosphorus and nitrogen concentrations of Salt Creek within the municipal limits of Lincoln, Nebr. Annual per capita contributions of phosphorus and nitrogen are estimated from the results and are compared to values reported for reaches of other streams that similarly receive urban wastes.

Large quantities of foam are present in Salt Creek where effluent from the city sewage-treatment plant enters the creek. Although such foam does not result directly from phosphorus and nitrogen, but rather from detergents with which they are associated, its presence indicates that high concentrations of phosphorus and nitrogen are present in the effluent. Phosphorus and nitrogen are undesirable because they stimulate growth of nuisance algae and other vegetation downstream from the sewage outfall and reduce the efficiency of any downstream water-treatment processes.

HYDROLOGIC SETTING

Salt Creek, which flows in a generally northeasterly direction and empties into the Platte River at Ashland, Nebr., drains an area of 1,640 square miles (fig. 1). A 6-mile reach of the creek is within the municipal limits of the city of Lincoln, population 155,000 (1968 Chamber of Commerce estimate). At U.S. Geological Survey gaging station 6–8035, which is located on Salt Creek where it flows out of the city, the drainage area is about 710 square miles, or about three-eighths of the creek's total drainage area.

Above the South Street bridge, which is near the point where Salt Creek enters the city, the drainage area is mostly rural. Three small towns having a combined population of less than 500 are in this part of the basin. Beal Slough, a stream entering Salt Creek about 1 mile upstream from the point where the creek enters the city, drains a little more than 2 square miles of residential property in the south part of Lincoln.

Most of the overland runoff emptying into the 6-mile reach within the city is derived from the areas drained by Middle, Oak, and Antelope Creeks. Middle and Oak Creeks enter from the west and Antelope Creek from the east.

The area drained by Middle Creek lies west of Lincoln and is almost wholly agricultural land, although a small residential area and a railroad switchyard are near the mouth of the creek. The discharge of Middle Creek, which is affected by two reservoirs for flood control and recreation, is estimated to average less than 5 cfs (cubic feet per second).

The area drained by Oak Creek also is largely agricultural. Four small towns having a combined population of less than 1,000 are in the upper and middle parts of the basin. The Lincoln Municipal Airport, the adjacent Arnold Heights residential area, sections of Lincoln known as West Lincoln and Belmont, and two lakes—Salt and Oak—are features of the lower part of the basin. Originally a natural feature, Salt Lake now is above the dredged channel of Oak Creek, and its level is maintained by water pumped from the creek. Oak Lake, on the other hand, is manmade and is on a sanitary fill in the wedge-shaped area lying between Oak and Salt Creeks; it, too, is maintained by pumpage from Oak Creek. During the period of study, part of the flow of Oak Creek was being impounded in a reservoir near the middle of the drainage basin and part was being pumped to maintain Salt and Oak Lakes. Thus, the discharge of Oak Creek at its mouth was much less than it would have been if the flow were not regulated. Discharges measured during this study ranged from 0.36 to 49.8 cfs and averaged 12.5 cfs.

Antelope Creek drains a much smaller area than either Middle or Oak Creeks. The upper half of the basin is mostly

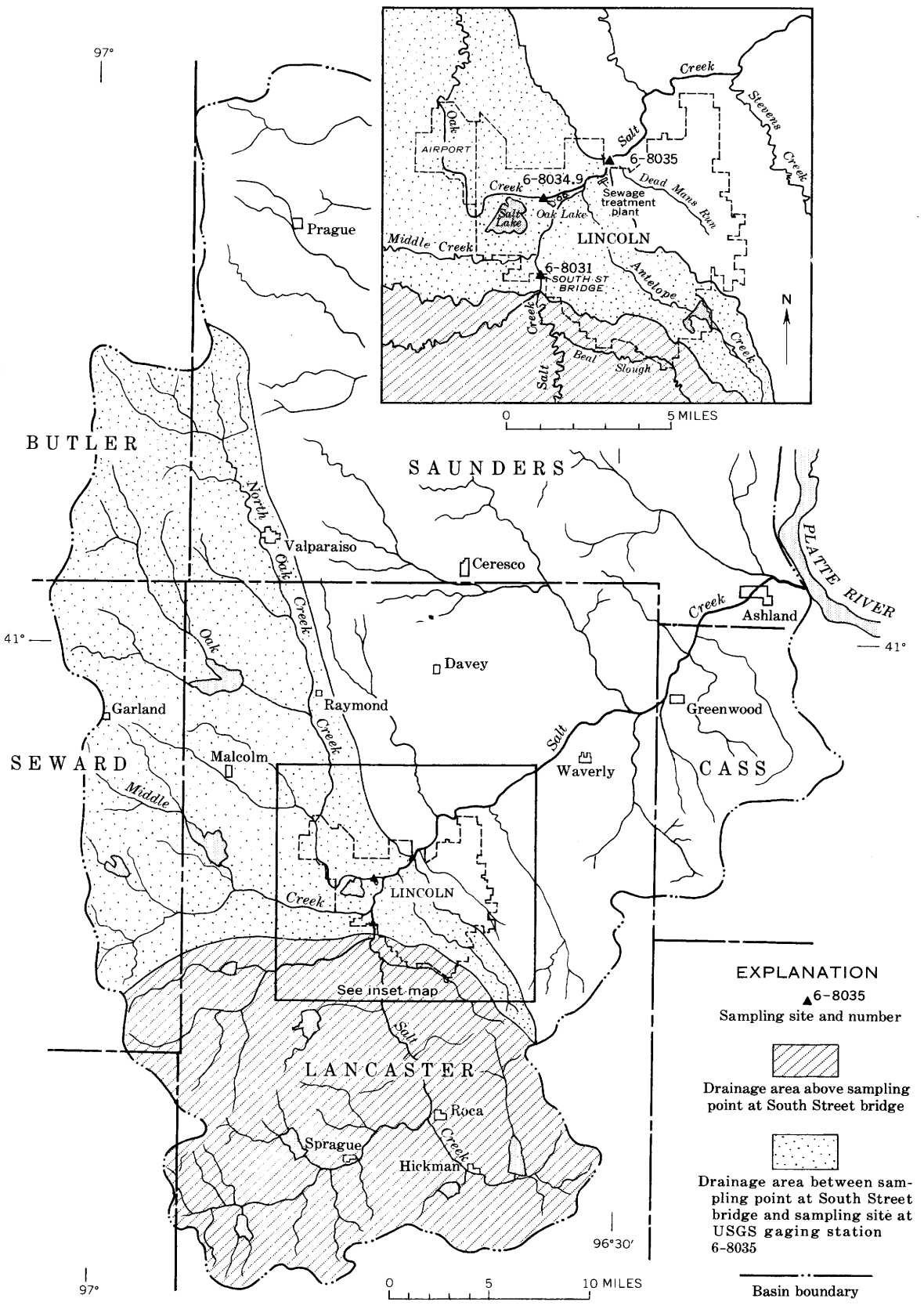

Figure 1.—Map of Salt Creek basin, Nebraska, showing sampling sites on Salt and Oak Creeks, area drained by Salt Creek above Lincoln, and area drained by 6-mile reach of Salt Creek within Lincoln's municipal limits.

agricultural land, but its lower half—an area of about 6 square miles—is wholly urbanized and includes about 35 percent of the city of Lincoln. At the upper end of the urbanized area is a flood-control dam and impoundment for recreational use. Except during times of storm runoff and snowmelt, the discharge at the mouth of Antelope Creek is very low. Average discharge, including storm runoff, is less than 5 cfs.

Runoff from another 30 percent of Lincoln, which includes the main business district, the city campus of the University of Nebraska, and the State fairgrounds also drains into the 6-mile reach via storm sewers and small unnamed creeks. Included in the contribution from the main business district and city campus is a small amount of water pumped from wells and used for air conditioning.

Effluent that has undergone secondary treatment at the Lincoln sewage-treatment plant constitutes an important contribution to the flow of Salt Creek at the lower end of the 6-mile reach. During the 1968 water year, the average discharge from the treatment plant was 27.3 cfs, or about 30 percent of the total flow at the gaging station. Monthly averages of flow during the 1968 water year ranged from 24.7 cfs in February and March 1968 to 31.2 cfs in August 1968, a 24 percent variation; daily ranges in flow were even greater. Virtually all the water passing through the plant was water that the municipal water-supply system imported by pipeline from a well field alongside the Platte River near the mouth of Salt Creek.

Between the South Street bridge, where Salt Creek enters the city, and gaging station 6–8035, where the creek leaves the city, the discharge of Salt Creek increases more than the visible inflow from streams, storm sewers, and effluent from the sewage-treatment plant. The additional pickup must be due to ground-water seepage from the adjacent alluvial deposits. Whether Salt and Oak Lakes are sources of significant amounts of seepage is not known.

Some waste water from the city reaches Salt Creek after it leaves the municipal limits. Overland runoff and storm-sewer outflow from about 30 percent of Lincoln reaches Salt Creek via Dead Mans Run, the mouth of which is about 0.3 mile below gaging station 6–8035. In addition, 1 percent of the sewage—that from the northeasternmost part of the city—is conveyed to a lagoon near the mouth of Stevens Creek, which is tributary to Salt Creek 5.5 miles downstream from the gaging station.

OTHER INVESTIGATIONS

Other researchers have investigated the various sources of phosphorus and nitrogen in waste waters and have determined per capita contributions of these elements to sewage effluent. Sherman (1952) indicated that data from 150 institutions in the United States show that the annual per capita contribution of phosphorus from human excrement ranges from a minimum of 0.5 pound to a maximum of 2.3 pounds and averages 1.3 pounds. The annual per capita contribution of phosphorus from detergents (United States only) was shown by Sawyer (1952) to have been 1.6 pounds in 1950, by Engelbrecht and Morgan (1959) to have been 1.9 pounds in 1955, and by an AWWA (American Water Works Association) Task Group (1967) to have been 2.1 pounds in 1958. Sawyer (1965) indicated that detergent-based phosphorus composed between 50 and 75 percent of the total phosphorus concentration in domestic waste water. The AWWA Task Group estimated total phosphorus in domestic sewage from both human wastes and detergents in the United States as 2.8 to 4.1 pounds per capita in 1958 and 1.7 to 4.2 pounds per capita in 1959. Investigations by Missingham (1967) indicated per capita per year contributions of phosphorus ranging from 2.0 to 2.8 pounds for four cities discharging wastes to the Grand River in Ontario, Canada. MacKenthun (1968, 1969) gave a national average for phosphorus, based on the work of several researchers, of 3.0 pounds per capita per year in sewage and sewage effluents in the United States. Feth (1966) indicated that the normal range of mineral pickup (concentration in sewage effluent) is 20 to 40 mg/l (milligrams per liter) as PO_4, which is about 7 to 14 mg/l as P. The AWWA Task Group report stated that a 1937 ASCE (American Society of Civil Engineers) committee found the annual per capita contribution of total nitrogen in the United States to range from 8 to 12 pounds and average 11 pounds. An average of 12 pounds per capita per year was given by Weibel (1969) for Cincinnati, Ohio. Feth (1966) indicated a concentration in sewage effluent of 20 to 40 mg/l total nitrogen.

METHODS OF INVESTIGATION

During the 17-month period of the study, 14 sets of samples were collected at three sites, one site at each end of the 6-mile reach of Salt Creek within Lincoln and one near the lower end of Oak Creek, which is the major tributary entering the reach. The sampling site at the upper end of the reach was Salt Creek at South Street (6–8031), and the sampling site at the lower end of the reach was the gaging station Salt Creek at Lincoln (6–8035). The sampling site on the tributary was Oak Creek at Lincoln (6–8034.9) and was about 1 mile upstream from the confluence of Oak and Salt Creeks.

Days chosen to collect samples were selected at random to allow an unbiased calculation of averages for the study period and to minimize the effect of variables, such as fluctuating sewage load on different days of the week. For example, Monday is traditionally laundry day and the detergent contribution to phosphorus loads that day of the week might be higher than average. Water discharge of Salt Creek at South Street and of Oak Creek was measured at the time the samples were collected. An instantaneous discharge was obtained for Salt Creek at Lincoln from the rating curve based on streamflow records.

Samples were packed in ice and taken to the U.S. Geological Survey laboratory in Lincoln, where the analyses were performed as soon as possible, usually within 24 hours, after

Table 1.—*Determinations of phosphorus and nitrogen in Salt and Oak Creeks at Lincoln, Nebr.*

[Locations of sampling sites are shown in figure 1]

Date	Salt Creek at South Street (6–8031)					Oak Creek at Lincoln (6–8034.9)					Salt Creek at Lincoln (6–8035)				
	Water discharge (cfs)	Dissolved phosphorus as P (mg/l)	Phosphorus, in tons per day	Total nitrogen as N (mg/l)	Nitrogen, in tons per day	Water discharge (cfs)	Dissolved phosphorus as P (mg/l)	Phosphorus, in tons per day	Total nitrogen as N (mg/l)	Nitrogen, in tons per day	Water discharge (cfs)	Dissolved phosphorus as P (mg/l)	Phosphorus, in tons per day	Total nitrogen as N (mg/l)	Nitrogen, in tons per day
10–12–67 . . .	[1]25	0.26	0.018	1.3	0.088	10.9	0.22	0.0065	1.6	0.047	78	2.3	0.48	9.7	2.0
11– 8–67 . . .	12.4	.28	.0094	.86	.029	12.2	.16	.0053	.66	.022	64	7.4	1.3	18	3.1
2– 2–68 . . .	20.2	.20	.011	1.6	.087	10.3	.12	.0033	1.5	.042	64	6.1	1.0	10	1.7
4–12–68 . . .	12.4	.22	.0074	2.0	.067	2.9	....	.....	2.5	.020	69	5.7	1.1	13	2.4
7–17–68 . . .	6.8	.31	.0057	1.2	.022	.36	.23	.0002	.88	.0009	69	5.6	1.0	12	2.2
9–23–68 . . .	55.2	.19	.028	1.8	.27	13.5	.28	.010	1.8	.066	130	5.0	1.8	13	4.6
10– 1–68 . . .	14.3	.30	.011	1.4	.054	6.8	.33	.0060	1.1	.020	81	10	2.2	8.9	2.0
10–16–68 . . .	37.5	.56	.057	.77	.078	49.8	.25	.034	2.1	.28	286	1.1	.85	2.1	1.6
12– 4–68 . . .	16.0	.23	.010	.30	.013	15.1	.22	.0090	1.7	.069	73	2.8	.55	5.9	1.2
12– 5–68 . . .	17.0	.24	.011	.38	.017	15.5	.13	.0054	.53	.022	69	2.0	.37	5.8	1.1
12–16–68 . . .	14.2	.23	.0088	1.9	.073	8.2	.17	.0038	.44	.010	66	2.8	.50	9.6	1.7
1– 6–69 . . .	12.9	.12	.0042	1.6	.056	9.6	.11	.0028	2.1	.054	68	2.4	.44	6.5	1.2
1– 9–69 . . .	17.9	.17	.0082	1.5	.072	10.7	.24	.0069	2.1	.061	62	1.2	.20	4.8	.80
2–18–69 . . .	[1]60	.41	.066	2.6	.42	9.6	.85	.022	2.9	.075	104	7.4	2.1	10	2.8

[1] Estimated.

the time of collection. Dissolved phosphorus and total nitrogen (sum of several constituents) were determined by standard U.S. Geological Survey methods (Rainwater and Thatcher, 1960).

RESULTS

Chemical analyses for each of the 14 sets of samples are shown in table 1. The highest concentrations of dissolved phosphorus in Salt Creek at South Street (6–8031) and in Oak Creek (6–8034.9) were 0.41 mg/l and 0.85 mg/l, respectively. Most of the phosphorus at these sites is agricultural in origin because, as previously indicated, very little urban runoff is contributed to either stream above these locations. Salt Creek at the gaging station (6–8035) downstream from the sewage outfall contained a high value of 10 mg/l phosphorus. Total nitrogen values were as much as 2.6 mg/l at South Street, 2.9 mg/l at Oak Creek, and 18 mg/l at the gaging station.

Inflow to the 6-mile reach from sources other than Salt Creek and Oak Creek can be determined from the discharges shown in table 1 for each set of measurements. Except on October 16, 1968, inflow ranged from 33 to 62 cfs and treatment-plant effluent accounted for at least half the amount. The other sources of water previously mentioned account for the rest of the flow. Rain was falling on October 16, 1968, when the difference amounted to 199 cfs, and storm-sewer outfall and urban runoff accounted for the greater part of inflow to the reach. The lowest concentrations of phosphorus and nitrogen at the gaging-station site occurred at this time.

Random sampling made possible the computation of overall averages for the period of study. The validity of the averages is indicated by the water-discharge record of the Salt Creek at Lincoln station (6–8035). The 14 sampling-day discharges averaged 92 cfs, which is within 5 percent of the 97-cfs average flow at the gaging station for the entire study period.

Table 2 shows the average amounts of phosphorus and nitrogen at each sampling site during the period of study. In addition, it shows estimates, based largely on those data, of the average amounts of phosphorus and nitrogen contributed to Salt Creek by the city of Lincoln. Taken into account in the making of these estimates were the concentrations of phosphorus (0.2 mg/l) and nitrogen (0.1 mg/l) in the Lincoln city water supply and the probable contributions of the almost wholly rural Middle Creek drainage basin and the rural upper part of the Antelope Creek drainage basin. The estimated values for effluent from the city—0.94 ton of phosphorus per day and 1.8 tons of nitrogen per day—are equivalent to 4.5 pounds per capita per year of phosphorus and 8.7 pounds per capita per year of nitrogen. These figures represent minimum values because about 30 percent of the overland runoff and storm-sewer outfall and about 1 percent of the sewage from the city enters Salt Creek either upstream or downstream from the 6-mile reach within the city and thus is not represented in the measured increases of phosphorus and nitrogen within the reach.

The computed values for phosphorus and nitrogen contributions from treatment-plant effluent and urban runoff need some qualification. They may be smaller than actual because runoff during the first part of a storm may contain phosphorus

Table 2.—*Average amounts of phosphorus and nitrogen determined for the period October 1967–February 1969 in Salt and Oak Creeks, and amounts computed for the city of Lincoln*

[Locations of sampling sites are shown in figure 1]

	Salt Creek at South Street (6–8031)	Oak Creek at Lincoln (6–8034.9)	Salt Creek at Lincoln (6–8035)	City of Lincoln
Phosphorus:				
Tons per day . . .	0.018	0.0089	0.99	0.94
Pounds per day. .	36	18	2,000	1,900
Pounds per capita per year.	.....	.....	.....	4.5
Nitrogen:				
Tons per day . . .	.096	.056	2.0	1.8
Pounds per day. .	192	110	4,000	3,700
Pounds per capita per year.	.....	.....	.....	8.7

and nitrogen derived from fertilizers as well as fixed nitrogen from lawns in amounts considerably larger than those measured in randomly collected samples. Furthermore, phosphorus is adsorbed on sediment readily, and such adsorbed phosphorus is either lost before runoff reaches the stream or is removed by filtration when samples are collected.

ANALYSIS OF DATA

Results obtained during this study compare favorably with those of earlier investigators. Although the value of 4.5 pounds of phosphorus per capita per year is greater than the AWWA Task Group's estimated maximum of 4.2 pounds per capita in 1959, it seems an acceptable result because use of detergents, including the "presoaks" that entered the market since 1959, has increased markedly in the interim. The per capita figures for nitrogen from sewage expectably would remain more nearly static than per capita figures for phosphorus because industrial advances involving nitrogen compounds have been modest compared to the detergent industry's advances involving phosphorus. The 8.7 pounds per capita per year of nitrogen is within the ASCE Committee's reported range of 8 to 12 pounds per capita per year.

If it is assumed that 90 percent of the 0.94 ton per day of phosphorus passes through the Lincoln sewage-treatment plant, the average concentration of phosphorus in the effluent would be 12 mg/l. This value is within the range of 7–14 mg/l given by Feth (1966). Ralph Langemeier, an official of the Environmental Health Department of the State of Nebraska, stated (oral commun., August 1970) that a sample of treatment-plant effluent collected December 18, 1968, by his agency contained 43 mg/l total phosphate as PO_4, or 14 mg/l phosphorus. That was the only sample of Lincoln sewage analyzed for phosphorus by his agency while this study was in progress, and the result compares well with the average concentration determined by this study. An average concentration of 23 mg/l nitrogen in the effluent was obtained by assuming that 90 percent of the 1.8 tons per day of nitrogen passes through the sewage-treatment plant. This value falls within the 20–40 mg/l range given by Feth (1966).

Dilution and other processes such as adsorption on sediments and biological activity reduce the concentration of total phosphorus and total nitrogen downstream from Lincoln. Regardless of the dilution and other processes, a certain amount of those constituents remain in solution and should, therefore, be considered in planning for any projected downstream use.

REFERENCES

American Water Works Association Task Group 2610P, 1967, Sources of nitrogen and phosphorus in water supplies: Am. Water Works Assoc. Jour., v. 59, no. 3, p. 344–366.

Engelbrecht, R. S., and Morgan, J. J., 1959, Studies on the occurrence and degradation of condensed phosphate in surface waters: Sewage Indus. Wastes, v. 31, no. 4, p. 458–478.

Feth, J. H., 1966, Nitrogen compounds in natural water–a review: Water Resources Research, v. 2, no. 1, p. 41–58.

MacKenthun, K. M., 1968, The phosphorus problem: Am. Water Works Assoc. Jour., v. 60, no. 9, p. 1047–1054.

———1969, The practice of water pollution biology: Federal Water Pollution Control Administration, 281 p.

Missingham, G. A., 1967, Occurrence of phosphates in surface waters and some related problems: Am. Water Works Assoc. Jour., v. 59, no. 2, p. 183–211.

Rainwater, F. H., and Thatcher, L. L., 1960, Methods for collection and analysis of water samples: U.S. Geol. Survey Water-Supply Paper 1454, 301 p.

Sawyer, C. N., 1952, Some new aspects of phosphates in relation to lake fertilization: Sewage Indus. Wastes, v. 24, no. 7, p. 768–776.

———1965, Problem of phosphorus in water supplies: Am. Water Works Assoc. Jour., v. 57, no. 11, p. 1431–1439.

Sherman, H. C., 1952, Chemistry of food and nutrition, 8th ed.: New York, The MacMillan Co., 721 p.

Weibel, S. R., 1969, Urban drainage as a factor in eutrophication, *in* Eutrophication–causes, consequences, correctives: Washington, D.C., National Academy of Sciences, p. 383–403.

PREDICTION ERROR OF REGRESSION ESTIMATES OF STREAMFLOW CHARACTERISTICS AT UNGAGED SITES

By CLAYTON H. HARDISON, Arlington, Va.

Abstract.—When the time-sampling error of a streamflow characteristic that is used in a multiple regression with basin characteristics is greater than the space-sampling error and when the average interstation correlation coefficient is less than 0.25 or greater than 0.75, the average standard error of prediction differs by more than 20 percent from the standard error of estimate of the regression. Graphs show how the relation between average prediction error and the regression error can be evaluated for any regression. A moderate increase in the length of record at the gaging stations used in the regression will seldom result in an appreciable decrease in the standard error of prediction.

To appraise the accuracy of streamflow information obtained by regression of a flow characteristic, such as a 50-year flood, with basin characteristics, such as drainage-area size and stream-channel slope, the standard error of the flow characteristic thus estimated is sometimes compared with the standard error of the same characteristic estimated from an observed record of given length. Although the standard error of estimate of the regression gives an approximation of the standard error of the flow characteristic, the standard error of prediction is really what should be used in making the comparison.

The standard error of prediction as used in this paper differs from the standard error of estimate of the regression in that it includes the error in the regression equation as well as the scatter about the equation. It is a measure of the difference between estimated and true values of the characteristic. As shown by Matalas and Gilroy (1968), the accuracy of a prediction depends in part on how much of the standard error of estimate is due to time-sampling error (error in the characteristic at the stations used in the regression) and how much is due to error in the underlying relation between the true values of the flow characteristic and the set of basin characteristics. Furthermore, it is different for the gaged sites used in the regression than it is for ungaged sites.

This paper evaluates the equation for ungaged sites given by Matalas and Gilroy (1968) and presents the results in a form more suitable for use in planning a program for the collection of streamflow information. The error in the underlying relation between a flow characteristic and a set of basin characteristics is here termed space-sampling error as it represents the interstation difference in flow characteristics that would remain as regression error even though the records at the gaging stations used in defining the regression were of infinite length. It is similar to the model error in a classical regression.

In this paper, standard error is expressed in percentage or in log units, and the corresponding variance is therefore expressed as the square of these units rather than as the square of a measurement unit. In most regressions of streamflow characteristics and basin characteristics, logarithmic transformation of all variables tends to normalize the variables and the residuals as well as tending to make the residuals homoscedastic as required in classical regression analysis. The resulting standard error of estimate for regressions of such transformed variables is in log units, but it can be converted to percentage where desired.

Acknowledgments.—Appreciation is expressed in various associates who made helpful suggestions regarding the content of this paper and especially to E.J. Gilroy for his help in relating the practical approach used in this paper to results given in previous papers of a more theoretical nature.

PREDICTION ERROR AT SPECIFIC SITES

The accuracy of a streamflow characteristic estimated from a regional regression depends on how the true values of the flow characteristic for fixed values of basin characteristics would compare with values of the flow characteristic estimated from regression equations based on many different sets of gaging-station data. The prediction error at a specific site thus depends on the accuracy of the given regression equation as well as on the scatter of the true values about that equation. In standard textbook regression, where the inaccuracy of the regression equation is usually small in comparison with the scatter about the equation, the standard error of estimate of the regression can be used as a reasonable estimate of the standard error of prediction. In a regression of a streamflow characteristic, however, the difference between the standard error of prediction and the standard error of estimate of the regression can be appreciable.

Where the time-sampling error contributes significantly to the standard error of estimate of the regression, Matalas and Gilroy (1968, equation 24) give an equation for the variance of a prediction at a site not used in the development of the regression. In different notation, this equation becomes

$$V_P = V_S\left[1+\frac{1}{k}+\frac{z^2}{k}\right]+\overline{V_T}\left[\rho+\frac{(1-\rho)}{k}+\frac{(1-\rho)z^2}{k}\right], \quad (1)$$

in which

V_P = variance of prediction at an ungaged site,
V_S = variance of the space-sampling error in a given regression,
$\overline{V_T}$ = average variance of the time-sampling error at the stations used in the regression,
k = number of stations used in the regression,
ρ = average (mean) interstation correlation coefficient as defined by Matalas and Gilroy, and
z = a weighted measure of the departure of the specific values of the independent variables (basin characteristics) from their means; in a regression on one independent variable, z is the number of standard deviation units from the mean at which the prediction is being made.

The reader is referred to the List of Symbols at the end of the paper for more comprehensive definitions of symbols.

Equation 1 reduces to

$$V_P = V_S + \rho\overline{V_T} + \frac{[V_S + (1-\rho)\overline{V_T}]\,(1+z^2)}{k}. \quad (2)$$

Because the term $[V_S + (1-\rho)\overline{V_T}]/k$ defines the accuracy of the regression equation at the mean of all the independent variables insofar as the accuracy is affected by k and by the scatter about the regression equation, it can be set equal to V_R/k, in which V_R is the square of the standard error of estimate of the regression. Thus

$$V_S = V_R - (1-\rho)\overline{V_T}, \quad (3)$$

and from equation 2

$$V_P = V_R - \overline{V_T} + 2\rho\overline{V_T} + \frac{V_R(1+z^2)}{k}. \quad (4)$$

Letting $b = V_R/\overline{V_T}$, $\overline{V_T}$ equals V_R/b and

$$\frac{V_P}{V_R} = \left[1+\frac{1}{k}+\frac{z^2}{k}\right] - \frac{1}{b}(1-2\rho). \quad (5)$$

This is the basic equation for the accuracy of prediction at a specific ungaged site. The evaluation of this equation is discussed in the remainder of this section.

The evaluation of $b = V_R/\overline{V_T}$ for use in equation 5 is complicated by the fact that V_T, the time-sampling variance, varies among stations and depends on the length of record and on the variability of the annual events. The average variability (coefficient of variation, C_v, or index of variability, I_v) for all the stations used in a regression has been found to be suitable for use in computing the average time-sampling variance if the corresponding average length of record is computed as the reciprocal of the average reciprocal of the length of records at the individual stations. Therefore, the average length of record thus computed, which is commonly called the harmonic mean, is used as N_G in this paper. For practical purposes, however, the arithmetic mean is a reasonably satisfactory estimate of N_G. Although the arithmetic mean is usually about 10 percent larger than the harmonic mean for a twofold variation in length of record, the effect on the computed standard error of prediction is usually less than 10 percent.

If a mean monthly discharge for a specific calendar month or the mean annual discharge are being regionalized, $\overline{V_T}$ for use in obtaining b to use in equation 5 is computed as $(100\,\overline{C_v})^2/N_G$ in which $\overline{C_v}$ is the average coefficient of variation of the annual events, such as October mean flows or the annual mean flows at the stations used in the regression. To make the units of V_R and V_S consistent with those for $\overline{V_T}$, the standard error of estimate in log units, $\sqrt{V_R}$, is converted to percentage error by use of table 1.

Table 1.—*Relation between standard error of estimate,* V_R, *in log units and in percent for a log-normal distribution of errors*

Log units	Percent	Log units	Percent
0.02	4.6	0.42	124
.04	9.2	.44	134
.06	13.9	.46	144
.08	18.6	.48	155
.10	23.3	.50	166
.12	28.2	.52	178
.14	33.0	.54	192
.16	38.1	.56	206
.18	43.2	.58	222
.20	48.6	.60	240
.22	54.0	.62	258
.24	59.8	.64	278
.26	65.6	.66	301
.28	71.8	.68	326
.30	78.2	.70	353
.32	84.9	.72	382
.34	92.0	.74	415
.36	99.4	.76	451
.38	107	.78	491
.40	116	.80	536

NOTE.—Errors in percentage are not normally distributed.

The relation between normally distributed log units (common logarithms) and percentage shown in table 1 is based on the relation $C_v^2 = \exp(\sigma_y^2) - 1$, in which σ_y is the standard error in units of natural logarithms and $100\,C_v$ is the standard error in percent. The percentages shown differ somewhat from those given by the conversion of the log units for one standard deviation to equivalent percent (Hardison, 1969, table 2). Although this previously published conversion is useful in that it gives the percentage bands that include two-thirds of the errors, it does not give the standard error in percent required in computing the ratio $V_R/\overline{V_T}$. For log units less than 0.30, however, the effect on $V_R/\overline{V_T}$ of using the previously published table is less than 5 percent.

If it is a T-year event that is being regionalized, $\overline{V_T}$ is computed from the R values shown in table 2 by the equation $\sqrt{\overline{V_T}} = SE_{xT} = R(\overline{I_v})/\sqrt{N_G}$, in which SE_{xT} is the standard error of the T-year event in log units, $\overline{I_v}$ is the average standard deviation of the logarithms of the annual events, and N_G is the harmonic mean length of record at the gaging stations used in the regression. The corresponding V_R needed to compute the ratio $V_R/\overline{V_T}$ equals $(SE_R)^2$ in which SE_R is the standard error of estimate of the regression in log units.

The standard error computed from the R values shown in table 2 represents the standard error of the T-year event that would be obtained by using the known population skew coefficient in conjunction with the mean and the standard deviation of the annual events in each sample. If the skew coefficient of the sample were to be used in computing the T-year event, the R values would differ somewhat from those shown in table 2. Therefore, if the T-year events, such as the 50-year floods used in a regression, are computed by fitting a log-Pearson Type III distribution to the mean, standard deviation, and skew coefficient of the logarithms of the observed annual peaks, the R values for 50-year and 100-year peaks shown in table 2 should be increased by 10 percent and 20 percent, respectively, to obtain the proper V_T to use in computing b for use in equation 5. These adjustments are based on random-number experiments using 5, 10, and 50 annual events per sample.

Accuracy equations for the time-sampling error of streamflow characteristics are summarized in table 3. The units for $\sqrt{V_T}$ indicated for each characteristic define the appropriate units for $\sqrt{V_R}$, $\sqrt{V_S}$, and SE_P as used in this paper also. The last two columns of table 3 are discussed later in this paper.

The evaluation of the average interstation correlation coefficient, ρ, shown in equation 5 is outside the scope of this paper, but for some characteristics it can be estimated from the streamflow records used in the regression. By random sampling of possible pairs of the gaging stations used in a regression study, for example, Benson (1962, p. A-25) found that the average interstation correlation coefficient between annual peak flows in New England was 0.26. Similarly, M. E. Moss (written commun., 1969) found that the average interstation correlation coefficient between monthly flows at stations in the Potomac River basin was about 0.7. Interstation correlation coefficients obtained in this manner are suitable for use in appraising the accuracy of mean events such as mean annual peak flow and mean October flow. Although it is likely that the average interstation correlation coefficient may vary with T, no information is available to indicate whether ρ tends to increase or to decrease as the recurrence interval becomes larger.

As k in equation 5 is the number of stations used in the regression, the only remaining variable to be evaluated is z. In

Table 2.—*Values of* R *for use in appraising accuracy of a T-year event estimated from observed annual events from a log-Pearson Type III population of known skew*[1]

T	R for indicated logarithmic skew coefficient of population of annual peaks								
	-1.5	-1.0	-0.5	-0.2	0	+0.2	+0.5	1.0	1.5
1.25	1.638	1.486	1.328	1.229	1.164	1.102	1.020	0.916	0.819
2	.845	.933	.983	.997	1.000	.997	.983	.933	.845
5	.819	.916	1.020	1.102	1.164	1.229	1.328	1.486	1.638
10	.926	1.029	1.148	1.258	1.350	1.454	1.629	1.956	2.325
20	1.006	1.134	1.276	1.414	1.534	1.674	1.921	2.416	3.010
25	1.026	1.163	1.316	1.500	1.591	1.747	2.013	2.560	3.228
50	1.075	1.246	1.433	1.608	1.763	1.950	2.288	3.006	3.093
100	1.107	1.313	1.538	1.742	1.925	2.146	2.554	3.438	4.574
Corresponding logarithmic skew coefficient for annual lows.	+1.5	+1.0	+0.5	+0.2	0	-0.2	-0.5	-1.0	-1.5

NOTE.—R equals $SE_{xT}\sqrt{N}/I_v$ in which SE_{xT} is the standard error of the estimated T-year event in log units, I_v is the standard deviation of the logarithms of the annual events, and N is the number of annual events. T is recurrence interval in years.

[1] For a 50-year peak computed using sample skew, indicated value of R should be increased 10 percent; for a 100-year peak, 20 percent.

Table 3.—*Accuracy equations for regionalized streamflow characteristics*

Characteristic	Time-sampling error		Accuracy of prediction in equivalent years of record	
	Equation	Units for $\sqrt{\overline{V_T}}$	Equation	Units for SE_P
Monthly or annual mean flow.	$\sqrt{\overline{V_T}} = \frac{100\overline{C_v}}{\sqrt{N_G}}$	Percent	$N_U = \left[\frac{100\overline{C_v}}{SE_P}\right]^2$	Percent
Standard deviation of monthly or annual flow.	$\sqrt{\overline{V_T}} = \frac{100\sqrt{1+0.75\,C_s^2}}{\sqrt{2N_G}}$	Percent	$N_U = \frac{0.5(1+0.75C_s^2)}{(SE_P/100)^2}$	Percent
Mean log of monthly or annual flow.	$\sqrt{\overline{V_T}} = \frac{\overline{I_v}}{\sqrt{N_G}}$	Log	$N_U = \left[\frac{\overline{I_v}}{SE_P}\right]^2$	Log
Standard deviation of logs of monthly or annual flow.	$\sqrt{\overline{V_T}} = \frac{\overline{I_v}\sqrt{1+0.75C_s^2}}{\sqrt{2N_G}}$	Log	$N_U = 0.5\left[\frac{\overline{I_v}}{SE_P}\right]^2 (1+0.75C_s^2)$	Log
T-year highs or T-year lows.	$\sqrt{\overline{V_T}} = \frac{R(\overline{I_v})}{\sqrt{N_G}}$	Log	$N_U = R^2\left[\frac{\overline{I_v}}{SE_P}\right]^2$	Log

NOTE.—V_T is time-sampling standard error, SE_P is standard error of prediction, values of R are as shown in table 2, other symbols are defined in List of Symbols.

a simple regression, z for a specific site can be computed as the distance measured in standard deviation units between a specific value of the independent variable and the mean of that variable. In a multiple regression, z^2 can be computed from the inverse of the variance-covariance matrix of the independent variables and the departure of the specific value of each variable from the mean of that variable (Davies, 1961, p. 229). When the results of a regression are used to help plan a program for collecting streamflow information at ungaged sites, however, an average value of z^2 at all possible sites should be used as discussed in the next section.

AVERAGE PREDICTION ERROR

The average accuracy of prediction at all ungaged sites in a region can be appraised by assuming that the values of the independent variables at the gaging stations used in the regression are an unbiased sample of a log-normally distributed population of values of the independent variables at all sites. Under such an assumption, the average z^2 to use in equation 5 as computed from an equation given by Kerridge (1967) equals $\frac{(k+1)m}{(k-m-2)}$, in which m is the number of independent variables. Thus from equation 5

$$\frac{\overline{V_P}}{V_R} = 1 + \left(\frac{2\rho - 1}{b}\right) + \frac{1}{k} + \frac{(k+1)m}{k(k-m-2)}, \qquad (6)$$

in which $\overline{V_P}$ is the average logarithmic variance of predictions made from a regression. Equation 6 can be used to evaluate $\overline{V_P}/V_R$ and SE_P/SE_R for selected values of k, m, ρ, and $b = V_R/\overline{V_T}$.

For a regression of a flow characteristic at 40 gaging stations and using three independent variables, the last term in equation 6 becomes 0.088 and the sum of the last two terms becomes 0.113 to make $\overline{V_P}/V_R$ equal 1.113 plus $(2\rho - 1)/b$. From this relation $\overline{V_P}/V_R$ can be evaluated for selected values of ρ and of b as shown in columns 3 and 4 of table 4. Since by equation 3

$$\frac{V_S}{\overline{V_T}} = \frac{V_R}{\overline{V_T}} - 1 + \rho \qquad (7)$$

the corresponding $V_S/\overline{V_T}$ can be computed as shown in column 2. For number of stations and number of independent

Table 4.—*Standard error of prediction of streamflow characteristics at ungaged sites estimated from a regression of 40 gaging stations and three basin parameters*

ρ	b = $V_S/\overline{V_T}$	$V_R/\overline{V_T}$	$\overline{V_P}/V_R$	SE_P/SE_R
0	0.00	1.00	0.113	0.336
	.25	1.25	.313	.559
	.50	1.50	.446	.668
	1	2	.613	.783
	2	3	.780	.883
	4	5	.913	.956
	8	9	1.002	1.001
.10	0	.9	.224	.473
	.25	1.15	.417	.646
	.50	1.4	.542	.736
	1	1.9	.692	.832
	2	2.9	.837	.915
	4	4.9	.950	.975
	8	8.9	1.017	1.008
.25	0	.75	.447	.669
	.25	1.00	.613	.783
	.50	1.25	.713	.844
	1	1.75	.827	.909
	2	2.75	.931	.965
	4	4.75	1.008	1.004
	8	8.75	1.056	1.028
.50	0	.50	1.113	1.055
	.25	.75	1.113	1.055
	.50	1.00	1.113	1.055
	1	1.50	1.113	1.055
	2	2.5	1.113	1.055
	4	4.5	1.113	1.055
	8	8.5	1.113	1.055
.75	0	.25	3.113	1.764
	.25	.50	2.113	1.454
	.50	.75	1.779	1.334
	1	1.25	1.513	1.230
	2	2.25	1.335	1.155
	4	4.25	1.231	1.110
	8	8.25	1.173	1.083
.90	0	.10	9.113	3.019
	.25	.35	3.399	1.844
	.50	.60	2.447	1.564
	1	1.1	1.840	1.356
	2	2.1	1.494	1.222
	4	4.1	1.308	1.114
	8	8.1	1.211	1.100
1.0	.10	.10	11.113	3.334
	.25	.25	5.113	2.261
	.50	.50	3.113	1.764
	1	1	2.113	1.454
	2	2	1.613	1.270
	4	4	1.361	1.167
	8	8	1.236	1.112

NOTE.—$SE_P/SE_R = \sqrt{\overline{V_P}/V_R}$ is ratio of standard error of prediction to standard error of regression, both in log units. Other symbols are defined in the List of Symbols at end of paper.

variables different than those used in the computation of table 4, $\overline{V_P}/V_R$ should be adjusted as shown in figure 1, which is based on an evaluation of the last two terms in equation 6.

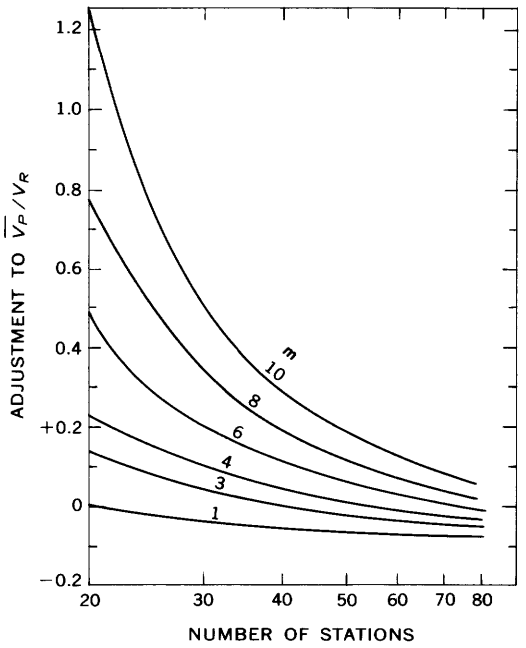

Figure 1.—Effect of number of variables and number of stations on average variance of prediction, $\overline{V_P}$. Parameter, m, is number of independent variables. V_R is variance of the regression. Adjustment is to be added to the $\overline{V_P}/V_R$ values for 40 stations and three basin parameters.

The ratio of the standard error of prediction to the standard error of regression shown in the last column of table 4 is the square root of $\overline{V_P}/V_R$. It is for use in converting standard error of regression to standard error of prediction.

Data from table 4 are plotted in figures 2 and 3 for illustration and for use in interpolation. The relations between the $\overline{V_P}/V_R$ ratios and the $V_S/\overline{V_T}$ ratios shown in figure 2 are the fundamental relations given by columns 2 and 4 of table 4, whereas the relations in figure 3, which are from the data given in columns 3 and 5, are more suited for practical application. The principal difference between figures 2 and 3 is that the values of $V_R/\overline{V_T}$ in figure 3 equal the values of $V_S/\overline{V_T}$ from the abscissa of figure 2 plus $(1.0 - \rho)$; the other difference is that SE_P/SE_R equals the square root of $\overline{V_P}/V_R$.

EQUIVALENT LENGTH OF RECORD

As the standard error of prediction of a streamflow characteristic depends largely on the variability of the annual events, it tends to be much larger in some sections of the country than in others. One way to remove this regional variability is to express the accuracy of prediction in terms of the equivalent years of record that would be required to give results of equal accuracy. This concept of equivalent-year accuracy is now being used in the design of streamflow data programs (Carter and Benson, 1970).

Equations for converting standard error of prediction to accuracy in equivalent years of record are given in the last two

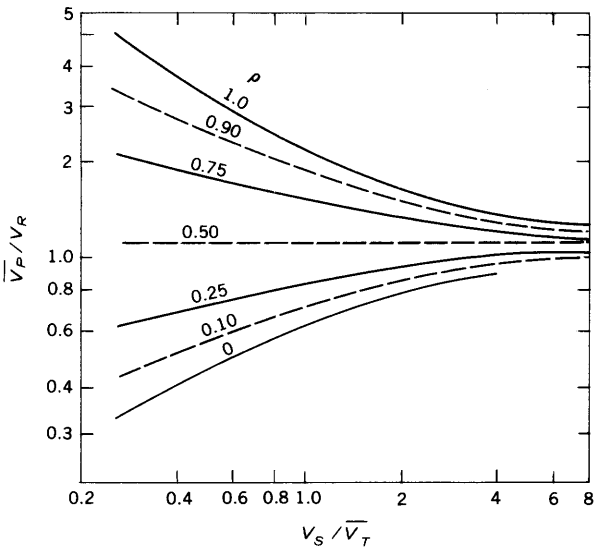

Figure 2.—Average variance of streamflow characteristics at ungaged sites estimated by regression with three basin parameters at 40 stream-gaging stations. $\overline{V_P}/V_R$ is ratio of average variance of prediction to the variance of the regression. Parameter, ρ, is average interstation correlation coefficient. $V_S/\overline{V_T}$ is ratio of space-sampling variance to average time-sampling variance.

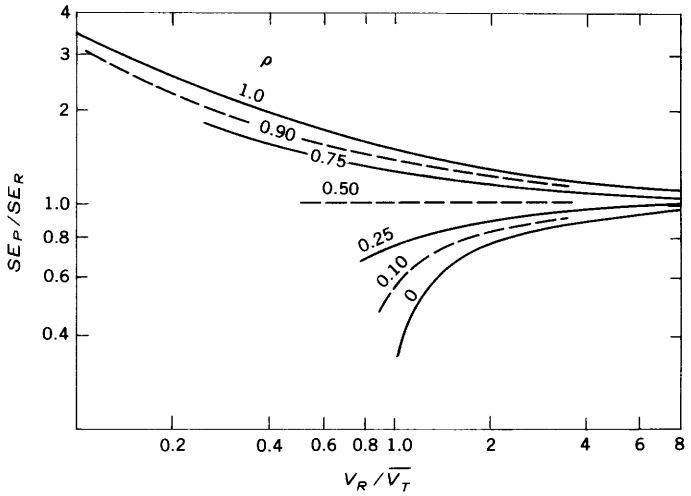

Figure 3.—Standard error of prediction of streamflow characteristics at ungaged sites estimated by regression with three basin parameters at 40 stream-gaging stations. SE_P/SE_R is ratio of standard error of prediction to standard error of estimate. Parameter, ρ, is average interstation correlation coefficient. $V_R/\overline{V_T}$ is ratio of regression variance to average time-sampling variance.

columns of table 3. If, for example, the coefficient of variation of the annual mean flows were 0.30 and the standard error of prediction were 10 percent, the accuracy of prediction in equivalent years of record is given by

$$N_U = \left(\frac{100C_v}{SE_P}\right)^2 = \left(\frac{30}{10}\right)^2 = 9 \text{ years.}$$

If the coefficient of variation and the standard error of prediction were both twice as large, the accuracy in terms of equivalent years of record would still be 9 years.

DISCUSSION

Table 4 shows that the standard error of estimate of a regression is a reasonably good estimate of the standard error of prediction when the average interstation correlation coefficient is 0.5 as the SE_P/SE_R ratio is then only 1.055 for all values of $V_S/\overline{V_T}$. When the average interstation correlation coefficient is greater than 0.5, the standard error of prediction is greater than the standard error of estimate, especially at low values of $V_S/\overline{V_T}$. When the average interstation correlation coefficient is appreciably less than 0.5, the standard error of prediction is less than the standard error of estimate, especially at low values of $V_S/\overline{V_T}$. When the space-sampling variance is more than 4 times the time-sampling variance, the difference between the standard error of prediction and the standard error of estimate is less than 10 percent in the usual range of ρ values. Thus the difference between the standard error of prediction and the standard error of estimate discussed in this paper is especially important when the space-sampling variance is less than 4 times the time-sampling variance and when the average interstation correlation coefficient differs appreciably from 0.5. For events such as flood peaks that tend to be somewhat independent this difference improves the accuracy of the estimates and thus improves the usefulness of the regression in estimating flow characteristics at ungaged sites. For events such as monthly discharge that tend to be fairly well correlated with monthly discharge at other sites, the difference impairs the accuracy and thus decreases the usefulness of the regression.

As the accuracy of a streamflow characteristic estimated by regression depends in part on the number of years of record at the gaging stations used in the regression and on the average interstation correlation, it is instructive to observe how much the accuracy of the estimates (standard error of prediction) could be improved by additional years of record or by a decrease in interstation correlation coefficient. (The effect of number of stations and of number of basin parameters can be evaluated by the curves shown in figure 1.)

The effect of an increase in the length of record at the gaging stations used in a regression of 40 stations and three basin parameters is indicated by the ratios in table 5, which show the effect of doubling the length of record. Although about half the percentage decrease in standard error of prediction indicated by these ratios would occur with only a 25-percent increase in length of record, it is obvious that the accuracy of the estimates would not usually be improved much by obtaining a few more years of record at the same gaging stations used to define the regression. The ratios shown in table 5 were computed from $\overline{V_P}/\overline{V_T}$ values obtained as the product of $V_R/\overline{V_T}$ and $\overline{V_P}/V_P$ for successive values of $V_S/\overline{V_T}$

Table 5.—*Decrease in standard error of prediction resulting from doubling the length of record at the gaging station used in a regression of 40 stations and three basin parameters*

Average interstation correlation coefficient	Ratio of final standard error of prediction to initial standard error of prediction, both in log units, for indicated $V_S/\overline{V_T}$				
	0.25	0.50	1.0	2.0	4.0
0.10	0.889	0.931	0.961	0.979	0.986
.25	.853	.901	.941	.967	.982
.50	.816	.866	.913	.949	.972
.75	.795	.842	.891	.933	.962
.90	.785	.830	.880	.925	.956

NOTE.—$V_S/\overline{V_T}$, the ratio of space-sampling variance to time-sampling variance, equals $(V_R/\overline{V_T} - 1 + \rho)$.

shown in table 4 by considering the fact that since $\overline{V_T}$, the time-sampling variance, varies inversely with the number of years of record in the sample, the successive values represent a doubling of the length of record. (V_S, the space sampling variance would of course remain constant for a given set of stations and independent variables.)

The effect of a change in the average interstation correlation coefficient on the accuracy of a streamflow characteristic obtained by regression is shown by the spacing of the curves in figure 3. It is evident that when the regression variance is greater than twice the time-sampling variance ($V_R/\overline{V_T}$ greater than two) that a substantial change in ρ, the average interstation correlation coefficient, is required to make a significant change in the computed accuracy of the estimates.

Whenever the product of the values of $V_R/\overline{V_T}$ and $\overline{V_P}/V_R$ given in table 4 is less than unity, the average variance of the estimates at the ungaged sites is less than the average time-sampling variance at the gaged sites. For such instances, the possible use of regression estimates at the gaged sites also should be considered, and the accuracy of such estimates should be evaluated by the use of the equation for gaged sites given by Matalas and Gilroy (1968, eq 13).

EXAMPLES FOR PLANNING

Given a logarithmic multiple regression of estimated 50-year peaks against drainage-area size, channel slope, channel length, pond area, and average annual snowfall in the Potomac River basin, which according to Thomas and Benson (1970, p. 32) gives a standard error of estimate of 0.167 log units, assume that we wish to know the average standard error of prediction of estimates made from this regression. The standard deviations of the logarithms of the annual peaks, I_v, at the gaging stations used in the regression average 0.279 with an average skew coefficient of 0.4, and the mean length of record at the 41 gaging stations used in the regression is 32 years. With these data known we can use an SE_P/SE_R ratio from figure 3 to obtain an estimate of the standard error of prediction and can refine this estimate by the use of figure 1.

A value of $V_R/\overline{V_T}$ to use in entering figure 3 can be obtained from the relation V_R equals $(SE_R)^2$ and from the equation $\sqrt{\overline{V_T}} = R(\overline{I_v})/\sqrt{N_G}$ given on the last line of table 3. For 50-year flood peaks with a known skew coefficient of 0.2, the R value given by table 2 is 1.950 and for a known skew coefficient of 0.5, it is 2.288. Interpolation for a skew coefficient of 0.4 gives an R of 2.175, but since the observed skew was used in computing the 50-year peaks used in the regression, this value should be increased by 10 percent as shown by the footnote on table 2 to give an R of 2.39. Then $SE_{xT} = \sqrt{\overline{V_T}} = R(I_v)/\sqrt{N_G} = 2.39\ (0.279)/\sqrt{32} = 0.1179$.

and $\dfrac{V_R}{\overline{V_T}} = \left(\dfrac{SE_R}{SE_{xT}}\right)^2 = \left(\dfrac{0.167}{0.1179}\right)^2 = (1.42)^2 = 2.0$. For this value of $V_R/\overline{V_T}$ and an assumed average interstation correlation coefficient of 0.25, figure 3 gives an 0.92 for SE_P/SE_R. As SE_R is 0.167 log units, SE_P would be 0.154 log units if k were 40 and m were 3. But since there are 41 stations (k = 41) and fire basin parameters (m = 5), the adjustment to $(SE_P/SE_R)^2$ is +0.07 according to figure 1 and the adjusted SE_P/SE_R is $\sqrt{(0.92)^2+0.07} = 0.957$ from which the standard error of prediction is 0.957 (0.167) or 0.160 log units.

If the accuracy goal for estimated 50-year floods had been set as the accuracy equivalent to what could be obtained with 20 years of observed annual peak flows, the accuracy goal for the distribution of annual peaks in this example would be

$$SE_{xT} = \sqrt{\overline{V_T}} = \frac{R(I_v)}{\sqrt{N}} = \frac{(2.39)\ (0.279)}{\sqrt{20}} = 0.149 \text{ log units.}$$

As this standard error is less than the 0.160 log units obtained for the standard error of prediction, the accuracy goal would not have been attained.

In order to help decide how the standard error of prediction might be improved, we can use the graphs and tables given in this paper. The ratio of space-sampling variance to the time-sampling variance as given by equation 7 is

$$\frac{V_S}{\overline{V_T}} = \frac{V_R}{\overline{V_T}} - 1 + \rho = 2.0 - 1 + 0.25 = 1.25,$$

and according to table 5 doubling the length of record for this value of $V_S/\overline{V_T}$ and for a ρ of 0.25 would reduce the standard error of prediction to 95 percent of the 0.160 log units obtained for the present regression. Thus, obtaining a few additional years of record at the gaging stations used in the present regression would do little toward improving the standard error of prediction. If by additional research the average interstation correlation coefficient were found to be only 0.10, the effect on SE_P would be only about 8 percent as indicated by the spacing of the curves in figure 3 at a $V_R/\overline{V_T}$ of 2.0.

Therefore, the only feasible way to increase the accuracy of estimated 50-year floods would be to improve the model by

adding additional basin parameters or by changing the transformations of the ones that were used. In other words, we would need to do a better job of indexing the physical and meteorological differences between basins within the Potomac River basin.

The average number of years of record required at ungaged sites to give estimated 50-year peaks as accurate as those given by the regression used in this example is helpful information to use in planning a streamflow data program. This information can be obtained from the equation given in the fourth column of the last line of table 3 as follows:

$$N_U = R^2 \left(\frac{\overline{I_v}}{SE_P}\right)^2 = (2.39)^2 \left(\frac{0.279}{0.160}\right)^2 = 5.71\,(3.04)$$

$$= 17.4 \text{ years.}$$

For a specific ungaged site, however, N_U would differ from 17.4 years because the standard error of prediction computed by equation 5 would differ from 0.160 depending on the specific values of the independent variables.

As another example, consider the mean flow for October for streams in the Potomac River basin, which in a regression against drainage area and precipitation (Thomas and Benson, 1970) has a standard error of estimate of 0.082 log units or 19.0 percent. The coefficients of variation of the October discharges at the 41 stations used in the regression range from 0.893 to 2.623 and average 1.426. The average length of record of October discharges is 29 years, and the harmonic mean length is 27 years. Using the arithmetic mean and the appropriate equation from table 3, the time-sampling standard error at the gaging stations used in the regression is computed as follows:

$$SE_{\bar{x}} = \sqrt{\overline{V_T}} = \frac{100\overline{C_v}}{\sqrt{N_G}} = \frac{142.6}{\sqrt{29}} = 26.5 \text{ percent.}$$

Thus, the $V_R/\overline{V_T}$ for use in entering figure 3 is given by

$$\frac{V_R}{V_T} = \left(\frac{SE_R}{SE_{\bar{x}}}\right)^2 = \left(\frac{19.0}{26.5}\right)^2 = 0.51.$$

For this value of $V_R/\overline{V_T}$ and an assumed average interstation correlation coefficient of 0.75, figure 3 gives 1.43 for SE_P/SE_R. But for the 41 stations and 2 basin parameters in this regression, figure 1 gives an adjustment of −0.03 to V_P/V_R. Thus, the adjusted SE_P/SE_R is $\sqrt{(1.43)^2 - 0.03} = 1.42$, and the average standard error of mean October discharge for ungaged sites estimated from the regression is 1.42(19.0) or 27.0 percent, which is only slightly larger than the average time-sampling standard error at the gaged sites used in the regression. (As indicated in the preceding section, it is possible for the estimates at the ungaged sites to be even more accurate than the computed values of the characteristic at the gaged sites used in the regression.)

In terms of equivalent years of record, the accuracy of October discharge estimated from the regression is given by

$$N_U = \left(\frac{100C_v}{SE_P}\right)^2 = \left(\frac{142.6}{27.0}\right)^2 = 27.9 \text{ years.}$$

Thus, it appears that the average accuracy of mean October discharge for ungaged sites predicted from the regional regression is so good that further attempt to improve it is not required.

The adjustment indicated by figure 1 was applied in the two examples given here to illustrate the method, but for practical purposes the ratios from figure 3 could have been used without adjustment. So long as the relation between number of stations and number of basin parameters is such that the adjustment indicated by figure 1 is between +0.10 and −0.10 the effect on the computed standard error of prediction will have little practical importance.

LIST OF SYMBOLS

- b . . . . . The ratio $V_R/\overline{V_T}$.
- C_s . . . Coefficient of skew of annual events.
- C_v . . . Coefficient of variation of annual events; $\overline{C_v}$ is average C_v.
- I_v. . . . . Index of variability equal to standard deviation of logarithms of annual events; $\overline{I_v}$ is average I_v.
- k . . . . . Number of stations used in the regression.
- N. . . . . Number of annual events.
- N_G . . . Harmonic mean of the number of annual events observed at stream-gaging stations used in the regression, in years; equals the reciprocal of the average reciprocal of the N's at all stations.
- N_U . . . Accuracy of estimated streamflow characteristic at a site not used in the regression, in equivalent years of record.
- m. . . . . Number of independent variables used in the regression.
- ρ . . . . . Average interstation correlation coefficient.
- R. . . . . Factor relating standard error of a T-year event to I_v and $\sqrt{N}$.
- SE_P . . . Standard error of prediction, in log units or in percent.
- SE_R . . . Standard error of estimate of a regression, in log units or in percent.
- SE_{x_T} . Standard error of estimated T-year event, in log units; equals $R(I_v)/\sqrt{N}$.
- $SE_{\bar{x}}$ . . . Standard error of estimated mean event, in percent.
- T. . . . . Average interval, in years, between recurrences of an annual event of equal or greater severity.
- V. . . . . Variance; equals $(SE)^2$, in which SE is in log units or percent.

V_P . . . Variance of predictions made from a regression; $\overline{V_P}$ is average V_P.

V_R . . . Variance of the regression; equals $(SE_R)^2$.

V_S . . . Variance due to space-sampling error; same as model error.

V_T . . . Variance of a streamflow characteristic estimated from observed annual events; equals $(SE_{x_T})^2$ or $(SE_{\overline{x}})^2$; $\overline{V_T}$ is average V_T.

z . . . . . A weighted measure of the departures of the specific values of the independent variables from their mean.

REFERENCES

Benson, M. A., 1962, Evolution of methods for evaluating the occurrence of floods: U.S. Geol. Survey Water-Supply Paper 1580-A, 30 p.

Carter, R. W., and Benson, M. A., 1970, Concepts for the design of streamflow data programs: U.S. Geol. Survey open-file report, 33 p.

Davies, O. L., 1961, Statistical methods in research and production, 3d ed.: New York, Hafner Publishing Co., 396 p.

Hardison, C. H., 1969, Accuracy of streamflow characteristics, *in* Geological Survey Research 1969: U.S. Geol. Survey Prof. Paper 650-D, p. D210–D214.

Kerridge, D., 1967, Errors of prediction in multiple regression with stochastic regressor variables: Technometrics, v. 9, no. 2, p. 309–311.

Matalas, N. C., and Gilroy, E. J., 1968, Some comments on regionalization in hydrologic studies: Water Resources Research, v. 4, no. 6, p. 1361–1369.

Thomas, D. M., and Benson, M. A., 1970, Generalization of streamflow characteristics from drainage-basin characteristics: U.S. Geol. Survey Water-Supply Paper 1975, 55 p., 16 figs.

PRECIPITATION DEPTH-DURATION-FREQUENCY RELATIONS FOR THE SAN FRANCISCO BAY REGION, CALIFORNIA

By S. E. RANTZ, Menlo Park, Calif.

Work done in cooperation with the U.S. Department of Housing and Urban Development

Abstract.—Precipitation depth-duration-frequency relations have been derived for the San Francisco Bay region, California. The regimen of precipitation in the region is such that depth-duration-frequency characteristics for a site are closely related to the mean annual precipitation for that site.

The purpose of this study was to derive precipitation depth-duration-frequency data for the San Francisco Bay region to be used as criteria for both local drainage design and the study of the stability of land slopes. The study region encompasses 7,416 square miles in the nine counties surrounding San Francisco Bay (fig. 1). The frequencies studied were those corresponding to recurrence intervals of 2, 5, 10, 25, 50, and 100 years; the durations studied ranged from 5 minutes to 60 consecutive days. Data for the shorter durations are required for local drainage design and also for the study of surface-erosion potential, with land slope and soil type as additional factors. Data for the longer durations, to be used in conjunction with land slope and soil and geologic factors, are needed for the study of land-slippage potential.

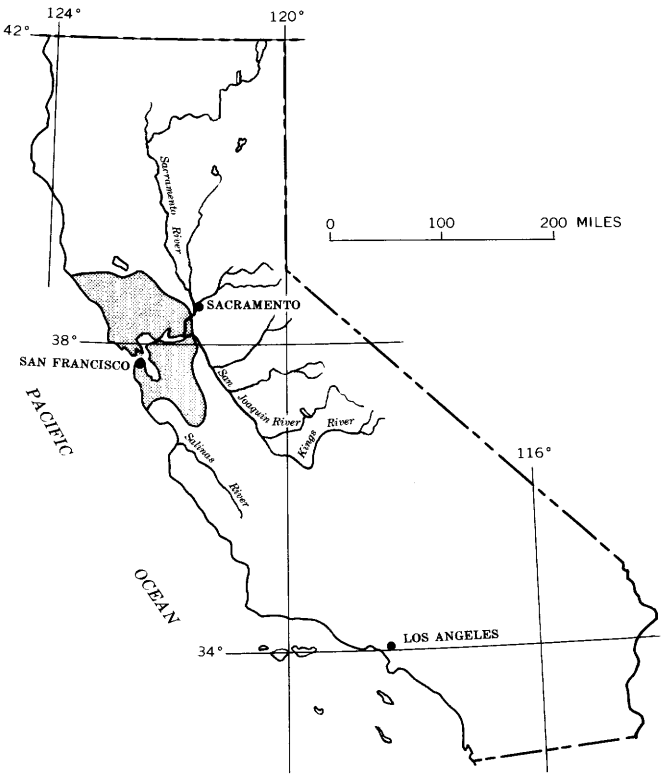

Figure 1.—Location map of California, showing report area (shaded).

REGIONAL REGIMEN OF PRECIPITATION

Precipitation in the region is highly seasonal; almost 90 percent of the annual precipitation occurs during the 6-month period November through April. The great bulk of that precipitation occurs in a series of general storms that reach all parts of the region, but the storm centers usually pass to the north of the region, and the result is a general tendency for precipitation to decrease from north to south. Altitude has a strong local influence on the depth of precipitation, and because altitudes range from sea level to 4,400 feet, there is a wide range in mean annual precipitation in the San Francisco Bay region—from 10 inches in low-lying valley areas in the east to 80 inches in some mountain areas in the north. Winter precipitation often occurs as snow at altitudes above 2,000 feet, but snowfalls are generally light, and snow does not remain on the ground for more than a few days. Snow, therefore, has an insignificant role in the hydrology of the region. Intense local convective storms are almost unknown in the region.

DATA AVAILABLE FOR ANALYSIS

The end product of this study, as mentioned earlier, is a set of precipitation depth-duration-frequency relations for use

anywhere within the study region. A preliminary step is the preparation of such data for climatological stations in and near the region. For each year of record at a station a tabulation is made of the maximum precipitation depth experienced for each of the duration periods under consideration. A theoretical statistical distribution is then fitted to the array of annual data for each individual duration period, and precipitation depths for selected recurrence intervals are computed. The California Department of Water Resources has such computations in its files and graciously made them available for this study. Included were data for 35 recording and 45 nonrecording stations. A Pearson type III distribution had been fitted to the arrayed precipitation depths. Duration periods used for the recording stations were 1, 2, 3, 6, 12, and 24 hours; duration periods used for the nonrecording stations were 1, 2, 3, 4, 5, 6, 8, 10, 15, 20, 30, and 60 consecutive days.

For the 35 recording stations, the mean annual precipitation ranged from 9 to 62 inches. For 32 of those stations, the number of years of record ranged from 11 to 28. The other three stations had much longer records—Sacramento, 66 years; San Francisco, 79 years; and San Jose, 60 years.

For the 45 nonrecording stations, the mean annual precipitation ranged from 9 to 73 inches. The number of years of record at the stations ranged from 17 to 94. However, 30 of the stations had more than 30 years of record, and of those, 15 had more than 60 years of record.

METHOD OF ANALYSIS

The reasoning behind the method used for obtaining depth-duration-frequency relations for ungaged sites was as follows: The bulk of the annual precipitation occurs in several general storms each year, and all areas in the San Francisco Bay region usually experience all these storms. Furthermore, intense local convective storms are almost unknown in the region. Although more rainy days occur at sites that receive greater annual precipitation, there usually is not a great difference among sites in the duration of any particular storm in the region. Therefore, we expect a relation to exist between the mean annual precipitation at a site and the depth of precipitation there for a given duration period and a given recurrence interval. In other words, if the total number of hours or days of precipitation does not vary greatly among sites in the region, there should be a general relation between precipitation intensity and total depth of precipitation. However, because the average annual number of rainy days at a given site is usually greater than the number at another site having less total precipitation, we do not expect the relation to be in the form of a direct ratio. For example, although site A experiences twice as great a mean annual precipitation as site B, we expect the storm precipitation for a short period at site A to be something less than twice that at site B. We also expect the departure from a direct ratio to be more pronounced for the shorter duration periods.

On the basis of the above reasoning, precipitation depths at all appropriate stations for each of the 17 duration periods (1 hour to 60 days) were correlated graphically with their mean annual values. An individual relation was determined for each of the six recurrence intervals chosen for study—2, 5, 10, 25, 50, and 100 years. This resulted in 102 curves of relation—six recurrence intervals for each of the 17 duration periods. Some of the relations were adjusted slightly for internal consistency, as will be explained later, and equations describing the final form of all 102 relations were obtained. These equations, to be used with mean annual precipitation values between 10 and 80 inches, are shown in table 1. Although it had been expected that the relations would not be in the form of a direct ratio, it was found that for the four largest recurrence intervals for 2-day storms and for all durations greater than 2 days, the departure from a direct ratio was insignificant. In other words, the value of a in the equations of table 1 was zero for the longer durations. All but nine relations were linear; those nine had curvilinear segments for values of mean annual precipitation less than 20 inches. The nine relations included all six of the relations for 1-hour precipitation and those for 2-hour precipitation for recurrence intervals of 2, 5, and 10 years.

To obtain precipitation depths for duration periods of less than 1 hour, an appropriate coefficient is applied to the precipitation depths computed for 1 hour. Table 2 gives the coefficients to be applied for durations of 5, 10, 15, and 30 minutes; the values of the coefficients do not vary with recurrence interval.

In all 102 correlations the plotted points showed considerable scatter, and the greatest scatter—in inches, not percentage—occurred at depths corresponding to large values of mean annual precipitation. Typical examples of this are shown in the scatter diagrams for the 3-hour and 15-day durations at the 25-year recurrence interval (figs. 2 and 3, respectively). After the 102 correlations had been made, all computed precipitation depths corresponding to a mean annual precipitation of 80 inches were used in plotting a family of frequency curves on extreme-value probability paper. (The frequency curves have been omitted from this report because of space limitations.) In order to have smooth frequency curves passing through, or very close to, all the plotted points, it was necessary to adjust the values of some of the points. This in turn made it necessary to adjust the coefficient b, or slope, of several of the preliminary depth-duration-frequency relations, but none of the coefficients required a change of more than about 3 percent. The purpose behind all these adjustments was to ensure internal consistency among the 102 derived relations, the reasoning being that the form of the derived relations in table 1 is such that if smooth frequency curves are achieved for precipitation depths corresponding to a mean annual precipitation of 80 inches, all frequency curves corresponding to lesser precipitation depths will likewise be smooth.

All equations given in table 1 are in their final adjusted form. To provide a measure of the scatter of the plotted points

Table 1.—*Regression equations for precipitation depths of various durations at selected recurrence intervals*

Duration (consecutive time units)	Recurrence interval, T (years)	Values of constants in regression equation: $P_T = a + bP_{MA}$[1]	
		a	b
1 hour	[2]2	0.32	0.0080
	[2]5	.40	.0105
	[2]10	.50	.0115
	[2]25	.60	.0130
	[2]50	.65	.0140
	[2]100	.70	.0150
2	[2]2	.40	.015
	[2]5	.50	.019
	[2]10	.55	.021
	25	.68	.022
	50	.75	.023
	100	.80	.025
3	2	.40	.023
	5	.50	.028
	10	.60	.031
	25	.70	.033
	50	.80	.034
	100	.90	.035
6	2	.50	.041
	5	.60	.054
	10	.70	.060
	25	.80	.066
	50	.90	.070
	100	1.00	.073
12	2	.32	.072
	5	.60	.084
	10	.80	.090
	25	.90	.100
	50	1.10	.105
	100	1.25	.110
1 day	2	0.20	0.100
	5	.30	.130
	10	.40	.150
	25	.50	.175
	50	.70	.190
	100	.80	.205
2	2	.20	.132
	5	.10	.190
	10	0	.230
	25	0	.275
	50	0	.305
	100	0	.340
3	2	0	.160
	5	0	.220
	10	0	.260
	25	0	.306
	50	0	.340
	100	0	.370
4	2	0	.175
	5	0	.240
	10	0	.285
4 days (con.)	25	0	0.340
	50	0	.380
	100	0	.420
5	2	0	.185
	5	0	.260
	10	0	.300
	25	0	.360
	50	0	.400
	100	0	.440
6	2	0	.200
	5	0	.280
	10	0	.325
	25	0	.385
	50	0	.430
	100	0	.470
8	2	0	.225
	5	0	.305
	10	0	.350
	25	0	.410
	50	0	.450
	100	0	.490
10	2	0	.245
	5	0	.330
	10	0	.380
	25	0	.440
	50	0	.480
	100	0	.520
15	2	0	.285
	5	0	.380
	10	0	.440
	25	0	.510
	50	0	.560
	100	0	.610
20	2	0	.310
	5	0	.425
	10	0	.490
	25	0	.570
	50	0	.630
	100	0	.680
30	2	0	.370
	5	0	.500
	10	0	.580
	25	0	.670
	50	0	.735
	100	0	.800
60	2	0	.530
	5	0	.720
	10	0	.825
	25	0	.950
	50	0	1.050
	100	0	1.130

[1] Where P_T = precipitation, in inches, corresponding to recurrence interval of T years; P_{MA} = mean annual precipitation, in inches; a and b are constants.

[2] Equation does not apply for values of mean annual precipitation (P_{MA}) less than 20 inches, because relation is curvilinear for short-duration precipitation in subhumid areas.

Table 2.—*Coefficients to convert 1-hour storm precipitation to storm precipitation for shorter duration periods*

Duration (minutes)	Coefficient[1]
5	0.29
10	.45
15	.57
30	.79

[1] Adapted from U.S. Weather Bureau (1961, p. 2, 5).

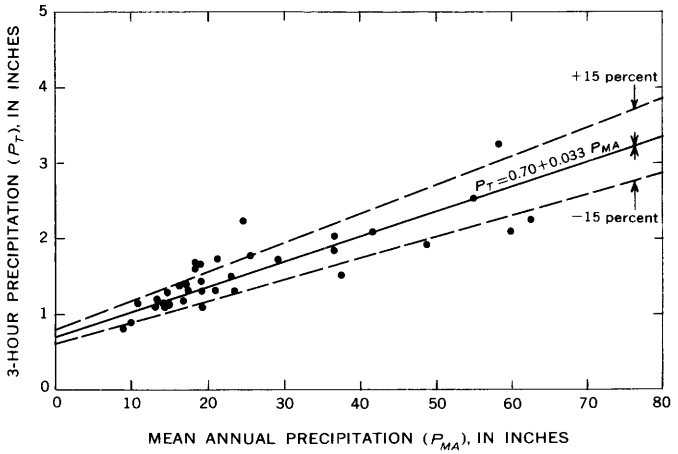

Figure 2.—Scatter diagram relating mean annual precipitation to 3-hour precipitation for the 25-year recurrence interval.

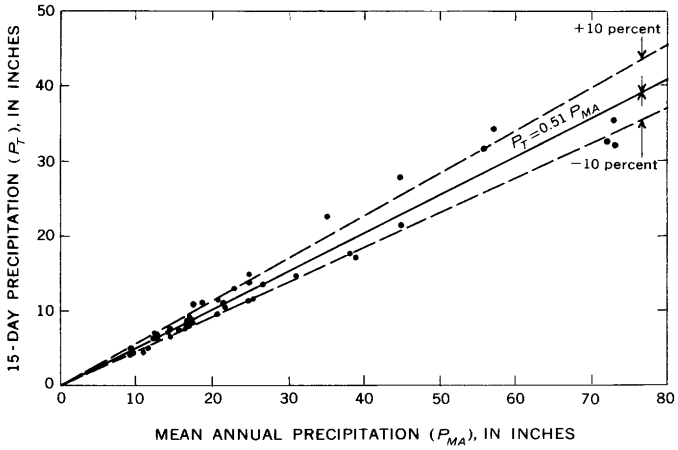

Figure 3.—Scatter diagram relating mean annual precipitation to 15-day precipitation for the 25-year recurrence interval.

in the 102 relations, the tabulation in the next column gives a generalized index of the standard error of the relations. The index shows the percentage deviation from the relations that includes about two-thirds of the plotted points. For example, the relation shown in figure 2 has two-thirds of the plotted points within the ±15 percent band; the relation in figure 3 has two-thirds of the plotted points within the ±10 percent band.

Duration (days)	*Recurrence interval (years)*	*Error index (percent)*
Less than 1	2, 5	±10
	10, 25	±15
	50, 100	±20
1–8	2, 5	±10
	10, 25, 50	±15
	100	±20
10–15	2, 5, 10, 25	±10
	50, 100	±15
20–60	All recurrence intervals	±10

USE OF THE DERIVED PRECIPITATION RELATIONS

To obtain depth-duration-frequency data for any given site in the San Francisco Bay region, first obtain the mean annual precipitation for that site from an isohyetal map. To that value apply the appropriate equations in table 1 for the durations and frequencies that are required. For storm durations of less than 1 hour, first obtain the precipitation for a 1-hour storm of the required frequency, then multiply that value by the appropriate coefficient from table 2. For sites whose mean annual precipitation is less than 20 inches, table 1 indicates that a curvilinear relation exists between mean annual precipitation and storm precipitation of duration shorter than 3 hours; therefore, do not use the first nine equations listed in table 1 for such sites. Space limitations preclude graphical depiction of the nine relations that are curvilinear; they are shown in the as yet unpublished original report from which this paper was abstracted.

EVALUATION OF RESULTS

As mentioned earlier, the 102 correlations involving storm depth and mean annual precipitation had graphical standard errors of estimate ranging from 10 to 20 percent. Much of this error can properly be ascribed to local departures from the regional relation, although no systematic geographical pattern of departure was evident. However, some of the error may arise from the time-sampling variation introduced by the combining of short-term records with long-term records. It is probable that estimates made from the regional relations are more accurate than estimates derived from short-term records, even at the location of the short-term station. The explanation for that statement is as follows: (1) The station data used in the analysis were derived, as stated earlier, by fitting a Pearson type III distribution to observed data; (2) the Pearson type III distribution uses the coefficient of skew as one of its parameters; (3) use of the coefficient of skew computed from a short array of data may often result in a biased distribution, particularly if unusually large or small values of precipitation are included in the short array of observed data.

The 102 correlations are independent of the isohyetal map to which they will be applied because the station values of mean annual precipitation used in the correlations were not

obtained from any map, but were the mean annual values computed for the various periods of record used in the analysis. The relations may therefore be used with any isohyetal map of mean annual precipitation for the study area; the more reliable the map, the more reliable the final results will be.

It is anticipated that this report may raise two questions in the mind of the reader, and it seems appropriate to conclude with a reply to those anticipated questions. It is easy enough for the reader to see the necessity for precipitation depth-frequency data of short duration for drainage design, but he may well ask: "Why must similar data be obtained for the longer durations for slope-stability studies, in view of the fact that storm precipitation correlates so well with mean annual precipitation; why not just use mean annual precipitation as an index of storm precipitation? Furthermore, why were data computed for so many different duration periods?" In answer to the first question, if we were interested in slope-stability problems solely in the San Francisco Bay region, the use of mean annual precipitation as an index of storm precipitation would probably be adequate. However if the results of slope-stability studies are to have transfer value for use in other regions, and if in those other regions differing relations of storm precipitation to mean annual precipitation exist, as they undoubtedly do, it is necessary that we use actual values of storm precipitation, rather than general index values. In answer to the second question, depth-duration-frequency data were provided for many duration periods because we cannot tell in advance which duration periods will be critical in slope-stability studies.

REFERENCE

U.S. Weather Bureau, 1961, Rainfall frequency atlas of the United States for durations from 30 minutes to 24 hours and return periods from 1 to 100 years: U.S. Weather Bur. Tech. Paper 40, 115 p.

ORIGIN AND SEDIMENTOLOGY OF 1969 DEBRIS FLOWS NEAR GLENDORA, CALIFORNIA

By KEVIN M. SCOTT, Garden Grove, Calif.

Prepared in cooperation with the California Department of Water Resources

Abstract.—Watersheds near Glendora yielded catastrophic volumes of debris slurry during the recordbreaking 1969 storms. Erosion rates sufficient to reduce the entire land surface by more than 2 inches occurred in several of a series of steep mountain-front basins which had suffered brush fires in 1968. The most concentrated damage from debris flows occurred among homes built directly at the mouth of a basin with a drainage area of 0.09 square mile and a relief of 1,400 feet. Triggered in part by surficial slope failures, the debris flows mobilized channel bed material and scoured channels to bedrock. This mechanism is probably the most common means of coarse-sediment transport in these and similar basins. Channel oaks were of considerable value in retaining debris and reducing the number and size of hillslope failures of the type which triggered the flows.

On January 22, 1969, in response to locally unprecedented rainfall throughout southern California, torrents of granular debris surged from small watersheds above Glendora, inundated residential areas, and damaged at least 175 homes. Muddy debris enveloped structures, poured through doors and windows, and surrounded the automobiles of residents attempting to flee the disaster. Such flows were among the most widely reported results of the catastrophic 1969 floods throughout the huge metropolitan area of southern California. Portrayal by national news media of the scenes of personal economic disaster caused by the flows was graphic evidence of the need for improvement in urban planning, zoning ordinances, and flood insurance in the area.

Sediment yields from the watersheds above Glendora locally exceeded 200,000 cu yd per sq mi (cubic yards per square mile) during the storm runoff in January and February 1969. Such a high yield exceeded the previous high seasonal debris-production rate in Los Angeles County of 130,000 cu yd per sq mi, recorded during the 1937–38 season. The purpose of this paper is to describe some of the factors that caused high rates of erosion and briefly to document the character of the debris flows and the way in which they formed.

ENVIRONMENT

Glendora, 20 miles east of downtown Los Angeles, is a valley community situated directly at the base of the east-west-trending San Gabriel Mountains (fig. 1). The city is dominated by the steep south front of the mountains, which rise precipitously from the flanking surface of coalesced alluvial fans on which urbanization has taken place. The mountains, part of the Transverse Ranges, are geologically young and tectonically active. Uplift of the mountain mass has occurred at a much greater pace than denudation, a situation resulting in a geomorphic setting wherein major storms trigger the production and transport of large quantities of sediment. Erosion is highly episodic, responding to the short-but-violent rainstorms that are characteristic of the area. Major storms like those of 1969 are separated by many years during which little or no movement of coarse detritus occurs.

The fans and fanheads at the foot of the mountain front have been built by the deposition of debris from past flash floods and debris flows issuing from the short, steep watersheds. They are the natural loci of deposition for debris from the same processes in the future. The recent growth of such valley communities as Glendora has included construction on the flank of the valley, so that large parts of many fans are now covered with homes. (An awareness of the slope stability problems that attend construction on the steeper slopes above the fans has restricted expansion into those areas.) These newly urbanized foothill areas, because of their positions on the fans and the recurrence of torrential rainstorms, are subject to damage by floods and debris flows from the small watersheds above. Damage from these phenomena, chiefly from debris flows, totaled $2,500,000 in the Glendora area in 1969. Residents of areas on the fans and fanheads that escaped damage in 1969 (see fig. 1) should, for the most part, consider their escape fortuitous because many characteristics of the flows are presently unpredictable—most notably, the positions of channels of transport across the fans may shift rapidly in response to changing factors such as: (1) sediment load, which varies greatly when debris transport is largely by debris-flow

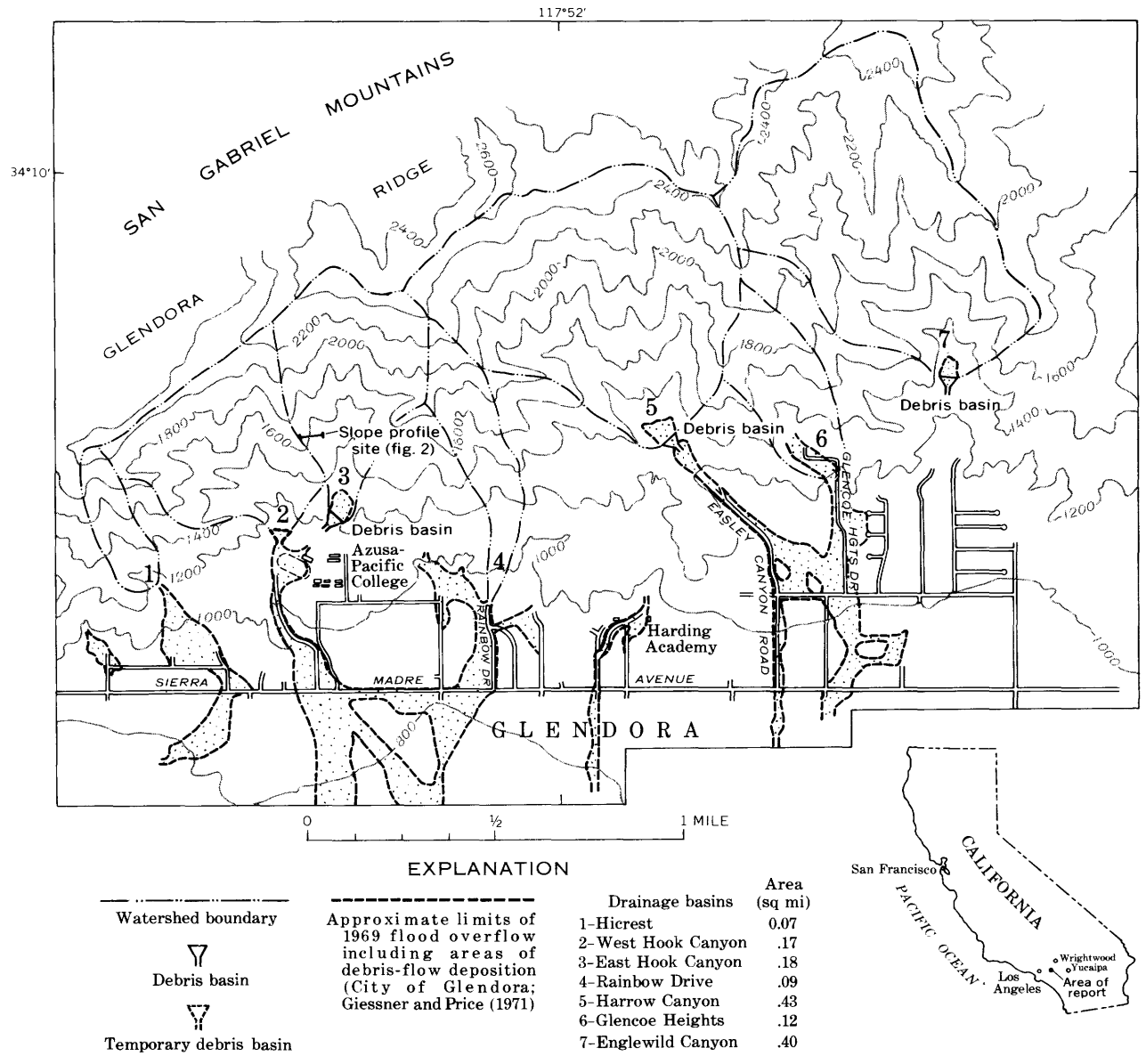

Figure 1.—Map of main watersheds above Glendora, Calif. Watersheds listed were those contributing greatest volumes of debris flow during the 1969 floods. Streets and facilities shown were sites of extensive damage from both debris flow and waterflow.

surges, leading to (2) local deposition during lulls in the storm or between debris flows, which may fill the old channel and divert subsequent flow into a new one, or (3) the formation of debris levees that may channel or divert subsequent flows.

The watersheds along the southern slopes of the San Gabriel Mountains resemble giant gullies when viewed from the air. Channel profiles are extremely steep, and hillslopes can be climbed only locally and with difficulty. Total relief of the main watersheds which contributed debris flows ranges from 900 to 1,400 feet, and the drainages range in area from 0.07 to 0.43 square mile. The most extreme example is the Rainbow Drive watershed, which has a relief of slightly more than 1,400 feet and an area of only 0.09 square mile (55 acres).

The bedrock of all the watersheds above Glendora is a complex of acid to intermediate granitic rocks most often described as highly weathered, though in fact the alteration is predominantly deuteric. The soil mantle consists of thin, sporadic, azonal mountain soils. The rock is highly fractured and is eroded from the hillslopes of the frontal watersheds at a rate sufficient to minimize soil-forming processes. Gravity is an important process acting to move debris such as colluvium and talus from hillslopes to channels during the dry season. Experiments by the U.S. Forest Service on nearby frontal watersheds showed that such dry-sliding, as the process is known locally, was an important debris transport mechanism following brush-fire denudation (Krammes, 1960). A number of major landslides were mapped within the Glendora watersheds (Morton and Streitz, 1969), but these large slope failures

were only indirectly related to the smaller surficial failures described below, which generated at least several of the debris flows.

Hillslopes in all the watersheds are covered with chaparral, a dwarf forest of shrubs and stunted tree forms, which are highly flammable during the dry season. The steep canyons act as natural flues for brush fires during the characteristic summer dry season and before the first good rain of the winter storm season. Canyon oaks rooted in channel alluvium and on basal hillslopes most often survive the fires and are instrumental in retaining debris within the watershed and preventing the mobilization of channel bed material, as will be described below, in addition to preventing erosion on lower hillslopes. Optimum conditions for the release of large quantities of debris include a dry-season burn, below-normal antecedent precipitation to inhibit regrowth of watershed cover, and a major runoff-producing storm. This set of circumstances occurred in the watersheds above Glendora during 1968–69.

STORMS AND DEBRIS FLOWS

The most devastating series of debris flows above Glendora occurred during the storm of January 18–27, 1969. This two-phase storm, however, was only the first of two major storms to bring locally unprecedented precipitation and runoff to southern California in 1969. Record rainfall and discharge figures set by the March 1938 storm were surpassed in many areas. The second of the 1969 storms, February 22–25, produced peak discharges that in most areas did not exceed those of January; renewed debris flow activity in the Glendora area did only minor damage.

The January storm began as a tropical low moving out of the Pacific Ocean from the southwest. A ridge of high pressure, present throughout much of the earlier winter season, deteriorated to permit onshore movement of the front. The main surge of the system occurred January 21–22, and mountain ranges oblique to the storm track, such as the San Gabriel range, received the most intense precipitation. A general comparison with the recurrence intervals of peak discharges from the nearest small drainage basins indicates that the January flooding in the Glendora area had a recurrence interval greater than 70 years and perhaps greater than 100 years (Giessner and Price, 1971).

The main series of debris flows occurred near the end of the initial phase of the January storm. The prelude to the disaster, however, had been staged the previous summer when most of the watersheds above Glendora were burned by brush fires in July and August 1968. Rainfall in the interval between the burns and the first storm was barely half of normal, and little vegetative recovery had occurred. Consequently, when the storm hit, initial rainfall was absorbed by the dry soil mantle, and the watersheds were rapidly saturated.

Conditions climaxed early January 22 when torrential rainfall struck the frontal watersheds, triggering many small slope failures and an intense sloughing of debris from hillslopes. Rainfall figures (Simpson, 1969) indicate that as much as 1.30 inches fell in 1 hour in the watersheds above Glendora near the peak of debris-flow activity. Recurrence intervals of total January storm precipitation were as much as 75+ years at higher elevations in the San Gabriel Mountains, where more than 45 inches fell at one station during the 10-day period.

The most concentrated damage due almost solely to debris flows occurred at the mouths of the Rainbow Drive and Glencoe Heights watersheds (fig. 1). Homes built in and along the active channels debouching from the mouths of these watersheds were in places totally destroyed. The small size of both watersheds illustrates the obvious economic infeasibility of debris-basin construction for every watershed in the frontal San Gabriel Mountains and suggests that the most practical alternative in areas destined for urbanization is land use planning in concert with flood control projects.

SEDIMENT SOURCES—HILLSLOPE EROSION, HILLSLOPE FAILURES, AND MOBILIZATION OF CHANNEL BED MATERIAL

The recordbreaking seasonal sediment yield in Los Angeles County of more than 200,000 cu yd per sq mi was measured in the debris basin in East Hook Canyon, one of three permanent basins constructed by the Los Angeles County Flood Control District in the area. Sediment yields measured in these basins, which functioned well in retaining the bulk of the debris under extreme circumstances, are summarized in table 1. Some debris passed the spillway of each basin during the storms, so that even these measured rates are slightly under the true values. Based on field observations, sediment yields per unit area in the Rainbow Drive and Glencoe Heights watersheds, although unmeasured, probably exceeded the above record yield.

The slope profile in figure 2 indicates local amounts of erosion on a typical slope in the East Hook Canyon watershed. The values represent vertical amounts of root exposure or the

Table 1.—*Sediment-yield data for watersheds in the Glendora area, California, during the 1969 storms*

[From Simpson (1969)]

Location of debris basin	Drainage area (sq mi)	Debris production	
		January storm period (cu yd per sq mi)	February storm period (cu yd per sq mi)
East Hook Canyon.	0.18	140,000	[1]83,000
Englewild Canyon.	.40	112,000	38,200
Harrow Canyon.	.43	122,000	25,200

[1] Estimated.

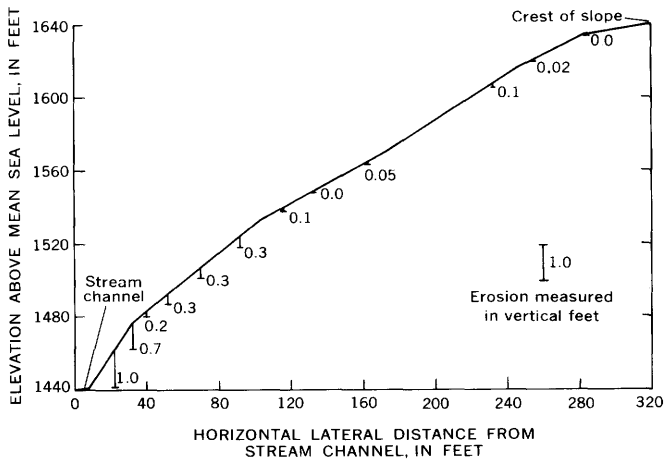

Figure 2.—Slope profile in the East Hook Canyon, Calif., watershed, showing net amounts of erosion caused by the 1969 storms.

height of large fragments preserved on storm-eroded pedestals. Gully formation throughout the watersheds was surprisingly minor in areal extent. Many slopes seemed to have shed sediment by a sheetlike sloughing of debris, especially on their lower, steeper segments. As in the erosion profile of figure 2, most hillslopes in the watersheds are convex upward. Also, as shown in figure 2, erosion occurred predominantly on the lowest and steepest segments, in a few places to the apparent near exclusion of the remainder of the slope.

Small slope failures were important as an erosional source of sediment. Such failures commonly involved only surficial rubble and dry-sliding deposits. Bedrock was involved in only a few instances. Crudely triangular in shape, the failures apparently generated many of the individual debris flows and accounted for surges in the debris flows from larger watersheds. Tracing and measuring the height of debris-flow levees upstream revealed that in many instances the depth of debris flow (d_{df} in fig. 3) increased abruptly at the sites of slope failures.

In at least one instance (Rainbow Drive watershed, fig. 3) a slope failure contributed flowing debris to a channel at a point above which there was no evidence of debris having moved down the channel.

Another major component of the debris flows was mobilized channel bed material. Study of root exposures permitted estimates of the net channel scour (d_s in fig. 3) that took place during the storm. Scour was greatest in intermediate reaches within the watersheds. Even in the lower reaches, where deposition might have been expected, scour was apparently continuous.

DEBRIS-FLOW CHANNELS

The most striking aspect of the channels within the watersheds shortly after the storms was the degree to which reaches in all parts of the watersheds had been scoured to bedrock. A part of this scour was caused by recession runoff,

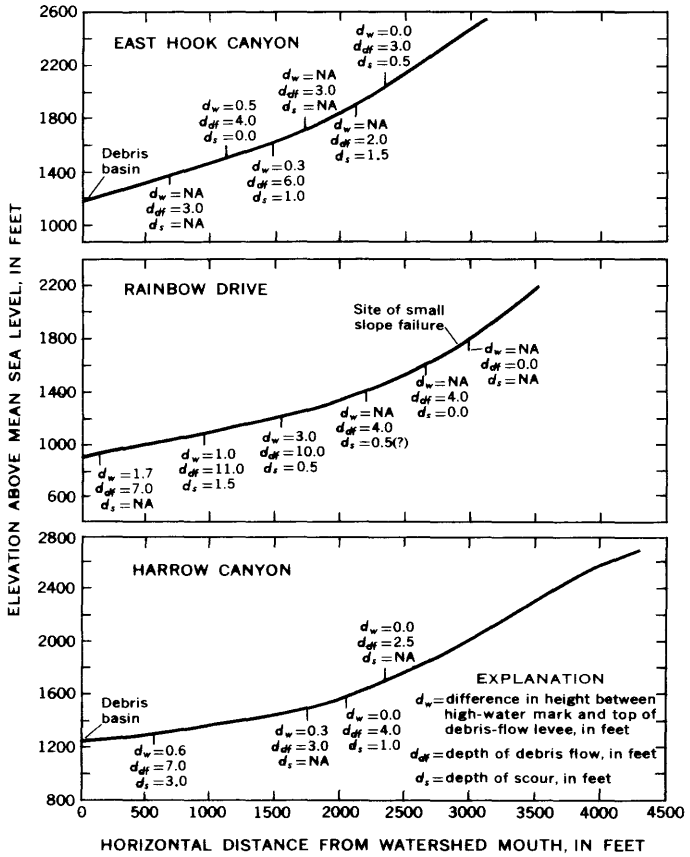

Figure 3.—Channel profiles of three typical Glendora, Calif., watersheds among those yielding debris flows in 1969. NA, not available.

which was not debris laden. Most of the scour, however, clearly was due to incorporation of coarse bed material into the debris flow. By the late summer of 1969, less than 6 months after the last of the storms, noteworthy quantities of debris again were being supplied laterally to the channels by gravitational processes.

Channel processes in the burned watersheds differed only in magnitude from those in unburned watersheds. The processes of sediment yield from both burned and unburned watersheds involve continuous supply from slopes during both dry and wet seasons, accompanied by periodic flushing of debris from the channels during major storms. Much of the debris supplied laterally to the channels is so coarse that significant downchannel transportation could be effected only in a viscous slurry such as a debris flow. The sedimentary characteristics of pre-1969 flood deposits in the watersheds indicate that debris-flow transportation also has predominated in the past.

Most of the debris in the boulder size range probably is removed from the watersheds by the debris-flow mechanism. Such a sediment regime is strikingly different from the situation in normal alluvial channels, where coarse debris that is supplied laterally or residual debris from times of greater runoff must commonly await size reduction by in-place weathering before transport. In fact, on the basis of study of channels in these watersheds and others nearby, a case could

Table 2.—*Textural data for debris flows in two Glendora watersheds and for mudflows near Wrightwood and Yucaipa, Calif.*

[Graphic statistical measures described by Folk (1964)]

Sample	Location		Type	Modal classes		Graphic mean particle size M_z	Inclusive graphic deviation σ_I	Inclusive graphic skewness SK_I	Total silt and clay (percent)	Roundness of ϕ–2 class (4–8 mm) (percent >0.15, the transition from angular to subangular)
	Watershed	Distance above mouth (miles)		Primary mode ϕ class	Secondary mode ϕ class					
3–1 . .	Rainbow Drive. . .	0.51	Dry-sliding (colluvium).	−1	−3	−1.2	2.5	+0.20	8.2	2
3–2 . .	. . .do. . .	.41	1969 debris flow.	−4	Not pronounced	−1.9	2.6	+.38	6.6	2
3–3 . .	. . .do. . .	.29	. . .do. . .	−5	. . .do. . .	−3.4	2.5	+.55	3.1	17
3–4 . .	. . .do. . .	.18	. . .do. . .	−3	None	−1.5	2.5	+.22	5.8	30
3–5 . .	. . .do. . .	.03	. . .do. . .	−3	None	−1.7	2.7	+.48	6.8	45
4–1 . .	Harrow Canyon . .	.44	Dry-sliding (colluvium).	−3	−1	−1.9	1.6	+.12	2.2	0
4–2 . .	. . .do. . .	.30	1969 debris flow.	−3	None	−2.6	2.2	+.29	2.9	8
4–3 . .	. . .do. . .	.23	. . .do. . .	0	None	−0.6	2.4	+.04	7.2	23
4–4 . .	. . .do. . .	.10	. . .do. . .	−1	None	−1.4	2.3	+.10	4.9	52
Wi–2[1]	Wildwood Canyon near Yucaipa, Calif.	. . . .	1969 mudflow	−3	5	0.7	3.7	+.49	28.7	. . .
Wr–1[1]	Heath Creek near Wrightwood, Calif.	. . . .	. . .do. . .	1	3	1.0	3.1	+.37	25.4	. . .

[1] Analyses by wet sieve and pipet.

be made for debris-flow or mudflow transport of the majority of coarse debris in most watersheds under 5 square miles in the San Gabriel Mountains.

The channels at low and intermediate elevations of the watersheds are lined with oaks. Each of these fire-resistant trees directly retained an estimated 15–100 cubic yards of debris in its root system. Additional, greater quantities of debris upslope were stabilized by many of the trees, and in some places the root structures acted as natural check dams, protecting from erosion the terraces formed of previous debris-flow deposits. The more time one spends in the watersheds, the more one is impressed with the importance of the canyon oaks in retaining debris, slowing erosion, and reducing sediment yields. Certainly, future phreatophyte eradication projects proposed in watersheds similar to those near Glendora should assess the role of the oaks in debris retention when benefit-cost ratios are computed.

DEBRIS-FLOW DEPOSITS

Texturally, the Glendora debris-flow deposits are similar to typical debris flows (American Geological Institute, 1957, p. 193) and distinctly different from known mudflows (American Geological Institute, 1957, p. 74). In none of the analyzed samples (table 2) did the mud content (total silt and clay <0.0625 mm, 4ϕ) exceed 10 percent. Such a mud content contrasts with values commonly in excess of 10 percent for many flows described as mudflows. The mudflows sampled for comparative purposes were those associated with the 1969 snowmelt in Heath Creek near Wrightwood and related to 1969 storm precipitation in Wildwood Canyon near Yucaipa (fig. 1).

The sorting (expressed as σ_I, table 2) of the debris-flow deposits is better than that of mudflows. It is still, however, in the poorly sorted range of Folk (1964). The sorting of mudflows commonly is extremely poor, as high as 7ϕ–8ϕ. In the series of samples representing traverses in two main watershed (Rainbow Drive and Harrow Canyon) channels (table 2), no downstream change in sorting of deposits is apparent in either channel after an initial upstream deterioration in the degree of sorting, as shown by comparison of the flow deposits with the sliding deposits. Once mixing of the variety of source materials has been accomplished, little selective sorting occurred within the watersheds.

Skewness of the debris-flow deposits is uniformly positive and is in the range indicating a strong bias toward the fines in the size distributions. This is typical of much alluvial sediment and many mudflows. In terms of skewness, there is little distinction between the debris-flow deposits and the two sampled mudflows.

Most mudflows and many debris flows have bimodal size distributions. The two sampled mudflows were strikingly and characteristically bimodal. Only four debris-flow deposits were bimodal, and those weakly so; the remainder showed no secondary mode.

Distinctive levees or berms of coarse debris accreting to channel sides were observed wherever a debris flow was known to have occurred. These striking features, differing from the deposits at the sides of known mudflow channels only in texture, are flat topped and in most reaches are coincident with or only slightly below high-water marks. Measurements of the difference in height between high-water marks and the tops of the levees (d_w in fig. 3) indicate the probable depth of water flow at the time of peak debris flow. From eyewitness accounts of other debris flows in frontal watersheds of the San Gabriel Mountains, and because of the unlikelihood that predominantly waterflow filled the channels to these levels, it is assumed that d_w is the depth of waterflow at the time peak debris-flow discharge occurred. Flow in the channels at times appeared to be in the form of a two-phase slurry in which the upper, substantially more fluid phase was less important as a transport mechanism.

Inspection of the channels indicates that normal indirect measurement of peak discharge would give extreme values and that sometimes the resultant values probably would exceed enveloping curves developed for maximum floods in small drainage basins in southern California. There can be little doubt that, at the time of formation of the high-water marks, the channels were passing substantial, if not peak, discharges of debris flow. Evidence of the upper, less viscous phase of the flow commonly is preserved in a thin layer of water-laid detritus at the top of the debris-flow levees. Material in that layer is better sorted and generally not as coarse as that in the debris-flow deposits.

An attempt was made to determine the relative importance of each sediment source by studying differences in roundness in an intermediate size fraction. Such information would be useful in watershed stabilization programs designed to reduce debris production. It was thought that the channel bed material, presumably having been subject to a history of fluvial processes, would be better rounded than debris supplied directly to the channel by sliding, slope failures, and sheet erosion and that this difference would remain during transport. Such, however, was not the case (table 2). Analysis of the ϕ-2 (4–8 mm) size fraction showed that debris-flow deposits in upper reaches of the watersheds contained clasts with roundness little changed from that of the almost totally angular roundness range (0–0.15) of sliding deposits. As expected, average roundness increased downstream (table 2) but appeared to do so relatively uniformly for all clasts in the size range studied, a finding that rules out simple dilution of angular clasts with better rounded particles and negates any determination of sources beyond a short interval of initial mixing. This conclusion, although negative in regard to determining debris sources, is in accordance with the model of debris production discussed above—lateral supply to channels by processes acting on slopes, followed by periodic transport out of the watersheds almost exclusively by debris flows.

REFERENCES

American Geological Institute, 1957, Glossary of geology and related sciences: Washington, D.C., Natl. Acad. Sci.–Natl. Research Council, Pub. 501, 325 p.

City of Glendora, 1969, 1969 storm report and recommendations: 13 p.

Folk, R. L., 1964, Petrology of sedimentary rocks: Austin, Tex., Hemphill's, 154 p.

Giessner, F. W., and Price, McGlone, 1971, Flood of January 1969 near Azusa and Glendora, California: U.S. Geol. Survey Hydrol. Inv. Atlas HA–424. [In press]

Krammes, J. S., 1960, Erosion from mountain side slopes after fire in southern California: Pacific Southwest Forest and Range Expt. Sta. Research Note 171, 7 p.

Morton, D. M., and Streitz, R., 1969, Preliminary reconnaissance map of major landslides, San Gabriel Mountains, California: California Div. Mines and Geology Map Sheet 15.

Simpson, L. D., 1969, Hydrologic report on storms of 1969: Los Angeles County Flood Control Dist., 286 p.

FOREST SPECIES AS INDICATORS OF FLOODING IN THE LOWER WHITE RIVER VALLEY, ARKANSAS

By M. S. BEDINGER, Little Rock, Ark.

Abstract.—The dominant environmental factor of forest habitats within the lower valley of the White River, Ark., is flooding. The flood plain consists of a series of terraces. Distribution of forest species on the terrace levels is related to flooding. The relationship is sufficiently distinct to permit determination of flood characteristics at a given site by evaluation of forest-species composition. The vegetation of the lower White River valley can be divided into four groups. Each group occurs on sites having distinctly different flooding characteristics. On sites flooded 29–40 percent of the time, the dominant species are water hickory and overcup oak. On sites flooded 10–21 percent of the time, a more varied flora exists—including nuttall oak, willow oak, sweetgum, southern hackberry, and American elm. The third group of sites is subject to flooding at intervals of from 2 to 8 years. This group is marked by presence of southern red oak, shagbark oak, and black gum. The presence of blackjack oak marks the fourth group (not flooded in historic times).

The forest vegetation of the lower White River valley in Arkansas is broadly classified by Küchler (1967) as a southern flood-plain forest, with oak, gum, and cypress predominating. However, any single descriptive term is inadequate to describe the varied forest assemblages that naturally inhabit the bottom lands of the White River.

The dominant characteristics of forest habitats within the flood plain are the frequency and duration of flood inundation. The flood plain consists of a sequence of levels or terraces. Upstream regulation of the White River, which has been significant since 1952, has resulted in a reduction of floodflows. Prior to regulation of the river by dams, the lowest extensive terrace, commonly called the first bottom, was flooded annually, with the average duration of flooding being about 29–40 percent of the time. Since regulation, the first bottom has been inundated about 15–20 percent of the time. The highest terrace that was flooded in historic times, sampled for this study, was flooded on the average about once in 8 years. Since regulation, this terrace has not been flooded. A higher terrace that has not been flooded in historic times was also sampled. The long-range effects of these changes in flooding on forest composition are not known. For example, it is not known whether or not areas now flooded 15–20 percent of the time will eventually contain some species characteristic of a higher terrace that was flooded 15–20 percent of the time prior to regulation. Flood characteristics used in this report to describe sites are for the period prior to significant regulation of the White River. For the present study, only forest trees 4 inches DBH (diameter at breast height, 4½ feet or larger), and presumed to have been established prior to significant regulation of flow, were sampled.

Acknowledgments.—The author is grateful for the advice and assistance of colleagues and associates during the planning and fieldwork of the study and the writing of the manuscript.

C. B. Sinclair, Chairman, Life-Sciences Department, University of Arkansas at Little Rock, and Richard L. Phipps, Research Botanist, U.S. Geological Survey, Arlington, Va., visited field sites with the author and made valuable suggestions. Raymond McMaster, Superintendent, White River National Wildlife Refuge, permitted access to the refuge. Sedge Watson, in charge of forest management at the White River National Wildlife Refuge, was helpful in discussions of the identification and distribution of tree species in the refuge.

DESCRIPTION OF STUDY AREA

The area studied (fig. 1) is in the Coastal Plain province (Fenneman, 1938). The lower White River valley can be divided topographically into a series of terraces. Each terrace level in the bottom land represents a former active level of river deposition. The lowest level is the most extensive areally and is marked by features such as backswamp areas, oxbow lakes, swales, and natural levees bordering the major waterways. The highest level, the Grand Prairie terrace, is about 40 feet above the lowest flood-plain level. Although the Grand Prairie, as its name indicates, is a natural prairie, "islands" of forested areas are found. The bottom land of the White River is naturally forested. The bottom-land soils are medium- to fine-grained silts and clays and are slowly to moderately permeable. The Grand Prairie soils of thick clays of very low permeability have not been flooded in historic times.

The hydrologic environment of the lower levels of the White River flood plain could be described as extreme or rigorous. The lower flood-plain levels are naturally flooded each year

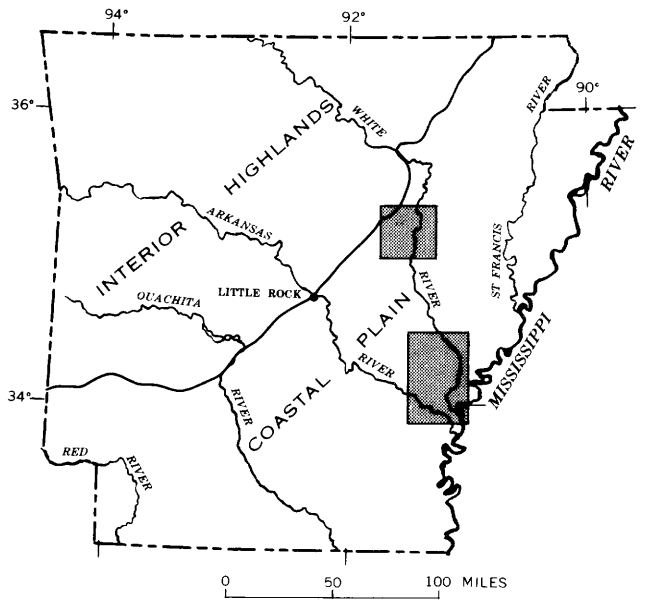

Figure 1.—Index map of Arkansas, showing study areas (shaded) in the White River valley.

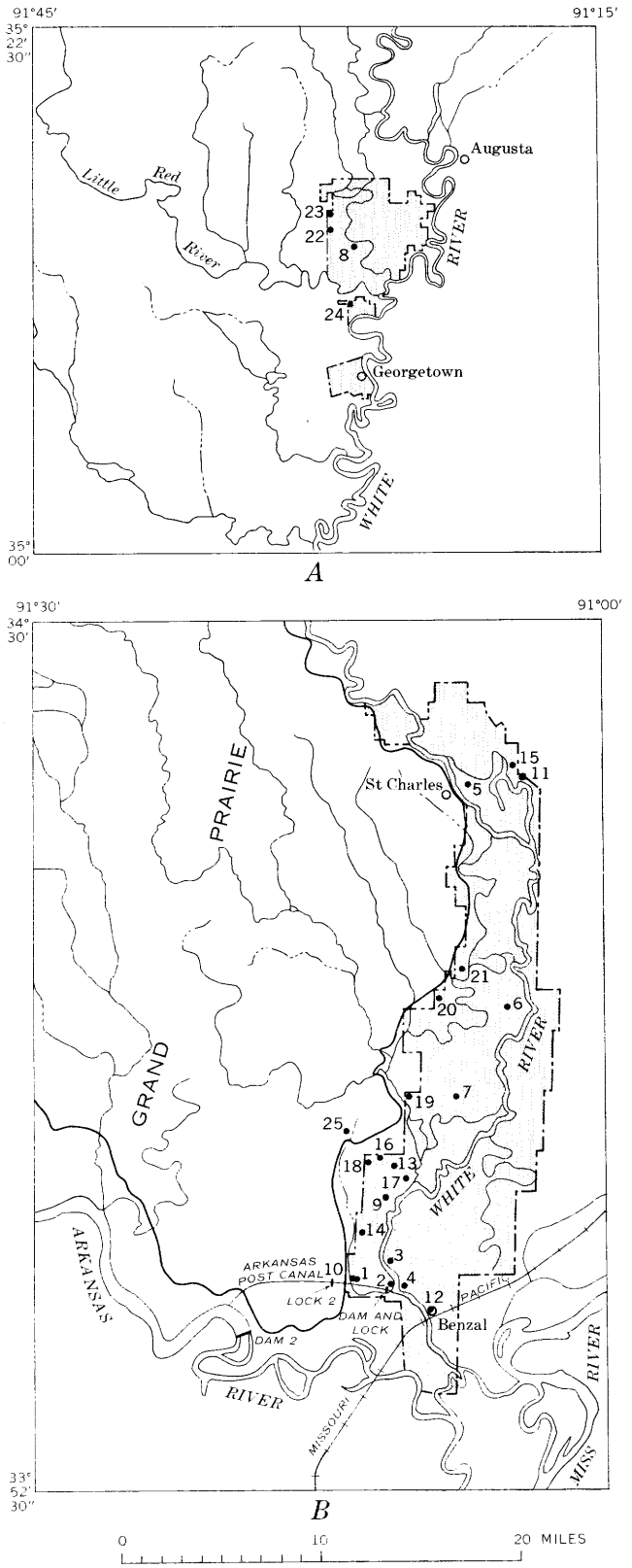

Figure 2.—Maps showing location of sampling sites (numbered dots). *A*, sites in the Hurricane Lake Public Hunting Area (shaded); *B*, sites in and near the White River National Wildlife Refuge (shaded).

about 40 percent of the time—a much longer duration than most flood plains in the Coastal Plain of Arkansas. Flooding generally occurs in winter and spring. The floodwaters generally recede in late spring or early summer, followed by flow below bankfull stage until late fall or winter. The nearest similar habitat to the lower White River valley is in the lower Ouachita River valley of south Arkansas that is also flooded for 35–40 percent of the time. It is interesting to speculate that the cause of flooding characteristics in both valleys is of similar geological origin. The streams drain areas with relatively small sediment yield and are tributary to streams with large sediment load. Sedimentation by the trunk streams (Arkansas and Mississippi) was much greater than that by the Ouachita and White—thus resulting in a rise in base levels of the Ouachita and White Rivers without a concomitant equal rise in the level of their flood plains by deposition.

PURPOSE AND METHODS OF STUDY

The purpose of this study was to determine the relation of tree species to the flooding in the forests in the lower White River valley. Flood frequency and duration of flooding are used as parameters to describe the flooding characteristics of each site sampled. Sites were selected to include the range of flooding in the valley. The areas for study of forest vegetation in the lower White River valley were practically limited to large forested tracts in which the natural forest has not been obliterated by timber operations or cleared for agriculture. The sites sampled for this study were centered in two areas: (1) The White River National Wildlife Refuge, near the mouth of the White River, and (2) the Hurricane Lake Public Hunting Area, near Augusta, Ark. (fig. 2). Timber management

in these areas may have altered the natural percentages of the forest species, but it is not believed that the species makeup has been changed. Each site is relatively level and homogeneous in habitat. Local drainage courses and depressions were avoided. Within each of 25 sites, 50 pairs of trees (100 trees) were selected, each tree at least 4 inches DBH. This sampling procedure, described below, is the random-pairs method of Cottam and Curtis (Phillips, 1959).

The first tree in each pair is the nearest tree to a predetermined point on a traverse. An area around the first tree is excluded from consideration in selecting the second tree. The excluded area is determined by the observer standing on the point and facing the nearest tree. Arms outstretched on both sides of the observer mark a 180° angle. No trees in front of the observer in the 180° sector containing the first tree are chosen. Rather, the nearest tree outside this area behind the observer is chosen as the second member of the pair. The diameter of each tree and the distance between them are measured and recorded. The species of each tree is recorded.

Specimens of most of the forest species were collected during the fall of 1970 and are now in the herbarium of the University of Arkansas at Little Rock, Ark. Duplicate collections of some of the species are in the herbarium of the University of Arkansas at Fayetteville.

Inundation characteristics of a flood plain can be described by the frequency of flooding and by the duration of time that the flood plain is under water. For areas frequently flooded, the duration of flooding is probably more significant than the frequency of flooding.

Flood frequency can be analyzed by either of two flood series—the annual-flood series or the partial-duration series. In the annual-flood series, only the highest peak stage in each water year (October 1 to September 30) is used. The partial-duration series includes all peaks higher than a selected base (Patterson, 1964).

Data on annual floods were readily available from gaging stations on the White River. Flood frequencies for this study were computed from the annual-flood series, using the formula (Dalrymple, 1960)

$$T = (n + 1)/m,$$

where T is the recurrence interval, in years, n is the number of years of record, and m is the order number, beginning with the largest flood as 1. The relation between the annual-flood series and the partial-duration series is shown in the following table (Langbein, 1949). The two flood series give practically the same results for recurrence intervals of 10 years or more.

Recurrence interval, in years	
Annual-flood series	*Partial-duration series*
1.16	0.5
1.58	1.0
2.00	1.45
2.54	2.00
5.52	5.0
10.5	10

Flood (stage) duration curves, based on stream-stage records through 1951, were computed for three gaging stations on the White River. Flood duration, the percentage of time that a given site is inundated, was used as a parameter in evaluating vegetation at sites flooded more frequently than once every 2.0 years. A flood-recurrence interval, based on the annual-flood series, is used for sites flooded at intervals of 2 years, or greater. The relation between flood frequency and flood duration for the White River is given in the following table. At each station, the 20-percent-duration stage was exceeded each year during the period of record.

Augusta		St. Charles		Benzal	
Frequency (years)	Duration (percent of time)	Frequency (years)	Duration (percent of time)	Frequency (years)	Duration (percent of time)
1.1	10	1.25	10	1.2	10
1.3	5	1.9	5	1.75	5
2.0	1.5	2.0	4.5	2.0	4
2.5	.8	2.5	4	2.5	2.5
3.5	.4	3.5	1.8	3.5	1.6
5	....	5	1.1	5	.9
8	....	8	.6	8	.5
10	....	10	.5	10	.4

REGULATION OF FLOODS IN THE WHITE RIVER

Construction of dams on the White River and its tributaries has altered the flood regimen in the study area. Flows on the White River were not significantly affected by reservoirs until 1952, when Bull Shoals Reservoir began operation. Prior to 1952, three reservoirs had been constructed—Lake Tanneycomo on the White River, Clearwater Reservoir on the Black River, and Norfork Reservoir on the North Fork River. Lake Tanneycomo, completed in 1913, and Clearwater Reservoir, completed in 1948, had an insignificant effect on flows in the White River. Norfork Reservoir, completed in 1943, had a small influence on floodflows in the study area. Since 1952, Beaver and Table Rock Reservoirs have been constructed on the main stem, and Greers Ferry Reservoir has been constructed on the Little Red River.

Flooding in the lower parts of the White River is affected not only by the flow in the White River, but also by the stage of the Mississippi River. Flows in the Mississippi River, upstream from its confluence with the White River, seem to have been affected by structures on the upper Mississippi River and tributaries and by construction of cutoffs on the river. The effect is noticeable in gross examination of hydrographs of the Mississippi, which shows a decrease in peak flows and stages of yearly floods.

Prior to construction of the Arkansas River Multiple-Purpose Project (ARMPP) in the 1960's, the lower White River was also affected by high stages in the Arkansas River. The construction of the ARMPP eliminated a natural cutoff between the White and Arkansas Rivers that had permitted flow between the rivers during high stages.

Stage records are available for several stations on the White River near the forest sites sampled for this study. Records used in flood analysis date back to 1934 at St. Charles, Ark., 1939 at Augusta, Ark., and 1937 at Benzal, Ark. (locations are shown in fig. 2).

The history of regulation on the White River indicates that the period through 1951 was the period of record most representative of natural, preregulated flow conditions on the river.

The stations at Benzal, St. Charles, and Augusta, Ark., provided the basis for assignment of flood-duration and flood-frequency values at each sampling site. Values of floodflow characteristics at sites between stations were based on the river gradient and the proportionate distance of each site from gaging stations. The gage at Georgetown, Ark., downstream from Augusta (fig. 2), was used in determining stream gradients for the sites in the Hurricane Lake Public Hunting Area.

STRATIFICATION OF FOREST TREES

The species distribution in the lower White River flood plain is related to habitat, particularly to the hydrologic factors of the habitat. Local features related to hydrology, that is, oxbow lakes, streambanks, river sandbars, bayous, and others, are associated with certain species such as cottonwood, willow, cypress, sycamore, and water tupelo (table 1). Though these species are present in the lower White River flood plain, they are species of special environments and are a small part of the flood-plain vegetation as a whole. The present study related the species of broad, generally homogeneous habitats in the flood plain to the hydrologic factor rather than to the species of the special or forest-edge habitat.

The vegetation of the sites sampled for this study can be grouped into four broad categories. The flood characteristics of the sites in each category are correspondingly similar. The sites in the first group are flooded annually, with the average duration of flooding ranging from 29 to 40 percent of the time. The sites in the second group are flooded from 10 to 21 percent of the time. The second group is inundated during most years. Sites in the third group are flooded on an average of from once every other year to once in 8 years. A fourth category includes one site on the Grand Prairie terrace that had not been flooded during historic times. A summary of the distribution of selected forest species with respect to flooding is given in table 2.

The forest of the first group (29–40 percent duration of inundation) is referred to as the water hickory-overcup oak group, and is composed primarily of six species. Water hickory and overcup oak are major species; southern hackberry, water locust, water elm, and swamp privet are minor species. On some sites, southern hackberry is a major species. On the lower sites in this group, these six species, with an occasional bald cypress, may compose the entire forest.

Table 1.—*Common and scientific names of trees in the lower White River Valley, Arkansas*

[Nomenclature after Moore (1960)]

Common name	Scientific name
Ash	*Fraxinus* spp.
Beech, blue	*Carpinus caroliniana* Walt.
Blackgum	*Nyssa sylvatica* Marsh.
Boxelder	*Acer negundo* L.
Cherry, black	*Prunus serotina* Ehrh.
Cottonwood	*Populus deltoides* Bartr.
Cypress, bald	*Taxodium distichum* (L.) Rich.
Dogwood, flowering	*Cornus florida* L.
Elm:	
American	*Ulmus americana* L.
Cedar	*Ulmus crassifolia* Nutt.
Water	*Planera aquatica* (Walt.) Gmelin
Winged	*Ulmus alata* Michx.
Hackberry, southern	*Celtis laevigata* Willd.
Hawthorn	*Crataegus* spp.
Hickory:	
Bitternut	*Carya cordiformis* (Wang.) K. Koch
Mockernut	*Carya tomentosa* Nutt.
Shagbark	*Carya ovata* (Mill.) K. Koch
Shellbark	*Carya laciniosa* (Michx. f.) Loud.
Water	*Carya aquatica* (Michx. f.) Nutt.
Locust:	
Honey	*Gleditsia triacanthos* L.
Water	*Gleditsia aquatica* Marsh.
Maple:	
Red	*Acer rubrum* L.
Silver	*Acer saccharinum* L.
Mulberry, red	*Morus rubra* L.
Oak:	
Blackjack	*Quercus marilandica* Muenchh.
Nuttall	*Quercus nuttallii* Palmer
Overcup	*Quercus lyrata* Walt.
Pin	*Quercus palustris* Muenchh.
Post	*Quercus stellata* Wang.
Shumard	*Quercus shumardii* Buckl.
Southern red	*Quercus falcata* Michx.
Water	*Quercus nigra* L.
White	*Quercus alba* L.
Willow	*Quercus phellos* L.
Pecan, sweet	*Carya illinoensis* (Wang.) K. Koch
Persimmon	*Diospyros virginiana* L.
Possumhaw	*Ilex decidua* Walt.
Privet, swamp	*Forestiera acuminata* (Michx.) Poir.
Redbud	*Cercis canadensis* L.
Sweetgum	*Liquidambar styraciflua* L.
Sycamore	*Platanus occidentalis* L.
Willow	*Salix* spp.

On the highest site of the first group (flooded 29 percent of the time), a more varied flora may be found—the additional species including American elm, cedar elm, persimmon, red maple, silver maple, and blue beech. Two other species, nuttall

Table 2.—*Distribution of forest species in relation to*

Designation and forest species	Flood duration (percent of time)	Flood frequency (years)	Site (fig. 2) Number	Site (fig. 2) Name	*Taxodium distichum*	*Planera aquatica*	*Gleditsia aquatica*	*Forestiera acuminata*	*Carya aquatica*	*Quercus lyrata*	*Quercus nuttallii*	*Celtis laevigata*	*Salix* spp.	*Fraxinus* spp.	*Crataegus* spp.	*Ulmus americana*	*Ulmus crassifolia*	*Gleditsia triacanthos*	*Acer rubrum*
Group 1	40	....	1	Flat Lake	....	9	28	14	18	15	...	16	....	....	....	....	....	....	....
Water hickory–overcup oak group (flooded 29–40 percent of time)	36	....	2	Wild Goose Bayou	....	3	19	9	30	34	...	5	....	....	....	....	....	....	....
	33	....	3	Pickle Bar	1	4	11	10	17	52	...	5	....	....	....	....	....	....	....
	32	....	4	Dam 1	....	3	7	18	24	37	...	11	....	....	....	....	....	....	....
	29	....	5	St. Charles	1	1	2	5	4	10	13	34	....	10	1	4	1	....	1
	33	....	6	Escronges Lake	1	10	12	7	14	44	...	4	1	7	....	....	....	....	....
	32	....	7	Prairie Lake	3	1	4	10	13	47	3	9	....	10	....	....	....	....	....
Group 2 Nuttall oak group	21	....	8	Glaise Creek	....	....	....	2	9	10	26	11	....	9	3	2	17	....	....
	19	....	9	Prairie Landing	....	....	....	....	10	23	20	7	....	4	3	3	3	....	1
	18	....	10	Arkansas Post Canal	....	....	....	6	6	16	14	35	....	5	1	10	....	1	....
	17	....	11	Indian Bay	....	....	....	1	2	4	6	20	....	2	1	4	5	1	1
	15	....	12	Benzal	....	....	....	3	5	17	12	26	....	9	3	....	....	....	....
	15	....	13	Wolf Bayou	....	....	....	....	22	27	13	6	....	23	1	1	....	....	....
	11	....	14	Prosperous Bayou	....	....	....	....	6	7	19	6	....	10	1	8	1	....	5
	10	....	15	Kelly Field	....	....	....	....	1	4	3	9	....	2	....	6	1	2	1
	10	....	16	East-West road	....	....	....	....	8	15	5	27	....	1	2	5	1	....	2
	10	....	17	Jacks Bay	....	....	....	....	1	2	10	24	....	3	2	8	9	....	....
Group 3 Shagbark hickory–southern red oak group (flooded at intervals of 2–8 years)	....	2	18	Section 3	....	....	....	....	....	7	1	...	....	....	....	5	....	....	7
	....	2	19	Hickory Ridge	....	....	....	....	....	8	1	15	....	7	2	9	6	....	....
	....	2.5	20	Briar Ridge	1	....	....	....	....	....	....	4	....	1	....	5	....	....	....
	....	3.5	21	Essex Bayou	....	....	....	....	....	....	....	...	....	2	....	3	....	....	....
	....	8	22	Hurricane Lake	....	....	....	....	....	....	....	...	....	2	....	2	....	....	....
	....	8	23	Picnic	....	....	....	....	....	....	....	...	....	2	....	....	....	....	....
	....	8	24	Little Red River	....	....	....	....	....	....	....	...	....	2	....	5	....	....	....
Group 4	([1])	([1])	25	Bell Gully	....	....	....	....	....	....	....	2	....	2	....	....	....	2	....

[1] Not flooded in historic times.

oak and ash, are present in the higher sites of the first group. These species become conspicuous in the second group of sites (inundated 10–21 percent of the time).

Forests of the second group of sites (inundated 10–21 percent of the time), referred to as the nuttall oak group, are persistently more varied in species composition than the first group. The major species are overcup oak, nuttall oak, southern hackberry, ash, and water hickory. Willow oak and sweetgum are present on most of these sites and are commonly conspicuous. Swamp privet is present on some of the lower sites in this group. Water locust is rare in this group of sites, having been replaced by honey locust. Hawthorn and persimmon, though minor species, are present in almost all sites of the group and reach their greatest populations in the nuttall oak group.

The third group of sites (flooded at intervals of 2–8 years) is referred to as the shagbark hickory–southern red oak group because these species are major constituents and persist throughout the group. Bitternut hickory and black gum are found on higher sites of this group. The shagbark hickory–southern red oak group is also characterized by the paucity of several species conspicuous in lower sites. Water hickory is absent, and nuttall oak and overcup oak are found only on the lower sites of the third group. Several minor species, cedar elm, red maple, and blue beech, are sparingly present on the lower sites in the group. Among the species present on higher sites in this group are white oak, shumard oak, post oak, and pin oak.

A single species—blackjack oak—that is not found on lower sites is present in the fourth group (not flooded in historic times).

CONCLUSIONS

The present study demonstrates a definite relationship between the distribution of forest species and the frequency and duration of flooding on the lower White River flood plain. The relationship is sufficiently distinct to permit determination of flood characteristics at a given site by evaluation of the forest-species composition. Although the results of the study do not show a cause-effect relationship between species distribution and flooding, such a relationship is strongly suggested. A reconnaissance by the author of tree species in stream valleys of south-central Arkansas reveals that hydrologic habitats similar to those of the White River valley support a similar assemblage of forest species. For example, the first bottom of the lower Ouachita River valley, near the Arkansas-Louisiana State line, is flooded on the average 35–40 percent of the time. The forest species in this area are similar to forest species in like habitats of the lower White River valley. By contrast, the smaller stream valleys of south-central Arkansas are flooded nearly every year, but for a relatively short duration—a hydrologic condition that is not found in the lower White River valley. The difference in hydrologic environment is reflected by a distinct difference in the forest-species assemblages.

flooding in the lower White River valley, Arkansas

Quercus phellos	*Liquidambar styraciflua*	*Diospyros virginiana*	*Ulmus alata*	*Carpinus caroliniana*	*Acer saccharinum*	*Populus deltoides*	*Platanus occidentalis*	*Ilex decidua*	*Quercus nigra*	*Morus rubra*	*Acer negundo*	*Carya tomentosa*	*Carya ovata*	*Quercus falcata*	*Nyssa sylvatica*	*Carya laciniosa*	*Cercis canadensis*	*Quercus alba*	*Quercus stellata*	*Quercus shumardii*	*Carya cordiformis*	*Quercus palustris*	*Cornus florida*	*Prunus serotina*	*Quercus marilandica*
....	....	....	....	....	....	....	....	....	....	....	....	....	....	....	....	....	....	....	....	....	....	....	....	....	....
....	....	....	....	....	....	....	....	....	....	....	....	....	....	....	....	....	....	....	....	....	....	....	....	....	....
....	....	....	....	....	....	....	....	....	....	....	....	....	....	....	....	....	....	....	....	....	....	....	....	....	....
....	....	7	....	1	1	1	3	....	....	....	....	....	....	....	....	....	....	....	....	....	....	....	....	....	....
....	....	....	....	....	....	....	....	....	....	....	....	....	....	....	....	....	....	....	....	....	....	....	....	....	....
....	....	....	....	....	....	....	....	....	....	....	....	....	....	....	....	....	....	....	....	....	....	....	....	....	....
1	2	1	7	....	....	....	....	....	....	....	....	....	....	....	....	....	....	....	....	....	....	....	....	....	....
8	10	8	....	....	....	....	....	....	....	....	....	....	....	....	....	....	....	....	....	....	....	....	....	....	....
....	....	5	1	....	....	....	....	....	....	....	....	....	....	....	....	....	....	....	....	....	....	....	....	....	....
5	11	2	....	9	....	....	1	....	8	12	5	....	....	....	....	....	....	....	....	....	....	....	....	....	....
6	10	6	....	....	....	....	....	3	....	....	....	....	....	....	....	....	....	....	....	....	....	....	....	....	....
....	2	5	....	....	....	....	....	....	....	....	....	....	....	....	....	....	....	....	....	....	....	....	....	....	....
9	23	5	....	....	....	....	....	....	....	....	....	....	....	....	....	....	....	....	....	....	....	....	....	....	....
9	11	4	2	16	....	....	....	....	17	12	....	....	....	....	....	....	....	....	....	....	....	....	....	....	....
17	11	2	....	....	....	....	....	....	1	3	....	....	....	....	....	....	....	....	....	....	....	....	....	....	....
25	5	6	1	....	....	....	....	....	3	1	....	....	....	....	....	....	....	....	....	....	....	....	....	....	....
5	36	....	14	....	....	....	....	....	1	3	....	8	2	7	4	....	....	....	....	....	....	....	....	....	....
22	1	1	18	1	....	....	....	....	5	3	....	....	....	1	....	....	....	....	....	....	....	....	....	....	....
9	25	2	4	2	....	....	....	1	5	4	....	....	10	14	2	6	5	....	....	....	....	....	....	....	....
19	2	1	26	....	....	....	....	....	....	....	....	....	5	23	....	3	....	5	10	1	....	....	....	....	....
....	4	....	3	....	....	....	....	....	4	....	....	35	6	19	4	....	....	10	7	1	....	....	3	....	....
4	7	....	9	....	....	....	....	....	....	1	....	5	11	24	4	....	....	5	13	....	8	....	5	2	....
13	1	1	5	....	....	....	....	....	....	....	....	5	4	43	....	....	....	7	2	7	1	4	....	....	....
....	....	....	2	....	....	....	....	....	....	5	....	39	3	27	....	....	....	....	10	....	5	....	....	1	2

The reporting of such a fundamental relationship between flooding and forest species at this time reveals indirectly how little is actually known of the relationship between the Coastal Plain forest species and their environment. Many questions arise immediately—what will be the long-range effect of streamflow regulation on forest species in terms of growth rates, propagation, influence on species distribution, forest-management practices, and wildlife practices and habitat? The present study, by demonstrating a relationship between flooding and forest species, is potentially useful in answering these questions and can aid in the understanding of the environmental relationship of flood-plain forests. The species-flooding relationship is also of potential use to the hydrologist who may use forest species as criteria to transfer flooding parameters from gaging stations to ungaged reaches of streams.

REFERENCES

Dalrymple, Tate, 1960, Flood-frequency analysis: U.S. Geol. Survey Water-Supply Paper 1543–A, 80 p.

Fenneman, N. M., 1938, Physiography of Eastern United States: New York and London, McGraw-Hill Book Co., Inc., 714 p.

Küchler, A. W., 1967, Potential natural vegetation: U.S. Geol. Survey Natl. Atlas sheet 90.

Langbein, W. B., 1949, Annual floods and the partial-duration flood series: Am. Geophys. Union Trans., v. 30, p. 879–881.

Moore, D. M., 1960 Trees of Arkansas: Arkansas Forestry Comm., 128 p.

Patterson, J. L., 1964, Magnitude and frequency of floods in the United States—Part 7, Lower Mississippi River basin: U.S. Geol. Survey Water-Supply Paper 1681, 636 p.

Phillips, E. A., 1959, Methods of vegetation study: New York, Holt, Rinehart and Winston, Inc., 107 p.

SUBJECT INDEX

[For major headings such as "Economic geology," "Geochemistry," "Ground water," see under State names or refer to table of contents]

AUTHOR INDEX

☆U.S. GOVERNMENT PRINTING OFFICE—1971: 483-323/1